marine reSEArch@CNR.it

Oceanography

National Research Council of Italy

Oceanography

Toward an Assessment of Ocean Acidification in the Adriatic Sea and Impacts on the Biogeochemistry of Marine Carbonate System

A. Luchetta, C. Cantoni, G. Catalano, S. Cozzi
Institute of Marine Sciences, CNR, Trieste, Italy
anna.luchetta@ts.ismar.cnr.it

Abstract

The increase of CO_2 amount in the atmosphere has created great concern: it will in all probability result in changes in temperature, precipitation and/or their seasonal amplitudes with consequences not only on sea level rise but also on chemical equilibrium of the CO_2 system in seawater, mainly reducing pH and carbonate ion concentration (Ocean Acidification). The process is now well documented in field data from all around the world. However is not sufficiently witnessed in the Mediterreranean Sea, due to the scarcity of good quality data. On this concern, results for the Adriatic Sea are presented: from experimental measures of pH and total alkalinity, two seasonal pictures of pH and carbonate system parameters have been drawn. In addition, a pH decrease of 0.063 pH^T units with related chemistry changes has been inferred in the North Adriatic Dense Water (NAdDW) over the two last decades. These results, although preliminary, merit attention as confirm that N. A. sea has been affected by OA, being sensitive to the climate forcing. Potential impacts of OA are several and should be assessed, as many might even exacerbate hyopoxia/anoxia events, already affecting the area. OA might also affetc the food web, as the carbonate reduction has the potential to alter the distribution and abundance of marine organisms that use calcium carbonate to build their shells or skeletons (corals, plankton) and the organisms that depend on them for survival (fishes, marine mammals).

1 Introduction

Over the past 250 years the carbon dioxide (CO_2) concentration in the atmosphere has continuously raised, reaching values up to 380 ppmv, that have never been experienced on Earth in the last 800,000 years [1]. It is now largely recognized that this increase was mainly determined by human activities related to the combustion of fossil fuels and deforestation, which, in all probability will result in changes in temperature, precipitation and/or their seasonal amplitudes with consequences on the stability of our climate. Since the beginning of the industrial age, between 1800 and 2000, mankind has emitted 361 Gt C to the atmosphere [2]. The ocean has absorbed approximately 155 Gt C: this make the world ocean the largest sink of anthropogenic CO_2, without it atmospheric carbon dioxide levels would be approximately 450 ppmv today [2, 3]. The uptake of CO_2 by the ocean is primarily due to physicochemical processes. As CO_2 solubilises in seawater, it behaves like a weak acid that

dissociates according to:

$$\begin{aligned} \mathrm{CO_2(atm)} &\rightleftharpoons \mathrm{CO_2(aq) + H_2O} \\ &\rightleftharpoons \mathrm{H_2CO_3(aq)} \\ &\rightleftharpoons \mathrm{H^+(aq) + HCO_3^-(aq)} \\ &\rightleftharpoons \mathrm{H^+(aq) + CO_3^{2-}(aq)}, \end{aligned}$$

leading to an increase of [H+] and to a decrease of pH value (pH = -log [H^+]). The overall process resulting in a reduction of pH and shifts in carbonate speciation is referred to as "Ocean Acidification" (OA). Climate change and ocean acidification are both caused by the increasing of atmospheric CO_2 levels and ocean acidification has been recently referred to as "The other CO_2 problem" [4]. However, if climate change forecasts suffer from some uncertainties, in contrast OA is a well predictable consequence of rising atmospheric CO_2. On global scale, OA is now documented with hydrographic surveys, time series data and well verified from models [5, 6, 7, 8, 9, 10].

Since preindustrial times, the average oceanic surface pH has fallen down by approximately 0.1 units, from approximately 8.21 to 8.10 [11], and is expected to decrease a further 0.3–0.4 pH units [9] if atmospheric CO_2 concentrations reachs 800 ppmv (the projected end-of-century concentration according to the Intergovernmental Panel on Climate Change (IPCC) business-as-usual emission scenario). Ocean acidification alters seawater speciation and biogeochemical cycles of many elements and compounds, including nitrogen, phosphorus, silicon and trace elements (iron, zinc), thus changing their availability for phytoplankton [4]. Acidification of ocean water occurs in tandem with decreases in carbonate ion ($CO_3^=$) concentration and saturation state of calcium carbonate minerals ($CaCO_3$), which directly impact the formation and dissolution. In the marine environment, carbonate formation is largely a biotic process: corals, foraminifera, coccoliths, bivalves and other marine organisms form shells and skeletons composed of a variety of carbonate minerals.

CO_2 solubility in seawater is the highest at low temperatures, thus the most pronounced effects of OA on marine ecosystems are expected to affect sub polar seas and not the Mediterranean Sea, a semi-enclosed water body in a temperate climate region [12]. In addition Mediterranean seawater is characterized, on average, by higher alkalinity than open ocean, that would increase the buffering capacity of the Mediterranean waters thus limiting OA. Notwithstanding, ocean acidification is particularly interesting to be investigated in the Mediterranean Sea as the basin is supposed to be very sensitive to the global climatic change (giving a rapid response), because of the faster water renewal (shorter residence times of water masses) compared to the oceans and the high anthropogenic pressure concurrently with the high CO_2 carrying capacities of the cold surface waters in the northernmost regions. Consequently the Mediterranean area would already present significant pH drops [12], especially in the regions where cold dense waters are formed. But the OA process in the Mediterranean Sea is not sufficiently witnessed, due to the scarcity of good quality pH measurements, particularly in the Eastern sub-basin [12, 13].

The Adriatic basin is one of the few sites where dense waters are formed in wintry season. This process represents an important driving engine for the circulation and ventilation of deep waters of the east-

ern Mediterranean Sea. Adriatic dense waters form either on the northern shallow shelf of this basin, North Adriatic Deep Water (NAdDW), and by the deep Southern Adriatic Pit, Adriatic Deep Water (ADW). Afterward, they usually sink and outflow through the Otranto Strait sill (750 m), which controls the export to Ionian and Eastern Mediterranean Seas [14]. The Adriatic Sea has been therefore considered the dominant source region of dense waters for the Eastern Med until the occurrence of the Eastern Mediterranean Transient [15], in the end of 1980's, which abruptly changed the deep circulation pattern. At present time, the deep circulation scheme seems to have switched back to pre-Transient conditions.

The Adriatic basin is subjected to high anthropogenic pressure, being surrounded by very industrialized regions that release CO_2 into the atmosphere. There carbon dioxide uptake and ocean acidification would be particularly effective, due to low temperature of surface waters, especially in the northernmost part which represents the largest shelf area of the entire Mediterranean region [14]. According to the deep and bottom layers circulation scheme the Adriatic dense water masses are expected to have the possibility of spreading acidified waters around, through the Eastern Mediterranean.

Therefore monitoring the interannual variability of pH and studying the forcings on the carbonate system in the Adriatic Sea appears worth and new. Here are presented the major findings of the research activity carried out by ISMAR Trieste in last few years, within a few national and european projects and in collaboration with local environmental agency.

2 Methods

The determination of pH was performed by the spectrophotometric method described by Dickson [16], values are expressed on the total H^+ scale (pH_T, $[H^+]$ in μmol H^+/kg_{SW}), at 25 °C (as recommended by protocols for quality control of results), with a precision of $\pm$ 0.003 pH units. To our knowledge the dataset is the first collected with such a precision over the whole basin. The Total Alkalinity (A_T) has been measured by potentiometric titration in an open cell, with precision of $\pm$ 3.0 $/kg_{sw}$, the accuracy was controlled against certified reference materials (CRM) supplied by Andrew Dickson (Scripps Institution of Oceanography, San Diego, USA). Both the *in situ* fugacity of carbon dioxide (fCO_2) and the *in situ* pH values were calculated with the CO_2 calculation program (CO_2SYS program) developed by Lewis and Wallace [17] by using the parameters pH_T, A_T, silicate, phosphate, T *in situ* and S for each discrete sample. However, pH distributions in Figures 1, 2, 3, are shown at fixed temperature (25 C) because fixing the temperature means "lock" the equilibrium reactions of the carbonate system, getting rid of the temperature contribution. Thus any comparison between different water masses and different seasons is more immediate.

3 Results and discussion

3.1 pH_T spatial and seasonal variability in the Adriatic Sea

In Figures 1 and 2 are reported the distributions of potential density (σ_t), apparent oxygen utilization (AOU) and pH_T gath-

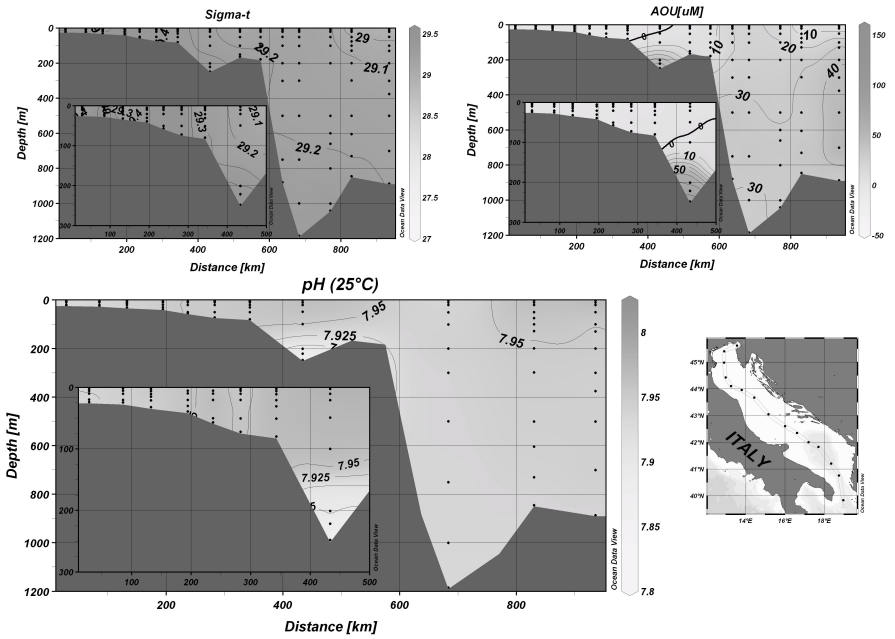

Figure 1: Potential density (σ_t), apparent oxygen utilization (AOU), pH_T at 25 C distributions along the Adriatic Sea in February 2008. In the smaller frames a more detailed view of the North Adriatic shelf area is given.

ered at meso scale in the Adriatic basin. They were measured during two surveys, conducted in February and October 2008, within the frame of VECTOR (national) and SESAME (EU FP-6) projects.

In February 2008 the North Adriatic shelf was involved in a dense water formation event, being shallow and exposed to cold dry winds (Bora) as reported also in the past [18]. The water column was well mixed, ventilated down to the bottom (mean AOU = -4.1 μM), cool (10.35 C) and dense ($\sigma_t > 29.3$ kgm^{-3}). The T/S properties were in agreement with those of NAdDW, that are among the densest of the Mediterranean Sea [19].

The whole water column was rich of DIN (1.00-7.00 μM) and SiO_2 (1.20–5.33 μM), even at surface, thus suggesting that intense primary production had not yet started. The pH_T values were homogeneously distributed in the water column, ranging between 7.917 and 7.973 pH_T units, with a mean value of 7.946 in the core of dense water mass (NAdDW). Biological processes such as primary production and remineralization of organic matter, could contribute to the final pH of seawater by consuming or adding CO_2. Such a homogeneous distribution of all parameters over an extended area mirrored the winter time conditions encountered. The pH_T values were driven by the high CO_2 solubility in cold seawater while intense biological pro-

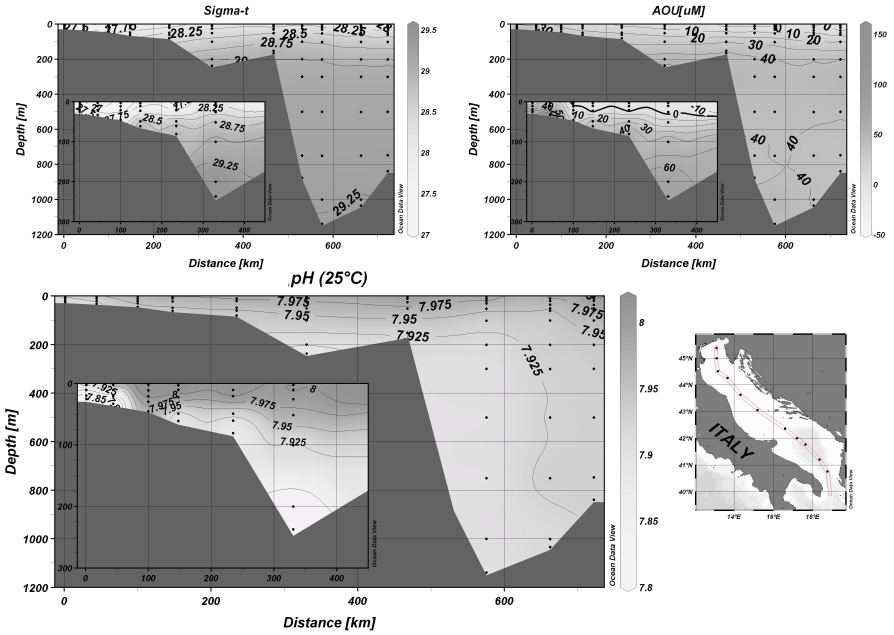

Figure 2: Potential density (σ_t), apparent oxygen utilization (AOU), pH^T at 25 C distributions along the Adriatic Sea in October 2008. In the smaller frames a more detailed view of the North Adriatic shelf area is shown.

cesses had not yet started (as indicated by AOU and nutrients values), that is typical of wintry season.

fCO_2 values calculated at fixed temperature (25°C) were high (avg 583 μatm) thus indicating that such cold and ventilated waters had adsorbed high CO_2 amount, that determined the decrease of pH_T value observeds. At the same time fCO_2 values, calculated at the *in situ* temperature, ranged from 222.4 to 334.6 μatm from surface to the bottom over the whole area. They resulted much lower than the equilibrium value with atmospheric CO_2 (398 μatm, mean value on measurements conducted on board). This clearly indicated the occurrence of under saturated conditions under which the northern Adriatic shelf region was a potential sink for atmospheric CO_2.

Generally, NAdDW water mass flows southward and accumulates at the bottom of the Meso and Southern Adriatic pits (250 and 1250 m, respectively) [14] as evidenced in Figure 1 by density, higher than 29.3 and 29.2 respectively, at the bottom. The dense waters of Meso Adriatic pit exhibited pH_T values lower ($<$ 7.880 pH_T units) than those on the northern shelf because the water mass was older (AOU higher than 65.0 μM), remineralisation processes had time to act releasing nutrients and CO_2 decreasing the pH, as indicated also by nutrients maxima ($SiO_2 >$ 6.0 μM , DIN $>$ 5.0 μM).

In the southern part of the section, a very clear event of deep convection was ob-

served on February 2008 in the deepest central stations, as pointed out by the homogeneous water column down to 600 m (σ_t around 29.15-29.16 kgm^{-3} down to 600 m, in Figure 1). pH_T had an average value of 7.947 $\pm$ 0.003 pH_T units, AOU was positive (15-35 μM) and nutrients were homogeneously distributed down to 600m. Such values suggest that the deep convection allowed mixing between surface and older (AOU $>$ 0) CO_2 enriched deep waters: for such reason surface AOU were positive in contrast to what occurring along the whole basin.

These results are in agreement to what reported in literature for the area, which is known to be dominated by a quasi-permanent cyclonic circulation intensifying in autumn and creating the conditions for the production of dense and oxygenated deep waters during winter deep convection events [14]. However fCO_2 *in situ* values, around 370-380 μatm, were still slightly lower than the equilibrium value with atmospheric CO_2 (398 μatm). At the beginning of October '08 the situation appeared completely changed as the whole Adriatic basin was characterized by the thermal and density stratifications typical of late summer conditions.

In the northern shallow shelf region sea water temperature varied between 13.0 C to 19.4 C from surface to bottom with an average value of 17.6, 7.3 degrees higher than February. The upper water column was characterized by higher pH_T values (between 7.960 and 8.050 pH_T units, Figure 2) than in February, due to primary production process witnessed by the release of oxygen (negative AOU values) and the depletion of all nutrients. In contrast, the layer below pycnocline, was strongly depleted of oxygen (AOU mean value = 102.3 μM), more acidic (7.784 pH_T units) and enriched in CO_2 and nutrients (DIN up to 22.9 μM; fCO_2>600 μatm) due to the remineralization of newly produced POC and labile DOC, all is characteristic of the autumn season.

The bottom water mass in the Meso Adriatic pit in October was about 0.1 °C colder than in February, less saline (0.1 psu) and more oxigenated (DO 20 μmol/L higher), thus indicating at least the partial renewal of this water mass with the NAdDW formed during previous winter on the northern shelf. Also in October pH_T mean value was low (7.861 pH_T units, in Figure 2) and mainly determined by remineralization processes as evidenced by high AOU values ($>$ 60 μM) and nutrient maxima (DIN up to 7.0 μM, SiO_2 up to 9.0 μM).

The southern part of the section was also characterized by late summer thermal and density stratifications (13.178 $<$ T $<$ 21.082 C), with the upper layer dominated by primary production processes (0 $<$ AOU $<$ 15) and characterized by higher pH_T (7.950 $<$ pH $<$ 8.0). In the layers below the pycnocline, remineralization processes prevailed as suggested by oxygen and nutrient values (AOU $>$ 40 μM; DIN $>$ 3.0 μM; SiO_2 $>$ 5.0 μM). Seasonal primary production provides POC (in different amounts) to the euphotic layers, which is available to the microbial community for remineralization during sinking to the bottom. This phenomenology was probably at the basis of the pH_T shift observed in the bottom water mass of the Southern Adriatic pit between February (pH_T = 7.937) and October (pH_T = 7.898).

This preliminary comparison between pH distributions and oceanographic conditions met in February and October 2008 pointed out the high spatial and seasonal variability of pH_T in the Adriatic sea. The fi-

nal values were determined by the combined effects of circulation patterns, temperature driven CO_2 solubility and biological processes (primary production, increasing pH_T values, and respiration of organic matter, lowering them).
However the most significant conclusion we can infer is the fact that the lower pH_T values of surface waters in winter were determined by the high dissolved CO_2 concentrations (due to atmospheric CO_2 forcing). In contrast the drawdown of dissolved CO_2 by photosynthetic planktonic organisms led to higher pH_T values in late summer.

3.2 Long term variability of pH_T in the dense waters of the northern Adriatic Sea

The first comparison between two sets of data related to the dense cold waters (Northern Adriatic Dense Water) formed, respectively, in winters 1982-1983 and 2007-2008 has been recently published [20]. Values of pH on the NBS scale from the old dataset were converted to the new "total hydrogen ion concentration scale" adopted for the new dataset and expressed in $^+/kg_{sw}$, as recommended by the international scientific community. Some results at 25 °C are summarized in Table 1, they show the decrease of both pH_T average value (-0.063 pH units) and carbonate ion concentration (-19.6 H^+/kg_{sw}), which named OA. In contrast, the total alkalinity, dissolved inorganic carbon and CO_2 fugacity exhibit net increases over the same period.

After an analysis of the different forcing (total alkalinity and dissolved carbon dioxide) impacting on water masses during the two seasons and between the two winters, the net increase of dissolved CO_2 resulted to be the driving factor of the observed inter-decadal acidification [20]. This important result confirms that the Adriatic Sea is sensitive to atmospheric gas solubilisation (as CO_2) and indicates that OA has been affecting the Adriatic marine waters for the last 25 years. It also indicates the need for a careful checking, in the coming decades, of the acidification rates as the impact on water quality, marine ecosystems and fishery resources could be not negligible. Although a determination of acidification rates is not possible on the base of only 2 specific years because interannual variations must also be considered, we inferred an approximate "acidification rate" over this time span. It corresponded to 0.0025 pH units/year, in agreement with acidification rates calculated in other oceanic regions from time series: at ESTOC station in the open ocean, Atlantic, Canary islands 0.0017 $\pm$ 0.0004 pH units/year [21] 0.0012 $\pm$ 0.0004 pH units/year, in the open Atlantic ocean, Bermuda Islands, [22].

3.3 Time series in the Gulf of Trieste (northern Adriatic Sea)

The acquisition of time series, at least by a few key sites such as those where dense water formation occurs in winter, is a promising strategy to monitor ocean acidification rates and impacts in the Mediterranean sea.
On this concern, ISMAR Trieste has recently started the collection of pH_T and other biogeochemical parameters time series in the Gulf of Trieste (very shallow, the northernmost of the Mediterranean Sea), which is representative of a coastal envi-

	Param.	Units	N° samples	Average	Std Dev	Median
1983	**pH_T**	µmol/kg_{sw}	33	8.010	±.046	8.005
	Tot. Alk	µmol/kg_{sw}	33	2584.5	±10.9	2584.8
	DIC	µmol/kg_{sw}	33	2256.3	±32.1	2260.9
	fCO_2	µatm	33	485.1	±63.6	489.2
	H_2CO_3	µmol/kg_{sw}	33	13.6	±1.8	13.7
	HCO_3^-	µmol/kg_{sw}	33	2003.8	±49.0	2011.1
	$CO_3^=$	µmol/kg_{sw}	33	239.0	±19.5	236.1
	Revelle		33	9.773	±0.469	9.809
	Ω_{Ca}		33	5.60	±0.46	5.54
	Ω_{Ar}		33	3.71	±0.30	3.66
2008	**pH_T**	µmol/kg_{sw}	56	7.946	±0.012	7.947
	Tot. Alk	µmol/kg_{sw}	61	2658.9	±18.1	2658.1
	DIC	µmol/kg_{sw}	54	2366.6	±21.6	2370.3
	fCO_2	µatm	54	593.4	±22.3	593.2
	H_2CO_3	µmol/kg_{sw}	54	16.6	±0.6	16.6
	HCO_3^-	µmol/kg_{sw}	54	2130.6	±23.9	2137.4
	$CO_3^=$	µmol/kg_{sw}	54	219.4	±4.9	219.5
	Revelle		54	10.491	±0.168	10.493
	Ω_{Ca}		54	5.14	±0.11	5.14
	Ω_{Ar}		54	3.40	±0.07	3.40

Table 1: Values of the carbonate system parameters (at 25 °C) in the Northern Adriatic Dense Water mass formed in winter 1983 and 2008.

ronment (Figure 3).

Since January 2008, pH_T, A_T and the mayor biogeochemical and physical parameters were acquired on monthly basis on the whole water column at the coastal site PALOMA (centre of the Gulf, 25m deep, close to the mast PALOMA - Advanced Oceanic Laboratory PlatforM for the Adriatic sea, 45° 37 N, 13° 34 E). First results evidenced a complex time evolution of pH_T, mainly driven by the combined effect of strong changes in both temperature and production/ remineralisation processes (Figure 3). During winter pH_T values were generally low (7.868-7.958, avg 7.920) and homogeneous owing to the increased CO_2 solubility driven by the low water temperature (down to 8.0°C) and by the absence of intense production processes. During spring and summer pH_T was highly variable and mainly driven by the biological processes: the highest values (up to 8.120, June 2008) were reached in the upper layer during high production events (AOU= -34 μM) and the lowest values (down to 7.648, August 2008) in the bottom layer during

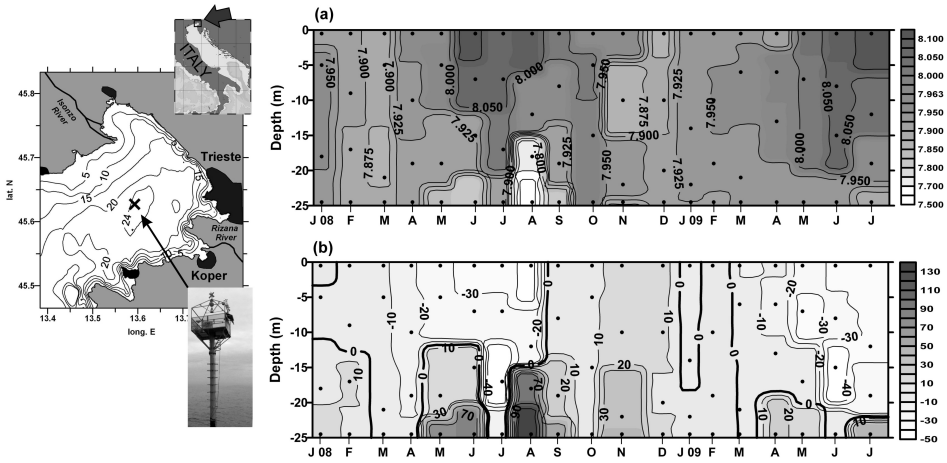

Figure 3: Map of the sampling site PALOMA in the Gulf of Trieste; distribution of monthly values of pH_T (a) and AOU (b) at PALOMA station from January 2008 to July 2009.

biomass remineralisation (AOU= 142 μM). During Jan-March 2008 the oceanographic properties (average σ_t = 29.35 kgm^{-3}, T = 8.84 °C) and pH_T values (7.907 $\pm$ 0.028) of site PALOMA, indicating dense water formation, fit well to the general North Adriatic Sea conditions over the same period. In summer, small scale biological processes prevailed in determining pH_T values both in PALOMA site and in the North Adriatic, depicting a more complex situation.

From such preliminary data, this site located in the centre of the Gulf of Trieste results to be a good indicator not only of coastal dynamics/ processes but also of sub-basin wide (North Adriatic Sea) processes and dynamics.

4 Impacts on biogeochemistry and marine ecosystem

The most significant indication we can draw from the preliminary study on NAdDW is that the observed pH decrease has affected the biogeochemistry of the carbonate system, causing speciation shifts (Table 1) as the decrease of carbonate ion concentration (from 236.1 to 219.5 $\mu{\cdot}\mathrm{mol} \cdot \mathrm{kg}_{\mathrm{sw}}^{-1}$) accompanied by the increases of bicarbonate ion and carbonic acid concentrations (from 2011.1 to 2137.4 $\mu{\cdot}\mathrm{mol} \cdot \mathrm{kg}_{\mathrm{sw}}^{-1}$, from 13.7 to 16.6 $\mu{\cdot}\mathrm{mol} \cdot \mathrm{kg}_{\mathrm{sw}}^{-1}$, respectively) that fit well to what generally observed in other oceanic regions [11]. Also the solubility ratios of calcite and aragonite show a decrease (Ω_{Ca} from 5.51 to 5.14, Ω_{Ar} from 3.66 to 3.40) during last 25 years but, being far from 1.0, they indicate that NAdDW is still oversaturated with respect to calcium carbon-

ate, as already observed for the Mediterranean Sea [6]. Therefore, the Adriatic Sea with its adequate carbonate saturations state seems to ensure still quite healthy growth conditions for calcifying organisms (from plankton to benthic molluscs, echinoderms and corals). The increase of the Revelle factor in the same period (R= 9.773 $\pm$ 0.469 and 10.491 $\pm$ 0.168, respectively) suggest a decrease of the buffering capacity of the whole carbonate system [23]).
There are several impacts of OA on the marine ecosystem which have not yet been investigated. For example the observed pH decrease might have impacted the carbon fixation capacity by photosynthetic organisms (calcifyer and non calcifyer), actually a few papers report the possibility of an increase of primary productivity [4] in response to ocean acidification. An increase of primary production might further affect hypoxia and anoxia events, already seasonally occurring in the northern Adriatic basin [24], through an increase of the microbial respiration of the surplus of organic matter. On another hand, the combined impacts of increased stratification, due to the global warming, and changes in the ocean biology, caused by ocean acidification, could cause a further decline in dissolved oxygen concentrations as recently forecast by Oeschlies [25]. If this would occur in the North Adriatic it might exacerbate hypoxia and anoxia. Another significant impact of OA in the North Adriatic could be represented by the increase of dissolved organic carbon (DOC) production as response to the increase of primary production induced by OA [26]. If the DOC increase would be assessed true also for the Adriatic Sea, it might have major effects on mucillages phenomena which affect the basin, as mucillages are aggregates of muchopolysaccharide and would be favoured by higher DOC concentrations.
In the end, all these aspects could have massive consequences on marine resources (fishery, aquaculture, tourism). Hence the Northern Adriatic Sea offers challenges for future research activities of high priority. Thus confirming to be an interesting basin where assessing the impacts of Ocean Acidification with the potential for marine organisms to adapt to increasing CO_2, and broader implications for marine ecosystems.

5 Acknowledgement

The authors thank: dr. Massimo Celio (ARPA-FVG) for the use of CTD data acquired at PALOMA station and dr. Vedrana Kovacevic (OGS-Trieste) for the use of CTD data acquired during VECTOR and SESAME campaigns. They are grateful to the captains and crews of R/V Urania (CNR) and Effevigi (ARPA-FVG). The study was funded by the VECTOR project of the Italian Ministry for University and Scientific Research and by the SESAME project of the European Commission.

References

[1] D. Lüthi, M. Le Floch, B. Bereiter, T. Blunier, J.M. Barnola, et al. High-resolution carbon dioxide concentration record 650,000-800,000 years before present. *Nature*, 453:379–382, 2008.

[2] C.L. Sabine, R.A. Feely, R.M. Gruber, N.and Key, and K. Lee et al. The oceanic sink for anthropogenic CO_2. *Science*, 305:367–371, 2004.

[3] C.L. Sabine and R.A. Feely. The oceanic sink for carbon dioxide. In: Greenhouse gas sink, D. Ready, N. Hewitt, J. Grace and K. Smith (editors). pages 31–49, 2007.

[4] S.C. Doney, V.J. Fabry, R.A. Feely, and J. A Kleypas. Ocean Acidification: The Other CO_2 Problem. *Annual. Reviews Marine Science*, 1:169–192, 2009.

[5] K. Caldeira and M.E. Wickett. Anthropogenic carbon and ocean pH. *Nature*, 425:365–365, 2003.

[6] A. Schneider, D.W.R. Wallace, and A. Koertzinger. Alkalinity of the Mediterranena Sea. *Geophys. Res. Letters*, 34(L15608), 2007.

[7] R.A. Feely, C.L. Sabine, K. Lee, W. Berelson, J. Kleypas, et al. Impact of anthropogenic CO_2 on the $CaCO_3$ system in the oceans. *Science*, 305:362–366, 2004.

[8] R.A. Feely, J. Orr, V.J. Fabry, J.A. Kleypas, C.L. Sabine, and C. Langdon. Present and future changes in seawater chemistry due to ocean acidifcation. In: Carbon sequestration and its role in the global carbon cycle, Brian J. McPherson and Eric T. Sundquist (eds.). *AGU Monograph*, 2009.

[9] J.C. Orr, V.J. Fabry, O. Aumont, L. Bopp, S.C. Doney, R. A. Feely, A. Gnanadesikan, N. Gruber, A. Ishida, F. Joos, R.M. Key, K. Linsay, E.M. Reimer, R. Matear, P. Monfray, A. Mouchet, R.G. Najjar, G.K. Plattner, K.B. Rodgers, C.L. Sabine, J.L. Sarmiento, R. Schlitzer, R.D. Slater, I.J. Totterdell, M.F. Weirig, Y. Yamanaka, and A. Yool. Anthropogenic ocean acidification over the twenty-first century and its impact on calcifying organisms. *Nature*, 437:681–686, 2005.

[10] S. Solomon, D. Quin, and M. Mannings et al. Climate Change 2007: the physical science basis: contribution of working group I to the Fourth Assessment Report of the Intergovernamental Panel on Climate change. New York (2007). *Cambridge Univ. Press*, 2007.

[11] Royal Society. Ocean acidification due to increasing carbon dioxide, Policy Document 12/05. 2005.

[12] A. Yilmaz et al. Impacts of acidification on biological, chemical and physical systems in the Mediterranean and Black Seas. In: CIESM Workshop Monographs N° 36. F. Briand editor, CIESM, Monaco. page 124, 2008.

[13] MEDAR Group. MEDATLAS/2002 database. Mediterranean and Black Sea database of temperature salinity and bio-chemical parameters. Climatological Atlas. IFREMER Edition (4 Cd). 2002.

[14] M. Gačić, A. Lascaratos, B.B. Manca, and A. Mantziafoul. Adriatic deep water and interaction with the eastern Mediterranean Sea. In: Physical Ocenaography of the Adriatic Sea. Past, Present and Future. In: B. Cushman-Roisin, M. Gačić, M.P. Poulain and A. Artegiani (eds.), Kluwer Academic Publishers, The Netherlands. pages 111–142, 2001.

[15] W. Roether, B. Manca, B. Klein, D. Bregant, D. Georgopoulos, V. Beitzel, V. Kovacevic, and A. Luchetta. Recent changes in the Eastern Mediterranean deep waters. *Science*, 271:333–335, 1996.

[16] A.G. Dickson, C.L. Sabine, and J.R Christian. Guide to best practices for ocean CO_2 measurements. *PICES Special Publication*, 3:191, 2007.

[17] E. Lewis and D.W.R. Wallace. Program Developed for CO_2 System Calculations. ORNL/CDIAC-105. Carbon Dioxide Information Analysis Centre, Oak Ridge National Laboratory, U.S. Department of Energy, Oak Ridge, Tennessee. 1998.

[18] P. Malanotte-Rizzoli. The northern Adriatic Sea as a prototype of convection and water mass formation on the continental shelf. In: Deep convection and deep water formation in the oceans. P.C. Chu and J.C. Gascard (eds.). *Elsevier Oceanography Series*, 57:229–239, 1991.

[19] A. Artegiani, E. Paschini, A. Russo, D. Bregant, F. Raicich, and N. Pinardi. The Adriatic Sea Circulation, Part 1: Air-sea interactions and water mass structure. *J. Phys. Oceanography*, 27:1492–1515, 1997.

[20] A. Luchetta, C. Cantoni, and G. Catalano. New observations of CO_2 induced acidification in the Northern Adriatiic Sea, over the last quarter century. *Chemistry and Ecology*, 26:1–17, 2010.

[21] J.M. et al. Santana Casiano. The interannual variability of oceanic CO_2 in the northeast Atlantic subtropical gyre at the ESTOC site. *Global Biogeochem. Cycles*, 21(GB1015), 2007.

[22] N.R. Bates. Interannual variability of CO_2 sink in the subtropical gyre of the North Atlantic Ocean over the last two decades. *J. Geophys. Res.*, 112, 2007.

[23] F.J. Millero. The marine inorganic carbon cycle. *Chemical Reviews*, 107:308–341, 2007.

[24] R. Marchetti. The problems of the Emilia Romagna coastal waters: facts and interpretations. In: Marine Coastal Eutrophication. pages 21–33, 1992.

[25] A. Oschlies, K.G. Schulz, U. Riebesell, and A. Schmittner. Simulated 21^{st} century's increase in oceanic suboxia by CO_2-enhanced biotic carbon export. *Global Biogeochemical Cycles*, 22, 2008.

[26] U. Riebesell, K. G. Schulz, R. G. J. Bellerby, M. Botros, P. Fritsche, Meyerhöfer, et al. Enhanced biological carbon consumption in a high CO_2 ocean. *Nature*, 450:545–548, 2007.

The Roads of the Sea - Can We Predict the Motion of Particles Carried by Ocean Currents?

A. Griffa[1], K. Schroeder[1], S. Aliani[1], A. Doglioli[2], A. Molcard[3], V. Taillandier[4], P.M. Poulan[5], T. Ozgokmen[6], A. Haza[6])
1, Institute of Marine Sciences, CNR, Pozzuolo di Lerici (SP), Italy
2, University of Marseille, Marseille, France
3, University of Toulon, Toulon, France
4, Laboratoire d'Océanographie de Villefranche-sur-mer, Villefranche-sur-mer, France
5, National Institute of Oceanography and Experimental Geophysics, Trieste, Italy
6, University of Miami, Rosenstiel School of Marine and Atmospheric Science, Miami, Florida
a.griffa@ismar.cnr.it

Abstract

Ocean currents play a fundamental role in the transport of substances and species. Being able to monitor and predict their effects is of great relevance for a number of applications, such as correct management of the coastal ecosystem, manage control in case of discharge of pollutants and understanding of pathways of invasive species. While transport by ocean currents is under many aspects very complex and dominated by turbulent and chaotic processes, it has been shown in recent works that it is often possible to find a hidden structure, at least for mesoscale motion, that guides the movement of the advected quantities. Barriers of motion exist in the ocean, related to the main "Lagrangian coherent structures", i.e. to structures such as gyres, jets and eddies. In this paper, we provide examples of methods to identify such barriers and applications in the Mediterrean Sea. The limits of these methods, that are based on the assumption that the velocity field is well known, are also discussed, and possible remedies in terms of Lagrangian assimilation are discussed.

1 Introduction

Currents are the roads of the sea. They transport physical properties such as temperature and salinity (T,S), chemical properties, pollutants, particulate and sediments as well as biological quantities such as phytoplankton, zooplankton, larvae and jelly fish. Being able to understand and predict transport by ocean currents is therefore crucial for a number of applications. They include climatic applications, for instance understanding heat transport or pathways of species invasions, as well as applications for a correct management of the coastal ocean ecosystem and for damage control in case of accidents at sea such as discharges of pollutants. Transport predictions is very challenging for a number of reasons [1]. To understand it, consider the basic equation of Lagrangian transport, i.e. the equation that describes particles advected by the current,

$$\mathrm{dx}/\mathrm{dt} = \mathbf{u}(\mathbf{x}, \mathrm{t}),$$

where **x** is the position of a particle and u is the velocity. The equation shows that the trajectory of a particle, **x**(t), is the integral of the velocity **u**(**x**,t). This implies that even small errors in the prediction of **u** (obtained from numerical models or measurements) tend to accumulate and grow in the prediction of **x**(t). Since in practice small errors in u are unavoidable, due to incomplete knowledge of forcing, topography, coastline and to the influence of small scale unresolved processes, we can expect that this will result in significantly amplified errors in trajectories. Also, the equation is inherently nonlinear, since **u** depends on the position **x**, and it has the property of being very often chaotic. This implies that even for very simple Eulerian flows **u** (in presence of time dependence) trajectories are highly sensitive to initial conditions. Predicting them is therefore very difficult, since even a slight difference in initial conditions in space and time can result in significantly different behaviours. Even though Lagrangian prediction is highly challenging, a number of methods have been put forth in the past decade that have helped increasing our skills in this direction. Different methods have been suggested for different applications. Methods based on statistical approaches are particularly suited for climatic problems. They consist in separating the mean component of the currents from the turbulent and fluctuating component and parameterizing the turbulent part for instance using stochastic methods [2, 3, 4]. Other methods are more suited for the prediction of specific events, and they are typically based on dynamical system theories. The basic concept here is that even though the motion of a single particle is extremely challenging to reproduce because of the high dependence on initial conditions and on the details of the flow, the description of the general pattern of transport is much more approachable. It has been suggested that ocean transport in quasi-geostrophic, quasi-2-dimensional situations is dominated by main "coherent structures" [5], such as vortices, eddies and jets, that are separated by invisible barriers, i.e. regions that particle trajectories cannot cross. Methods from nonlinear dynamical system theory have been proposed to locate such barriers, that can be used to provide information on the general fate of a particle launched in a certain area. Details on the specific trajectory might be difficult to determine, but its general behaviour is expected to be determined by such barriers. In this context, the knowledge of the location of hyperbolic points (HPs) that separate different structures appears especially relevant. Various methods can be used to identify such barriers and HPs, ranging from direct identification in terms of flow invariants to methods based on local dispersion properties, such as Finite Time (FTLE) or Finite Size (FSLE) Lyapunov Exponents [5, 6]. Dynamical system methods appear to have a great potential for practical ocean applications. Nevertheless it is important to point out that they are "diagnostic" tools, in the sense that they can be used with great results only as long as the velocity field u is known with a certain degree of accuracy. This is the case for instance for velocity fields from extensive HF (High Frequency) radar measurements, or from accurate ocean circulation models. In many cases, though, predictions from circulation models are still incomplete and the structures can be considered known only with some approximation. In order to increase our knowledge of such structures and therefore our prediction capability, assimilation methods can

be used, that combine information from real time data with model results. In particular, since we are interested in Lagrangian predictability, we can expect that assimilation of Lagrangian data will be especially fruitful. For Lagrangian data we mean data from floating instruments that follow the current with good approximation, either at the ocean surface (drifters) or in the ocean interior (SOFAR, RAFOS and Argo floats) communicating their position via satellite or acoustically. In the last few years, new methods for Lagrangian data assimilation have been proposed in the literature and tested using simplified models [7, 8, 9]. Some of these methods have been recently applied to in situ data and the results appear very promising in terms of flow correction and increasing transport prediction skills. In this paper we provide a brief summary of results that have been obtained in the last few years at CNR-ISMAR in collaborations with a number of national and international laboratories aimed at increasing the predictability of particles in ocean flows. We focus on two main issues. In Section 2, we review the development and implementation of methods from dynamical system theory focusing especially on the FSLE tool [10] to highlight flow features and barriers. We provide some examples of applications in the Adriatic and Ligurian Sea, testing the result using independent Lagrangian data. The presented results are among the very first examples of applications of the theory to real ocean flows. In Section 3, we provide a summary of work aimed at improving flow prediction using Lagrangian data assimilation. The development of a method based on a variational approach is briefly reviewed and examples in coastal flows are shown, using different types of Lagrangian data from Argo floats moving at 350 m to drifters at the surface. These results are the first successful applications of Lagrangian data assimilation using in-situ data, and the method is now transitioned toward operational systems. The potential of these findings for practical applications and the strategies for further developments are discussed in Section 4.

2 Computing transport barriers using FSLEs

The Finite Size Lyapunov Exponents (FLSEs) are a diagnostic tool that can be used to identify the main transport barriers and flow structures such as eddies, jests and boundary currents. They are based on the computation of maps of relative dispersion in the flow field, and are relatively simple to implement. In order to compute FSLEs the velocity field u has to be known, either from high resolution measurements (HF radar) or from models. The computations of FSLEs is performed seeding particles in small clusters (typically of three particles each) throughout the flow domain and numerically advecting them forward and backward. Formally FSLEs are defined as the time that takes for particles initially separated of a given distance d0 to reach a distance d1=a d0 where a is a specified factor. Forward advection highlights regions of high dispersion, while backward advction identify convergence regions. An example of computation of FSLEs using results from an NCOM NRL model in the Adriatic Sea [10] is shown in Figure 1 (left panel). The red (blue) lines indicate concentration (dispersion) lines. The superposition of lines indicate "ridges", i.e. areas that act as transport barriers between different flow regions and

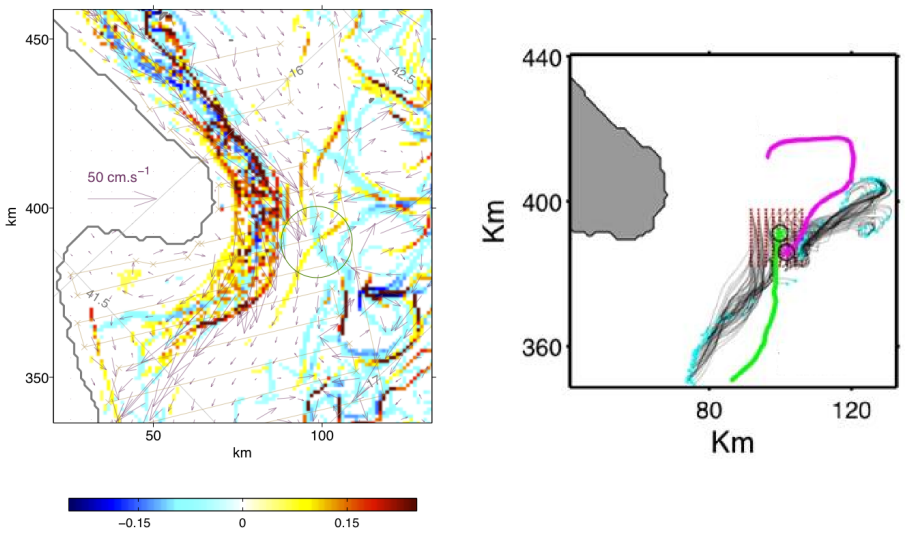

Figure 1: (left) Forecasted surface velocity from NCOM model during DART06 experiment. Superimposed are the 2-day model based FSLE field and the location of a hyperbolic point (green circle). (right) 2 day trajectories for real drifters (green and purple) and numerical drifters (black lines). Adapted from [10].

that cannot be crossed by particle trajectories. Hyperbolic points are indicated by the crossing of blue and red lines, as indicated by the circle in Figure 1 off the Gargano Cape. These points are central to understand Lagrangian pathways, since they separate different structures and are characterized by directions in which stretching can cause particles to diverge from the structures (unstable manifolds) as well as to converge (stable manifolds). Particles located close to a hyperbolic point can easily separate, following the different manifolds. FSLEs cmputations have been performed and tested during two recent field experiments in collaboration with NURC-NATO, NRL, OGS, University of Miami and University of Toulone. The two experiments took place in the Adriatic Sea (DART06, [10]) and in the Ligurian Sea (MREA07-POET, [11, 12] respectively. During DART06, FSLEs have been computed using the NCOM circulation model with 1 km resolution, and FSLE maps (Figure 1, left panel) were used in real time to guide drifter launches from ship. The goal was to identify regions of high hyperbolicity so that the launched drifters would tend to quickly separate, inducing a maximum coverage of the area. The presence of an hyperbolic point in the area off the Gargano Cape have been suggested in previous works through the analysis of historical drifter data [13], but the hyperbolic point is known to be present only at certain times, and to depend on the flow structure. For this reason, model results are needed to pinpoint the exact time and location of the

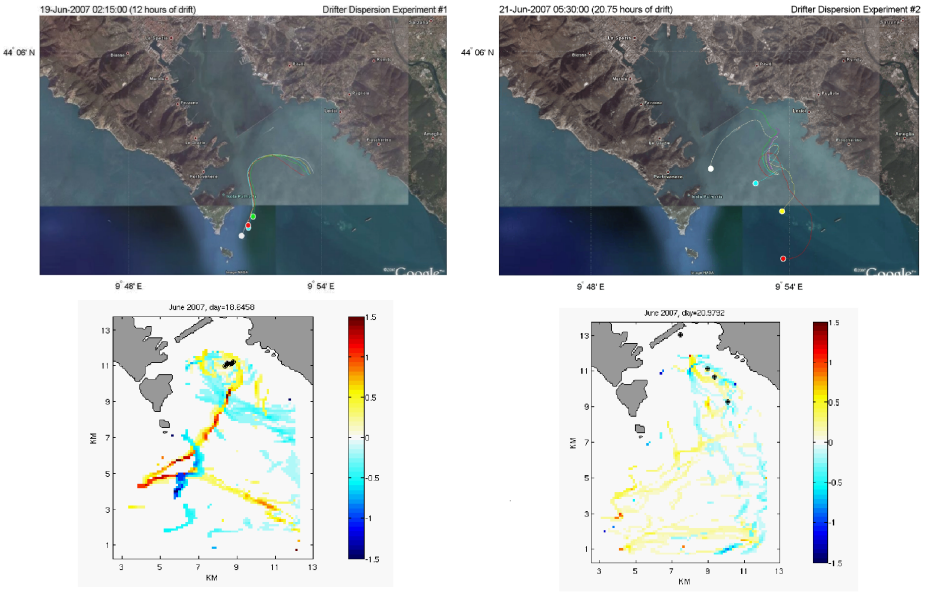

Figure 2: Top panels show the trajectories of two drifter clusters launched from the same location two days apart in the Gulf of La Spezia during the POET experiment (June 2007). Bottom panels show FSLE maps computed from VHF radar at the time of the launches. The superimposed stars indicate the position of the drifters.

point. During DART06 three launches of drifter pairs have been performed guided by model forecasts, and two over three show the presence of an hyperbolic point that induces drifter trajectories to quickly separate and diverge. An example is shown in Figure 1, right panel, where the observed drifter trajectories (green and purple lines) appear to separate quickly, one going to the north and the other to the south, in agreement with the model results, as shown by the numerical trajectories in black. During the third launch, instead, the drifters did not separate and moved together toward the north. This launch actually acted as an inadvertent "control" experiment in the sense that the circulation model was indeed predicting at the time that the presence of the hyperbolic point was cancelled by a strong wind episode. The ship, though, due to logistic reasons performed the drifter launches in any case, and the observed and numerical trajectories did not show separation. This clearly indicates that a) the hyperbolic point is not present at all times and b) the model forecast is able to correctly capture its time dependence. The second experiment took place in the Ligurian Sea and had two components: a large scale component with drifter launches in open ocean [12], and a more coastal component in the Gulf of La Spezia with significantly smaller scales of the order of 5-7 km (POET experiment, [11, 14]. Dur-

ing POET, clusters of five drifters were launched in the Gulf. Results from two launches performed two days a part from the same initial conditions are presented in Figure 3 (upper panels), showing a dramatically different trajectory behaviour. During the first launch (left) the drifters move coherently in a cyclonic way exiting the Gulf after 12-15 hours. During the second launch, instead, the drifters quickly separate and end up sampling the whole Gulf, exiting after more that 20 hours. During POET, a VHF coastal radar was operated in the area providing maps of velocity fields at resolution of 250 m every 30 minutes. FSLE maps were computed from the radar velocity and used to understand and quantify the different type of dynamics acting during the two launches. Snapshots of FLSLEs during the two launches are shown in Figure 3 (lower panels). During the first launch, a clear ridge is depicted that separate the area of the Gulf in two different regions. The drifters move along the evolving ridge and do not cross it as they flow through the Gulf. This can be partially seen by comparing the drifter trajectories and the FSLE snapshot in Figure 3 (left panels) but it is much more clear considering the animation depicting drifter motion superimposed to the evolving FSLE maps (http://www.rsmas.miami.edu/personal/ahaza/radar/LaSpezia_fsle_clusters.gif). During the second launch (right panel), no clear ridges separating the Gulf are detected and the structures are less marked, even though the presence of an hyperbolic point very close to the launching region of the drifters can be detected, indicated by the crossing of blue and red lines. This explains the initial separation of the cluster with drifters moving in different direction. The animation of drifter/FSLEs evolution shows that the drifters indeed follow the manifold lines stemming from the hyperbolic point. The results show that even at small coastal scales, where the dynamics are complex and driven partially by the large scale boundary current intruding in the Gulf and partially by local forcing, Lagrangian transport can be interpreted in terms of barriers between dominant structures well captured by FSLEs.

3 Improving transport prediction using assimilation

The results in Section 2 provide positive indications on the feasibility of forecasting the main transport properties, since they suggest that particle motion is mostly dominated by barriers between the main coherent structures, rather than by smaller scale flow feautures. As a consequence, when the main coherent structures are well represented and forecasted by the models, we can expect that also particle transport is well represented at least in terms of general behaviour, even though the details of single trajectories might be missing. On the other hand, the nature of these coherent structures is still only partially understood and in many cases circulation models are only partially able to capture them. A common problem with models, for instance, is related to the propagation velocity of the structures, so that there might be phase shift errors involving the exact location of the structures at a given time. A very effective avenue to improve model performance is to use real time data to correct model results using methods of data assimilation. In particular, in our case, since we are interested in transport prediction, we can expect that Lagrangian data from float-

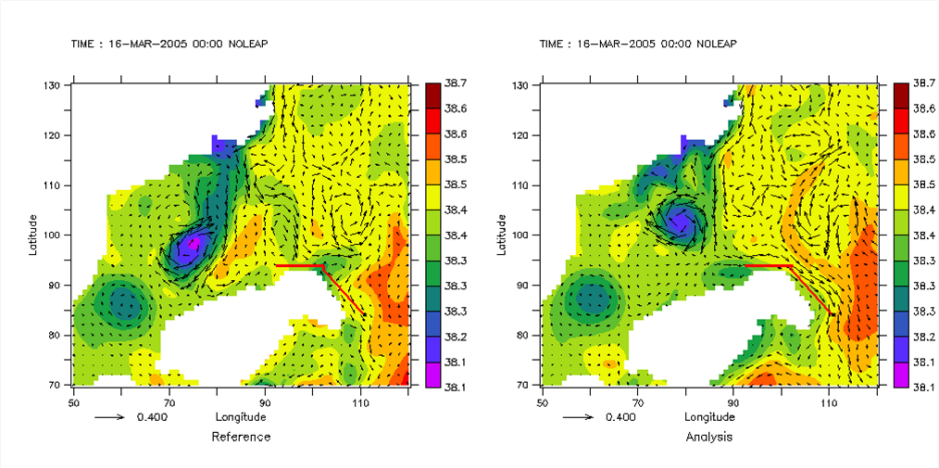

Figure 3: Left (right) panel shows an example of OPA model results in the Balearic Sea without (with) assimilation of Argo float trajectories. Arrows indicate vector velocities, color the salinity field and the superimposed brown-orange lines indicate the observed 10 day drift of the assimilated float. Adapted from [15].

ing instruments that directly sample current advection will be especially useful. A new method to assimilate Lagrangian data have been developed by CNR-ISMAR in collaboration with the University of Miami and Toulone. The method is based on correcting the velocity field at the level where the instruments are transported by the currents (i.e. in the interior ocean for Argo floats and at the surface for drifters) by requiring minimization of the distance between observed positions and positions of numerical trajectories launched in the model [7, 8]. Once the velocity field is corrected, the other variables of the model, i.e. the mass variables T,S and the sea surface height (SSH), are adjusted using some simplified dynamical requirements such as geostrophy and mass conservation (Ozgokmen et al., 2003). The method has been implemented using a variational approach and it has been first applied to Argo floats [15] in the Mediterranen Sea as part of the MFS (Mediterranean Forecasting System) project. Mediterranean Argo floats (MedArgo) are programmed to drift at a parking depth of 350 m, resurfacing at approximately 5 day intervals, and providing information on their position and on TS profiles. Lagrangian assimilation uses the position information to correct the drift at 350m. An example of results obtained assimilating MedArgo floats in the region close to the Balearic Islands is shown in Figure 4. Results without assimilation (left panel) can be compared with results with assimilation (right panel). The superimposed orange-brown lines indicate the observed drift of one float during 10 days, the arrows indicate velocity vectors and the color indicates the salinity field S. As it can be seen, the assimilation of the Argo float data induces a jet along the eastern coast of the island that was not present without

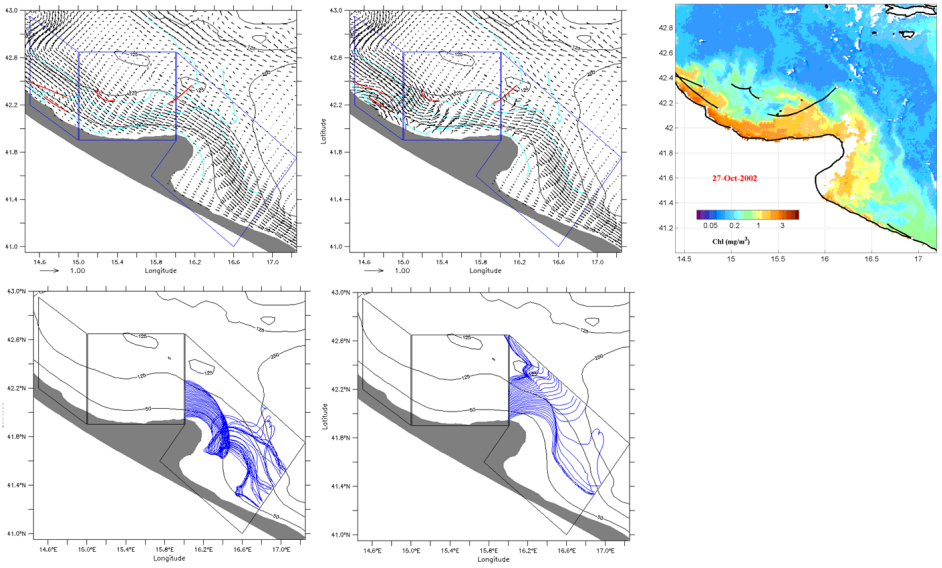

Figure 4: Left (central) panels show an example of ROMS model results in the Adriatic Sea without (with) velocity correction from surface drifters. Top panels depict the velocity field, with superimposed the 2 day trajectories (red lines) of the drifters used in the correction, while the bottom panels depict numerical trajectories launched along a section. Right panel shows a Modis satellite image taken at the same time as the model results. Adapted from [16].

assimilation, in keeping with the observed float drift. Notice also that there are differences in the S fields between the two panels, due to the dynamical adjustment performed during the assimilation. The Lagrangian assimilation of MedArgo has been recently performed in the framework of a multivariate system, i.e. as part of the MFS observing system including T,S profiles from MedArgo and XBTs and satellite SSH and SST [17]. Results are very positive and the Lagrangian MedArgo assimilation is now in the process of being transitioned to the operative MFS system. Further investigations are presently carried out on the assimilation of surface drifters. Assimilation of surface drifters is expected to be more challenging than for Argo floats mostly because they sample the very surface of the ocean (from 15 m to 1-2 m), that is characterized by small scales fluctuations and dynamics that significantly deviate from geostrophy. This poses two significant question. The first one is related to which scales should be filtered and which ones retained in the model correction, while the second one is related to the correction of the mass variables, that has to be performed differently than in the case of Argo floats. A simple geostrophic balance in fact cannot be used since the upper meters are strongly influenced by Ekmn dynamics, so that a more complex dynamical decomposition has to be adopted. So far,

we have been working on the first step of assimilation, i.e. the velocity correction at the surface using drifter data, and we have not attacked the problem of mass correction yet. Results on surface correction are very promising [16], as shown in the example in Figure **??** for the Adriatic Sea. The left (central) panels show results from the ROMS model without (with) correction, for a snapshot of velocity (top panels) and for numerical trajectories (bottom panels) launched along a section. The small red lines in the top panels indicate two day trajectories of four drifters used for the correction. As it can be seen, the velocity correction appears small, but it has a significant impact on trajectories. The trajectories of the non corrected model in fact appear retained inside the boundary current, while they tend to exit from it in the case of correction, more in keep with what suggested by MODIS satellite data (right panel) indicating significant intrusion from the boundary current in the interior. Of course this is not a quantitative test of results yet, and work is in progress to quantify the improvement using independent data

4 Summary and discussion

In this paper, we have discussed methods to improve the prediction of particles transported by ocean currents. Results are very encouraging and they show that, even though the problem is extremely challenging, significant improvements can be obtained using appropriate techniques. On the other hand, a number of questions are still open as discussed in the following. The results in Section 2 strongly suggest that the motion of particles is controlled by barriers between the main coherent structures in the flow, such as mesoscale eddies, jets and boundary currents. The size of these structures depends on the flow environment and in particular on the Rossby radius of deformation, ranging from more than 10 km in the open sea in the Adriatic and Ligurian sea, to few km in small coastal gulfs such as the Gulf of La Spezia. Flow features smaller than these mesoscale structures do not appear to directly influence the main characteristics of particle transport, even though they can influence the details of single trajectories. This result, if confirmed in other regions of the world ocean and shown to be general, is expected to be extremely important for what concerns practical applications. The result in fact implies that the resolution of circulation models can be limited to correctly reproduce mesoscale structures, while capturing submesoscale or smaller processes is not crucial for the problem of Lagrangian transport, that is central to many practical applications of operational prediction systems. Looking at the existent literature, results in other parts of the world show similar and compatible results, for instance the studies of relative dispersion in the Gulf of Mexico and in the Norwegian Sea [18]. On the other hand, other results in the California Current seem to suggest that submesoscale and smaller scales might be relevant for flow advection properties [19]. This might be related to the fact that the California Current is characterized by supwelling and significant vertical motion, that is often dominated by submesoscale structures. Overall, the central issue of the role of submesoscale and smaller features is still open and it requires significant further investigations. Different regions of the ocean might have to be treated differently [20], and it is crucial to

understand what are the physical reasons for these differences and the consequences for the transport of biogeochemical properties and their modeling and prediction. For what concerns assimilation methods, the results in Section 3 show that they can be extremely useful to correct model forecasts, for instance repositioning and shaping coherent structures that are not correctly reproduced by the models. Assimilation has been successfully implemented in the case of Argo subsurface floats, and it is now in the process of being transitioned to operational systems. Work is in progress for surface drifters and the main questions to be addressed are conceptually related to the ones discussed above. We have to decide whether or not the signature of small scale processes present in the data have to be maintained and used in the assimilation or filtered away, and which type of dynamics have to be used, beyond geostrophy. In order to do that, an increased knowledge of air sea interaction processes is necessary, as well as an improved understanding of the role played by vertical motion in the mixed layer. Finally, it should be pointed out that while Lagrangian data are certainly a natural choice to improve transport prediction, other types of data can also be used, and fusion between models and various data is expected to be very important in the future. As an example, work has already started to use satellite data (SAR and visible) to improve transport prediction in case of accidents at sea such as oils spill events [21].

5 Acknowledgements

The authors wish to acknowledge collaborations with G. Gasparini, M. Rixen, A. Poje ,L. Piterbarg, N. Pinardi and S. Dobricic. The work was supported by the EU projects MFSTEP and ECOOP and by ONR (Ofice of Naval Research).

References

[1] L. Piterbarg, T.M. Özgökmen, A. Griffa, and A.J. Mariano. Predictability of Lagrangian motion in the upper ocean. 2007.

[2] S. Aliani and A. Molcard. Hitch-hiking on floating marine debris: macrobenthic species in the Western Mediterranean Sea. *Hydrobiologia*, 503:59 –67, 2003.

[3] M. Veneziani, A. Griffa, A. Reynolds, Z. Garraffo, and E. Chassignet. Parameterization of Lagrangian spin statistics and particle dispersion in the presence of coherent vortices. *J. Mar. Res*, 63:1057–1084, 2005.

[4] A. Doglioli, M. Veneziani, B. Blanke, S. Speich, and A.Griffa. Lagrangian analysis of Indian-Atlantic interocean exchange in a regional model. *Geophys. Res. Lett*, 33:L14611, 2006.

[5] S.C. Shadden, F. Lekien, and J. E. Marsden. Definition and properties of Lagrangian coherent structures from finite-time Lapunov exponents in two-dimensional aperiodic flows. *Physica D*, 212:352–380, 2005.

[6] V. Artale, G. Boffetta, A. Celani, M. Cencini, and A. Vulpiani. Dispersion of passive tracers in closed basins: Beyond the diffusion coefficient. *, Phys. Fluids*, 9:3162–3171, 1997.

[7] A. Molcard, L. Piterbarg, A. Griffa, T.M. Ozgokmen, and A.J. Mariano. Assimilation of drifter positions for the reconstruction of the Eulerian circulation field. *J. Gephy. Res*, 107:3154–3171, 2003.

[8] V. Taillandier, A Griffa, and A. Molcard. A variational approach for the reconstruction of regional scale Eulerian velocity fields from Lagrangian data. *Ocean Modelling*, 13:1–24, 2006.

[9] L. Kuznetsov, K. Ide, and C. K. R. T. Jones. A method for assimilation of Lagrangian data. *Mon. Weather Rev*, 131:2247–2260, 2003.

[10] A. Haza, A. Griffa, P. Martin, A. Molcard, T.M. Ozgokmen, A.C. Poje, R. Barbanti, J. Book, P.M. Poulain, M. Rixen, and P. Zanasca. Model-based directed drifter launches in the Adriatic Sea: Results from the DART experiment. *Geophys. Res. Letters*, 34:L10605, 2007.

[11] A. Molcard, P.M. Poulain, P. Forget, A. Griffa, Y. Barbin, J. Gaggelli, J.C. De Maistre, and M. Rixen. Comparison between VHF radar observations and data from drifter clusters in the Gulf of La Spezia (Mediterranean Sea). *J. Mar. Sys.*, 78:S79–S89, 2009.

[12] K. Schroeder, A. Griffa, P.M. Poulain, A. Haza, and T.M. Ozgokmen. Relative dispersion in the Ligurian Sea. 2010.

[13] M. Veneziani, A. Griffa, and P.M. Poulain. Historical drifter dataand statistical prediction of particle motion: a case study in the Adriatic Sea. *J. Atmos. Ocean Tech*, 24:235–254, 2007.

[14] A. Haza, T.M. Ozgokmen, A. Griffa, A. Molcard, P.M. Poulain, and G. Peggion. Transport properties in small scale coastal flows: relative dispersion from VHF radar measurements in the Gulf of La Spezia. 2010.

[15] V. Taillandier, A. Griffa, P.M. Poulain, and K. Beranger. Assimilation of ARGO float positions in the North Western Mediterranean Sea and impact on ocean circulation simulations. *Geophys. Res. Lett*, 33:L11604, 2006.

[16] V. Taillandier, A. Griffa, P.M. Poulain, R. Signell, J. Chiggiato, and S. Carniel. Variational analysis of drifter positions and model outputs for the reconstruction of surface currents in the Central Adriatic during fall 2002. *J. Geophys. Res*, 113:C04004, 2008.

[17] V. Taillandier, S. Dobricic, P. Testor, N. Pinardi, A. Griffa, L. Mortier, and G.P. Gasparini. Integration of ARGO trajectories in the Mediterranean Forecasting System and impact on the regional analysis of the Western Mediterranean circulation. *J. Geophys. Res*, 2010.

[18] J. LaCasce and C. Ohlmann. Relative dispersion at the surface of the Gulf of Mexico. *J. Mar. Res*, 61:285–312, 2003.

[19] X. Capet, J. McWilliams, M. J. Molemaker, and A. Shchepetkin. Mesoscale to Submesoscale Transition in the California Current System. Part II: Frontal Processes. *J. Phys.Ocean*, 38:44, 2008.

[20] A. Griffa, R. Lumpkin, and M. Veneziani. Cyclonic and anticyclonic motion in the upper ocean. *Geophys. Res. Lett*, (35):L01608, 2008.

[21] A. Mercatini, A. Griffa, L. Piterbarg, E. Zambianchi, and M. Magaldi. Estimating surface velocities from satellite data and numerical models: implementation and testing of a new simple method. *Ocean Modelling*, 2010.

Monitoring and Scientific Analysis of the Sea Level in the Venice Area

A. Tomasin[1,2]
1, Department of Applied Mathematics, University "Ca' Foscari", Venezia, Italy
2, Institute of Marine Sciences, CNR, Venezia, Italy
tomasin@unive.it

Abstract

At Venice and in the nearby coastal area the sea level is always observed with obvious care. The scientific effort is documented here for analysis and forecasting of the the tide. The different factors are considered, from the astronomical forcing whose effects can be altered by human modifications of the environment, to the storm surges and the long-term evolution of mean sea level. Surges are the day-to-day alarming nightmare in the autumn-winter season, since they quickly add up to the normal tide and flood large parts of the towns of the lagoon. Also the mean sea-level change is of concern, especially in these decades when a strong rise is possibile due to climatic change, in addition to the old problem of sinking of the city and its surroundings.

1 Introduction

The sea level of the northern Adriatic, and particularly of the Venice lagoon, stimulates particular interest. In fact, unlike in the largest part of the Mediterranean, here the tidal oscillations are large, and the anomalies due to atmospheric forcing are severe. This creates the concern for the secular 'acqua alta' (high water) phenomenon in a city, like Venice, that the world admires for its historical treasures. The Adriatic is like a long bay, 800 km long and 100 wide approximately, with a narrow opening into the central Mediterranean it is shallow in its northern part, and all this gives it a proper period of oscillation (22 hours, and, secondary, 11 hours) very close to the tidal forcing (24 and 12 hours), as it will be explained below. What matters here is that the ordinary (astronomical) tide has a range of the order of one meter, three times more than observed in most areas close to it (British sailors in the past used to report that 'in the Mediterranean there is no tide...').

In addition, the morphology of the Adriatic favours the amplification of the wind effect. Sirocco wind (south-easterly) piles up water towards the dead end, and the flood is easy. An obvious addition comes from climate change with a real increase of mean sea level that sums, not to be forgotten, to the subsidence of the plain contiguous to the Lagoon, and finally to the peculiar lowering of the Venice area likely due, in the recent past, to human activity. The three factors listed above (astronomical tide, surges and general sea-level rise) will be analyzed with respect to the scientific activity. Other effects, like the ones due to precipitations or tsunamis, will not be considered here.

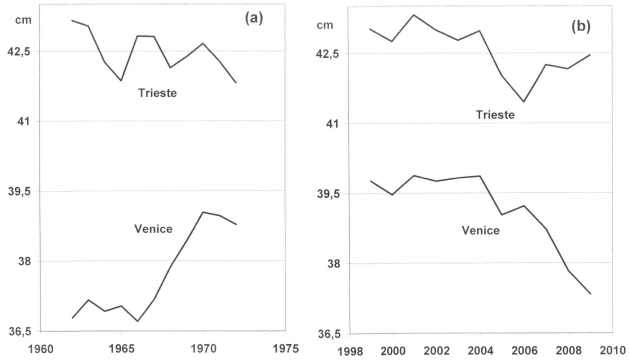

Figure 1: Spring-tide amplitude (M2+S2) at Trieste and Venice: (a) anomalous increase at Venice in 1965-1970, (b) variations in recent years (updated to 2009).

2 The ordinary tide

The ordinary tide, generated by the Sun-Moon-Earth dynamics, is successfully described by the expansion in harmonic components [1]: it permits the analysis of the data collected by level recordings in the various sites. Needless to say, one can compute, without experimental data, the ideal, gravitational level of tide in whatever point (equilibrium tide): in real life, water tends to such equilibrium, with a delay and reduction/amplification, whence the need for measurements models will try to explain the reasons. At Venice, the heritage of tide-gauge measurements is due to the Ufficio Idrografico (now ISPRA), the ICPSM of the City of Venice and the local CNR branch. The tool used here (good also for other sites) to estimate the constants of the harmonic components is a software developed at CNR, named Polifemo [2]: it works with the least-square method which is "hole tolerant" (meaning that the possible lack of some data can be tolerated), does not require observations at regular times and can be used with sequences of extremes (high and low tides) instead of the usual (and more precise) hourly data. A convenient feature of this algorithm is its matching the long-term astronomical variations (consciously left out by the harmonic development), thus avoiding further corrections.

Given the constants for a place, predictions are possible for the astronomical tide, and in Venice they are yearly published thanks to cooperation of the local office for this activity (ICPSM), the branch of a national institute for protection (ISPRA) and the CNR researchers (ISMAR), [3].

A more precise description of the scientific effort is required, since the harmonic expansion mentioned above is not computed once forever: many sites (notably: the city of Venice) are not immutable, in the sense that the morphology of their surroundings is not fixed. Reference is made to the lagoon (that can be dredged), and in particular to the three inlets by which the Adriatic communicates with the lagoon: by monitoring the harmonic constants year by year, the effect of environmental changes (mostly of human origin) is detected. A pe-

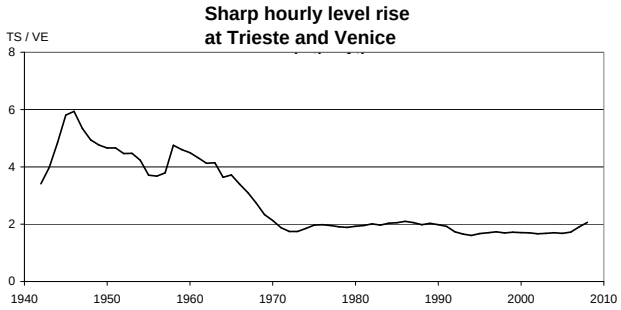

Figure 2: The lagoon inlets can mitigate more or less the violence of the external surges. The cases of sharp increase of water level at Trieste and at Venice (at least .2 m in an hour) are considered. The ratio of the yearly numbers in the two cities is shown (updated to 2009, three-year moving average). The lower is the ratio, the easier is the entrance of quick surges.

riod of heavy interventions on the lagoon (1965-1970) was clearly revealed by such survey by CNR [4]. Moreover, an important tool of comparison can be introduced, i.e., the parallel tidal recordings of Trieste, collected by the local CNR-ISMAR office. This city is ideal for comparison, being at about hundred kilometres from Venice, situated at the closed end of the Adriatic like the lagoon, but substantially not subject to morphological changes of the coast. The coupled analysis of the harmonic constants shows in the period mentioned above (1965-1970), but also in the most recent years, particular trends in the astronomical tide at Venice, revealing some kind of human intervention (Figure 1).

There is another intriguing remark about the effect of morphology on the water level observed inside the lagoon. Tides have fundamental periods of one day or half a day. What happens with phenomena of shorter periods, that can occur with surges? This will be considered in what follows.

3 Level anomalies due to meteorology

The most severe troubles for Venice originate from atmospheric forcing. A little difficulty arises from the definition of such effect that is totally called ‘surge’: it is the deviation from the expected ordinary tide, but one has to deal with long-term variability of sea level, even along the seasons (also due to circulation). Here the definition is sharp: from the observed value one subtracts the astronomical oscillations assumed at zero mean (i.e., one subtracts only a few sinusoids) and subtracts the yearly mean-level value. Clearly, this way the surge is something independent of the tide gauge zero and the yearly variations that could also include the sinking of the area. But the definition could be different. Scientists would also be careful about this definition, since considering an addition denies possible interactions between tide and surge (non-linearitiy). But indirect proofs allow such an assumption to a good

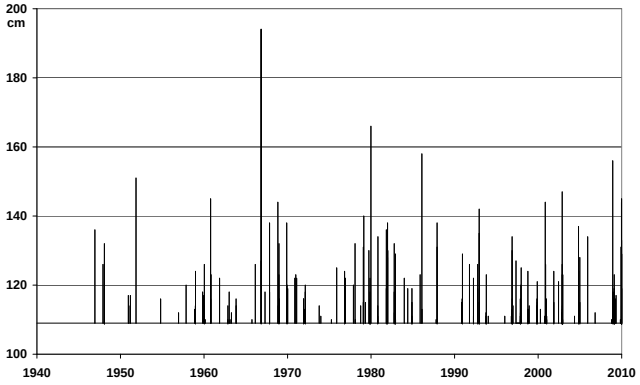

Figure 3: The cases of flood of Venice (i.e. when the water level exceeds 1.10 m over a fixed reference in the city) updated to 2009.

level, for example by observing the absence of tide interactions with itself (overtide or compound tides).

Since the astronomical tide cannot cause a flood (at least, in the present conditions of mean sea level), only surges can give it. But this can occur both with a high tide and even a moderate surge, and vice versa: the nightmarish case of 1966 occurred with a negative tide, and this reminds us that there is no upper limit to surges. It is well known that the forcing on the Adriatic is done by SE winds (sirocco, blowing along the axis of the sea towards the closed end) and atmospheric depressions passing over the Adriatic. A catalogue over the last half-century involved also the local CNR branch [5].

As anticipated above, the morphology of the lagoon has a strong influence on everything coming from the open sea: the simplest check one can perform is the count of cases in which the water level at Venice sharply increases, let us consider 0.2 m in an hour. This number obviously changes for yearly variability, but again the comparison with Trieste can help. The ratio of numbers of such events between Trieste and Venice gives an inverse idea of the "permeability" of the lagoon inlets (Figure 2). Again something interesting turns out - to be investigated using models [6] - showing periods in which the lagoon is more or less protected against surges. Indeed, it is clearly demonstrated that "quick" storms, originating spikes in the Adriatic level, could be cut by the low efficiency of the inlets [5].

Another question about surges concerns their frequency: the floods, hence the storms, are more or less frequent in different years, and the suggestion of regular fluctuations appears from simple graphs (Figure 3). From the above distinctions, it seems more interesting to consider the surges, and in fact a simple correlation emerges between yearly number of surges (over a certain threshold) and the solar activity, as measured by the Wolf's sunspot number [7]: it is presumably a cue for further investigations (Figure 4).

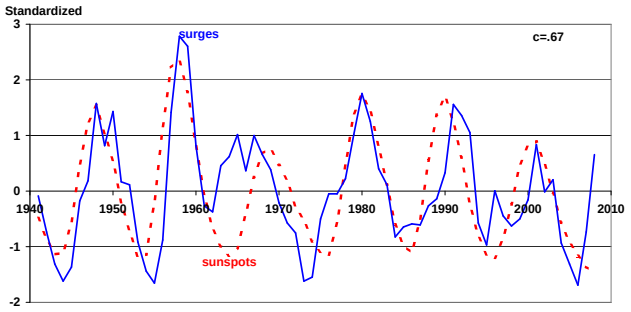

Figure 4: Frequency of surges of meteorological origin and frequency of sunspots (Wolf's number); surges not less than .50 m high. The samples are standardized, updated to 2009, and a 3-year moving average is applied. Correlation index is .67.

4 Free oscillations of the Adriatic

Related to surges, a peculiarity of the Adriatic dynamics is relevant, i.e., seiches. They are the free oscillations of the Adriatic that follow the pulse of a storm. They persist for many days, and they are interesting for many reasons. In the prediction of floods they are very important [8], and it can occur that a storm surge comes out of phase with respect to tide, but the next return of the seiche is instead in phase and a flood occurs when the storm was forgotten (Figure 5).

Another feature about seiches is the fact that they reveal the proper period of oscillation (eigenperiod, for scientists) of the Adriatic. The morphology of the sea determines the main oscillation, with a period between 21 and 22 hours, and a secondary one close to 11 hours [9]. This shows why the tide is strong in this sea, much more than in the rest of the Mediterranean: the well-known astronomical periodicities (about 24 and 12 hours) are close to resonance in this basin. The semi closed shape of the sea and the mechanism of onset by wind are the cause of all that [8].

5 Models and facts about the mean sea level

The sea depth is one of the morphological elements that determines the above periodicities: indeed, a sea-level rise will possibly be a consequence of climate change: what about seiches and tides in this case? An analysis was performed, in a cooperation including ISMAR-CNR [3] for this hypothesis: beyond details, we briefly remind here that if only the depth is modified (by an increase) the proper periods of the sea would go more distant of the astronomical periods, and a tidal reduction would occur. The mean sea-level remains in the background of the above discussions, and it is extremely relevant. As mentioned above, it will possibly rise, with a menace to coastal settlements, but so far the short-term considerations (the last five- or ten-year trends) turn out deceiving. As one can see in the plot (Figure 6), also the mean sea level shows possible oscillation [10]. Another

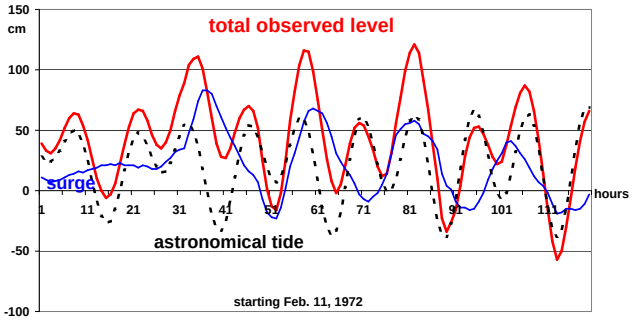

Figure 5: Showing the seiche, or free oscillation of the sea after a storm: the meteorological anomaly continues for a few days, and getting in phase with the tide gives origin to an unexpected flood.

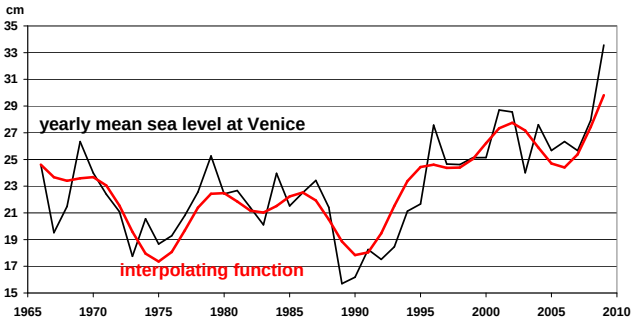

Figure 6: The yearly mean sea level at Venice, updated to 2009: two oscillations (period: 7.8 and 16.0 years) seem to act, and short-term linear trends would be deceiving.

important chapter would treat the sinking of the Venice area [11]: in fact, one considers, for the city, the relative mean sea level, combining the two effects of subsidence and real sea-level rise. But this is studied in other sections of the local research.

6 Acknowledgements

The various institutions, mentioned in the present work, cooperating with CNR-ISMAR, are warmly acknowledged, first of all for their activity in favor of Venice, the lagoon, and people of the northern coast of the Adriatic.

References

[1] A. T. Doodson. The harmonic development of the tide-generating potential. *Proc. Roy. Soc., A*, 100:305–329, 1922.

[2] A. Tomasin. The software "Polifemo" for tidal analysis, Tech. Note 202. 2005a.

[3] P. Canestrelli, M. Ferla, and F. Trincardi. Previsioni delle altezze di marea per il bacino San Marco e delle velocità di corrente per il Canal Porto di Lido, Laguna di Venezia, valori astronomici. 2010.

[4] A. Tomasin. Recent changes in the tidal régime in Venice. *Rivista Italiana di Geofisica*, 23:275–278, 1974.

[5] P. Canestrelli, M. Mandich, P. A. Pirazzoli, and A. Tomasin. Wind, depressions and seiches: tidal perturbations in Venice (1950-2000). 2001.

[6] L. Zampato, G. Umgiesser, and S. Zecchetto. Storm surge in the Adriatic Sea: observational and numerical diagnosis of an extreme event. *Advances in Geosciences*, 7:371–378, 2006.

[7] A. Tomasin. Forecasting the water level in Venice: physical background and perspectives. In: Flooding and Environmental Challenges for Venice and its Lagoon: State of Knowledge. pages 71–78, 2005b.

[8] A. Tomasin, G. Umgiesser, and L. Zampato. (c) On the dynamics of the Adriatic seiche, in: Scientific research and safeguarding of Venice. pages 65–74, 2005.

[9] A. R. Robinson, A. Tomasin, and A. Artegiani. Flooding of Venice: phenomenology and prediction of the Adriatic storm surge. *Quart. J. Roy. Met. Soc*, 99:688–692, 1973.

[10] P. A. Pirazzoli and A. Tomasin. Sea level and surges in the Adriatic Sea area: recent trends and possible near-future scenarios. 166:61–83, 2008.

[11] L. Carbognin, P. Teatini, and L. Tosi. Relative land subsidence in the lagoon of Venice, Italy, at the beginning of the new millennium. *J. Mar. Sys*, 51:345–353, 2004.

The Sea Between Image and Imagination-the Investigation of the Underwater World from the Renaissance to the Age of Enlightenment

A. Ceregato
Institute of Marine Sciences, CNR, Bologna, Italy
alessandro.ceregato@bo.ismar.cnr.it

Abstract

The roots of modern Marine sciences as commonly meant stemmed from the work of Luigi Ferdinando Marsili (Bologna, 1658 - 1730), an eclectic military architect who produced the first "scientific" descriptions of the seabed and its inhabitants. Coeval of the natural philosopher Vallisneri and introduced by Newton to the Royal Society of London, Marsili represents an ideal link between the observation of Nature according to the method developed in the sixteenth century by his co-citizen Ulisse Aldrovandi and the modern oceanographic disciplines. Curiously but perhaps not accidentally, the Institute of Marine Geology of CNR, now incorporated into the ISMAR, was founded by Raimondo Selli in Bologna, Marsili's birthplace and Selli himself named after his ancient precursor one of the most impressive submarine volcanoes of the Mediterranean.

1 Introduction

The modern approach to the history of science (and to history in general) tends to investigate rather the context than finding the "first", the "precursor" or the "father" of a discipline or of a theory. Nonetheless, individual people undoubtedly boosted the evolution of science, or they made a discovery before anybody else, with very diverse outcomes according to many variables.

It is commonly accepted that the development of the marine sciences (the term "oceanography" appeared much later, after the 1872-1876 Challenger expeditions), took place after the work of Luigi Ferdinando Marsili (1658-1730) (Figure 1), in particular from two of his published works, *Osservazioni intorno al Bosforo Tracio* [1] written during his earlier career, and the programmatic *Histoire Physique de la Mer* [2] published in the Netherlands just five years before Marsili's death, at the end of a life entirely spent on the field, through all over the Mediterranean from the Bosporus to Gibraltar. The first work cited above contains analytical results of the investigations on some physical features of the sea performed by Marsili during his first diplomatic mission from Venice to the Ottoman Empire and his return trip to Venice, that can be considered as one of the first oceanographic surveys. The *Histoire Physique* represents somehow the completion of this research, presenting new data on the seawater currents, temperature and salinity, but also descriptions of the seabottom and of the marine organisms [3, 4, 5].

Figure 1: Portrait of Luigi Ferdinando Marsili. (Courtesy of G.B Vai. University of Bologna)

As a matter of fact, the most original element of the approach of Luigi Ferdinando Marsili to investigation and to the dissemination of his observations is due to the application of the scientific method codified some decades earlier by Galilei, Descartes and Bacon, but also to the wide use of the image as a scientific tool, introduced by Ulisse Aldrovandi (Figure 2) in Marsili's hometown Bologna, about a century before.

2 Imagine versus imagination

The combined use of image and text as a tool for describing the natural objects (man included) is well known from the antiquity to medieval treatises, but except of some medical herbals and of particular bestiaries like the *De arte venandi cum avibus* by Emperor Frederick II [6], the role of images was primarily ornamental or symbolic, and their accuracy was poor or even fantastic. Until the Renaissance, most of the written knowledge about nature consisted of a transmittance from generation to generation of a mix of Latin texts, translations from Arabic authors and Arabic versions of Greek literature. These handwritten books were enriched by comments (the "glossae") and sometimes by drawings only occasionally taken from a real model even in the case of depicted herbals or medical treatises; more commonly, texts and images were simply copied from volume to volume. This way of transmission of knowledge favoured the creation of stereotypical, simplified images, whose significance carried rather symbolic significances than real features of the natural objects.

Figure 2: Portrait of Ulisse Aldrovandi (copy from the original by Pelagio Pelagi, early 1800) Courtesy of G.B. Vai. (Photo Mattei-Zannoni, BUB, ASUB)

Starting from the XV century, the strong interaction between art and science and a renewed attention to the physical reality led to an increased accuracy of the images.
The new fame of the *Naturalis Historia* of Pliny and novelties imported from the voyages of exploration explosively expanded the list of terrestrial and marine organisms, forcing the natural philosophers to review the old classifications and try to build a new inventory of the world.
The introduction of printing and of more accurate and analytical illustrations, fed an irreversible process of liberation from the old scholasticism, based on a dogmatic interpretation of Aristotle (filtered from medieval tradition) which conditioned most of the knowledge on nature.
Leonardo Da Vinci (1452-1519), in search of proving a geocentric, "protoscientific" Theory of Earth based on the Neo-Platonist relationship between Man's Microcosm and Nature's Macrocosm, demonstrated that fossils are the remains of ancient organisms that the Deluge could not carry to the highest mountains [7].
At the end of the XV century, Leonardo in Italy and Albrecht Dürer (1471-1528) in Germany, started two different approaches to the figurative description of natural objects: while Leonardo, drawing natural objects and anatomic studies, always tended to represent the dynamism, the continuous transformation of the objects and the relationship between the subject and its context in order to stress their evocative power, on the other hand Dürer isolated the objects to concentrate the analysis on the physical nature of the objects themselves; the best techniques to achieve the finest detail were

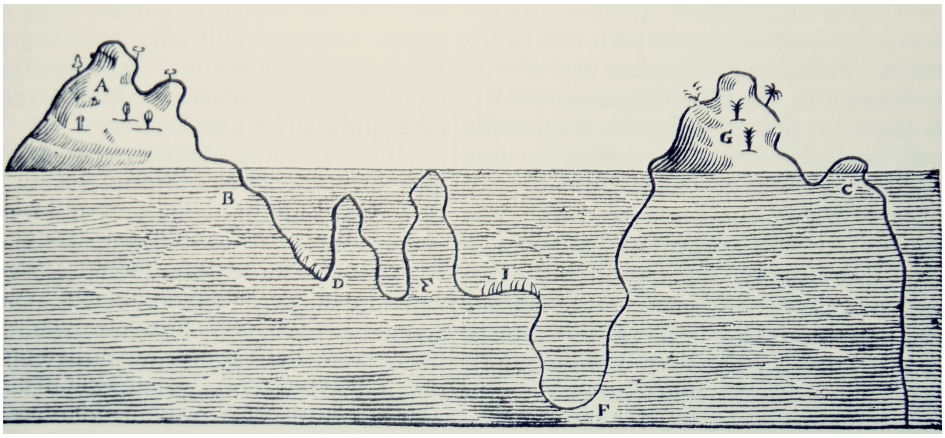

Figure 3: Section of the Earth surface with the hypothetical profile of the seabed. A. Kircher, *Mundus Subterraneus* (III Ed. 1678), Cap. XV, p. 97. G.B. Vai (2004) Ed., Critical reprint by A. Forni Editore. (A. Ceregato, personal archive and photo)

the drawing by ink pen, the engraving and a mix of tempera and watercolors [8].

The new generation of natural philosophers will choose the model proposed by Dürer and his pupils as the best for their descriptions. The Swiss Conrad Gessner (or Gesner;1516-1565) will attempt for first to build an updated inventory of the Three Kingdoms of Nature: Animalia, Plantae and Mineralia. The technique of engraving on wood and later on copper sheets developed by Dürer was immediately adopted for printing the new treatises [9]. The Counter-Reformation limited the freedom of Italian natural philosophers (Galileo Galilei and Giordano Bruno were only the most famous victims), who were denied to venture interpretations dangerously dissonant with the Scriptures, but did not prevent to investigate the "order" of Nature: Ulisse Aldrovandi (Bologna, 1522-1605) set up the first natural history museum at home, a microcosm of Nature tended to show as more comprehensively as possible the diversity of natural objects, animals, plants and minerals and to compose a natural history rich in images as much accurate as possible. For this purpose Aldrovandi created an artistic laboratory within his home museum and invited some of the best illustrators and engravers of his time to take their drawings directly from his specimens; he also acquired and exchanged watercolours and engraved images from his correspondents and collectors as the Archidukes of Tuscany and the Duke of Mantua. He personally maintained for years some artists, and looked at Dürer's legacy when he decided to print his books, so he hired Cornelius Schwindt and Christopher Lederlein (Cristoforo Coriolano) who produced more than 3000 woodcuts at the end of 1598 (i.e. [10]; see also [11] for a complete reference review).

A part of four volumes (*Ornithologiae... I, II, III* and *De Animalibus Insectis*) published from 1599 to 1603, the remaining

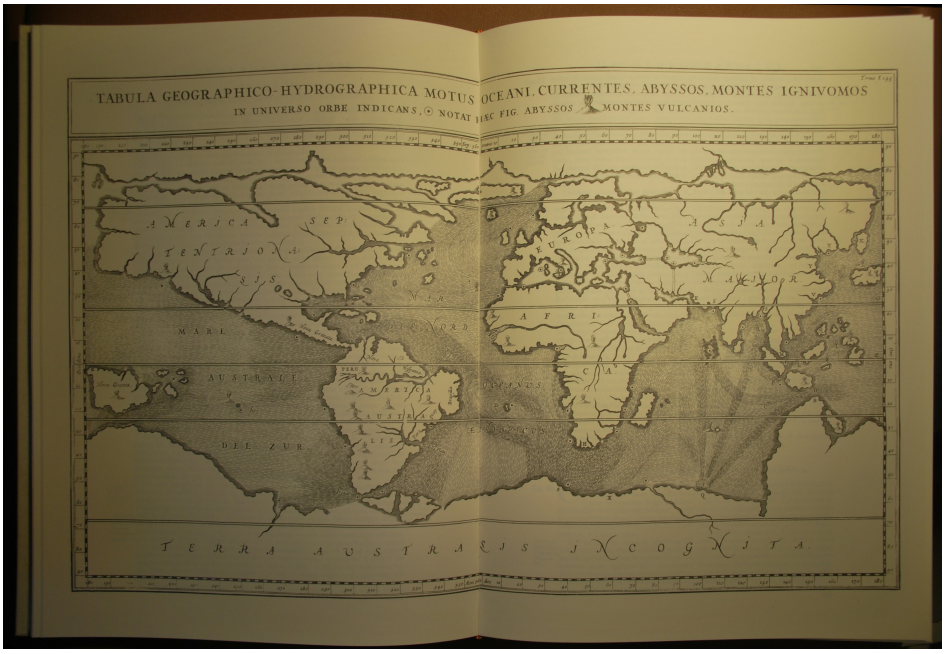

Figure 4: Map of the surface oceanic currents after Athanasius Kircher. Kircher did not perform any direct measurement, differently from what Marsili did some decades later, but it is one earliest attempt of representing the sea currents. From Athanasius Kircher, *Mundus Subterraneus* (III Ed. 1678). Crit. Ed. by G.B. Vai, 2004. A. Forni ed. (A. Ceregato, personal archive and photo)

books of the Ulisse Aldrovandi's *Historia Naturalis* were printed after his death, often remarkably modified by the curators and only one of the planned botanical volumes was published in 1668. According to the common approach of that age, the taxonomy was adapted from those of Aristotle or, as Aldrovandi tended to prefer, from Pliny. Each section included a review of the previous knowledge about a group of natural objects, not only "scientific" descriptions but also symbolic attributes and their eventual pharmaceutical use. The originality of these works was in the personal observations Aldrovandi made directly on the specimens and the accuracy of the images. He also was used to list all the current, popular, foreign names referred to each "species", both within his books and in his collection of more than 2000 colour drawings he used also for his lessons as the first professor of Natural History at the Bologna University.

The XVII century is apparently characterized by a paradox: on one hand, it is the age of the Scientific Revolution introduced by Galileo Galilei, Renè Descartes and Francis Bacon, of the experimental methodology, of the discovery of the new order of the Universe, introduced by Galilei and perfected by Newton at the end of the century; on the other hand the Natu-

ral History collections appeared since the Renaissance, from which the new ideas originated, progressively lost their scientific significance in favour of the aesthetic attributes, becoming *Cabinets of Curiosities* (also known as *Wunderkammern*) [12]. From the work of Aldrovandi and Gessner, forgotten the scientific descriptions, the Baroque readers prefer the anedoctal contents, so the old authors will be cited for their descriptions of monsters and drakes: the Aldrovandi's *Monstrorum Historia*, published in 1642 by Bartolomeo Ambrosini, then one of his most appreciated works and largely cited by Athanasius Kircher in his *Mundus Subterraneus* (1664), will be ridiculized a century later by the Enlightened scientists. Nonetheless, some scientists continued to follow the lesson of Aldrovandi, in particular those who were involved in the debate on the nature of fossils and of the structure of the Earth: Fabio Colonna (1567-1640), Niels Stensen (1638-1686) and Agostino Scilla (1629-1700) largely used the images for clarify their observations. Colonna within the *De Glossopetris dissertatio* (1616), demonstrated the organic nature of *Glossopetrae* with a use of images not dissimilar to that of Aldrovandi, Niels Stensen completed the demonstration made by Colonna with a figure of *Canis Carchariae* with a detail of a tooth (following the original Gessner's intuition) and the *Prodromus* (1669) with some simplified figures to describe the different facies of Earth before and after the Deluge [13, 14]. Agostino Scilla, artist rather than scientist titled his most famous work on the real origin of fossils (1670) drawing a frontispiece with two: *La vana speculazione disingannata dal senso* (trad.: the vain speculation disillusioned by the sense), and he accompanied his discussion with accurate figures. Athanasius Kircher described his theories on the *Mundus Subterraneus* through a number of sections of the Earth very imaginative but easy to understand, sometimes populated by the drakes taken from Aldrovandi's works. A few decades later, his hypothesis that the maximum depth of the sea was equal to the highest mountain (Figure 3) influenced the early observations by Marsili. In another chapter of *Mundus Subterraneus* he put one of the first attempts of represent the oceanic currents that is not conceptually so dissimilar from our present charts (Figure 4). If the use of images by natural philosophers is sometimes oscillating between loyalty to the real and the imaginary (the sea is still populated by mysterious sea monsters), in the same years, the development of the cartographic disciplines led to the creation of more reliable maps even in three dimensions, such as those by the Dutch Willem Blaeu (1571-1638) and his sons and the globes made by the Italian Coronelli (1650-1713). Although until the eighteenth century the problem of longitude remains unresolved, maps and nautical books become even more faithful and detailed, and some attempts to describe the seabottom achieved better results. Luigi Ferdinando Marsili, holder of a large collection of natural specimens on the model of that of Ulisse Aldrovandi, immediately understands the importance of considering a good representation as a fundamental tool both for investigation and for dissemination of his observations [15]

3 Towards a new perspective of the Sea

It is easy to imagine how the first area of investigation of the natural philosophers

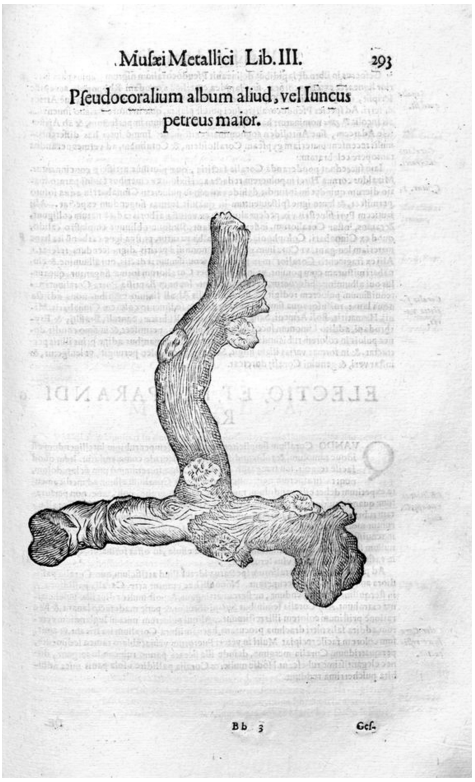

Figure 5: "Pseudocoralium album aliud, seu Iuncus petreus maior" From: Ulisse Aldrovandi (Ed. B. Ambrosini, 1648) *Musaeum Metallicum...* BUB. Fondo Aldrovandi. Courtesy of the Biblioteca Universitaria Bolognese, (Director Dr Biancastella Antonino)

turned to the sea was the ichthyology, or more generally the marine zoology. Introduced by Aristotle and cultivated by scholars from around the Mediterranean, the study of fishes and other marine organisms had a first major boost when the first transoceanic navigators returned back from their explorations with their finds from unknown animals and their rich imaginative and often anecdotal reports on terrible monsters appeared from the oceanic abysses. Nevertheless, the updated classification of marine animals also developed among the stalls of the fishermen, the first attempts of Guillaume Rondelet and scans of his young disciples Paolo Giovio and Ulisse Aldrovandi within the markets of Rome. By these first experiences Aldrovandi will distinguish for the first time between bone and cartilagineous fishes, even if he will not still recognize dolphins and whales as mammals [16]. Meanwhile Georg Bauer (Agricola) and Conrad Gessner began to describe not only the most geological objects but groped their interpretation: they never take the sea, but through their comments on the mainland will begin to ask questions about the nature of

Figure 6: Sketch of the stratigraphic unconformity between a folded substrate (continuing below the sea level) and a soil deposited on its depression.BUB, Fondo Marsili, ms. 90 c.44. Photo A. Ceregato.

the "petrefatti di creature marine" which will culminate in seventeenth-century debate about the nature of fossils, only concluded at the end of the next century. The questions posed by Gessner and Agricola had already been resolved decades ago - but not transmitted - by Leonardo da Vinci, who noted (especially on the famous *Codex Leicester*) even his ideas on the organic nature of fossils and the behavior of water and seabed. Ulisse Aldrovandi devoted a huge space to marine objects, animate and inanimate. It is interesting to extrapolate from his papers the richest correspondence with other collectors along the Adriatic coast. Many of the invertebrates documented in his *De Reliquis Animalibus Exanguibus* (1606) came from the Adriatic coast and from the nets of fishermen from that area. Within his collection of illustrations, we can find rocks colonized by date mussels, squid and dogfish eggs attached to the substrate, a rich repertoire of molluscs typical of sandy bottoms of the Adriatic (i.e. *Chamelea gallina, Pecten jacobeus, Acanthocardia spp., Modiolus sp., Aporrhais pespelecani* and even a branch of the yellow coral *Dendrophyllia cornigera* (Figure 5) [16, 17]. After Aldrovandi the observation and research of a natural order of things, starting point of the founders of modern science such as Descartes, Galileo and Bacon, continues in the seventeenth century through a dichotomy between the collections of "Naturalia et Mirabilia" (the *Wun-*

Figure 7: Sketch of the unconformity between the bodies deposited along the submarine slope and forming sands, gravels and shelly/coral concretions. BUB, Fondo Marsili, Ms. 90 c.45. Photo A. Ceregato.

derkammern) and research based on experiment and observation that, with regard to the geology, will see the first assertion of the cornerstones of the modern discipline with Steno and Colonna at the beginning of a century that will be shut down, just at the time of Marsili, with the major debates on Theory of the Earth and the nature of fossils, and with the development of dissemination until the *Encyclopédie*, twenty years after Marsili's death. As previously seen, The preconditions for the Marsili's insight are ultimately given by the results of natural philosophy, collectionism and the birth of the great academies and scientific societies through which the scientific method, developed between the late sixteenth and seventeenth century, comes to be the only possible epistemological approach to investigate the physical world. During his formative years, Marsili also because his military career, received an irregular instruction and he never achieved a graduation even if he attended many courses at the Bologna and Padua Universities, but he formed his own cultural background by the friendship with the most active scientists of his hometown: Geminiano Montanari and Marcello Malpighi among others. His most formative training was given by direct experiences and observations made since his earliest diplomatic missions in the Ottoman empire and in the Balkans [1, 2, 3, 18, 4, 5]. He knew the works by Steno and Scilla and he had direct contacts with Johann Jakob Scheuchzer and Antonio Vallisneri Sr. who

Figure 8: *Corallium rubrum*. Original specimen figured in *Hist. Phys. de la Mer*, T. XXVIII. Museum of Zoology, Bologna. Courtesy Bruno Sabelli, Photo A. Ceregato.

unvealed to him the first discoveries on the structure of mountains and their stratigraphy, but he also was very influenced by the works of physics like Hooke, Newton and by the John Woodward's theory of the Deluge. He was not really an eclectic intellectual, but more a passionated military technician who investigated as many aspects as possible of the territories and seas he visited for diplomatic or military purposes. In the second part of his life he devoted all his energies to the creation of an Instituto Scientiarum based on the model of the foreign Academies of Science but also following the way indicated by his predecessor Aldrovandi, that is stimulating the interaction between art and science, mixing together the Institute with the Clementine Academy of Arts and reforming the obsolete University of Bologna introducing the experimental method. He did not see his project completely realized, even if it was formally ratified during the period 1709-1712, because of the opposition of the old teachers and of the Bolognese Senate who did not give the necessary funds because of the concurrent poverty of the town. In spite of all that, he left to the Institute a huge collection of natural and archaeological specimens, some fundamental books on marine sciences and geology and a rich library. During his scientific activity, Marsili intro-

Figure 9: *Corallium rubrum*. Detail from *Hist. Phys. de la Mer* (Dutch Ed., 1785), T. XXVIII. BUB, Fondo Marsili. Photo A. Ceregato.

duced the experimental method for measuring many oceanological parameters and drew sections and profiles of the seabottoms from a modern point of view (Figure 6,7). He did not recognized the real nature of the corals but his descriptions of *Corallium rubrum* (Figure 8,9), and deep water madreporarians, such as *Dendrophyllia cornigera* and *Madrepora Oculata* (Figure 10) were cited for a long time after the final taxonomic placement of the Cnidaria. He made many descriptions on the benthic environments and on the anatomy and the behaviour of marine organisms. As Vai [19] noted, he had some remarkable insights on that process we today know as isostasy. Lacking of regular academic training he always needed help to translate his texts in Latin or in French (later the great Dutch naturalist Boerhaave translated the whole *Histoire Physique* for a new edition printed by the Company of Indies), but after three centuries the recent literature returned him the right role in the history of science. Count Marsili, engineer and military, by its own admission only an occasional frequenter of the Humanae Litterae, had better luck at the Académie de France than in his hometown. Two centuries later, tells Renzo Sartori, Raimondo Selli returns a double tribute to Marsili founded in Bologna, the Institute of Marine Geology and dedicate one of the largest underwater volcanoes in the Mediterranean ([3], Vai, pers. comm.).

Figure 10: Complete specimens and details of *Dendrophyllia cornigera* and *Madrepora oculata*. Detail from *Hist. Phys. de la Mer* (Dutch Ed., 1785), T. XXX. BUB, Fondo Marsili. Photo A. Ceregato.

4 Acknowledgements

I am indebted to dr Laura Miani and dr Maria Cristina Bacchi (Biblioteca Universitaria Bolognese) for their kindness and their helpful suggestions concerning the manuscripts by Marsili. Thanks are due also to the Director of the BUB, dr Biancastella Antonino, and to the Director of the Museum of Zoology of the Bologna University, prof Bruno Sabelli, for the permission of taking photographs of the Marsili's collections for this work. Prof Gian Battista Vai, Director of the Museum of Geology G. Capellini (University of Bologna), friendly let me free to dig into his personal archive. This is the ISMAR CNR contribution n. 1674.

References

[1] L.F. Marsili. Osservazioni intorno al Bosforo Tracio overo Canale di Costantinopoli Rappresentate in lettera ala Sacra Reale Maestà di Cristina Regina di Svezia da Luigi Ferdinando Marsili. pages 1–10, 1681.

[2] L.F. Marsili. Histoire Physique de la Mer. Ouvrage enrichi de figures dessinées d'après le Naturel. pages 1–173, 1725.

[3] R. Sartori. Luigi Ferdinando Marsili, founding father of oceanography. *Four Centuries of the Word Geology. Ulisse Aldrovandi 1603 in Bologna.*, pages 169–177, 2003.

[4] A. Lodovisi. Luigi Ferdinando Marsili e l'Olanda. page 239, 2006.

[5] N. Pinardi. Misurare il mare. Luigi Ferdinando Marsili nell'Egeo e nel Bosforo 1679-1680. page 83, 2009.

[6] Federico II di Svevia. L'Universo degli Uccelli - Il trattato di ornitologia del grande imperatore naturalista. (Critical edition of De arte venandi cum avibus, from various manuscripts, sec. XIII). pages 1–231, 1988.

[7] S.J. Gould. I Fossili di Leonardo e il Pony di Sofia. (Orig.: Leonardo's mountains of Clams and the Diet of Worms). pages 1–448, 2004.

[8] L. Tongiorgi Tomasi. L'immagine naturalistica: tecnica e invenzione. In: Natura-Cultura. L'interpretazione del mondo fisico nei testi e nelle immagini. Atti del Convegno Internazionale di Studi, Mantova, 5-8- Ottobre 1996. pages 133–151, 2000.

[9] C.M. Pyle. Art as science: scientific illustration, 1490–1670 in drawing, woodcut and copper plate. *Endeavour*, 24(2):69–75, 2000.

[10] G. Olmi. Il museo o "microcosmo di natura". In: Natura Picta. Ulisse Aldrovandi. pages 19–37, 2007.

[11] M. Folia Campos and C. Magnani. Bibliografia su Ulisse Aldrovandi. In: Natura Picta - Ulisse Aldrovandi. pages 620–660, 2007.

[12] M. Beretta. Storia Materiale della Scienza. Dal Libro ai Laboratori. pages 1–336, 2002.

[13] N. Morello. The question on the nature of fossils in the 16th and 17th centuries. In: Four Centuries of the Word Geology. Ulisse Aldrovandi 1603 in Bologna. pages 127–152, 2003.

[14] N. Morello. Steno, the fossils, the Rocks, and the calendar of the Earth. In: The Origins of Geology in Italy. *GSA Special Paper*, 411:81–94, 2006.

[15] G. Olmi. L'illustrazione naturalistica nelle opere di Luigi Ferdinando Marsigli. In: Natura-Cultura. L'interpretazione del mondo fisico nei testi e nelle immagini. Atti del Convegno Internazionale di Studi, Mantova, 5-8- Ottobre 1996. pages 255–303, 2000.

[16] P. Tongiorgi. Dalle profondità dei mari del XVI secolo. In: Natura Picta - Ulisse Aldrovandi. pages 89–93, 2007.

[17] W.D.I. Rolfe and A. Ceregato. “A fossilized nut?”: a drawing from Aldrovandi in the Paper Museum of Cassiano dal Pozzo. *Archives of natural history*, 36(1):160–163, 2009.

[18] B. Soffientino and M.E.Q. Pilson. The Bosporus Strait - A Special Place in the History of Oceanography. *Oceanography*, 18(2):17–23, 2005.

[19] G.B. Vai. Isostasy in Luigi Ferdinando Marsili’s manuscripts. In: The Origins of Geology in Italy. 411:95–127, 2006.

Particle Fluxes and Transport Processes Along the Continental Margins and in Deep Sea Environments

A. Boldrin[1], L. Langone[2], S. Miserocchi[2], M. Turchetto[1]
1, Institute of Marine Sciences, CNR, Venezia, Italy
2, Institute of Marine Sciences, CNR, Bologna, Italy
alfredo.boldrin@ismar.cnr.it

Abstract

Assessing processes involved in particle dynamics in the marine environment is an important step in order to understand the role of oceans in the global cycle of carbon and related elements. The sinking of particles represents one of the most important processes of exchange from the upper to deep ocean, and the export of organic carbon, produced by phytoplankton in the photic layers, gives the estimation of the efficiency of the biological pump.
In the framework of several national and international projects, vertical fluxes of particulate matter and their biogenic components were analysed in the Adriatic and Ionian seas and in the Sicily strait, below the photic layer and near the bottom to define the principal processes affecting the dynamics of suspended matter in the open sea and along the continental margins.
In open seas, the pool of particulate organic carbon is mainly determined by autotrophic production occurring in the upper layer of the water column, supported by the seasonal mixing, deep convection events and coastal-offshore exchange. The export of particles depends on production, consumption and decomposition controlled by physical and biological processes with high seasonal and interannual variability. Near the sea floor, advective transport and resuspension of bottom sediment influence the fluxes. In the Southern Adriatic, the Bari Canyon is an efficient conduit in delivering suspended sediment from the continental shelf to the deep basin.

1 Introduction

The increase of atmospheric CO_2 and the associated global warming could modify the chemical and physical cycle of nutrients with important effects on biological processes (e.g., [1, 2] and on the functioning and efficiency of the biological pump in the oceans.
Open oceans are considered key areas for their role in the global cycling of matter and energy. The annual uptake of CO_2 by the surface ocean has been estimated to range from 1 to 3 Gt of carbon [3], and the biological processes involving the organic carbon production in upper oceans and transport in deep layers, highly affect the CO_2 budget. The uptake of carbon by marine phytoplankton and the consumption of this organic material by zooplankton and marine bacteria form the basis of the "biological pump". These surface-dominated processes develop and regulate the flux of sinking particles to depth.

Assessing processes involved in particle dynamics in the marine environment is an important step in order to understand the role of oceans in the global cycles of carbon and related elements and the sinking of particles, the "marine rain", represents one of the most important processes linking the upper to deep ocean. In open seas, the pool of particulate organic carbon - POC - is mainly determined by autotrophic production occurring in the upper layer of the water column, supported by the seasonal mixing, deep convection events and coastal-offshore exchange. The export of organic carbon, produced by phytoplankton in the photic layers, gives the estimation of the efficiency of the biological pump [4].

The export of particles depends on the equilibrium among production, consumption and decomposition controlled by physical and biological processes with high seasonal and interannual variability. Several physical and biological factors, affecting the transport efficiency of POC as it sinks through the mesopelagic zone, are of considerable importance to predictions of C sequestration in the deep sea [5].

In open sea environments, productivity may be estimated by the amount of organic matter that falls out from the photic zone thus vertical fluxes could be related to new production processes [6].

Particle fluxes to the sea floor and physical-chemical transformations occurring while settling through the water column are investigated analysing the composition of the material caught in intercepting sediment traps. The collection of sinking particles by means of sediment traps has revealed a relationship between exported fluxes and primary productivity of overlying waters.

Particle dynamics is generally related to the transport of material from the source areas, generally located in the surface layer, to the sea bed, that could represent the final sink of the material.

In this process continental margins give an important contribution to the total budget of material transferred to the deep environments and peculiar geo-morphological structures, as canyons, are generally assumed to play an important role in water and sediment transport from the shelf to the deep sea. The central Mediterranean because of its geo-morphology and water circulation is particularly exposed to climate changes, so that studying the distribution and the exchange between the upper and deep sea is considered highly important, the southern Adriatic and Ionian seas being relevant regions in the dynamics of the basin. Studies on the physical oceanography of these regions showed a high variability at seasonal and interannual time scale [7, 8] but the influence of these rapid changes on production and transport of suspended matter is not yet completely understood [9].

Since 1994, in the framework of several national and international projects (e.g., EU-OTRANTO, EU-EUROMARGE, EU-MATER, EU-EUROSTRATAFORM, EU-HERMES, EU-HERMIONE, VECTOR, OBAMA) particle fluxes were determined in deep areas of the Southern Adriatic (1200 m depth) and northern and western Ionian Sea at 2400 and 3300 m depth, respectively (Figure 1), deploying moorings equipped with sediment traps, below the photic zone (150 m depth) and near the sea floor. Moreover, to point out the influence of shelf areas and the transport along the slope to the deep basin, 3 stations were analysed in the Bari canyon area (600 m depth) and 2 stations in the Gela basin (Sicily strait area, 600 m depth), an area characterised by the presence of submarine slides (Figure 1).

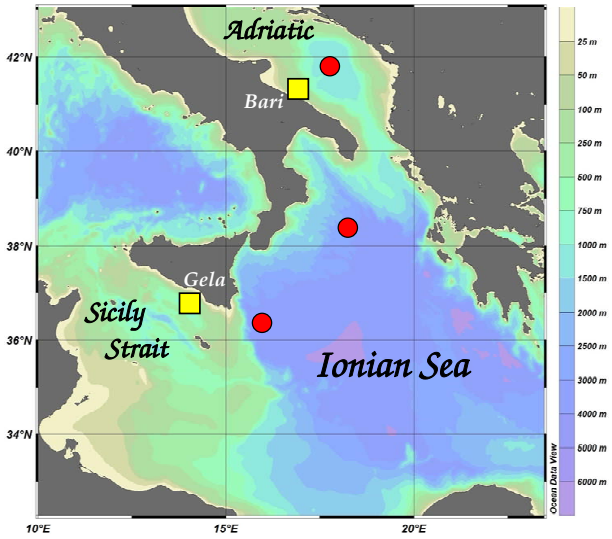

Figure 1: Map of the sites where time-series samples were collected by sediment traps. Circles indicate the deep areas in the Ionian (two stations) and Adriatic seas, squares indicate the continental margins investigated: the Bari canyon (three stations) and the Gela basin (two stations). Plot realized by Ocean Data View program [10].

These investigations permitted to define:

- the temporal and spatial variability of particulate material, its production, transfer and sedimentation processes;
- the influence of the hydrological and dynamical structures on production and transfer of particulate material to the sea floor;
- the export of particulate organic carbon from the photic zone and the relation with productivity processes.

2 Role of biological processes on vertical fluxes

According to the low suspended matter concentration, the Southern Adriatic and Ionian Sea can be considered as representative of oligotrophic systems. The availability of different inorganic or organic nutrient forms, related to the water column structure and circulation dynamics, affected the structure of phytoplankton communities, primary production rates and the characteristics and composition of the vertical fluxes [12]. The phytoplankton communities in both areas are composed of organisms living in an often nutrient-limited environment where relatively fast blooms of the larger sized fraction occur. Two modes of the food web operation in the photic zone can be identified [13]: a winter situation, characterised by the nutrient uptake carried out by larger organisms, with a late winter-early spring maximum sedimentation rate, followed in summer by the growth of the

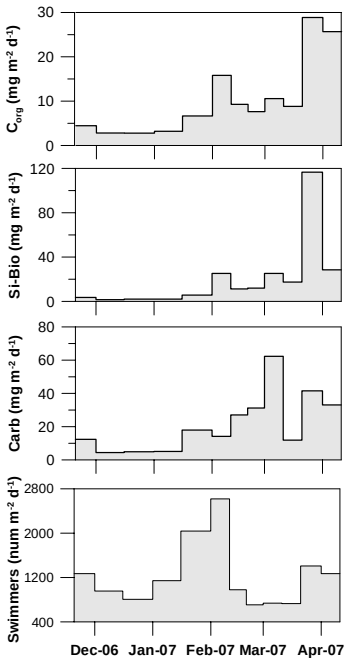

Figure 2: Time series of vertical fluxes of organic carbon (C^{org}), biogenic silica (Si-Bio), carbonate (Carb) and number of swimmers measured from November 2006 to April 2007 in the south Adriatic Pit below the photic zone, at 168 m depth.

small phytoplankton fraction with a low sinking rate [14]. In the southern Adriatic, the influence of waters coming from the northern Adriatic is evident at the surface of the western side of the basin. The phytoplankton community is mainly represented by diatoms and nanoflagellates. In the northern Ionian, particulate matter concentration was lower compared to the Adriatic and the phytoplankton community was dominated by nanoflagellates and coccolithophorids [12]. Phytoplankton growth and primary production rate might be strictly related to vertical fluxes of particulate matter thus the vertical fluxes measured reflect the different trophic status of the two basins. The Ionian vertical fluxes are lower than the Adriatic ones (average of 36 and 105 mg m^{-2} day^{-1}, in the upper trap, in Ionian and Adriatic, respectively). With the same trend, the C-export in the Ionian was halved in respect to the Adriatic (5 and 10 mg C m^{-2} d^{-2}, respectively). The downward C-flux showed high seasonality and episodic events (Figure 2). The C-flux peaks, observed in late winter-spring, generally last for a single sampling period (10-15 days), and can account for up to 50% of the annual C-flux. Maxima of C fluxes are strictly correlated with high biogenic silica and carbonate fluxes, e.g., in the Adriatic in a

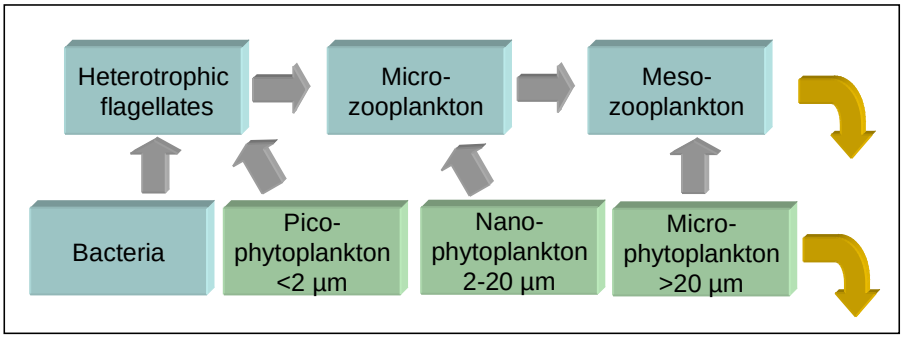

Figure 3: Schematic food web (redrawn from [11]). The Micro-phytoplankton and Meso-zooplankton communities control the export of particles from the upper photic layer to the deep sea.

single 15-day long event in spring 2007 the biogenic silica flux accounted for about 40% of the total 6-months flux (Figure 2). These events of high export, normally limited in time, could be correlated to blooms of different micro-planktonic communities, with silicate (e.g., diatoms and radiolarian) or carbonate (e.g., coccolithophorids and forams) skeleton organisms. After or simultaneously, a higher abundance of faecal pellets and swimmers was found in the traps Figure 2, highlighting the role of the zooplankton grazing in the vertical transfer of carbon. These observations confirm the importance of the micro-phytoplankton and of meso-zooplankton in the export of particles from the upper water column (Figure 3). Early-spring blooms have been related to the vertical mixing of the upper water column supplying deep inorganic nutrients in the photic layer. In the southern Adriatic the vertical mixing convection is considered the dominant process, increasing primary production and downward fluxes of particulate matter [15, 16]. The intensity and duration of the convective vertical mixing is related to heat fluxes and shows an interannual variability as observed comparing the different cooling periods in winters 1996-97 and 1997-98. The longer period in spring 1998 determined a deeper convection process which increased the primary productivity in the photic layer and the vertical fluxes (Figure 4). In both areas a positive coupling between the carbon flux in the upper trap and productivity measured in the same periods was observed [12] and the coupling of pelagic phytoplankton abundance and downward flux in the Otranto Strait was also described by [17]. The organic carbon export with respect to the primary production (f-ratio) showed low values (<5-10 %, Figure 5). Calculated at annual scale, at the Adriatic station the f-ratio was 3.4% for the upper trap and 2.7% for the lower trap. At the Ionian station the f-ratio was 3.9% below the upper layer and 0.8% at the deepest trap. These low values indicate high carbon utilisation and/or high efficiency of particulate organic matter degradation, i.e. fast recycling in the upper water column.

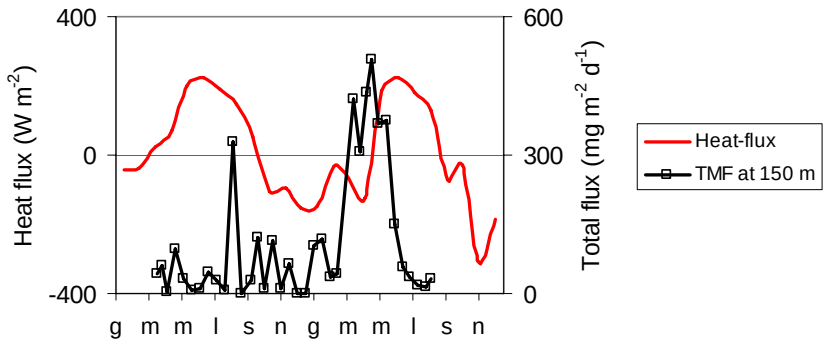

Figure 4: Influence of climatology (from calculated heat fluxes) on the export of particles in the South Adriatic Pit from January 1997 to November 1998. The lower heat fluxes measured in late-winter/early spring 1998 respect to the previous year determined a deeper mixing and, consequently, an increase of primary production and vertical flux of particles.

3 Continental margins: active area for advective transport

In the South Adriatic Pit, particle fluxes near the bottom (on average 201 mg $m^{-2}day^{-1}$) show higher values in respect to those measured just below the surface productive layer and these higher values are likely due to horizontal and advective contributions of material transported into the basin by mesoscale circulation.

In the Adriatic sea this process can be correlated to the spreading of bottom waters from shelf areas along the continental slope. In particular the morphological structure determined by the Bari canyon represents an efficient conduit in delivering suspended sediment from the continental shelf to the deep southern Adriatic basin [18].

It is known that canyons act as trapping areas for sediments and provide a direct conduit for sediment transport from the continental shelf to the deep sea depositional systems [19]. Furthermore, canyons influence the water flow along the continental margins by forcing a cross-shelf exchange [20] and canalizing dense water to the deep basins [21], thus modulating in turn also the amount of particle export. For example, in the Gulf of Lions, downward particle fluxes differ up to three orders of magnitude over a 6- year period [22] with interannual variability caused by both particulate inputs and the intensity of the oceanic transport processes including storms, fluctuation of cyclonic currents and dense water cascading [23, 24].

The Bari Canyon is the main canyon system along the Adriatic margin and plays an important role in the water dynamics of the southern Adriatic basin. An integrated approach including hydrological measurements, i.e. suspended matter dis-

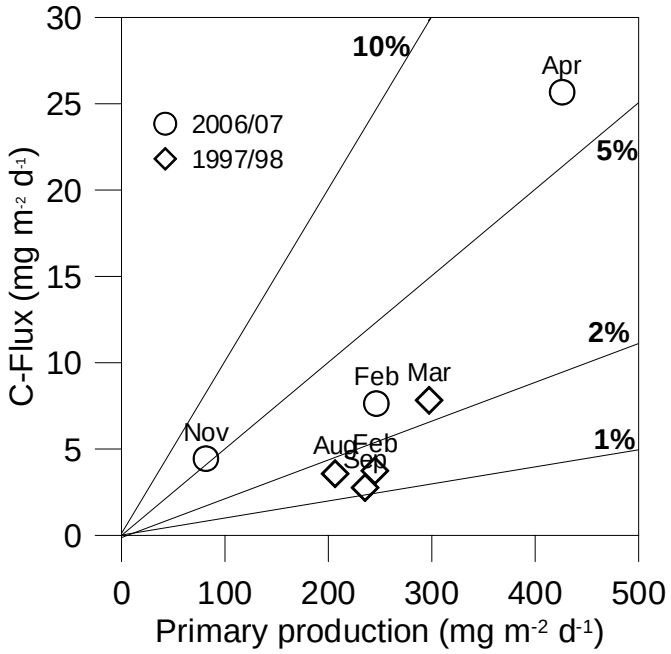

Figure 5: Relationship between primary production and organic carbon export (C-Flux) in the south Adriatic Pit in two different sampling periods. Organic carbon export represents generally less then 10% of primary production (values of primary production from Malaguti, pers. comm.).

tribution, water dynamics, water-column particle fluxes and sedimentary data, allowed to define the main processes occurring in the canyon [18].

Total mass fluxes measured by sediment traps near the bottom in the canyon area, inside the two main branches of the canyon and on the open slope, at 600 m depth, were one order of magnitude higher (ranging from 3000 to 8000 mg m^{-2} day^{-1} on average) than the ones measured in the deep Adriatic (1200 m depth). The highest particle fluxes were recorded in spring, a period characterized by the lowest water temperatures and the highest current speeds (up to 72 cm^{-1}) along the canyon axes that can be related to a vein of North Adriatic Dense Water (NAdDW) flowing southward along the Adriatic shelf. The temporal variability of total mass fluxes, showing maximum values in the stations located inside the canyon and on the slope area, suggests that similar processes of sediment transport are active along the entire southern Adriatic margin, but that they are amplified in the Bari canyon system, highlighting that the canyon is an efficient conduit in delivering suspended sediment from the conti-

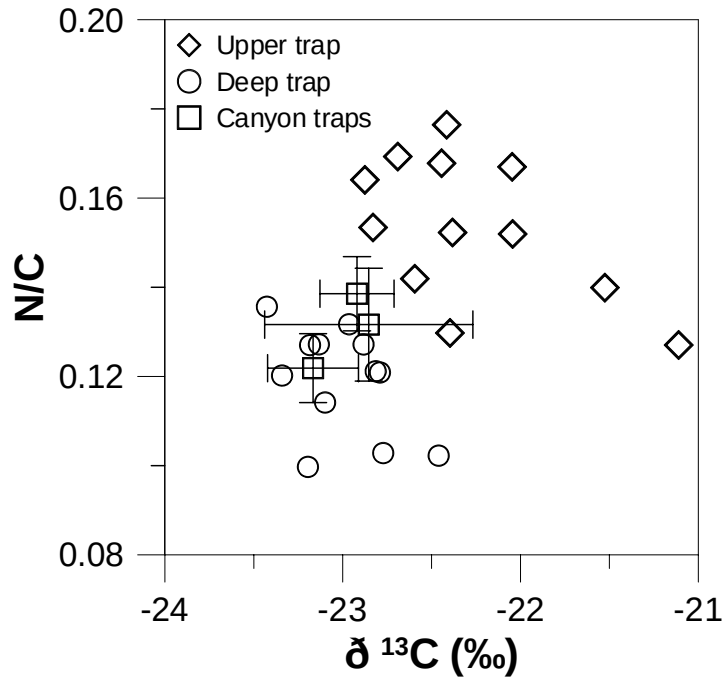

Figure 6: Biochemical composition of sediment-trap samples collected in southern Adriatic Pit below the photic layer (upper trap) and near the bottom (deep trap) compared with the sediment-trap-samples collected near the bottom of the Bari canyon showing similar compositions between the deeper traps. N/C = total particulate nitrogen/particulate organic carbon molar ratio; $\delta\ ^{13}$C(‰) = stable isotopes of organic carbon.

nental shelf to the deep southern Adriatic basin.

Downcore profiles of ^{210}Pb in sediments collected below the traps in the Bari canyon and on the slope areas have been used to estimate sediment mass accumulation rates (MARs) on a century scale. On the open slope, the annual trap flux recorded in 2004-2005 was lower than MAR. On the contrary, in the Bari Canyon, the annual trap flux was higher than MAR, indicating that the lateral advection of particles becomes predominant and that a fraction of the particles intercepted by sediment traps was only in transit through the canyon. On the open slope area the discrepancy between the two estimated rates could be attributed to under-trapping effects or to interannual variability of NAdDW formation and spreading [18].

The biogeochemical comparison of surficial sediment samples from the western Adriatic shelf and material collected by the sediment traps excludes the direct transport of material from the inshore region to the slope (e.g., via river floods or wave-

induced resuspension) during the observed period. Conversely, the material trapped on the slope exhibits an organic matter composition comparable to the sediment of the outer shelf [25]. This suggests a relatively long retention of sediments on the inner shelf before reaching the outer shelf, and that current-resuspension of sediment on the southern outer shelf contributes to the down-slope flux in the Bari Canyon. Moreover, the similarity in organic matter biochemical composition between the Adriatic deep basin and the Bari canyon area (Figure 6) confirms the link between the shelf-slope area and the deep basin.

The results of the mooring experiment in the submarine slides in the Gela basin (Sicily strait area) conflict the sedimentological and stratigraphic evidences: mass fluxes and current speeds are low and current directions seem not to be influenced by the land-slide induced morphology.

The origin of this disagreement may be due to the small-scale spatial complexity. Submarine slides occasionally impact a certain slope and basin sector. Seasonally modulated events, as bottom-hugging dense water events, which normally occur at the end of winter, may be captured by the induced morphological indentation (i.e., the NW Mediterranean canyons and Bari canyon). Our results show that these events were absent in the Gela area during the experiment interval. In contrast, other stochastic events, as turbidite currents, may have affected the sediment instability of the deep-seated and highly steep headscarp of the southern slide.

4 Conclusions

From long-term sediment trap studies we have learned much of what we know about the biological pump and transfer of particulate organic material from the surface ocean to the deep sea. Deep-sea pelagic and benthic organisms depend on the rain of particles from above, and benthic time series have illustrated how communities respond to climate-induced changes in sedimentation. Investigations on the vertical fluxes of particles along the water column in deep central Mediterranean areas permitted to highlight and evaluate the complex interactions among climatological events, biological processes, geomorphology and water masse dynamics. All these components concur to determine the variability and intensity of the vertical transfer of material and energy to the bottom. Early important results from deep time-series sediment trap studies included the discovery of a tight coupling between surface seasonal patterns in primary production and the deep sea, resulting in a strong seasonality in deep-ocean particle fluxes, and the important role of episodic flux events in rapid transport of biogenic material to depth [26]. The role of large planktonic organisms both autotrophic and heterotrophic is relevant in the fluxes below the upper layer that show high-seasonality and short time events. Episodic, short-lived, high-flux events in the deep sea that are not associated with the spring bloom are important in the delivery of highly labile organic material and can account for a significant proportion of the export flux of bioavailable C for mesopelagic and deep-sea benthic organisms. These episodic events have been linked to physical forcing such as physical perturbation, related to the interaction between the general water circulation and the geomorphologic structures.

5 Acknowledgements

The PRIN-project OBAMA (Osservatorio off shore per ricerche ecologiche a lungo termine (L-TER) sulla Biodiversità e funzionamento degli ecosistemi marini profondi in Mar Mediterraneo, prot. 2008N2Y5C7), funded by MIUR, supported authors while preparing the manuscript.

References

[1] R. J. Matear and A. C. Hirst. Climate change feedback on the future oceanic CO_2 uptake. *Tellus Series B-Chemical and Physical Meteorology*, 51(3):722–733, 1999.

[2] J. L. Sarmiento, T. M. C. Hughes, R. J. Stouffer, and S. Manabe. Simulated response of the ocean carbon cycle to anthropogenic climate warming. *Nature*, 393(6682):245–249, 1998.

[3] M. Battle, M.L. Bender, P.P. Tans, J. W. C. White, J. T. Ellis, T. Conway, and R.J. Francey. Global carbon sinks and their variability inferred from atmospheric O_2 and $\delta^{13}C$. *Science*, 287(5462):2467–2470, 2000.

[4] H.W. Ducklow, D.K. Steinberg, and K.O. Buesseler. Upper Ocean Carbon Export and the Biological Pump. *Oceanography*, 14:50–58, 2001.

[5] K.O. Buesseler, A.N. Antia, M. Chen, S.W. Fowler, W.D. Gardner, et al. An assessment of the use of sediment traps for estimating upper ocean particle fluxes. *Journal of Marine Research*, 65(3):345–416, 2007.

[6] R.W. Eppley and B.J. Peterson. Particulate organic matter flux and planktonic new production in the deep ocean. *Nature*, 282:677– 680, 1979.

[7] N. Pinardi and E. Masetti. Variability of the large scale general circulation of the Mediterranean Sea from observations and modelling: a review. *Palaeogeography Palaeoclimatology Palaeoecology*, 158(3-4):153–174, 2000.

[8] W. Roether, B. B. Manca, B. Klein, D. Bregant, D. Georgopoulos, V. Beitzel, V. Kovacevic, and A. Luchetta. Recent changes in eastern Mediterranean deep waters. *Science*, 271(5247):333–335, 1996.

[9] G. Civitarese and M. Gačić. Had the Eastern Mediterranean transient an impact ore the new production in the Southern Adriatic? *Geophysical Research Letters*, 28(8):1627–1630, 2001.

[10] R. Schlitzer. Interactive analysis and visualization of geoscience data with Ocean Data View. *Computers & Geosciences*, 28(10):1211–1218, 2002.

[11] P.W. Boyd and P.P. Newton. Does planktonic community structure determine downward particulate organic carbon flux in different oceanic provinces? *Deep-Sea Research Part I-Oceanographic Research Papers*, 46(1):63–91, 1999.

[12] A. Boldrin, S. Miserocchi, S. Rabitti, M.M. Turchetto, V. Balboni, and G. Socal. Particulate matter in the southern Adriatic and Ionian Sea: characterisation and downward fluxes. *Journal of Marine Systems*, 34:389–410, 2002.

[13] T. F. Thingstad and F. Rassoulzadegan. Nutrient Limitations, Microbial Food Webs, and Biological C-Pumps - Suggested Interactions in a P-Limited Mediterranean. *Marine Ecology-Progress Series*, 117(1-3):299–306, 1995.

[14] S.W. Fowler, L.F. Small, and J. La Rosa. Seasonal Particulate Carbon Flux in the Coastal Northwestern Mediterranean-Sea, and the Role of Zooplankton Fecal Matter. *Oceanologica Acta*, 14(1):77–85, 1991.

[15] M. Gačić, G. Civitarese, S. Miserocchi, V. Cardin, A. Crise, and E. Mauri. The open-ocean convection in the Southern Adriatic: a controlling mechanism of the spring phytoplankton bloom. *Continental Shelf Research*, 22(14):1897–1908, 2002.

[16] G. Civitarese, M. Gačić, V. Cardin, and V. Ibello. Winter convection continues in the warming southern Adriatic. *Eos*, 86(45):445–451, 2005.

[17] A. De Lazzari, A. Boldrin, S. Rabitti, and M.M. Turchetto. Variability and downward fluxes of particulate matter in the Otranto Strait area. *Journal of Marine Systems*, 20(1-4):399–413, 1999.

[18] M. Turchetto, A. Boldrin, L. Langone, S. Miserocchi, T. Tesi, and F. Foglini. Particle transport in the Bari Canyon (Southern Adriatic Sea). *Marine Geology*, 246(2-4):231–247, 2007.

[19] P. Puig and A. Palanques. Temporal variability and composition of settling particle fluxes on the Barcelona continental margin (Northwestern Mediterranean). *Journal of Marine Research*, 56(3):639–654, 1998.

[20] A.M. Davies and H.X. Xing. Modelling processes influencing shelf edge exchange of water and suspended sediment. *Continental Shelf Research*, 25(7-8):973–1001, 2005.

[21] P.T. Shaw and S.Y. Chao. Effects of baroclinic current on a sinking dense water plume from a submarine canyon and heton shedding. *Deep-Sea Research Part I-Oceanographic Research Papers*, 50:357–370, 2003.

[22] A. Monaco and S. Peruzzi. The Mediterranean Targeted Project MATER - a multiscale approach of the variability of a marine system - overview. *Journal of Marine Systems*, 34:3–21, 2002.

[23] J.P. Bethoux, X.D. de Madron, F. Nyffeler, and D. Tailliez. Deep water in the western Mediterranean: peculiar 1999 and 2000 characteristics, shelf formation hypothesis, variability since 1970 and geochemical inferences. *Journal of Marine Systems*, 34:117–131, 2002.

[24] M. Canals, P. Puig, X.D. de Madron, S. Heussner, A. Palanques, and J. Fabres. Flushing submarine canyons. *Nature*, 444(7117):354–357, 2006.

[25] T. Tesi, L. Langone, M. A. Goñi, M. Turchetto, S. Miserocchi, and A. Boldrin. Source and composition of organic matter in the Bari canyon (Italy): Dense water cascading versus particulate export from the upper ocean. *Deep-Sea Research Part I-Oceanographic Research Papers*, 55(7):813–831, 2008.

[26] W.G. Deuser. Seasonal and interannual variations in deep-water particle fluxes in the Sargasso Sea and their relation to surface hydrography. *Deep-Sea Research Part I-Oceanographic Research Papers*, 33:225–246, 1986.

Antarctic Shelf Slope Dynamics and Deep Ventilation of the Southern Ocean

A. Bergamasco[1], P. Del Negro[2], S. Aliani[3], K. Schroeder[3], M. Celussi[2], S. Carniel[1], M. Sclavo[1]
1, Institute of Marine Sciences, CNR, Venezia, Italy
2, Department of Biological Oceanography, National Institute of Oceanography and Experimental Geophysics, Trieste, Italy
3, Institute of Marine Sciences, CNR, Pozzuolo di Lerici (SP), Italy
andrea.bergamasco@ismar.cnr.it

Abstract

Polar regions are among the most sensitive locations in responding to climate change, and host key processes driving these changes. Yet, they are also regions where least is known, partly because of the historical paucity of observations. In particular, Shelf-Slope dynamics are characterized by sinking of dense waters, that trigger the austral circumpolar branch of the global ocean thermohaline cell (THC). The THC is the main mechanism through which the ocean contributes to controlling the global radiative budgets, therefore triggering main climate induced changes. During the last decade three national programs, the U.S. "Antarctic Slope" experiment and the two Italian Projects "Climate Long-term Interaction of the Mass balance of Antarctica" and "Polar Deep Ocean VEntilation", have significantly advanced our understanding of processes through intensive measurements in the northwest Ross Sea. In the paper some analysis of 2006-2008 transport measurements and evolutions of physical properties of the water masses associated with the Antarctic Slope Front near the Cape Adare Shelf Break are presented. We will show also some estimate of Antarctic Bottom Water production and a first estimate of the Carbon export within the bottom boundary layer during february 2006 overflow sinking across the slope. Looking at the data acquired during the sea cruise, a plume thickness of 150 m average was measured. If a 10 km plume wide is assumed, a transport rate of 0.25 Sv AABW could be estimate. At the same time using the DOC measured during the 2006 sea cruise, a Carbon Export in the order of 100 ton $C \cdot s^{-1}$ can be estimate.

1 Introduction

In the Pacific sector, High Salinity Shelf Water (HSSW) is a key constituent of the Antarctic Bottom Water (AABW) [1] that plays an important role in ventilating the global deep ocean. HSSW is formed by brine release during sea ice formation. Cold katabatic winds, infact, generate new sea ice by freezing but at the same time sea ice is mechanically removed and pushed away, producing important polynya phenomena mainly in southern Victoria Land near Terra Nova Bay (TNB). HSSW fills up the whole Drygalsky basin as bottom water, dense enough to flow northward and trigger downslope processes to the abyssal depths near Cape Adare region [2, 3, 4]. During February 2006, within the XXI°

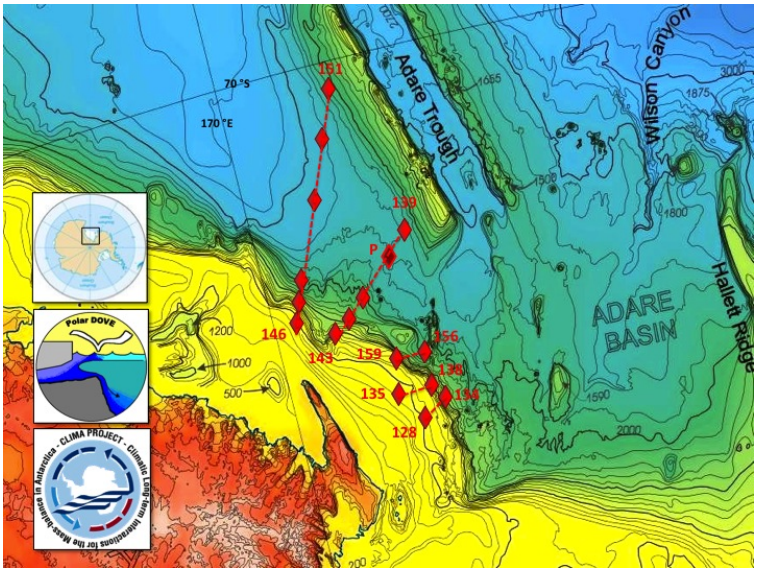

Figure 1: Bathymetry of the NW Shelf Break off Cape Adare (Ross Sea) with station locations of the selected transects from the 2005-2006 austral summer Polar DOVE and CLIMA oceanographic cruises.

PNRA expedition, CLIMA (Climate Long-term Interaction of the Mass balance of Antarctica) and PolarDOVE (Polar Deep Ocean VEntilation) Projects, explored the shelf-slope system behaviour by selected transects of the shelf break and by a benthic boundary layer mooring deployed off the Cape Adare at 2300 meter depth. The mooring was recovered successfully in January 2008 providing of two-year long time series of the evolution of the bottom boundary layer during IPY period. This paper focuses on the February-March ADCP record, allowing a first estimate of the organic carbon export as well as the AABW formation within the downslope cascading plume.

2 Data and Methods

PolarDOVE primary goal was to assess the role of the Antarctic Bottom Waters formation and dispersion (particularly the Ross Sea Bottom Water) in the global perspective of the thermohaline cell regulation in the Pacific sector. During February 2006 the observation of temperature and salinity fields, as well as the acquisition of physical variables using CTD-rosette samples were carried out adding some deep casts to the network sampled by CLIMA IV Project to complement these measurements looking at the AABW fate. Within the PolarDOVE project, at the end of the observational period, we deployed a small mooring to sample the bottom boundary layer dynamics, off the Cape Adare at 2300 m depth. It was recovered in February 2008.

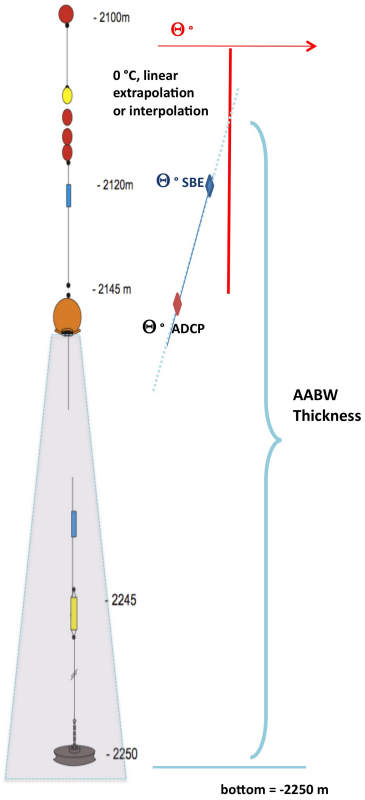

Figure 2: Schematic of the mooring P setup. The potential temperature extrapolation scheme is illustrated..

Figure 1 shows the studied area.
Profiles of temperature, salinity, dissolved oxygen, fluorescence and transmittance were obtained using a Sea-bird Electronics SBE911+ CTD system. Water samples were collected using a 24 position SBE 32 Carousel sampler with 12 l water sample bottles from Ocean Test Equipment. A SBE 43 dissolved oxygen sensor was incorporated into the CTD sensor array. At CTD stations water samples were drawn from selected rosette bottles for dissolved oxygen analyses using the Winkler method.
Mooring P belongs to the project Polar-DOVE devoted to the study of the deep ocean ventilation. The mooring was deployed over a sea bottom of 2300 m depth (point P in Figure 1), at a height of 150 m above the seafloor (Figure 2). It was equipped with an SBE 37 Microcat at 2245 m, that unfortunately did not work properly and data was not recovered. A downward-looking ADCP (RDI WH 300 KHz) was

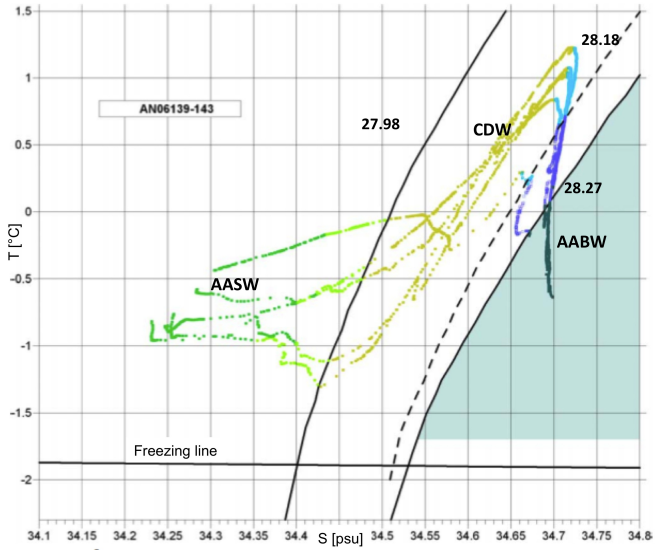

Figure 3: Plot of T-S diagram of CTD casts ensemble of AN06139-143.

positioned at 2145 m depth and provided a 2-year data set of velocity profiles with a bin size of 4 m and a depth range of about 70 m below the instrument. Just above the current profiler, an SBE 39 temperature recorder was positioned at 2120 m.
During CTD downcasts a pre-analysis of the water profile characteristics was done and during upcasts seawater samples for dissolved organic carbon measurements and bacterial activity were collected at depths with significant signals. Samples for DOC analyses were filtered on board, and analysed in Italy, details of sampling, analysis and methods can be found in a paper actually under preparation.

3 Hydrographic Observations on the Cape Adare Shelf

An accurate T/S, T/h, S/h analysis was performed grouping together the stations in order to document the types of water that make up the spreading phase of the downslope plume phenomenon.
In Figure 3 the T/S diagram (Temperature is always Potential Temperature) of AN06139-143 casts is shown, as well as freezing line as function of salinity and the neutral density curves 27.98 and 28.27 (solid lines). Dashed line is neutral density anomaly γ^n = 28.18 that we can consider as CDW core in an average view.
Following Orsi et al. [5] we can point out the importance of neutral density γ^n equal to 27.98, 28.18 and 28.27. Neutral density anomaly less than γ^n = 27.98 [kg·m^{-3}]

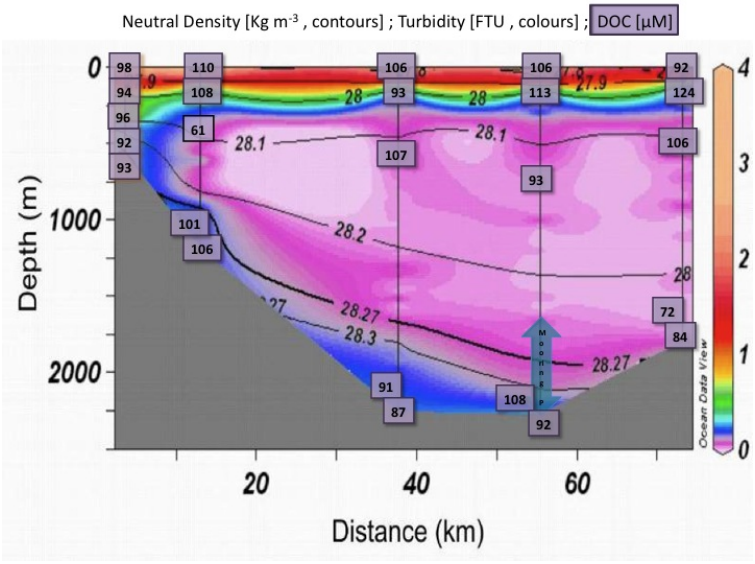

Figure 4: Neutral Density, Turbidity and DOC concentrations along transect AN06143-139. The location of mooring P is marked by an arrow.

can be defined as Antarctic surface water. Looking in fact at the depth of this kind of water we can recognize waters within the photic region, often less than 100 m and always less than 200 m.

Neutral density anomaly between the values of γ^n = 27.98 and γ^n = 28.27 define Circumpolar Deep Water CDW, in particular if temperature is positive, and the Modified Circumpolar Deep Water (MCDW) if temperature is negative. Neutral density between 28.18 and 28.27 characterizes water masses of the lower CDW, the ambient water that can interact with the gravity driven shelf water sloping down the continental shelf break. Temperature less than -1.7 °C define Shelf Waters that can be separated upon T-S properties into High Salinity Shelf Water (HSSW) for salinity greater or equal of 34.8 and Ice Shelf Water (ISW) if temperature is below of the surface freezing point [6].

In the Figure 3 we coloured in light blue the region with T/S characteristics of the Antarctic Bottom Waters (AABW) ($\gamma^n >$ 28.27 kg·m^{-3} — T> -1.7°C).

The mooring transect is plotted in Figure 3, where neutral density [kg·m^{-3},contours], turbidity [FPU, colours] and DOC concentrations [box] are shown. Potential temperatures < 0 °C in the benthic layer mark the presence of AABW, with salinity values of 34.68 and neutral density $>$ 28.27 (T & S not shown).

The benthic AABW is characterized by an increasing turbidity, whose distribution follows almost exactly the displacement of the 28.27 kg·m^{-3} neutral density surface. These features suggest that the suspended sediments have been transported down from the shelf along with the HSSW, that mixes with the lower CDW.

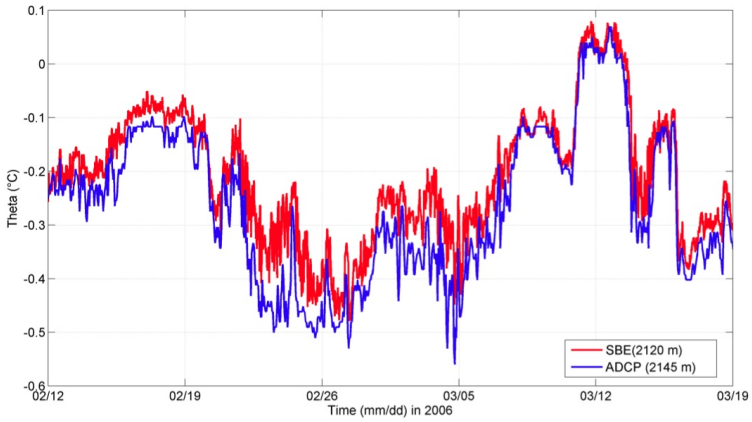

Figure 5: Potential Temperature time series recorded by SBE (2120m.) and ADCP (2145m.) in the period February 12, 2006 - March 19, 2006.

Further, the turbidity signal suggests that the AABW production is an efficient way to export particles (organic and inorganic) from the shelf region to the deep ocean, thus to export carbon from the near-surface layers to the deep waters.

4 Mooring data analysis

Mooring P schematic is shown in Figure 2. In particular temperature is measured by both the SBE 39 at 2120 m depth and by the ADCP internal temperature sensor at 2145 m. Both time series were transformed to potential temperature and their comparison gave a good agreement, with an almost constant θ difference of 0.06 °C, the temperature at 2120 m being warmer (see also Figure 5). The mean temperature of the whole time series (from February 2006 to February 2008) was -0.22 $\pm$ 0.13 °C (min= -0.70 °C, max=0.16 °C). Figure 5 show in red potential temperature of SBE sensors, while blue one is the ADCP measure.

Since tide plays a key role in modulating the periodic outflows of cold water [7, 8], the first step in the current meter measurements analysis was to de-tide the data (using the whole dataset). This has been done by using the standard harmonic analysis [9] to obtain the tidal ellipses of the main components. The most energetic components are the diurnal components O1 and K1. Here we focus on the first period of the record, in order to have a quasi synoptic view with respect to the CTD sampling. The analysis of the whole data set will be discussed in a future paper, while here we concentrate on the beginning of the time series when an episode of strong temperature decrease was recorded, it began at the end of February 2006 and lasted about one week. From the difference between the two temperature data at different depth, see the scheme in Figure 2, we can extrapolate the depth of 0°C potential temperature, the signature of the AABW interface.
The down flow episode associated strong flows of AABW shows an abrupt temper-

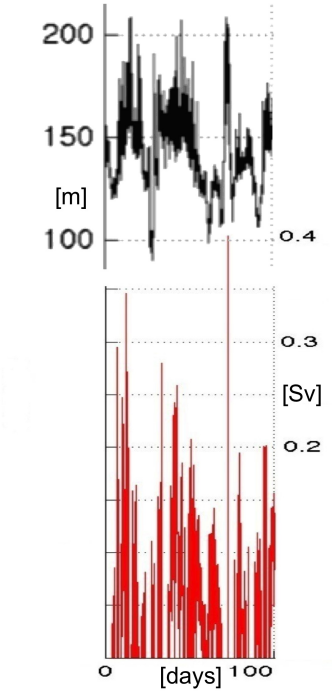

Figure 6: Upper panel in black: estimate of AABW thickness in m during the first 100 days of mooring measurements , bottom panel in red: estimate of AABW transport in Sverdrup during the same period.

ature decrease of almost 0.4 °C and is accompanied by an initial abrupt change in the current regime, with speed increases of almost 30 cm·s^{-1}. During this event the mean flow direction was 135° (± 0.6°), while the velocity range was 20 ± 7 cm·s^{-1}. The enhanced sediment transport due to AABW cascading is a link of fundamental importance between the shelf and the deep southern ocean.

5 AABW formation estimate and carbon sequestration

Looking at the data evolution, we can extrapolate the velocity structure shown for this episodes down to the bottom (2250 m). For the period February March 2006 the plume thickness average was 150 m. Looking at the data acquired during the sea cruise we can estimate a 10 Km wide of the plume, this give us a first estimate of AABW transport rate for April 2006 period of 0.25 Sv, see Figure 6. At the same time, if we derive the Carbon concentration from

DOC measurements acquired during 2006 sea cruise, we can estimate the Carbon Export in the order of 100 ton C·s^{-1}. Overall, down slope processes play a key role to ventilate the abyssal layer. There was a clear signal of high microbial metabolic processes within the newly formed AABW. The benthic boundary layer is dominated by entrainment processes during plume descending events.

6 Acknowledgements.

This work was carried out in the framework of the Polar Dove & Clima projects of PNRA. We are greatly thankful to all colleagues participating in these projects.

References

[1] G. Budillon, M. Pacciaroni, S. Cozzi, P. Rivaro, G. Catalano, C. Ianni, and C. Cantoni. A multiparameter mixing analysis of the shelf waters in the Ross Sea. *Antarctic Science*, 15:105–118, 2003.

[2] P.G. Baines and S. Condie. Observations and modelling of Antarctic downslope flows: a review. *Antarctic Research Series*, 75:29–49, 1998.

[3] A. Bergamasco, V. Defendi, G. Budillon, and G. Spezie. Downslope flow observations near Cape Adare shelf break. *Antarctic Science*, 16(2):199–204, 2004.

[4] S.S. Jacobs. On the nature and significance of the Antarctic slope front. *Marine Chemistry*, 35:9–24, 1991.

[5] A. Orsi, G.C. Johnson, and J.L. Bullister. Circulation, mixing, and production of Antarctic Bottom water. *Progress in Oceanography*, 43:55–109, 1999.

[6] G. Budillon, S. Gremes Corder, and E. Salusti. On the dense water spreading off the Ross Sea shelf (Southern Ocean). *Journal of Marine System*, 35:207–227, 2002.

[7] L. Padman, S.L. Howard, A.H. Orsi, and R.D. Muench. Tides of northwestern Ross Sea and their impact on dense outflows of Antarctic Bottom Water. *In: Gordon, A., Padman, L., Bergamasco, A. (Eds.), Deep-Sea Research II. [doi:10.1016/jdsr2.2008.10.026]*, 2008.

[8] S.Y. Erofeeva, G.D. Egbert, and L. Padman. Assimilation of ship mounted ADCP data for barotropic tides: Application to the Ross Sea. *J. Atmos., Ocean. Technol.*, 22(6):721–734, 2005.

[9] R. Pawlowicz, B. Beardsley, and S. Lentz. Classical tidal harmonic analysis including error estimates in MATLAB using T_TIDE. *Computers and Geosciences*, 28:929–937, 2002.

Marine Dynamics and Biological Records: the *Adamussium colbecki* Multi-Proxy

A. Bergamasco[1], A. Trevisiol[6], S. Aliani[2], S. Schiaparelli[5], M. Taviani[3], S. Donnici[1], S. Carniel[1], M. Sclavo[1], M. Sprovieri[4]
1, Institute of Marine Sciences, CNR, Venezia, Italy
2, Institute of Marine Sciences, CNR, Pozzuolo di Lerici (SP), Italy
3, Institute of Marine Sciences, CNR, Bologna, Italy
4, Institute for Coastal Marine Environment, CNR, Capo Granitola (TP), Italy
5, University of Genova, Italy
6, University of Siena, Italy

andrea.bergamasco@ismar.cnr.it

Abstract

During the oceanographic expedition of the PNRA (National Antarctic Research Program) in the austral summer 2005-2006, the PolarDove project research group carried out an experiment to verify the feasibility of using the indigenous bivalve *Adamussium colbecki* (Smith, 1902) as an environmental-climate proxy, exploiting the connection between the mineralogical composition of molluscs' shell and the water masses characteristics (temperature, salinity, etc.) in which they grow [1]. In order to it, a mooring was installed near shore of Terra Nova Bay (Ross Sea), 145 m depth, equipped to measure the hydrodynamic parameters and with 2 cages, in which 60 living A. clobecki specimens stayed for 1 year. After the mooring recovery, some selected specimens shells were sampled to analyze the isotopic (δ^{18}O and δ^{13}C) and trace element composition. In this study we present the mooring logistic preparation, data analysis and multi-proxy methodology of the experiment. We discuss also preliminary interpretations of the δ^{18}O signal as a temperature proxy, with particular attention at the shell growth rate impact [2]. Because of its longevity [3], wide circumpolar distribution [4] and availability of fossil fragments [5], the use of *A. colbecki* as proxy is a powerful mean to inferred climatic information at high temporal resolution about either known or less known Antarctic regions.

1 Introduction

Water masses dynamics in the Antarctic region is a key issue for the comprehension of the global thermo-haline circulation and variability, that play a crucial role on climate control. The two Antarctic basins, Weddel Sea and Ross Sea contribute mostly to the production and export of dense water, the Antarctic Bottom Water (AABW) that constitutes the ocean bottom water at global extent [6]. During the last years the PolarDove (Polar Deep Ocean Ventilation) project has focused on the study of the deep ventilation in the Ross Sea, connected to the HSSW (High Salinity Shelf Water) formation processes, that take place in the Terra Nova Bay region,

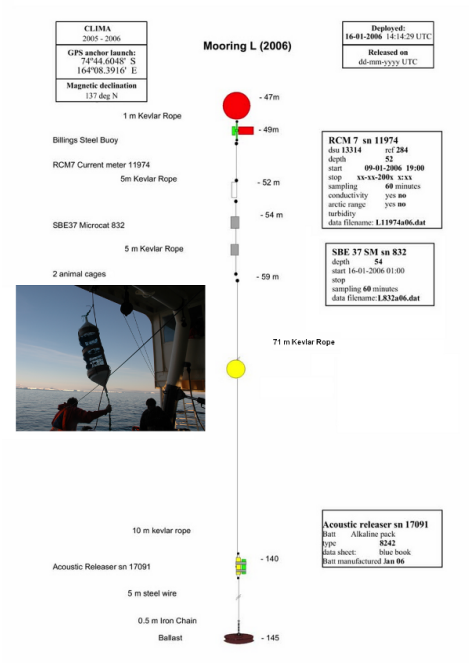

Figure 1: L mooring configuration with a photo of the *A. colbecki* bivalves cage deployment.

and to the HSSW northward flow that produces across the continental shelf slope the AABW new formation. The project deals with this issue with different approach, an experimental one, through the data analysis of the classical oceanographic instruments, a modelling approach and a multiproxy approach. The last exploits the information recorded in the carbonatic matrix of animal species living in the water column. Since the 1950s [7] it's well-known the possibility to use biogenic carbonates as climate-environmental proxies, analyzing the isotopic (e.g. δ^{18}O, δ^{13}C) and trace element (e.g. Mg/Ca, Sr/Ca) composition. This, indeed, depends on the environmental conditions (such as temperature, salinity, primary production…) in which the mineralization occurs (isotopic equilibrium) and on merely biological effects, connected to the metabolism of the considered specie and specimen (kinetic and ontogenetic effects). The analysis of isotopic ratios and trace element composition has been applied with success to foraminifera, corals, ostracodes and molluscs [8, 9]. The Antarctic bivalve *Adamussium colbecki* (Smith, 1902) was selected as target specie to obtain high time resolution information about temperature and salinity of the water, in which it lives, from the isotopic and trace element analysis of its shell. The choice of the *A. colbecki* is due to its longevity [3], that allows to investigate a decadal time window, and to the wide geographic distribu-

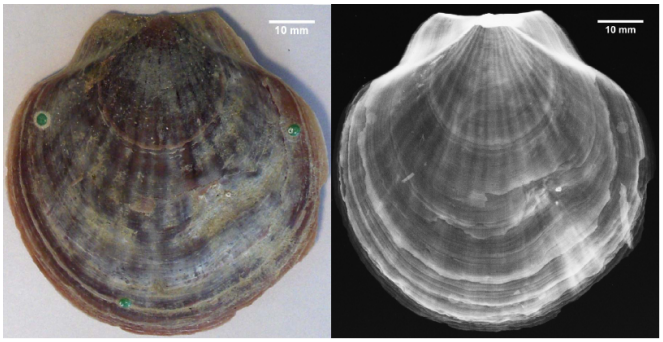

Figure 2: Photo and mammography of one *A. colbecki*'s left shell.

Sample	H_0 (cm)	H_1 (cm)	ΔH (cm)	L_0 (cm)	L_1 (cm)	ΔL (cm)
B3	6.85	7.03	0.18	6.90	7.29	0.39
B9	7.20	7.42	0.22	7.20	7.32	0.12
G5	7.30	7.69	0.39	7.20	7.84	0.64
G19	7.55	7.79	0.24	7.60	7.98	0.38
V11	6.75	7.23	0.48	6.60	7.25	0.65
V14	6.80	7.00	0.20	6.80	7.00	0.20

Figure 3: Table with height (H) and length (L) of sampled specimens (see text for definition). 0 and 1 index refers to the deployment (January 2006) and to the recovery (January 2007) times respectively. ΔH (ΔL) are the differences between H1 (L1) and H0 (L0).

tion [4], that allows to infer information from other Antarctic regions, that are not monitored with traditional oceanographic instruments. Moreover, the possibility to recover some fossil fragments or individuals makes the multi-proxy approach a powerful tool to provide precious information for paleo-climatic models.

In this paper we will describe the methodology and the achievement of a first experiment carried out during the PNRA (National Research Program in Antarctica) oceanographic campaigns in the austral summer 2005-2006 and 2006-2007 in order to verify the feasibility to use the *A. colbecki*. Furthermore we deal with the issue of the isotopic equilibrium and the relative weight of kinetic and ontogenetic effects on the temperature-δ^{18}O relation. In the Ross Sea the *A. colbecki* experience extreme conditions, characterized by a temperature range of $\sim$2°C, but often, during winter season, with little excursions around the sea water freezing point. In these conditions the variations of δ^{18}O signal are not only temperature dependent, but it's necessary to consider also the salinity variability. A contemporary measure of stable isotopes and trace element seems to be fundamental to fair estimate both the temperature and the salinity signals at high time resolution [10].

	Captivity	B3	B9	G5	G19	V11	V14
δ^{18}O ‰ (VPDB)	Mean	3.48	3.24	1.99	2.90	2.15	3.51
	St. Dev.	*0.61*	*0.37*	*0.80*	*0.58*	*1.45*	*0.19*
	Minimum	2.18	2.81	0.98	1.97	-0.68	3.33
	Maximum	4.30	4.07	3.62	3.83	3.86	3.98
δ^{13}C ‰ (VPDB)	Mean	1.19	1.46	-0.84	1.35	1.12	1.10
	St. Dev.	*0.26*	*0.23*	*0.94*	*0.14*	*0.36*	*0.14*
	Minimum	0.80	1.17	-1.93	1.12	0.57	0.96
	Maximum	1.46	1.81	1.31	1.63	1.57	1.42
	Previous Period						
δ^{18}O ‰ (VPDB)	Mean	4.25	3.47	3.30	3.69	2.25	3.38
	St. Dev.	*0.65*	*0.49*	*0.55*	*0.27*	*1.10*	*0.36*
	Minimum	2.83	2.47	2.09	3.05	-0.23	2.87
	Maximum	5.23	4.29	4.07	4.00	3.72	4.00
δ^{13}C ‰ (VPDB)	Mean	1.43	1.63	0.89	1.48	1.54	1.18
	St. Dev.	*0.20*	*0.19*	*0.58*	*0.19*	*0.22*	*0.35*
	Minimum	1.07	1.18	-0.82	0.97	1.06	0.71
	Maximum	1.86	1.92	1.46	1.84	1.90	1.95

Figure 4: Table containing mean, standard deviation, minimum and maximum values of δ^{18}O and δ^{13}C measurements for each specimen for both the captivity and the previous period.

2 Materials and Methods

The experiment was set up in the Terra Nova Bay (Ross Sea), placing 2 cages at -59 m depth along the Kevlar wire of the mooring L (position: 74°44'.604 S, 164°08'.391 E; depth: 145 m), which was equipped with a current meter Aanderaa RCM 7 to measure the current speed and the temperature (sampling time: 60') and with a MicroCAT SBE probe to measure temperature, pressure and conductivity (sampling time: 20') (Figure 1). The instruments were installed on 16th January 2006 and were recovered on 31st January 2007. The current meter worked correctly during the period, whereas the probe worked very partially, inhibiting the data recover.

In the cages (Figure 1), specially made from molluscs breeding lanterns, were placed 60 *A. colbecki* specimens, previously collected near the Italian Mario Zucchelli Station and identified with numbered labels on the shell. During the yearlong deployment, 5 of the 60 initial individuals died. Before the deployment and after the recovery the maximum dimension along the dorso-ventral axis from umbo to the ventral margin (H) and the maximum dimension parallel to the hinge (L) were measured for each specimen's shell with a calibre (accuracy: 0.01 cm).

The shells of 6 specimens, whose we have also the mammography plates and that aren't damaged at the margin, are available to analyse the isotopic and trace metal composition. The shells were cleaned via ultrasonic baths in milliQ water and drying in oven at 50°C.

The central zone of the left valve [11] were sectioned by hand with a drill and were sampled through a micromill sampling sys-

tem (New Wave Research). The sampling occurred drilling in continuous from the shell ventral margin toward the umbo; for one step the sampled distance was 1/12 of the specimen's growth in captivity during the experiment. Step by step the photographs of the sampled shell were acquired in order to measure a posteriori the actual sampling distance. For each specimen we collected 36 samples to cover a time window of about 3 years. The samples' powder were sent to the geochemical laboratory IAMC-CNR of Naples (Italy) to proceed with the isotopic analysis of δ^{18}O and δ^{13}C, using an automated, continuous-flow carbonate preparation GasBenchII device and a ThermoElectron Delta Plus XP mass spectrometer. The reference standards are the Carrara marble (internal) and the international NBS19 (external). Standard deviations of carbon and oxygen isotope measures were estimated to be 0.1 and 0.08‰. All values are reported using delta notation (δ) in parts per mil (‰) relative to the VPDB [Vienna Pee Dee belemnite] standard.

From one part of the shell, remained after the cut with the drill, we obtained a 500-700μm thick slice on glass slide by incorporating in epossidic resin. The slices were photographed at the stereoscope. 3 specimens were also photographed near the margin at the Scanning Electron Microscope.

3 Results

The Figure 2 shows a photo and a mammography plate of one *A. colbecki*'s left valve, before the micromill sampling. The table in Figure 3 reports the identification codes and the morphometric parameters of the 6 studied specimens. The differencesΔH andΔL measure the specimens' growth during the captivity in the H and L directions. The error associated toΔH andΔL is 0.02 cm by propagating the calibre error. We calculated from the Stereoscopic and SEM photographs the shell thickness, that is 150-600μm in the sampled part. The thickness is not uniform, but shows some discontinuities due to periodic slow down or break of the shell growth.

The table in Figure 4 reports the base statistics for each specimen, while the graphs in Figure 5 show the trend of measured δ^{18}O and δ^{13}C for B9 and V14 specimens. The origin coincides with the ventral margin. Both in the Figure 4 and in the Figure 5 we distinguish the captivity period from the previous one.

For the captivity and previous period we observed that B3, B9, G19 and V14 have δ^{18}O and δ^{13}C mean values comparable within one standard deviation; whereas G5 and V11 show a high δ^{18}O variability and mean values lower than the other. In general the δ^{18}O the and δ^{13}C mean values are lower during the captivity than in the previous period.

The δ^{18}O and δ^{13}C trend is variable for the different specimens in both considered periods (see Discussion). Moreover the statistical standard deviation is higher than the analytical error; that is the data variation is an actual variation in the signal recorded by the animal.

For 4 specimens δ^{18}O and δ^{13}C are significantly ($p<0.001$) correlated with correlation coefficient higher than 0.82 for the captivity and/or the prevous period.

Figure 6 represents our data for the captivity period on a (δ^{18}O, δ^{13}C) plane and compares them with the predicted ones for conditions of isotopic equilibrium mineralization. The vertical lines mark two δ^{13}C extreme values for spring and summer,

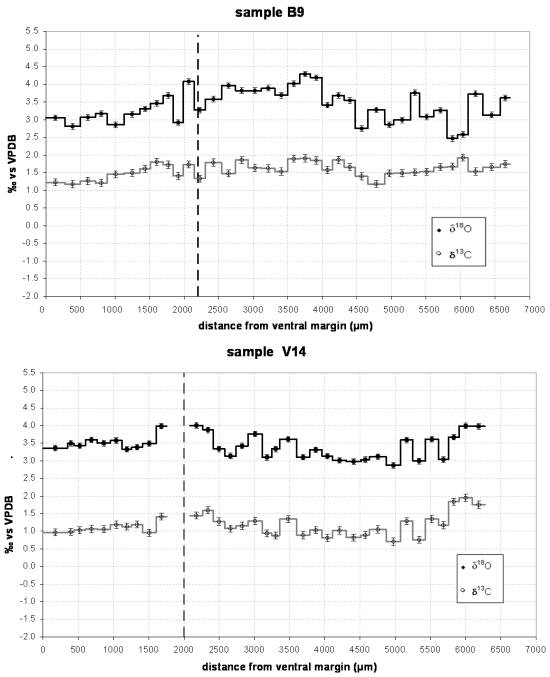

Figure 5: Sequences of measured δ^{18}O and δ^{13}C from the ventral margin (origin of the axes) toward the umbo for B9 and V14 specimens. The horizontal scale extends to the whole sampled region and it is different for B9 and V14. The sampling rate is about 1/12 ofΔH and the error bars are equal to the analytical error (0.08 and 0.10 ‰ for δ^{18}O and δ^{13}C respectively). The captivity ranges from the origin to the vertical dashed line.

such as reported by Barrera et al. [11] and calculated from water δ^{13}C(DIC), pH and temperature near McMurdo Sound (Ross Sea). The horizontal lines delimit the δ^{18}O interval, that is predicted from temperature data, measured at the mooring L, and based on the equation (*) for the isotopic equilibrium mineralization, that was obtained by Kim and O'Neil and reported by King and Howard [12], in the following form:

(*) T(°C) =16.1-4.64 (δ^{18}Os-δ^{18}Ow) + 0.09 (δ^{18}Os - δ^{18}Ow);

2δ^{18}Os is the measured δ^{18}O of the sample and δ^{18}Ow is the δ^{18}O of the water, where the mineralization of the sample occurred. Both are expressed as ‰ VPDB. In our case δ^{18}Ow is equal to -0.38‰ SMOW, that was converted in the VPDB scale by subtracting 0.27‰. This δ^{18}Ow value was measured from a water sample collected during the Italian 1987-1988 austral summer oceanographic campaign in a site nearby the mooring L at 50 m depth [13]. The most of the data stay within the predicted interval for δ^{13}C and the δ^{18}O data are centred in the interval calculated from the equation (*). A better agreement would be possible, if we had

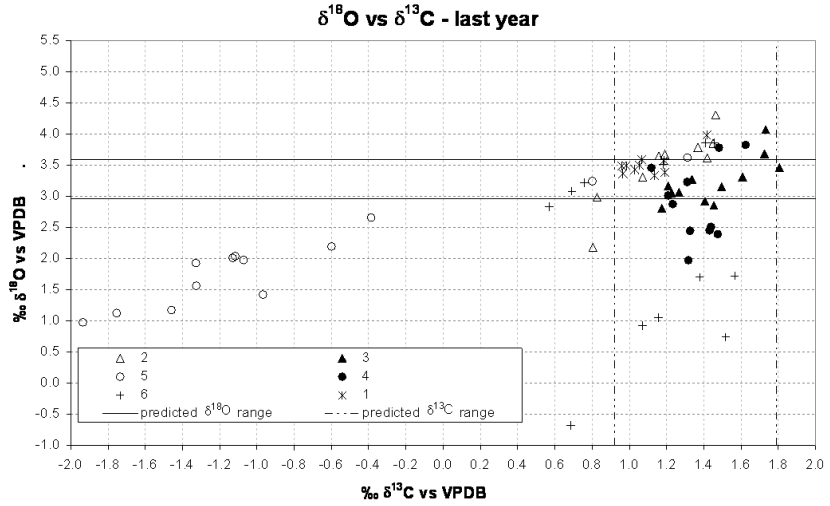

Figure 6: Scatter plot of (δ^{18}O, δ^{13}C) pairs for the captivity period. The vertical dashed lines indicate extreme values for δ^{13}C(DIC) in spring and summer as discussed inside the text, while the horizontal lines represent the extreme predicted values for δ^{18}O, based on the (*) equation and for δ^{18}Ow equal to -0.38 ‰ SMOW.

also a measure of δ^{18}Ow for winter conditions. The G5 and V11 data don't lie in the predicted zone; they already show some differences in the δ^{18}O and δ^{13}C mean values and they are the specimens with the higher growth rate.

4 Discussion

The low specimens' mortality and the growth rate survey argue the success in the experiment achievement. Based on the Von Bertalanffy's equation parameters [14] and on the data in Figure 3, we established an age between 10 and 12 years for the individuals in January 2006. The growth rates are comparable with those revealed in the literature [15, 16].

Absolutely the δ^{18}O values are compatible with the ones measured both by Heilmayer et al. [14] and by Barrera et al. [11]. The former reported values between 3.04‰ and 3.92‰ for 2 specimens and the latter between 3.65‰ and 4.75‰ for one specimen. Furthermore Barrera at al. [11] measured δ^{13}C values varying in the range 0.09-2.50‰, that are compatible with our data with the exception of G5 specimen. The lower mean values in the captivity period in comparison with the previous are due to the different conditions which the animals experienced and are also due to a decrease of the stable isotopic ratios on the shell from the umbo to the ventral margin. This trend was already pointed out by Richardson [1] and is the result of the sum of kinetic effects and the signal integration during the life time, because of the growth bands overlapping in the shell formation.

The correlations between δ^{18}O and δ^{13}C

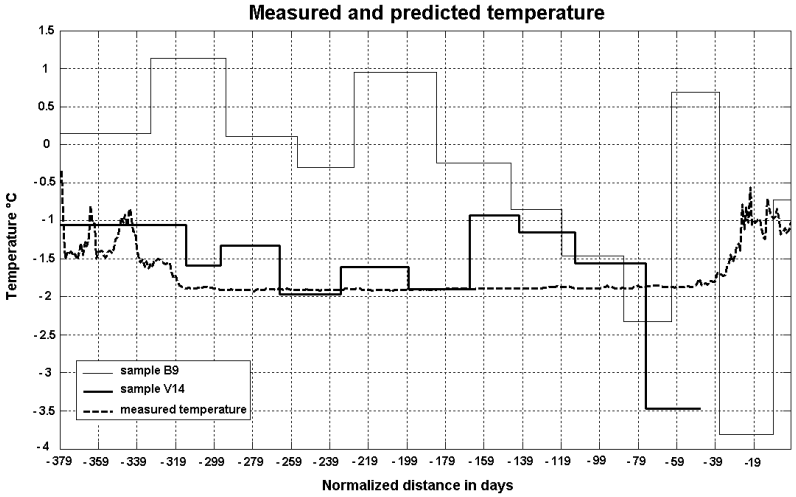

Figure 7: Trend of the mooring L measured temperature (daily averaged) and the predicted temperature from B9 and V14's δ^{18}O data, using (*) equation for δ^{18}Ow = -0.38‰ SMOW.

in B3, B9 and G5 for the captivity period may be considered an indicator of presence of kinetic effects, that are consequence of an incomplete isotopic fractionation of the CO_2 during the mineralization, as suggested by the McConnaughey's model [17] for the biogenic carbonates. According to the same model the biogenetic effects and, in particular, the incorporation of CO_2 derived from the respiration, should be the reason of the low δ^{13}C value, that we revealed for the G5 specimen. In Owen et al. [2] a similar shift in the (δ^{18}O, δ^{13}C) plane for the G5 and V11 specimens occurs for higher growth rate shells and is ascribed to a sum of kinetic and variable metabolic effects. In fact G5 and V11 are the specimens with the highest growth rate in our specific dataset. In Figure 7 we report in detail the comparison between the measured temperature (daily mean in °C) and the predicted one (from (*) equation). The δ^{18}O signal is uniformly normalized for the captivity period (379 days), by supposing an uniform growth of the individuals during the year. The graph reports the trend for B9 and V14 specimens. The latter, which has a low growth rate and doesn't show δ^{18}O-δ^{13}C correlation during the captivity, has the better agreement between measured and predicted temperature.

In general, our data overestimate the temperature. Klein et al. [10] highlighted similar results with differences of $\sim$10°C, that were due to the salinity variations. The classical isotopic equilibrium equations, like (*), don't take into account these variations. Indeed, the salinity impact is expressed by the δ^{18}Ow term, that generally is forced to be constant and equal to a seasonal mean value [9]. To deal with this question a second experimental phase has be planned, in which the trace metal composition on the shell will be mea-

sured along the dorso-ventral axis via laser ablation and mass spectrometry (ICP-MS) technique. E.g. for other biogenic carbonates Mg/Ca and Sr/Ca ratios were already used as temperature proxies, unaffected by salinity variations [10]. The measure of trace element composition would allow an independent evaluation of the temperature and to estimate separately the salinity and temperature contribution to the δ^{18}O.
Moreover, it is impossibly to superimpose directly the measured and predicted temperature trends by scaling uniformly the captivity period, but it would be necessary to take into account the seasonal growth rate of each specimen. Though there aren't direct field measures, we reasonably suppose that there is a slow down or a break in the growth of *A. colbecki* in the winter, based on the thickness discontinuities and on the observations for growth rate in laboratory experiments [16]. In such a case, our data would be compared only with summer temperatures and this would partially justify the temperature overestimation. The comparison is also affected by theΔH error, that causes a $\sim$30 days uncertainty for the dates in the Figure 7.

5 Conclusions

The experiment succeed in the technical achievement and demonstrated the feasibility of using the living *A. colbecki* specimens as target for similar experiments and perspective developments, because of the low mortality of the individuals during the experiment.
The stable isotopes analysis showed that the mean δ^{18}O and δ^{13}C values are in the range predicted for the isotopic equilibrium, according to the equation of Kim and O'Neil, for the low shell growth rate individuals. Conversely, in our dataset the individuals with higher shell growth rate differ from the equilibrium because of kinetic and variable metabolic effects [2]. A direct comparison between measured and predicted temperature showed that the temperature alone is not enough to take into account δ^{18}O evolution. This result is in agreement with the hypothesis that the salinity contribute to δ^{18}O signal isn't negligible. In our particular conditions *A. colbecki* experience temperature range of about 2°C, often near the freezing point and salinity of the new formed HSSW could play a crucial role in the recorded signal. This question is under study by carrying out some measures of the shell trace element composition via laser ablation and ICP-MS technique.
This study highlighted the critical issue of matching the sequences measured on the shells and the time series revealed by the instruments. This is due to the uncertainty on the time life of the shell when mineralization occurred, especially in case of slowing down or breaking of the shell growth in the winter season.

6 Acknowledgments

Thanks are due to Dr. Peruzzo for the help in the realisation of SEM images at IGG-CNR laboratory of Padova and to Prof. Mazzoli for the availability to use the micro-mill device at University of Padova. We are grateful to Dr. Montagna and Prof. Chiantore for fundamental suggestions and scientific contributions. This work was realized through the PolarDove's grants, funded by PNRA.

References

[1] C.A. Richardson. Mollusks as archives of environmental change. In: Oceanography and Marine Biology: An Annual Review. 39:103–164, 2001.

[2] R. Owen, H. Kennedy, and C. Richardson. Isotopic partitioning between scallop shell calcite and seawater: effect of shell growth rate. *Geochimica et Cosmochimica Acta*, 66(10):1727–1737, 2002.

[3] P.A. Berkman. The population biology of the Antarctic Scallop, Adamussium colbecki (Smith, 1902) at New Arbour, Ross Sea. In: Antarctic Ecosystems. Ecological Change and Conservation. pages 281–288, 1990.

[4] S. Schiaparelli and K. Linse. A reassessment of the distribution of the common Antarctic scallop Adamussium colbecki (Smith, 1902). *Deep-Sea Research II*, 53:912–920, 2006.

[5] M. Lavelle, C.R. Fielding, M.A. Hall, and M.R.A. Thomson. Molluscan Stable Isotope Temperature Estimates of the Southwestern Ross Sea during the Early Oligocene and Early Miocene,CRP-2/2A and CRP-3, Victoria Land Basin, Antarctica. *Terra Antartica*, 8(4):439–444, 2001.

[6] A.H. Orsi and C.L. Wiederwohl. A recount of Ross Sea waters. *Deep-Sea Research II*, 56:778–795, 2009.

[7] S. Epstein, R. Buchsbaum H.A. Lowenstam, and H.C. Urey. Revised carbonate-water isotopic temperature scale. *Bull. Geol. Soc. Amer.*, 64:1315–1326, 1953.

[8] D. W. Lea. Elemental and Isotopic Proxies of Past Ocean Temperatures. In: Treatise on Geochemistry. 6, 2003.

[9] J.A. Hickson, A.L.A. Johnson, T.H.E. Heaton, and P.S. Balson. The shell of the Queen Scallop Aequipecten opercularis (L.) as a promising tool for palaeoenvironmental reconstruction: evidence and reasons for equilibrium stable-isotope incorporation. *Palaeogeography, Palaeoclimatology, Palaeoecology*, 154:325–337, 1999.

[10] R.T. Klein, K.C. Lohmann, and C.W. Thayer. Bivalve skeletons record sea-surface temperature and δ18O via Mg/Ca and 18O/16O ratios. *Geology*, 24:415–418, 1996.

[11] E. Barrera, M.J.S. Tevesz, and J.G. Carter. Variations in Oxygen and Carbon Isotopic Composition and Microstructure of the Shell of Adamussium colbecki (Bivalvia). *Palaios*, 5:149–159, 1990.

[12] A.L. King and W.R. Howard. δ18O seasonality of planktonic foraminifera from Southern Ocean sediment traps: Latitudinal gradients and implications for paleoclimate reconstructions. *Marine Micropaleontology*, 56:1–24, 2005.

[13] M. Dini and B. Stenni. Oxygen Isotope Characterization of Terra Nova Bay Seawater. In Ross Sea ecology: Italiantartide Expeditions (1987-1995). 2000.

[14] O. Heilmayer, T. Brey, M. Chiantore, R. Cattaneo-Vietti, and W.E.Arntz. Age and productivity of the Antarctic scallop, Adamussium colbecki, in Terra Nova Bay (Ross Sea, Antarctica). *Journal of Experimental Marine Biology and Ecology*, 288:239–256, 2003.

[15] M. Chiantore, R. Cattaneo-Vietti, and O. Heilmayer. Antarctic scallop (Adamussium colbecki) annual growth rate at Terra Nova Bay. *Polar Biology*, 26:416–419, 2003.

[16] O. Heilmayer, C. Honnen, U. Jacob, M. Chiantore, R. Cattaneo-Vietti, and T. Brey. Temperature effects on summer growth rates in the Antarctic scallop, Adamussium colbecki. *Polar Biology*, 28:523–527, 2005.

[17] T. McConnaughey. 13C and 18O isotopic disequilibrium in biological carbonates: I. Patterns. *Geochimica et Cosmochimica Acta*, 53:151–162, 1989.

Hydrological and Biogeochemical Characteristics of the Sardinian Sea (Western Mediterranean) during March-April 2001

A. Perilli[1], M. Marcelli[2], L. Massi[3], A. Olita[1], A. Ribotti[1], M. Sinerchia[1]
1, Institute for Coastal Marine Environment, CNR, Oristano, Italy
2, University of Tuscia, Viterbo, Italy
3, University of Firenze, Firenze, Italy
angelo.perilli@cnr.it

Abstract

This paper presents the results of a study on the hydrological and biogechemical properties of the Sardinian Sea (SaS), located in the eastern part of the Algerian Basin (AB), an area that altimetric data identified as one of the most energetic of the whole Western Mediterranean Sea. However, the oceanographic features of this Sea have been so far poorly investigated.
The explorative cruise MedGOOS-2, conducted in spring 2001, confirmed that the SaS is located in a complex area in which two different hydrological and biogeochemical regions were identified. The northern region, north of 40.50°N, was characterized by the densest, coldest, freshest water and deepest upper mixed layer (UML). In this region, chlorophyll was uniformly distributed within the UML. The southern region was dominated by mesoscale phenomena, mainly anticyclonic eddies (AEs). Chlorophyll was distributed as sub-surface deep chlorophyll maximum (DCM). In the two largest AEs, the DCM, nutrient distributions and UML appeared to be modulated as typical for anticyclones. Shallow and more intense DCM occurred in the area of denser and more nutrient rich water. In the southern large AE, extending near the Sardinian coast, the eddy interacts with resident coastal water masses and have a biological relevance for this area. It is located NW of a coastal upwelling area and seems to be responsible of capturing and transporting chlorophyll rich upwelled water from the coast to the oligotrophic off-shore area of the AB.

1 Introduction

Hydrological and remote sensing data from the last 20 years, have emphasized the role of mesoscale phenomena on the dynamical structures of the Algerian Basin (AB) and on the general circulation of the Western Mediterranean sea [1, 2, 3, 4, 5]. Ocean colour data and in situ data have also evidenced the importance of the mesoscale activity on the biological and nutrient distribution of the water masses [6, 7, 8].
In the AB, the Algerian Current, flowing along the northern African coast, is markedly unstable (EUROMODEL group 1995, [9, 10]). It generates intense mesoscale coastal eddies, both cyclonic and anticyclonic. The cyclonic eddies have short life, while the Anticyclonic Eddies (AEs) can grow in size and become in-

creasingly larger and deeper. They may reach a diameter greater than 150 km and a depth greater than 800 m. During its eastward flow, some AEs may detach from the coast and migrate toward the central AB. These AEs, called open eddies, may stay for months and sometimes for years in this basin [4, 5].
Most of the eddies flow along the African coast up to the Sardinian Channel (SaC). The bathymetry of the channel does not permit to the largest and deepest AEs to propagate eastward toward the Sicily Channel and Tyrrhenian Sea. Due to the morphology of the bottom between the Sardinian island, the SaC and African coast, these large eddies can stay blocked for month, changing in form and dimensions before detaching toward the central part of the basin following a cyclonic circuit. The SaS is located in the eastern part of the AB, which, at mesoscale, is one of the most energetic area of the whole Mediterranean Sea [11, 12]. In this area, the eddies dynamic is not yet completely clarified because most of the information are derived from satellite-based study. Through altimetric data, some authors, (e.g. [12, 11]) deduced these AEs may deviate northwards along the Sardinian coast up to about 40°N. At this latitude they may move from Sardinian coast westwards in the open AB, following a cyclonic circuit. In the last few years, Fuda et al. [4] reported the presence and formation in the area of mesoscale eddies having a different origin, not related to the Algerian Current. They evidenced a series of eddies, located at about 40°N, propagating westward from Sardinian coast toward the central AB approximately along the North Balearic Front (NBF). They named these structures Frontal Eddies (FEs). However, these authors could not provide any theoretical explanation about their formations.
Geographical position of the Sardinian Sea is therefore critical to understand the dynamics of these energetic anticyclonic eddies. This is also a crucial area for determining the dynamics of the water masses at intermediate level because these eddies, located in proximity of the Sardinian coast, seem to be responsible for detaching of lens Levantine Intermediate Water LIW and Tyrrhenian Deep Water (TDW) from the coast [13]. Anyway, although its geographical importance, the historical hydrological data for the SaS are disomogeneous and scarce [14, 13]. The nutrient and chlorophyll-a distribution, particularly around 40°N, and its relation to mesoscale phenomena are largely unknown.
In this work, we present the results of the explorative oceanographic cruise MedGOOS-2, realized in a large area of the SaS during spring 2001, in order to study the hydrological and biogeochemical characteristics of the water masses in proximity of the Sardinian coast. We also investigate the hydrological characteristics of large anticyclonic eddies, frequently observed from SST and altimetric data, and its related chlorophyll-a and nutrient distribution.

2 Material and methods

The MedGOOS-2 cruise was conducted, between 23 March 2001 and 03 April 2001, on board the R/V Urania. This explorative cruise was performed on a large area, between 38.00°N to 41.50°N, in latitude, and between 07.00°E to 09.00°E, in longitude (Figure 1). Sixty-eight hydrographic stations were positioned in a quasi-regular grid of about 28 Km. The grid was intensified around the Gulf of Oristano, ($\sim$

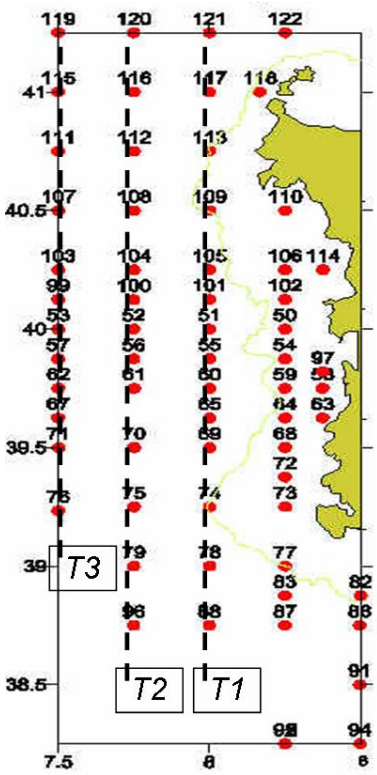

Figure 1: The survey area and the location of stations during the MedGOOS-2 cruise. Numbers indicate the location of the stations. Lines denote, from coastal to open ocean, the bathymetry of 200 m, 500 m and 1000 m.

39.80°N, 008.50°E), with stations at about 14 Km in longitude.

For each hydrographic station, a standard SBE 911 CTD was used. A 4000 Digiquarz (pressure), a SBE-3/F (temperature), a SBE-4 (conductivity) and a SBE-13 (oxygen) were installed on the probe. In situ active induced chlorophyll-a fluorescence was measured by means of a Seatech 90S fluorometer connected to the SBE carousel. Data were archived, processed and reduced using SeaSoft vers. 5.26 modules. The hydrographic data were represented in horizontal maps (at 5, 30, 50 and 80 m) and in vertical South-North sections, interpolated by a kriging method utilising a linear variogram [15].

In the high resolution grid, around the Gulf of Oristano, water samples were collected in 38 stations by a standard G.O. 1016 I, 10 litres 24 Niskin bottle carousel. In these stations, 193 samples, for nutrients, and 166 samples, for photosynthetic pigments analyses, were collected at fixed depths (0, 25, 50, 75, 100, 150, 250, 500 m) and at the deep chlorophyll maximum (DCM) depth. Nutrients and chlorophyll a and phaeopigments have been sampled, stored and an-

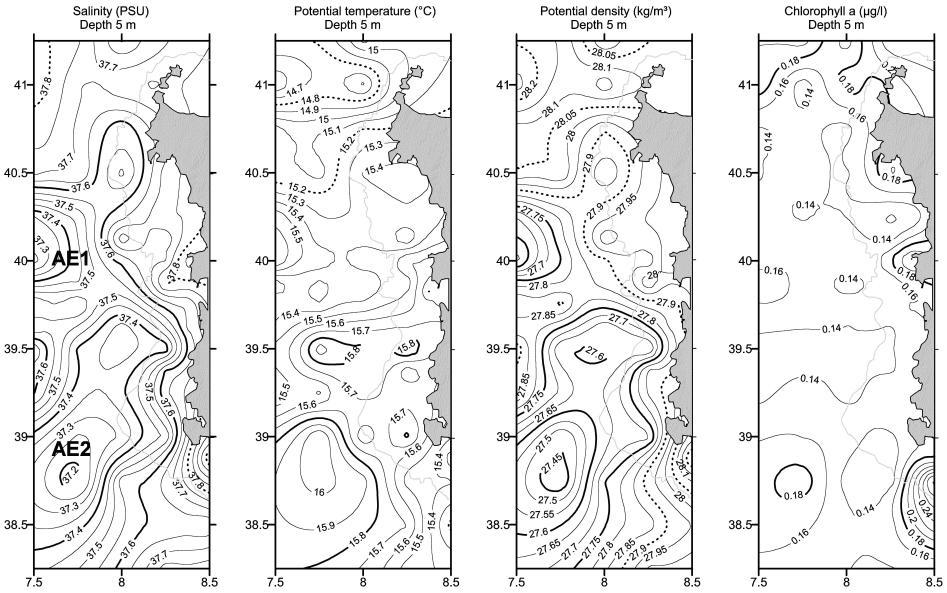

Figure 2: From left to right panel: contour maps of 5 m salinity, potential temperature, potential density, chlorophyll concentration. Bold solid lines, in salinity, temperature and density, delimited the area interested by the anticyclonic eddies. Dotted line denotes the external area, not interested by the anticyclones.

alyzed according to standard methods described in Innamorati et al. 1990. The chlorophyll a concentration (mg·m^{-3}) has been used to calibrate the Seatech 90S fluorescence data (Fl) with following orthogonal (major axis) regression: Chl = 0.666*Fl + 0.011 (n = 166, r^2 = 0.6466).

3 Results

3.1 Horizontal and vertical hydrological fields

At surface (5 m), the salinity, potential temperature and potential density maps (Figure 2) reveal the presence of two large anticyclonic eddies, south of 40.50°N. These AEs have a core of warmer, and in particular less dense (27.45) and fresher water (S <= 37.4). They occupy most of the off shore area. The large northern eddy, denominated AE1, is located in the off shore area at a latitude between 39.75°N and 40.50°N. The diameter of this structure was estimated to be around 70 km. The core of AE1 is characterized by S <=37.3, Theta >=15.6°C and SigmaT<=27.60.

The large southern eddy, AE2, is centered at about 38.75°N and 07.70°E. It is characterized by S<=37.2, Theta>=15.8 °C and SigmaT<=27.45. The core of AE2, at the surface, has lower salinity, density and higher temperature than AE1. In each map, the boundaries of the two AEs are better delimited by the salinity and density fields. The contour of AEs (bounded line), identified by high horizontal salinity and den-

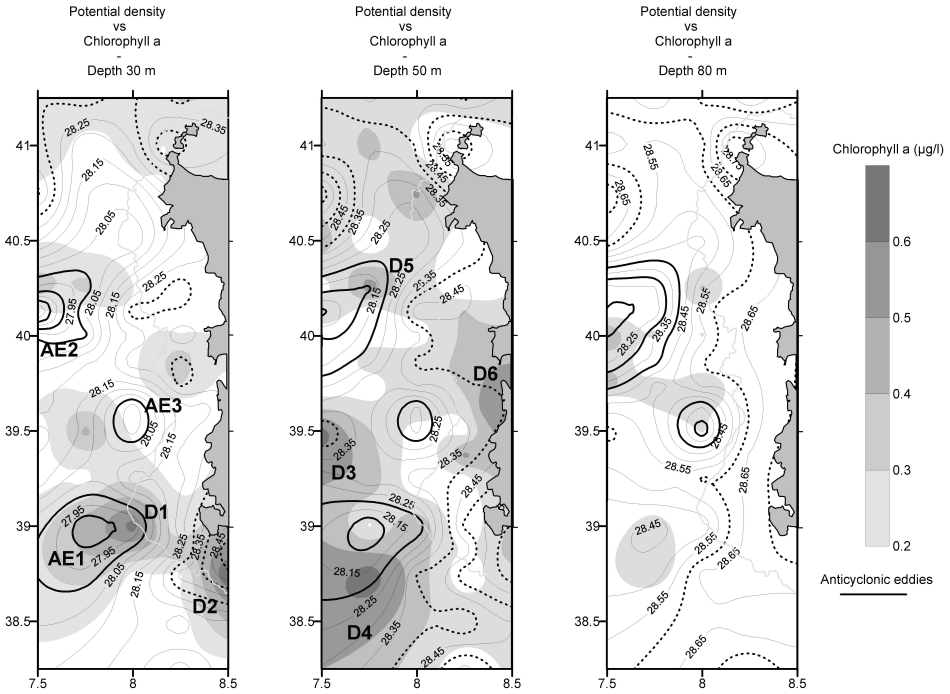

Figure 3: Contour maps of potential density overlapped to chlorophyll concentration, at 30 m, 50 m and 80 m. Bold solid lines indicate the border and the core of three anticyclonic eddies. Dotted line denotes the limit of the external area, not interested by the anticyclones.

sity gradients, are enclosed approximately by the isohaline S>=37.6 and isopycnal sigmaT<=27.90, for AE1, and S>= 37.4 and sigmaT<=27.75, for AE2. North of 40.50° N, AE1 stretches northerly in the coastal area, while a different hydrological regime with colder and denser water, is detected in the open ocean.

In the sub-surface maps at 30 m, 50 m and 80 m, the density is overlapped to the chlorophyll-a contours (Figure 3). As for the surface map, the density field indicates the presence of the two large anticyclonic eddies (AE1, AE2). North North-East of AE2, at about 39.50°N and 08.00°E, these maps evidence another quasi circular line characterized by low salinity and density. This structure is well evidenced in the map at 80 m. The density field suggests it is an isolated and small AE. We called this structure AE3.

These three anticyclonic structures are also evident in the South-North vertical density field sections of the upper 200 m. These sections, from the coastal to the off-shore area, are denominated respectively transects T1 (sts. 88 to 121), T2 (sts. 96 to 120) and T3 (sts. 76 to 119). The density field indicates that the inshore transect T1 (Figure 4) intersects the eastern part of

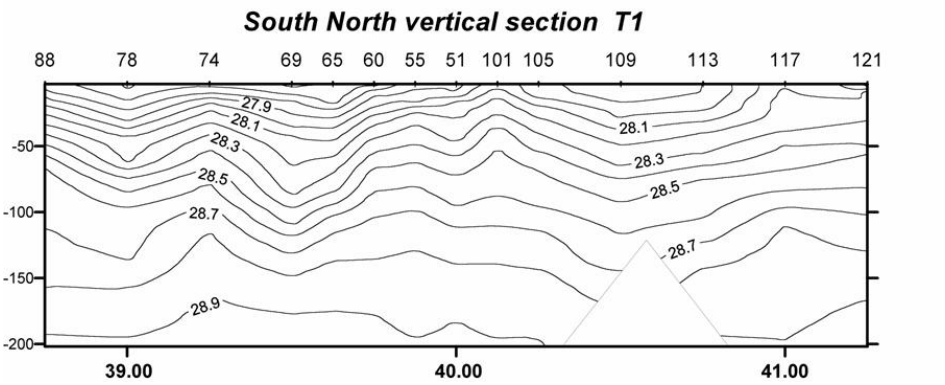

Figure 4: South-North vertical section of density in the upper 200m along in-shore transect T1. Transect T1 cuts the eastern part of the southern eddy AE2 (sts. 88 to 74), the core of AE3 (sts. 69 to 60) and the northern coastal elongation of AE1 (sts. 105 to 117).

AE2 (sts. 88 to 74), the core of AE3 (sts. 69 to 60) and the northern coastal elongation of AE1 (sts. 105 to 117). Details of the large anticyclonic eddy AE2 are not well resolved by the spatial resolution station grid of the southern surveyed area.

The structure of the anticyclone AE1 is instead well evidenced in the offshore South-North section denominated T3 (Figure 6). The rotational forces of AE1 affect the vertical density distribution between stations 71 to 111. In the upper 50 m, a surface mixed layer, delimited approximately by the isopycnals 27.8 to 28.1, is detected in all stations of AE1, except for station 57.

Below the upper 30 m, the convergence of AE1 is well detected by isopycnals sloped downward from the periphery (sts. 111 and 71) to the centre (sts. 99 and 103). The hydrological characteristics of the northern large eddy AE1 are well evidenced in nine significant vertical profiles of potential temperature, potential density and salinity (Figure 5). The effect of the anticyclone AE1 is well distinguished in the six profiles of the stations 99, 103, 57, 62, 71 and 111 (blue lines). The density decreases from the centre (st. 99) to the border (sts. 71 and 111) of the anticyclone. The Upper Mixed Layer (UML) is deeper in the centre (hUML=34m) than in periphery (hUML<=15m). The temperature has a more complex behavior due to the presence of a double isothermal layer and low horizontal temperature gradients. As also evidenced by the surface maps, the borders of the anticyclone AE1 are better identified in salinity and density. The northern offshore area, not interested by the AEs (red lines, sts. 115, 116 and 119), is characterized by a different hydrological regime with colder, heavier and saltier water and by a deepest UMLs (hUML>45m).

AE1 is located, just south to the area occupied by the southern part of the Northern Balearic Front [16]. Its water mass characteristic (higher salinity then AE2), its the position and dimension suggests is could not be an Algerian eddies moved northward along the Sardinian coast but it is probably a Frontal Eddies (FE) as suggested by Fuda et al. [4].

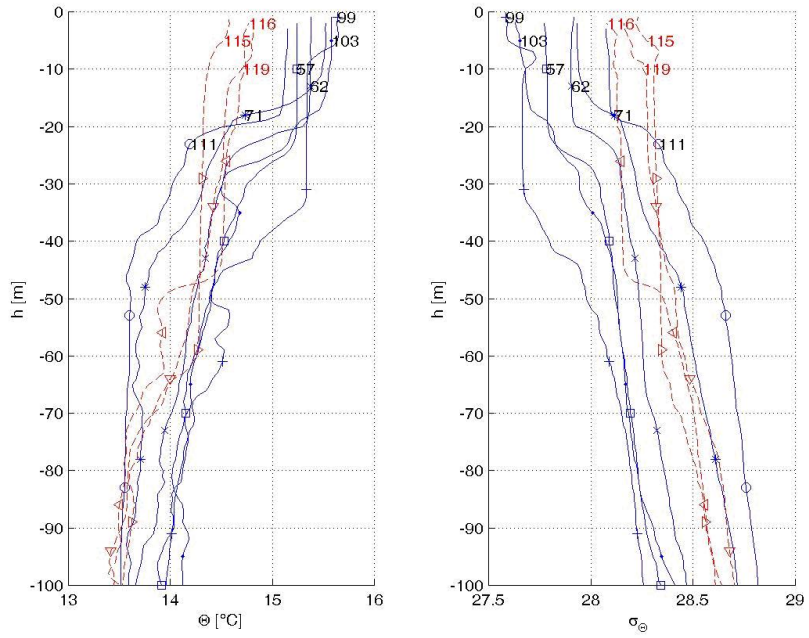

Figure 5: Nine selected potential temperature and potential density profiles in the offshore area for stations within the AE1 areas (blue) and outside the AEs (red).

In the survey area (map at 5 m), chlorophyll-a fluorescence is very low, except for the South-East limit (at Lon 8.5 °E) of the survey area (Figure 2). In the subsurface maps, chlorophyll-a distribution is patchy.

The highest concentrations (Chl-a >= 0.5 mg/m3) are identified as D1 to D6 (Figure 3). At 30m depth, D2 is located at the South-East limit of the survey area. This is a region characterized by the heaviest waters. A similar situation, with colder and saltier waters, occurs also in the surface waters (maps at 5 m), we suppose it denote an upwelling. D1 is located in the eastern part of AE2. At 50 m, D6 is located in a large area around the Gulf of Oristano. The other higher chlorophyll-a concentrations (D3, D4 and D5) are localized at the border of the anticyclonic eddies. This is consistent with the hypothesis of Yentsch [17], suggesting that the growth of phytoplankton could be highest in the proximity of a frontal area, at the extremities of anticyclonic eddies. At 80 m, the higher chlorophyll-a concentrations are detected approximately in the centre of the AEs.

In the upper 200 m, the undulation of the DCMs is evident in the North-South offshore chlorophyll-a vertical section (Figure 6). This is due to the rotational forces of the anticyclone AE1, as indicated by the isopycnals 28.6. The DCMs are shallow ($\sim$ 50 m) and more intense, in the doming area of

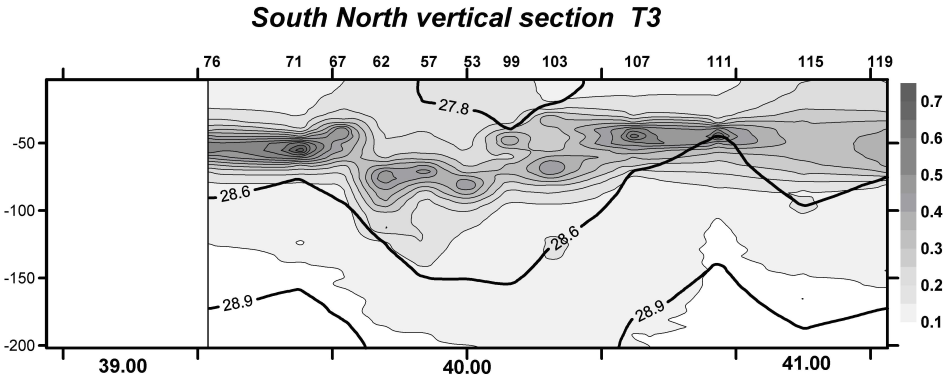

Figure 6: Off-shore South-North section of chlorophyll distribution, with 3 superimposed isopycnals. Isopycnal 27.8 indicates the limit of the UML, isopycnals 28.6 and 28.9 denote the convergence zone in AE1.

AE1 (sts. 71, 67, 107 and 111) and deeper ($\sim$ 70 m) in the convergence zone (from sts. 62 to 103).
Below the deeper DCM the isolines of chlorophyll-a are sloped downward, toward the centre of AE1 (sts. 99 and 103), following the isopycnal slope (see $\sigma\theta$ = 28.9).
The northern area where AEs are absent, also the distribution of chlorophyll-a in the water column is different. It is almost uniformly distributed in the deepest UML (sts 115 and 119 in figure 6). It is not DCM and patch distributed.

3.2 Nutrients distribution

Water samples for nutrient were collected in the region behind the Gulf of Oristano, covered by a higher resolution grid. It corresponds approximately to the area occupied by the anticyclone AE1. In the UML, surface water has a low chlorophyll-a concentration (<0.20 mg/m3) and it is nutrient-depleted. Nutrients (NO_2 + NO_3) are present at different concentrations at the surface and at 25 m, however generally lower than 1 microMol.
The effect of the anticyclone is more evident just below the UML where, for each transect, the vertical sections of nutrients concentrations (Figure 7) present an elevated analogy with the density field. The nutrients isopleths are sloped down toward the core of AE1. These concentrations are higher in denser and saltier water and lower in lighter and fresher water. The horizontal gradients of the nutrients concentration are positive from the core to the periphery of AE1. The gradients are highest in the off-shore transect T3, intersecting the core of AE1, where the convergence is stronger. Along this transect, a tongue of poor nutrient water (5 microMol) reaches 250 m depth. At this depth, nutrient concentration ranges between 5 microMol in the core (st. 103) and 9 microMol in the southern periphery (st. 71). This indicates that the effect of the anticyclone on the nutrient distribution is still detected at this depth.
The nutrients isopleths are also well related to the chlorophyll-a concentration.

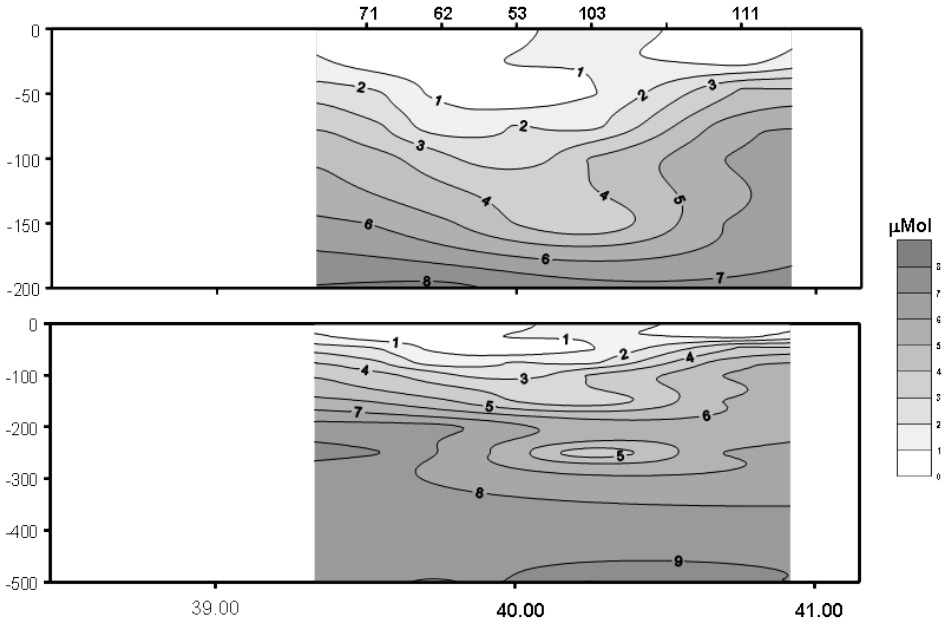

Figure 7: South-North vertical sections of NO_2 + NO_3 (microMol) concentration in the off-shore transect T3, in the upper 200m (upper panel); and from surface to 500m (lower panel).

The 2 microMol isopleth has the same undulation of the depth of the DCM. It is shallower (∼50m) in the periphery and deeper (∼75m) in the centre of AE1. However, chlorophyll-a concentration is higher where the 2 microMol isopleth is shallower. We suppose this is due to the photoactive range (PAR) being higher near the surface.

The in-shore section T1 does not present a significant south-north gradient (Figure 8). However the relationship between nutrient distribution and density field is identified in the small anticyclone AE3. In the core of AE3 (st. 69), there is a minimum of nutrient (Figure 8), between 25 m and 100 m, in correspondence of a minimum in density (Figure 5).

At 500 m, nutrient concentration does not present significant south-north variability but a positive coast to off-shore gradient is detected. The highest nutrients concentrations are found along the off-shore transect T3 ($>$ 9 microMol) and not along the in-shore transect T1 ($>$ 7.5 microM).

4 Discussion

Results from the explorative cruise, MedGOOS-2, suggests that the SaS is characterized by complex dynamics. The surveyed area is dominated by mesoscale phenomena, mainly anticyclonic eddies, that cover the majority of the surveyed area, with the exception of the open ocean North of 40.50°N. This observation sug-

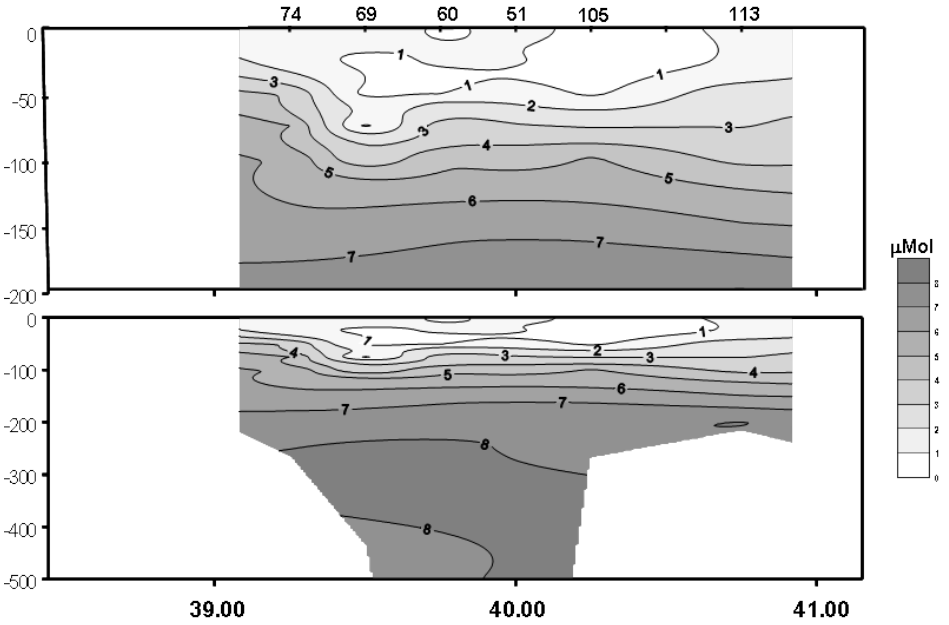

Figure 8: South-North vertical sections of NO_2 + NO_3 (microMol) concentration in the off-shore transect T1, in the upper 200m (upper panel); and from surface to 500m (lower panel).

gests the occurrence of two different hydrological regimes, separated approximately at this latitude of 40.50°N. These two regimes have different hydrological but also biogeochemical characteristics at the surface. In the northern area, the water is heavier, colder and saltier and the UML is deeper. In the southern region, three AEs cover the majority of the mesoscala area from the coast to the open ocean. The two largest eddies, AE1 and AE2, extend up to the open ocean while the smaller AE3 is located between these and the Sardinian coast. In this mesoscala region, the rotational forces, acting on these anticyclone, affect the slope of isopycnals and the depth of the UML. The effect of the rotational forces are more evident in the largest and deepest eddy (AE1), which is located in the northern part of this mesoscale region, covered with an higher resolution sampling grid. The isopycnals are domed upward at the edge and downward at the centre of AE1. The UML is shallower in the periphery and deeper in the core of these AEs. In addition in the southern area, the upper layer is more homo-thermal. With the exception of the warmer core of AE2, the temperature ranges between 15.2°C and 15.8°C from coast to open ocean in all the mesoscala area. The smoothed horizontal gradients, during March-April 2001, and the high cloud cover of the satellite data (not shown) does not permit to have a synoptic view, to identify the border, the extension and the variability, in space and time,

of these anticyclones. The only northern border of AE1 is well detectable in temperature because it is located in proximity of the region of separation between the two regimes where the greater gradients in temperatures are encountered.
The surface and subsurface hydrological maps in spring 2001 suggest that density and salinity are better indicators of these AEs than temperature. This is not only due to the smoothed horizontal thermal gradients of the mesoscale area but, we suppose, it is also due to the origin of these AES.
This is, in fact, coherent with the assumption that these AEs are water masses of Atlantic origin with a strong signature in salinity. Anyway, the core of AE2 is fresher and warmer than AE1. The position and the water masses characteristics suggest AE2 can be an eddy of Atlantic origin directly detached from the Algerian Current. AE1 is locate at the border of the two hydrodynamic regions, just in proximity of the separation area between the two regimes.
The location of AE1 and its dimension could suggest that it is not an AE directly detached from the Algerian Current but it can be a Frontal eddy, as indicated in Fuda et. al [5]. The two regions have also different chlorophyll-a and nutrient distributions. In the northern region, chlorophyll-a is uniformly distributed along the UMLs, while in the southern region it occurs as DCM. The chlorophyll and nutrient distributions are strongly influenced by the physical processes due to these anticyclones. In particular, in the eddies AE1 and AE3, there is the typical distribution of the chlorophyll-a into the anticyclone, as described by Yentch et. al [17]. In the convergence zone, the DCM and nutrients isopleths are sloped downward toward the centre, following the isopycnals. Denser and more nutrient rich water is observed in the periphery, where a shallower and more intense DCM is present. Less dense and nutrient poor waters are identified in the centre, where the DCM is deeper. The effect of the anticyclone on the nutrient distribution is detected down to a depth of 250 m. These anticyclonic eddies are elongated near the coastal areas and therefore, even at surface level, they strongly interact with surface resident water, often rich in terms of chlorophyll-a concentration. Hydrological data and chlorophyll distribution highlighted the presence of a coastal upwelling in the South-East part of the sampling area. This upwelling, probably triggered by N-Westerly Mistral winds, seems to be a peculiarity of the region. Such structure was revealed by thermal images to be present also in other periods of the year (not shown). In this cruise, the eddy AE2 is located in the proximity of the coastal area. Hydrologic data suggest that AE2 is responsible for capturing and transporting the upwelled chlorophyll-a rich water from the coast to the open ocean.

5 Conclusion

The study focused on a hydro-dynamically important area of the eastern part of the Algerian basin, the Sardinian Sea. The explorative cruise, MedGOOS-2, conducted on a large area, allowed to gain a better understanding of the physical and biogeochemical properties of this area.
Two different hydrological and biogeochemical regimes were detected separated at a latitude of about 40.3°N. The northern region is characterized by coldest, saltiest, densest and with chlorophyll-a uniformly distributed in the deepest UML. The south-

ern region is dominated by the mesoscala phenomena, mainly anticyclonic eddies. Three AEs cover the major surveyed area. In this region, the chlorophyll-a is DCM distributed. The two largest AEs strongly modulate the depth and the intensity of these DCMs and also of the nutrient distribution. However these eddies seems to have a different origin. AE1 is located just in proximity of the frontal area between the two regimes. We suppose it is a frontal eddies, as indicated by Fuda et. al [5]. The characteristics of the water masses, the position and dimension of AE2 seem instead to indicate it is an Algerian eddy directly detached by the Algerian Current. This southern eddy is located in proximity to the Sardinian coast just N-W to the upwelling. It seems also responsible for capturing and transporting rich nutrient and biomass upwelled water from the coast toward the oligotrophic off-shore area. The interaction between mesoscala phenomena with resident water seems therefore to be dependent on different factors: eddies location and distance from the coast. We also suppose these relationships may depend on the eddies history and origin.

It would be desirable to conduct a more detailed analysis including extensive use of multisensor satellite data (altimetric, ocean colour, and sea surface temperature) that would permit to analyze the life history of these eddies.

Finally, a high resolution eddy resolving model could represent an ideal tool for better understanding dynamic processes, such as the formation of frontal eddies and their interaction with dynamic features. This would allow to gain a further insight in the complex relationships between chlorophyll-a distribution and mesoscale phenomena.

References

[1] C. Millot. Some features of the Algerian current. *J. Geophys. Res.*, 90(C4):7169–7166, 1985.

[2] C. Millot, I. Taupier-Letage, and M. Benzohra. Circulation off Algeria inferred from the Mediprod-5 current meters. *Deep-Sea Research*, 44(9-10):1467–1495, 1997.

[3] C. Millot. Circulation in the Western Mediterranean sea. *Journal Marine Systems*, 20:423–442, 1999.

[4] J.L Fuda, C. Millot, I. Taupier-Latarge, U. Send, and J.M. Bocognano. XBT monitoring of a Meridian section across the Western Mediterranean Sea. *Deep-Sea Research*, 47:2291–2218, 2000.

[5] I. Puillant, I. Taupier-Letage, and C. Millot. Algerian Eddies life time can near 3 years. *Journal Marine Systems*, 31:245–259, 2002.

[6] A.R. Arnore and P.E. La Violette. Satellite definition of bio-optical and thermal variation of coastal eddies associated with African current. *Journal Geophysical Research*, 91:2351–2364, 1986.

[7] G. Gorsky, L. Prieur, I. TaupierLetage, L. Stemmann, and M. Picheral. Large particulate matter in the Western Mediterranean I. LPM distribution related to mesoscale hydrodynamics. *J. Mar. Syst.*, 33-34:289–311, 2002.

[8] P. Raimbault, B. Coste, M. Boulhadid, and B. Boudjellal. Origin of high phytoplankton in Deep Chlorophyll Maximum (DCM) in a frontal region of Southwestern Mediterranean Sea (Algerian Current). *Deep-Sea Research*, 40(4):791–804, 1993.

[9] C. Millot. Mesoscale and seasonal variabilities of the circulation in the western Mediterranean. *Dynamics of atmospheres and oceans*, 15:179–214, 1991.

[10] M. Benzohra and C. Millot. Hydrodynamics of an open sea Algerian eddy. *Deep-Sea Research*, 42:1831–1847, 1995.

[11] N. Ayoub, P.Y. Le Treon, and P. De Mey. A description of the Mediterranean surface circulation from combined ERS-1 and TOPEX/POSEIDON altimetric data. *Journal Marine Systems*, 18(1-3):3–40, 1998.

[12] S. Vignudelli. Potential use of ERS-1 and Topex/Poseidon altimeters for resolving oceanographic patterns in the Algerian Basin. *Geophysical Research Letters*, 24(14):1787–1790, 1997.

[13] A. Ribotti, I. Puillat, R. Sorgente, and S. Natale. Mesoscale circulation in the surface layer off the southern and western Sardinia Island in 2000-2002. *A. Chemistry and Ecology*, 20(5):345–363, 2004.

[14] A. Perilli, R. Sorgente, and A. Ribotti. A preliminary analysis of the seasonal variability of the LIW water mass characteristics from historical hydrological data. *In Archivio di Oceanografia e limnologia. Ed. IBM-CNR (VE)*, 22:51–58, 2001.

[15] R. Barnes. The Variogram Sill and the Sample Variance. *Mathematical Geology*, 23(4):673–678, 1991.

[16] A. Olita, A. Ribotti, R. Sorgente, L. Fazioli, and A. Perilli. SLA–chlorophyll-a variability and co-variability in the Algero-Provençal Basin (1997–2007) through combined use of EOF and wavelet analysis of satellite data. *DOI: 10.1007/s10236-010-0344-9*, 61(1):98–102, 2010.

[17] C.S. Yentsch and D. A. Phinney. Rotary motion and convection as a means of regulating primary production in warm core rings. *Journal Geophysical Research*, 90(C2):3237–3248, 1985.

Tyrrhenian Sea Circulation: Observations and Model Results

A. Vetrano[1], K. Schroeder[1], G.P. Gasparini[1], E. Napolitano[2] , R. Iacono[2]
1, Institute of Marine Sciences, CNR, Pozzuolo di Lerici (SP), Italy
2, ENEA, Casaccia Research Center, Roma, Italy
anna.vetrano@sp.ismar.cnr.it

Abstract

Hydrological and current measurements, collected in the Tyrrhenian Sea during May-June 2004, are analyzed with an inverse box-model (IBM) to establish the mean circulation patterns of the basin during spring 2004. These patterns are compared with those provided by a high resolution, primitive equation model (POM) implemented over the area in order to simulate the mean basin circulation during the survey. The good agreement between the two circulation fields, despite the differences and the respective limitations of the employed methods, represents a solid evidence for the reliability of the estimated dynamical structures. Moreover, the POM reveals the short spatial variability of the basin not always resolved by IBM because of the low spatial resolution of the in-situ measurements. The comparative study indicates the Tyrrhenian basin as a highly dynamically active region of the Mediterranean Sea, characterized by a rich mesoscale dynamics. This work provides, for the first time after more than 25 years, a novel qualitative assessment of the Tyrrhenian Sea spring circulation.

1 Introduction

The Tyrrhenian Sea (TS hereafter) is a deep basin of the Mediterranean characterized by a complex bathymetry. It is delimited by the Italian coast to the East, by Corsica and Sardinia to the West, and by Sicily to the South (see Figure 1). The TS has a narrow and shallow northern opening towards the Ligurian Sea (the Corsica channel) and a much larger and deeper opening in the south, corresponding to a 250 Km wide passage between Sardinia and Sicily. Beyond this aperture, are present a western deep communication towards the western Provençal basin (Sardinia channel) and a eastern shallow connection to the Eastern Mediterranean basin (Sicily strait). The Tyrrhenian water column can be schematized as a three layers system: a surface layer filled by waters of Atlantic origin, the Atlantic Water (AW hereafter); an intermediate layer containing the Levantine Intermediate Water (LIW hereafter) and a bottom layer of resident Tyrrhenian Deep Water (TDW hereafter). The latter results from the mixing between waters of western and eastern origin: The Western Mediterranean Deep water (WMDW, hereafter), and the transitional Eastern Mediterranean Deep Water (tEMDW hereafter) [1]. A significant part of the incoming LIW mixes with the surrounding water masses, inducing a downwelling into the TDW layer, and an upward flux into the surface AW layer [2]. In winter and spring, the sur-

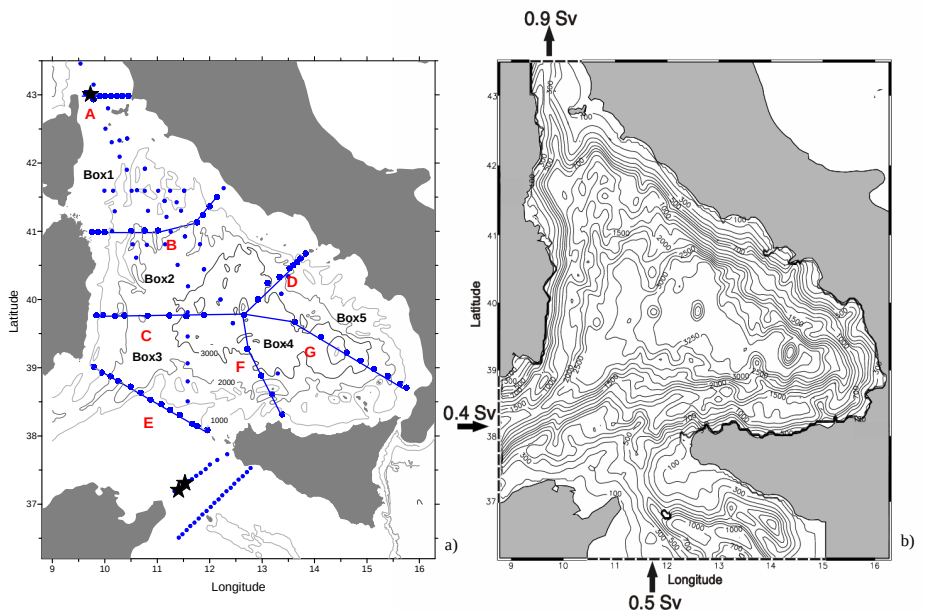

Figure 1: a) Study area subdivided in five boxes and locations of the CTD measurements. The seven transects used for the IBM application are denoted by letters. Stars indicate the locations of the moored instruments; b) Computational domain and model bathymetry for the POM simulation. The net barotropic transports (Sv) imposed at the three open boundaries (dashed lines) are also indicated.

face and intermediate waters entering the TS from the southern opening circulate along an approximately cyclonic route inside the basin, and leave partly through the same opening and partly through the Corsica channel [2]. In summer and autumn, the southern opening is the main connection with the rest of the Mediterranean Sea. Several studies of the TS circulation have been conducted in the last two decades, some dedicated to the description of the large scale circulation patterns [3], while others focused on local processes, either in the northern basin [4] or in the southern opening region [5]. A recent work [6] describes the Tyrrhenian surface circulation from drifters and altimetric data. A review of the TS circulation and forcings has first been proposed by Astraldi and Gasparini [2] from existing literature and available historical data. However, a detailed characterization of the basin dynamics, at all relevant spatial scales, is still missing. The modern common description of the global TS circulation is not very different from that developed long ago by Krivosheya and Ovchinnikov [7], who derived large-scale geostrophic circulation patterns from composite hydrographic datasets, including sparse in-situ measurements over several decades. This hydrological dataset can be regarded as one of the most complete ever collected in the TS, and the resulting circulation is still a

reference for modeling work. In the last decades, no other extensive observational study has been conducted in the area and details of the TS circulation have received limited attention from the modeling community. This work is aimed to achieve a better understanding of the typical spring circulation patterns of the TS, based on the observations collected during recent basin-wide hydrographic surveys. Between May and June 2004, two dedicated oceanographic campaigns were consecutively conducted in the study area (Figure 1a), providing a comprehensive description of the hydrographic conditions of the whole basin over the period. The absolute geostrophic flow is estimated with a linear Inverse Box Model (IBM hereafter), essentially using i) the hydrographic dataset, ii) long-term current measurements (in the Sicily strait and in the Corsica channel), and iii) the average ECMWF wind stress data. The IBM method [8] provides a correction for the geostrophic velocity field, assuming conservation of water properties inside boxes, which are closed volumes of water bounded by the geographical margins (coastline and bottom) and by the hydrographic transects. The IBM assessment of the circulation has been compared with that resulting from a high-resolution numerical simulation (about 4 Km of horizontal grid spacing) using [9] the Princeton Ocean Model (POM hereafterforced) with ECMWF wind stress fields averaged over the cruise period. The paper is organized as follows: the next section gives a short description of both the experimental measurements and the two methods used to estimate the mean circulation. The hydrological characteristics of the different water masses are examined in the successive section. Section 4 focuses on the horizontal circulation patterns produced by IBM and POM for the AW and LIW layers. Finally, a discussion on results and future work is given in the last section.

2 Data and Methods

2.1 *In situ* Measurements

The *in situ* measurements used in this study come from CTD and current-meters. Two consecutive hydrological campaigns have been carried out during spring 2004 in the TS. The first one (May 8-21, 2004) has mostly surveyed the northern part of the basin, while the second (May 26 - June 14, 2004) has covered the central basin. Hydrological data have been collected over a wide number of CTD stations (see Figure 1a). The 61 measurement points placed along the seven transects have been used in the IBM geostrophic computation, while all the stations have been exploited for the dynamic heights computation. It is worth noticing that, since the distance between adjacent stations on transects ranges from 5 Km to 50 Km (mean distance of about 15 Km), it is not always possible to resolve the small-scale spatial variability (the Rossby radius of the area is 10-15 Km). The continuous vertical profiles of conductivity, temperature and pressure have been acquired from surface to bottom by means of a CTD-rosette system consisting of a CTD SBE 911 plus, and a General Oceanics rosette with 24 Niskin Bottles for water samples. The probe calibration has been made before and after the cruise at the NATO Undersea Research Center (NURC) in La Spezia, Italy. The full depth vertical profiles have been sub-sampled every 25 m (giving a good compromise between vertical resolution and number of IBM system unknowns) and potential density values

have been calculated at each depth. Three historical current velocity time-series have also been used: one from a mooring in the Corsica channel (since 1985), and the others from arrays placed at the two sills of the Sicily strait (since 1993). Starting from the vertical geostrophic profiles adjusted to the current time series [1], the estimated mean fluxes have been calculated and used to force the flow at the northern and southern TS openings. The ECMWF wind field, averaged over the same period, has been employed to estimate the surface Ekman transport for each transect.

2.2 The Inverse box model

The hydrological, stationary, and geostrophic IBM, first introduced by Wunsch [8], employs inverse theory to estimate the geostrophic circulation of an ocean region on the basis of water properties conservation inside boxes of water delimited horizontally by hydrographic transects and coastlines, and vertically by interfaces of equal potential density. IBM allows to efficiently combine different types of data (i.e. hydrological, direct current measurements, and climatological), to provide robust estimates of horizontal and vertical mass transports, and associated errors [8, 10]. A delicate task for the IBM application is the definition of the interfaces between water masses. After accurate examination of the potential temperature-salinity diagram of the along transect measurements, two isopycnals have been selected to define three vertical layers: AW lays between the sea surface and sigma=28.9, LIW between sigma=28.9 and sigma=29.1, and TDW between sigma=29.1 and the bottom. A fourth layer between the sea-surface and the bottom is considered as well. In the present IBM application, six horizontal boxes are defined for each water mass, namely the five boxes delimited by the seven transects of Figure 1a, plus a sixth box for the entire basin (on the latter, we impose the balance of the net flows through the northern and southern openings). The absolute geostrophic currents are obtained by imposing near-conservation of mass, salt, and heat inside boxes, tolerating an a-priori error is in the conservation equations. Two additional flux equations take into account the transports obtained from direct current measurements at the Corsica channel and the Sicily strait. The solution of the resulting system is found by inverse methodologies [8] and provides the velocity adjustment, or reference velocity, along the interface between LIW and TDW (sigma=29.1). Diffusive and advective exchanges between layers are also allowed and the evaporative air-sea exchange at surface is considered, together with the transport induced by the wind at surface. Details on how these equations are solved can be found in previous application by Wunsch [8], and Vetrano et al. [11].

2.3 The numerical model

The basic numerical experiment is aimed at simulating the Tyrrhenian mean state during the period covered by the in-situ measurements (May 8 - June 14, 2004). The simulation is made with POM [9], a three-dimensional, free-surface, primitive-equations, hydrostatic model, with sigma coordinates in the vertical direction. The computational domain covers the whole Tyrrhenian basin (see Figure 1b). The horizontal, regular grid is made of 188x186 points, yielding an average resolution of about 4 Km. This is sufficient to resolve mesoscale and sub-mesoscale eddies, since, as mentioned in the previous sec-

tion, the internal Rossby radius for the central Mediterranean is 10-15 Km. The vertical grid consists of 40 sigma levels, which are smoothly distributed along the water column to better resolve the surface and intermediate layers. Bathymetry is interpolated from the Digital Bathymetric Data Base-Variable resolution (DBDB-V) from the U.S. Naval Oceanographic Office, which has a 1' resolution. To avoid the large pressure gradient errors inherent to the use of sigma coordinates over steep topography, a Laplacian smoothing has been applied. Initial and boundary conditions are obtained by interpolating on the POM grid the temperature, salinity, velocities, and surface elevation fields produced by the Mediterranean Forecast System, which is a coarser resolution (1/16°) model of the whole Mediterranean circulation, and runs operationally since 2001. Both the initial and the boundary data are averaged over the cruise period. At the three boundaries connecting the basin to the rest of the Mediterranean Sea (see Figure 1b), we impose the net mean barotropic transports simulated by MFS: a net outflow of 0.9 Sv at the northern boundary (the Corsica channel), which is balanced by net inflows of 0.4 Sv at the Sardinia channel and 0.5 Sv at the southern boundary (the Sicily channel). On the other hand, the baroclinic velocities are left free to radiate out of the domain, according to the Orlanski condition. Therefore, although the total transports at the open boundaries are prescribed, the internal velocities are left free to adjust to the density field. Finally, the model is forced at the surface with the average May 2004 wind stress field from the ECMWF analysis, that has a spatial resolution of ½° both in latitude and longitude. The model is integrated for sixty days. After an adjustment phase, it rapidly reaches a new quasi-equilibrium, and after thirty days, the mean volume kinetic energy remains approximately constant. The circulation patterns shown in the following are obtained by averaging the velocity field over the last thirty days of integration.

3 Hydrological and dynamical analysis

In this section, we describe the TS hydrology of spring 2004 and perform a preliminary dynamical analysis of the main hydrographic structures, which will be examined in detail in the next section. Figure 2 gives the horizontal distributions of salinity minimum, salinity maximum, and dynamic heights at both 75 m (mean depth for the AW) and at 400 m (mean depth for the LIW). The AW occupies the entire surface layer of the TS and it is identified by a shallow salinity minimum. It enters the Mediterranean through the strait of Gibraltar with very low salinities, and meanders toward east along the Algerian and Tunisian coasts, gradually increasing its salt content. By the Sicily strait, the AW stream divides in two veins, one flowing through the strait into the eastern Mediterranean, and the other entering the TS. The route of the latter vein inside the basin can be traced from the Smin distribution (Figure 2a) and from the surface dynamic heights (Figure 2b). From these figures the AW inflow is seen to occurs in the eastern part of transect E, where the lowest salinity of the whole survey has been found (S=37.3). At the opposite side of the transect, the AW exits the basin with salinity values of about 38.1, which corresponds to an increase of about 0.8 with respect to that of the inflow. Besides the

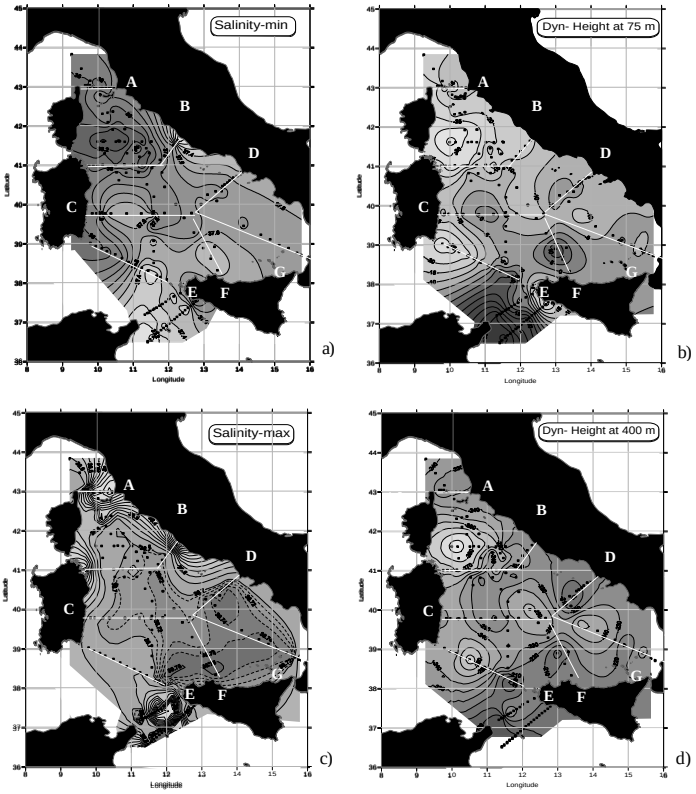

Figure 2: Horizontal distributions of (a) salinity minimum, (b) dynamic heights at 75 m, c) salinity maximum and (d) dynamic heights at 400 m. Panels a) and b) are representative for the AW layer; panel c) and d) describes the LIW layer. The Dynamic heights units are dyn. cm. (figure extracted from [11])

low salinities at transect E, two other low salinity patches are highlighted in Figure 2a (transect C and F) corresponding to anticyclonic gyres in Figure 2b. This indicates that the inflowing AW further separates into a vein that proceeds along the Sicilian shelf (Smin=37.5), and another one that recirculates westward toward transect C (Smin=37.6). Another low salinity anticyclonic patch (Smin=37.7) is observed offshore the Campania coast, while the Bonifacio gyre is clearly visible as a high salinity area (S=38.2). The AW flowing out of the basin through the Corsica channel has a salinity value of 38. Let us now examine the hydrological characteristics of the intermediate layer. The LIW originates in the eastern Mediterranean and enters the western basin through the two shallow and narrow sills of the Sicily strait. It is known from the literature [2] that the LIW is topographically constrained to enter the TS, deviating its route towards northeast. The route of this vein can be traced from

the Smax distribution (Figure 2c) and from the corresponding dynamic heights (Figure 2d). The figures clearly show the LIW entering the basin at the three easternmost stations of transect E, along the Sicilian slope, with the maximum salinity values of 38.75. Another vein is seen to enter the basin shifted toward the central part of transect E, with Smax of 38.65. Although it appears to come from the eastern basin (due to lack of data in the Sardinia channel), it indeed represents the old LIW coming from the western Mediterranean after a complete recirculation of the basin [1]. On the Sardinian side of the same transect, the isohaline 38.65 delimits the LIW flowing out of the TS. These findings appear consistent with what is known about the main cyclonic circulation of the basin [7, 2]. However, some peculiar pathways can be outlined. For example, intermediate salinities at transect C are higher than salinities along the western edge of transect B, indicating that a branch of LIW does not reach transect B, but recirculates through transect C. The Bonifacio gyre is well defined in the same figure, with very low dynamic heights values. The bottom of the Tyrrhenian basin is occupied by the TDW, with salinities ranging between 38.48 and 38.6 (not shown). As told in section 1, the TDW is composed of tEMDW, WMDW, and local deep waters, modified by heat and salt vertical exchanges with the overlaying LIW. The entrance into the basin of the tEMDW can be identified by a salinity value of 38.58 at the eastern trench of the Sardinia-Sicily transect. The WMDW, produced in the Gulf of Lion during winter convective processes, flows into the TS along the deeper part or the eastern wall of the Sardinia channel (transect E). It is characterized by salinity of 38.5, low temperatures and high oxygen content (not shown). Above the WMDW and along the western wall of the deep Sardinia channel, the TDW leaves the basin, with the salinity value of 38.54, which represents an average between the salinities of the two inflowing water masses. The dynamic heights distribution for the bottom layer (not shown) does not allow to properly define the TDW hydrological structures due to insufficient measurement points: it is only possible to verify the nearly cyclonic circulation inside the basin. Therefore, the TDW is not considered for the further estimates of the basin circulation field. Summarizing, the hydrological and dynamical analysis confirm the main known characteristics of the TS, providing new insights on particular regions.

4 Circulation patterns

In this section a qualitative description of the average circulation patterns for spring 2004 is given, as reproduced by both IBM and POM results. Let us start by examining the surface circulation. Figure 3a shows the IBM estimated geostrophic velocities (small arrows perpendicular to transects) at a depth of 75 m, superimposed to the dynamic heights distribution (dotted curves) at the same depth, referenced to the surface. By combining information from both fields, a sketch of the main AW patterns (continuous curves) has been drawn, and will be compared with a similar sketch resulting from the horizontal velocity field of the POM simulation (panel b of the same figure). Before analyzing the circulation patterns, let us consider the surface dynamical structures that can be clearly pointed out in both panels (a and b of Figure 3). We have identified ten dynamic structures, distributed all over the basin, and we have

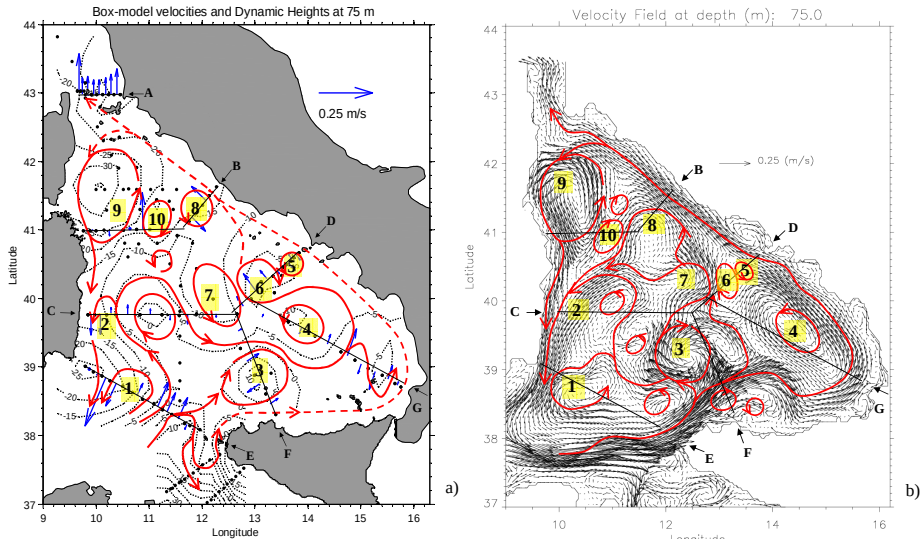

Figure 3: Comparison between IBM and POM current fields at 75 m (AW). Numbers refer to the dynamic structures individuated in both panels. Continuous curves represent a deduced sketch of the surface circulation. Velocity values are in ms^{-1}. (a) IBM estimated geostrophic velocities perpendicular to the transects (thin arrows) superimposed to the dynamic heights distribution (dotted curves). (b) High resolution current velocity field estimated by POM during the survey (figure extracted from [11])

numbered them likewise in the two panels, tolerating small differences in position and shape. The largest structure is the Bonifacio gyre (9), which is a permanent cyclonic circulation due to the year-round westerly jet of wind blowing through the Bonifacio strait. This gyre displays remarkably close features in the two estimates. According to both the dynamic heights and the POM simulations, the gyre elongates in the north-south direction for about 170 Km, with a zonal extension of about 100 Km and maximum velocities of about 12 cm s^{-1}. It is known from the literature [7], that the Bonifacio gyre has an anticyclonic companion to the southeast. In this region, we find a narrow anticyclonic area (10) in both IBM and POM. Moving south, good agreement is found for the anticyclone 3, just above the Sicily tip, and for the cyclonic circulation 4, more to the east, despite the few available IBM estimates. The smaller structures 5 and 7, located along transect D, also show reasonably good agreement (note that 5, not clearly distinguishable in Figure 3b, is revealed by a full resolution not shown), although 7 is slightly displaced to the north in the POM simulation. The eddy 8, which is deduced by IBM from only two arrows of opposite directions along transect B, is well developed in POM, as a wide current meander. Finally, both results show a cyclonic structure (1) in the western part of transect E, and another one (2) off the Sardinian east cost, which is however more

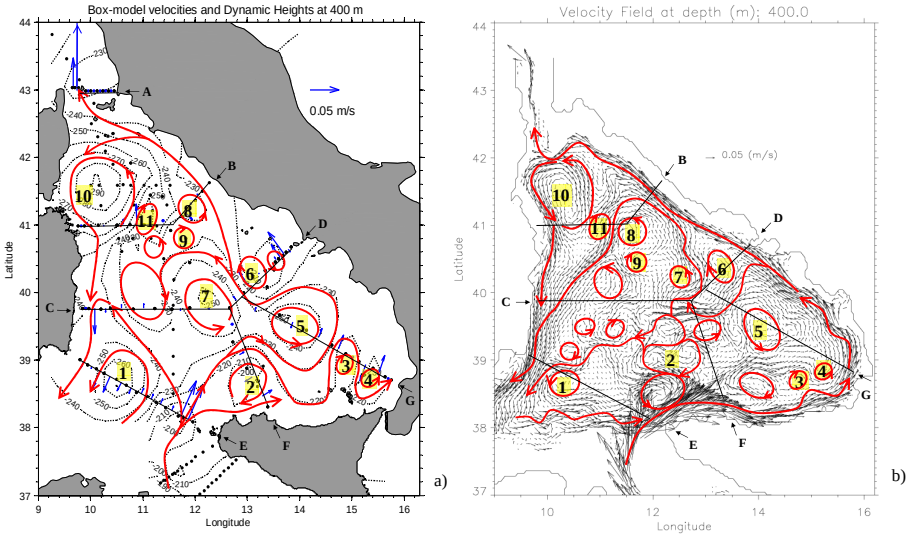

Figure 4: Comparison between IBM and POM current fields at 400 m (LIW). Notations are as in Figure 3 (figure extracted from [11])

elongated towards north-east in the POM simulation, partly overlying a region that, according to IBM, is interested by a circulation of opposite sign. Another difference is found in the southeastern part of the basin, where IBM indicates the presence of two eddies (along the eastern side of transect G), that are absent in the velocity field computed by POM. Let us now come to the surface circulation patterns. Just after the entrance, the AW splits in two veins: one turns north/northeast and generates the anticyclonic gyre 3, while the other proceeds further eastward along the Sicilian coast. The latter vein circles around the cyclone 4, which, according to POM, is embedded in a wide, coherent cyclonic region. IBM indicates a more complex structure of the flow in the area, with the presence of additional eddies to the north of the Aeolian archipelago. After rounding 4, the flow progresses cyclonically along the coast in both fields, encompassing several gyres, both cyclonic (5, 7 and 8) and anticyclonic (6). The flow patterns given by the two estimates appear consistent in this area. POM shows the presence of a well-defined northern current along the Italian coast, which is probably wider than in reality, because of the smoothed topography. Just above 42°N, the AW splits into a northward vein exiting the basin through the Corsica channel, and a cyclonic southward flow, entrained in the Bonifacio gyre. The surface circulation patterns described above appear broadly consistent with the classical picture of the geostrophic winter-spring circulation of Krivosheya and Ovchinnikov [7] with two wide cyclonic regions to the north-east and south-east of Sardinia, and a third one more to the east (the area around gyre 4). The latter region, however, appears smaller in our results, and leaves room for a more complex structure in the

central part of the basin, where the gyres 3, 6, 7, and 8 are located. In the POM output, this central region is interested by an ascending, meandering branch of the AW, which finally rejoins the northern coastal current. Because of data scarceness, the existence of such a branch is neither clearly supported nor refuted by IBM. The intermediate circulation at a depth of 400 m is shown in Figure 4. The LIW circulation patterns deduced by the two estimates appear fairly coherent with the respective surface patterns. The main LIW inflow occurs along the eastern side of transect E, through the narrow trench connecting the eastern basin with the TS. The velocity distribution of this inflow is not properly resolved by IBM for the presence of a steep bottom topography, which makes it difficult to obtain a satisfactory reconstruction of the geostrophic velocity field in the deep region. Despite this, the imposed flux of 0.94 Sv, distributed over layers 2 and 3 is fully satisfied. On the other hand, the coastal vein is well resolved in the POM simulation, where it is characterized by velocities of about 20 cm s^{-1}, in good agreement with instantaneous current measurements from an Acoustic Doppler Current Profiler. In both fields, a fraction of the inflowing LIW turns westward, and recirculates out of the basin around gyre 1, which is coherent with its surface counterpart. In IBM, part of this branch is involved in an anticyclonic circulation located west to gyre 7, which is coherent to the surface layer but is missing in the POM field. The principal LIW vein proceeds eastwards, reproducing both the surface anticyclone (2) to the north of Sicily, and the same surface pair of cyclonic-anticyclonic small eddies resolved by IBM (3 and 4, now also present in the POM reconstruction), and finally feeds a northern coastal current, particularly evident in the POM field. The central part of the basin is dominated by a large bi-lobate cyclonic structure (gyres 5 and 7) that is present in both models, although with differences in position and shape. This large circulation makes the LIW meander far from the coast and reside longer in the central area of the basin, favoring the exchange of properties with surrounding waters. In this area, the POM velocity field shows an ascending meandering vein of LIW, which appears consistent with the corresponding path found in the surface field. Coming back to the coastal current, it is seen in both fields that it produces several cyclonic/anticyclonic eddies (5, 6, 7, 8 and 9) as it proceeds northward. Most of these are coherent with the corresponding surface structures, indicating a strong barotropic component of the current. A fraction of the intermediate coastal current leaves the basin through the Corsica Channel, while the main LIW vein turns south following the bathymetry and exits the basin through the Sardinia-Sicily transect. In this region, the Bonifacio gyre (10) is again present with very similar characteristics in both estimates. Summarizing, the horizontal dynamics of the surface and intermediate waters reproduced by IBM and POM are generally in good agreement. Differences may reflect the intrinsic limitations of both the two estimates (coming from their basic hypotheses) and choices taken in their respective implementations. Nevertheless, the previous discussion clearly shows that the combined use of the two approaches can overcome some of these limitations.

5 Discussion and conclusion

We have analyzed observations collected in the TS during two dedicated oceanographic cruises carried out between May 8 and June 14, 2004. These recent basin-wide surveys, coming decades after the extensive experimental activities summarized in the classical work of Krivosheya and Ovchinnikov [7] provide the opportunity to get a novel description of the TS spring circulation. In this work, we have discussed the hydrological properties of the main water masses of the TS, and characterized the mean horizontal circulation patterns for both AW and LIW layers, through the combined use of an inverse box model (IBM) and of a primitive equation numerical model (POM), simulating the mean circulation over the survey period. Despite the differences between the two estimates and the respective limitations of the approaches, the resulting picture of the TS mean circulation is fairly coherent. Embedded in a broad, basin-wide cyclonic circulation, typical of wintertime, there is a pretty large number of dynamical structures that appear in both reconstructions, with similar features. They have spatial scales ranging from over 100 Km for the wide Bonifacio gyre to few tens of kilometers for several mesoscale gyres through the basin. Most of them have a strong barotropic signature, i.e. they appear both in the surface and in the intermediate layers. The majority of these gyres is absent in the large scale mean geostrophic winter flows of Krivosheya and Ovchinnikov [7], whose main structures are the cited Bonifacio gyre and another wide cyclonic area between Sardinia and Sicily (this is the cyclonic patterns that encompasses gyres 1 and 2 in our surface circulation patterns), with a smaller anticyclone in between. In particular, there is a numbers of gyres, (2, 7, 6, 4 in the surface patterns, from west to east), that appear to follow the arc formed by the submerged volcanoes present in the central part of the TS. Moreover, there is a strong anticyclonic gyre just to the north of the Sicily tip, around which circulates part of the AW in its path towards east, and part of the beneath LIW entering from the Sicily strait. Most of the established features, as well as other bifurcations and recirculations (such as that occurring around gyre 6, which moves away from the coast part of the coastal streams of AW and LIW, to rejoin the central ascending stream), are not described in the works of Krivosheya and Ovchinnikov [7]. The overall results indicate the presence of a rich mesoscale dynamics, until now poorly resolved, which is likely to be strongly influenced by the interaction of the surface forcing with the complex bathymetry of the basin. The good agreement found between the geostrophic velocity reconstruction of IBM and the velocity patterns of POM represents a solid evidence for the reliability of the estimated dynamical structures, giving new insights for the surface and intermediate spring circulation of the TS.

6 Acknowledgments

We gratefully acknowledge the technical support by Mireno Borghini during the cruises and the pre-processing phase. Hydrographic cruises were carried out on board of the R/V Urania, whose officers and crew provided continuous support during operation at sea. Measurements were supported by EC MASTER Project EUROMODEL I and II (MAST – CT 90-0043-C

and MAS-CT93-0066), SALTO (93-AVI-065) , MATER (MAS3-CT96-0051). Part of the modeling work was supported by the project PRIMI ("PRogetto pilota Inquinamento Marino da Idrocarburi") of the "Agenzia Spaziale Italiana" (ASI).

References

[1] A. Astraldi, G.P. Gasparini, S. Sparnocchia, M. Moretti, and E. Sansone. The characteristics of the water masses and the water transport in the Sicily strait at long time scales. pages 95–115, 1996.

[2] M. Astraldi, , and G.P. Gasparini. The seasonal characteristics of the circulation in the Tyrrhenian Sea. 46:115–134, 1994.

[3] V. Artale, M. Astraldi, G. Buffoni, and G.P. Gasparini. Seasonal variability of gyre-scale circulation in the northern Tyrrhenian Sea. *Journal of Geophysical Research*, 99(C7):14127–1413, 1994.

[4] G. Budillon, G.P. Gasparini, and K. Schroeder. Persistence of an eddy signature in the Central Tyrrhenian Basin. *Deep Sea Res. II*, 56:713–724, 2009.

[5] A. Vetrano, G.P. Gasparini, R. Molcard, and M. Astraldi. Water flux estimates in the central Mediterranean Sea from an inverse box model. *Journal of Geophysical Research*, 109(C01019), 2004.

[6] E. Rinaldi, B. Buongiorno Nardelli, E. Zambianchi, R. Santoleri, and P.-M Poulain. Lagrangian and Eulerian observations of the surface circulation in the Tyrrhenian Sea. *Journal of Geophysical Research*, 115(C04024), 2010.

[7] V.G. Krivosheya and I. M. Ovchinnikov. Peculiarities in the Geostrophic circulation of the Waters of the Tyrrhenian Sea. Oceanology. 13:822–827, 1973.

[8] C. Wunsch. The ocean circulation inverse problem. page 442, 1996.

[9] G.L. Mellor. User's Guide for a Three-Dimensional, Primitive Equation Numerical ocean Model. 2004.

[10] K Schroeder, V. Taillandier, A. Vetrano, and G.P. Gasparini. The circulation of the western Mediterranean in spring 2005 as inferred from observations and from model outputs. *Deep-Sea Research I*, 55:947–965, 2008.

[11] A. Vetrano, E. Napolitano, R. Iacono, K. Schroeder, and G.P. Gasparini. Tyrrhenian Sea circulation and water mass fluxes in spring 2004: observations and model results. *Journal of Geophisical Research*, in press, 2010.

Influence of the Increasing Mediterranean Sea Surface Temperature on Local Wind Regimes in Leghorn Area

A. Scartazza[1], B. Doronzo[1,2], G. Rossini[1], S. Taddei[1,2], L. Pellegrino[1], G. Brugnoni[1,2], B. Gozzini[1,2], F.P. Vaccari[1]
1, Institute for Biometeorology, CNR, Firenze, Italy
2, LaMMa Consortium, Laboratory of Monitoring and Environment Modelling for the Sustainable Development, Sesto Fiorentino (FI), Italy
scartazza@libero.it

Abstract

The global warming has not only large scale effects but it is also influencing local climate. In this work we show the correlation between the increase of the Mediterranean sea surface temperature (SST) and the characteristic wind regimes of the Leghorn area. In particular the comparison between the Mediterranean SST values and the wind data measured by the Historical Observatory Pietro Monte in Leghorn shows that the SST increase in the last 40 years is associated with frequency and intensity changes of the wind regimes. The Historical Observatory Pietro Monte has a very long anemological series of about 140 years, only partially in digital form, completed in recent years by data from a weather station of the Consorzio LAMMA (Laboratory of Monitoring and Environmental Modelling for the Sustainable Development). Further studies and the complete digitalization of the wind series are in progress.

1 Introduction

One of the most evident sign of the global warming is undoubtedly the increase of the Sea Surface Temperature (SST). This increase, which accelerates the evaporation and the consequent release of large amounts of energy in the atmosphere, can change the atmospheric circulation pattern and increase the likelihood of extreme events. Although much attention has been given to the effects of SST on the thermo-pluviometric regimes, there has been little discussion of prospective changes in the wind regimes. Understanding the effects of climate change on wind speed and directions, is important for example to study the hydrodynamics and coastal processes that influence the coastal morphological changes (erosion, accumulation of sediments, shape and nature of beaches, loss of land) [1, 2]. Furthermore these informations are very important also for many human activities depending by wind regimes, like wind energy industry and related problematic [3]. Wind regimes in the Mediterranean basin are dominated by the atmospheric circulation pattern which in turn could be potentially affected by sea thermal changes [4, 5]. The analysis of changing wind regimes and extreme events requires detailed impact studies based on ac-

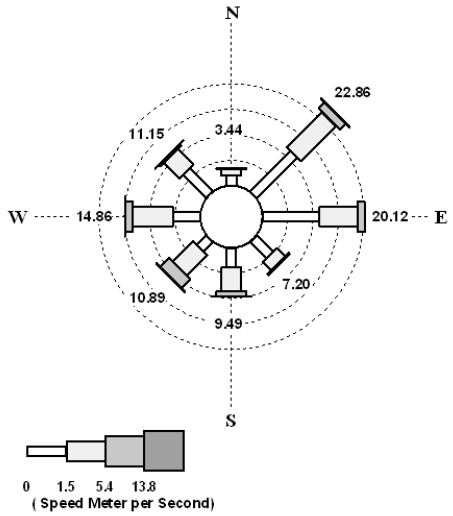

Figure 1: Wind rose for daily series (Leghorn, 1934-2009)

curate historical analysis of wind datasets at both global [6] and local levels. In this paper we analyze the effect of SST increase on the wind regimes in the Leghorn area (Livorno: coord. 43°33'7"N, 10°18'29"E datum WGS84). We focus our study on Leghorn for two remarkable reasons: first since it is located in the most important cyclogenetic region of the Mediterranean Sea [7, 8]; second since a meteorological data collection of about 140 years long is available. These data, coming from the ancient meteorological observatory named "Pietro Monte" in Leghorn, extended in recent years by the LAMMA and RMN (Rete Mareografica Nazionale) datasets, represent one of the longest historical series on Mediterranean coast.

2 Datasets and methods

In order to study the climate and to evaluate the possible effects of climate changes on both frequency and intensity of wind regimes in a given area, it is necessary to perform a climatological analysis, based on a statistical processing of numerical data consisting of at least a thirty years dataset. It is not always possible to have long descriptive documentary observations, i.e. meteorological measurements that provide direct information about the weather and climate. In the Leghorn area is available a long sequence of meteorological data coming from an ancient meteorological observatory, founded by Pietro Monte in 1856. This observatory has been operative until recently, providing detailed reports on the weather of the city. In the present study we examine a time wind series that, except a few cases of short interruptions, covers the time period from 1934 to 2009. Although the Pietro Monte series started from 1856, only the period defined above has been digitized until now. Since 1996 to 2009 we integrate the wind sequence

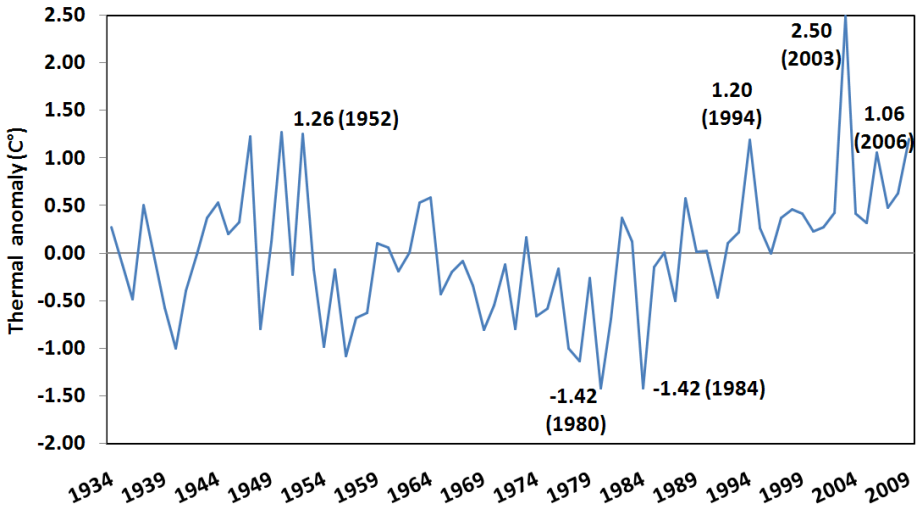

Figure 2: Time series of SST summer anomalies.

with the RMN (1998 - 2003) and LAMMA (2004 - 2009) datasets. The wind data were collected at three different times (7 AM, 1 PM, and 6 PM) based on observations of ten minutes; in order to estimate the daily series, reported in this study, we calculate the average of these three daily values. The SST data are monthly averages at 2 degrees of resolution (center: 42°N, 10°W), taken from a large dataset extracted from the NOAA NCDC ERSST (Extended Reconstruction Sea Surface Temperature) archive. This ERSST dataset is updated with the available GTS ship and buoy data. The thermal anomalies are computed for each month with respect to a 1934-2009 month climatology. The study is conducted, at first, by analyzing the thermal anomalies and, secondly, assessing their possible influence on the Leghorn wind regimes during the same period. We focus our attention on the frequency distribution of wind events divided into wind direction and class intensity, with particular emphasis to Libeccio (SW) and Grecale (NE) that represent the strongest and the most frequent wind in Leghorn area respectively [9, 10]. For this purpose all the wind data are distributed into four classes with increasing intensity and the wind frequency variation within each class has been calculated. Concerning the wind directions, the wind rose is divided into eight sectors to better standardize all data series and to easily compare historical wind values with more recent ones.

3 Results and discussion

The analysis of the 1934 - 2009 period confirms the wind climatology of the Leghorn area [9, 10] Figure 1 shows that the prevailing wind, i.e. the most frequent wind, is Grecale. This wind blows with a yearly frequency of about 23%. On the other hand, the Libeccio wind blows with greater in-

Years	Summer temperature anomalies (C°)	Frequency of Libeccio wind (%)				
		0-1.5 m/s	1,5-5.4 m/s	5.4-13.8 m/s	>13.8 m/s	TOT
1934-2009		3.18	6.76	2.31	0.08	12.32
1952	1.26	3.62	8.33	2.54	0.00	14.49
1994	1.20	5.20	3.72	4.83	0.00	13.75
2003	2.50	4.92	9.29	4.37	0.00	18.58
2006	1.06	2.58	7.38	5.17	1.11	16.24
1980	-1.42	1.45	2.90	0.00	0.00	4.35
1984	-1.42	5.70	4.94	3.42	0.00	14.07

Table 1: Thermal anomalies in summer and frequency distribution.

tensity. Approximately the 60% of events of strong or more intense winds, with respect the Beaufort scale, comes from the SW direction. In particular, by observing the historical data, we note the presence of rather strong Grecale, especially in the early morning, at 7 AM, during the entire year. Generally, the Leghorn wind regimes are typical of maritime regions, where the east winds prevail in autumn-winter while the west ones prevail in spring-summer [11]. To better understand the Leghorn wind regimes and the possible influence of the Mediterranean Sea warming, we need to point out a few matters. It is well known that in the spring-summer period the breeze regime is the factor that affects primarily the wind frequency of the eastern and western quadrants. This justifies the prevalence of the eastern winds in the 7 AM observations set, because of the residual effects of land breezes. In the same period, at the 13 PM and 19 PM observations, we notice higher prevalence of the western quadrant winds. This phenomenon is due to the influence of sea breezes, typical of the warmest months. During the winter, the more frequent winds blow from the eastern direction during the whole day, although the western winds occur with greater intensity. A primary role in the Leghorn wind regimes is played by the complex topography around the western Mediterranean Sea. On that side the sea is surrounded by mountains like Pyrenees, the Massif Central, the Alps and the Apennines and by a series of mountainous islands like Corsica, Sardinia and Balearics. In the autumn-winter period, the Leghorn area is influenced by the arrival of both moist and unstable currents coming from the Balearic Islands and from the arctic-polar dry and cold currents. These currents are deviated from the alpine range, reaching the Tyrrhenian Sea via the Rhone valley [12]. In particular, a Ligurian Gulf low pressure area, due to the Alpine-Mediterranean cyclogenesis and marine thermal effect, generates a baric reinforcement for the north cold currents [13, 14, 15]. When the thickness of cold air, coming from the North, settles at a height of about 3000 meters, the Alpine barrier is no longer an obstacle; therefore, these air masses can easily

Years	Autumn temperature anomalies (C°)	Frequency of Grecale wind (%)				
		0-1.5 m/s	1,5-5.4 m/s	5.4-13.8 m/s	>13.8 m/s	TOT
1934-2009		14.68	15.31	2.67	0.30	32.96
1953	0.77	6.52	22.46	1.09	0.00	30.07
1961	0.74	11.96	20.65	1.45	0.00	34.06
1987	0.87	17.00	15.02	11.86	0.00	43.87
2004	1.04	2.59	37.04	7.04	0.00	46.67
2006	1.14	2.17	35.14	3.99	0.00	41.30
2009	1.81	4.80	37.27	3.69	0.00	45.76
1978	-0.75	30.80	3.26	0.00	0.00	34.06
1996	-1.01	31.32	7.92	0.00	0.00	39.25

Table 2: Thermal anomalies in autumn and frequency distribution.

reach the Tyrrhenian areas as a milder Grecale wind [16]. It is interesting to assess if the changes in the SST of Tyrrhenian area, leads to an increase in intensity of the wind regimes for both the typical spring-summer breezes and the cold winds of the autumn-winter months. The results reported in this study show that this is generally true for all the wind directions, although for Libeccio and Grecale, this increase is more evident in the summer and autumn months when the thermal contrast on the Tyrrhenian Sea is more noticeable. For this reason, we analyze the correlation between the highest thermal anomalies during the summer-autumn period and the frequency distribution for both Libeccio and Grecale in the 1934-2009 period (see Tables 1,2). Concerning the Libeccio, we find high positive anomalies in the summer of the years 1952 (1.3° C), 1994 (1.2° C), 2003 (2.5° C) and 2006 (1.1) (see Figure 2). Associated to these positive anomalies, there is a significant shift toward more intense classes of frequency distribution (see Table 1). Until now the summer of 2003 is historically the most important, because the SST hits record values [17]. It worth to recall that in that period the thermal anomaly was about 3° C (the highest in the last three thousand years) and in Leghorn there were very intense Libeccio events, with gusts that reached respectively 80 km/h (1-2 July 2003) and 90 km/h (27-31 August 2003) and caused numerous problems both offshore and on land. This positive thermal anomaly was evident also during October 2003 (with temperatures close to 26° C), associated with events of very intense rain and gust winds of Libeccio that reached 100 km/h. During these years the positive thermal anomalies were associated to very low pressure values on the Ligurian Gulf, affecting the cyclogenesis in the medium-high Tyrrenian sea (Herding, 2009). It is noteworthy also to note that a preliminary study indicates a shorter duration of extreme wind events of libeccio with respect to the past (data not show). On the contrary, in years with high negative thermal anoma-

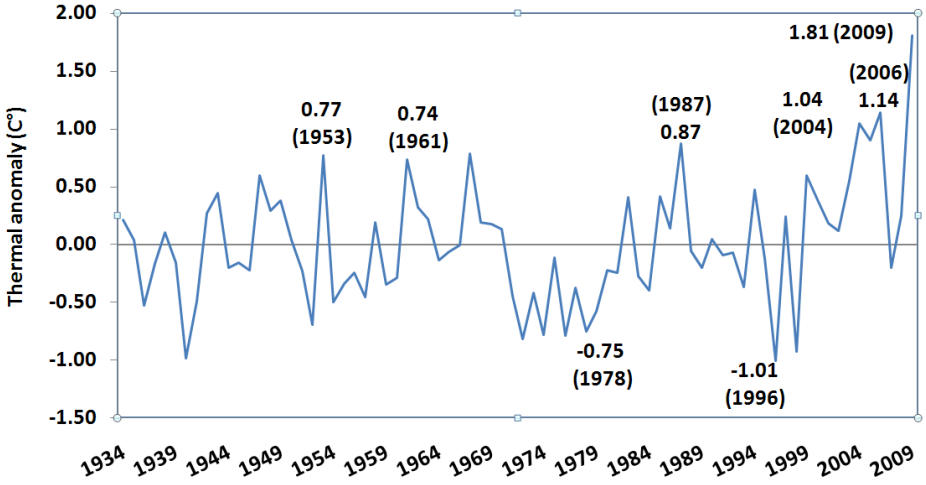

Figure 3: Time series of SST autumn anomalies.

lies, such as 1980 and 1984 (-1.4° C), we note a general decrease of all the classes of frequency (1980) or a decrease of the second class (1984). Looking at the Grecale wind we consider some events related to positive thermal anomalies, recorded in the autumns of the years 1953, 1961, 1987, 2004, 2006, 2009 (see Figure 3). The reference wind rose, for the autumn period, is shown in Figure 4, where the frequency distribution of wind speed for each of the eight directions has been highlighted for the entire historical series. It is evident that the observed positive thermal anomalies are associated to a frequency increase of the highest classes Table 2and Figures 5, 6, 7). For example, in 1953 we observe a reduction of about 50% of the first class and an increase of about 30% of the second one. Similarly, for the positive anomaly of about 0.9°C in the autumn of 1987, we note that the second class do not show any significant change while the third class shows a frequency four times higher. In 2004, the first class shows a strong decrease, while the second class increases more than twice and the third class triples. Finally, in 2006 and in 2009, we observe a significant decrease of the breeze and calm winds, with a consistent increase of both second and third classes. Conversely, for negative thermal anomalies, in the autumn of 1978 (-0,8°C) and 1996 (-1°C.), there is a strong reduction of the second class and the third class disappears (see Table 2).

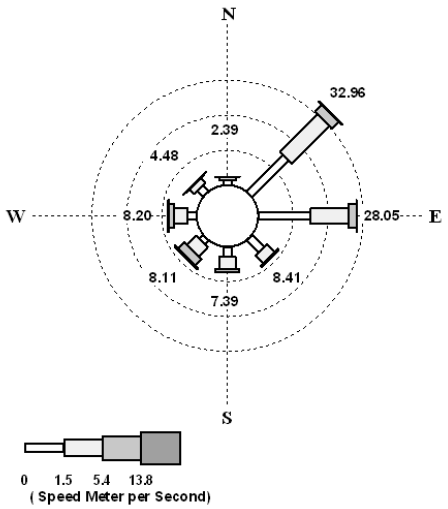

Figure 4: Wind rose for the daily series (Autumn 1934-2009).

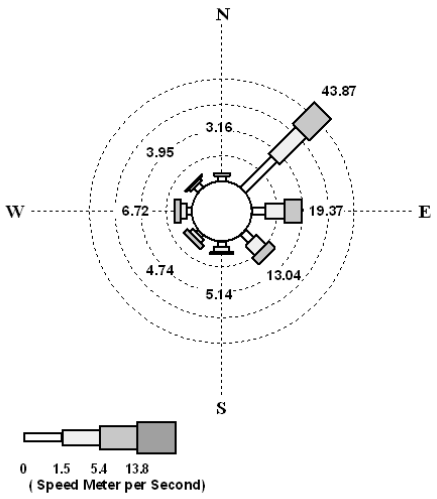

Figure 5: Wind rose for the daily series (Autumn 1987).

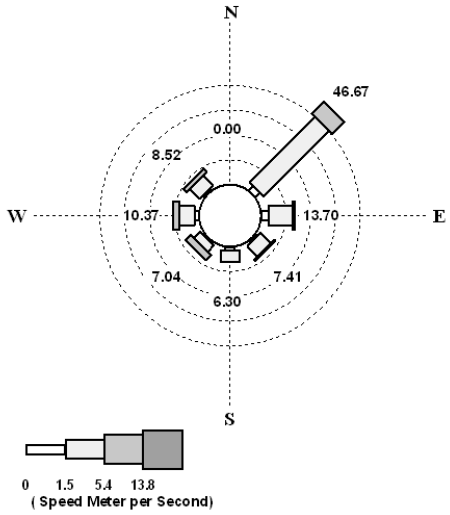

Figure 6: Wind rose for the daily series (Autumn 2004).

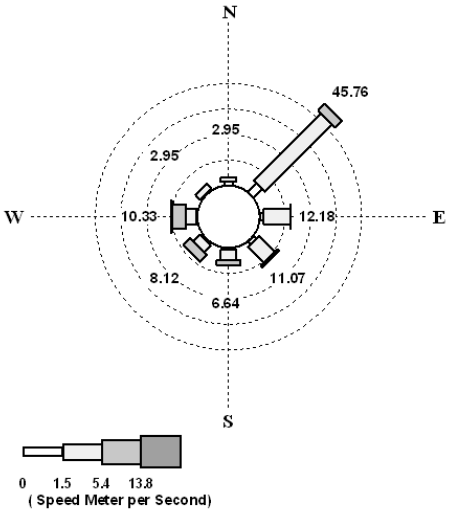

Figure 7: Wind rose for the daily series (Autumn 2009).

4 Conclusion

Although these historical and statistical analysis cannot provide a definitive answer on the relationship between the climate change and the frequency distribution of Libeccio and Grecale in the Leghorn area, our preliminary results indicate an increase of the more intense classes associated with positive thermal anomalies and a decrease in their duration with respect to the past. However since we analyzed only a significant sample of thermal anomalies, a further study of the historical series, taking into account also the other meteorological parameters, is necessary to completely verify this hypothesis. For this reason the complete digitalization of the Pietro Monte time series, including pressure, relative humidity and air temperature, is in progress. This study represents one of the first contribution to the analysis of a possible impact of thermal anomalies on the cyclogenesis in the medium-high Tyrrhenian, that affects the wind regimes at local level. In order to give more evidence to this phenomenon it is necessary to extend the analysis to other historical datasets along the Tyrrhenian coastline. A deeper study of these local phenomena can bring a better contribution to the coastal monitoring and management activity. Particularly, a possible frequency increase of extreme events, could have a large impact on coastal erosion, beach recession, flooding and all the other alterations that affect this complex coastline structure.

References

[1] P. Lionello, J. Bhend, A. Buzzi, PM Della-Marta, S. Krichak, A. Iansà, P. Maheras, A. Sanna, IF Trigo, and R. Trigo. Cyclones in the Mediterranean region: climatology and effects on the environment. *Mediterranean climate variability*, pages 324–372, 2006.

[2] N.K. Soumendra, D. Yan Sam, and S.Y.Wang.

[3] S.C. Pryor and R.J. Barthelmie. Climate change impacts on wind energy: A review. *Renewable and Sustainable Energy Reviews*, 14:430–437, 2010.

[4] P. Lionello, S. Cogo, M.B. Galati, and A. Sanna. The Mediterranean surface wave climate inferred from future climate scenarios. *Global and Planetary Change*, 63:152–161, 2008.

[5] P. Alpert, B.U. Neeman, and Y. Shay-El. Intermonthly variability of cyclone tracks in the Mediterranean. *J. of Clim.*, 3:1474–1478, 1990.

[6] M. Burlano. The synoptic-scale surface wind climate regimes of the Mediterranean Sea according to the cluster analysis of ERA-40 wind fields. *Theor Appl Climatol.*, 96(1-2):69–83, 2009.

[7] J. Campins, A. Genovés, M. A. Picornell, and A. Jansà. Climatology of Mediterranean cyclones using ERA-40 dataset. *Int. J. of Clim.*, 2010.

[8] A. Herding et al. The Climate System. *The Physical Geography of the Mediterranean*, pages 69–88, 2009.

[9] L. Meini, G. Mucci, and S. Vittorini. Ricerche Meteomarine sul Litorale Toscano: Centoventi Anni di Osservazioni Meteorologiche a Livorno. *Bollettino della Società Geografica Italiana*, VIII(X):449–474, 1979.

[10] A. Scartazza, G. Brugnoni, B. Doronzo, B. Gozzini, L. Pellegrino, G. Rossini, S. Taddei, F. P. Vaccari, and G. Maracchi. Analisi climatologica degli eventi estremi di Libeccio a Livorno. *Clima e cambiamenti climatici: le attivita' di ricerca del CNR*, pages 245–248, 2007.

[11] S. Sannino. Meteorologia Nautica. 1998.

[12] C.D.Whiteman. Mountain Meteorology. 2000.

[13] I.F. Trigo, T.D. Davies, and G.R. Bigg. Objective Climatology of Cyclones in the Mediterranean Region. *J. Climate*, 12:1685–1696, 1999.

[14] R.G. Barry and R.J. Chorley. Atmosphere and Wheather Climate. 1998.

[15] H. Flocas, P. Maheras, T. Karacostas, I. Patrikas, and C. Anagnostopoulou. A 40-year climatological study of relative vorticity distribution over the Mediterranean. *Int. J. of Clim.*, 21:1759–1778, 2001.

[16] L. Rusca, F. Castino, and G. Solari. Analisi probabilistica della velocità e direzione del vento. page 193, 1999.

[17] L. Genesio et al. Segnali Climatici - Il Cambiamento Climatico: dagli Scenari Globali alle Strategie locali. 2004.

Influence of Physical Processes on the Spring Bloom in the MEDOC Area (Northwestern Mediterranean Sea)

C. Pizzi, F. Bignami
Institute of Atmospheric Sciences and Climate, CNR, Roma, Italy
cinzia.pizzi@artov.isac.cnr.it

Abstract

This work has been carried out at the ISAC-CNR UOS Roma (Italy) and focuses on the North Balearic Front (NORBAL) oceanographic research project. The study area is off the Gulf of Lions, i.e. the MEDOC area (42-44°N e 3-6°E) in which Western Mediterranean Deep Water (WMDW) is formed and which hosts the Mediterranean Sea's most important algal bloom. The main objective is the study of the influence of physical processes on the bloom's development. Hydrological and biogeochemical data have been collected during the five cruises (2000-2003) and the data analysis of the three spring cruises (NORBAL 1, 4 e 5; 24 March-22 April 2000; 03-25 March 2003; 17-25 April 2003) is presented here, together with an analysis of the bloom as resulting from SeaWiFS chlorophyll satellite imagery. Results suggest: (1) high interannual variability in bloom strength and duration; (2) WMDW recent formation via deep convection; (3) WMDW diffusion in the basin; (4) intense mesoscale dynamics associated to the "recapping" process of the convection columns, as the spring season advances; (5) the surface nature of the bloom in the MEDOC area and, vice versa, the presence of a Deep Chlorophyll Maximum (DCM) regime more to the south; (6) strong modulation of the chlorophyll field due to both recapping and doming processes in the center of the MEDOC area, the latter being associated to WMDW formation.

1 Introduction

One of the most up-to-date oceanographic research themes is the estimate and prediction of ocean primary production through analysis of the space-time distribution of phytoplanktonic biomass. Such distribution proves to be highly nonlinear because it is the end result of physical and biological processes whose complexity is tied both to different levels of biomass functional organization, from genetic to ecosystem level, and to the inter- and intra-specific relationships that are established at different spatial and temporal scales [1, 2]. Physical processes, instead, include vertical transport associated with deep and intermediate water mass formation that redistribute organisms in the water column and supply nutrients to the euphotic layer. Such processes are associated to mesoscale dynamics (thermohaline fronts, surface eddies and meanders, turbulent mixing phenomena, etc.) which further contributes to biomass and nutrient redistribution within the water column [3, 4, 5]. Deep water formation is one of the most impor-

tant physical phenomena linked with the development of algal blooms. Indeed, a tight correlation between deep water formation and algal blooms is observed in several regions of the global ocean. The above is also true for the Mediterranean Sea (MED) where high biomass concentrations of varying duration and extent are found in correspondence of terrigenous input from river outflow or deep convection processes [6]. In particular, in the MEDOC area (42-44°N e 3-6°E [7]) offshore of the Gulf of Lions, the deep vertical convection process which forms the Western Mediterranean Deep WateR (WMDW) [8] is set up by fall/winter cold air outbreaks, due to the northerly Mistral and Tramontane winds, which cause isopycnal doming accentuation and surface density increase through strong cooling and evaporation within the permanent Gulf of Lions cyclonic gyre [9, 8, 7]. Therefore, vertical stability weakens and denser surface waters sink to the bottom replacing subsurface waters that are displaced toward the surface and carry nutrients to the euphotic zone [10]. In spring, at the end of the convective process, restratification, optimal illumination and nutrient availability in the euphotic layer allow the growth of an extensive algal bloom [11, 12]. Also, mesoscale dynamics affects the redistribution of the algal biomass. The latter is linked to both the recapping phase of the convective columns by surface waters after the WMDW formation process [13, 14, 15] and to the baroclinic instabilities composed of warmer and/or less saline vortices at the gyre's borders, i.e. the Northern Current in the northern coastal area and the North Balearic Front (NBF) to the south. The algal biomass is also strongly modulated by the less intense springtime atmospheric forcing that mixes the water column down to intermediate depths [16] guaranteeing nutrient supply continuity to the euphotic layer and allowing for a two-month long phytoplankton bloom (February-April). The present work is in the framework of the North Balearic Front oceanographic project (NORBAL, 2000-2003, funded by the Italian Space Agency and within the ESA-ENVISAT Announcement of Opportunity) coordinated by CNR-ISAC UOS Roma (Italy) in collaboration with Italian (CNR-ISMAR, Trieste, SZN, Naples, Univ. Florence) and foreign research institutes (LODYC, Paris, RSMAS UMIAMI, Miami). The project aims to characterize the influence of physical processes on the evolution of the algal bloom in the MEDOC area by analyzing in situ and satellite data. In particular, the bloom has been observed by means of SeaWiFS chlorophyll satellite image time series using MedOC4, a bio-optical chlorophyll Mediterranean Sea algorithm developed at CNR-ISAC [17] see also: [18, 19, 20, 21]. Also, the area has been surveyed in situ during five oceanographic cruises onboard the R/V Urania (2000-2003), organized by CNR-ISAC UOS Rome. Section 2 describes the satellite and in situ datasets acquired during 3 of the 5 NORBAL cruises (2000-2003). Section 3 reports results on both spring bloom variability (satellite) and in situ data relative to the NORBAL 1 (spring 2000), NORBAL 4 and NORBAL 5 (spring 2003) cruises. In section 4 conclusions are presented.

2 Materials and methods

Level 1A LAC SeaWiFS data of the 1998-2005 period (6000 images) were reprocessed to produce chlorophyll maps with the regional Mediterranean Sea MedOC4

algorithm [17]. The maps have been used to describe the interannual variability of the MEDOC phytoplankton spring bloom (Figure 1). Moreover, 81 hydrographic stations were analyzed for the NORBAL 1 (24 Mar.-22 Apr. 2000), 118 for NORBAL 4 (3-25 Mar. 2003) and 41 for NORBAL 5 (17-25 Apr. 2003) cruises respectively (Figure 2). These experimental surveys were guided by the satellite data acquired in Rome and received onboard (AVHRR-derived SST and SeaWiFS-derived chlorophyll, *chl*) to precisely locate the MEDOC area and the phytoplankton spring bloom. Pressure, temperature, conductivity, dissolved oxygen, light transmission and fluorescence were sampled at all stations with a SBE 9/11 plus CTD - General Oceanics Rosette system. Water samples at selected stations were taken to calibrate CTD temperature, salinity and dissolved oxygen and to measure nutrients (phosphates, nitrates, silicates), dissolved carbon and nitrogen (DOP, DOC, DON), particulate organic carbon (POC), chlorophyll-a (*chl*), photosynthetic pigments and phytoplanktonic species. CTD conductivity and oxygen sensors were calibrated with a Portasal Salinometer and by Winkler analysis, respectively. The fluorimeter was calibrated to yield chlorophyll profiles, by comparison with *chl* water samples. CTD temperature calibration was performed via SIS digital reversing thermometers attached to the Rosette system. The other biochemical water samples were processed with the mass spectrometer (nutrients), UV photolitic oxydation (DOP and DON), catalytic high temperature oxydation (DOC), HPLC and spectrophotometric analysis (chl and pigments) and microscope phytoplankton species recognition. Continuous measurements included: surface temperature and salinity (hull-mounted thermosalinograph); Photosynthetically Available Radiation (PAR; Satlantic OCI200 waveband radiometer); water leaving IR spectra for SST calculation and surface IR budget (M-AERI spectroradiometer of RSMAS Univ. of Miami, USA); surface current and fluorescence (hull mounted Acoustic Doppler Current Profiler, ADCP, and continuous flow Turner fluorimeter, respectively); meteorological and radiative parameters (R/V Urania and RSMAS automatic weather stations).

3 Results

3.1 Spring bloom variability in satellite observations

The 1998-2001 SeaWiFS MedOC4 chlorophyll temporal suite in the MEDOC area reveals high interannual variability in the bloom's strength and evolution period, the latter being typically between February and May (Figure 1). However, there are common features in each year's bloom. That is, first, very low chlorophyll concentrations are always found at the center of the MEDOC area (a circle of $\sim$ 100 Km radius centered in 42°N 5°E [8, 22, 23], indicating a "mixed patch" (dark blue hues in Figure 1, leftmost column) from the second half of January to the end of February in the years 1999, 2000 and 2001. This is in agreement with the timing and location of WMDW formation, whose deep convection processes distribute biomass throughout the water column, thus causing low surface concentrations.

Next, the bloom initiates between the end of February and March 15, i.e. in a relatively short lapse of time, and is seen to terminate between the end of April and the first decade of May, with peaks in mid

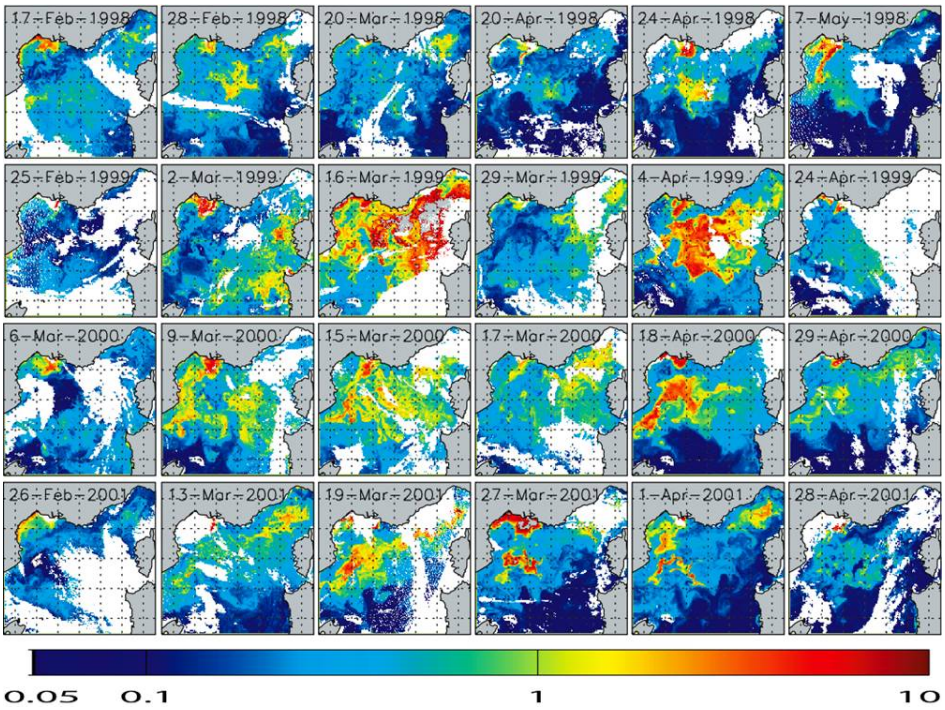

Figure 1: Evolution of the NW Mediterranean spring bloom in the years 1998 to 2001 from SeaWiFS chlorophyll ($\mathrm{mg \cdot m^{-3}}$) imagery.

March and April (Figure 1) alternated by weakening, particularly evident in the 1999 row of Figure 1. Besides these common basic features, a high year-to-year variability is observable in the bloom's evolution. Indeed, 1998 surface chlorophyll is always quite low in the whole basin, while 1999 seems to be the most prominent event. Also, the March images (Figure 1) show that there are initially two separate high chlorophyll regions, i.e. the MEDOC and the Ligurian Sea -western Corsica areas. These two patches seem to join in a unique feature (see 18 Mar 1998 image) in 1999, 2000 and 2001, but not during the weak bloom of 1998. Also, they separate again in April, when the bloom is waning (1998, 2001; Figure 1).

During the 1999 bloom, a dramatic decrease in *chl* occurs in the WMDW formation region in late March, when the low *chl* mixed patch reappears (Figure 1). This suggests that air-sea interaction plays a dominant role in bloom modulation and that also minor variations in the chlorophyll field, such as the milder bloom weakening of March 17 2000, are probably due to wind events of intermediate intensity. Similarly, the long (two month) duration of the bloom may find an explanation in the existence of post-convection atmospheric events. Indeed, Lévy et al. [24] show that wind bursts during the bloom, combined with related vertical motions due to related

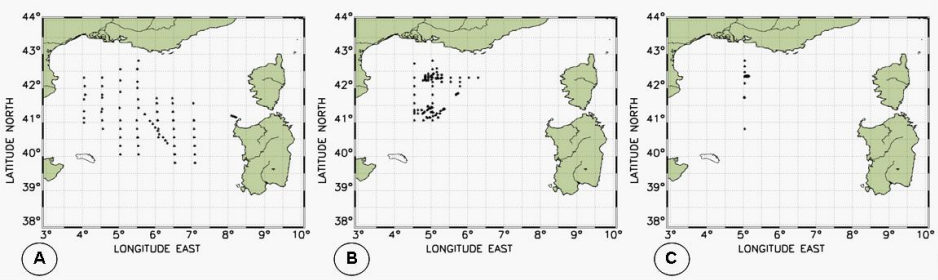

Figure 2: Hydrographic stations: (a) NORBAL 1 (March-April, 2000), (b) NORBAL 4 (March, 2003) and (c) NORBAL 5 (April, 2003).

mesoscale activity and restratification due to solar heating and Ekman transport of lighter stratified peripheral waters towards the MEDOC area are the elementary causes of bloom intermittency and, possibly, of long bloom duration, given the rapid nutrient depletion of such extensive primary production events and the nutrient supply represented by vertical mixing events. A study of the MEDOC spring bloom combining ocean color imagery, atmospheric model output time series as well and in situ data described below is planned, to experimentally confirm these issues.

3.2 Intermediate and deep in situ hydrography and dynamics

In order to illustrate WMDW formation, two N-S sections were selected from the NORBAL 1 cruise (March-April, 2000) in the Sardinian Sea (transect 1-8, Figure 3) and MEDOC area (transect 58-24, Figure 4). Figure 3 shows that the 150-1000 m range includes maximum θ and S associated with the Levantine Intermediate Water (LIW) layer. However, a fresher and more oxygenated water column is found in sta. 4, with values typical of deeper waters in the transect (θ=12.09-13.02 °C, S = 38.41-38.47 psu, O_2= 4.22-4.49 ml·l^{-1}) and within WMDW average values (12.72-12.90 °C e S = 38.40-38.50 psu [25]). This water could have first been formed locally by deep convection and subsequent recapping. Alternatively, since the transect is far from the MEDOC area, we may hypothesize this structure to be a Subsurface Coherent Vortex (SCV) advected away from the MEDOC area, also because its diameter (15 km), depth (1km) and anticyclonic rotation (Figure 3D) correspond to those of SCVs, as described by Testor et al. [26].
Transect 58-24 (Figure 4) in the MEDOC region again shows interruption of the LIW layer, by a fresher and more oxygenated homogeneous water column (θ=12.90-13.20°C, S=38.47-38.49 psu, $O_2\sim$4.41 ml·l^{-1}; Figure 4A-4C) centered at station 40, about 50 km wide and characterized by WMDW properties. This is a residual of deep convection, its surface portion being partly topped by incipient stratification, as seen in Figure 7 below. In the northern part of the transect, ν (Figure 4D) indicates westward flow in the upper 1000 m, following the northern margin of the basin, in agreement with the Northern Current pattern (e.g.[25]). South of sta. 40, the flow is

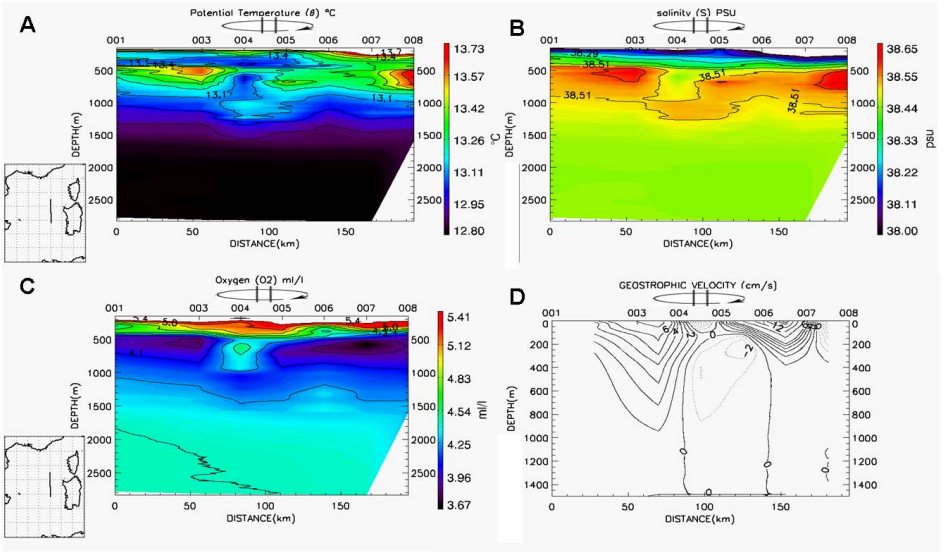

Figure 3: NORBAL 1 cruise, Transect of stations 1-8, Sardinian Sea (150 m-bottom). (A) potential temperature θ (referenced to 0 db); (B) salinity S; (C) dissolved oxygen O_2, (D) and geostrophic velocity ν normal to the transect. Continuous (dashed) lines indicate eastward (westward) velocities, i.e. into (out of) the page. The northernmost part of the transect corresponds to the left side of each plot and location is shown in the map (inset); the subsurface water anticyclonic circulation shown in (D) is drawn atop the figure.

eastward and constitutes the closure of the MEDOC cyclonic gyre and the NBF.

NORBAL 4 (2003) spring data (Transect 88-95 transect; Figure 5) also indicate an evident convection signature, from 500 m to the bottom, in the O_2 vertical pattern at stas. 90 and 93 (Figure 5C). Also, a stronger intermediate recapping is evident, compared to NORBAL 1 Transect 58-24 (Figure 4), suggesting that the convection event has taken place earlier, with respect to the cruise period.

We note that at sta. 90 and below 1000 m (Figure 5A-5C), the WMDW that is warmer and saltier (12.94-13.0°C, 38.46-38.48 psu) than the water of the isolated lenses found in the southern portion and the bottom of the transect (sta. 94 and 95). The differences between this water mass and more offshore deep waters suggest that the former may be water formed by strong evaporative cooling on the shelf of the Gulf of Lions and rapid sinking along the submarine canyons of the continental slope, as described by Bethoux et al. [27].

A summary chart of the convection sites found in the NORBAL 1, 4 and 5 cruises is presented in Figure 6A, together with a monthly mean climatological wind intensity (Figure 6B), in order to stress how such sites line up southeastward along the line of maximum wind intensity towards the Sardinian Sea and are thus probably the wintertime convection locations.

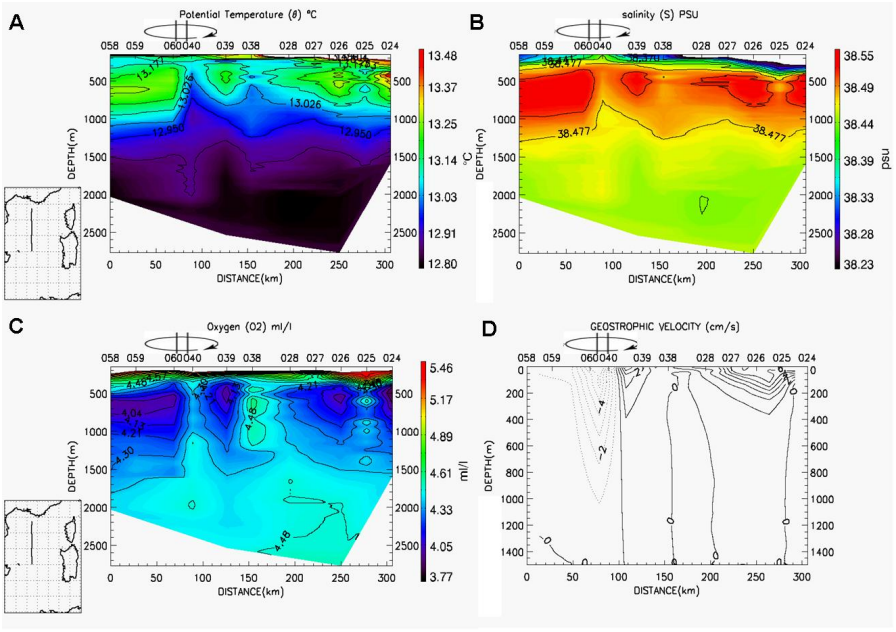

Figure 4: NORBAL 1, Transect 58-24, MEDOC area (150 m-bottom). (A) θ, (B) S, (C) O_2, (D) ν. Cyclonic circulation schematized atop each figure. The left side of each section corresponds to the northernmost part of the transect.

3.3 Surface hydrography, dynamics, nutrients and chlorophyll

The upper 150 m situation hydrography in Figure 7A,7B,7C (NORBAL 1 Transect 58-24) shows that colder and saltier waters found in the north are associated to the MEDOC isopycnal doming. The isoline uplifting observed between stations 28 and 24 to the south (Figure 7A-7C) is associated with warmer and fresher waters, with values close to those of the Modified Atlantic Water (MAW) (13.87-14.85°C, 37.52-38.18 psu) found south of the NBF. The transect thus intersects the NBF, whose northern limit is between station 38 and 28. The nutrient distribution (Figure 7D-7F) follows the density pattern (Figure 7C), with low concentrations to the south (DIN = 0.02-0.80 μmol·dm^{-3}, PO_4 = 0.03-0.08 μmol·dm^{-3}, $SiOH_4$ = 1.08-2.15 μmol·dm^{-3}) and high concentrations to the north, especially in nitrogen and silicates (DIN = 1.86-4.31 μmol·dm^{-3}, PO_4 = 0.09-0.10 μmol·dm^{-3}, $SiOH_4$ = 3.25-4.85 μmol·dm^{-3}), the latter also probably linked to both vertical and horizontal transport of Rhone river waters (stas. 58, 59).
The nutricline is only 50 m deep to the north and reaches the surface at sta. 40, confirmining recent convective events and suggesting that the biomass (*chl*, Figure 7G) has not entirely used up the upwelled nutrients. The surface *chl* bloom (stas. 58-38) in the upper 60 m reaches the nutri-

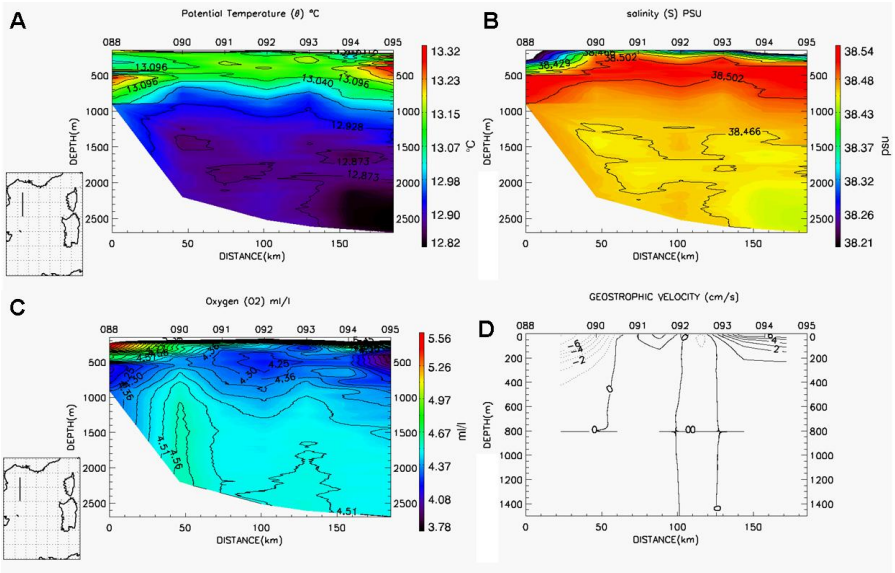

Figure 5: NORBAL 4 Transect 88-95, MEDOC area (150 m-bottom). (A) θ, (B) S, (C) O_2, (D) ν. The left side of each section corresponds to the northernmost part of the transect.

cline in the central part of the transect suggesting that it is still in the growing phase, while further north a small surface bloom, in warmer silica-rich waters (Figure 7A, 7G, 7F) appears to originate from coastal nutrient input rather than MEDOC convection.

To the south, the deep *chl* maximum (DCM) at 40 m has lower concentrations (1.13-1.49 mg$\cdot$l^{-1}) than the surface bloom, is located south of the NBF and is shallower than the nutricline. In other transects (not shown) the depth of the DCM is controlled by the density gradient between MEDOC and southern surface oligotrophic waters, which intrude into the MEDOC area as mesoscale instabilities, deepening the bloom.

The Redfield ratio R is everywhere greater than 16 (Figure 7H) indicating PO_4 limitation except south of the NBF where $R<16$, with DIN limitation. Finally, both the surface bloom and DCM regime regions are characterized by R values close to theoretical equilibrium (about 18), suggesting that the entire algal biomass is in an active production phase, unlike the declining phase observed in the surface portion of Transect 1-8 in the Sardinian Sea (not shown).

We now briefly exemplify the situation in the 2003 spring bloom by presenting Transect 88-95 (Figure 8) relative to the NORBAL 4 cruise (Mar. 3-25 2003). The NBF is centered in sta. 93 and the waters to south of it occupy a short portion of the transect (Figure 8A-8C), while to the north a strong dilution is observed, S decreasing from 38.40 to 38.19 psu from sta. 90 to sta. 88 (Figure 8B), caused by the influence of the fresher waters of the Northern Cur-

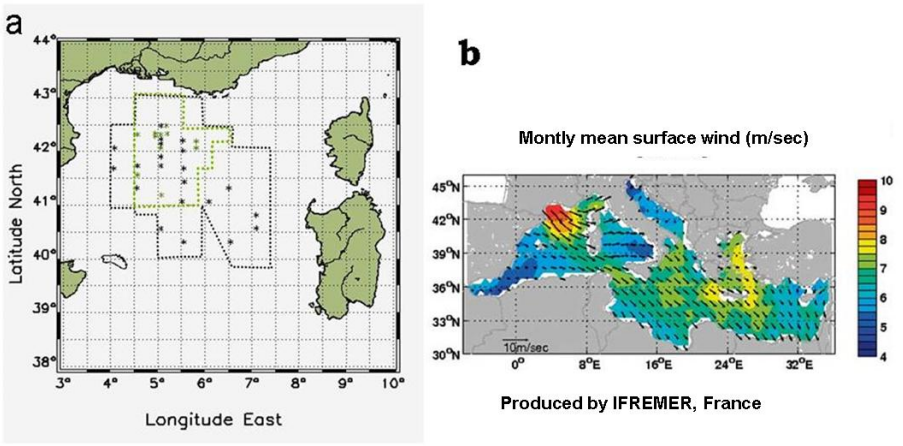

Figure 6: Map of observed convection sites (a). Black (green) polygons and stars respectively indicate the sampled area and the stations in which convection residual water columns were observed in NORBAL 1 (NORBAL 4 and 5) (b) Monthly mean surface wind ($\mathrm{m{\cdot}sec^{-1}}$; from http://www.ifremer.fr).

rent and possibly from the contribution of the Rhone river. The σ_θ and ν distributions (Figure 8C, 8D) show the isopycnal doming peaked at sta. 90, where a convection site is located as seen in Figure 5, the westward Northern Current to the north and the eastward flow of the waters south of the NBF. An small anticyclonic region at the of center of the transect (sta. 91-93, Figure 8D) together with warmer and saltier surface waters (Figure 8A, 8B) likely indicates a mesoscale eddy or NBF meander towards the MEDOC gyre center. The nutrient distribution (Figure 8E-8F) matches the other properties' pattern and is characterized by NO_3 = 0.49-4.04 $\mu\mathrm{mol{\cdot}dm^{-3}}$, PO_4 = 0.04-0.23 $\mu\mathrm{mol{\cdot}dm^{-3}}$, $SiOH_4$ = 0.72-3.0 $\mu\mathrm{mol{\cdot}dm^{-3}}$ (not shown here, same distribution as NO_3) that increase significantly between 50 and 150 m to (i.e. to NO_3 = 4.04-6.25 $\mu\mathrm{mol{\cdot}dm^{-3}}$, PO_4 = 0.23-0.41 $\mu\mathrm{mol{\cdot}dm^{-3}}$, $SiOH_4$ = 3.0-5.55 $\mu\mathrm{mol{\cdot}dm^{-3}}$).

The nutricline depth is approximately 50 m, typical of the MEDOC area, except for st. 92 where it is at the surface. The *chl* pattern (Figure 8G) indicates a surface bloom to the north (1.69-4.05 $\mathrm{mg{\cdot}m^{-3}}$) and a 40-50 deep DCM regime to the south (1.69 $\mathrm{mg{\cdot}m^{-3}}$) with sta. 92 being the separation point of the two regimes. The surfacing of the nutricline at sta. 90 therefore possibly indicates production scarcity at this separation point. The highest *chl* concentrations are found at stas. 90-91 close to the deep convection site (Figure 5). This bloom and the DCM are in the upper 40 m where values of *R* (14.13, Figure 8H) are closest to system equilibrium, indicating active productivity.

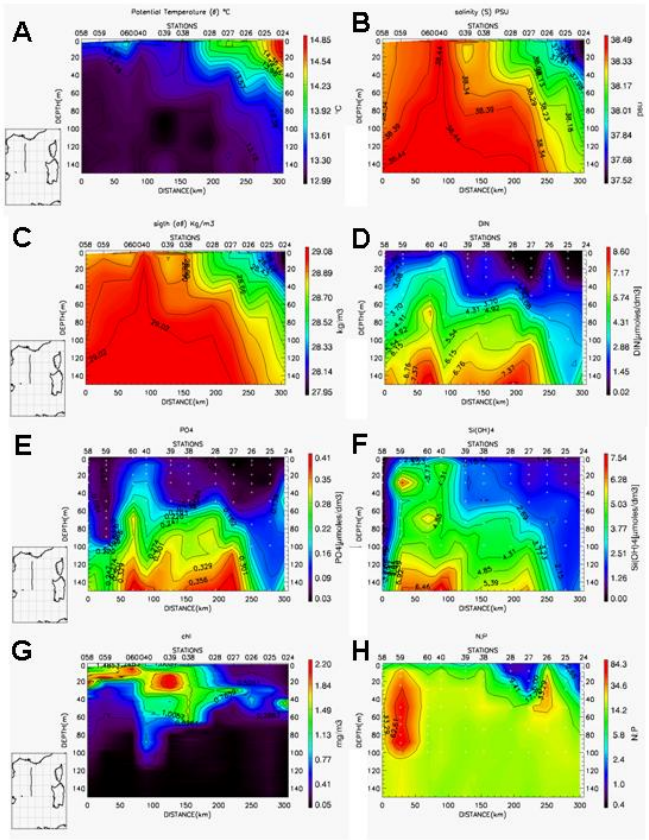

Figure 7: NORBAL 1, Transect 58-24, upper 150 m; (A) θ, (B) S, (C) σ_θ, (D) DIN, (E) PO_4, (F) $SiOH_4$, (G) *chl*, (H) Redfield ratio_R = N:P. The left side of each section corresponds to the northernmost part of the transect.

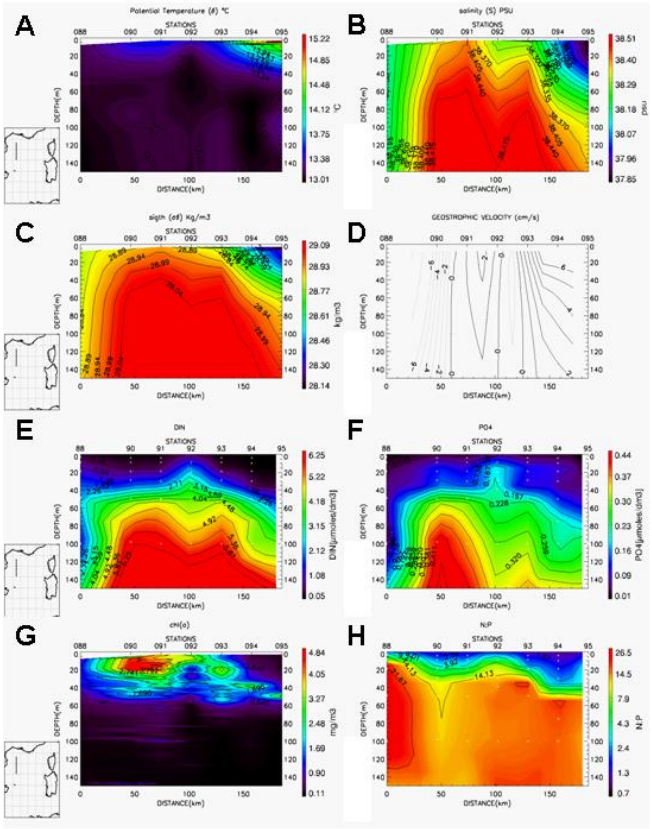

Figure 8: NORBAL 4 Transect 88-95 (0-150 m); (A) θ, (B) S, (C) σ_θ, (D) ν, (E) DIN, (F) PO_4, (G) *chl*, (H) R = N:P. The left side of each section corresponds to the northernmost part of the transect.

4 Summary and conclusions

This work is the initial step of a study of the physical-biological interactions in the MEDOC spring bloom, the Mediterranean Sea's most extensive algal bloom, as inferred by chlorophyll SeaWiFS satellite imagery and the five NORBAL project cruises onboard R/V Urania, organized by CNR-ISAC in the 2000-2003 period.

SeaWiFS data (1998-2001) show that deep water formation events are detectable in the satellite chlorophyll images as a low-*chl* mixed patch in February, because of plankton dilution in the entire water column. The images show that separate blooms occur in the MEDOC area and the Ligurian Sea between the end of February and the first days in March, and later join into a single extended bloom covering both sites. There is an evident correspondence between the end of deep water formation and the onset of the bloom, in agreement with numerous modelling studies [28, 29, 30, 31, 14, 15, 24]. In contrast, there are some discrepancies with the analysis performed by Morel and André [23], mainly in the timing of the event. Indeed, these authors indicate mid-March as the end of the convection period and mid-April as the beginning of the bloom, with a month's interval between the two phenomena. The SeaWiFS images show no such time interval these discrepancies could be either due to the excessive smoothing in the time averaged images used by Morel and André [23], or in a substantial change in the physical-biogeochemical conditions of the area since the 90's.

High interannual variability is seen in bloom evolution and strength and investigation using atmospheric forcing data is planned, to determine the role of air-sea interaction in modulating bloom characteristics. Also, the reasons for the length of the bloom have to be experimentally more accurately pinpointed, given the number of complex vertical mixing phenomena participating to primary production variability evidenced by the modelling effort of Lévy et al. [24]. The NORBAL spring 2000 and 2003 cruise data clearly show local convection sites of WMDW formation and that newly formed WMDW is differentiated in a warmer and saltier type probably formed in the MEDOC offshore center and a colder and fresher type, possibly formed on the Gulf of Lions shelf and reaching the bottom via the shelf break canyons, as proposed by Bethoux et al. [27]. The data also reveal the presence of a convection-like structure in the Sardinian Sea; however, its anticyclonic dynamics suggests that this may be a Subsurface Coherent Vortex (SCV) [26] migrating southeastward from the MEDOC area. The post-convection restratification and recapping processes are also evident from the observed warmer surface waters and the confinement of the convective columns to the deep layer, while the LIW layer is still interrupted by the presence of the latter columns. Finally, the observed convective column locations agree well with the spatial distribution of the strongest northeasterly winds in the area.

In situ chlorophyll data indicate that algal biomass forms a surface bloom in the MEDOC area, while a Deep Chlorophyll Maximum (DCM) regime dominates to the south, in the North Balearic Front area. Higher *chl* concentrations, nutrient and Redfield ratio R distributions suggest high and active primary production in the surface bloom and declining production in the southern DCM regime. Also, a thin surface

secondary bloom is seen offshore of the Rhone river delta, possibly connected to the latter's nutrient input. An investigation is planned in which plankton species will be analyzed, so as to determine the nature of this secondary bloom. Chlorophyll vertical distribution is evidently conditioned by frontal structures and mesoscale features: the waters south of the NBF or intruding into the MEDOC gyre area are always oligotrophic, thus confirming modulation of phytoplankton distribution by mesoscale dynamics ([24]and references therein). In other words, the NBF waters seem to be a barrier for the biomass and the DCM regime observed south of the area is interpretable as a vertical depression of the surface bloom by NBF waters.
Nutrient (DIN, PO_4 and $SiOH_4$) values are coherent with former observations [32, 33] and confirm the higher concentrations of the deep nutrient pool (150 m-bottom) in the Western Mediterranean Sea with respect to the Levantine basin. Nutricline depth is always greater than that of the biomass indicating nutrient consumption in the surface layer. Redfield ratios in the pool are about 20, indicating phosphorus limitation. R values in the surface bloom are closer to equilibrium values ($R \leq 16$), suggesting active production. On the other hand the DCM regime to the south has lower R values ($2 < R < 4$) indicating productivity decline.

5 Acknowledgments

We thank Drs. F. D'Ortenzio, D. Iudicone (SZN-OCE, Naples, Italy) and Cristophe Brunet (SZN-OCE, Naples) for the essential contribution in data analysis, Dr. V. Saggiomo (SZN-MECA, Naples) for providing the in situ chlorophyll data, Drs. V. Ibello, and G. Civitarese of OGS (Trieste, Italy) for providing the in situ nutrient data. All of the above are also thanked for the organization of and participation in the NORBAL project and cruises, together with the R/V Urania crew and technicians.

References

[1] M. Kaennel. Biodiversity: a diversity in definition. pages 71–81, 1997.

[2] J.L. Innes and B. Kock. Forest biodiversity and its assessment by remote sensing. *Global Ecol. Biogeogr. Lett.*, 7:397–419, 1998.

[3] A.J. Watson, C. Robinson, J.E. Robinson, P.J. Le B. Williams, and M.J.R. Fasham. Spatial variability in the sink for atmospheric carbon dioxide in the North Atlantic. *Nature*, 350:50–53, 1991.

[4] A.R. Robinson, D.J. McGillicuddy, J. Calman, H.W. Ducklow, M.J.R. Fasham, F.E. Hoge, W.G. Leslie, J.J. McCarthy, S. Podewski, D.L. Porter, G. Saure, and J.A. Yoder. Mesoscale and upper ocean variabilities during the 1989 JGOFS bloom study. *Deep Sea Research II*, 40:9–35, 1993.

[5] J.A. Yoder, J. Aiken, R.N. Swift, F.E.Hoge, and P.M. Stegmann. Spatial variability in near-surface chlorophyll a fuorescence measured by the Airbone Oceanographic Lidar(AOL). *Deep Sea Research II*, 40:33–53, 1993.

[6] D. Antoine, A. Morel, and J.M. André. Algal Pigment Distribution and Primary Production in the Eastern Mediterranean as Derived from Coastal Zone Color Scanner Observations. *Journal of Geophysical Research-Oceans*, 100(C8):16193–209, 1995.

[7] J.C. Gascard. Mediterranean deep water formation, baroclinic eddies and ocean eddies. *Oceanologica Acta*, 1:313–315, 1978.

[8] MEDOC-Group. Observation of formation of deep water in the Mediterranean Sea. *Nature*, 227:1037–1040, 1970.

[9] M. Crépon, M. Boukthir, B. Barnier, and F. Aikman. Horizontal ocean circulation forced by deep-water formation. Part 1: An analytical study. *Journal of Physical Oceanography*, 9:1781–1793, 1989.

[10] P.D. Killworth. The mixing and spreading phases of MEDOC. *Progress in Oceanography*, 7:59–90, 1976.

[11] G.A. Riley. The relationship of vertical turbulence and spring diatom flowerings. *Journal of Marine Research*, 5:67–87, 1942.

[12] H.U. Sverdrup. On Conditions for the Vernal Blooming of Phytoplankton. *Journal of Cons. Int. Explor. Mer.*, 18:287–295, 1953.

[13] G. Madec, F. Lott, P. Delecluse, and M. Crepon. Large-scale preconditioning of deep-water formation in the northwestern Mediterranean Sea. *Journal of Physical Oceanography*, 26:1393–1408, 1996.

[14] M. Lévy, M. Visbeck, and N. Naik. Sensitivity of primary production to different eddy parameterizations: A case study of the spring bloom development in the northwestern Mediterranean Sea. *Journal of Marine Research*, 57(3):427–448, 1999a.

[15] M. Lévy, L. Mémery, and G. Madec. The onset of the Spring Bloom in the MEDOC area: mesoscale spatial variability. *Deep-Sea Research Part I-Oceanographic Research Papers*, 46(7):1137–1160, 1999b.

[16] P.G. Falkowski and J.O. Matthew. Mix and match: how climate selects phytoplankton. *Nature Reviews Microbiology*, 5:813–819, 2007.

[17] G. Volpe, R. Santoleri, V. Vellucci, M. Ribera d'Alcalà, S. Marullo, and F. D'Ortenzio. The colour of the Mediterranean Sea: global versus regional bio-optical algorithms evaluation and implication for satellite chlorophyll estimates. *Remote Sensing of Environment*, 107:625–638, 2006.

[18] A. Bricaud, E. Bosc, and D. Antoine. Algal biomass and sea surface temperature in the Mediterranean Basin - Intercomparison of data from various satellite sensors, and implications for primary production estimates. *Remote Sensing of Environment*, 81(2-3):163–178, 2002.

[19] H. Claustre, A. Morel, S.B. Hooker, M. Babin, D. Antoine, K. Oubelkheir, A. Bricaud, K. Leblanc, B. Queguiner, and S. Maritorena. Is desert dust making oligotrophic waters greener? *Geophysical Research Letters*, 29(10):1469, 2002.

[20] F. D'Ortenzio, S. Marullo, M. Ragni, M. Ribera d'Alcalà, and R. Santoleri. Validation of empirical SeaWiFS algorithms for chlorophyll- alpha retrieval in the Mediterranean Sea - A case study for oligotrophic seas. *Remote Sensing of Environment*, 82(1):79–94, 2002.

[21] W.W. Gregg and N.W. Casey. Global and regional evaluation of the SeaWiFS chlorophyll data set. *Remote Sensing of Environment*, 93(4):463–479, 2004.

[22] K.D. Leaman and F. Schott. Hydrographic structure of the convection regime in the Gulf of Lions: Winter 1987. *Journal Of Physical Oceanography*, 21:573–596, 1991.

[23] A. Morel and J.M. André. Pigment Distribution and Primary Production in the Western Mediterranean as Derived and Modelled from Coastal Zone Color Scanner Observations. *Journal of Geophysical Research-Oceans*, 96(C7):12685–698, 1991.

[24] M. Lévy, L. Mémery, and G. Madec. Combined effects of mesoscale processes and atmospheric high-frequency variability on the spring bloom in the MEDOC area. *Deep-Sea Research Part I-Oceanographic Research Papers*, 47(1):27–53, 2000.

[25] C. Millot. Circulation in the Western Mediterranean Sea. *Journal of Marine Systems*, 20:423–442, 1999.

[26] P. Testor and J.C. Gascard. Post-convection spreading phase in the North western Mediterranean Sea. *Deep-Sea Research I*, 53:869–893, 2006.

[27] J.P. Béthoux, X. Durieu de Madron, F. Nyffeler, and D.Tailliez. Deep water in the western Mediterranean: peculiar 1999 and 2000 characteristics, shelf formation hypothesis, variability since 1970 and geochemical inferences. *Journal of Marine Systems*, 33:117–131, 2002a.

[28] M. H. Tusseau, C. Lancelot, J. M. Martin, and B. Tassin. 1-D coupled physical-biological model of the northwestern Mediterranean Sea. *Deep-Sea Research Part Ii-Topical Studies in Oceanography*, 44(3-4):851–880, 1997.

[29] M. Lévy, L. Mémery, and J.M. André. Simulation of primary production and export fluxes in the Northwestern Mediterranean Sea. *Journal of Marine Research*, 56(1):197–238, 1998a.

[30] M. Lévy, M., Mémery, L. Madec, and G. Madec. The onset of a bloom after deep winter convection in the northwestern Mediterranean Sea: mesoscale process study with a primitive equation model. *Journal of Marine Systems*, 16(1-2):7–21, 1998b.

[31] M. H. Tusseau-Vuillemin, L. Mortier, and C. Herbaut. Modeling nitrate fluxes in an open coastal environment (Gulf of Lions): Transport versus biogeochemical processes. *Journal of Geophysical Research-Oceans*, 103(C4):7693–7708, 1998.

[32] J.P. Béthoux, P. Morin, and D.P. Ruiz-Pino. Temporal trends in nutrient ratio: chemical evidence of Mediterranean ecosystem change driven by human activity. *Deep sea Research II*, 49:2007–2016, 2002b.

[33] M. Ribera d'Alcalà, G. Civitarese, F. Conversano, and R. Lavezza. Nutrient ratios and fluxes hint at Mediterranean Sea. *Journal of Geophysical Research*, 108(C9):16, 2003.

Climate Change and the Marine Habitat in the Polar Regions

C. Verde, D. Giordano, R. Russo, G. di Prisco
Institute of Protein Biochemistry, CNR, Napoli, Italy
c.verde@ibp.cnr.it

Abstract

The polar regions are instrumental parts of the Earth system. The largest challenge facing humankind is the management of the Earth system to ensure a sustainable human future in the context of natural and anthropogenic changes. Climate change is having a major impact on marine and terrestrial systems and will therefore influence biodiversity. All regions are undergoing environmental changes, to nature and man. This awareness is spreading within the public opinion, despite resistance from commercial interests. Global Warming appears to be the master driver of changes, and produces effects on physiology and ecology. Compared to temperate and tropical latitudes, warming has stronger impacts in the Arctic, but Antarctica, which has a decisive role in driving the world's climate, is not spared. The Western Peninsula is undergoing one of the fastest changes on the planet. Predictions of the physiological costs and evolutionary consequences of global warming are strictly dependent on the knowledge gained on the structure/function of polar ecosystems. Thus, ongoing change is generating growing interest in polar organisms and their evolution at cold temperatures. In this contribution, our purpose is manifold. Firstly, international research will be described, with the EBA programme and the ACCE report. Secondly, the consequences on Biodiversity produced by Global Warming will be discussed. Finally, our recent results on adaptations will be summarised.

1 The scenario for international research

1.1 EBA: Evolution and Biodiversity in the Antarctic - The Response of Life to Change ("Describe the past, understand the present and predict the future")

Environmental changes drive evolution. The polar regions offer an immensely valuable, regionally focussed model for studying the biological response to climate change. Small temperature changes may have great impacts on the physiology of organisms as well as on the extent of sea ice, hence on the life history and biology of many species. Many organisms are susceptible to current temperature changes, and those of the marine environment are particularly vulnerable (even though warming is more evident in the air than in the sea), because of their stenothermal nature, which (especially in the Antarctic) allows a small window of tolerable temperatures. Changes will continue to influence biodiversity. The Scientific Committee on Antarctic Research (SCAR) has three Sci-

entific Groups, on Life Sciences, Physical Sciences and GeoSciences. SCAR endorses five Programmes, namely Evolution and Biodiversity in the Antarctic - The Response of Life to Change (EBA, Life Sciences), Antarctica and the Global Climate System (AGCS, Physical Sciences), Antarctic Climate Evolution (ACE, Earth Sciences), Subglacial Antarctic Lake Environments (SALE, cross-disciplinary), and Interhemispheric Conjugacy Effects in Solar-Terrestrial and Aeronomy Research (ICESTAR, Physical Sciences). The polar regions are instrumental parts of the Earth System. The study of their biotic history is intimately linked to climate and tectonic history, an essential feature because of the intimate interconnection between the living and abiotic environments. Consequently, SCAR is pursuing cross-linkages among the three Groups. EBA, co-chaired by G di Prisco and P Convey (UK), was launched in 2004. It aims at understanding the role of biodiversity in the Earth System by providing the Antarctic context. It assembles the whole world's Antarctic biological community. Its role in addressing climate change is to provide the best estimate possible of the possible consequences of continued environmental change. Revealing the response of species adapted to extreme conditions allows extrapolation of analyses to lower latitudes. It is a reference item for funding agencies and decision makers, consolidates the community, and establishes linkages/dialogue with funding agencies and other stakeholders, including industry, companies, science associations and other projects/programmes. In view of the importance of both polar regions in climate change, EBA includes the Arctic. Some Arctic Programmes of the International Polar Year (IPY, 2007-2009), e.g. Marine Fishes of NE Greenland (TUNU-MAFIG), Svalbard Research Base (SVALBASE), Arctic Marine Ecosystems Research Network (ARCTOS), are linked to EBA. The Arctic (together with the Sub-Antarctic) is less extreme than isolated Antarctica. Its climate exhibits spatial and temporal variability, leading to regional differences in ecological and climatic features, which are intermediate between polar and temperate latitudes. The Arctic is undergoing massive changes associated with progressive and fast decrease of sea and land ice, with ecological and socio-economic implications. The response of Arctic species to global warming provides additional information to analyse and foresee the impact of changes at lower latitudes. The International Polar Year (2007-2008) has seen a worldwide science effort. Its life span has included the major IPY scientific activities. Some 620 EBA scientists participated in IPY. EBA is an overarching umbrella. It provides advise to the Antarctic Treaty Consultative Meetings (ATCM) and the Commission for the Conservation of Antarctic Marine Living Resources (CCAMLR). It has close links with other international SCAR/IPY programmes, e.g. Census of Antarctic Marine Life (CAML), Antarctic Benthic Deep-Sea Biodiversity-System Coupling (ANDEEP-SYSTCO), International Collaborative Expedition to Collect and Study Fish Indigenous to Sub-Antarctic Habitats (ICEFISH, led by C Verde), Marine Biodiversity Information Network (MarBIN), Microbiological and Ecological Responses to Global Environmental Changes in Polar Regions (MERGE), and many other. The cooperative and cross-disciplinary ongoing research of EBA is a long-range IPY legacy. EBA is establishing contact with the general public (Outreach and Education). It places information sources into an accessi-

ble format (www.scar.org), connecting research with the public domain, including the educational sectors, and building on existing (but often inaccessible) information. It encourages training of PhD students and postgraduates, and promotes web sites, media coverage, publications, conference proceedings, input to databases. Dissemination encourages involvement of the public opinion by establishing an interface to the public and private sectors to enable understanding and acceptance of Antarctic science. EBA will end in 2013. The EBA community began discussing its future, and the next SCAR Open Science Conference (2010) will be a forum for selecting future pathways.

1.2 Antarctic Climate Change and the Environment (ACCE)

The first comprehensive review of the state of Antarctica's climate and its relationship to the global climate system was published on December 1st, 2009, by SCAR (www.scar.org). It offers the latest research from the icy continent, identifies areas for future scientific research, and addresses the urgent questions that policy makers have about Antarctic melting, sea-level rise and biodiversity. It represents the Antarctic counterpart of the recently published report [1] Arctic Climate Impact Assessment (ACIA). ACCE and ACIA make constant reference to the Intergovernmental Panel on Climate Change (IPCC). Based on the latest evidence from 100 world-leading scientists from many countries, the review focusses on the consequences of rapid warming of the Antarctic Peninsula and the Southern Ocean; rapid ice loss in parts of Antarctica and increase in sea ice around the continent; impact of climate change on Antarctica's plants and animals; unprecedented increase in carbon dioxide levels; connections between human-induced global change and natural variability and the extraordinary finding that the ozone hole has shielded most of Antarctica from global warming. A summary of ACCE has been published [2]. According to Colin Summerhayes, Executive Director of SCAR, "Antarctica is an unrivalled source of information about our planet. ACCE describes what we know now and illustrates how human activity is driving rapid climate change. By integrating this multidisciplinary evidence into a single source we will help scientists and policy makers understand the distinction between environmental changes linked to the Earth's natural cycles, and those that are human induced. The work is particularly important because it puts Antarctic climate change into context and reveals the impact on the rest of the planet." John Turner of the British Antarctic Survey is the Lead Editor of the review: "For me the most astonishing evidence is the way that one man-made environmental impact - the ozone hole - has shielded most of Antarctica from another - global warming. Understanding the complexities surrounding these issues is a challenge for scientists - and communicating these in a meaningful way to society and to policy makers is essential. There is no doubt that our world is changing and human activity is accelerating global change. This review is a major step forward in making sure that the latest and best evidence is available in one place. It sets the scene for future Antarctic Research and provides the knowledge that we all need to help us live with environmental change." The Editorial Committee of ACCE is as follows (Fig-

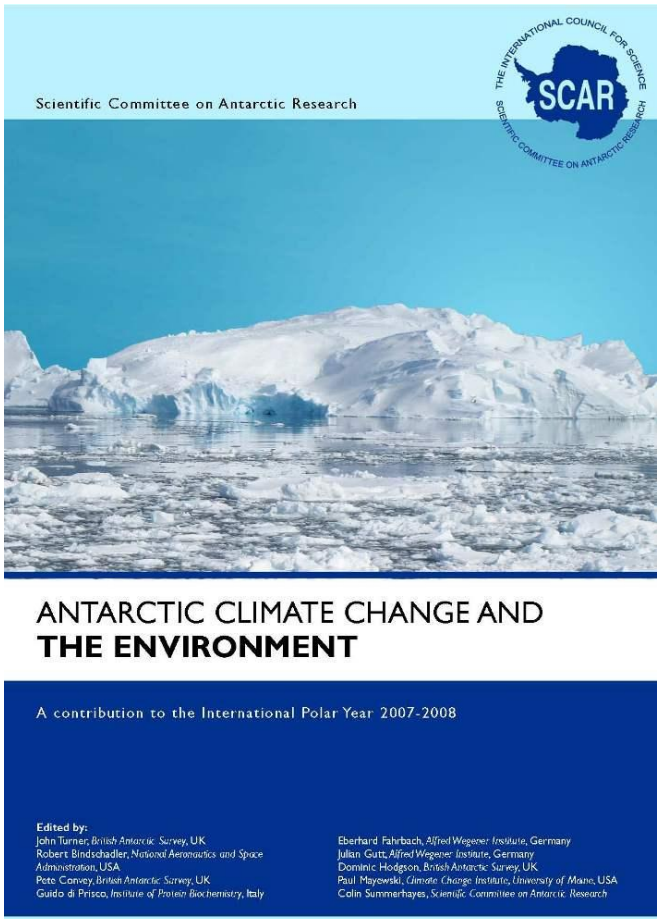

Figure 1: Cover of the ACCE Report.

ure 1): Robert Bindschadler, NASA, USA; Peter Convey, British Antarctic Survey (BAS), Cambridge, UK; Guido di Prisco, Institute of Protein Biochemistry, CNR, Naples, Italy; Eberhard Fahrbach, Alfred Wegener Institute (AWI), Germany; Julian Gutt, AWI, Germany; Dominic Hodgson, BAS, Cambridge, UK; Paul Mayewski, University of Maine, USA; Colin Summerhayes, Executive Director, SCAR, Scott Polar Research Institute, Cambridge, UK; John Turner, BAS, Cambridge, UK. ACCE draws together important information from different disciplines (such as meteorology, glaciology and biology) and therefore different aspects of the global climate system. The key findings from the review are highlighted in 85 key points. In summary:

- Hole in ozone layer shields most of Antarctica from global warming
- Warming of the Southern Ocean will cause ecosystem changes

- Plant communities across the Antarctic Peninsula are rapidly increasing
- Rapid ice loss in parts of the Antarctic
- Increase in sea ice around the Antarctic
- CO_2 levels increase at fastest pace in 800,000 years
- Sea-ice loss directly affects krill levels and penguin colonisation
- Antarctica is predicted to warm by around 3°C over this century
- West Antarctic ice loss could contribute to 1.4-m sea level rise
- Improved modelling is required for accurate predictions

1.3 The Role of Biodiversity: Threats by Climate Change

1.3.1 Biodiversity

The largest challenge facing humankind is the management of the Earth System to ensure a sustainable human future in the context of natural and anthropogenic changes. Human health is closely connected to the health of Earth, hence to changes in the environment. The concept of "sustainable world" is strongly linked to the concept of "biodiversity". All life becomes possible because biodiversity makes the planet what it is. Biodiversity (Figure 2) refers to the diversity of genes, individuals, species, and habitats on Earth, as well as - above all - their interconnections and relationships. Climate change is impacting marine and terrestrial systems, influencing biodiversity. All regions are undergoing environmental changes, often due to the combined effects of nature and man. The anthropogenic impact (e.g. accelerated global warming, increased levels of UVB due to ozone depletion, uncontrolled fishing) is crucial in accelerating/causing environmental change. Despite resistance due to commercial interests, this awareness is steadily spreading within the world public opinion. Present patterns of biodiversity and distribution are a consequence of factors and processes working on both evolutionary and ecological timescales. Global warming appears to be the master driver of changes, producing effects on the physiology and ecology of many species.

1.3.2 The "polar amplification"

The urge to investigate biodiversity at high latitudes is increasing. Compared to temperate and tropical latitudes, warming is having stronger impacts in the Arctic. Antarctica, known to have a decisive role in driving the world's climatic features, is also not spared. The ozone hole generates contradictory trends, but the western side of the Antarctic Peninsula is undergoing one of the fastest rates of change on the planet. Large reduction of annual sea ice causes disappearance of key fish species of the trophic web, whose reproduction processes, being closely associated to sea ice, are upset. Thus, in both polar environments, changes have complex and interacting effects. In fact, an impact on the lowest or highest level in a food web can propagate through to affect other taxa. For example, the progressive disappearance of sea ice in the Arctic will eventually lead to extinction of the polar bear. A "polar amplification" of the anthropogenic warming has been predicted and is supported by accelerations of glacier retreat, sea-ice thinning and permafrost degradation. The vulnerability of species does raise the possibility of a major extinction event in the near future, brought about by strong acceleration of climate change due to human influence. Debates are under way to urgently launch new policies aimed at reducing the human im-

Figure 2: Representation of biodiversity.

pact. The awareness of global warming has prompted scientists and governments to seriously consider the risk of extinction of marine species depending on sea ice. Such an event may be averted only by resorting to concerted, multidisciplinary, international programmes aimed at understanding life processes, evolution and adaptations, and finally protecting polar life. EBA (see above) is such a programme. It aims at gaining knowledge of the ways in which evolution has driven (and is driving) life, and of how life is likely to change. It is the only programme having this major goal, and is endowed with the relevant human resources, expertise, and capability. Besides the need to tackle these questions in all biological fields, integration with programmes investigating climate and tectonic history are essential because intimate feedback between the living and abiotic environments have modulated both. Among the ecological factors controlling distribution patterns and biodiversity of the modern Antarctic biota, the most important are temperature, water availability in the terrestrial ecosystems, and ice cover, oxygen, light, UVB and wind in the marine systems. EBA is investigating all of these aspects, providing information on the resistance and recoverability of Antarctic communities. Many of these arguments also apply to Arctic marine biodiversity. It would be useful to develop an overarching programme also in the North. The evolution of polar organisms has taken million of years to build cold adaptations suitable to allow survival and reproduction during gradual establishment of the current extreme conditions. Hence, insights on the ability of cold-adapted organisms and communities to cope with changes is likely to

provide useful information for analysing changes at lower (our) latitudes.

2 Evolutionary adaptations of marine organisms

Understanding molecular adaptations in response to cooling is essential, because temperature affects the kinetic energy of molecules, it modifies molecular interactions, macromolecular stability/functioning and membrane features. This section discusses some adaptations evolved by fish and bacteria in response to cold. The central role of O_2 and oxidative stress in regulating adaptive responses is also highlighted. Variation in environmental O_2 availability has played an important role in the evolution of polar marine organisms, as suggested by the physiological and biochemical strategies adopted by these organisms to acquire, deliver and scavenge O_2. Why use fishes and bacteria for studying environmental adaptations? The complexity of multicellular animals such as fishes allows addressing physiological mechanisms at multiple levels of biological organisation, from molecules to whole organism, including responses to climate changes. However, the most significant constraint to research on polar fish is the lack of genomic-sequence data. This is not a major problem for microorganisms and their small genomes. The possibility to sequence whole bacterial genomes may provide the necessary data for understanding protein thermal adaptation. Thanks to short generation times, bacteria are often used to study the combination of physiological responses, genetic variation and ability to evolve, since the responses of multiple generations to selective forces (e.g. environmental conditions) can be followed relatively easily and rapidly in selection experiments.

2.1 Molecular adaptations in Antarctic fish

In extreme polar marine environments, one of the most important driving force in the evolutionary adaptations is the enhanced O_2 solubility [3]. These environmental conditions may cause the production of high levels of reactive O_2 species (ROS), able to oxidise proteins, DNA and lipids and leading to injury of cellular components and cell death. The dominance of notothenioid fishes is the result of evolutionary biological responses to the advent of the extreme conditions of the southern ocean. Living in a stable, extremely cold, and well-oxygenated marine environment, this group has evolved adaptations in biochemical/physiological functions, several of which are unique. Specialised hematological features are striking adaptations developed by the ichthyofauna during evolution at low temperature. Red-blooded notothenioids differ from temperate and tropical species in having fewer erythrocytes and reduced hemoglobin (Hb) concentration and multiplicity [4]. The blood of the 16 "icefish" species of Channichthyidae, the most phyletically derived family, lacks Hb . The increased solubility of O_2 in water allows icefish to transport sufficient O_2 in physical solution rather than by a specific O_2 carrier; this feature would be deleterious, if not lethal, in warmer waters. These fish cope with the lack of an O_2 carrier with increased blood volume and higher cardiac output; they have large gills, and highly vascularised, scale-

Figure 3: Neuroglobin in the brain of icefish (*Pagetopsis macropterus*). In the picture it is reported the structure of mouse neuroglobin (PDB ID: 1Q1F).

less skin, which favours cutaneous respiration. The recent discovery of the neuroglobin (Ngb) gene in the brain of red-blooded notothenioids and in at least 13 of the 16 icefish species (Figure 3) suggests a crucial biological function of Ngb [5, 6, 7]. The finding that icefish retain the Ngb gene despite having lost Hb, and myoglobin in most species, may have important implications in the physiology and pathology of the brain. Ngb, a monomeric heme-containing globin, expressed in retinal neurons and fibroblast-like cells, is able to bind O_2 and NO [8, 9, 10]. Although a number of hypotheses have been produced, its functional role is still uncertain. There is no doubt that Ngb has an essential, conserved function, is beneficial to neurons [8]) and supplies O_2 to the retina, similar to myoglobin in the myocardium and skeletal muscle. One of the most important physiological function attributed to Ngb is the ability to neutralise the neurotoxic effects of ROS [11] and reactive nitrogen species. In an extreme O_2-rich environment, this neuroprotective role has potential implications in our understanding of the function of this protein and suggests future avenues of investigation.

2.2 Molecular adaptation of the Antarctic bacterium *Pseudoalteromonas haloplanktis* TAC125

Cold-adapted bacteria are generally acknowledged to adopt adaptive strategies to maintain activity and metabolic function despite challenging conditions. Best performances are made possible by peculiar features which altogether lead to higher flexibility of key parts of the molecular structure of many proteins. The genome sequence and annotation of the psychrophilic Antarctic bacterium *Pseudoalteromonas haloplanktis* TAC125 [12], isolated in coastal sea water near the French station Dumont d'Urville (Terre Adélie), provides a unique opportunity to explore the strate-

gies adopted by cold adapted bacteria to cope with cold and high-O_2 concentration. Cold-adapted bacteria have developed programmed responses to strong oxidative stress. The genome sequence of *P. haloplanktis* TAC125 reveals that the bacterium copes with increased O_2 solubility by enhancing production of O_2-scavenging enzymes and deleting entire metabolic pathways, e.g. those which generate ROS as side products. The deletion of the ubiquitous molybdopterin-dependent metabolism in the *P. haloplanktis* TAC125 genome and the number of proteins involved in scavenging chemical groups can be seen in this perspective. A further sign, which may be related to the features of the Antarctic habitat, is the synthesis of bacterial Hbs and flavoHbs, versatile proteins serving several biological functions. These Hbs fulfil important physiological roles, including protecting the cell from nitrosative and oxidative stress and delivering O_2 to respiring cells. Multiple genes encoding 2-on-2 (2/2) Hbs and one for flavoHb have been discovered in the genome of *P. haloplanktis* TAC125 [12, 13], suggesting that specific and different functions may be associated to these two classes of proteins [13]. Similar to Antarctic fish Hbs and Ngb, the *P. haloplanktis* TAC125 recombinant 2/2Hb [13] shows predominance of a hexacoordinated form in ferric and ferrous Hbs [7]. The physiological role of hexacoordinated Hbs is not well understood, even in these monomeric Hbs, and several roles have been suggested. Probably, the finding of hexacoordination in monomeric and tetrameric cold-adapted Hbs suggests a common physiological mechanism for protecting cells against oxidation due to high O_2 concentration. In the genome of *P. haloplanktis* TAC125, besides the hexacoordinated 2/2Hb gene, there is also a gene encoding for a flavoHb, a protein with the heme-containing O_2-binding domain, and a FAD-containing reductase domain, involved in detoxification of NO. The presence of 2/2Hb and flavoHb genes in *P. haloplanktis* TAC125 raises the questions on the structural and functional features evolved (in comparison with their mesophilic counterparts) in response to thermal adaptation and the ability to cope with extreme environments.

2.3 Arctic fishes and climate change

Studies on the vulnerability of Arctic fishes are timely and important. Parallel to global warming and the ongoing and indisputable decrease of sea ice, human-induced stresses rapidly increase into hitherto pristine and little studied parts of the Arctic ocean. Observations and model simulations of surface air temperature indicate that the nature of the current warming is distinct from the earlier warm period, suggesting that the former is linked to anthropic factors [1]. While wholesale extinctions of entire Arctic species are unlikely, some fish may possibly become geographically or ecologically marginalised [14]. Hence, many high-latitude species are currently at their physiological limits and likely to be very sensitive to future shifts in climate. These constraints could be compensated evolving adequate genotypes, but this step is probably too slow for long-lived species. Thus, climate change will favour species with wide thermal windows and with a range of genotypes [15]. Arctic fishes are important because: (i) they are taxonomically complex, (ii) they are believed to be extremely temperature sensitive, (iii) they constitute

the key-link in the food chain between the lower trophic levels and the apex predators, (iv) they are believed to grow and reproduce slowly (e.g. prolonged generation span) and may be particularly vulnerable to harvesting, and (v) they have evolved an array of unique physiological and biochemical mechanisms to sustain low temperatures, thus being very useful for comparison with Antarctic fishes. The polar cod (*B. saida*, family Gadidae) is a key species in the Arctic food chain, spends much time associated with sea ice and lives in Arctic waters throughout its life cycle. It displays physiological and biochemical cold adaptations [16, 17, 3]. Other cods found in the Arctic include Atlantic cod, Pacific cod, Greenland cod, and Arctic cod (*Arctogadus glacialis*). The Atlantic cod (*G. morhua*) is the most abundant species in the North Atlantic. The polar and Arctic cods have already shifted their distribution northwards, presumably in response to water warming. The ongoing northward shifts of Atlantic stocks probably involve direct warming impacts on cod, linked to thermal windows, and indirect food-web effects [15]. Unlike Antarctic notothenioids, Arctic gadidis display Hb multiplicity, a sign of phylogenetic and molecular adaptation. For the Arctic ichthyofauna, it may be advantageous to maintain multiplicity, considering the need to adapt to a much more variable environment than the Antarctic one, whose conditions, including lower temperatures, are highly stable because of isolation caused by the Antarctic Polar Front. The different selective pressures on Arctic and Antarctic Hb genes depend on the respective habitats, and correlation with environmental conditions may have had a driving role [3, 17]. Studies suggest that the optimal temperature for cod growth decreases with size and age and that the specific effects of temperature are also dependent on the Hb genotype [18].

3 Conclusions

An important outcome of the Arctic-Antarctic comparison shows that, under the constant Antarctic conditions, teleost phylogeny in fish globins (zoarcoids with notothenioids, gadids as sister-group to both) is recovered in the phylogenetic trees. In contrast, although the alpha-globin tree mostly recovers the Arctic species tree, gadid beta globins show high sequence variation, interpreted as an effect of the perturbation of the available mutational space in these sequences, possibly due to the variability of thermal conditions experienced by most Arctic fish, in comparison with the thermal stability in the life style of zoarcoids and notothenioids, that display unperturbed phylogenetic signal [4, 19]. The studies summarised in this contribution are in the framework of climate changes. Any prediction of the physiological costs and evolutionary consequences of global warming is strictly dependent on the knowledge gained on the structure and functioning of polar ecosystems. More importantly, life sciences are not the only area gaining key insights from studying biological communities inhabiting the poles, because organisms, oceans and atmosphere are strongly linked in the polar regions influencing each other in complex pathways. EBA and ACCE contain the general guidelines for the future work of our team.

4 Perspectives

Polar marine organisms are of major interest because they are thought to be amongst

the most vulnerable species to climate change. In all the examples addressed, we imply that the combination of molecular studies at various levels of biological organisation will lead us to an understanding of the evolutionary consequences of global warming. The contemporary challenges to the research community include identifying links between tectonics, climate evolution, and evolution in the Northern and Southern regions. Such approaches are imperative to follow in the coming years to understand adaptation in biology. Ecosystem level responses depend on a cascade of responses from the genomic through cellular to physiological and ecological. Understanding the complexity of this cascade requires a very broad scale cross-disciplinary approach.

References

[1] ACIA. Arctic Climate Impact Assessment. page 1018, 2005.

[2] P. Convey, R. Bindschadler, G. Di Prisco, E. Fahrbach, et al. Antarctic climate change and the environment. *Antarctic Science*, pages 541–563, 2009.

[3] C. Verde, A. Vergara, L. Mazzarella, and G. Di Prisco. The hemoglobins of fishes living at polar latitudes - Current knowledge on structural adaptations in a changing environment. *Current Protein and Peptide Science*, 9:578–590, 2008.

[4] C. Verde, M. Balestrieri, D. De Pascale, D. Pagnozzi, G. Lecointre, and G. Di Prisco. The oxygen-transport system in three species of the boreal fish family Gadidae. Molecular phylogeny of haemoglobin. *Journal of Biological Chemistry*, 281:22073–2208, 2006.

[5] C.H.C. Cheng, G. Di Prisco, and C. Verde. Cold-adapted Antarctic fish: the discovery of neuroglobin in the dominant suborder Notothenioidei. *Gene*, 433:100–101, 2009.

[6] C-H.C. Cheng, G. Di Prisco, and C. Verde. The "icefish paradox". Which is the task of neuroglobin in Antarctic haemoglobin-less icefish? *International Union of Biochemistry and Molecular Biology IUBMB Life*, 60:29–40, 2009.

[7] C. Verde, D. Giordano, R. Russo, A. Riccio, et al. Hemoproteins in the cold. *Marine Genomics*, 2:67–73, 2009.

[8] T. Burmester, B. Weich, S. Reinhardt, and T. Hankeln. A vertebrate globin expressed in the brain. *Nature*, 407:520–523, 2000.

[9] A. Pesce, S. Dewilde, M. Nardini, L. Moens, P. Ascenzi, et al. Human brain neuroglobin structure reveals a distinct mode of controlling oxygen affinity. *Structure*, 11:1087–1095, 2003.

[10] B. Vallone, K. Nienhaus, M. Brunori, and G.U. Nienhaus. The structure of murine neuroglobin: Novel pathways for ligand migration and binding. *Proteins*, 56:85–92, 2004.

[11] M. Brunori, A. Giuffrè, K. Nienhaus, G.U. Nienhaus, et al. Neuroglobin, nitric oxide, and oxygen: functional pathways and conformational changes. *Proceedings of the National Academy of Sciences of the USA*, 102:8483–8488, 2005.

[12] C. Médigue, E. Krin, G. Pascal, V. Barbe, et al. Coping with cold: the genome of the versatile marine Antarctica bacterium Pseudoalteromonas haloplanktis TAC125. *Genome Research*, 15:1325–1335, 2005.

[13] D. Giordano, E. Parrilli, A. Dettaï, R. Russo, G. Barbiero, G. Marino, et al. The truncated hemoglobins in the Antarctic psychrophilic bacterium Pseudoalteromonas haloplanktis TAC125. *Gene*, 398:69–77, 2007.

[14] O.A. Anisimov, D.G. Vaughan, T.V. Callaghan, C. Furgal, et al. Climate Change 2007: impacts, adaptation and vulnerability. Contribution of Working Group II to the Fourth Assessment. Report of the Intergovernmental Panel on Climate Change (IPCC). pages 653–685, 2007.

[15] H.O. Pörtner and A.P. Farrell. Physiology and climate change. *Science*, 322:690–692, 2008.

[16] C. Verde, E. Parisi, and G. Di Prisco. The evolution of thermal adaptation in polar fish. *Gene*, 385:137–145, 2006.

[17] C. Verde, D. Giordano, and G. Di Prisco. The adaptation of polar fishes to climatic changes: structure, function and phylogeny of haemoglobin. *International Union of Biochemistry and Molecular Biology IUBMB Life*, 60:29–40, 2008.

[18] M.F. Petersen and J.F. Steffensen. Preferred temperature of juvenile Atlantic cod Gadus morhua with different haemoglobin genotypes at normoxia and moderate hypoxia. *Journal of Experimental Biology*, 206:359–364, 2003.

[19] A. Dettaï, G. Di Prisco, G. Lecointre, E. Parisi, et al. Inferring evolution of fish proteins: the globin case study. *Methods in Enzymology*, 436:539–570, 2008.

Antarctic Marine Bacteria as Sources of New Cold-Adapted Lipolytic Enzymes with Wide Range of Biotechnological Applications

D. de Pascale, C. De Santi
Institute of Protein Biochemistry, CNR, Napoli, Italy
d.depascale@ibp.cnr.it

Abstract

Micro-organisms that thrive at low temperatures produce cold-adapted enzymes which generally display high catalytic efficiency; these biocatalysts are particularly interesting either for investigating stability/flexibility relationships, or for their quite wide applications. Psychrophilic lipases and esterases from microbial sources have attracted attention because of their increasing use in the organic synthesis of chiral intermediates due to their low optimum temperature and high activity in cold conditions, which are favourable properties for the production of relatively frail compounds. In addition, these enzymes have an advantage under low water conditions due to their inherent greater flexibility, wherein the activity of mesophilic and thermophilic enzymes are severely impaired by an excess of rigidity. The different experimental strategies available for the search of psychrophilic biocatalysts and their application to discover novel cold-adapted lipolytic enzymes will be outlined. Some structural features that justify the unusually high enzymatic activity at low temperature will be discussed, in view of the recent achievements concerning the use of cold-adapted lipases and esterases in the synthesis of fine chemicals.

1 Introduction

The largest proportion of biomass on earth is generated at cold temperatures ($\leq$5°C). This is mainly due to the contribution of vast numbers of micro-organisms in the oceans, although the cold biosphere extends to permanently cold alpine regions, caves, upper atmosphere, and polar regions, in addition to seasonally cold environments. Numerous organism and in particular bacteria, yeasts, unicellular algae and fungi have been isolated and characterised from these cold environments. A variety of these microrganisms has been isolated in Antarctica; some are specialised to very low temperatures (steno-psychrophilic bacteria, with optimal growth temperature $<$15°C), and some tolerate temperature up to 20°C (eury-psychrophiles) [1]. These cold-adapted micro-organisms have been found to not only endure, but to flourish under the harsh conditions of permanently low-temperatures. In fact, for some, this environment is not only optimal, but mandatory for sustained cell proliferation, with moderate to high temperatures (e.g. $>$12°C) being deleterious [2]. Clearly, adaptations at level of structural and physiological organisation have occurred, which allow these psychrophilic micro-organisms

Bacteria	**Source**	**References**
Moraxella sp. strain TA144	Antarctic habitat	G. Feller et al., 1991
Psychrobacter immobilis strain B10	Antarctic habitat	JL. Arpigny et al., 1993
Pseudomonas sp. strain B11-1	Alaskan soil	DW. Choo et al., 1998
Pseudomonas fluorescens	Refrigerated human placental extracts	J. Preuss et al., 2001
Pseudomonas sp. strain KB700A	Subterranean environment	N. Rashid et al., 2001
Psychrobacter sp. Ant 300	Antarctic habitat	L. Kulakova et al., 2004
Photobacterium lipolyticum M37	Marine habitat	HS. Ryu et al., 2006
Psychrobacter sp. 7195	Antarctic habitat	J. Zhang et al., 2007
Moritella sp. 2-5-10-1	Antarctic habitat	X. Yang et al., 2008
Fungi		
Candida antarctica	Antarctic habitat	JC. Rotticci-Mulder et al., 2001
Candida antarctica	Antarctic habitat	K. Blank et al., 2006

Table 1: Micro-organism producing cold-active lipases.

to overcome key obstacles inherent to life at low temperatures [3]. The key to all this adaptation in response to low temperature is the activity of enzymes which perform the necessary metabolic conversions. Psychrophilic enzymes are of great interest in the scientific community, and are currently under study to characterize their physical and chemical properties in an attempt to understand the molecular basis of cold adaptation. It is frequently observed that enzymes from psychrophiles are thermolabile and more flexible than their counterparts from thermophiles. Many cold-adapted enzymes have regions of local flexibility, particularly around the active site, which allows better interaction with substrates, and by lower activation energy requirements in comparison with their mesophilic and thermophilic counterparts. The higher structural flexibility of psychrophilic enzymes could be the result of a combination of several features: weakening of intramolecular bonds (fewer hydrogen bonds and salt bridges as compared to mesophilic and thermophilic homologs have been shown):

• a decrease in compactness of the hydrophobic core,
• an increase in the number of hydrophobic side chains that are exposed to the solvent,
• longer and more hydrophilic loops,
• a reduced number of proline and arginine residues, and a higher number of glycine residues [4].

Among enzymes displaying low evolutionary rate, it is interesting to analyse lipolytic enzymes, also because of the key role in the metabolic pathway. At the moment, several microbial sources of cold-active lipases are available. As shown in Table 1, the most of cold-active lipases/esterases producing micro-organisms are cold-adapted bacteria, mostly isolated from Antarctic and polar regions. Other powerful sources of cold-active lipolytic enzymes are bacterial genera isolated from deep-sea water and sediments or refrigerated milk and food samples. The investigations on cold-active lipases are also extended to mycotic sources (Table 1). Even though only a few lipolytic fungi were reported to produce cold-active lipases, an extensive research has been carried out on the cold-active lipase B of Candida antarctica (CAL-B), which is widely

used in industrial applications. The first example of isolation of cold-active lipolytic enzymes from a psychrophilic bacterium was from the Antarctic strain *Psychrobacter sp.* TA144 (previously called Moraxella TA144) [5]. Recently, the isolation of a cold-active lipase from the Antarctic deep-sea psychrotrophic bacterium *Psychrobacter sp.* 7195 and its characterization has been described [6].

2 Description of catalytic site

Lipids are a complex class of biomolecules arising from esterification of fatty acids with an alcohol moiety. Due to their structural/functional similarities, it is still difficult to predict a priori if a lipolytic enzyme is an esterase or lipase, but the most reliable tool to classify it, is testing the substrate specificity: water-insoluble long-chain acylglycerols ($\geq$C10) are very good substrates for lipases, while esters with short-chain fatty acids ($\leq$C10), at least partially soluble in water, are hydrolysed by esterases. Due to their respective solubility, esterase activity occurs in aqueous solution, while lipolytic reactions occur at the lipid–water interface, implying that the kinetics cannot be described by Michaelis–Menten equations, as these are valid only if the catalytic reaction takes place in one homogenous phase. The best-known phenomenon emerging from early kinetic studies of lipolytic reactions became known as 'interfacial activation', describing the fact that the activity of lipases is enhanced towards insoluble substrates that form an emulsion. Lipases, in contrast to esterases, were therefore defined as carboxylesterases acting on emulsified substrates that catalyses the hydrolysis of long-chain acylglycerols. The superfamily of carboxyl ester hydrolases (which comprises also lipases and esterases) includes ubiquitous enzymes of great physiological function with a wide range of substrate specificities; they are member of the alfa/beta hydrolase family. Enzymatic catalysis utilises a 'catalytic triad' of residues that is usually comprised of a serine (nucleophile), a histidine and an aspartic acid that occur after the same secondary structure elements in the alfa/beta structure – as shown in Figure 1. The Asp/Glu and His residues of the catalytic triad are usually located in a loop containing two reverse turns at the end of strands 7 and 8 respectively. The catalytic triad is a particularly useful arrangement of amino acids and has probably arisen several times during the course of evolution – the overall structures of the serine proteases and the alfa/beta hydrolase fold enzymes are quite different and their triads are clearly related by convergent evolution. Although the catalytic machinery of alfa/beta hydrolase enzymes is very similar, the way by which they bind substrates varies from protein to protein. In most cases, substrate binding occurs in a "cap" domain that sits over the catalytic triad. The cap domains are built from one or more peptides that emanate from the C-terminal ends of strands 4, 6, 7 or 8. The active site of lipases was found to be covered by a surface loop, which was called the lid (or flap). Upon binding to the interface, this lid moves away, turning the 'closed' form of the enzyme into an 'open' form, with the active site now accessible to the solvent; at the same time, a large hydrophobic surface is exposed, which is thought to facilitate binding of the lipase to the interface.

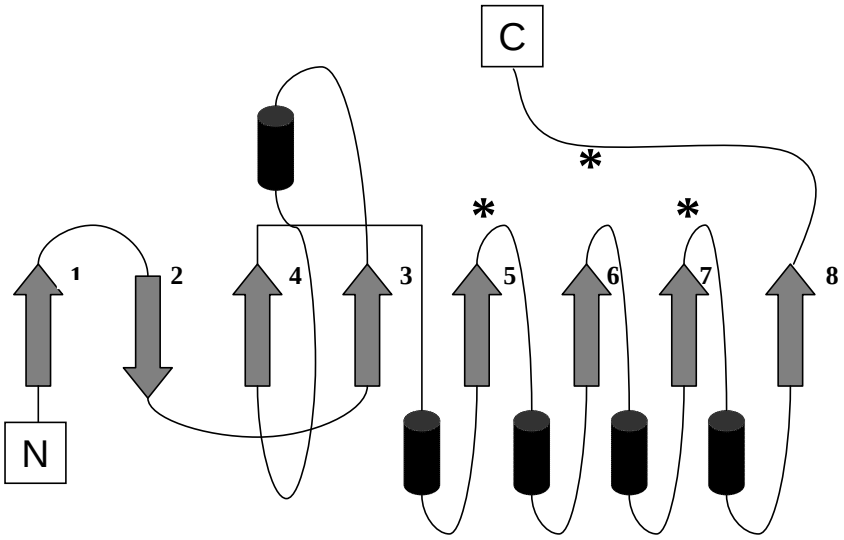

Figure 1: Schematic representation of alfa/beta hydrolase canonical fold. * represent the catalytic residues.

3 Methodologies to discover novel biocatalists

The isolation of novel enzymes with specific properties is the result of several experimental strategies that could be distinguished in: classical, genomic and metagenomic approach. The three approaches differ significantly in the expected size of the enzymatic repertoire potentially accessible to the screening procedures. Recent paper reports the isolation of cold-active LipP from *Moritella sp*.2-5-10-1 by classical approach [7]. In fact, classical and genomic approaches require the microbial source isolation and its cultivation in laboratory conditions. The isolation of novel enzymes can also be achieved by combining in silico genome analysis with in vivo functional characterization. Genomic approach requires the knowledge of the whole genome sequence of the microbial source. Nowadays, several genomes of psychrophilic micro-organisms are available and their number in steadily increasing (Table 2). The genome of the Antarctic organism contains several genes annotated as putative esterase/lipase encoding sequences; for example, the Gram-negative Antarctic bacterium *Pseudoalteromonas haloplanktis* TAC125 (*P. haloplanktis* TAC125), reports two examples of cold-active lipolytic enzyme characterization. The major limitation of the two described methodologies, classical gene cloning and genomic approach, is the need to cultivate the lipase-producing micro-organisms in laboratory conditions. In spite of the great variety of potential sources of novel enzymes, it is extimated that more than 99% of the

Species/strain	**Source**	**References**
Colwellia psychrerythraea 34H	Artic marine sediment	BA. Methe et al., 2005
Desulfotalea psychrophila LSv54	Marine sediment, Svarlbard	R. Rabus et al., 2004
Methanococcoides burtonii DSM6242	Ace lake Vestfold Hills Eastern Antarctica	NF. Saunders et al., 2003
Pseudoaltermonas haloplanktis TAC125	Antarctic sea-water	C. Médigue et al., 2005
Psychromonas ingrahamii 37	Under-ice sea-water, Alaska	AJ. Auman et al., 2006
Photobacterium profundum SS9	Amphipod, Sulu Trench	S. Campanaro et al., 2005
Psychrobacter arcticus 273-4	Tundra permafrost, Siberia	C. Bakermans et al., 2006
Psychrobacter cryohaloentis K5	Cryopeg, Siberia	C. Bakermans et al., 2006

Table 2: Sequenced genomes of cold-adapted bacteria.

prokaryotic organisms are so far unculturable [8] and therefore not accessible for biotechnology and basic research. However, valuable resources from uncultivable microbial communities can be exploited by using metagenomic approach. This approach is based on the culture-independent retrieval of genomic DNA from microbial communities living in particular environments [9]. Metagenomic libraries construction involves the same methods as the cloning of genomic DNA of individual micro-organisms; that is, DNA fragmentation by restriction-enzyme digestion or mechanical shearing, insertion of DNA fragments into an appropriate vector system, and transformation of the recombinant vectors into a suitable host. Once established, metagenomic libraries can be accessed and tested by multiple screening methodologies to discover novel biocatalysts. The principal testing criteria include the functional screening [10, 11], the identification of interesting genes based on sequence homology through PCR or random sequencing [12] and the large-scale shotgun sequencing [13, 14], the hybridization [15] or the detection of substrate induced gene expression [16]. Several cold-active lipases have been identified by the metagenomic approach during the last years. A novel low temperature active lipase was isolated from a metagenomic library of Baltic Sea sediment bacteria [17]. A fosmid library with inserts of 24-39 kb was generated and screened for clones producing lipolytic activity. A 978 bp open reading frame was selected encoding a putative lipase/esterase, called h1Lip1. Further characterization of the recombinant enzyme confirmed that it was a lipase. The same strategy was adopted to search another cold-active lipase from the sea sediment samples at Edison Seamount, South West Pacific [18].

The sequence analysis of the selected fosmid clone revealed the presence of an open reading frame (EML1) showing similarities to lipases. EML1 enzyme was then recombinantly produced in *E. coli* BL21, and purified for biochemical characterization. Based on the data of optimum conditions for the recombinant enzyme activity and the calculated activation energy, it was suggested that EML1 is cold-active, consistent with the origin of the sample. The reported examples show that metagenomic approach, using extreme environment samples, can provide an opportunity to isolate enzymes perfectly adapted to extreme working conditions which display unique primary sequence. On the other hand, the method suffers the general limitations of the heterologous gene-expression screening in *E. coli* which have been discussed in full details elsewhere [19].

4 Esterases and lipases in fine chemical synthesis

All mentioned properties of cold adapted biocatalysts make these enzymes of great interest in many industrial applications, where a high catalytic efficiency in a low temperatures processes is required and the easy inactivation of the added catalysts by moderate heating is an added value. New catalytic synthetic methods in organic chemistry that satisfy increasingly stringent environmental constraints are in great demand by chemical industry. Enzyme-catalysed chemical transformations are now widely recognized as effective alternative to traditional (non-biological) organic synthesis, and as convenient solutions to certain intractable synthetic problems. Esterases and lipases are the most applied biocatalysts in industrial applications. Lipase, due to their high catalytic efficiency, selectivity, and the "far than harsh" conditions in which they operate, are used to produce some of industrially important chemicals, traditionally manufactured from fats and oils by chemical processes, with greater rapidity and better specificity under mild conditions [20]. The increasing interest in bacterial lipases is based on their potential to catalyze the hydrolysis of fats (their natural function), trans-esterification, alcoholysis and esterification among other reactions. Indeed lipases, that cleave ester bonds of triacylglycerols with the subsequent release of free fatty acids, diacylglycerols, monoacylglycerols and glycerol are also able to catalyze the reverse reactions (esterification, inter-esterification and trans-esterification) provided that the aqueous medium is replaced by an organic or a biphasic aqueous/organic medium. Indeed, various esters and lactones are among the substances synthesized using bacterial lipases [21], moreover the high selectivity of these enzymes is a key feature of these biocatalysts which are used in the resolution of racemic mixtures for preparation of optically pure compounds. Esterases and lipases are the most applied biocatalysts in industrial applications. The reasons of this success are numerous and related to the wide diversity in the substrates recognised, combined to the exquisite chemoselectivity, regioselectivity and stereoselectivity frequently displayed by this class of enzymes. Furthermore, they are readily available in large quantities because many of them can be produced in high yields from microbial organisms and the crystal structures of many lipolytic enzymes have been solved, making possible the design of rational engineering strategies. Finally, they do not usu-

ally require cofactors nor do they catalyse side reactions. These properties make lipolytic enzymes the most widely used group of biocatalysts in numerous industrial applications and in organic chemistry. In the field of fine chemicals, *C. antarctica* lipase B is an excellent biocatalyst which provides some specific examples of stereoselective biotransformations. The use of *C. antarctica* lipase B in the synthesis of monoester of pyridoxine (vitamin B6) was investigated [6]. Ester derivatives of the most important form of commercial vitamin B6, have broad applications in food industry, cosmetics and medical supplies but regioselective esterification of pyridoxine is a difficult task since the pyridine-ring possesses three hydroxyl groups of similar reactivity. As a result, it is very difficult to discriminate among these three groups from a chemical point of view. The lipase enzymatic reactions were used to provide an helpful option to achieve regioisomer of pyridoxine ester; *C. antarctica* lipase B catalyzed esterification of pyridoxine provides not only an effective selection of one out of the three hydroxyl groups thus leading to synthesis of regioselective monoester. In addition, the use of enzymes for polymer synthesis allows to carry out ester-interchange reactions in the absence of heavy metals, at lower temperatures, and with increased selectivity. Modern methods of genetic engineering combined with growing knowledge of structure and function allow further adaptation to industrial needs and exploration of novel applications.

References

[1] K.S. Siddiqui and R. Cavicchioli. Cold-Adapted enzymes. *Annu. Rev. Biochem.*, 75:403, 2006.

[2] Y. Xu, Y. Nogi, C. Kato, Z. Liang, et al. Moritella profonda sp.nov. and Moritella abyssi sp. nov., two psychropiezophilic organisms isolated from deep Atlantic sediments. *Int. J. Syst. Evo.l Microbiol.*, 53:533, 2003.

[3] R.R. Margesin, F. Schinner, J.C. Marx, and C. Gerday. Editors Psychrophiles: from Biodiversity to Biotechnology. 2008.

[4] G. Gianese, F. Bossa, and S. Pascarella. Comparative structural analysis of psychrophilic and meso- and thermophilic enzymes. *Proteins*, 47:236, 2002.

[5] G. Feller, M. Thiry, J.L. Arpigny, and C. Gerday. Cloning and expression in Escherichia coli of three lipase-encoding genes from the psychrotrophic Antarctic strain Moraxella TA144. *Gene*, 101(111), 1991.

[6] J. Zhang, S. Lin, and R. Zeng. Cloning, expression, and characterization of a cold-adapted lipase gene from an antarctic deep-sea psychrotrophic bacterium, Psychrobacter sp 7195. *J. Microbiol. Biotechnol.*, 17:604, 2007.

[7] X. Yang, X. Lin, T. Fan, J. Bian, and X. Huang. Cloning and expression of lipP, a gene encoding a cold-adapted lipase from Moritella sp.2-5-10-1. *Curr. Microbiology*, 56:194, 2008.

[8] M.S. Rappe and S.J. Giovannoni. The uncultured microbial majority. *Annu. Rev. Microbiol.*, 57:369, 2003.

[9] M.R. Rondon, P.R. August, A.D. Bettermann, S.F. Brady, et al. Cloning the soil metagenome: a strategy for accessing the genetic and functional diversity of uncultured micro-organisms. *Appl. Environ. Microbiol.*, 66:2541, 2000.

[10] P. Entcheva, W. Liebl, A. Johann, T. Hartsch, and W. Streit. Direct cloning from enrichment cultures, a reliable strategy for isolation of complete operons and genes from microbial consortia. *Appl. Environ. Microbiol.*, 67:89, 2001.

[11] A. Knietsch, T. Waschkowitz, S. Bowien, A. Henne, and R. Daniel. Construction and screening of metagenomic libraries derived from enrichment cultures: generation of a gene bank for genes conferring alcohol oxidoreductase activity on Escherichia coli. *Appl. Environ. Microbiol.*, 69:1408, 2003.

[12] D.E. Gillespie, S.F. Brady, A.D. Bettermann, N.P. Cianciotto, M.R. Liles, et al. Isolation of antibiotics turbomycin A and B from a metagenomic library of soil microbial DNA. *Appl. Environ. Microbiol.*, 68:4301, 2002.

[13] J.C. Venter, K. Remington, J.F. Heidelberg, A.L. Halpern, et al. Environmental genome shotgun sequencing of the Sargasso Sea. *Science*, 304:66, 2004.

[14] S.G. Tringe, C. von Mering, A. Kobayashi, A.A. Salamov, et al. Comparative metagenomics of microbial communities. *Science*, 308:554, 2005.

[15] J.L. Stein, T.L. Marsh, K.Y. Wu, H. Shizuya, and E.F. DeLong. Characterization of uncultivated prokaryotes: isolation and analysis of a 40-kilobase-pair genome fragment front a planktonic marine archaeon. *Bacteriology*, 1996(178):591.

[16] T. Uchiyama, T. Abe, T. Ikemura, and K. Watanabe. Substrate induced gene-expression screening of environmental metagenome libraries for isolation of catabolic genes. *Nat. Biotechnology*, 23:88, 2005.

[17] F. Hårdeman and S. Sjöling. Metagenomic approach for the isolation of a novel low-temperature-active lipase from uncultured bacteria of marine sediment. *FEMS Microbiol. Ecol.*, 59:524, 2007.

[18] J.H. Jeon, J.T. Kim, Y.J. Kim, H.K. Kim, H.S. Lee, S.G. Kang, S.J. Kim, and J.H. Lee. Cloning and characterization of a new cold-active lipase from a deep-sea sediment metagenome. *Appl. Microbiol. Biotechnol.*, 81:865, 2009.

[19] R. Daniel. The Metagenomics of soil. *Nat. Rev. Microbio.*, 3:470, 2005.

[20] E.N. Vulfson. Industrial applications of lipases. page 271, 2004.

[21] B. Joseph, P.W. Ramteke, and G. Thomas. Cold active microbial liapses: some hot issues and recent developments. *Biotechnol. Adv.*, 26:457, 2008.

Role of Physical Forcings in Modulating Primary Production in the Coastal Upwelling Area of the Sicilian Channel

B. Patti[1], C. Guisande[2], A. Bonanno[1], G. Basilone[1], A. Cuttitta[1]
1, Institute for Coastal Marine Environment, CNR, Capo Granitola (TP), Italy
2, University of Vigo, Vigo, Spain
bernardo.patti@cnr.it

Abstract

Wind-induced upwelling is generally considered a very important mechanism for the enhancement of primary production in coastal areas. Coastal upwelling is a common feature of the marine ecosystems along the western coasts of continents (or, alternatively, of the eastern sides of the main oceanic basins), also known as Eastern Boundary Upwelling Ecosystems (EBUEs), where the dominant winds are equatorward (i.e., southward in the northern hemisphere and northward in the southern hemisphere). The Sicilian Channel is an area of favourable upwelling winds, which ought to support primary production. However, the values for primary production are low when compared with other Mediterranean areas and very low compared with the most biologically productive regions of the world's oceans. This work aims at showing the role of various physical forcings in controlling satellite-based estimates of primary production in the Sicilian Channel, starting from the analysis of the modulation of its monthly changes. Results show that monthly changes in primary production are mostly driven by the mixing of water column and wind-induced and/or circulation-related upwelling processes operating there, which are believed to have been able to compensate for the negative effects on primary production generated by the general warming trend characterizing surface waters over the last three decades.

1 Introduction

Wind-induced upwelling is generally considered as an important mechanism for the enhancement of primary production in coastal areas. For instance, coastal upwelling is a common feature of the very productive marine ecosystems along the western coasts of continents (or, alternatively, of the eastern sides of the main oceanic basins), also known as Eastern Boundary Current (EBC) upwelling systems or Eastern Boundary Upwelling Ecosystems (EBUEs), where the dominant winds are equatorward (i.e., southward in the northern hemisphere and northward in the southern hemisphere) [1, 2]. The Sicilian Channel is an area of favourable upwelling winds, which ought to support primary production. However, the values for primary production are low when compared with other Mediterranean areas and very low compared with the most biologically productive regions of the world's oceans [3]. The Mediterranean is characterized by oligotrophic conditions and it has been suggested that there is a decreas-

ing trend over time in chlorophyll concentration. This has been associated with increased nutrient limitation resulting from reduced vertical mixing due to a more stable stratification of the basin, in line with the general warming of the Mediterranean [4]. Behrenfeld et al.[5] have also suggested that the decreasing trend in ocean primary production is due to climatic changes that allow surface warming which determines an increase in the density contrast between the surface layer and underlying nutrient-rich waters. This in turn leads to enhanced stratification which is able to suppress nutrient exchange through vertical mixing. Global warming, therefore, should be able to lead to a decrease in primary production in the Mediterranean. However, the Mediterranean Sea presents considerable spatial heterogeneity in primary production [6, 7]. Therefore, it is interesting to determine whether this potential limitation of primary production due to the more stable stratification of the basin suggested to be the case for the Mediterranean [4] is also observed in the upwelling area which characterizes the northern sector of the Strait of Sicily, an area very important for the nutrient concentrations encountered in Mediterranean waters [8]. This study aims at further investigating the role of various physical forcings in controlling primary production levels in the Sicilian Channel, starting from the results of a previous study [3] based on satellite-based chlorophyll a concentration (chl-a) and using in addition satellite-based estimates of net primary production (NPP).

2 Materials and Methods

2.1 Data set description

This study is mainly based on in situ and satellite environmental information available for each of the three sites shown in Figure 1 over the period September 1997 – December 2007. Information on turbulence was gathered across the period September 1997 – May 2007. Average data values over a 1ºx1º degree of latitude and longitude cells were employed for all factors. Although some of the datasets used in this chapter are accessible on the Internet at higher resolutions, 1°x1° resolution was chosen in order to meet the available spatial resolution of the International Comprehensive Ocean-Atmosphere Data Set (ICOADS). 1°x1° box locations were selected by choosing along the southern Sicilian coast those sites closer to the coast and better able to represent the features of the local upwelling system (see Figure 2).

2.1.1 Offshore Ekman transport

Monthly Ekman transport estimates used herein were based on monthly wind stress data, as available from the Simple Ocean Data Assimilation (SODA) database, accessible at 0.5° resolution, by assimilating the available field observations (http://ingrid.ldeo.columbia.edu/SOURCES/.CARTON-GIESE/.SODA/.v2p0p2-4/ [9]. Specifically, Ekman transport components were calculated according to Bakun [10]:

$$\mathrm{Qx} = \tau\mathrm{y}/(\mathrm{f} * \rho) * 1000,$$

$$\mathrm{Qy} = -\tau\mathrm{x}/(\mathrm{f} * \rho) * 1000,$$

where Qx and Qy are Ekman transport along the x (zonal) and y (meridional) axes,

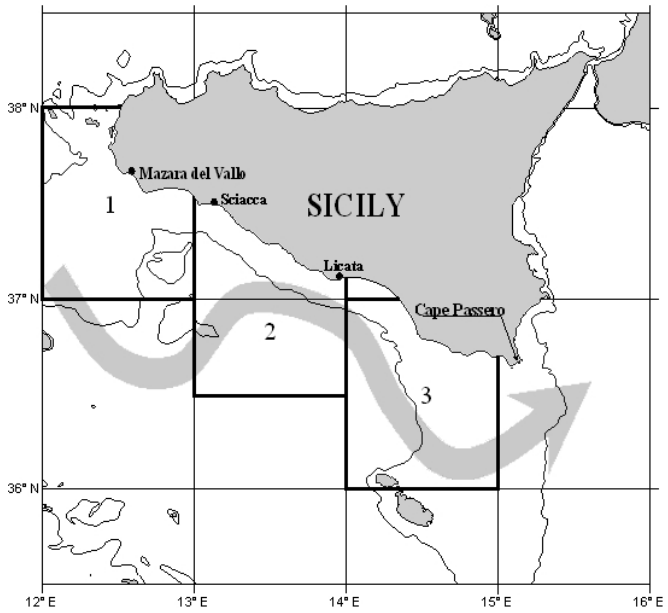

Figure 1: Map showing the 1° x 1° of latitude and longitude boxes in the Sicilian Channel area where chl-a concentration, Net Primary Production, Ekman transport, wind mixing, nutrient concentration, and water column stability were estimated or extracted from the available databases. The average path of the Atlantic Ionian Stream (AIS) area and 200 m isobath are superimposed.

respectively, in $m^3 \cdot s^{-1} \cdot km^{-1}$, ρ = 1025 kgm^{-3} (water density), f is the (latitude dependent) Coriolis factor in s^{-1}, and τx and τy are the wind stress components (in $N \cdot m^{-2}$, i.e. kilogram $\cdot$ meter^{-1} $\cdot$ second^{-2}) over the sea. The resultant vectors of Qx and Qy components was used as an index of wind-induced alongshore upwelling intensity.

2.1.2 Chlorophyll-a concentration and Net Primary Production

Chl-a data herein used were obtained from the NASA Sea-viewing Wide Field-of-view Sensor (SeaWiFS) Project, distributed as a Level 3 Standard Mapped Image product [11]. Specifically, monthly composite images for the period September 1997 – December 2007 were downloaded from the http://oceancolor.gsfc.nasa.gov/cgi/l3 website in Hierarchical Data Format (HDF). These images have 2160 by 4320 pixels and a resolution of about 9 x 9 km2. To match the resolution of I-COADS data, average pigment concentration values were obtained for each of the 1° x 1° boxes of Figure 1. Although we have not directly measured primary production, it has been demonstrated that chlorophyll concentration estimated from SEAWiFS ocean colour data is a good indicator of primary production [12]. In addition, for compar-

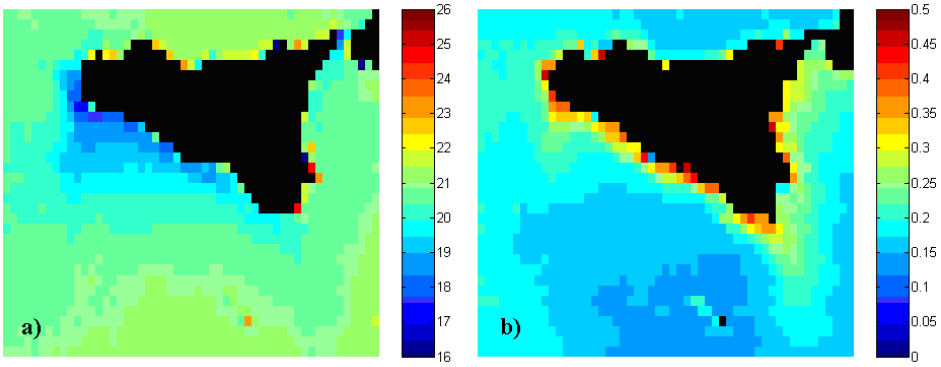

Figure 2: Climatologies of: (a) SST (degree C), and (b) chl-a concentration (mg m-3) over the study area, obtained respectively from the AQUA MODIS mission (period: January 2002 – February 2008) and the SeaWiFS mission (period: September 1997 – December 2007).

ison purposes, satellite-based estimates of Net Primary Production (NPP) were also used. Specifically, NPP data, expressed in mg C m-2 day-1 and available on request as global 2160x4320 hdf files with an approximate resolution of about 9x9 square kilometers, were downloaded from the web site http://web.science.oregonstate.edu/ocean.productivity/index.php. They refer to products generated using the standard algorithm for the Vertically Generalized Production Model (VGPM) [13]. The VGPM is a "chlorophyll-based" model that estimates net primary production from chlorophyll using a temperature-dependent description of chlorophyll-specific photosynthetic efficiency. For the VGPM, net primary production is a function of chlorophyll, available light, and the photosynthetic efficiency. Similarly to chl-a data, the original resolution was lowered by averaging pixels to obtain a data set at one-degree resolution, compatible with the I-COADS data.

2.1.3 Wind-mixing index

The energy transferred through the water column by the wind creates turbulence in the surface layers. Therefore, a wind-mixing index in the upper layer is usually calculated as the cube of wind speed. We used this index as an indicator of turbulence in the surface layers. Wind speed data from September 1997 to May 2007 for wind-mixing index calculation were extracted from the Global Marine Monthly Summaries in the International Comprehensive Ocean Atmosphere Data Set (I-COADS), as available on the Data Support Section of the University Corporation for Atmospheric Research (UCAR) website (http://dss.ucar.edu/datasets/ds540.1/).

2.1.4 Sea surface temperature

Monthly 1° x 1° (spatial resolution) optimal interpolation (OI) sea surface temperature (SST) data [14] used for this study were provided by the NOAA Operational Model Archive Dis-

tribution System from their website http://nomad3.ncep.noaa.gov/ncep_data/index.html. From the global data set, covering the period November 1981 – present, we extracted SST time series for the 1° x 1° boxes located along the southern Sicilian coast (Figure 1). Further SST data, downloaded from http://oceancolor.gsfc.nasa.gov/cgi/l3 and used for the mapping of the climatological SST field over the Sicilian channel, were taken from the AQUA MODIS mission, spanning the period January 2002 – February 2008.

2.1.5 Water column stability

Water column stability was estimated using the methodology described by Guisande et al. [15]. Specifically, for each of the three sites of Figure 1 and for the period September 1997 – December 2007, monthly density values were calculated using temperature and salinity data extracted at the standard depths of 5, 15, 25, 36, and 47 m taken from the Simple Ocean Data Assimilation (SODA) (http://ingrid.ldeo.columbia.edu/SOURCES/.CARTON-GIESE/.SODA/.v2p0p2-4/) database [9]. With the aim of detecting trends, the entire available time series, starting from January 1958, was also used.
The Brunt-Väisälä or buoyancy frequency equation (N) was used to measure the strength of the density gradients:

$$\mathrm{N} = (\mathrm{g}/\rho\mathrm{med} * \mathrm{d}\rho/\mathrm{dz})^{0.5}$$

where ρ is the density of the water (in $\mathrm{kg{\cdot}m^{-3}}$), ρmed is the mean ρ of the water column, g is the acceleration due to gravity, and z is the depth. The integrated buoyancy frequency estimated using the trapezoid method was used as an indicator of stability of the water column (S). Low values of S (presented as cycles $\mathrm{h^{-1}}$) indicate that the water column is mixed whereas high values indicate that the water column is stratified.

2.2 Statistical analysis

For each of the considered sites (see Figure 1), Pearson correlation coefficients were calculated between each of the available environmental factors' monthly series (regressors: Ekman transport, SST, water column stability, and wind-mixing index) and ch- a (regressand). For comparison purposes, the same analysis was repeated using satellite-based NPP estimates as regressand. Each series was firstly deseasonalized by subtracting from each monthly value the corresponding monthly average for the entire time series. In addition, as the deseasonalized anomalies so obtained were not in general trend-stationary, a linear trend was removed from all data prior to regression. For each model, correlation coefficients were computed and tested for significance at lags 0, 1, and 2. The multiple hypothesis testing issue was taken into account by using two alternative methods. According to a first, more conservative, criterion based on Bonferroni correction [16], individual correlation coefficients can be considered significantly different from zero if the related significance level is lower than a critical p-value given by the ratio between alfa (i.e., the significance levels: 0.05, 00.1 and 0.001) and m, the number of models contemporarily tested (in this case, m = 4 (factors) x 3 (boxes) x 3 (lags) = 36). A second, less conservative approach was based on False Discovery Rate (FDR) control [17] which is a statistical method in which a list of rejected hypotheses is able to control the expected proportion of in-

correctly rejected null hypotheses. Specifically, a rough FDR (RFDR) control under dependence assumptions was adopted [18], obtained by multiplying alfa by the factor (m+1)/(2*m).

3 Results

The results of the linear regression analysis between detrended anomalies of chl-a (regressand) and Ekman transport, SST, stability, and wind-mixing index (regressors) are given in Table 1. Specifically, the Pearson correlation coefficients and related significance levels resulting from the adoption of both Bonferroni correction and RFSR control for all linear regressions tested are shown. The relationship between Ekman transport and chl-a was not significant (with the only exception of the westernmost box site with RFDR control). Conversely, a significant positive linear relationship between SST and chl-a was detected at lag 0 in all the easternmost box site (in all sites using RFDR control). As expected, estimated R values were positive for Ekman transport and negative for SST, as the upwelling of nutrient-rich subsurface waters is related to a decrease in the surface temperature regime (see Figure 2). However, chl-a showed a generally stronger relationship with SST compared to Ekman transport. Additionally, where R values for Ekman transport were lower, the R coefficients for SST were higher (in absolute value), with a decreasing eastward trend for Ekman transport and increasing eastward trend for SST. Positive relationships with the wind-mixing index were also observed to occur, with a significant R value in one out of three geographical boxes (in all sites with RFDS approach). As far as concerns water column stability, none of the estimated correlation coefficients were significantly different from zero (with the only exception of the easternmost box site if applying RFDR control). The results obtained using NPP as regressand in correlation analysis, generally comparable to those obtained using chl a estimates (Table 2), further emphasizes the role of wind mixing and circulation-related upwelling processes.

4 Discussion

In the Mediterranean Sea the prevailing westerly winds produce offshore-directed Ekman transport and coastal upwelling off the southern sides of the bigger islands [19]. Several authors have observed a frequent local occurrence of upwelling events for the south coast of Sicily, which is certainly associated with local winds [20, 21, 22, 23, 24, 25, 26, 27]. This upwelling regime is observed to occur off the southern coast of Sicily, whereas downwelling processes are expected to occur along the eastern coast of Tunisia on the opposite side of the Strait [28]. However, south-eastward winds alone are not the only factor responsible for coastal upwelling, a persistent feature off the southern Sicilian coast. Surface circulation is controlled by the flow of modified Atlantic water (MAW), which is locally referred to as the Atlantic Ionian Stream (AIS) [22]. The AIS, when passing through the Sicilian Channel, produces two large cyclonic vortices, one over Adventure Bank and a second one off Cape Passero, at the southernmost tip of Sicily. The signature of the upwelling of subsurface cold waters associated with these vortices is visible in the averaged satellite SST (Figure 2a). In addition, along the AIS trajectory

1	2	3	4	5	6	7	8	9	10
Box	**Lat N**	**Lon E**	**Regressor**	**lag**	**df**	**R**	**p-value**	**Significance1**	**Significance2**
1	37.5	12.5	ET	2	120	0.28	0.0021	NS	**
2	37.0	13.5	ET	0	122	0.12	0.1979	NS	NS
3	36.5	14.5	ET	1	121	0.12	0.1805	NS	NS
1	37.5	12.5	SST	0	122	-0.28	0.0019	NS	**
2	37.0	13.5	SST	0	122	-0.25	0.0045	NS	**
3	36.5	14.5	SST	0	122	-0.33	0.0002	**	**
1	37.5	12.5	Stability	0	122	-0.06	0.5220	NS	NS
2	37.0	13.5	Stability	0	122	-0.06	0.4861	NS	NS
3	36.5	14.5	Stability	1	121	-0.21	0.0182	NS	*
1	37.5	12.5	Wind-mixing index	0	115	0.36	0.0001	**	***
2	37.0	13.5	Wind-mixing index	0	115	0.25	0.0067	NS	*
3	36.5	14.5	Wind-mixing index	0	115	0.27	0.0028	NS	**

Table 1: Statistical results of linear regression models relating chl-a (regressand) and Ekman transport (ET), SST, stability, and wind-mixing index (regressors). For each geographical 1° x 1° box of Figure 1 – identified in the columns 1, 2, and 3 (coordinates refer to the centre of 1° x 1° cells) – four linear models have been fitted by regression between trend-removed monthly time series, one for each available regressor. For each model, Pearson's correlation coefficients (R) between regressors and regressand (chl-a) reported in column 7 represent the maximum absolute values obtained among tested regressions at lags 0, 1, and 2 (column 5), with degrees of freedom given in column 6. Column 8 indicates the p-values of the estimated correlation coefficients. Column 9 shows the significance of p-values on the basis of Bonferroni correction (m = 36 "*" -> $p < 0.05/m$; "**" -> $p < 0.01/m$; "***" -> $p < 0.001/m$). The critical p-value at the 0.05 significance level, with Bonferroni correction, is 0.0014. Column 10 reports the significance of p-values according to the RFDR control (m = 36 "*" -> $p < 0.05*(m+1)/(2*m)$; "**" -> $p < 0.01*(m+1)/(2*m)$; "***" -> $p < 0.001*(m+1)/(2*m)$. The critical p-value at the 0.05 significance level, with RFDR control, is 0.0260.

a density front to the left of the current, facing downstream, is observed to occur. The AIS anticyclonic meander characterizing surface flow in the central part of the southern Sicilian coast determines the uprising of the underlying LIW to the surface, due to geostrophic adjustment processes [29, 27]. This also causes the fertilization of coastal waters, as also visible in averaged satellite chl a products (Figure 2b). Finally, another possible mechanism able to affect local phytoplankton biomass is simply by lateral advection of the relatively more enriched MAW waters coming from the North African coast. The question addressed in this study concerns which physical factors may be considered as most responsible for the monthly modulation of primary production levels. The relatively low fraction of variance in chl-a (and NPP) explained by Ekman transport (ET), the higher correlation values between primary production (both chl-a and NPP) and SST compared to ET, and the apparent inverse eastward pattern in the R coefficients for ET and SST factors (decreasing for ET and increasing for SST) would suggest the importance of general surface

1	2	3	4	5	6	7	8	9	10
Box	**Lat N**	**Lon E**	**Regressor**	**lag**	**df**	**R**	**p-value**	**Significance1**	**Significance2**
1	37.5	12.5	ET	2	120	0.26	0.0045	NS	**
2	37.0	13.5	ET	0	122	0.13	0.1412	NS	NS
3	36.5	14.5	ET	1	121	0.12	0.1907	NS	NS
1	37.5	12.5	SST	0	122	–0.38	<0.0001	***	***
2	37.0	13.5	SST	0	122	–0.31	0.0005	*	**
3	36.5	14.5	SST	0	122	–0.45	<0.0001	***	***
1	37.5	12.5	Stability	0	122	–0.07	0.4430	NS	NS
2	37.0	13.5	Stability	2	120	0.04	0.6689	NS	NS
3	36.5	14.5	Stability	2	120	–0.13	0.1252	NS	NS
1	37.5	12.5	Wind-mixing index	0	115	0.25	0.0059	NS	*
2	37.0	13.5	Wind-mixing index	0	115	0.36	0.0001	**	***
3	36.5	14.5	Wind-mixing index	0	115	0.47	<0.0001	***	***

Table 2: Statistical results of linear regression models relating NPP (regressand) and Ekman transport (ET), SST, stability, and wind-mixing index (regressors). (see Table 1 caption for details)

circulation and local topography in influencing the coastal upwelling and, through the related input of nutrients, the productivity levels off the southern coast of Sicily. The analysis of linear trends characterizing the time series gives further insights. The SST has been subjected to a significant increasing trend ($p < 0.001$) over the last 30 years, with less significant but still important growth rates over the last decade, due to the intrinsic increased variability in monthly values. Conversely, stability did not show any significant increasing trend, even considering the longer time span of the SODA data (1958–2007). The same was observed to occur in the satellite-based chl a and NPP. So, the limiting mechanism for primary production which is related to the enhanced stratification processes resulting from the general warming trend of global open ocean [5], also suggested to occur in Mediterranean waters [4], is not active over most of the northern sector of the Sicilian Channel. Actually, in the context of a general decreasing chl a trend in Mediterranean waters, especially over the basin interior, it has been observed that some coastal areas follow an opposite tendency [4]. On the basis of SeaWiFS data for the last decade, this appears to be the case in the near-coastal zones off the south Sicilian coast, at least over the two more westerly 1° x 1° cells investigated in this study. Specifically, wind-induced and surface circulation-related processes operating there are believed to be able to compensate for the negative effects on primary production generated by the general warming trend of the surface waters, as recently observed in most EBUEs [30]. In fact, correlation analysis showed that chl-a (and NPP) monthly changes are not driven by stratification, at least during the time span covered by the SeaWiFS mission (last decade). Indeed, the positive correlations between wind-mixing index and primary produc-

tion (both chl a and NPP) observed during the last decade would testify to the importance of wind-induced mixing processes as an explanation for phytoplankton biomass (and productivity) variation, independent of induced upwelling. These results do not support, at least for most of the coastal areas investigated, the hypothesis that a limiting mechanism for primary production is related to the enhanced stratification processes resulting from the general warming trend of Mediterranean waters.

References

[1] A.C. Thomas, P.T. Strub, M.E. Carr, and R. Weatherbee. Comparison of chlorophyll variability between the four major global eastern boundary currents. *Int. J. Remote Sens.*, 25:1443–1447, 2004.

[2] B. Patti, C. Guisande, A.R. Vergara, I. Riveiro, I. Maniero, et al. Factors responsible for the differences in satellite-based chlorophyll a concentration between the major global upwelling areas. *Est. Coast Shelf Sci.*, 76:775–786, 2008.

[3] B. Patti, C. Guisande, A. Bonanno, G. Basilone, A. Cuttitta, and S. Mazzola. Role of physical forcings and nutrient availability on the control of satellite-based chlorophyll a concentration in the coastal upwelling area of the Sicilian Channel. *Scientia Marina*, 74(3):577–588, 2010.

[4] V. Barale, J.M. Jaquet, and M. Ndiaye. Algal blooming patterns and anomalies in the Mediterranean Sea as derived from the SeaWiFS data set (1998-2003). *Remote Sens. Environ.*, 112:3300–3313, 2008.

[5] M.J. Behrenfeld, R.T. O´Malley, D.A. Siegel, C.R. McClain, et al. Climate-driven trends in contemporary ocean productivity. *Nature*, 444:752–755, 2006.

[6] M. Estrada. Primary production in the northwestern Mediterranean. *Scientia Marina*, 60:55–64, 1996.

[7] G. Crispi and M. Pacciaroni. Long-term numerical evolution of the nitrogen bulk content in the Mediterranean Sea. *Est. Coast Shelf Sci.*, 83:148–158, 2009.

[8] A. Karafistan, J.-M. Martin, M. Rixen, and J.M. Beckers. Space and time distributions of phosphate in the Mediterranean Sea. *Deep-Sea Res. I*, 49:67–82, 2002.

[9] J.A. Carton, G. Chepurin, X. Cao, and B. Giese. A simple ocean data assimilation analysis of the global upper ocean 1950-95. *J. Phys. Oceanogr. I*, 30:294–309, 2000.

[10] A. Bakun. Coastal upwelling indices, west coast of North America 1946-71. *NOAA Tech Report NMFS*, 671:1–103, 1973.

[11] G.C. Feldman and C.R. McClain. Ocean Color Web. SeaWiFS Reprocessing 5.http://oceancolor.gsfc.nasa.gov/. 2007.

[12] I. Joint and S.B. Groom. Estimation of phytoplankton production from space: Current status and future potential of satellite remote sensing. *J. Exp. Mar. Biol. Ecol.*, 250:233–255, 2000.

[13] M.J. Behrenfeld and P. G. Falkowski. Photosynthetic rates derived from satellite-based chlorophyll concentration. *Limnology and Oceanography*, 42:1–20, 1997.

[14] R.W. Reynolds, N.A. Rayner, T.M. Smith, D.C. Stokes, and W. Wang. An improved in situ and satellite SST analysis for climate. *J. Climate*, 15:1609–1625, 2002.

[15] C. Guisande, J.M. Cabanas, A.R. Vergara, and I. Riveiro. Effect of climate on recruitment success of Atlantic Iberian sardine (*Sardina pilchardus*). *Mar. Ecol. Prog. Ser.*, 223:243–250, 2001.

[16] R.G. Miller. Simultaneous Statistical Inference. 2nd ed. 1981.

[17] Y. Benjamini and Y. Hochberg. Controlling the false discovery rate: a practical and powerful approach to multiple testing. *Journal of the Royal Statistical Society, Series B Journal of the Royal Statistical Society, Series B (Methodological)*, 57:289–300, 1995.

[18] Y. Benjamini and D. Yekutieli. The control of the false discovery rate in multiple testing under dependency. *Annals of Statistics*, 29:1165–1188, 2001.

[19] A. Bakun and V. Agostini. Seasonal patterns of wind driven upwelling/downwelling in the Mediterranean Sea. *Scientia Marina*, 65:243–257, 2001.

[20] A. Piccioni, M. Gabrielle, E. Salus, and E. Zambianchi. Wind-induced upwellings off the southern coast of Sicily. *Oceanol. Acta*, 11:309–314, 1988.

[21] P.F.J. Lermusiaux. Estimation and study of mesoscale variability in the strait of Sicily. *Dynam. Atmosph. Oceans*, 29:255–303, 1999.

[22] A.R. Robinson, J. Sellschopp, A. Warn-Varnas, W.G. Leslie, et al. The Atlantic Ionian Stream. *J. Mar. Syst.*, 20:129–156, 1999.

[23] A. Warn-Varnas, J. Sellschopp, P.J. Haley Jr., W.G. Leslie, and C.J. Lozano. Strait of Sicily water masses. *Dynam. Atmosph. Oceans*, 29:437–469, 1999.

[24] A. Molcard, L. Gervasio, A. Griffa, G.P. Gasparini, L. Mortier, and T.M. Özgökmen. Numerical investigation of the Sicily Channel dynamics: density currents and water mass advection. *J. Mar. Syst.*, 36:219–238, 2002.

[25] M. Astraldi M., G.P. Gasparini, A. Vetrano, and S. Vignudelli. Hydrographic characteristics and interannual variability of water masses in the central Mediterranean: a sensitivity test for long-term changes in the Mediterranean Sea. *Deep-Sea Research I*, 49:661–680, 2002.

[26] R. Sorgente, A.F. Drago, and A. Ribotti. Seasonal variability in the Central Mediterranean Sea circulation. *Ann. Geophys.*, 21:299–322, 2003.

[27] K. Béranger, L. Mortier, G.P. Gasparini, L. Gervasio, M. Astraldi, and M. Crépon. The dynamics of the Sicily Strait: A comprehensive study from observations and models. *Deep-Sea Res. II*, 51:411–440, 2004.

[28] V.N. Agostini and A. Bakun. "Ocean triads" in the Mediterranean Sea: physical mechanisms potentially structuring reproductive habitat suitability (with example application to European anchovy, *Engraulis encrasicolus*). *Fisheries Oceanography*, 11:129–142, 2002.

[29] J. García-Lafluente, A. García, S. Mazzola, L. Quintanilla, et al. Hydrographic phenomena influencing early stages of the Sicilian Channel Anchovy. *Fish Oceanogr.*, 11:31–44, 2002.

[30] H. Demarcq. Trends in primary production, sea surface temperature and wind in upwelling systems (1998-2007). *Prog. Oceanogr.*, 2009.

Use of Satellite Data to Study the Mediterranean Sea Physical and Biological Dynamics

E. Rinaldi, G. Volpe, B. Buongiorno Nardelli, R. Santoleri
Institute of Atmospheric Sciences and Climate, CNR, Roma, Italy
eleonora.rinaldi@artov.isac.cnr.it

Abstract

Satellite and in situ data give a complementary view of the processes occurring in the oceans. The advantage of using remote sensing is that it can provide long-term, synoptic and global estimates of key parameters of the oceans, covering a larger geographic area more frequently than field sampling. The Gruppo di Oceanografia da Satellite (GOS) of the Istituto di Scienze dell'Atmosfera e del Clima (ISAC) is responsible for the production of ocean colour and sea surface temperature (SST) data over the Mediterranean basin and Black Sea in the framework of several national and international projects. However, the GOS activity is not limited to the operational processing of satellite data but focuses also on their scientific analysis, which often includes other kinds of data, both remotely-sensed and collected in situ. A brief summary of the main results obtained in two of the most recent GOS works is presented herafter. The first one describes the analysis of the relation between physical and biological processes affecting the Mediterranean surface layer [1], and the second one focuses on the study of the Tyrrhenian Sea surface circulation from the combination of surface drifters and altimeter data [2].

1 Introduction

Satellite and in situ data give a complementary view of the processes occurring in the oceans. The advantage of using remote sensing is that it can provide long-term, synoptic and global estimates of key parameters of the oceans, covering a larger geographic area more frequently than field sampling. However, they may only provide measurements of surface parameters and they also need to be validated through available in situ measurements. On the opposite, in-situ measurements provide more complete and localized information but they generally cannot provide a dense and wide spatial coverage. This inadequate resolution and coverage issue is an important limitation for the study of spatially inhomogeneous parameters (like chlorophyll). The Gruppo di Oceanografia da Satellite (GOS) of the Istituto di Scienze dell'Atmosfera e del Clima (ISAC) is responsible for the production of ocean colour and sea surface temperature (SST) data over the Mediterranean and Black seas in the framework of several national and international projects. However, the GOS activity is not limited to the operational processing of satellite data but focuses also on their scientific analysis, which often include other kind of data both remotely-sensed and collected in situ. In the last years, the GOS has published many papers based on the analysis and integration of different satellite sen-

sors, also with in situ data [see for example [3, 4, 5, 6, 7, 8, 9, 10, 11, 12], collaborating with many different groups inside and outside Europe (among others, Rosenstiel School of Marine and Atmospheric Science (RSMAS), University 'Parthenope' of Napoli, Istituto Nazionale di Oceanografia e di Geofisica Sperimentale (OGS), National Oceanography Centre Southampton (NOCS), Agenzia nazionale per le nuove tecnologie, l'energia e lo sviluppo economico sostenibile (ENEA)). This work gives an overview of GOS activity summarizing the main results of the two most recent GOS works, namely Volpe et al. [1] and Rinaldi et al. [2]. The first describes the analysis of the relation between physical and biological processes affecting the Mediterranean surface layer in the period 1998-2006 (Section 3.1). The second is a study of the Tyrrhenian Sea surface circulation from the combination of surface drifters and altimeter data between December 2001 and February 2004 (Section 3.2). The paper is organized as follows: Section 2 describes the data used and the methodologies adopted within the two works. Section 3 discusses the main results while conclusions are drawn in Section 4.

2 Data and Methods

2.1 MADT Dataset

The altimeter data used here are produced by Ssalto/Duacs and distributed by Aviso, with support from Cnes (http://www.aviso.oceanobs.com/duacs/).
The 2001-2004 altimeter data time series is the Mediterranean Absolute Dynamic Topography (MADT) built from four altimetric satellites: Jason-1, Envisat or ERS-2, Topex/Poseidon and Geosat Follow-On GFO. Standard corrections have been applied to data by Ssalto/DUACS [13]. Data were merged and interpolated on a weekly basis over a regular 1/8° grid using an optimal interpolation [14]. Finally, the mean dynamic topography (MDT) was added to the sea level anomalies (SLA), as detailed in Rio et al. [15].

2.2 The SST Dataset

The SST time series is the optimally interpolated re-analysis product [OISST, [6]], widened to include the 2006 measurements. The re-analysis is based on Pathfinder SST time series. The data span from January 1998 to December 2006 and they cover the Mediterranean area at 1/16° resolution. To match the MADT spatial domain the northern Adriatic Sea was masked out (because of its shallowness). The daily SST time series were averaged over 8-day "week" intervals of which there are 45 in a year of 360 days.

2.3 The Chlorophyll Dataset

SeaWiFS ocean colour data were acquired and processed by the receiving station HROM at GOS from 1998 to 2006, The MedOC4 [5] algorithm for chlorophyll (CHL) retrieval in case-1 waters was applied to the remote sensing reflectance. CHL maps were remapped at the spatial resolution of 1.1x1.1 km over an equirectangular grid covering the Mediterranean Sea. The 1/16° resolution grid map was achieved by averaging the base-10 log-transformed chlorophyll values (LCHL, to differentiate from CHL), to account for chlorophyll lognormal distribution [16]. This spatial resolution matches the resolution of the SST OI maps developed in

the context of the Mediterranean Forecasting System Towards Environmental Prediction (MFSTEP) project. Similarly to SST time series, the northern Adriatic Sea was masked out. 8-day averages were then computed and used as input to DINEOF analyses for data interpolation and hence to EOF analysis for studying the field space-time variability.

2.3.1 DINEOF interpolation

The EOF analysis needs complete time series of input data, with no data voids. While the SST and the MADT time series were interpolated by data provider, the LCHL maps present several data voids due to persistent cloud cover. So, before any further analysis, an interpolation algorithm was applied to the LCHL time series. The Data INterpolating Empirical Orthogonal Functions (DINEOF) method developed by Beckers and Rixen [17] and used by Beckers et al. [18] was used for the reconstruction of missing data. This technique recognizes the areas that have different sources of space-time variability, through iterative EOF estimation. The method operates as follows: the time average is removed from valid observations and anomaly data are stored in a matrix X. Missing data are set to zero, which is the equivalent of using, as first guess, the temporal average of each marine pixel. Simultaneously, a set of good pixels is set aside as reference. These pixels are set to zero within X. Data initially missing are replaced with the reconstructed field using the first EOF mode. This process is iterated, truncating the time series reconstruction to the ith mode, until convergence is reached. Convergence is defined as the error evaluated in the reconstructed time series with respect to the reference pixels. In the present work, the same steps as in Beckers and Rixen [17] were followed and it was found that the error continued to decrease up to the 31st iteration. However, the variance explained by the 31st mode was well below the variance explained by noise. In fact, the first mode associated with a random-filled matrix of the same dimensions as X explains the same variance as the 20th EOF mode from LCHL. Therefore, this variance level was adopted as the limit to stop the iterations and thus define the number of useful modes. The interpolated dataset and associated EOFs were obtained by reconstructing the time series using this truncated set of modes. Finally, when comparing the spatial patterns obtained from EOF analysis computed over different variables, it is useful to have a measure of their similarity, i.e., to correlate different spatial patterns. In a similar way, the temporal lagged correlation coefficient measures the correlation between amplitudes of different modes of different variables. This latter parameter may be useful in identifying the time response of one variable to the forcing of the others. All correlation values were tested for significance (99.9% level) through the Student T-test.

2.4 Drifting buoy data-set

The drifting buoy dataset used in this study consists of 53 satellite-tracked modified CODE drifters data spanning from December 2001 to February 2004. As first step, before data are interpolated at 2-hour intervals using a kriging technique, raw drifter data were corrected for spikes and outliers [19]. To remove high frequency current components, data were then filtered using a low-pass filter. This filtered time series was sub-sampled at 6-hour intervals, and resulting surface velocities calculated

through centred finite differencing of the filtered positions. Pseudo-Eulerian statistics were estimated from this dataset (for the definitions of pseudo-eulerian statistics see Emery and Thomson, [20]). The pseudo-Eulerian approach consists of subdividing the domain under study into regions (bins) within which the flow is assumed to be homogeneous and stationary and by calculating the mean field as the average of all the velocity measurements available in the bin. In this study bins of 0.25° x 0.25° were used [21]; for a thorough methodological discussion see [22].

2.4.1 Wind data

To estimate the Ekman component from the velocity field as deduced by drifters, the operational analysis of wind data provided by the European Centre for Medium-range Weather Forecast (ECMWF) measurements were used. Wind data were interpolated at the time of observation and at the drifter positions using a bilinear scheme. In this work the formula for the Mediterranean proposed by Mauri and Poulain [23] was applied.

$$\mathrm{Uwind} - \mathrm{driven} = 0.012\exp(-\mathrm{i}24)\mathrm{Uwind}$$

After the removal of the Ekman component from drifter velocities, the same binning scheme as the original drifter data was applied to the resulting Ekman-corrected drifter observations.

3 Results

3.1 Phytoplankton response to physical processes in the Mediterranean Sea: EOF analysis of satellite observations

The ocean can reduce the atmospheric CO_2 concentration through the so-called biological pump (i.e., which refers to the sinking of organic matter from the surface productive layers to deep waters in the ocean [24]). In this context, the quantification of the carbon flux into the ocean through the marine primary productivity and of the mechanisms that might control it is of crucial importance. This work provides a direct and powerful scheme linking the upper ocean dynamics to the mechanisms that can force the phytoplankton variability, on a seasonal scale. With the scope of defining the scales of co-variability and eventually assess the its timing, the analysis was carried out in two steps. First, to isolate physical and biological processes EOF analysis was performed over SST and LCHL separately. Once different processes have been clearly identified, a spatial and temporal correlation analysis should permit the investigation of the coupling between phytoplankton biomass and the upper ocean dynamics, ultimately letting for the timing of the biological response to the physical forcing to be defined.

3.1.1 Basin scale variability

The first LCHL EOF mode (explaining 74% of total variance) is characterized by a large-scale signal with the spatial pattern positive almost everywhere (Figure 1a). The EOF pattern shows an E-W gradient, with most of the variability located

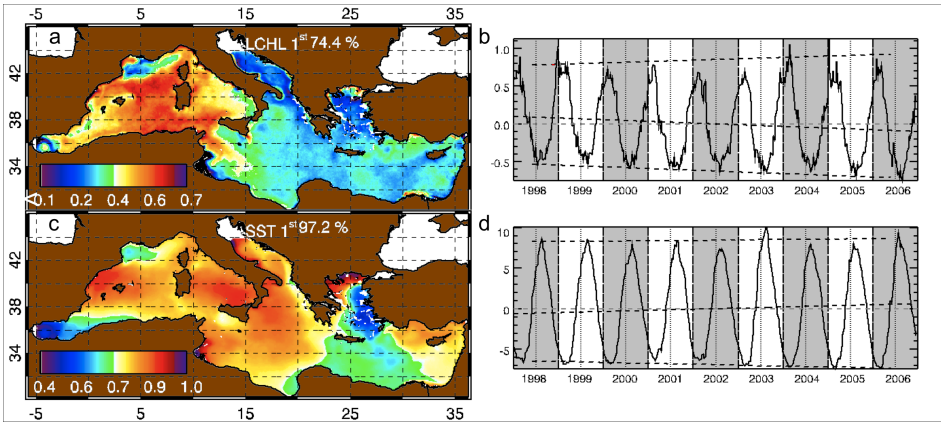

Figure 1: First EOF mode computed over LCHL (a-b) and SST (c-d) data time series. Units are in Log10(mg m-3) for LCHL and °C for SST. Negative values (Gulf of Gabes (Tunisia), and of the Gibraltar inflow to the Alboran Sea) are indicated by black colour. Temporal amplitudes and spatial patterns are normalized on the spatial pattern maximum value for each mode. Trend line (among the maxima, minima and for the whole time series) and zero value are represented by black and grey dashed lines.

Variable 1 (mode #)	Variable 2 (mode #)	Time r	Time lag	Space r
LCHL (1)	SST (1)	0.91	0	0.2
LCHL (2)	SST (2)	-0.7	5.5 months	0.6

Table 1: Space-time correlation between two variables. Variable 1 follows variable 2 in the temporal correlation analysis with a time lag as defined in the relevant column.

in the WMED basin. The LCHL amplitude presents maxima commonly recurring from mid-January to April and minima from July to September (Figure 1b). This annual cycle can be described in terms of water stratification as already shown by Behrenfeld et al. [25] global scale. In fact, the amplitude of this mode (Figure 1b) is highly anti-correlated (r=-0.9, see Table 1) with the amplitude of the first mode of SST (Figure 1d) at zero time lag: in other words, during winter when the water column is less stratified due to stronger heat loss from the ocean surface, high biomass levels occur. This increase is reasonably attributable to the stronger nutrient entrainment into the upper mixed layer.This is confirmed by trends related to the maximum and minimum values of two variables (Figure 1b,d). In fact, during the summer season, there is an increase of maximum values for SST leading to a decrease of minimum values for Chl. So a greater stratification corresponds to a lower intake of nutrients in the surface layer and hence to an increase oligotrophy. Nevertheless, the seasonal heating determines a reply of SST almost spatially uniform. Higher variability is present

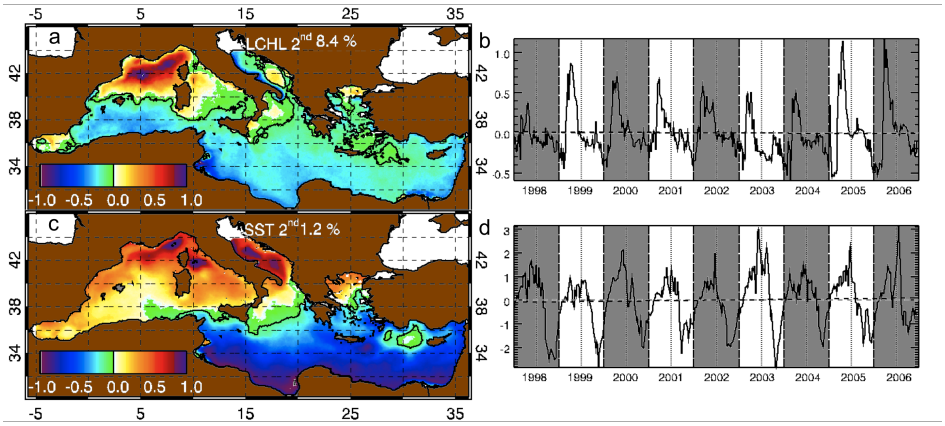

Figure 2: Second EOF mode calculated from LCHL (a-b) and SST (c-d) data. See Figure 1 for details.

only in those areas where repetitive wind regimes play a major role in regulating the seasonal air-sea heat flux: Mistral in the NW MED, and the Etesian in the Aegean Sea and south of Crete [26, 27]. Moreover the inflow of Atlantic waters, with strong and permanent mesoscale dynamics acting in the Alboran Sea [Pujol and Larnicol, 2005], leads to a reduction of the variability of the seasonal air-sea flux in this region. This explains the poor spatial correlation between LCHL and SST patterns (r=0.2, Table 1). High values of LCHL variability spreads eastward into the Sicily channel where the transport of surface Modified Atlantic Waters [MAW, see among others [28, 29] has already been shown to display a clear annual cycle with maxima in April [30]. Indeed the phytoplankton meridional distribution of the region is forced by the seasonal variability of MAW transport across the Sicily Channel with the southern sector being more susceptible to seasonal variations than the northern one. Similarly to the dynamics of the western Alboran Gyre, of the Adriatic coastal current and of the shallow Gulf of Gabes, the Ligurian Sea–Gulf of Lion area presents weaker variability as compared to the rest of the WMED, in this mode (Figure 1a). The variability of these areas is clearly described in the second mode (Figure 2, see next section), where regional processes rule their dynamics.

3.1.2 Regional scale variability

The second LCHL EOF mode, that explains the 8% of total variance, displays some peculiar areas inside the Mediterranean Sea related to the main open ocean spring blooms (Figure 2a). The spatial pattern shows strong maxima in the northwestern MED and to a lesser extent in the Bonifacio Gyre, along the eastern coast of Calabrian peninsula (southern Italy), and in the southern Adriatic and Rhodes Gyres. The comparison between this LCHL mode with the corresponding second SST mode (Figure 2c-d) reveals that the phytoplankton response is linked to the succession from autumn-winter water column mixing

to spring re-stratification. This succession is evident from the analysis of the temporal amplitudes of both SST and LCHL second modes (Figure 2b-d), and from respective spatial patterns (Figure 2a-c). In fact, in the LCHL amplitude a strong positive bloom-like pulse during spring always follows a strong negative signal during winter (Figure 2b). These winter minima are a signal of the deep mixing associated with open ocean deep-water formation (DWF). The SST second mode pattern identifies the same phenomenon (Figure 2c); high variability in the WMED coincides with the areas where preconditioning to DWF occurs in late autumn-beginning of winter [Stommel, 1972], and highlighted by the minima in the corresponding amplitude (Figure 2d). This means that the phytoplankton biomass dilution, coinciding with DWF events, is followed by the spring bloom that co-occurs with the gradual re-stratification of the water column. The significant spatial (r=0.6) and temporal (r = -0.7, 5.5 months lag; Table 1) correlations support this finding. Five and a half months is the time lag between the preconditioning phase to the DWF phenomenon and the spring bloom which coincides with the re-stratification of the water column, when phytoplankton can efficiently utilize the nutrients made available into the surface layer [31, 32, 33]. This phenomenon is characterized by evident interannual variability with a minimum in 1998 and exceptional high values during 2005 and 2006. Several study in the north WMED area found an unusual location for the newly formed deep water in the Ligurian basin [34] during this "anomalous" period. The unusually high values in 2005 and 2006 can be described by the fact that the Ligurian Sea might have acted as an additional area in terms of nutrient source. The southern Adriatic Gyre, where deep mixing generally takes place [35, 36], determines the signal of higher variability in the Adriatic Sea (Figure 2a). Moreover, positive values can be seen to correspond to the Rhodes Gyre, though less clearly. The Calabrian coast shows an opposition of phase with respect to the rest of the Ionian Sea, and probably due to the seasonal upwelling of the area [37]. During autumn another less intense peak occurs. This is due to the first response of phytoplankton to seasonal nutrient entrainment in the upper layers after summer stratification (St Martin Summer bloom [38]).

3.2 Lagrangian and Eulerian observations of the surface circulation in the Tyrrhenian Sea

The Tyrrhenian surface circulation was studied analyzing surface drifters data deployed in the area between December 2001 and February 2004 and coincident satellite remotely-sensed altimeter data, covering the same period. The interpolated fields of altimeter data are obtained by original altimeter data collected along tracks. These are located several kilometres apart, with an instantaneous field of view of $\sim$9 km, and a repetitivity ranging between 10 days and 35 days. Unlike, drifter data present large data gaps, both in space and time, due to the purely Lagrangian sampling. However, drifters data may or may not include the ageostrophic components of the flow, providing different measurements of the surface circulation in terms of dynamical components. In order to unequivocally assess and define the surface circulation features of the Tyrrhenian Sea, this work aims to estimate the limitations and representativeness of both datasets in terms of dy-

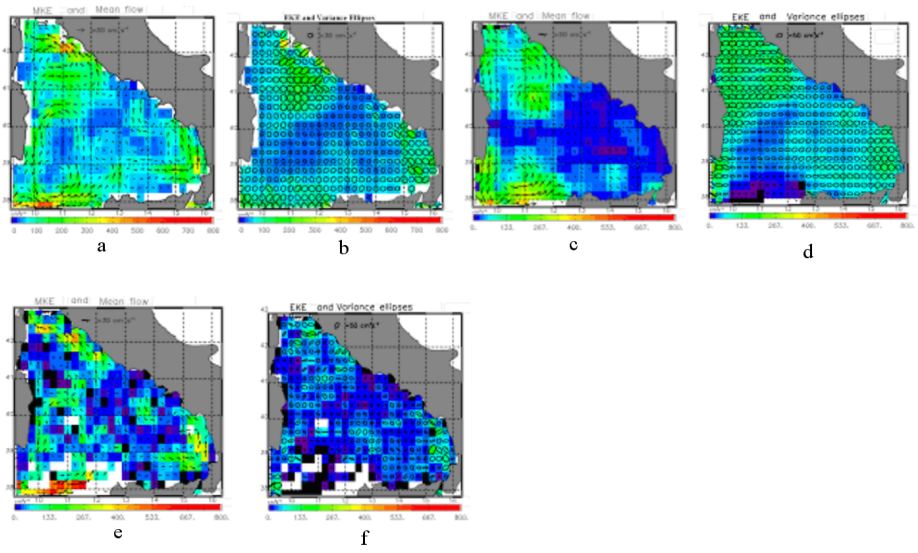

Figure 3: Pseudo-Eulerian statistics. (a) Mean Kinetic Energy with superimposed the mean flow vectors from altimeter data; (b) Eddy Kinetic Energy with superimposed the variance ellipses form altimeter data; (c) MKE and mean flow vectors obtained from smoothing fields of drifters data; (d) EKE and variances ellipses obtained from smoothing fields of drifters data; (e) MKE and mean flow vectors computed using altimeter data sampled in correspondence of the drifter measurements; (f) EKE and variances ellipses computed using altimeter data sampled in correspondence of the drifter measurements.

namical factors or sampling rate issues.

3.2.1 Overview of the surface circulation as described by the altimeter data

In this subsection the surface circulation traced by altimeter data is described (Figure 3a and Figure 3b). In the northern region of Tyrrhenian Sea the main structure of the circulation is the North Tyrrhenian Cyclone, NTC, (Figure 3a). The coastal current leaving the Tyrrhenian Sea through the Corsica Channel represents the eastern boundary of the NTC. Characterized by lower energy values than NTC, the North Tyrrhenian Anticyclone (NTA) works as its southern boundary. The outflow at the western side of the Sardinia Channel in Figure 3a can be attributable to the presence of a double core cyclonic gyre in the western side of the basin, as already shown by independent hydrological measurements [39, 40]. The northern margin of this gyre corresponds to the westward flow of the NTA. It extends south of 38°N and captures the major portion of the AW entering the Tyrrhenian basin. This structure presents the highest values of MKE ($>$135 $\mathrm{cm}^2 \cdot \mathrm{s}^{-2}$) in the southward flow along the Sardinian coast and in the southern area of this vortex (MKE $>$300 $\mathrm{cm}^2 \cdot \mathrm{s}^{-2}$). Be-

tween 12-13 °E and 39-40 °N an anticyclonic vortex captures a minor portion of the AW (this anticyclone will be referred to as the South Tyrrhenian Anticyclone, STA). This vortex has a circular shape with a diameter of ∼100 km and MKE level of around 70 $cm^2 \cdot s^{-2}$. At the eastern corner of the basin, an anticyclonic circulation is visible close to the northern coast of Sicily. Higher energy levels, at its eastern side, are located in correspondence of a cyclonic gyre that extends up to 40 °N. A second anticyclonic recirculation is visible offshore the Gulf of Naples. Contrary to previous studies, here the AW does not follow the coast to give rise a "simple" cyclonic circulation. In fact, due to the presence of the above-mentioned eddies the AW, entering the Tyrrhenian Sea through the eastern part of the Sardinia Channel, gives origin to a more complex surface circulation in the whole southeastern domain. The EKE map (Figure 3b) has a distribution of energy value similar to the MKE one. The maxima are present in correspondence of the divergence zone of the NTC and NTA (EKE $>$ 135 $cm^2 \cdot s^{-2}$), along 38°N and along the eastern side of the cyclonic gyre in front of the Calabrian coast (between 15-16 °E, 38-40 °N). In this area the eccentricity of variance ellipses demonstrates that the variability of the mean flow is prevalently oriented along the northwest-southeast direction (Figure 3b). Low values of EKE are present in the central area of the Tyrrhenian Sea, except for the region occupied by the STA. Over the whole basin, the MKE is generally higher than the EKE.

3.2.2 Joint pseudo-Eulerian analysis of altimeter and drifter data

The same procedure used for drifter data was applied also to altimeter data, so that the altimeter geostrophic velocities were first binned over the same 0.25° x 0.25° grid used for Lagrangian data and then used to compute the statistics. To make the two datasets as comparable as possible, the ageostrophic component due to the wind-driven Ekman transport has been calculated from the ECMWF wind data and subtracted from the drifter velocities. Moreover, drifters data have been smoothed using a moving average with a square boxcar of dimension of ∼100 Km. This length is comparable to the scales of spatial decorrelation used in the optimal interpolation of altimeter data. The resulting fields are shown in Figure 3c and Figure 3d. MKE and EKE average values are 73 $cm^2 \cdot s^{-2}$ and 66 $cm^2 \cdot s^{-2}$ respectively. West of 12°E the smoothed drifter data (Figure 3c) have almost the same qualitative (spatial distribution of local energy minima and maxima) and quantitative (MKE values) patterns displayed by the altimeter data of Figure 3a. This is particularly evident for the eastern side of NTC, in which the highest values of energy (∼170 $cm^2 \cdot s^{-2}$) distinguish the current along the Italian coast and the flow in the Corsica Channel. Nevertheless, on the eastern side of the Tyrrhenian Sea the values are still rather diverse. This is attributable to the fact that the circulation in this region is dominated by the mesoscale fields. On the contrary, the western area of the basin is characterized by sub-basin scale structures. Hence, the different sampling rates of the two instruments might be responsible for such a discrepancy. The values of the smoothed EKE calculated from drifter data

are greater than the altimeter EKE ones (Figure 3d and Figure 3b, respectively). In fact, the relative difference between altimeter and drifter smoothed maps is of the order of 43% with a correlation of 0.37. Ultimately, the pseudo-Eulerian statistics have been estimated from altimeter data re-sampled along drifter trajectories (Figures 3e, 7f). The MKE map of this new dataset (Figure 3e) is now more similar to the drifters MKE map (Figure 3c), with a MKE average value of 88 $cm^2 \cdot s^{-2}$ and 84 $cm^2 \cdot s^{-2}$ respectively, and the correlation of 0.7 (99% significance level). On the contrary, the EKE maps are still very different both in terms of energy (the average altimeter EKE is 29 $cm^2 \cdot s^{-2}$ against 66 $cm^2 \cdot s^{-2}$) and in terms of size and variance ellipses orientation (these are more regular and smaller than those from smoothed drifters data). Despite these differences, the correlation between Figure 3f and Figure 3d is increased to 0.45 (99% significance level). It is worth reminding that drifters are smoothed spatially but not temporally, while altimeter data, though representative of a particular day, are obtained interpolating data collected at different times, which are then smoothed through statistical interpolation. Although differences between the two datasets can be partly imputed to the above-mentioned intrinsic space-time sampling capabilities, this analysis shows that an important part of the drifters EKE is probably associated with ageostrophic signals.

4 Conclusions

In the work on phytoplankton response to physical processes in the Mediterranean Sea the principal component analysis of the SeaWiFS chlorophyll concentration (LCHL) time series (1998-2006) has been used to asses the coupling between phytoplankton biomass variability and surface physical dynamics. The spatial and lagged correlation between LCHL EOF modes and analogous modes estimated from SST has allowed to describe the first modes in terms of biological response to known physical processes or dynamical changes observed in the Mediterranean Sea. At basin scale, the phytoplankton concentration is linked to the annual cycle of the water column stratification, as already shown at global scale [25]. This is particularly evident in the areas previously identified D'Ortenzio and Ribera d'Alcalà [41] as intermittently or non-blooming: basically the whole WMED except those areas characterized by permanent and seasonal dynamical structures such as the Gulf of Lions-Ligurian Sea area and the Alboran Sea. The coupling between phytoplankton biomass variability and the water column stratification is supported by the high correlation found between LCHL and SST first modes. Conversely, the northwestern MED is interested by completely different mechanism. In fact, the delayed response of phytoplankton to local surface cooling connects the MED open ocean spring bloom to the DWF processes via the pre-conditioning phase. On one hand, the total amount of nutrients accessible in the offshore surface waters depends on the deep convection events occurring in late winter [31, 32]. On the other hand, the space-temporal extent of the DWF phenomenon is directly linked to the intensity of the pre-conditioning phase, during which the surface stratification is significantly reduced. This pre-conditioning is due to the combination of more powerful sub-basin scale cyclonic circulations and strong buoyancy fluxes associated with in-

tense atmospheric events. However, phytoplankton can efficiently utilize the nutrients of the upper mixed layer only during the re-stratification phase: i.e., the spring bloom. This analysis demonstrates that the pre-conditioning phase is decisive in determining the amount of nutrients and consequently the spatio-temporal extents of the spring bloom. Therefore the present study was able to associate the physical and biological variability with specific dynamical signals and phenomena observed at different space and time scales using the EOF decomposition method. The study of the Tyrrhenian surface and near surface circulation was achieved studying 53 CODE drifters and 4 years of altimetric data. This study has drawn a circulation pattern very different from the one described in literature. Here new circulation structures were identified in the southern region of the basin. These are modulated by a series of mesoscale/sub-basin structures, of both transient and semi-permanent nature. The importance of these structures is particularly evident in the southern sub-basin where they overcome by far the mean flow picture. The dynamical differences as obtained by drifter and altimeter measurements, primarily due to their different sampling rates and resolutions, were clearly shown up by the pseudo-Eulerian statistics computed with the two datasets. When altimetric data were sub-sampled over pre-smoothed drifter trajectories, the MKE levels of energy resulted in good agreement. Nevertheless, the variance ellipses and the EKE levels still displayed very different values, with the altimetric levels of energy always smaller than those from drifters. Therefore, it is possible conclude that, the standard interpolated products of altimeter data lose a considerable part of the signal, even if they ensure a wider and more regular sampling than drifters.

References

[1] G. Volpe, B. Buongiorno Nardelli, P. Cipollini, R. Santoleri, and I.S. Robinson. Seasonal to interannual phytoplankton response to physical processes in the Mediterranean Sea from satellite observations. *Under review in Remote Sensing of the Environment*, 2010.

[2] E. Rinaldi, B. Buongiorno Nardelli, E. Zambianchi, R. Santoleri, and P.-M. Poulain. Lagrangian and Eulerian observations of the surface circulation in the Tyrrhenian Sea. *J. Geophys. Res.*, 2010.

[3] F. Bignami, E. Böhm, E. D'Acunzo, R. D'Archino, and E. Salusti. On the dynamics of surface cold filaments in the Mediterranean Sea. *J. Mar. Sys.*, 74(1-2):429–442, 2008.

[4] F. Bignami, R. Sciarra, S. Carniel, and R. Santoleri. The variability of Adriatic Sea coastal turbid waters from SeaWiFS imagery. *J. Geophys. Res.*, 112(C3), 2007.

[5] G. Volpe, R. Santoleri, V. Vellucci, M. Ribera d'Alcala, S. Marullo, and F. D'Ortenzio. The colour of the Mediterranean Sea: Global versus regional bio-

optical algorithms evaluation and implication for satellite chlorophyll estimates. *Remote Sensing of Environment,*, 107:625–638, 2007.

[6] S. Marullo, B. Buongiorno Nardelli, M. Guarracino, and R. Santoleri. Observing the 580 Mediterranean Sea from space: 21 years of Pathfinder-AVHRR sea surface temperatures(1985 to 2005): re-analysis and validation,. *Ocean Science*, 3:299–310, 2007.

[7] E. Böhm, T.S. Hopkins, L.J. Pietrafesa, and J.H. Churchill. Continental slope sea level and flow variability induced by lateral movements of the Gulf Stream in the Middle Atlantic Bight. *Progress in Oceanography*, 70:196–212., 2006.

[8] B. Buongiorno Nardelli, O. Cavalieri, M.-H. Rio, and R. Santoleri. Subsurface geostrophic velocities inference from altimeter data: application to the Sicily Channel (Mediterranean Sea),. *J. Geophys. Res.*, 111(C04007), 2006.

[9] B. Buongiorno Nardelli and R. Santoleri. Methods for the reconstruction of vertical profiles from surface data: multivariate analyses, residual GEM and variable temporal signals in the North Pacific Ocean. *J. Atmos. Ocean. Tech.*, 22(11):1763–1782, 2005.

[10] G. Volpe, V.F. Banzon, R.H. Evans, R. Santoleri, A.J. Mariano, and R. Sciarra. Satellite observations of the impact of dust in a low-nutrient, low-chlorophyll region: Fertilization or artifact? *Global Biogeochem. Cycles*, 2009.

[11] B. Buongiorno Nardelli, S. Colella, R. Santoleri, M. Guarracino, and A. Kholod. A re-analysis of Black Sea Surface Temperature. *J. Mar. Sys.*, 2009.

[12] E. Rinaldi, B. Buongiorno Nardelli, E. Zambianchi, R. Santoleri, and P.M. Poulain. Lagrangian and Eulerian observations of the surface circulation in the Tyrrhenian Sea. *J. Geophys. Res. doi:10.1029/2009JC005535*, 115(C04024), 2010.

[13] P.Y. Le Traon and F. Ogor. ERS-1/2 orbit improvement using TOPEX/POSEIDON: The 2cm challenge. *Journal of Geophysical Research-Oceans*, 103(C4):8045–8057, 1998.

[14] N. Ducet, P.Y. Le Traon, and G. Reverdin. Global high-resolution mapping of ocean circulation from TOPEX/Poseidon and ERS-1 and -2. *J. Geophys. Res.*, 105(19,477–19,), 2000.

[15] M.E. Rio, P.-M. Poulain, A. Pasqual, E. Mauri, G. Larnicol, and L. Santoleri. A mean dynamic topography of the Mediterranean Sea computer from the altimetric data and in situ measurements. *J. Mar. Sys*, page 484–508, 2007.

[16] J.W. Campbell. The Lognormal-Distribution as a Model for Biooptical Variability in the Sea. *Journal of Geophysical Research-Oceans*, 100(C7):13237–1325, 1995.

[17] J.M. Beckers and M. Rixen. EOF calculations and data filling from incomplete oceanographic datasets. *J. Atmos. Oceanic Tech.*, 20(12):1839–1856, 2003.

[18] J.M. Beckers, A. Barth, and A. Alvera-Azcárate. DINEOF reconstruction of clouded images including error maps - application to the Sea-Surface Temperature around Corsican Island. *Ocean Science*, 2:183–199, 2006.

[19] P.-M. Poulain, R. Barbanti, R. Cecco, C. Fayos, E. Mauri, L. Ursella, and P. Zanasca. Mediterranean Surface Drifter Database: 2 June 1986 to 11 November 1999. Tech. Rep. 78/2004/OGA/31, OGS, Trieste, Italy. 2004.

[20] W.J. Emery and R.E. Thomson. Data analysis methods in physical oceanography. *Pergamon, Elsevier Science Ltd*, 1998.

[21] M.S. Swenson and P.P. Niiler. Statistical analysis of the surface circulation of the California Current. *J. Geophys. Res.*, 101:22631–2264, 1996.

[22] S. Bauer, M.S. Swenson, A. Griffa, A.J. Mariano, and K. Owens. Eddy-Mean flow decomposition and eddy-diffusivity estimates in the Tropical Pacific Ocean – 1. *Methodology, J. Geophys. Res.*, 103:30855–308, 1998.

[23] E. Mauri and P.-M. Poulain. Wind-driven currents in Mediterranean drifterdata. Tech. Rep. 01/2004/OGA/1, OGS, Trieste, Italy, 25 pp. 2004.

[24] C.M. Lalli and T.R. Parsons. Biological Oceanography, An Introduction. *The Open University*, page 314, 1997.

[25] M. Behrenfeld, R.T. O'Malley, D. Siegel, C. McClain, J.L. Sarmiento, G.C. Feldman, A.J. Milligan, P. Falkowski, R. Letelier, and E. Boss. Climate-driven trends in contemporary ocean productivity. *Nature. doi:710.1038/nature05317*, 444:752–755, 2006.

[26] S. Zecchetto and F. De Biaso. Sea surface winds over the Mediterranean basin from satellite data (2000-04): Meso- and local-scale features on annual and seasonal time scales. *Journal of Applied Meteorology and Climatology*, 46(6):814–827, 2008.

[27] M. Burlando. The synoptic-scale surface wind climate regimes of the Mediterranean Sea according to the cluster analysis of ERA-40 wind fields,. *Theoretical and Applied Climatology*, 96, 2009.

[28] G.M.R. Manzella, T.S. Hopkins, P.J. Minnett, , and E. Nacini. Atlantic water in the Strait of Sicily. *Journal of Geophysical Research*, 95:1569–1575, 1990.

[29] A.R. Robinson, J. Sellschopp, A. Warn-Varnas, W.G. Leslie, C.J. Lozano, P.J. Haley, L.A Anderson, and P.F.J. Lermusiaux. The Atlantic Ionian stream. *Journal of Marine Research*, 20:129–156, 1999.

[30] K. Béranger, L. Mortier, , and M. Crépon. Seasonal variability of water transport through the Straits of Gibraltar, Sicily and Corsica, derived from a high-resolution model of the Mediterranean circulation. *Progress in Oceanography*, 66(2-4):341–364, 2005.

[31] M. Levy, L. Memery, and G. Madec. The onset of a bloom after deep winter convection in the northwestern Mediterranean sea: mesoscale process study with a primitive equation model. *Journal Of Marine Systems*, 16:7–21, 1998.

[32] M. Levy, L. Memery, and G. Madec. The onset of the Spring Bloom in the MEDOC area: mesoscale spatial variability. *Deep-Sea Research Part I, Oceanographic Research Papers*, 46(7):1137–1160, 1999.

[33] V. Barale, J.M. Jaquet, and M. Ndiaye. Algal blooming patterns and anomalies in the Mediterranean Sea as derived from the SeaWiFS data set (1998-2003). *Remote Sensing of Environment*, 112:3300–3313, 2008.

[34] R.O. Smith, H.L. Bryden, and K. Stansfield. Observations of new western Mediterranean deep water formation using Argo floats 2004-2006. *Ocean Science*, 4:133–149, 2008.

[35] G. Civitarese and M. Gacic. Had the Eastern Mediterranean transient an impact ore the new production in the Southern Adriatic? *Geophysical Research Letters*, 28(8):1627–1630, 2001.

[36] R. Santoleri, G. Volpe, S. Marullo, and B. Buongiorno Nardelli. Open Waters Optical Remote Sensing of the Mediterranean Sea. 2008.

[37] F. D'Ortenzio, S. Marullo M. Ragni, and M. Ribera d'Alcala. Did biological activity in the Ionian Sea change after the Eastern Mediterranean Transient? Results from analysis of remote sensing observations. *Journal of Geophysical Research-Oceans*, 108(C9), 2003.

[38] A. Zingone, R. Casotti, M. Ribera D'Alcala, M. Scardi, and D. Marino. St-Martins summer – the case of an autumn phytoplankton bloom in the Gulf of Naples (Mediterranean Sea). *Journal of Plankton Research*, 17(3):575–593, 1995.

[39] S. Sparnocchia, G.P. Gasparini, M. Astraldi, M. Borghini, and P. Pistek. Dynamics and mixing of the eastern Mediterranean outflow in the Tyrrhenian Basin. *J. Mar. Syst. doi:10.1016/S0924-7963(98)00088-8*, 20:301–317, 1999.

[40] M. Astraldi, G.P. Gasparini, A. Vetrano, and S. Vignudelli. Hydrographic characteristics and interannual variability of water masses in the central Mediterranean: A sensitivity test for long term changes in the Mediterranean Sea. *Deep Sea Res. Part I, doi:10.1016/S0967-0637(01)00059-0*, 49(4):661–680, 2002.

[41] F. D'Ortenzio and M. Ribera d'Alcala. On the trophic regimes of the Mediterranean Sea: a satellite analysis. *Biogeosciences Discussions*, 5:2959–2983, 2008.

Temporal Physical and Chemical Bottom Water Changes in the Middle Adriatic Depressions

E. Paschini[1], M. Marini[1], A. Russo[2], F. Grilli[1], A. Campanelli[1]
1, Institute of Marine Sciences, CNR, Ancona, Italy
2, Polytechnic University of Marche, Ancona, Italy
e.paschini@ismar.cnr.it

Abstract

A physical and chemical dataset collected in the Jabuka (Pomo) depression area (Middle Adriatic Sea) was analysed for seasonal and interannual changes in temperature, salinity, density, dissolved oxygen and nitrates. The historical dataset collected from 1980 to 1997 has been enriched with 30 oceanographic cruises carried out between 1998 and 2008 in the framework of the SINAPSI research program. The bottom water masses of the Jabuka pits are periodically renewed by Northern Adriatic Deep Water (NAdDW) at 1- to 3-year intervals. During late winter-early spring, the new water eventually flows into the western pit and then into the central and the eastern ones. During 1 year of residence in the pits, the bottom water nitrates increase 3-fold and dissolved oxygen decreases by 28% due to mineralisation processes. Some aspects of recently observed decadal climatic anomalies in the Northern Adriatic Sea, in particular the average winter sea surface warming, are revealed by the analysed dataset. Connections may be established with the Eastern Mediterranean Transient (EMT), and indications that after 1999 the Adriatic Sea is returning to be a major producer of the Eastern Mediterranean Deep Water can be inferred. These facts confirms the value of the mesoadriatic depressions as an easily accessible recording site for the interannual oceanographic variations of the Adriatic basin.

1 Introduction

The Adriatic sea is the most continental basin of the Mediterranean Sea. It lies between the Italian peninsula and the Balkans and is elongated longitudinally, with the major axis (about 800 Km versus 200 km) in NW-SE direction. The basin shows clear morphological differences along both the longitudinal and the transversal axis and has been divided into a northern, a central and a southern sub-basin [2]. The northern sub-basin - spanning from the northernmost part to the 100 m bathymetric line - is characterised by an extremely shallow mean depth (about 30 m) with a very weak bathymetric gradient along the major axis, and by a strong river runoff; indeed, the Po and the other northern Italian rivers are believed to contribute about 20% of the whole Mediterranean river runoff [3]. The Middle Adriatic is a transition zone between northern and southern sub-basins, the latter showing some open sea conditions. This central zone spans from the 100 m contour to the Palagrüza (Pelagosa) sill (about 170 m depth), which is located on the line connecting Vieste to Split (Figure

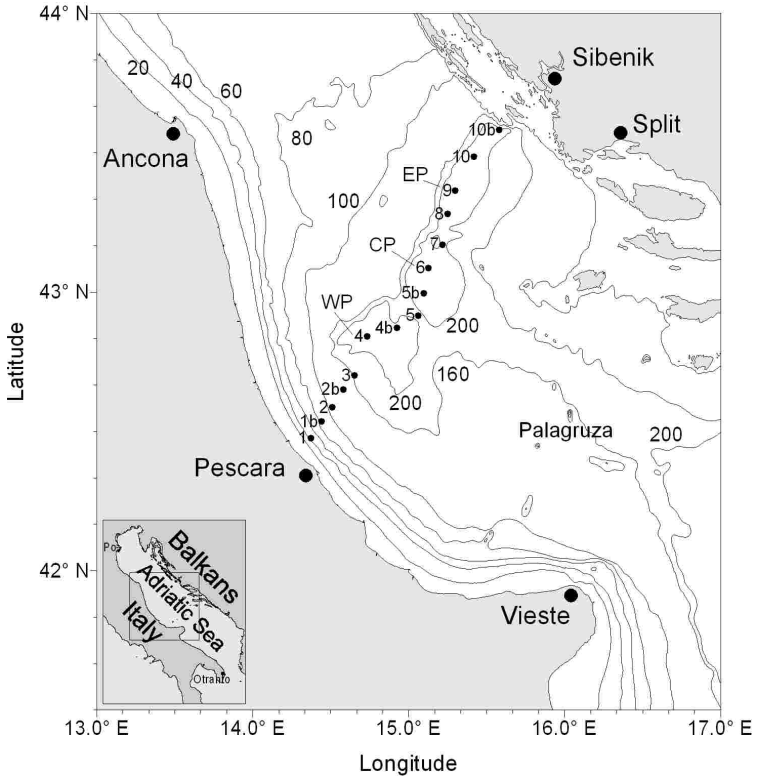

Figure 1: Geographical position of stations in the studied area [1].

1). This area exhibits three depressions, the Jabuka (or Pomo) pits, which reach a maximum depth of about 270 m. The southern sub-basin is characterised by a wide depression exceeding 1200 m in depth. Water exchange with the Mediterranean takes place through the Otranto Straits, which has an 800 m deep sill. Being a continental basin, the Adriatic Sea circulation and water masses are strongly influenced by atmospheric conditions, primarily winds. Main winds blowing over the Adriatic Sea are east-northward Bora and sud-eastward Sirocco. Bora is a cold wind, which in specific points of the Adriatic eastern coast is very intense due to katabathic effects. In winter Bora occurrence causes strong heat losses in the Northern Adriatic and formation of the Northern Adriatic Deep Water (NAdDW). Another factor influencing the NAdDW formation is the water flux, mainly governed by the Po river runoff, which can lower the salinity, and hence the density, of the NAdDW. Vilibić [4] demonstrated the relationships between NAdDW formation and both heat fluxes and autumn Po river runoff. A certain amount of the Adriatic bottom water (NAdDW) masses originate inside the northern subbasin, while intermediate ones mainly originate outside the Adriatic Sea and are modified in the basin [5]. The main interme-

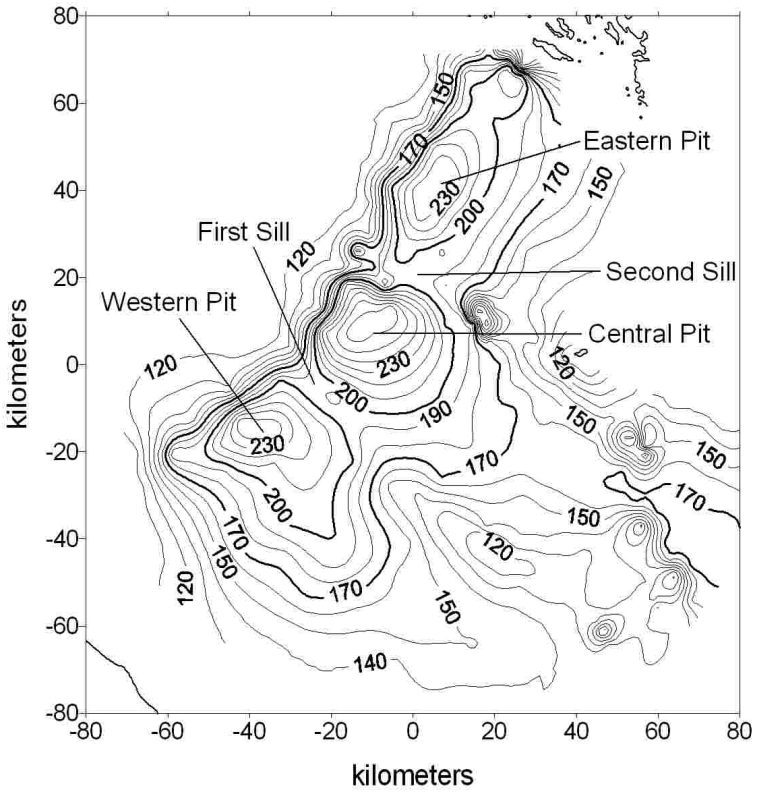

Figure 2: Bathymetric map of Jabuka Pits area [1].

diate water mass is the Levantine Intermediate Water (LIW, formed in the Levantine basin), which enters the Adriatic Sea through the Otranto Straits and then flows along the eastern coast with the Eastern Adriatic Current [6]. Decadal climatic anomalies have been recently evidenced in the Adriatic Sea, likely related to the Eastern Mediterranean Transient (EMT) [7]. In recent years, the LIW entering in the Adriatic Sea has been mostly replaced by the Cretan Intermediate Water (CIW, formed in the Cretan Sea), characterized by a slightly higher salinity; high salinity surface waters were also detected entering through Otranto Straits [8]. The Northern Adriatic surface waters waere changed, with an evident mean temperature increase for every season in the 1988-1999 period in respect to pre-1987 historical data [9]; salinity showed more complicated variations, which can be related to Po river runoff. The mesoadriatic depressions are an interesting site to monitor the changes of Adriatic water masses, especially bottom and intermediate ones. The main feature of this zone is a relatively large area lying below the Palagrüza sill (which marks the boundary between Middle and Southern Adriatic), where a peculiar water mass

(MAdDW, Middle Adriatic Deep Water) resides throughout the year [2]. Three distinct, adjacent pits (western, central and eastern) can be distinguished, with maximum depths of ca. 255, 270, and 240 m, respectively (Figure 2). The MAdDW standing in the Jabuka depressions is renewed primarily by new NAdDW, which forms in winter in the North Adriatic shelf and then flows toward southeast offshore the Italian coast [10, 11, 12]. Renewal generally occurs in late winter - early spring, though not every year, and causes a marked increment in density and oxygen concentrations and a reduction in temperature and nutrients [13]. Between renewals, bottom density declines owing mainly to rising bottom temperature. In some cases renewals have been seen to occur without marked cooling in the presence of low MAdDW density and/or high salinity of the new dense water. In the interval between two subsequent renewals, mineralization processes of organic matter take place in the bottom, explaining dissolved oxygen consumption and the concurrent increase in dissolved nutrients [13]. In the following, material and methods are reported, then the results of the 1998-2008 field work are described. A discussion, including comparison with previous measurements to infer some short-term Northern Adriatic Sea climate variations, follows and finally conclusions are drawn.

2 Material and methods

In the framework of the SINAPSI project, ISMAR-CNR carried out 30 oceanographic cruises in the Jabuka pits from January 1998 to June 2008, acquiring 275 CTD casts and collecting 122 seawater samples. A typical transect (Figure 2) from the western to the eastern Adriatic coast was near-seasonally monitored, performing CTD stations and samplings along the water column to measure physical (pressure, temperature, conductivity, fluorescence, turbidity, density) and chemical (dissolved oxygen and nutrient salts) parameters. The CTD data were collected using a SeaBird Electronic SBE911plus instrument coupled to an SBE Carousel water sampler. The CTD probe was equipped with sensors measuring pressure, temperature, conductivity, fluorescence (Sea Tech Fluorimeter), turbidity (Sea Tech backscattering) and distance from the bottom (Datasonic altimeter). Data were acquired and processed according to UNESCO [14] standards, obtaining pressure-averaged data (0.5 db interval). Seawater was sampled at fixed depths, with a smaller number of sampling points in winter and autumn, when the water column is more homogeneous, and a larger number in spring and summer. Water samples for nutrient salt analyses were filtered (GF/F Whatman, diameter 25 mm), immediately stored at -22 °C in polyethylene vials, and analyzed at the ISMAR-CNR laboratory (Ancona-Italy) using the colorimetric method [15] with a Technicon TRAACS 800 autoanalyzer. Dissolved oxygen was directly analyzed on board according to Winkler[16], samples were immediately fixed and stored in the dark and then analyzed within 24 h using the potentiometric method.

3 Results

In Figure 3 the time evolution of bottom density along the Jabuka pits transect is showed. The evident density increment in 1999, 2002, 2003, 2004, 2005 and 2006

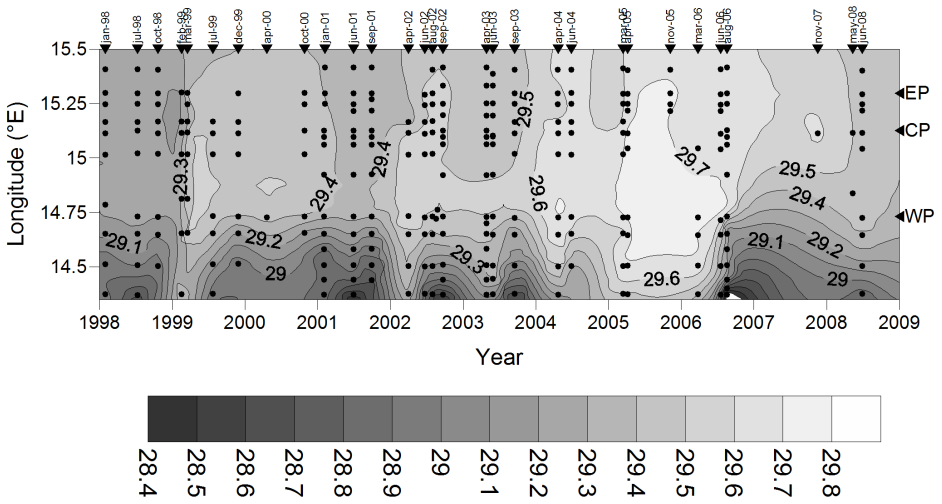

Figure 3: Time evolution of bottom density anomaly ($\mathrm{kg{\cdot}m^{-3}}$) from January 1998 (left) to June 2008 (right) along the transect of Figure 1.

immediately reveals that a bottom water renewal occured in those years. The figure gives also a quite clear indication that the new dense water came from the western side in both cases. This fact is confirmed by looking at selected sections showed in Figures 4, 5, 6. It can be seen (best for April 2002) that the new dense water mass had the features of NAdDW [2, 5, 17] which forms in the north Adriatic in the winter: i.e. very low temperature, comparatively low salinity (not showed) and high density. In February 1999 (Figures 4, 5, 6), a water mass - homogeneous from the bottom to 140 m - was detected in the western pit. Bottom physical characteristics (relatively low density: 29.2 $\mathrm{kg{\cdot}m^{-3}}$; and comparatively high temperature: 12.5 ºC), combined to high nitrate concentrations, indicated that it had not been renewed. In the spring, the NAdDW recently formed in the Northern Adriatic reaches the middle sub-basin, and, if it is denser than the water standing in the western pit, it flows into it below the 170 m bathymetric line, reaching the bottom (254 m). In fact, in March 1999 (not shown) the temperature and density data of the first two pits evidenced MADdW replacement with denser (29.5 $\mathrm{kg{\cdot}m^{-3}}$) and colder (10.7 °C) water, while the eastern pit was still occupied by old MAdDW. From the western pit the NAdDW flows into the central one (270 m) over the first 190 m sill, and subsequently into the eastern pit (240 m) over another 190 m sill. In July 1999 (Figure 4), dense (29.5 $\mathrm{kg{\cdot}m^{-3}}$) water was observed in the same two pits and at the level of the second sill (190 m) below 200 m throughout the area; the fact that dense water was also sampled at the level of the second sill suggests that analogous conditions were obtained in the eastern pit. The similar density data (29.4-29.5 $\mathrm{kg{\cdot}m^{-3}}$) recorded in

all three pits in December 1999 (Figure 5) lend substance to this hypothesis. In 2001 MAdDW was not renewed by new NAdDW, so October 2001 maps (Figure 5) are a good example of conditions ruling the pits when MAdDW is not renewed: at the bottom, temperature is increased, density decreased, and, more evident, dissolved oxygen saturation percentage is low while nitrates are high because of mineralisation processes. In April 2002 (Figure 6) the western and central pits bottom waters were renewed (density 29.6 $\mathrm{kg{\cdot}m^{-3}}$, temperature 10.4 °C and oxygen $>$ 90 % saturation). Since at the level of the second sill (190 m) values were incompatible with a renewal, the dense water had not yet reached the eastern pit. In June 2002 (Figure 6) all the three pits contained dense water (density 29.5 $\mathrm{kg{\cdot}m^{-3}}$, temperature 10.5 °C and oxygen saturation $>$ 90 %). The sections (Figures 4, 5, 6) illustrate that the dense and cold NAdDW mass entered first the western pit and then the central and the eastern pit in succession, flowing over the two sills at 190 m. The water mass standing in the pits was probably displaced by the new water, as described by Franco [10] for the western pit, and pushed over the Palagrüza sill to flow south. The time diagram (Figure 7) of the bottom values measured at the stations located in the three pits shows clearly the abrupt changes in temperature and density, the increase in dissolved oxygen and the fall in nitrates taking place at the time of the 1999 and 2002 renewals. Dissolved oxygen saturation and nitrates time diagrams also shows that another renewal occured in April 2000, but with different characteristics in respect to 1999 and 2002 ones. In fact bottom density increased slightly, and the salinity time diagram reveals that the renewal happened because of saltier NAdDW. Between April 2000 and June 2001, when the deep water was not ostensibly renewed by water from the north, the three pits exhibited a 0.0501 % daily consumption of dissolved oxygen saturation, obtained from:

$O_2\%\mathrm{sat} = O_2\%$ i.v. – 0.0501 tday,

where O_2 %sat is the per cent saturation value of dissolved oxygen after a given period of time; O_2 % i.v. is the initial dissolved oxygen value of the water that has just flowed into the pits; and tday is the time since water inflow into the pit. The increase in nitrates in the pits over the same period was also calculated as follows:

$NO_3 = NO_3$ i.v. + 0.0085 tday,

where NO_3 is the nitrate concentration ($\mu\mathrm{M{\cdot}l^{-1}}$) in the water flowing southward from the pits after a given period of time; NO_3i.v. is the initial value of nitrate concentration ($\mu\mathrm{M{\cdot}l^{-1}}$) in the water that has just flowed into the pits, and tday is the time since water inflow into the pit. According to this calculation, the nitrates in the pit increase after the renewal episode by ca. 3 $\mu\mathrm{M{\cdot}l^{-1}}$ a year.

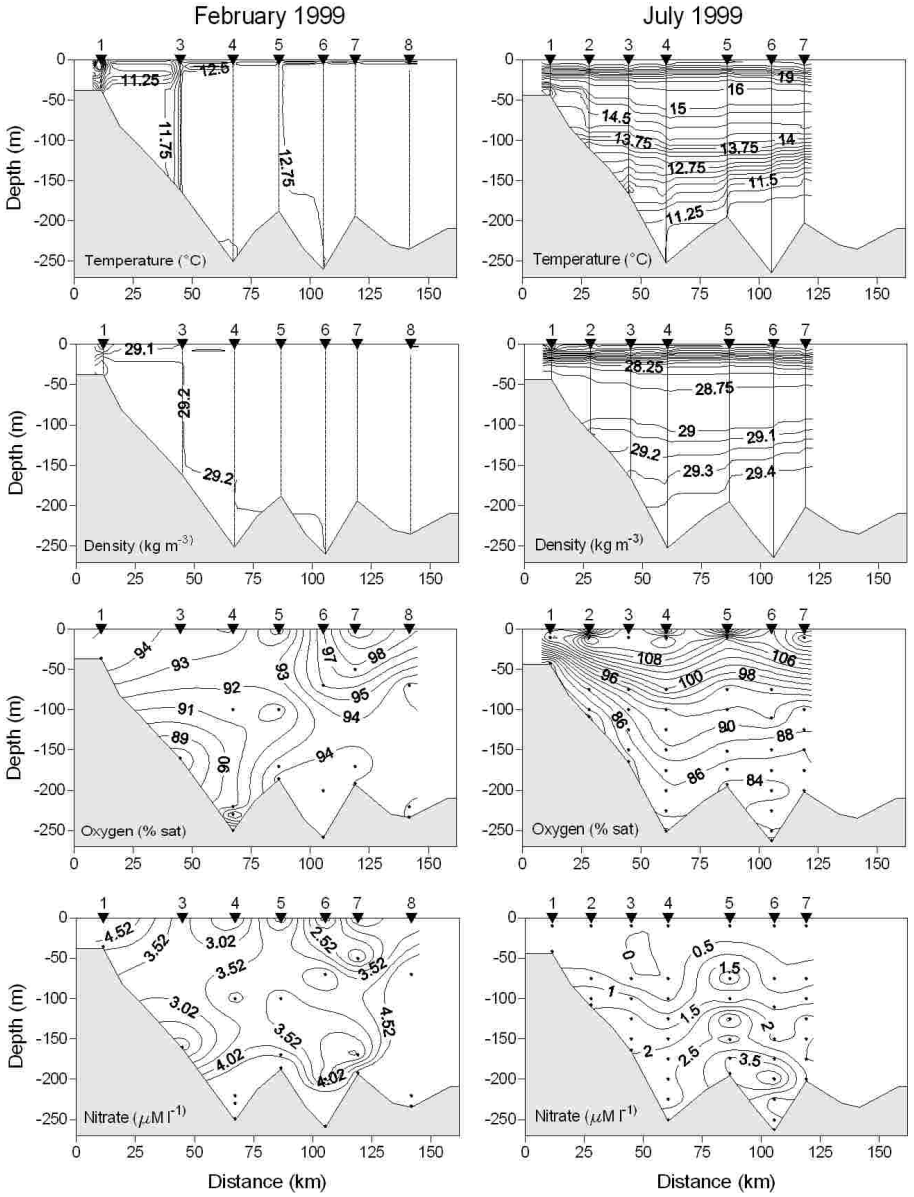

Figure 4: Vertical distribution of temperature (°C), density anomaly ($\mathrm{kg{\cdot}m^{-3}}$), oxygen saturation percentage (%) and nitrate ($\mu\mathrm{M{\cdot}l^{-1}}$) along the transect in February 1999 and in July 1999. The contour interval is variable (from [1]).

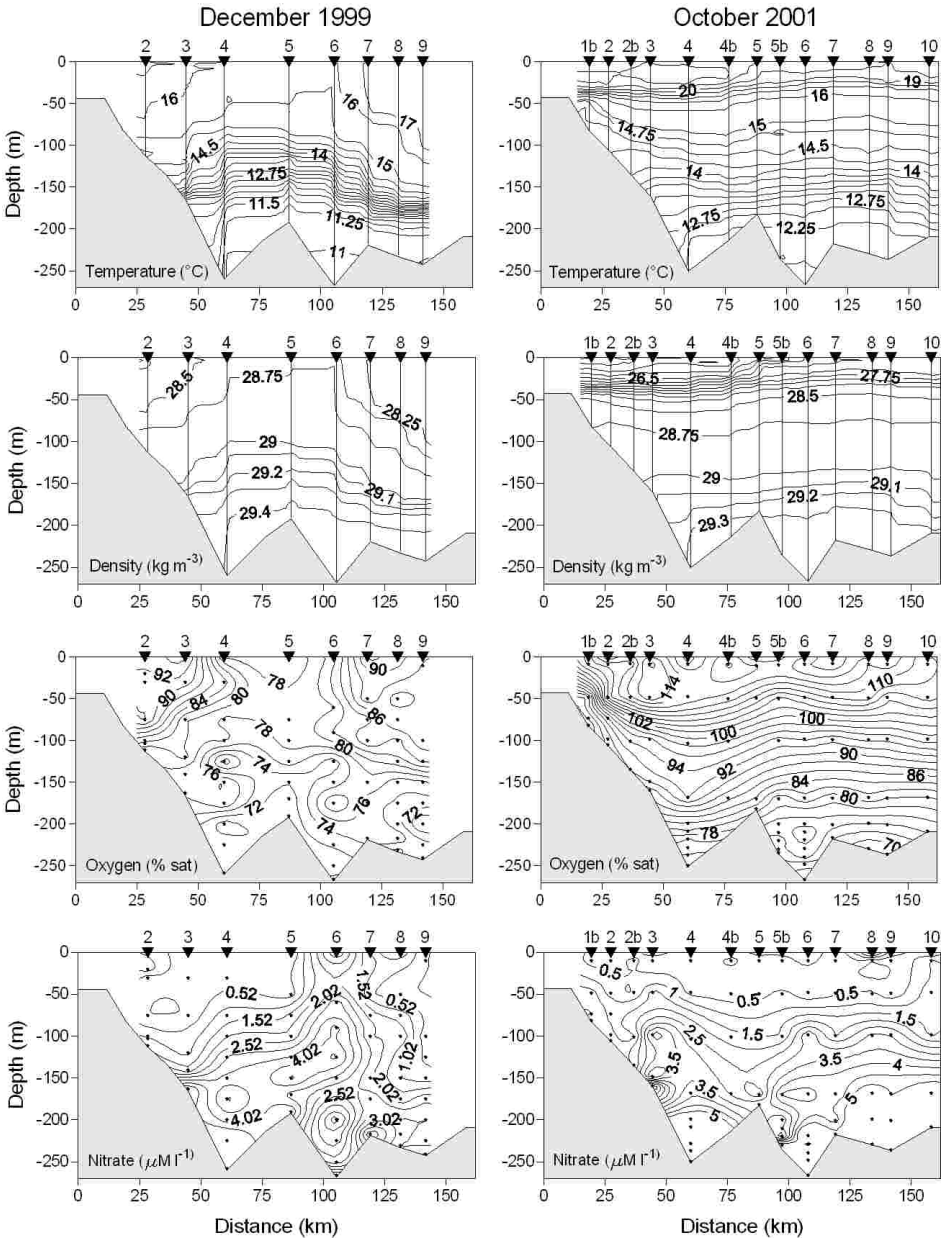

Figure 5: Vertical distribution of temperature (°C), density anomaly ($\mathrm{kg{\cdot}m^{-3}}$), oxygen saturation percentage (%)and nitrate ($\mu\mathrm{M{\cdot}l^{-1}}$) along the transect in December 1999 and in October 2001 (from [1]).

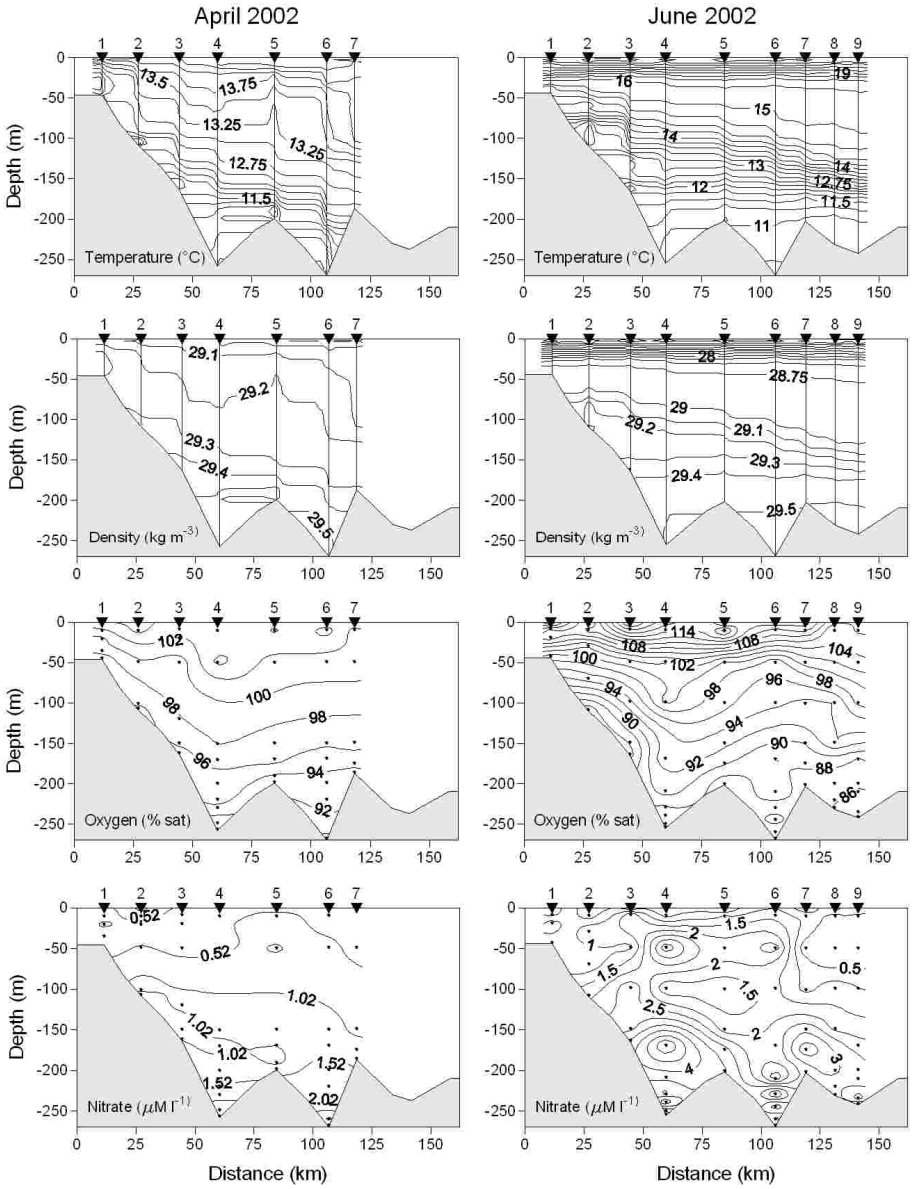

Figure 6: Vertical distribution of temperature (°C), density anomaly ($\mathrm{kg \cdot m^{-3}}$), oxygen saturation percentage (%) and nitrate ($\mu \mathrm{M \cdot l^{-1}}$) along the transect in April 2002 and in June 2002 (from [1]).

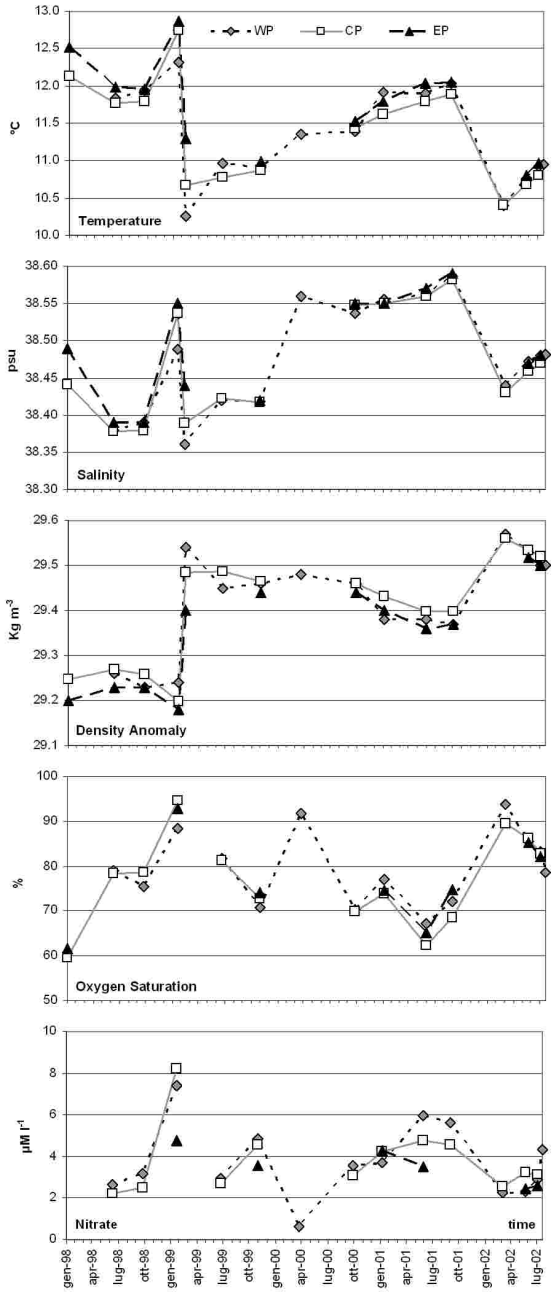

Figure 7: Time evolution of temperature (°C) (a), density anomaly ($\mathrm{kg \cdot m^{-3}}$) (b), oxygen saturation percentage (%) (c) and nitrate ($\mu \mathrm{M \cdot l^{-1}}$) at the bottom in the pits (redrawn from [1]).

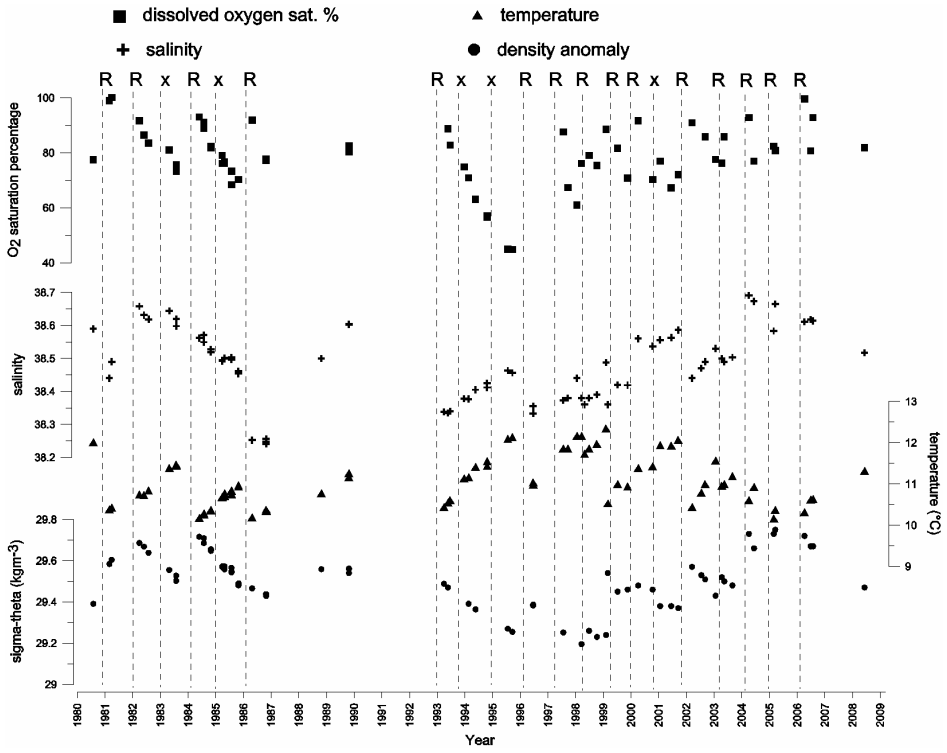

Figure 8: Time evolution of temperature (°C), salinity, density anomaly ($\mathrm{kg}\cdot\mathrm{m}^{-3}$) and oxygen saturation percentage (%) at bottom in the western Jabuka pit, "R" indicate the time of the renewal, "x" indicate the time of the not renewal.

4 Discussion

During the study period (1998-2008), the pits evidently received new water six times, the first in February-March 1999, then in March-April 2002, April-June 2003, April-June 2004, March-April 2005 and March 2006. During these renewals the dense water mass flowing into the pits came from the western side of the Adriatic Sea and had the features of NAdDW [2, 5, 17], which forms in the North Adriatic in the winter: i.e. very low temperature, comparatively low salinity and high density. In late winter - early spring, this water mass reaches the middle sub-basin, and when it is denser than the water standing in the western pit it flows into it below the 170 m bathymetric line, reaching the bottom (254 m). From this it flows into the central pit (270 m) over the first 190 m sill and subsequently into the eastern pit (240 m) over another 190 m sill (Figure 2). The old MAdDW and part of the new NAdDW can enter the South Adriatic Basin. If the NAdDW reaching the Middle Adriatic is less dense than the resident MAdDW, it is not able to occupy the deepest part of the depressions and it continues to flow southward along the western side of the basin to the southern sub-basin. In 2000 (when unfortunately only the western pit was sampled), the MAdDW renewal was not evidenced by an abrupt change of temperature and density, but the evident dissolved oxygen increase and the contemporary nitrates decrease (Figure 7) are indicative of new water entered in the western pit. Temperature slightly increased, but density increased too, due to higher salinity. Observations collected in the Northern Adriatic basin confirm that in 2000 dense and salty NAdDW formed, roughly 1.0 °C warmer and 0.1 $\mathrm{kg \cdot m^{-3}}$ less dense than the 2002 NAdDW [18], about the same difference between western Jabuka pit bottom water characteristics in 2000 and 2002. Analysing the 28 year time-series collected by ISMAR in the western pit (Figure 8) shows the bottom temperature, salinity, density and dissolved oxygen saturation), several considerations can be drawn. Starting from the period 1987-1992, bottom temperature shows a clear increasing trend (progressively higher minima and maxima); this is in agreement with the seasonal average sea surface temperature increase of the period 1988-1999 compared to the previous years found for the Northern Adriatic by Russo et al. [9]. During the last decade of 1990, while the temperature of the NAdDW renewing Jabuka pit bottom waters was increasing, its density was decreasing; a density minimum was reached in 1998. The bottom density minima reached in the pits during the period 1994-1998 are concomitant with the minimum production of Adriatic Bottom Water (ABW) from the Southern Adriatic, a consequence of the EMT. Starting from 1999, the decreasing density trend in the mesoadriatic depressions reversed: temperature decreased (but it remained still higher than pre-1987 values) and above all salinity increased. The salinity increase is due to a major ingression of Cretan surface and intermediate waters, characterized by high salinities, which were detected in the Northern Adriatic starting from about 1999. The bottom density increase in the mesoadriatic depressions, detected starting from 1999, is an indication that ABW production restarted, as found by Manca et al [7] on the basis of data collected in the Ionian Sea in 1999.

5 Conclusions

In the course of the study period, the Jabuka pits underwent six complete water renewals, in 1999, 2002, 2003, 2004, 2005 and 2006. The denser and colder water from the north (NAdDW) entered first the western pit and then the central and eastern ones over the two 190 m sills separating them before flowing south over the Palagrüza sill (170 m). In April 2000 there are evidences of a renewal due a warmer but denser NAdDW (due to its higher salinity). Dissolved oxygen saturation of the water mass standing in the three pits showed a negative trend approximately from 90% to 65%, between April 2000 and June 2001, exhibiting a total decrease of 28%. Over the same period, nitrates increased 5-fold from ca. 1 μM$\cdot$l^{-1} to ca. 4.8 μM-1; this indicates that the MAdDW flowing south over the Palagrüza sill after a year or more in the pits brings a considerably greater concentration of nitrates into the southern sub-basin than the NAdDW flowing directly into it. Bottom temperature and salinity in the Mesoadriatic depressions show trends which are in agreement with the decadal climatic changes evidenced for the Northern Adriatic Sea and with the recent variations of the Eastern Mediterranean water masses. These facts confirm that the mesoadriatic depressions are an optimal site where to monitor Northern Adriatic Sea water mass variations at seasonal scale an integrated signal of the, and information obtained from this site can also be relevant to the whole Adriatic and Eastern Mediterranean.

6 Acknowledgements

The authors are grateful to the crews of R/V G. Dallaporta, R/V Urania and R/V Alliance for their help in sample collection. The research was supported by the "Seasonal INterannual, and decAdal variability of the atmosPhere, oceanS and related marIne ecosystems" (SINAPSI) programme funded by the Italian MIUR.

References

[1] M. Marini, A. Russo, E. Paschini, F. Grilli, and A. Campanelli. Short – term physical and chemical variations in the bottom water of the Middle Adriatic Depressions. 2006.

[2] A. Artegiani, D. Bregant, E. Paschini, N. Pinardi, F. Raicich, and A. Russo. The Adriatic Sea general circulation. Part I. Air-sea interactions and water mass structure. 1997.

[3] T.S. Hopkins. The structure of Ionian and Levantine Seas. *Reports in Meteorology and Oceanography. Harvard Univ.*, 41(2):35–56, 1992.

[4] I. Vilibic. An analysis of dense water production on the North Adriatic shelf. 2003.

[5] A. Russo and A. Artegiani. Adriatic Sea hydrography. 1996.

[6] A. Artegiani, D. Bregant, E. Paschini, N. Pinardi, F. Raicich, and A. Russo. The Adriatic Sea general circulation. Part II: Baroclinic Circulation Structure. 1997.

[7] B.B. Manca, G. Budillon, P. Scarazzato, and L. Ursella. Evolution of dynamics in the eastern Mediterranean affecting water mass structures and properties in the Ionian and Adriatic Seas. 2003.

[8] B. Klein, W. Roether, B.B. Manca, D. Bregant, et al. The large deep water transient in the Eastern Mediterranean. 1999.

[9] A. Russo, S. Rabitti, and M. Bastianini. Decadal Climatic Anomalies in the Northern Adriatic Sea Inferred from a New Oceanographic Data Set. 2002.

[10] P. Franco, D. Bregant, and D. Voltolina. Oceanography of the Middle Adriatic Sea. Data from the crises December 1970, March-April 1971 and March 1972. 1982.

[11] A. Artegiani and E. Salusti. Field observation of the flow of dense water on the bottom of the Adriatic Sea during the winter of 1981. 1987.

[12] M. Gacic, A. Lascaratos, B.B. Manca, and A. Mantziafou. Adriatic deep water and interaction with eastern Mediterranean Sea. 2001.

[13] A. Artegiani, M. Marini, R. Pariante, E. Paschini, and A. Russo. Evolution of Physical parameters and Chemical observation in the middle Adriatic depressions. 2001.

[14] UNESCO. The acquisition, calibration, and analysis of CTD data. 1988.

[15] J.D.H. Strickland and T.R. Parsons. A practical handbook of seawater analysis. 1972.

[16] L.W. Winkler. Die Bestimmung des im Wasser gelosten Sauerstoffes. 1888.

[17] M. Gacic, P.M. Poulain, M. Zore-Armanda, and V. Barale. Physical Oceanography of the Adriatic Sea. 2001.

[18] A. Russo, M. Marini, F. Grilli, P. Fornasiero, et al. Ruolo dei fattori oceanografici nella formazione delle mucillagini nell'Adriatico settentrionale: processi termoalini, circolazione e valutazione dei flussi di acqua e nutrienti. 2003.

On Sea-Level Changes in the Mediterranean Sea with Focus on the Adriatic Sea

F. Raicich
Institute of Marine Sciences, CNR, Trieste, Italy
fabio.raicich@ts.ismar.cnr.it

Abstract

Mean sea level rise represents an increasing concern for most Countries due to its impact on the coastal environment. The sea level evolution is determined by several factors, such as changes of ocean mass and volume (eustatic), of water density by temperature and salinity variations (steric) and vertical ground movements (isostatic). Areas sensitive to sea level changes can be found in the Mediterranean Sea and particularly in the northern Adriatic, where the effect of global mean sea level rise is enhanced by local ground subsidence. Only few Mediterranean sea level records are long enough to describe secular sea level variability, moreover, they are concentrated along the northern coasts (northwestern Mediterranean and northern Adriatic). From all time series, a uniform sea level rise is observed until about 1960, followed by steady conditions for about 30 years, and a new rise afterwards. In the second half of the 20th century in the northern Adriatic severe storm surge events appear to have become less frequent and intense, on average. By contrast, the frequency and intensity of moderate events have remained almost constant or slightly increased. Seasonal sea level exhibits significant correlations with some climate indicators. Winter sea level is correlated with the NAO index, with decreasing strength going eastwards. Autumn sea level exhibits correlation on the interannual time scale with indices tropical precipitation, such as those of the Indian Monsoon and Sahel.

1 Introduction

The coastal environment has long been attractive for human settlement due to the abundance of natural resources in the adjacent sea and the possibility of establishing commercial relationships. As a consequence, large portions of the World coastlines are densely populated and large cities have developed.

Mean sea level rise represents an increasing concern for most Countries due to its impact on the coastal environment. Sea level changes can produce a significant impact on the coastal areas, thus affecting human activities and interests. Clearly, the impact is expected to be more severe along low-lying sandy or muddy coasts and on tropical atolls, rather than along high and rocky coasts. Although the mean sea level rise is a global issue, the sensitivity to its consequences depends on local conditions. Large cities and harbours lie on the Mediterranean coastline. A large part of it is low and, therefore, threatened by sea level rise in terms of flooding, salt wedge penetration and erosion.

In this paper, after defining some useful quantities (Section 2), we outline the factors that control sea level changes (Section 3). Recent mean sea level variations are

summarized in Section 4 and the evolution of extreme events is discussed in Section 5. Section 6 provides some conclusive remarks.

2 Some definitions

Sea level elevation can be quantified in two ways, namely as the distance between the sea surface and a reference plane connected with the ground, or the distance between the sea surface and an altimeter mounted on a satellite orbiting around the Earth.
In the first case the reference frame can be the sea floor or a land-based benchmark. It is local and the measurement provides the "relative" sea level, depending on the vertical motions that may affect the site.
In the second case the reference frame is global and corresponds to the geoid, which is defined as "the equipotential surface of the Earth's gravity field which best fits, in a least squares sense, global mean sea level". A geometric approximation to the geoid is the ellipsoid. Since the geoid shape is determined by the gravity field, which depends on the Earth mass distribution, it is quite irregular with major positive deviations from the ellipsoid in the North Atlantic-Europe and West Pacific Ocean regions, and negative deviations in the Indian Ocean and the Ross Sea regions. The height difference between minima and maxima amounts to about 200 m. The geoid is obtained as the mean sea level measured by the altimeter, thus the reference frame depends on the measurements themselves. In practice the geoid definition has to be changed from time to time to account for the additional data that are collected (at present only 19 years of data are available).
Except when explicitly noted, in the following we will refer to relative sea level, which is more relevant for studying the impact on the coastal areas.

3 Factors that control sea level changes

The sea level evolution is determined by several factors, such as changes of ocean mass and volume (eustatic), of water density by temperature and salinity variations (steric) and vertical ground movements (isostatic).
The ocean water mass is in equilibrium with the water mass stored on land and within the ground, namely ice sheets, glaciers, lakes and aquifers, and the water present in the atmosphere. According to recent estimates, the ocean represents more than 97% of the water in the Earth system and receives water from precipitation as well as river and coastal runoff, while it looses water to the atmosphere by evaporation. Approximately 2% of the global water can be found in the ice sheets, less than 1% underground, while less than 0.1% is present in the atmosphere, biosphere, surface reservoirs (lakes and rivers) and soil. All the processes involved in the hydrologic balance are affected by climate changes, but the role played by the ice sheets is crucial.
A glacier, ice cap or ice sheet gains mass by accumulation of snow, which is gradually transformed into ice, and looses mass mainly by melting at the surface or base with subsequent runoff or evaporation of the melt water. Ice may also be removed by discharge into a floating ice shelf or glacier tongue, from which it is lost by melting at the base and calving of icebergs. Almost 89% of continental ice can

be found in Antarctica, approximately 7% in Greenland and the remaining 4% in mountain glaciers. Changes in the components of the cryosphere occur at different time scales. All parts of the cryosphere contribute to short-term climate changes, with permafrost, ice shelves and ice sheets also contributing to longer-term changes. Greenland and West Antarctica are critical regions with regard to sea level variations, since the melting of their ice would imply a global sea level rise by 5-6 m. Note that if all the World ice sheets melted sea level would rise by about 75 m.

Relative sea level changes observed at a certain location are caused both by global and local factors. The spatial and time scales of the forcing are related to each other, therefore the effect of local factors prevails at intedecadal, interannual, seasonal and shorter time scales, while global factors prevail on multidecadal, secular and longer time scales. A recent review on this subject can be found in [1].

The spatial and temporal variability of sea level in ocean basins is maintained by atmospheric pressure and air-sea fluxes of momentum (surface wind stress), heat and fresh water (precipitation, evaporation, and water runoff from the land). As the ocean warms, the density decreases and thus, at constant mass, the volume of the ocean increases. Thermal expansion (or steric sea level rise) is one of the major contributors to recent sea level changes. Salinity changes also have a significant impact on the local density and thus local sea level, but have little effect on global average sea level change. Through the inverse barometer effect, a local increase in surface air pressure over the ocean produces a depression in the sea surface of 1 cm per hPa. Since water is practically incompressible, this cannot lead to a global-average sea level rise, but a long-term trend in surface air pressure patterns could influence local sea level trends.

The Eastern Mediterranean Transient [2] is an example of regional effects of combined atmospheric and ocean properties changes. In the early 1990's transient changes in the thermohaline properties of deep water masses and in the wind regime produced a reversal of the Ionian Sea circulation, and caused significant sea level changes in the region [3].

4 Mean sea level changes

The history of past sea level fluctuation can be reconstructed mainly from geological data, while direct measurements are available in very few sites only for the last 300 years. After the glacial peak about 21000 years before present (BP), the global mean sea level has always been rising, on average, although at variable rate. Between 2000 and 100 years BP the mean rate has been less than 2 cm per century. Direct sea level observations at several stations allow to estimate the global sea level rise rate from the late 19th century onwards. In addition, satellite altimetry provides a global coverage since 1992.

The main source of sea level data during the past century is the monthly and annual tide gauge data set of the Permanent Service for Mean Sea Level (PSMSL) [4]. Several estimates of mean sea level linear trend during the 20th century have been made, often using observations at stations considered geologically stable, i.e. not affected by significant vertical ground movements. Different results have been found, depending on the sea level time series analysed and the technique used to estimate possible vertical land motion trend,

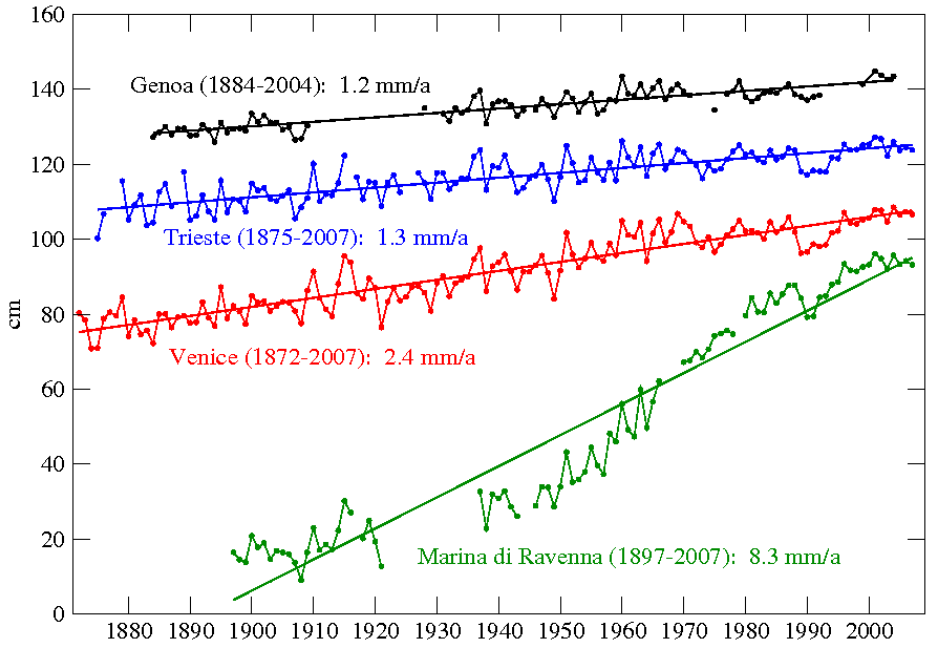

Figure 1: Time series of annual sea level at Genoa, Trieste, Venice and Marina di Ravenna, together with the linear trends.

to be removed from the data. The PSMSL data set, in fact, is characterized by uneven temporal and spatial distributions of observations, with higher station density and longer time series in Europe and North America.

A recent estimate by [5], using data since 1870, provides a mean sea level rise of 1.7 $\pm$ 0.3 mm·a^{-1}, consistent with the 1.5-2.0 mm·a^{-1} range proposed by the IPCC Third Assessment Report [6] and confirmed by the Fourth Assessment Report [7]. [5] also found a sea level rise acceleration of 1.3 $\pm$ 0.5 mm·a^{-1} per century. An acceleration cannot be detected using only 20th century data; therefore it was suggested that its onset occurred in the 19th century.

The rise in global mean sea level is accompanied by considerable decadal variability. For the period 1993-2003, the sea level rise rate estimated from satellite altimetry data is 3.1 $\pm$ 0.7 mm·a^{-1} [8], significantly higher than the average rate. The interpretation of this result and its comparison with sea level rise estimates from tide gauge station data must be made with caution due to the short time interval analysed. Only few Mediterranean sea level records are long enough to describe secular sea level variability, moreover, they are concentrated along the northern coasts (northwestern Mediterranean and northern Adriatic). Excluding the Black Sea, there are only five stations having 80 years of data or more, namely Trieste (since 1875), Genoa (1884), Marseille (1885), considered to

be geologically stable, and Venice (since 1872) and Marina di Ravenna (1896), the latter two stations being affected by marked ground subsidence partly due to gas and water extraction from beneath the sea floor, that occurred between 1930's and 1970's [9].

From the Mediterranean stable stations the mean sea level rise for the 20th century is estimated to be 1.1-1.3 mm·a^{-1}, on the lower edge of global estimates [10, 11, 12, 13]. In the Adriatic Sea Venice exhibits a mean sea level rise rate of 2.4 mm·a^{-1} and Marina di Ravenna of 8.3 mm·a^{-1}, compared to 1.3 mm·a^{-1} at Trieste, which is considered to be stable (Figure 1).

The fact that Mediterranean sea level rise seems somewhat slower than the global one is due to the peculiar behaviour of the basin. From all time series, a uniform sea level rise is observed until about 1960, followed by steady conditions for about 30 years, and a new rise afterwards. Fluctuations are superimposed onto this long-term changes, mostly connected with those of the atmospheric pressure, due to the inverse barometer effect, and in some cases with the wind regimes. The stationary sea level period during 1960-1990 does not mirror a similar behaviour of the Ocean. In the literature this anomalous condition is attributed both to decadal variability of the atmospheric forcing, in particular a relatively high pressure phase over the Mediterranean Sea connected with the North Atlantic Oscillation (NAO), and to internal processes of the Mediterranean basin [10, 14, 15, 13]. Among the latter we mention the steric changes related to a salinity increase of the intermediate and deep water masses, possibly due to a change in the hydrological balance, with higher evaporation and lower precipitation and river runoff, and the Eastern Mediterranean Transient, characterized by changes in the basin circulation.

The peculiar behaviour of the Mediterranean Sea in the second half of the 20th century puts in evidence that remarkable differences relative to the World Ocean can be observed also at a relatively long temporal scale (30 years). The absence of a significant sea level acceleration in the Mediterranean basin is essentially related to the anomalous conditions of the 1960-1990 period.

Mediterranean seasonal sea level exhibits significant correlations with some climate indicators. Winter sea level is correlated with the NAO index, through the inverse barometer effect, with decreasing strength going eastwards [16]. An exception is represented by the stations close to Gibraltar Strait, whose peculiar dynamics prevails over the atmospheric pressure effect. Statistically, sea level is lower in connection with the higher atmospheric pressure regime that usually characterizes mild winters in the region.

Sea level exhibits significant anticorrelation on the interannual time scale with indices of tropical precipitation, such as those of the Indian Monsoon and Sahel [17]. The peak in the correlation between sea level and precipitation indices always occur in autumn, and mostly concern the northern Mediterranean coasts. These areas seem to respond quite regularly to positively correlated pressure anomalies developing two months after Indian Monsoon and Sahel maximum precipitation anomalies, that occur in boreal summer, therefore the sea level response to tropical circulation appears to be delayed. The northern Mediterranean is outside the direct range of influence of the descending branch of the Hadley circulation, so the relevant mechanism, still to be fully understood, must be indirect.

The overall picture of sea level behaviour around the Adriatic Sea coast is to a large extent uniform at interannual and interdecadal time scales. This also holds for the seasonal cycle and its variations [18] . The similarity indicates that the dominant signals at interannual and interdecadal time scales are of basin wide character although it does not mean that all signals are all expressed with the same strength everywhere in the basin. For instance, the inverse barometer effect is observed everywhere, but it is more and more effective going northwards.
Also at the daily time scale the sea level varies coherently to a large extent, as it occurs at longer time scales, but it is possible to put in evidence a non-negligible internal variability connected with the wind components [19]. The atmospheric pressure plays the major role, producing a uniform sea level response also at the daily time scale, but meridional and zonal sea level gradients can be observed too, although their signals are weaker than that due to pressure. These gradients are connected with southerly wind (Sirocco), and easterly wind (Bora), respectively.
The high coherence of daily mean sea level anomalies at Trieste, Venice and Marina di Ravenna is illustrated in Figure 2. These time series are also compared to Trieste atmospheric pressure anomalies (which represent well the northern Adriatic). The inverse barometer effect can be clearly seen. The small differences that appear between the sea level time series are essentially due to the wind regime. For example, a positive Trieste-Marina di Ravenna sea level gradient is connected with Bora.

5 Extreme events

The impact of sea level change on human activities occurs mainly via the extreme levels, rather than as a direct consequence of mean sea level changes. Sea level extremes are generally connected with storm surges generated by tropical or extra tropical cyclones (tsunamis are an exception, but they are not produced by the atmospheric forcing).
The frequency and intensity of sea level extremes exhibits great variability, connected with that of the atmospheric forcing, i.e. of storminess. In general, during the 20th century there is evidence for a worldwide increase in the occurrence of extreme high water events related to storm surges. Variations in extremes in this period are related to the general mean sea level rise and the variability of storminess. However, the effect of the wind regimes is not uniform worldwide, producing different consequences on a regional basis. For instance, during the last 50-60 years, the trend of extremes is positive at San Francisco [20] and negative at Brest [21, 22].
In the second half of the 20th century in the northern Adriatic severe storm surge events appear to have become less frequent and intense (although trends are often only marginally significant), on average, as a consequence of a decreasing occurrence of strong and persisting Sirocco events [23, 24, 25]. By contrast, the frequency and intensity of weak and moderate events have remained almost constant or slightly increased [23]. As a consequence, the coastal flood frequency has increased because the frequency of weak storm surges has not significantly changed while, in the meantime, mean sea level has been rising.

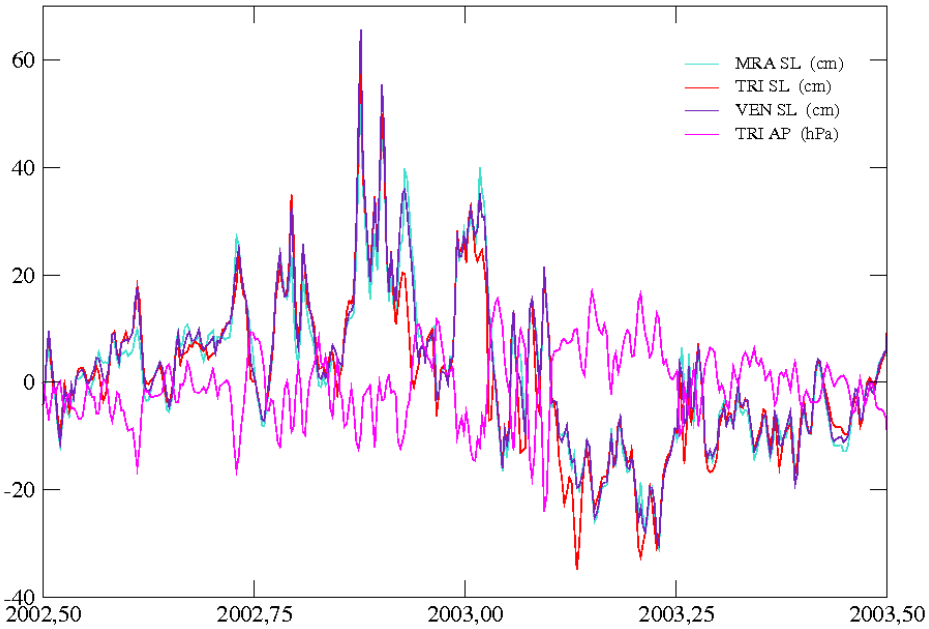

Figure 2: Comparison between Trieste, Venice and Marina di Ravenna daily sea level and Trieste atmospheric pressure from July 2002 to June 2003. The data are anomalies relative to the long-term mean.

6 Conclusive remarks

A growing concern exists about the consequence of mean sea level rise and the occurrence of extreme sea level events on the coastal environment. A direct connection exists between global sea level rise and atmospheric temperature increase, mainly in terms of ocean thermal expansion and ocean mass increase by continental ice melting. The ocean warming propagates from the surface into the interior, therefore its effect is expected to be felt with a delay of several years.

Although the future cannot be predicted, due to the incomplete knowledge of atmospheric and oceanic processes and limitations in model performance, current projections indicate that global sea level is expected to rise by several tens of centimetres during the 21st century. There are indications of a milder storm surge regime in the Adriatic region during the second half of the 20th century and for the present century, although large interdecadal variability can be expected. This may imply less frequent and less severe storm surges.

In planning the strategies for coastal protection local situations must be taken into account, because they may critically determine the impact of both the mean sea level rise and the extreme events occurrence.

References

[1] H.P. Plag. Recent relative sea-level trends: an attempt to quantify the forcing factors. *Phil. Trans. R. Soc. A*, 364:821–844, 2006.

[2] B. Klein, W. Roether, B.B. Manca, D. Bregant, V. Beitzel, V. Kovačević, and A. Luchetta. The large deep water transient in the Eastern Mediterranean. *Deep-Sea Res. I*, 46:371–414, 1999.

[3] J. Del Río Vera, F. Criado-Aldeanueva, J. García-Lafuente, and F.J. Soto-Navarro. A new insight on the decreasing sea level trend over the Ionian basin in the last decades. *Glob. Planet. Change*, 68:232–235, 2009.

[4] P.L. Woodworth and R. Player. The Permanent Service for Mean Sea Level: an update to the 21st century. *J. Coast. Res.*, 19:287–295, 2003.

[5] J.A. Church and N.J. White. A 20th century acceleration in global sea-level rise. *Geophys. Res. Lett.*, 33:L01602, 2006.

[6] J.A. Church, J.M. Gregory, P. Huybrechts, M. Kuhn, K. Lambeck, M.T. Nhuan, D. Qin, , and P.L. Woodworth. Changes in Sea Level. In. Climate Change 2001: The Scientific Basis. Contribution of Working Group I to the Third Assessment Report of the Intergovernmental Panel on Climate Change.Changes in Sea Level. In. Climate Change 2001: The Scientific Basis. pages 639–694, 2001.

[7] N.L. Bindoff, J. Willebrand, V. Artale, A. Cazenave, J. Gregory, S. Gulev, K. Hanawa, C. Le Quéré, S. Levitus, Y. Nojiri, C.K. Shum, L.D. Talley, , and A. Unnikrishnan. Observations: Oceanic Climate Change and Sea Level. In: Climate Change 2007: The Physical Science Basis. Contribution of Working Group I to the Fourth Assessment Report of the Intergovernmental Panel on Climate Change. pages 385–482, 2007.

[8] A. Cazenave and R.S. Nerem. Present-day sea level change: observations and causes. *Rev. Geophys.*, 42:RG3001, 2004.

[9] L. Carbognin, P. Teatini, and L. Tosi. Eustacy and land subsidence in the Venice Lagoon at the beginning of the new millennium. *J. Mar. Syst.*, 51:345–353, 2004.

[10] M.N. Tsimplis and T.F. Baker. Sea level drop in the Mediterranean Sea: an indicator of deep water salinity and temperature changes? *Geophys. Res. Lett.*, 27:1731–1734, 2000.

[11] M. Orlić and M. Pasarić. Sea-level changes and crustal movements recorded along the east Adriatic coast. *N. Cimento*, C23:351–364, 2000.

[12] F. Raicich. A study of early Trieste sea level data (1875-1914). *J. Coast. Res.*, 23:1067–1073, 2007.

[13] M. Marcos and M.N. Tsimplis. Coastal sea level trends in Southern Europe. *Geophys. J. Int.*, 175:70–82, 2008.

[14] M.N. Tsimplis and M. Rixen. Sea level in the Mediterranean Sea: The contribution of temperature and salinity changes. *Geophys. Res. Lett.*, 29:L02136, 2002.

[15] S.C. Painter and M.N. Tsimplis. Temperature and salinity trends in the upper waters of the Mediterranean Sea as determined from the MEDATLAS dataset. *Cont. Shelf Res.*, 23:1507–1522, 2003.

[16] M.N. Tsimplis and S. Josey. Forcing the Mediterranean Sea by atmospheric oscillations over the North Atlantic. *Geophys. Res. Lett.*, 28:803–806, 2001.

[17] F. Raicich, N. Pinardi, and A. Navarra. Teleconnections between Indian monsoon an Sahel precipitation and the Mediterranean. *Int. J. Clim.*, 23:173–186, 2003.

[18] M. Marcos and M.N. Tsimplis. Variations of the seasonal sea level cycle in southern Europe. *J. Geophys. Res.*, 112:C12011, 2007.

[19] M.N. Tsimplis, F. Raicich, L. Fenoglio-Marc, A.G.P. Shaw, M. Marcos, S. Somot, and A. Bergamasco. Recent developments in understanding sea level rise at the Adriatic coasts. (Accepted). *Phys. Chem. Earth*, 2009.

[20] P.D. Bromirski, R.E. Flick, and D.R. Cayan. Storminess variability along the California coast: 1858-2000. *J. Climate*, 16:982–993, 2003.

[21] M. Bondesan, G.B. Castiglioni, C. Elmi, G. Gabbianelli, R. Marocco, P.A. Pirazzoli, and A. Tomasin. Storm surges and sea level rise: coastal areas at risk in northeast Italy. *J. Coastal Res.*, 11:1354–1379, 1995.

[22] R. Bouligand and P.A. Pirazzoli. Les surcotes et les décotes marines à Brest, étude statistique et évolution. *Oceanol. Acta*, 22:153–166, 1999.

[23] F. Raicich. Recent evolution of sea-level extremes at Trieste (Northern Adriatic). *Cont. Shelf Res.*, 23:225–235, 2003.

[24] P. Pirazzoli and A. Tomasin. Sea-level and surges in the Adriatic Sea area: recent trends and possible near-future scenarios. *Atti Ist. Ven. Sc., Lett. Arti*, 166:61–83, 2008.

[25] P. Lionello, L. Cavaleri, K.M. Nissen, C. Pino, F. Raicich, and U. Ulbrich. Marine storminess in the Northern Adriatic: characteristics and trends. (Accepted). *Phys. Chem. Earth*, 2009.

Chemical-Physical Dynamics in the Sicily Channel (Central Mediterranean Sea)

F. Placenti[1], M. Sprovieri[1], A. Bonanno[1], P. Rumolo[2], S. Bonomo[1], G. Cerrati[2], S. Genovese[1], S. Zgozi[4], G.M. Zuppi[5],
1, Institute for Coastal Marine Environment, CNR, Capo Granitola (TP), Italy
2, Institute for Coastal Marine Environment, CNR, Napoli, Italy
3, Marine Environment Research Center "S. Teresa", ENEA, ENEA-CRAM, PZ (affiliazione non presente, segnalare)
4, Marine Biology Research Centre, Tajura (Tripoli), Libia
5, Institute of Environmental Geology and Geoengineering, CNR, Roma, Italy
francesco.placenti@iamc.cnr.it

Abstract

The Mediterranean Sea is an oligotrophic basin characterized by low nutrient levels and productivity rates. In the eastern Mediterranean, the molar ratio of nitrate to phosphate (N:P) in the deep water is $\sim$28:1, far in excess of the normal Redfield ratio (16:1) found in the oceans' deep water. At present, there are different hypotheses to explain why the eastern Mediterranean is a phosphorus limited basin. In order to investigate the biogeochemical water mass properties of the Sicily Channel, a sampling plan from Sicilian to Libyan coasts was performed in July 2008. The θ-S diagrams highlight the presence of three main water masses: Modified Atlantic Water (MAW), Levatine Intermediate Water (LIW) and Deep Water (DW) with different chemical-physical features. Analysis of nutrients reveal the oligotrophic character of the area with strong reduction of concentration in surface layers, due to the assimilation of phytoplankton in the euphotic zone and evident increase below 200 m caused by organisms' re-mineralization. This contribution presents a synthesis of vertical and horizontal variability of dissolved inorganic nutrients and argues on their detected anomalous stoichiometric ratios.

1 Introduction

The Mediterranean Sea is an oligotrophic basin, with the Eastern area characterized by ultra-oligotrophic features. The Mediterranean system is enriched with out-of-the-system matter flows coming from fluvial systems and aeolic materials mainly deriving from the Sahara desert and the industrialized European continental areas. Some authors showed the primary role of the atmospheric inputs as primary source of nitrogen (N) and phosphorus (P) to the basin [1]. In the eastern Mediterranean, the molar ratio of nitrate to phosphate (N:P) in the deep water is 28:1, far in excess of the normal Redfield ratio (16:1) found in the oceans' deep water. At present, there are different hypotheses to explain why the Eastern Mediterranean is phosphorus limited. Some authors, such as Bethoux et al.[2], Sachs and Repeta [3], Ribera d'Alcalà et al. [4] ascribe this phenomenon to nitrogen fixa-

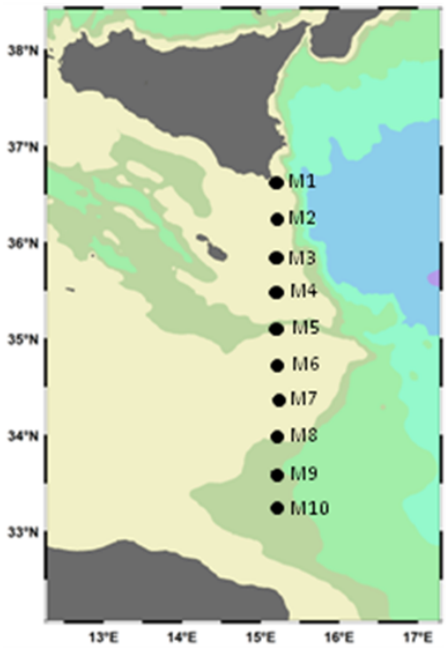

Figure 1: Location map of the sampled stations.

tion processes mainly present in the Eastern Mediterranean. According to Krom et al. [1], high N:P ratio may be caused by the high N:P values (N:P=117:1) in the atmospheric inputs to the Eastern Mediterranean. The main objective of this contribution is to provide a unprecedented and high-quality nutrients dataset from the Strait of Sicily, gateway from Eastern and Western Mediterranean basin, and argue on the main mechanisms driving the unbalanced Redfieldian biogeochemistry of the studied area.

2 Materials and methods

In July 2008, an approximately 400 Km-long N-S transect was sampled onboard of the R/V Urania. The transect (Figure 1) extends from the Sicilian to the Libyan coasts. A total of 10 stations were sampled for analysis of dissolved nutrients (nitrates, nitrites, orthphosphates and orthosilicates) and physical parameters. The nutrients' concentration was later determined in the laboratory using a Brän-AutoAnalyzer Luebbe. Details of analytical methods for nutrient analyses are reported in Grasshoff et al.[5]. Table 1 shows detection limits and accuracy of for the different analyzed nutrients.

Accuracy (µM)	Detection limit (µM)	Nutrients
0.003	0.01	Nitrate
0.003	0.01	Nitrite
0.005	0.01	Phosphate
0.01	0.05	Silicate

Table 1: Accuracy and detection limits for the analyzed nutrients.

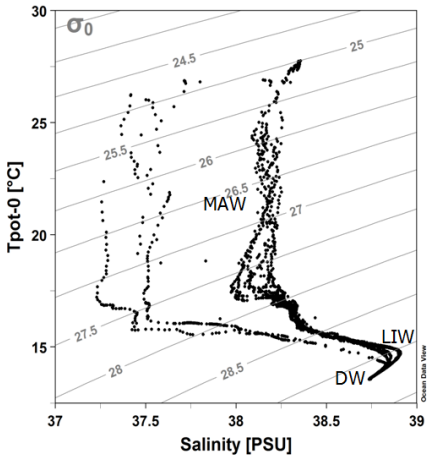

Figure 2: θ-S (potential temperature and salinity) diagrams of the sampled stations.

3 Results and discussion

3.1 Characteristics of water masses

A number of chemical and physical parameters (pressure, salinity, potential temperature, dissolved oxygen and fluorescence) were measured in order to identify and characterize the water masses in the studied area. The θ-S (potential temperature and salinity) diagram highlights the presence of three main highly stratified water masses: the surface Modified Atlantic Water (MAW), the Levantine Intermediate Water (LIW) and Deep Water (DW) with different chemical-physical features (Figure 2). MAW occupies the first 150-200 m of the water column with a salinity, temperature and density of $<$ 38.3 psu, $>$ 15.8 °C, $<$ 28.8 kg·m^{-3}, respectively (Figure 3a). Generally, the minimal salinity of 37.3-37.4 psu values was measured especially in the northern area of the Sicily-Lybia transect (Figure 3a). Below the MAW, a transition water mass (the well-known Levantine Intermediate Water [LIW] core goes from east to west at a depth of about 310 e

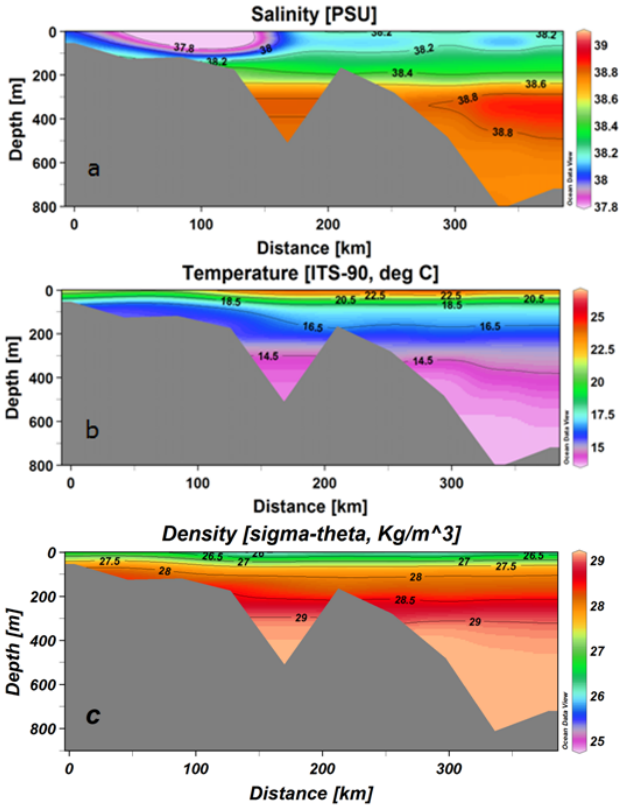

Figure 3: a) salinity, b) temperature and c) density vertical profiles.

350 and an average salinity value of 38.85-38.9 psu, a temperature ranging between 14.6 and 14.8 °C and a density of 29.05-29.08 kg·m^{-3}. Finally, the lower part of the water column (>500 m) is occupied by the DW with homogenous value of salinity (38.7 psu), temperature (13.7 °C) and density (29.15 kg·m^{-3}). Surface water at M1 station with high values in salinity (38.2 psu), especially when compared with the other sampling sites, appears strongly influenced by the presence of Ionian Surface Water (ISW). The M2-M4 sampling stations at the core of the Atlantic Ionian Stream (AIS), show a less salted and thin surface water layer. In these two stations the LIW (salinity and density $<$ 38.83 psu-$<$ 29.1 kg·m^{-3} respectively) appears shallower ($<$160 m). The evident slope of the LIW water mass is likely related to the effect of regional seafloor morphology rather than to direct effects of local impact on the seawater circulation (Figure 4a). Surface waters of the M3 and M4 stations show the lowest salinity values (37.2 psu) and peaks in dissolved oxygen (8.7 mg·l^{-1}) that can be associated to a Deep Chlorophyll Maximum (0.15-0.17 μg·l^{-1}) at depths of about

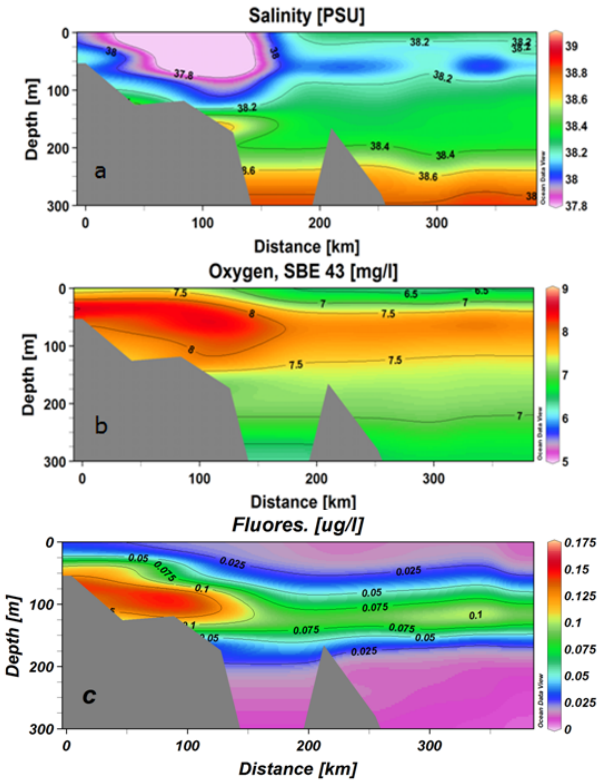

Figure 4: a) salinity, b) dissolved oxygen and c) fluorescence vertical profiles.

100 m (Figure 4b and 4c).

3.2 Nutrients distribution

The distribution of nutrients in the different water masses is controlled by interactions between physical and biogeochemical processes and external sources, as well as by water age directly influenced by accumulation of inorganic nutrients [6]. Results from the Sicily-Libya transect evidence classic nutrient reduction in surface waters (0-200 m) with mean concentrations of 0.22±0.38 μmol·l^{-1} of nitrates, 0.02±0.02 μmol·l^{-1} of orthophosphates and 0.76±0.18 μmol·l^{-1} of orthosilicates due to the effects of phytoplankton assimilation in the euphotic zone. Accordingly, deep waters show increase in nutrient values up to the highest mean concentrations of 4.93±0.74 μmol·l^{-1} of nitrates, 0.15±0.03 μmol·l^{-1} of orthophosphates and 5.86±1.1 μmol·l^{-1} of orthosilicates (Figure 5a, 5b and 5c). The highest concentrations of nitrates (6.6 μmol·l^{-1}) and orthophosphates (0.21 μmol·l^{-1}) are present in the LIW. Othosilicates do not follow that trend since they undergo a slower re-mineralization process as reported by Minas et al.[7]. The average con-

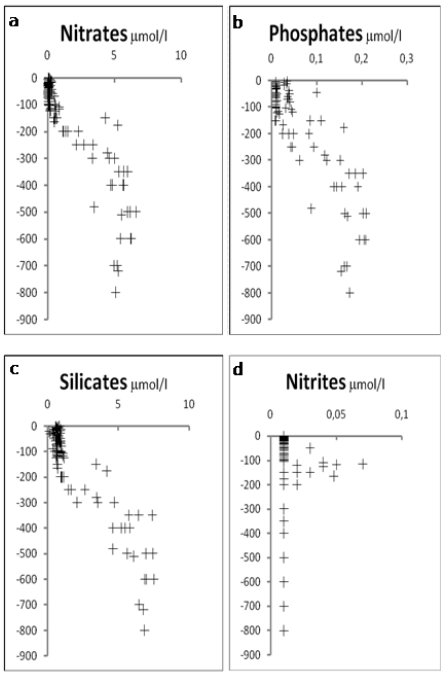

Figure 5: Distribution patterns of nitrates, orthophosphates, orthosilicates and nitrites along the water column in the Strait of Sicily.

centration of orthosilicates in the deep water is $\sim$2 μmol$\cdot$l^{-1}, higher than the average concentration in the intermediate water. Also nitrates show a similar trend even if the increase in their average concentration is 1 μmol$\cdot$l^{-1}. The measured average N:P is $\sim$10 in surface waters, while, in the intermediate and deep waters, it approximates $\sim$28 and 21 respectively. These values are comparable to those previously reported for the Strait of Sicily by Ribera d'Alcala et al. [4]. The average values of Si:N range between 3 in surface water and 1.1-0.96 in intermediate and deep waters, respectively. These ratios testify the important unbalance of Redfield ratios in the Mediterranean. Moreover, a high nutricline depth (150-200 m) is evident from Figures 6a, 6b, 6c, 6d. In the studied area a Deep Chlorophyll Maximum (DCM) at about 100-150 m, particularly in proximity of the Sicilian coastal stations (Figure 6e) occurs. Finally, an evident primary nitrite maximum (PNM) has been ascribed to a combination of incomplete assimilatory reduction of nitrate by phytoplankton and chemoautotrophic oxidation of ammonium by nitrifying bacteria (Figure 5d) [8].

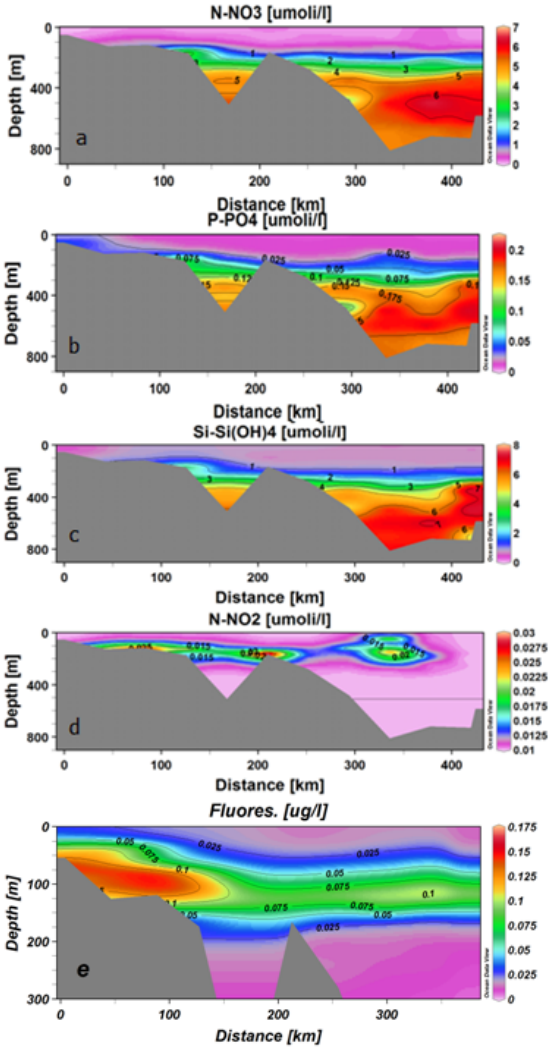

Figure 6: Nutrients (a, b, c, d) and fluorescence vertical profiles.

4 Conclusions

The main objective of this contribution is to provide a unprecedented and high-quality nutrients dataset from the Strait of Sicily, gateway from Eastern and Western Mediterranean basin. Evidence of a very shallow LIW water close to the Sicilian coast testifies a key role played by the seafloor morphology on the 3-D dynamics of the Sicilian strait. The LIW water mass appears enriched in nitrates and orthophosphates by effect of vertical demineralization of organic matter [6] while the DW shows the highest values of orthosilicates testifying a different kinetic in the dissolution of the two groups of nutrients along the water column [7]. The detected different values of the N:P ratios in the LIW and in the DW water masses confirm previously reported unbalanced Redfieldian biogeochemistry of the Mediterranean sea with respect to the global ocean [9]. No evidence of specific contribution on the biogeochemistry of the Sicily channel by effect of Saharan aeolian input emerges from the achieved dataset thus suggesting a primary role played by the 3D dynamics of the Mediterranean basin on the biogeochemistry of the strait.

References

[1] M.D. Krom, B. Herut, and F. Mantoura. Nutrient budget for the Eastern Mediterranean, implications for P limitation. *Limnol. Oceanogr.*, 49:1582–1592, 2004.

[2] J. P. Bethoux, P. Morin, and D.P. Ruiz-Pino. Temporal trends in nutrient ratios:chemical evidence of Mediterranean ecosystem changes driven by human activity. *Deep-Sea Research II*, 49:2007–2016, 2002.

[3] J. P. Sachs and D. J. Repeta. Oligotrophy and nitrose fixation during eastern Mediterranean sapropel events. *Science*, 286:2485–2488, 1999.

[4] M. Ribera d'Alcalà, G. Civitarese, F. Conversano, and R. Lavezza. Nutrient ratios and fluxes hint at overlooked processes in the Mediterranean Sea. *J. Geophys. Res.*, 108:1–15, 2003.

[5] K. Grasshoff, K. Kremling, and M. Ehrhardt. Methods of Seawater Analysis. 1999.

[6] K. Schroeder, G.P. Gasparini, M. Borghini, G. Cerrati, and R. Delfanti. Biogeochemical tracers and fluxes in the Western Mediterranean Sea, spring 2005. *Journal of Marine Systems-Available online*, 2009.

[7] H.J. Minas, B. Coste, P. Le Corre, M. Minas, and P. Raimbault. Biological and geochemical signatures associated with the water circulation through the strait of Gibraltar and in the western Alboran Sea. *J. Geophys. Res.*, 96:8755–8771, 1991.

[8] J.E. Dore and D.M. Karl. Nitrite distributions and dynamics at Station ALOHA. *Deep-Sea Research II*, 43:385–402, 1996.

[9] M.D. Krom, E.M.S. Woodward, B. Herut, N. Kress, P. Carbo, R.F.C. Mantoura, G. Spyres, T.F. Thingstad, P. Wassmann, C. Wexels-Riser, V. Kitidis, C.S. Law, and G. Zodiatis. Nutrient cycling in the south east Levantine basin of the eastern Mediterranean: Results from a phosphorus starved system. *Deep-Sea Research II*, 52:2879–2896, 2005.

Relationship of Yearly Changes of Phytoplanktonic Fluorescence to Upwelling in the Straits of Messina

F. Azzaro, F. Decembrini, F. Raffa, E. Crisafi
Institute for Coastal Marine Environment, CNR, Messina, Italy
filippo.azzaro@iamc.cnr.it

Abstract

Large gradients of tidal displacements as well as topographic constrictions determine upwelling of deeper waters to the surface layer in the Straits of Messina. This work describes the seasonal variability of surface distribution of phytoplankton biomass depending on upwelling phenomena. Temperature, salinity, nitrates and phytoplankton fluorescence were measured in 1994 and 1995 by continuous underway surface real-time measurements on board dedicated research boats. Each survey was performed following the dynamic phases of flooding and ebbing tides. Large spatial gradients of physical-chemical and biological parameters were mainly found at low water slack, while at high water slack a diffused phytoplankton fluorescence was observed only in autumn, concurrent with the seasonal thermocline. Generally, during winter, the upwelling distribution was limited to narrow zones, while in summer it involved the middle of the Straits and southern zones. During spring in the southern zone of the Straits, maximum of chlorophyll-a fluorescence was detected (0.32 $\mu g \cdot l^{-1}$ Chl-a) in summer, when back and forth tidal movements become intense between the Tyrrhenian and the Ionian seas, values was everywhere lower. The Straits system can be compared to an "intermittent pump" which, during the different seasons, before enriched itself and then it provides nutrients to the surrounding basins.

1 Introduction

Hydrodynamical processes affect the spatial distribution and temporal development of phytoplankton biomass of the global ocean and seas. Among the hydrographic events, the divergent current bring nutrients into the upper layer of the water column and modulates the chlorophyll-a distribution [1]. Upwelling is a hydrographic phenomenon that strongly impacts the marine ecosystem. In fact, upwelling systems belong to the most productive marine environments, and are characterized by increased 'biological richness' in all levels of the trophic chain. Low water temperature is one of the indicators of upwelling, and the difference of sea-surface temperatures between an upwelling zone and the surrounding waters is a parameter for defining upwelling intensity [2]. In these environments, phytoplankton growth is primarily regulated by the availability of allochthon nutrients, primarily nitrates, which stimulate the production of phytoplankton [3].

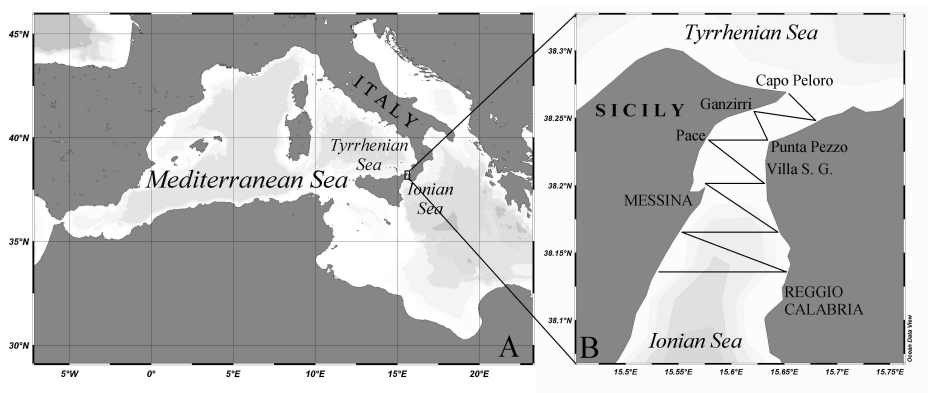

Figure 1: Geographical location of the Straits of Messina (A) and automatic surface tracking (B).

1.1 Description of the study area

The Straits of Messina, at the center of the Mediterranean Sea (Figure 1A), is an area where strong currents determine fast changes in the oceanographic conditions. This system, separating the Italian peninsula from Sicily, is an amphidromic point for the tides of the Tyrrhenian to the northwest and the Ionian seas to the southeast (Figure 1B). Morphologically, the Strait resembles a funnel-shaped geometry with a north-south length of 40 km and a west-east width ranging from 3 km near the Tyrrhenian edge, to about 25 km at the Ionian open boundary. The narrowest section (Ganzirri-Punta Pezzo), which coincides with the sill region, has a depth of 80 m and divides the area into northern and southern sectors. The sea bottom slopes steeply downward to a depth of 1000 m at 19 km south of the sill. The northern sector has a gentler slope, and the 400 m isobath is located 15 km north of the sill toward the Tyrrhenian Sea. The Straits exhibits strong tidal currents driven by both barotropic and baroclinic processes, due to strong bathymetric constraints exerted by the sill and coastal morphology [5]. Large gradients of tidal displacements are encountered in the Straits of Messina, because the predominantly semi-diurnal north and south tides are approximately in phase opposition. Due to both phase opposition and topographic constrictions, the current velocities can attain values as high as $3.0\mathrm{m{\cdot}s^{-1}}$ in the sill region, and are related to the position of the sun, the phase of the moon, the wind speed and direction, and the air pressure distribution [4, 6]. Surface water turbulence in the Straits is mainly influenced by two types of circulation, a steady surface current and a turbulent mixing, both of which generate discontinuity of the thermo-haline distribution in the surface layer (Figure 2). The steady current has a maximum speed of $2\mathrm{m{\cdot}s^{-1}}$ and a prevalently north to south direction at the surface (0-30 m). Water turbulence is caused both by internal waves and by tidal currents [7, 8, 9]. Internal waves are caused

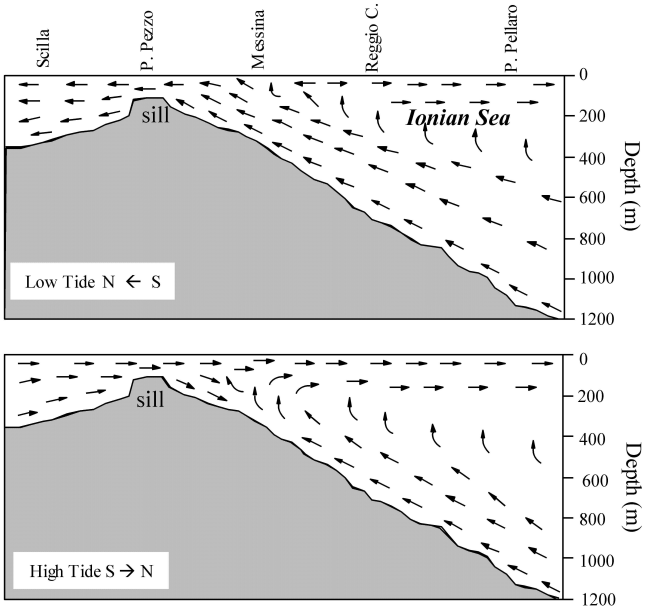

Figure 2: Straits of Messina: schematic distribution of the tidal currents during the maximum speed in the low and high tide flow [4]. Sill location refer to Figure 3.

by differences in water mass densities of the two basins that are facing in the Straits. Tidal currents are caused by opposite tidal oscillations of the two basins (max 27 cm) with almost the same amplitude and period (about 6 1/4 hours). These conditions lead to the upwelling of deeper water of Levantine Intermediate Water origin which is colder, more salty and more nutrient-rich compared to the Tyrrhenian Surface Waters (Atlantic Water origin). Harmonic oscillations of the current flowing from the Tyrrhenian Sea waters into the Ionian Sea (high tide current), and from the Ionian water into the Tyrrhenian Sea (low tide current) are encountered, with a brief slack water interval (balancing flow). Because of these particular environmental features, the Straits have been studied by many researchers in order to define forcing factors that determine its current regimen [4, 10, 11]. Many hydrobiological studies have been conducted over the last few decades to describe the influence of complex hydrodynamic conditions on biological parameters [12, 13, 14, 15].

1.2 Background and approach

The majority of previous hydrographic research has been conducted along the principal north-south axis using traditional oceanographic methods that, due to the time limitations of sampling, have produced an incomplete characterization of the horizontal extent and timing of the variability of the Straits of Messina. In recent years, oceanographic investigations using

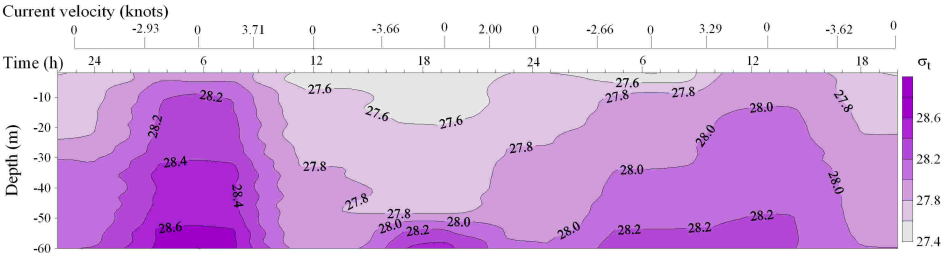

Figure 3: 48-hours behaviour of density at sill station surveyed with a frequency of 1-hour at syzygy (December 1993). Estimated current direction (+=S→N; -=N→S) and speed (Knots) from ≪Tavole di Marea I.I.M.M.≫. Reference to Figure 2.

innovative strategies and techniques have led to the observation of the upwelling of deeper water, not only in restricted zones (sill), but also in the wider areas of the system. These recent contributions have led to a better understanding of the system [16, 17, 18], but despite the development of new study approaches, proved to be limited in time. Conceivably, the concomitant ubiquitousness of water currents of different densities in the Straits, provokes natural vertical instability and an increase of deeper waters (upwelling). A conventional 48-h hydrographic survey (with a 1-h sampling interval) in a fixed sill station is representative of the frequent upwelling occurrence, as indicated by the detected density inversion (see the example of Figure 3). It is then assumed below that the timing of these overturns is highly coincident with the slack water interval when the rearrangement of the stable water column occurs as a result of instability. Near the end of the advective unsteadiness and during the onset of water slack, natural vertical vorticity and turbulent tidal currents occur. Flow continuity requires an upward flow from deeper waters to the south to maintain the divergence. As the vorticity and the associated cyclonic meander dissipate, upwelling should cease. The subsequent tidal stream could sweep the cold anomaly out of the Straits, and cause the temperature to rise again, setting the stage for the next tidal event. A data set from continuous and repeatable sampling of water temperature and chlorophyll-a fluorescence has allowed the study of different time-space scales in the Straits of Messina. Due to high hydrodynamic system variability, the surface tracking was performed during the slack water, when the advective current can be considered negligible and the turbulent moving water is replaced by upwelling water. Not surprisingly, temperature records indicate that this is the onset of massive upwelling of cold water from depths. In fact, the more evident chemical-physical and biological variation was observed during the rise of deeper waters. The aim of the present study was to assess the seasonal influence of the strong tidal variability on the surface phytoplankton distribution (estimated as chlorophyll-a fluorescence) in the water upwelling into the Straits of Messina system. The results covered an annual cycle at monthly scale, narrowly focused on providing a first-order description of the observed seasonal variability of the physical-chemical and bio-

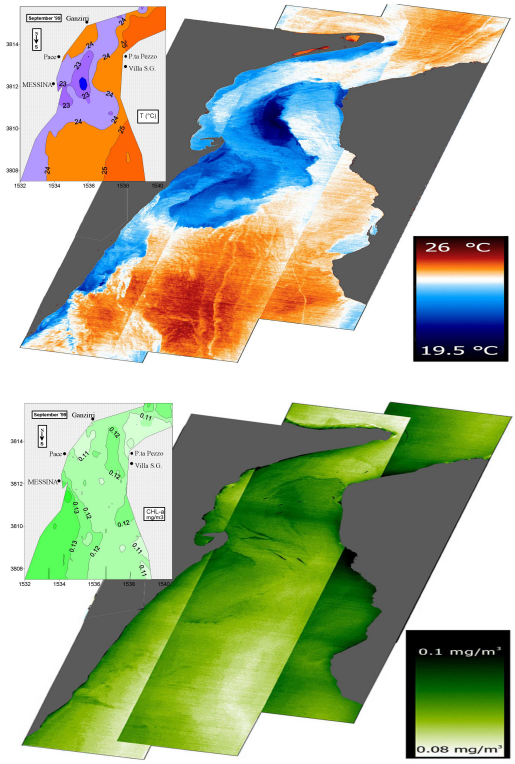

Figure 4: Map comparison of surface water temperature and chlorophyll-a fluorescence produced by data of sailing boat (left) with airborne images (MIVIS, right) data (25th September 1999).

logical parameters.

2 Materials and methods.

Spatial and temporal distribution patterns of physical-chemical (temperature, salinity, and nutrient concentrations) and biological (chlorophyll-a measured by in situ fluorescence emission) parameters were monitored for 25 months during a local research project, and data are presently available for the central-northern side of the Straits of Messina. Discrete water samples (nutrients, chlorophyll-a, etc.) based on conventional methods were collected during the surveys. The wind, air temperature and pressure were measured during each hydrographic cruise. Automatic real-time data were obtained by monthly surface tracking, from December 1993 to December 1995, in the area between Capo Peloro (Sicily) to the north and Reggio Calabria to the south. This area was covered on the R/B "Delfo" using zig-zag cruise tracks between the Calabrian and Sicil-

Figure 5: Effect of diurnal variability of spring-tide on the surface distribution of salinity (left) and nitrate (μM, right) during December 1993 and April 1994 in the slack water after low tide (upper panel) and high tide currents (lower panel).

ian coasts, adopting the lagrangian method in order to follow the wave of tide in the Strait. The location of the area and the track followed by the boat in each survey is displayed in Figure 1B. It is well known that the maximum intensity (more than $3 \mathrm{m \cdot s^{-1}}$) of the tidal currents occur during spring tides, corresponding to syzygy lunar phases. Measurements were carried out when the water slackens during the spring tide period to individuate the upwelling of deeper waters. Prior to taking measurements, the current forecast from "Tide tables of the Istituto Idrografico della Marina, Genova" was used in order to seize the quasi-stationary situations following the dynamic phases of high (high tide current, 3 h/cruise) and low (low tide current, 3 h/cruise) tides. The above-mentioned local sampling strategy (Figure 4) was recently repeated, and results showed that the images obtained simultaneously by MIVIS (Multispectral Infrared Visible Imaging Spectrometer) can be superimposed onto the measures at sea as reported in [19]. Seasonal real-time tracking of surface water temperature, salinity and fluorescence by chlorophyll-a were automatically measured (at a frequency of 30 sec.) using a CTD probe (Meerestechnik Elektronik) implemented with a fluorometer (Haardt-1101LP). The sensors were positioned inside a steel tank where the water flowed, drawn by a membrane pump at the back of the system; the sensors outputs were transmitted to a computer for display and storage. In addition to the above parameters, nitrate-nitrite automatic assays were performed in the winter and spring of 1994 (at a frequency of 30 sec.) in two different surveys onboard the R/V "Urania" using an Alliance Integral analyzer

(analytical accuracy of 0.15 μM). CTD-Fl data quality for salinity, fluorescence by chlorophyll-a and nitrate were assessed by comparison with laboratory analysis according to [20, 21, 22].

3 Results and discussions

As a part of several studies related to the influence of the physical forcing on the first level of the trophic chain, the hydrobiological behavior of surface waters from December 1993 to December 1995 are presented. Nitrate and salinity trends in winter and spring seasons are shown to point out the upwelling process. Among the cruises, four monthly surveys both in low and in high tides were chosen in order to represent the seasonal phytoplankton fluorescence and temperature conditions depending on the tidal current pattern.

3.1 Nitrate and salinity distributions

The high frequency real-time measurements of surface nitrates and salinity distributions observed in December 1993 and April 1994 are shown in Figure 5. In the winter season during the low water slack tide, the maximum nitrate concentrations were found along the Sicilian (1.51 μM - Pace) and Calabrian coasts (1.36 μM - Punta Pezzo) and were associated with the maximum salinity (38.24) and the minimum temperature (15.3°C). In the high water slack tide, the nitrate concentration increase was located near Villa S. Giovanni (1.2 μM of NO_3 and salinity of 38.22). Lower nitrate concentrations, close to undetectable values and associated with a salinity of 37.50, were measured in the northern zone of the Straits. During the spring season surveys, higher nitrate concentrations and wider upwelling zones were detected compared to winter surveys. Major NO_3 values during spring (3.67 μM) in the low water slack were associated with maximum salinity (38.39) and were located between Capo Peloro and Punta Pezzo, while the highest concentration (2.81 μM) was recorded between Pace and Punta Pezzo at the high water slack. The correlation analyses of nitrate concentration and thermo-haline parameters showed direct correlations with salinity ($r=0.52$, $p<0.01$, $n=1560$), and an inverse correlation with temperature ($r=0.84$, $p<0.01$, $n=1560$), [23]. A direct correlation (n=1560 Dec.'93 and Apr.'94) was observed between chlorophyll-a fluorescence and salinity ($r=0.22$ $p<0.01$) and nitrate levels ($r=0.12$ $p<0.01$), while an inverse correlation was observed with temperature ($r=0.23$ $p<0.01$). It is likely that tidal pumping is an important contributor to the nutrient supply of this area, which suggests that the NO_3 concentration could be a conservative parameter of the upwelled water in the Straits of Messina [12]. Upwelled water is cooler and saltier than the original surface water, and has much higher concentrations of nutrients such as nitrate, which sustain the biological primary production. The high values of chlorophyll-a fluorescence at the boundary of the divergence zone are likely determined by the upward flux of nutrients to the euphotic zone and by the intense tidally-induced vertical mixing.

Winter (Dec-Jan-Feb)

	T	*S*	*F*
HWS			*LWS*
T		-0.052	0.020
S	-0.101		-0.050
F	0.370	-0.319	

Spring (Mar-Apr-May)

	T	*S*	*F*
HWS			*LWS*
T		-0.393	-0.686
S	-0.481		0.219
F	-0.584	0.133	

Summer (Jun-Jul-Aug)

	T	*S*	*F*
HWS			*LWS*
T		-0.126	-0.556
S	-0.745		0.366
F	-0.732	0.292	

Autumn (Sep-Oct-Nov)

	T	*S*	*F*
HWS			*LWS*
T		-0.424	-0.375
S	-0.707		0.232
F	-0.560	0.370	

Table 1: Correlation matrix for the seasonal (1994-95) data: low water slack (upper right); high water slack (lower left); number of data for each set: >1000. Significance of correlation coefficients: r = 0.062 (P = 0.05); r = 0.081 (P = 0.01).

3.2 Seasonal trend of phytoplankton fluorescence and temperature distribution

The hydro-biological parameters recorded monthly during 1995 during both low and high water slack tide are described. The correlation matrices for both slack tides, based on 1000 individual datapoints for each component (Table 1), show some significant correlations. Thus, during spring, summer and fall seasons, fluorescence is positively correlated with salinity and negatively correlated with temperature, while in winter the correlation is inverted in high water slack and in low water slack there is a lack of correlation. The spatial distribution among the different seasons is clear evidence of the tidally-induced upwelling character of the zone. The contour plots of sea-surface temperature and chlorophyll-a fluorescence (SST and Chla-Fl hereinafter) and seasonal distribution patterns are displayed in Figures 6 and 7 . General uniformity of the surface thermo-haline horizontal structures were observed during winter months in slack water; water temperature ranged between 14.35°C and 15.67°C, and salinity ranged from 37.44 to 38.12. In the low water slack tide, SST was lower (15.30°C in January 1995, Figure 6) in the northern zone bounded by the Ganzirri-Punta Pezzo section. In the high water slack, SST was found to be lower (15.20°C in January 1995, Figure 7) mainly in the central zone along the Sicily coast. During winter, phytoplankton fluorescence was low and was uniformly distributed in the area (around 0.16 $\mu g \cdot l^{-1}$ Chl-a) in both slack waters (Figures 6 and 7). However, in the low water slack tide, a slight increase in the Chla-Fl concentration at the middle of the southern zone and in the western part of the central zone were found, whereas at high water slack tide (Figure 7)

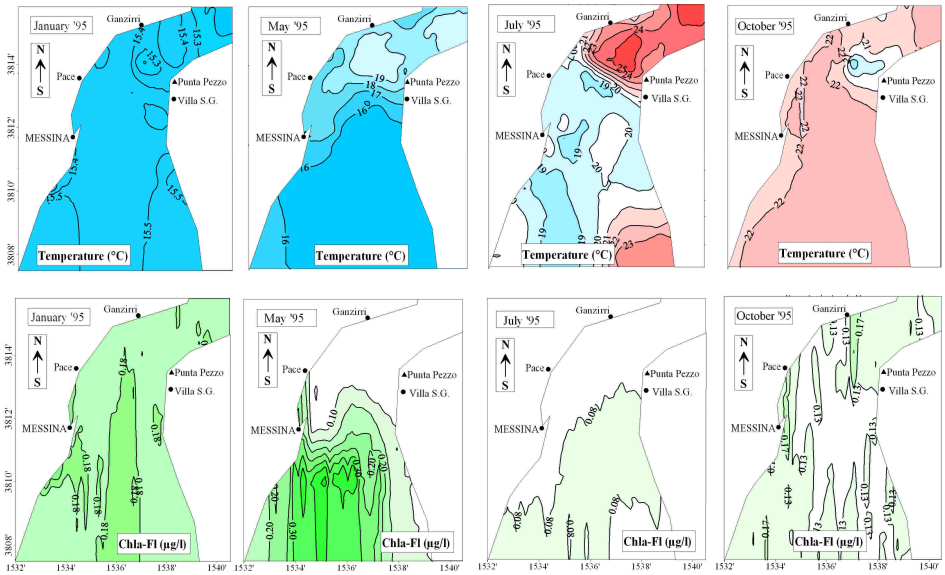

Figure 6: Effect of diurnal variability of spring-tide on the surface distribution of temperature (°C, upper panel) and chlorophyll-a fluorescence ($\mu g \cdot l^{-1}$ Chl-a, lower panel) during January, May, July and October 1995 in the slack water after low tide current.

in the upwelling zone, between Ganzirri-Punta Pezzo, a decrease of Chla-Fl values was measured (0.14 $\mu g \cdot l^{-1}$ Chl-a). During the spring season, the upwelling zone found in the winter gradually extended to the south (15.50°C in May 1995, Figure 6) during both low and high slack waters. In particular, during low water slack tide (Figure 6), the maximum phytoplankton fluorescence (0.32 $\mu g \cdot l^{-1}$ Chl-a) was recorded in the southern part, whereas in the high water slack, Chla-Fl was extremely low with a slight increase in the southern sector (more than 0.12 $\mu g \cdot l^{-1}$ Chl-a). The maximum SST range occurred in the low water slack after higher currents velocity (more than $2 m \cdot s^{-1}$) during the summer; a narrow temperature front (25.53-18.54°C) (Figure 6) and salinity front (37.80-38.35) were found in the northern zone of the system. In the opposing current phase (high water slack, Figure 7), SST ranged between 27.93°C and 22.88°C and the salinity ranged from 37.50 to 38.30. Moreover, the upwelling zone mainly extended along the Sicilian coast, while higher temperature values were recorded in the northern zone (27.93°C) (Figure 7). During summer, lower Chla-Fl values (<0.09 $\mu g \cdot l^{-1}$ Chl-a) were recorded coincident with highest surface thermo-haline discontinuities at slack water after both tidal flows and were localized in the southeastern area. In autumn, SST values were influenced by summer heating, and consequently there were higher annual averages with less variation (20.75 $\pm$ 2.47°C). Moreover, in October, the previously described phytoplankton fluorescence conditions become inverted (Figure 7): at low water slack high

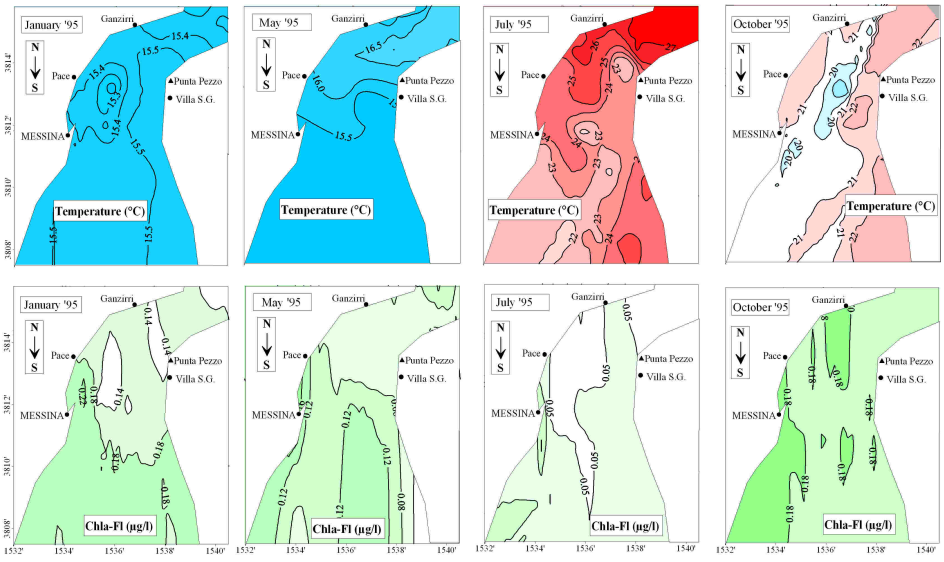

Figure 7: Effect of diurnal variability of spring-tide on the surface distribution of temperature (°C, upper panel) and chlorophyll-a fluorescence ($\mu g \cdot l^{-1}$ Chl-a, lower panel) during January, May, July and October 1995 in the slack water after high tide current.

tide, values and homogeneous distributions (0.13 $\mu g \cdot l^{-1}$ Chl-a) were found; in the divergence areas, higher Chla-Fl values (0.18 $\mu g \cdot l^{-1}$ Chl-a) were observed at both slack waters. In fact, the distribution of biomass in autumn was influenced by the presence of a thermocline. A report by [9] on high-resolution hydrographical measurements carried out in October 1995 approximately at slack waters after both tidal flows, showed that when south of the Straits sill, the thermic profile was characterized by the presence of a well-mixed near-surface layer with a thickness of about 40 meters. The astronomic conditions imply that advective velocities of the waters are stronger in spring through late summer, which could favor some of the phenomena discussed here (greater shear, more mixing). On the other hand, the simultaneous development of the autumnal thermocline would hinder the pumping of nutrients and other particles into the euphotic zone from deep waters. These counteracting influences are likely responsible for the biological cycle of the well mixed layer, and any reliable description of the seasonal cycle requires more in situ data. Seasonal temperature and chlorophyll-a maps (Figures 6 and 7) suggest the following features during most of the year: seasonal temperature depicts upwelling cores with cold and very rich in particles surface waters, but biologically poor patches. The chlorophyll-a maps depict a southward tongue of water rich in chlorophyll-a connected to the upwelling zone in such a way that high chlorophyll-a concentrations are found in calmer waters, far from the upwelling zone.

4 Conclusions

The seasonal variability of phytoplankton fluorescence exhibits low values in the tidally induced upwelling zone due to the strong vertical mixing, except during autumn, when thermocline is also present in the Straits and the vertical exchange in the water column is limited [13]. The data show the existence of an annual cycle with an upwelling peak in late spring through the late summer. During autumn and winter seasons, the upwelling is confined to the central zone of the Straits. In spring, the divergence zones occur both in the central and southern sectors of the system. During the summer season, the upwelling takes place in the middle area of the Straits spreading to the south. The principal correlation features are consistent with the assumption that main variations in hydrobiological characteristics are directly related to the seasonal trends of the tide currents, strongly evident during warm seasons compared to the cold ones. Moreover, the lack of correlation is due to winter homothermy of the water column. In the study area, ranges of surface physical-chemical and biological parameters increase after the low tide. The highest chlorophyll-a fluorescence values were observed during the spring season in the low water slack, while in the opposite high water slack only during autumn. The effects of seasonal variability recorded in autumn, with the high occurrence of phytoplankton biomass in divergence zones, are caused by the formation of a thermocline layer with a lower intensity of upwelling processes [9]. The gradual warming and expansion of the surface layer establishes the stratification and nutrients are recycled in the upper layer [13]. In stratified conditions, when the exchange in the water column is limited, nutrients are likely supplied to the photic level by lateral transport and faster remineralization above the thermocline. This particular combination means that phytoplanktonic organisms find optimal conditions for their growth at the surface layer, where there is low vertical mixing, light and nutrient availability. In the summer months, despite the input of nutrient-rich deeper waters [17], the low autotrophic biomass is due to high vertical hydrodynamics. Additional variability would be generated by wind force, irradiance, advection from adjacent areas, none of which were a major factor of modulation of the hydrographic conditions due to tides at the time of the present study. Although surface data alone are not enough to discriminate what physical process is forcing the biological response, mixing events at the sill region of the Straits of Messina are likely mechanisms for the fertilization of the upper layer. The evidence of mixing allows us to define the Straits as a pulsating upwelling area, because the mechanisms regulating the mixing events are tidally induced. As a formal model, the Straits of Messina may be compared to an 'intermittent pump' that compresses and nutrient-enriches during autumn and winter while in spring it expands and stimulates phytoplankton both locally and in the adjacent zones [16, 24]. During the summer season, the surface water is enriched with nutrients and is advected towards the surrounding areas, where a decrease of nutrients and increase of chlorophyll-a occurs, namely in the north (Gulf of Gioia Tauro [25]) and along the southeastern Sicilian coast [10, 26, 27].

References

[1] F. Gomez, G. Gorsky, E. Garcia-Gorriz, and M. Picheral. Control of the phytoplankton distribution in the Straits of Gibraltar by wind and fortnightly tides. *Estuarine, Coastal and Shelf Science*, 59:485–497, 2004.

[2] D.L. Tang, H. Kawamura, and L. Guan. Long-time observation of annual variation of Taiwan Straits upwelling in summer season. *Advances in Space Research.*, 33(3):307–312, 2004.

[3] C.T.A. Chen, L.Y. Hsing, C.L. Liu, and S.L. Wang. Degree of nutrient consumption of upwelled water in the Taiwan Strait based on dissolved organic phosphorus or nitrogen. *Marine Chemistry*, 87(3-4):73–86, 2004.

[4] F. Vercelli. Crociere per lo studio dei fenomeni nello Stretto di Messina. Il regime delle correnti e delle maree nello Stretto di Messina. II, 1925.

[5] T.S. Hopkins, E. Salusti, and D. Settimi. Tidal forcing of the water mass interface in the Straits of Messina. *Journal Geophysical Research*, 89:2013–2024, 1984.

[6] A. Defant. Physical Oceanography. 2, 1961.

[7] W. Alpers and E. Salusti. Scylla and Charybdis observed from space. *Journal of Geophysical Research*, 88(3):1800–1808, 1983.

[8] W. Alpers, P. Brandt, A. Rubino, and J.O. Backhaus. Recent contributions of remote sensing to the study of internal waves in the Straits of Gibraltar and Messina. *Dynamics of Mediterranean straits and channels*, 17:21–40, 1996.

[9] P. Brandt, A. Rubino, D. Quadfasel, W. Alpers, J. Sellschopp, and H. Fiekas. Evidence for the influence of Atlantic-Ionian stream fluctuations on the tidally induced internal dynamics in the Straits of Messina. *Journal of Physical Oceanography, Notes and Correspondence*, 29:1071–1080, 1999.

[10] E. Böhm, G. Magazzù, L. Wald, and M.L. Zoccolotti. Coastal currents on the Sicilian shelf south of Messina. *Oceanologica Acta*, 10:137–142, 1987.

[11] F. Mosetti. Some news on the currents in the Straits of Messina. *Bollettino di Oceanologia Teorica ed Applicata*, 6(3):119–201, 1988.

[12] E. De Domenico. Caratteristiche fisiche e chimiche delle acque nello Stretto di Messina. *Le Détroit de Messine (Italie). Doc. et Trav. IGAL*, 11:225–235, 1987.

[13] G. Magazzù, V. Bruni, A. Piccione, T. Platt, B. Irwin, and S. Rao. Picoplankton: Contribution to Phytoplankton Production in the Straits of Messina. *Marine Ecology*, 8(1):21–31, 1987.

[14] F. Azzaro, F. Decembrini, and F. Raffa. Hydrobiologic observations in syzygy in a latitudinal section in the Messina Straits. *Rapp. Comm. Int. Mer Médit.*, 37:483, 2004.

[15] F. Azzaro, F. Decembrini, F. Raffa, and E. Crisafi. Hydrobiologic observations in the water column from the quadrature to the syzygy in the Straits of Messina. *Biol. Mar. Medit.*, 11(2):481–485, 2004.

[16] F. Azzaro, F. Decembrini, and E. Crisafi. Continuos survey of upwelling in the Straits of Messina. *Rapp. Comm. Int. Mer Médit.*, 34:167, 1995.

[17] B. Cescon, F. Azzaro, S. Creazzo, F. Decembrini, and G. Magazzù. Processes affecting upwelling and primary productivity of the Straits of Messina. *Bollettino di Geofisica Teorica e Applicata*, 38(1-2):137–147, 1997.

[18] F. Azzaro, F. Decembrini, and E. Crisafi. Sequenza temporale delle condizioni termo-aline e distribuzione della biomassa fotoautotrofa nello Stretto di Messina. *Biol. Mar. Medit.*, 7(1):541–548, 2000.

[19] F. Azzaro, R.M. Cavalli, F. Decembrini, S. Pignatti, and C. Santella. Biochemical and dynamical characteristics of the Messina Straits water by means of hyperspectral data. *Hyperspectral Remote Sensing of the Ocean.*, 4154:240–249, 2001.

[20] J.H.D. Strickland and T.R. Parsons. A practical handbook of seawater analysis. 167(2nd ed.), 1972.

[21] M. Innamorati, I. Ferrari, D. Marino, and M. Ribera d'Alcalà. Metodi nell'Ecologia del Plancton Marino. 1990.

[22] K. Grasshoff. Determination of nitrate. *Methods of seawater analysis.*, pages 143–150, 1983.

[23] R.A. Fischer. Statistical Methods for Research Workers. 1946.

[24] F. Decembrini, F. Azzaro, E. Paschini, and G. Magazzù. Influenza dei fenomeni di upwelling sulla produzione e biomassa fitoplanctoniche nello Stretto di Messina. *Atti A.I.O.L*, 12(2):159–171, 1998.

[25] M. Innamorati, L. Massi, and C. Nuccio. Indipendenza delle biocenosi fitoplanctoniche dalle masse d'acqua circostanti le isole Eolie. *ATTI DEL 11° CONGRESSO*, 11:645–654, 1996.

[26] F. Decembrini, T.S. Hopkins, and F. Azzaro. Variability and sustenance of the deep-chlorophyll maximum over a narrow shelf, Augusta Gulf (Sicily). *Chemistry and Ecology*, 20(Suppl. 1):S231–S247, 2004.

[27] F. Raffa and T. S. Hopkins. Circulation and water mass structure over a narrow shelf, Augusta Gulf (Sicily). *Chemistry and Ecology.*, 20(Suppl. 1):S249–S266, 2004.

Multidisciplinary Investigations at Panarea (Aeolian Islands) after the Exhalative Crisis of 2002

G. Bortoluzzi[1], S. Aliani[2], M. Ligi[1], F. D'Oriano[1], V. Ferrante[1], F. Riminucci[1], C. Carmisciano[3], L. Cocchi[3], F. Muccini[3]
1, Institute of Marine Sciences, CNR, Bologna, Italy
2, Institute of Marine Sciences, CNR, Pozzuolo di Lerici (SP), Italy
3, National Institute of Geophysics and Volcanology, La Spezia, Italy
g.bortoluzzi@ismar.cnr.it

Abstract

Panarea and surrounding Islets form a volcanic edifice, that is part of the Eastern sector of the Aeolian Arc, Southern Tyrrhenian Sea. It is now considered inactive, since last documented activity is 20 Ka old. However, on 2002-11-03, gas started to flow violently from the seafloor in an area E of the Island, mainly along NE and NW structural lineaments, and lasting up to 2003-2004 with a consistent flux, orders of magnitude larger that 'steady-state' fumarolic activity documented there in historical times. On the same period a strong effusive activity of Stromboli (10 NM to NNE) was present. Since then, several investigations have been conducted at sea and on land, with the aim of focusing on the problem of effusive activity at sea, mainly in the light of volcanic surveillance and risk. Among these investigations, some of which have been repeated over years, we present and discuss some data and results from: (a)visual inspection and sampling by divers and ROV, (b)GPS networks and mapping by multibeam and LIDAR, (c) oceanographical measurements by current meters and CTD, and water flux and dynamics measurements, (d)magnetic and gravimetric surveys, (e) multichannel reflection Seismic with OBS and land station networks. Data were used for compilation of high resolution bathymetric, magnetic and gravimetric maps, including the emerged and submerged portions of the edifice.

1 Introduction and setting

On 2002-11-03 a burst of gas occurred in the marine area E of Panarea, lasting for years with a consistent flux from fractures and sinkholes on the seafloor, mostly near the islet of Bottaro (Figure 1). Investigation started immediately to monitor this event from geological and geochemical point of views, also in the light of volcanological surveillance and risk [1, 2, 3, 4, 5, 6, 7], and on the possible connection to regional tectonics [8, 9, 10, 11]. This paper aims at providing a review of the geophysical investigations carried out in the area of the eruption since 2002. The Aeolian Islands are part of the volcanic arc formed by the convergence of the African and Eurasian plates and by the subduction and southeastward rollback of the Ionian lithosphere [12, 13, 14, 15, 16, 17, 18], and is characterized by compression in the western sector, strike-slip faulting and extension in the central and eastern ones. The archipelago is formed by 7 islands and minor islets, including to-

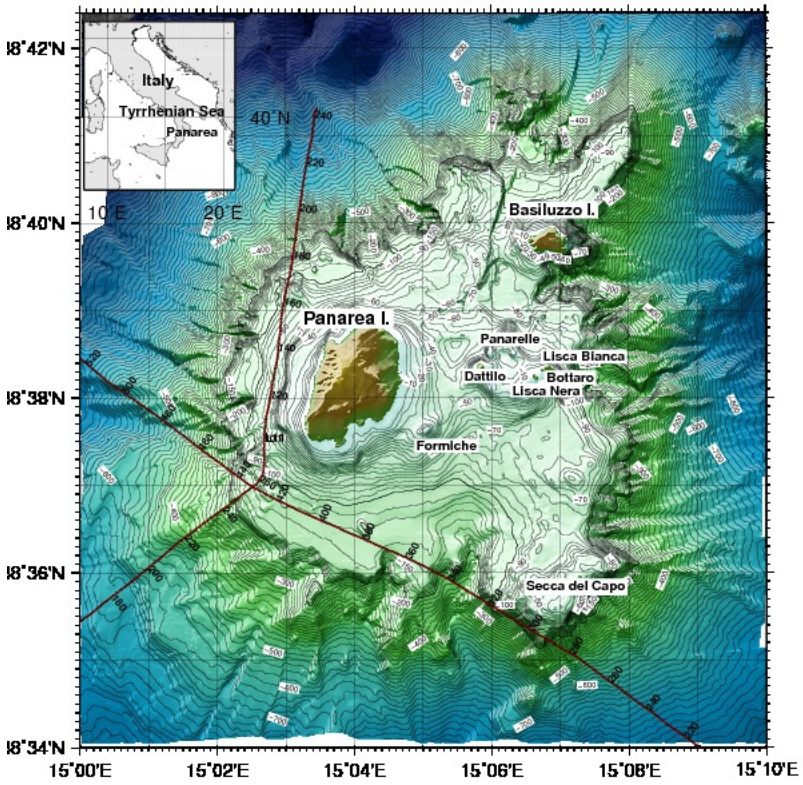

Figure 1: Panarea volcanic complex. Bathymetries from ISMAR. Also shown position of MCS lines L09, L10, L11.

day's active Stromboli volcano. Panarea is considered inactive, however [19] have shown possible recent volcanic outcrops near Basiluzzo; present deformation patterns are likely connected to NE-SW trending faults [20].

The gas release of 2002-11-03 in the area E of Panarea, known since historical times for fumarolic activities [21], generated 6-7m diameter columns of bubbles from the seafloor to the surface. Several active spots were identified by divers and ROVs' and by repeated multibeam surveys [3, 5]. The most impressive one was just SW of Bottaro (PEG1, Figure2) with gas reaching the surface from 15m depth, from an elliptic depression produced by the explosive collapse of the seafloor; a plume of suspended sediments was present at the sea surface for days.

During the most active degassing up to mid 2003, the emissions were found to be an emulsion of CO_2-dominated gas phase with suspended sediments, colloidal sulfur; the water was acidified by dissolution of SO_2, HCl and HF [2, 7]. [1] estimated a

RESP	CRUISE	Date	Ship	Mapping	F	C	M	G	D	R
ISMAR	1994	1996-11-01	J.Charcot	Sim.EM1000						X
ISMAR	TIR96	1996-09-01	Gelenzhik	Sim.EM12			X			
ISMAR	TIR96	1999-02-01	Strakhov	Sim.EM12			X			
ISMAR-INGV	P2002-11	2002-11-07	Thetis			X			X	X
ISMAR	P2002-12	2002-12-10	Alsea	Res.8125	X		X		X	
ISMAR	P2003-01	2003-01-20	Thetis							
ISMAR	P2003-07	2003-07-27	Alsea	Res.8125		X	X			
ISMAR	P2003-09	2003-09-02	L.Sanzo		X	X			X	X
ISMAR	P2003-12	2003-12-10	Alsea	Res.8125					X	
ISMAR-NERC	P2004-04	2004-04-20	plane	LIDAR		X				
ISMAR	P2006-01	2006-01-20	Alsea	Res.8125					X	
ISMAR-IMM-INGV	P2006-04	2006-04-15	Aretusa	Kon.EM3000			X			
INGV		2006-04-15	land					X		
ISMAR	P2006-05	2006-05-02		SeaInterf.						
ISMAR	PANA07	2007-08-01	Urania	Res.8160						
ISMAR-INGV	CALA08	2008-04-02	Urania	Res.8160				X		
ISMAR-INGV	PANSTR10	2010-02-01	Urania	Kong.EM710			X	X		

Table 1: Data Acquisition Cruises. Measurements: F=Water-gas Fluxes; C=CTD; M=Magnetics, G=Gravity; D=dive; R=ROV.

gas output of $10^9 \mathrm{l \cdot d^{-1}}$ (November 2002, all emissions) and of 4 to 2 x $10^7 \mathrm{l \cdot d^{-1}}$ (May to July 2003, PEG1), orders of magnitude higher than the total gas output of $10^6 \mathrm{l \cdot d^{-1}}$ measured within the Islets in the 1980's [21]. [22] measured the water fluxes at PEG1, deriving also the gas fluxes. The plumes affected the marine environment with changes in the biota [23, 24] and in the water properties [25]. Figure 2a shows the location of the major emissions (named PEG1,2,3,8).

2 Materials and Methods

Several cruises were performed in the area for obtaining geophysical and oceanographic data and to monitor the geomorphological features of the seabed and the evolution of the gas outflow after the 2002-11 crisis. The investigations were coordinated by the Italian Department of Civil Protection (DPC) and 'Commissione Grandi Rischi' and were carried out from immediately after the gas burst up to 2008 (Table 1).

Multibeam data from different cruises and instruments were processed with the Kongsberg's Neptune and RESON's PDS2000 software. Gridding was performed in the geographical and UTM33 projections, at spatial resolution ranging from 10-15m for deeper areas, to 0.20-0.25m for local, shallow areas. Some datasets have been processed separately due to large number of points acquired. Furthermore, a particular attention was paid to the analysys of the gas emissions (Figure2) included in the multibeam data [3]. A LIDAR flight was performed by NERC on April 2004 by the *Airborne Remote Sensing Facility* using an Optechh ALTM 3033 laser scanner; the processed data included first and last pulses and ob-

tained data at the resolution of ∼0.2m [26]. Magnetic data were acquired during cruises TIR96, TIR99, P2002-12, P2003-07 and PANSTR10, with GEM GSM19D and Marine Magnetics Sea-Spy 'Overhauser' magnetometers; during cruise P2006-04 the Geometrics G-800 'Cesium magnetometer was used [27]. Data underwent filtering, de-spiking, cross-over error reduction, application of IGRF Models with 2005 coefficients for calculating anomalies and reduction to the Pole.

Multichannel data (48 active, 12.5 m group interval, 2xGI Harmonic mode), were acquired during cruise PANA_07, complementing MESC2001 ISMAR's cruise (http://www.ismar.cnr.it/prodotti/reports-campagne). On the same cruise a seismic network was set on Islets and on the seafloor by deploying seismometers and OBSs from INGV and University of Trieste. Seismic shots sequences were performed along lineaments connecting the instruments. The gravity data on land [27] were sampled using a pair of LaCoste&Romberg microgravimeters (Aliod model) equipped with a digital data acquisition system, GPS tracking and automatic tide corrections, with a nominal resolution of 1 μgal. Marine gravity data were acquired with a Lacoste&Romberg 'AirSea' gravimeter, directly interfaced to DGPS, during cruises CALAMARE08 and PANSTR10 (http://www.ismar.cnr.it/prodotti/reports-campagne). Data were de-spiked, corrected for drifts and Eötvös effects, and Free air and Bouguer anomalies were calculated.

Flux of water entering the vent at PEG-1 was estimated by geometry of the ascending gas column and by measuring water velocities inside and outside the gas column. Rotor (Aanderaa and Datasonics) and ADCP current meters were positioned 1m above the sea floor in the gas, and few m away, respectively (Figure 4). Estimates of the venting surface was done by divers and high resolution bathymetries, since multibeam used were able to detect the gas in the water column. Once obtained the water fluxes entering at the base and exiting the vent, the gas fluxes were estimated by applying reduction factors accounting for (a) the bubble sizes and voids, as seen by divers and ROV, and (b) considerations about reduced velocities at the boundary layers of the cell.

R/V Thetis and R/V L.Sanzo deployed ROV systems, on 2002-11, few days after the burst, 2003-01 and 2002-09. During this last deployment the instrument was also moored on bottom in front of the degassing area for hours, aiming at recording flagged poles on seafloor and dye releases able to visualize the water dynamics at the base of the vent. ROV records confirmed the bathymetric and divers investigations about changes in topography and geometry of the gas column.

CTD investigations were performed on 2002-07, 2002-09 and 2004-04, to evaluate possible plumes and modifications of water column properties. Standard sensors mounted on SBE probe were used and pH was found to be particularly effective for tracing the acid fluid releases.

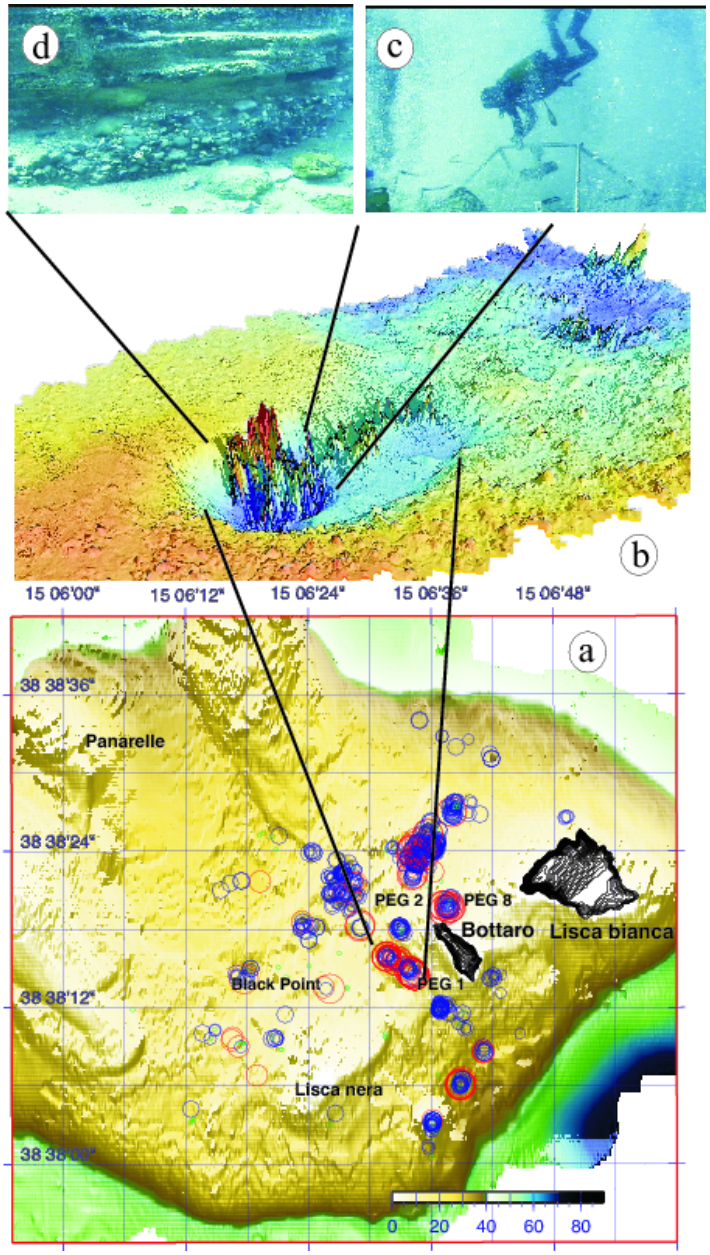

Figure 2: Gas emitting points (a) and 3D rendering of PEG1 multibeam data (b). Photos on top: (c) the divers' positioning the lander with a rotor current meter into the gas column, and (d) the exposed cemented breccia at the vertical borders of the sinkhole. Images from [2,4], modified.

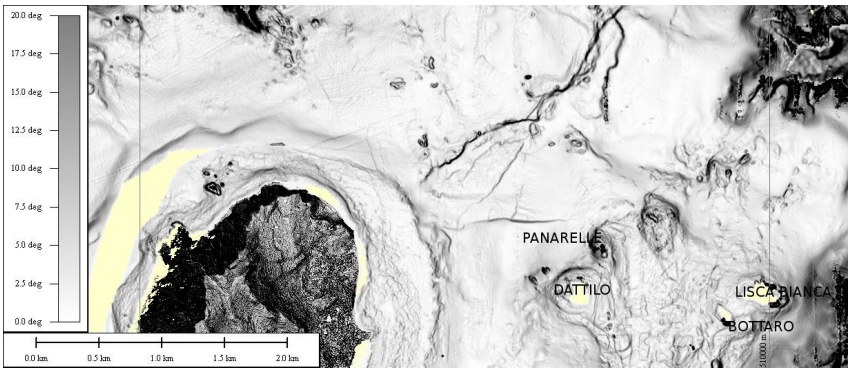

Figure 3: Area E of Panarea (slope shading). Topography by NERC's LIDAR flight.

Figure 4: September 2003 flux-measurement experiment: the ADCP and rotor current meter (within gas, on the frame) are visible.

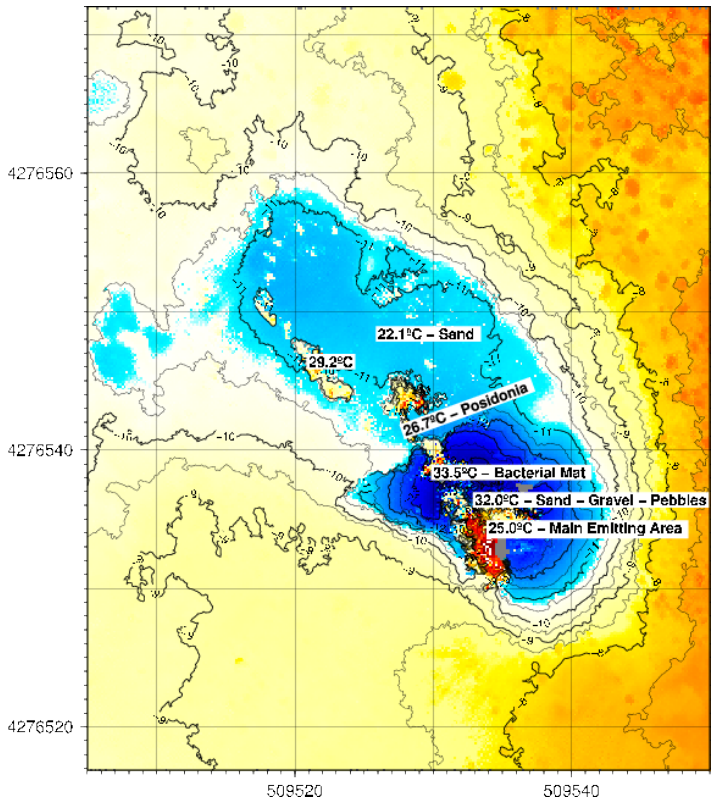

Figure 5: Bathymetry and diving observations on 2002-12. Also shown the temperature measured at the seafloor close to emitting spots. Sea water temperature was ∼17°C.

3 Results and Discussion

3.1 Bathymetry

ISMAR performed a high resolution multibeam bathymetric cruise on 1994 [29]. A wide portion of the Aeolian Central sector was imaged down to ∼800 m depth, except for very shallow waters, including the area of the Islets. The TIR96 and TIR99 cruises [30] mapped the deeper portions. After 2002 crisis several cruises were able to map almost entirely the submerged edifice, collecting also data near the shoreline of Panarea and Islets.

Panarea and islets (Figure 1, 3, [31]) emerge from a volcanic edifice (diameter of ∼18 km at the -1000 m isobath), dissected by gullies and channels and largely dismantled by erosion and by neo- and volcano-tectonics. Its flat summit, with edge at about 80-130 m bsl, is almost totally covered by volcanoclastic sedimentation, arranged in its upper part in sequences of terraced, wedge-shaped prograding units [32]. Several, partly buried, primary volcanic features are present and partially outcrop in the southern sector, among them the

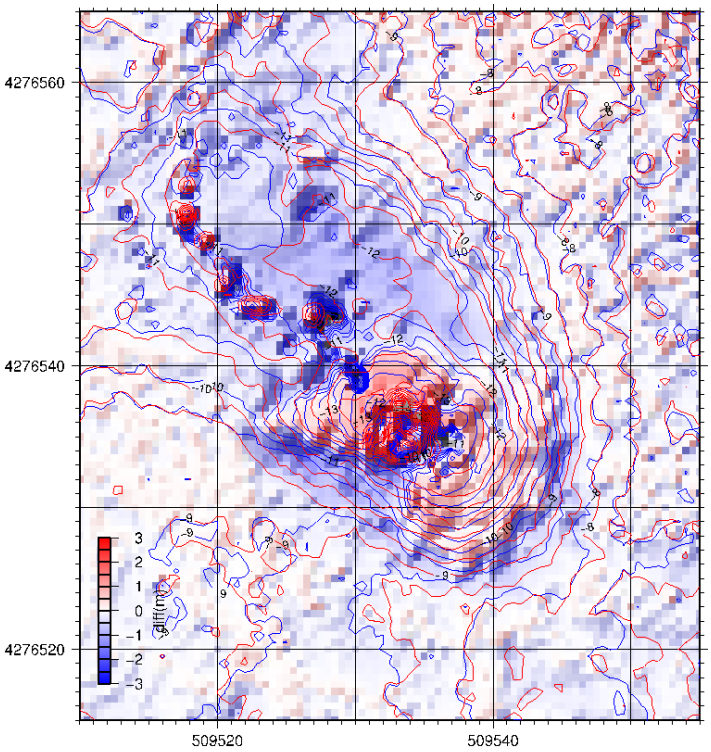

Figure 6: Bathymetry 2002-12, 2003-12, one year after. Also shown the difference in depth.

shoal of Secca del Capo [33, 34, 19, 29, 35].

East of the island, a relief of $\sim$ 1.5km diameter is present at depth $<$ 30m, partially emerging in the Islets and enclosing depressed areas where intense exhalative activity occured. The northeastern summit of the edifice presents a NNE-SSW and NE-SW structural lineament (on the $\sim$ 20 m high fault scarps, fresh rocks and mineralization as well as gas venting are present [36, 29, 35]) and further extends from Basiluzzo with NE-SW direction.

The repeated bathymetries over the years on the PEG1 area 5 showed that less than a year after the gas burst, the depression was already partially infilled by sediments transported from the flanks by the dismantling of the sub-vertical wall to the N, exposing cemented breccias and rocks of holocene age [5] (Figure6). The survey of 2006-01 further confirmed this infilling, producing variation of bathymetries of 2-3m. Pebbles rolling on the seafloor under wave and current dynamics kept on filling the sinkhole and very likely will produce a new non-active meter size depression filled with sandy or gravel materials similar to others discovered in the area by multibeam. On 2006 and 2007 the flux of gas was visibly reduced to a small area, and similarly the transport caused by entrainment at the

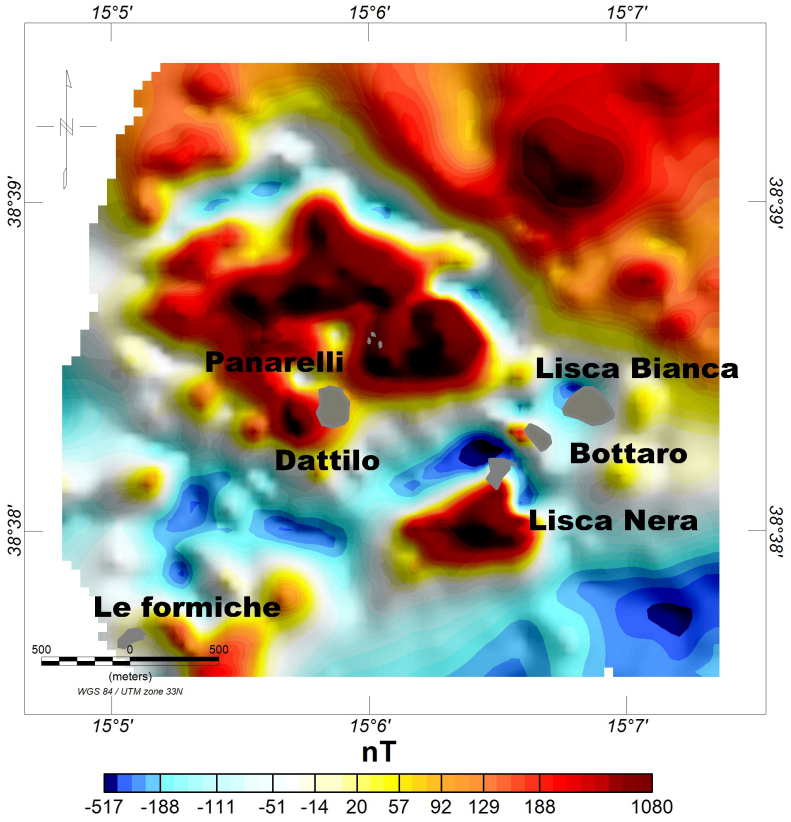

Figure 7: Magnetic anomaly data. 2002-12 Alsea cruise.

base of the degassing cell also reduced. The wave and current dynamics will probably be able to continue the filling process on the medium period. On the plateau just N of the depression, a wide area was covered by sediments, very likely ejected during the explosive collapse of 2002-11-03, and the sizes and water depth seem suitable for bedload transport and distribution. ROV on the field few days after revealed sand dunes and ripples crossing at 30-40°.

3.2 Magnetics and Gravity

On 2002-12 ISMAR collected high resolution data within the Islets (Figure7). The same pattern of lines was repeated by Geophysics and Marine Technology Unit of Istituto Nazionale di Geofisica e Vulcanologia (INGV) of Portovenere in Spring 2006, together with gravity data on the islets and on Panarea [27]. Magnetic anomaly pattern of islets area is dominated by the high positive (500-750 nT) north of Panarelli shoal in correspondence of a topographic high. This anomaly seems related with the

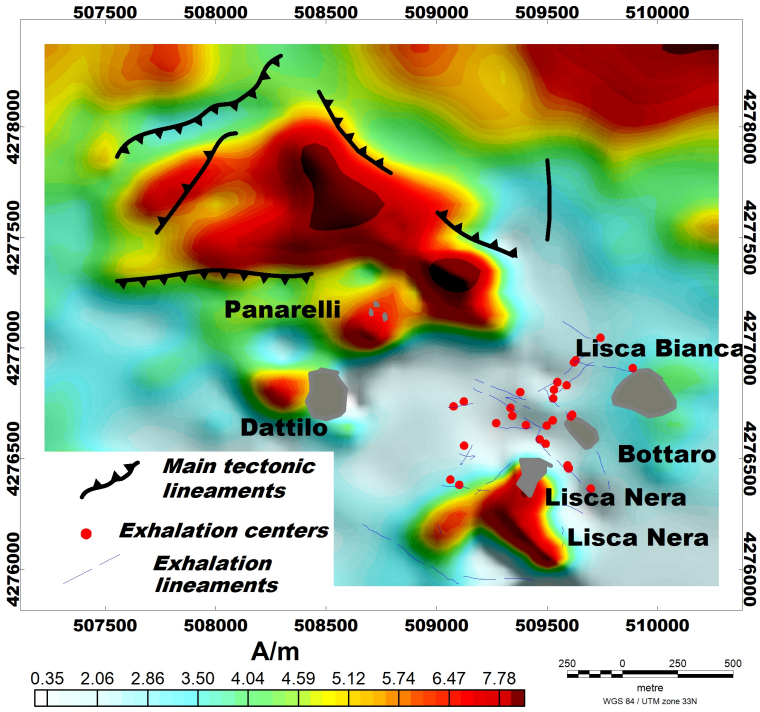

Figure 8: 2D Apparent magnetization map. Structural lineaments from [5], exhalative centers from [28].

main tectonic lineaments and it can be interpreted as the signature of an ensemble of magmatic sources. Rock-sampling by [5] showed andesitic lava products correlated to a shallow cryptodome-like structure. A 2D inversion of the data was performed to evaluate the magnetization pattern of the area, using an FFT-algorithm (Parker inverse approach, [37, 38]), applied to a crustal portion of 1Km below sea bottom. Figure 8 suggests a clear separation between the high magnetized region between Dattilo and Basiluzzo and the region among Lisca Bianca, Bottaro and Lisca Nera where the exhalative crisis of 2002 occurred. In this region the magnetization pattern decreases with a null-value strongly driven by the hydrothermal alteration which affects the seafloor.

During cruise CALAMARE08 marine gravity data around Panarea and Islets were acquired, and were integrated with the above cited survey on land (see Figure 9). The two dataset were collected by different methodologies and instruments, and the merging was achieved without any fictitious grid-knitting process but using the absolute gravity data from a station in Panarea for reducing the offsets. The offshore gravity mapping shows several gap, making these results preliminary, while awaiting for on-going data processing of

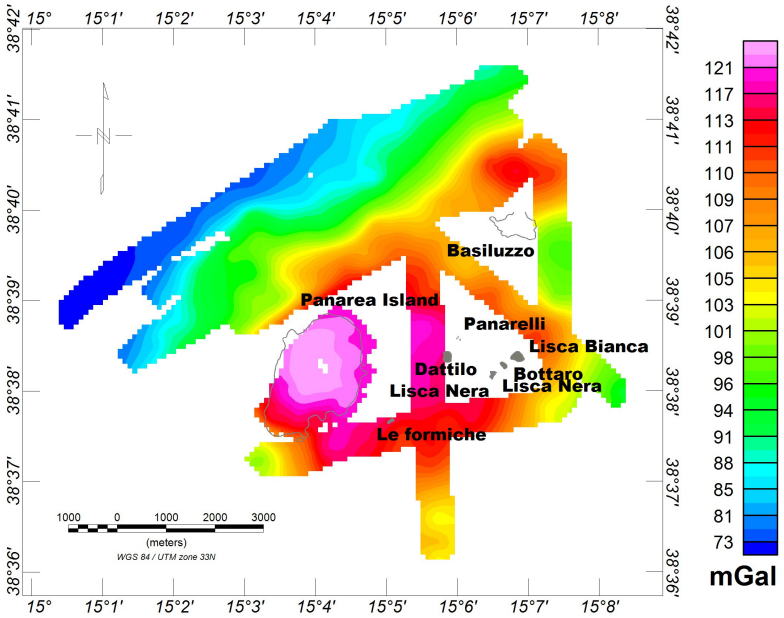

Figure 9: Free Air gravity anomaly map.

cruise PANSTR10.
Multichannel seismic acquired during cruise PANA07 were shot for investigating the regional tectonic and setting, other than for illuminating the OBS and land station seismological network. The data provide important information on plio-quaternary sediment thickness, to be used for proper gravimetric analysis and modelling. Some examples of the lines are on Figures 10, and 11 (positioning data in Figure1).

3.3 Flux estimation and Oceanography

The water and gas fluxes that we estimated for the main emission at PEG1 [22] are of the same order of magnitude of those calculated as in [1]. The experiment of December 2002 encountered problems because of the gas flowing violently from the depression; divers experimented strong ascensional force and heavy ballasts had been used for securing the instrumentation on bottom. Similarly [1] was able to measure the flux of gas at PEG1 only on 2002-05, due to such difficulties. Figure 12 shows the data obtained during the 2003-09 experiment and the instruments' deployment. The ADCP data have been influenced by tidal components, while rotor current meter data had a rather constant flux, being anchored well into the gas column. The ADCP to the E measured a much higher number of erratic values, and this is probably due to the beams being invested directly by gas bubbles, which are known to strongly reduce the data quality. These errors depend on the entrainment of gases at intermediate depths, in contrast, with data of 2002-12 when the gas ascending

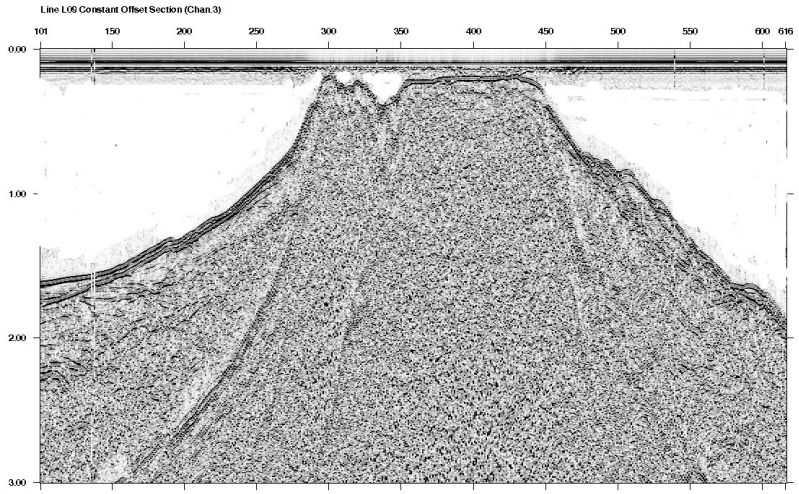

Figure 10: MCS Line L09, neartrace.

speed was higher and diverged at the surface without reaching buoyancy at intermediate depths. The CTD data of 2003-07 were able to depict a plume of acidified water (pH <6.5) centered on the PEG1. The data of 2004 cruise, instead, showed pH anomaly mostly centered on the PEG8 site to the N, which is up to now the lonely active emitting area left.

4 Conclusions

The Panarea area has been largely investigated through a number of geophysical surveys in the area and a comprehensive description of the event was achieved trough an intensive and continuous monitoring. A further step in multidisciplinary knowledge of degassing events was put forward and a number of papers has been published. A lot of scientific discussion arose from this large work and many new insights have been highlighted. This brief description summarizes some of the results.

- High resolution bathymetric surveys have imaged important structural lineaments and morphologies, and helped in studying the evolution of gas emissions near the Islets;
- High resolution magnetic and gravity data provided insights into the volcanic complex; a marked decrease of magnetization is present in the exhalative areas, due to hydrothermalism alteration, whereas strong values were found just to the N and NW of Dattilo and the Panarelli;
- The importance of measuring the effects of the eruptions on seawater properties and dynamics has been stressed, also as a possible new tool for monitoring the evolution of hydrothermal acitvity over time. Strong pH anomalies were reported and seawater was largely acidified. The effects of the acidification of seawater is an imporant issue and shallow vent systems are excellent sites where the effects of ocean acidification can be studied. Diving and morphobathymetric in-

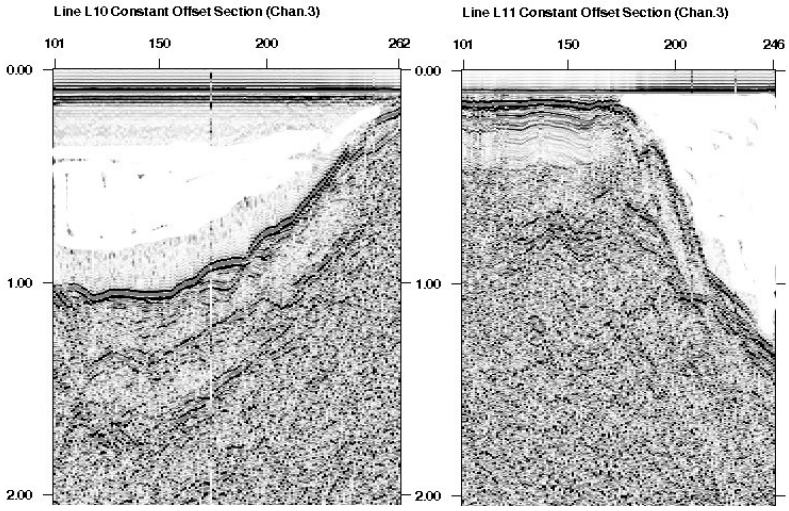

Figure 11: MCS Lines L10 and L11, neartraces.

vestigations reported of the infilling of PEG1 by sediment transport, suggesting a fate similar to other depressions found in the area.

5 Acknowledgments

We thank E. Bonatti, who supported our research and involved ISMAR since the early beginning. The project was funded by INGV/Dipartimento Protezione Civile and CNR. We thank the Coast Guard of Lipari for logistic support, the friends of Coastal Consulting Exploration of Bari, F. De Giosa and S. Lippolis, the Captain and crew of R/V L. Sanzo, Pippo Arena of Arenasub. The inhabitants of Panarea, especially Pina, her husband and family made the work a lot easier with their great hospitality and help. The 1994 multibeam survey was funded by Italian Ministry of Industry. We also acknowledge NERC (UK) that kindly provided LIDAR data. Most of the maps and figures were done by the Paul Wessel's GMT package [39]. Dr. Alina Polonia of ISMAR and the Hydrographic Institute of the Italian Navy helped with R/V Urania and Aretusa ship time. Finally, we would like to remember the work that was done in November 2002 and January 2003 at Panarea and Stromboli by R/V Thetis, which sunk dramatically on August 2007.

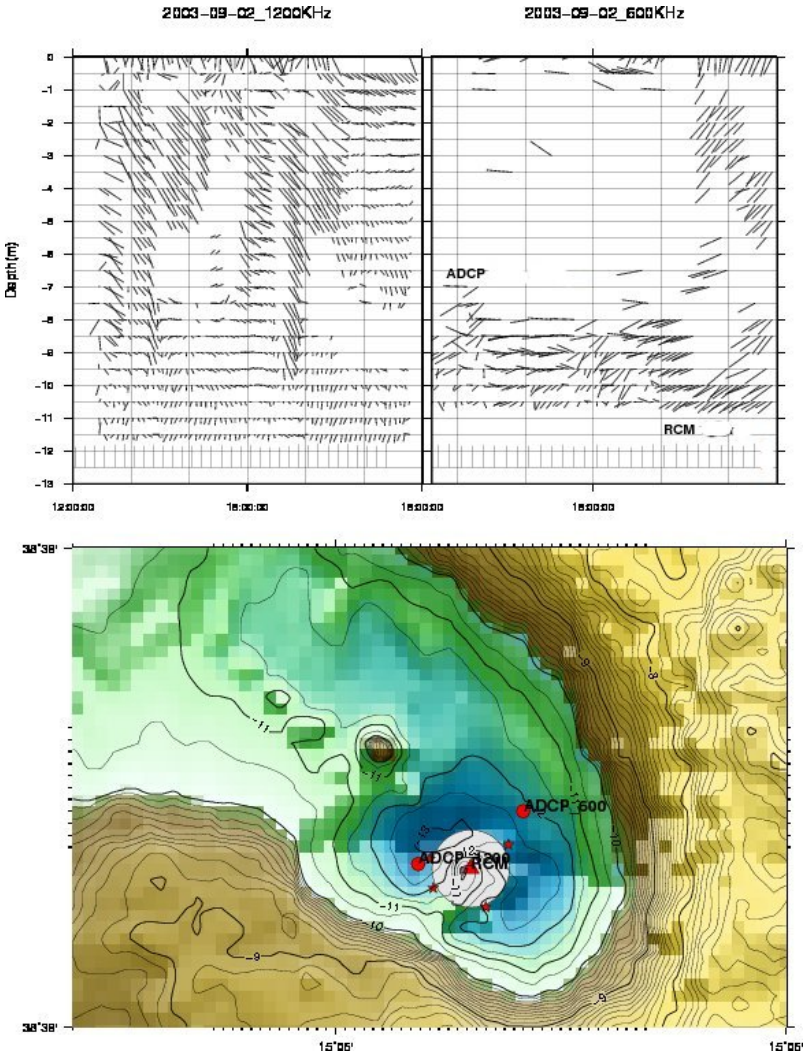

Figure 12: September 2003 flux-measurement experiment.

References

[1] S. Caliro, A. Caracausi, G. Chiodini, M. Ditta, F. Italiano, M. Longo, C. Minopoli, P.M. Nuccio, A. Paonita, and A. Rizzo. Evidence of a recent input of magmatic gases into the quiescent volcanic edifice of Panarea, Aeolian Islands, Italy. *Geophys. Res. Lett.*, 31:L07619, 2004. doi:10.1029/2003GL019359.

[2] B. Capaccioni, F. Tassi, D. Vaselli, D. Tedesco, and P.L. Rossi. The November 2002 degassing event at Panarea Island (Italy): the results of a 5 months geochemical monitoring program. *Annals of Geophysics*, 48(4-5):755–765, 2005.

[3] M. Anzidei, A. Esposito, G. Bortoluzzi, and F. Degiosa. The high resolution map of the exhalative area of Panarea (Aeolian Is., Italy). *Annals of Geophysics*, 48(6):899–921, 2005.

[4] A. Caracausi, M. Ditta, F. Italiano, M. Longo, P.M. Nuccio, A. Paonita, and A. Rizzo. Changes in fluid geochemistry and physico-chemical conditions of geothermal systems caused by magmatic input: The recent abrupt outgassing off the island of Panarea (Aeolian Islands, Italy). *Geochim. Cosmochim. Ac.*, 69(12):3045–3059, 2005. doi:10.1016/j.gca.2005.02.011.

[5] A. Esposito, G. Giordano, and M. Anzidei. The 2002-2003 submarine gas eruption at Panarea volcano Aeolian Islands, Italy: volcanology of the seafloor and implications for the hazard scenario. *Marine Geology*, 227:119–134, 2006.

[6] G. Chiodini, S. Caliro, G. Caramanna, D. Granieri, C. Minopoli, R. Moretti, L. Perrotta, and G. Ventura. Geochemistry of the submarine gaseous emissions of Panarea (Aeolian Islands, Southern Italy): magmatic vs. hydrothermal origin and implications for volcanic surveillance. *Pure Appl. Geophys.*, 163(4):759–780, 2006. doi:10.1007/s0024-006-0037-y.

[7] B. Capaccioni, F. Tassi, O. Vaselli, D. Tedesco, and R. Poreda. Submarine gas burst at Panarea Island (Southern Italy) on 3 November 2002: A magmatic versus hydrothermal episode. *J. Geophys. Res.*, 112:B05201, 2007.

[8] J. Heinicke, F. Italiano, R. Maugeri, B. Merkel, T. Pohl, M. Schipek, and T. Braun. Evidence of tectonic control on active arc volcanism: The Panarea-Stromboli tectonic link inferred by submarine hydrothermal vents monitoring (Aeolian arc, Italy). *Geophys. Res. Lett.*, 36:L04301, 2009. doi:10.1029/2008GL036664.

[9] V. Acocella, M. Neri, and T.R. Walter. Structural features of Panarea volcano in the frame of the Aeolian Arc (Italy): Implications for the 2002-2003 unrest. *J. Geodyn.*, 47(5):288–292, 2009. doi:10.1016/j.jog.2009.01.004.

[10] A. Billi and R. Funiciello. Concurrent eruptions at Etna, Stromboli, and Vulcano: casualty or causality? *Annals of Geophysics*, 51(4):655–725, 2008.

[11] T.R. Walter, R. Wang, V. Acocella, M. Neri, H. Grosser, and J. Zschau. Simultaneous magma and gas eruptions at three volcanoes in southern Italy: an earthquake trigger? *Geology*, 37(3):251–254, 2009.

[12] F. Barberi, P. Gasparini, F. Innocenti, and L. Villari. Volcanism of the Southern Tyrrhenian Sea and its geodynamic implications. *J. Geophys. Res.*, 78(23):5221–5232, 1973.

[13] F. Barberi, F. Innocenti, G. Ferrara, J. Keller, and L. Villari. Evolution of the Eolian arc volcanism (Southern Tyrrhenian Sea). *Earth Planet. Sc. Lett.*, 21(3):269–276, 1974. doi:10.1016/0012-821X(74)90161-7.

[14] A. Argnani and C. Savelli. Cenozoic volcanism and tectonics in the Southern Tyrrhenian Sea: space time distribution and geodynamic significance. *J. Geodyn.*, 27(4-5):409–432, 1999.

[15] A. Argnani. The Southern Tyrrhenian Subduction System: Recent Evolution and Neotectonic Implications. *Annals of Geophysics*, 43(3):585–607, 2000.

[16] N. Calanchi, A. Peccerillo, C.A. Tranne, F. Lucchini, P.L. Rossi, P. Kempton, W. Barbieri, and T.W. Woo. Petrology and geochemistry of volcanic rocks from the island of Panarea: implications for mantle evolution beneath the Aeolian island arc (Southern Tyrrhenian sea). *J. Volcanol. Geoth. Res.*, 115(3-4):367–395, 2002. doi:10.1016/S0377-0273(01)00333-X.

[17] G. De Astis, G. Ventura, and G. Vilardo. Geodynamic significance of the Aeolian volcanism (Southern Tyrrhenian Sea, Italy) in light of structural, seismological, and geochemical data. *Tectonics*, 22(4):1040, 2003. doi:10.1029/2003TC001506.

[18] G. Bortoluzzi, M. Ligi, C. Romagnoli, L. Cocchi, D. Casalbore, T. Sgroi, F. Caratori Contini, M. Cuffaro, F. D'Oriano, V. Ferrante, A. Remia, and F. Riminucci. Interactions between volcanism and tectonics in the Western Aeolian sector, Southern Tyrrhenian Sea. *Geophys. J. Int.*, 183:64–78, 2010. doi: 10.1111/j.1365-246X.2010.04729.x.

[19] F. Gamberi, M. Marani, and C. Savelli. Tectonic, volcanic and hydrothermal featues of a submarine portion of the Aeolian arc (Tyrrhenian Sea). *Marine Geology*, 140:167–181, 1997.

[20] F. Lucchi, C.A. Tranne, N. Calanchi, and P.L. Rossi. Late Quaternary deformation history of the volcanic edifice of Panarea, Aeolian Arc. *Bull. Volcanol.*, 69:239–257, 2007.

[21] F. Italiano and P.M. Nuccio. Geochemical investigations of submarine exhalations to the east of Panarea, Aeolian Islands, Italy. *J. Volcanol. Geoth. Res.*, 46:125–141, 1991.

[22] S. Aliani, G.Bortoluzzi, G. Caramanna, and F. Raffa. Seawater dynamics and environmental settings after november 2002 gas eruption off Bottaro (Panarea, Aeolian Islands, Mediterranean Sea). *Cont. Shelf Res.*, 30(12):1338–1348, 2010.

[23] C. Gugliandolo, F. Italiano, and T. Maugeri. The submarine hydrothermal system of Panarea (Southern Italy): biogeochemical processes at the thermal fluids - sea bottom interface. *Annals of Geophysics*, 49(2-3), 2006.

[24] E. Manini, G.M. Luna, C. Corinaldesi, D. Zeppilli, G. Bortoluzzi, G. Caramanna, F. Raffa, and R. Danovaro. Prokaryote diversity and virus abundance in shallow hydrothermal vents of the Mediterranean Sea (Panarea Island) and the Pacific Ocean (North Sulawesi-Indonesia). *Microbial Ecol.*, 55(4):626–639, 2008.

[25] F. Tassi, B. Capaccioni, G. Caramanna, D. Cinti, G. Montegrossi, L. Pizzino, F. Quattrocchi, and O. Valselli. Low-pH waters discharging from submarine vents at Panarea Island (Aeolian Islands, southern Italy) after the 2002 gas blast: Origin of hydrothermal fluids and implications for volcanic surveillance. *Appl. Geochem.*, 24(2):246–254, 2009.

[26] M. Fabris, M. Anzidei, P. Baldi, G. Bortoluzzi, A. Pesci, and S. Aliani. The high resolution combined topographic model of Panarea island (Aeolian island, Italy). In *EGU General Assembly*, 2010. Vienna, 02-07 Maggio.

[27] L. Cocchi, F. Caratori Tontini, C. Carmisciano, P. Stefanelli, M. Anzidei, A. Esposito, C. Del Negro, F. Greco, and R. Napoli. Looking inside the Panarea Island (Aeolian Archipelago, Italy) by gravity and magnetic data. *Annals of Geophysics*, 51(1):25–38, 2008.

[28] M. Anzidei, P. Baldi, G. Casula, F. Riguzzi, and L. Surace. La rete Tyrgeonet. *Bollettino di Geodesia e Scienze affini*, LIV(2):1–20, 1995.

[29] F. Gamberi, C. Savelli, M.P. Marani, M. Ligi, G. Bortoluzzi, V. Landuzzi, and M. Costa. Contesto morfo-tettonico e depositi idrotermali di solfuri ed ossidi di ferro in una porzione sommersa dell'arco eoliano (in base ad indagini ad alta definizione). *Boll.Soc.Geol.It.*, 117(1):55–71, 1998.

[30] M.P. Marani, F. Gamberi, G. Bortoluzzi, G. Carrara, M. Ligi, and D. Penitenti. Tyrrhenian sea bathymetry. In M.P. Marani, F. Gamberi, and E. Bonatti, editors, *From seafloor to deep mantle: architecture of the Tyrrhenian backarc basin*, volume 44 of *Mem. Descr. Carta Geologica d'Italia*. APAT, 2004.

[31] C. Romagnoli, D. Casalbore, G. Bortoluzzi, A. Bosman, F.L. Chiocci, F. D'Oriano, F. Gamberi, M. Ligi, and M .Marani. Bathy-morphological setting of the Aeolian Islands. In F. Lucchi, A. Peccerillo, J. Keller, C.A. Tranne, and P.L. Rossi, editors, *Geology of the Aeolian Islands*, Memoirs. Geological Society, London, 2010. Special Issue, in press.

[32] F.L. Chiocci and C. Romagnoli. Terrazzi deposizionali sommersi nelle Isole Eolie (Sicilia). *Mem. Descrittive della Carta Geologica d' Italia, APAT*, 58:81–114, 2004.

[33] G. Gabbianelli, P.Y. Gillot, G. Lanzafame, C. Romagnoli, and P. L. Rossi. Tectonic and volcanic evolution of Panarea (Aeolian Islands, Italy). *Marine Geology*, 92:313–326, 1990.

[34] G. Gabbianelli, C. Romagnoli, P.L. Rossi, and N. Calanchi. Marine geology of the Panarea-Stromboli area (Aeolian Archipelago, Southeastern Tyrrhenian Sea). *Acta Vulcanol.*, 3:11–20, 1993.

[35] F. Gamberi, C. Savelli, M.P. Marani, M. Ligi, G. Bortoluzzi, V. Landuzzi, A. Luppi, M. Badalini, and M. Costa. Carta morfo-batimetrica e dei depositi idrotermali in una porzione sommersa dell'arco eoliano. *Boll.Soc.Geol.It.*, 117(1), 1998. Supplement.

[36] M.P. Marani, F. Gamberi, and C. Savelli. Shallow-water polymetallic sulfide deposits in the Aeolian island arc. *Geology*, 25(9):815–818, 1997.

[37] L. Cocchi, F. Caratori Tontini, C. Carmisciano, P. Stefanelli, D. Embriaco, and M. Anzidei. Magnetic and Gravimetric model of Panarea (Aeolian islands). In *Convegno Nazionale MGMEESV*, 2006. Catania, 27-29 Settembre 2006.

[38] F. Caratori Tontini, L. Cocchi, and C. Carmisciano. Potential-field inversion for a layer with uneven thickness: The Tyrrhenian Sea density model. *Phys. Earth Planet. In.*, 166(1-2):105–111, 2008.

[39] P. Wessel and W.H.F. Smith. New version of the Generic Mapping Tools released. *Trans. Am. Geophys. Union (EOS)*, 76:329, 1995.

Interannual Variability in the Mediterranean Sea: a Long-Term Monitoring Strategy

G.P. Gasparini[1], K. Schroeder[1], S. Sparnocchia[2], M. Borghini[1]
1, Institute of Marine Sciences, CNR, Pozzuolo di Lerici (SP), Italy
2, Institute of Marine Sciences, CNR, Trieste, Italy
gasparini@sp.ismar.cnr.it

Abstract

Recent studies have shown that the Mediterranean Sea is far from being in a steady state. Important and abrupt changes in the stratification and in the thermohaline circulation have occurred both in the eastern basin (during the 90s) in the western basin (since 2005).
A continuous monitoring of the Mediterranean circulation is necessary to detect possible changes when they happen and to understand their time scales. Straits and channels form an important network inside the basin. Long-term monitoring of Mediterranean straits together with repeated observations in deep-basin sites of special interest demonstrated the capability to determine the evolution of the water mass characteristics and the transport variability at a basin scale. The on field activity developed during the last twenty years permitted to follow the interannual variability of Mediterranean water mass properties and circulation, while provided significant insight on the main involved processes.

1 Introduction

Recent studies have evidenced that significant changes in the climate conditions are not always related to centenary or millenary time scales, but may also happen in much shorter periods [1]. This is particularly true for the Mediterranean, where space/time scales are one order of magnitude less than in the ocean and where, starting from the 80s, a rapid and extended change in the thermohaline circulation of the eastern Mediterranean (EMED) has been observed.
An important task is to define a realistic survey strategy, focalized on a continuous monitoring of key regions, and to capitalize the existing time series, to understand the time scales of variability and to provide elements for the comparison and verification of models.

2 Recent changes

The properties of the WMDW experienced significant changes after two winters in which a remarkably different dense water has been formed by deep convection: winter 2004/2005 and winter 2005/2006 [2, 3]. In winter 2004/2005 the deep water formation (DWF) processes led to a salty and warm new deep water mass mainly in the Gulf of Lions and the Catalan subbasin. The event was probably triggered by strong atmospheric forcings and a very high salt content in the intermediate layer. In the fol-

lowing winter 2005/2006, the deep water was formed mainly in the Ligurian Sea.
The deep water properties and their variability are a consequence of the hydrographic structure of the water column (heat and salt content) before the onset of convection, and to the atmospheric forcings (heat, freshwater and buoyancy fluxes) acting on it. The deep convection is a result of the synergy between the surface losses and the lateral advection of heat and freshwater. In a steady state it is supposed that there is a balancing between the removal of heat and freshwater by the atmosphere and the supply of those properties by the ocean. The long-term monitoring of the hydrographic and dynamic properties of water masses in the Sicily Channel and in other key positions of the western Mediterranean (WMED) during the last 20 years permitted to follow the interannual variability of the east-west exchanges, considering the propagation of the Eastern Mediterranean Transient (EMT) signature toward the WMED [4].
The changes produced by this event in the deep thermohaline circulation of the EMED modified the properties of the Sicily Channel outflow and deeply influenced the hydrographic structure of the WMED water. More specifically, an acceleration of the increasing temperature and salinity trends in the deep and intermediate layers has been produced. During recent years, those changes were able to play a key role in modifying the WMED deep water production. The abrupt increase of the heat and salt contents in the deep layer of the basin can be largely attributed to an increased heat and salt lateral advection.

3 Approaches

A continuous monitoring of the Mediterranean circulation is necessary to detect possible changes when they happen and to understand their time scales. Straits and channels form an important network inside the basin. Their monitoring permits to determine, at a basin scale, the evolution of the water mass characteristics and the transport variability. Therefore an adequate survey strategy would consist in (Figure 1):

1. Long-term monitoring of Mediterranean straits, to define the main interbasin exchanges, and some few regions characterized by relevant processes (moorings in the Straits of Sicily and Corsica since 25 years);
2. Repeated observations in sites of special interest, to maintain a deep-basin monitoring with repeated CTD casts at fixed stations in deep basins (Ionian and Tyrrhenian since more than 20 years, 1-2 casts per year);
3. Large-scale monitoring, through basin wide hydrographic surveys, a necessary tool for budget calculation, e.g. by means of box models (Figure 2), to initialize and validate general circulation models, and to be assimilated in models to improve their forecast capability.

Recently, wide-ranging dedicated field experiments have been carried out to get a quasi-synoptic view of the circulation in the WMED (Figure 2b). A first comprehensive estimate of water fluxes in the WMED was obtained by means of a physically robust approach, aimed to an intercomparison of differently achieved results. Three approaches have been adopted to describe the WMED circulation and velocity field, resolving different spatial-temporal scales and components of the motion, in order to evaluate their degree of accordance:

a geostrophic approach, a direct approach and a modeling approach. The results confirm the qualitative overall circulation pattern, providing a solid quantitative basis to be used for budget estimates of different chemical/biological properties. Despite several advances in recent years, there are still huge gaps in current knowledge, as well as the need of a monitoring effort of the anomaly, including not only physical, but also biogeochemical, sedimentological and biological parameters. The main knowledge gaps regarding this event are both specific and general (Table 1).

Priorities for future research on the dynamics of Mediterranean deep waters should therefore include attempts to answer the following questions:

1. Reconstruction and monitoring of the transient event which is occurring in the western Mediterranean Sea.
   - Evolution in time and space: Which is the extent of the event occurring in the western Mediterranean, in terms of salt and heat contents increases in the deep layers and in terms of uplifting of the resident deep water? Which are the involved mixing processes? What are the ventilation times and the ages of the involved water masses?
   Achievements: to contribute to the knowledge of the evolution of this climatic event, reconstructing its spatial and temporal variability, the transit times and the mixing fraction of the involved water masses, both resident and newly formed.
   - Causes and forcings: Which forcings have determined the observed anomaly in the deep western basin?
   Achievements: to identify processes at different time-scales and to test hypotheses on the mechanisms and causes of the abrupt alterations in the physical properties of deep water masses, by using on-purpose models and the time-series of observations.
   - Possible impacts and repercussions: To which degree the anomaly will contribute to the general warming and salinification of the Mediterranean basin? How fast is the anomaly propagating in the interior of the basin? To which extent the straits control this propagation? Which might be the possible repercussions on the Mediterranean Outflow? Which are the involved temporal scales?
   Achievements: to identify and quantify the effects the anomaly observed in the western basin induces on adjacent areas (eastern Mediterranean and Atlantic Ocean).
2. Documentation and understanding of the interactions between the western and the eastern Mediterranean, studying the physical tracers and the factors that modulate their variability.
   - Internal variability: Which is the degree of variability of the thermohaline circulation and the physical properties of each basin?
   Achievements: to set the background of the more recent changes, thus improving the interpretation and synthesis capability of the new available observations.
   - Modulation of the variability: Which are the mechanisms that modulate the internal variability in each basin? How do the feedbacks between Strait of Sicily - Strait of Gibraltar - deep water formation areas act?
   Achievements: to define the relationship between exchanges through the straits and internal variability of the basins; to assess the possible feedbacks of the Mediterranean dynamics on the global climatic system.

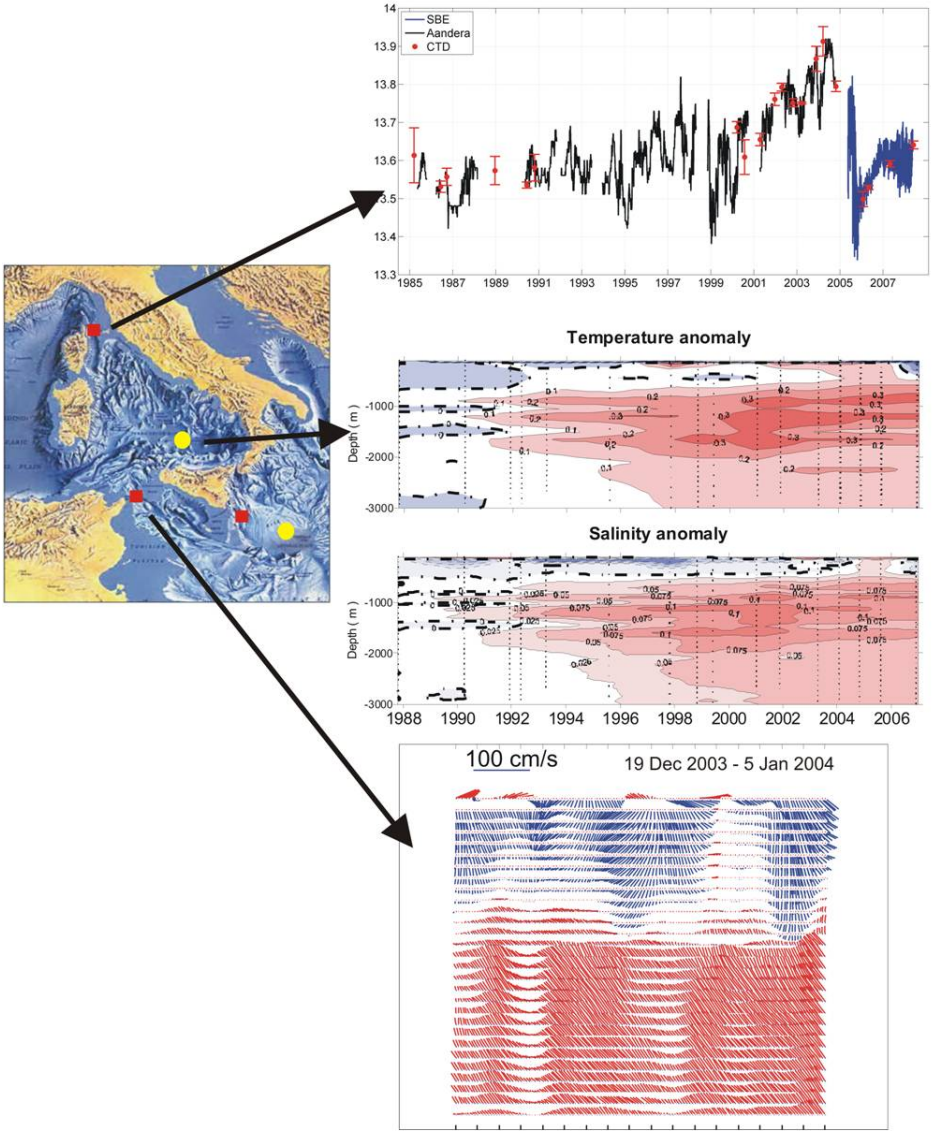

Figure 1: Location of moored chains (red squares in the map) and sites of special interest (yellow circles in the map). Examples of data collected: (up) time series of potential temperature in the Corsica Channel (moored instruments since 1985, different colours refer to different instruments used); (centre) temperature and salinity anomalies in the central Tyrrhenian basin (repeated CTD casts since 1988, red contours are positive anomalies, blue contours are negative anomalies); (bottom) current profiles in the Sicily Strait (moored instruments since 1994 red sticks are N-NE-NW currents, blue sticks are S-SE-SW currents).

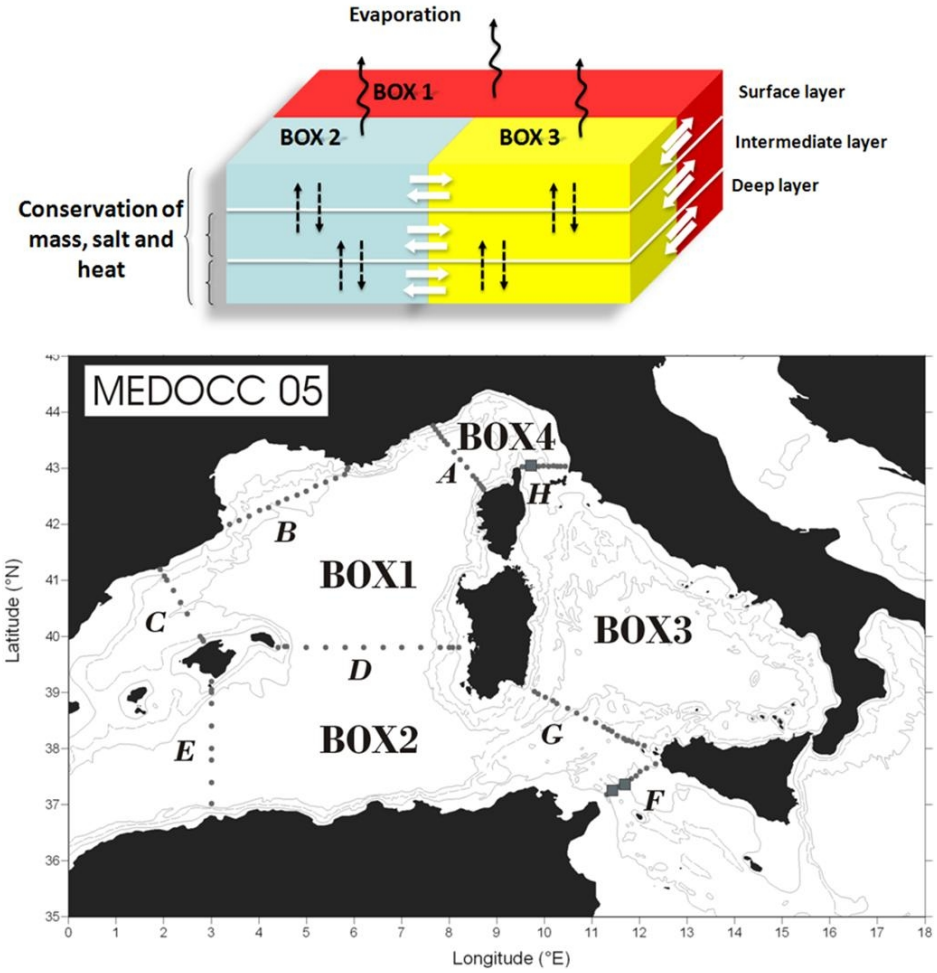

Figure 2: (a) Box model scheme and (b) definition of real boxes using data from a cruise in the Western Mediterranean [3]

Specific needs	General needs
Identification of the causes that triggered the event (atmospheric forcings vs lateral advection?)	Better understanding of the thermohaline stability and variability in the Mediterranean Sea, as well as identification of the factors that modulate this variability.
Determination of the origin of the greatly increased salt and heat transports across the Strait of Sicily (Cretan Intermediate Water, Levantine Intermediate Water…?), which is still continuing.	Reconstruction and monitoring of the post-transient evolution, which occurred and is still occurring in the eastern Mediterranean Sea.
Availability of data to estimate the DWF relevance in the winters 06/07, 07/08 and 08/09.	Reconstruction and monitoring of the event presently occurring in the western Mediterranean Sea.
	Assessment of the degree to which a relevant deep water production in one year may influence the production of the following years (*memory* of the system).

Table 1: Specific and general needs of further investigations

4 Conclusion

The interannual variability of the hydrographic conditions evidences how the influence of the EMT in the Mediterranean is far to be concluded. Recent observations in the Sicily Channel suggest the arrival of new dense waters from the EMED. The experience of the propagation of the EMT demonstrates that straits and channels are suitable points to provide early warning of anomaly propagation.

The long-term monitoring of the straits of Sicily and Corsica permitted to detect important changes in the circulation and hydrography at basin-scale, giving important information concerning the investigation strategy for the basin interior. This is done by providing time-series of repeated CTD casts in the deep layers of both the western (Tyrrhenian) and the eastern (Ionian) Mediterranean, as well as performing basin-wide surveys, that provide quasi-synoptic views of the hydrographic and dynamic features.

Even though the recent western anomaly has several similarities with the EMT, in terms of intensity and effects, it has not received the same attention. Therefore the future research priorities should aim to make up for this lack, scheduling the monitoring of the event and addressing the study of the causes (remote or local) that may have induced it and of the possible repercussions.

New available technologies are able to significantly improve the present monitoring in term of space/time resolution and extending the coverage to biogeochemical parameters. A more close interaction with model simulations is a further important task able to improve both the model results and interpretation of observational data permitting to provide more confident scenarios of the Mediterranean conditions for the next decades.

References

[1] W. Roether, B. Manca, B. Klein, D. Bregant, et al. Recent changes in the Eastern Mediterranean deep waters. *Science*, 271:333–335, 1996.

[2] K. Schroeder, G.P. Gasparini, M. Tangherlini, and M. Astraldi. Deep and Intermediate water in the western Mediterranean under the influence of the Eastern Mediterranean Transient. *Geophysical Research Letters*, 33(L21607), 2006.

[3] K. Schroeder, V. Taillandier, A. Vetrano, and G.P. Gasparini. The circulation of the Western Mediterranean Sea in spring 2005 as inferred from observations and from model outputs. *Deep Sea Research I*, 55:947–965, 2008.

[4] G.P. Gasparini, A. Ortona, G. Budillon, M. Astraldi, and E. Sansone. The effect of the Eastern Mediterranean Transient on the hydrographic characteristics in the Strait of Sicily and in the Tyrrhenian. *Deep Sea Research I*, 52(6):915–935, 2005.

Po River Plume Influence on Marine Biochemical Properties along the Western Adriatic Coast

M. Marini, A. Campanelli, F. Grilli
Institute of Marine Sciences, CNR, Ancona, Italy
m.marini@ismar.cnr.it

Abstract

An international research program was devoted to understanding the dynamic properties of the mesoscale circulation in the Adriatic Sea such as fronts, eddies, coastal filaments, river inflow and study the effects of forcing by winds and river run-offs. The present work focuses specifically on the impact of the Po river outflow on the biochemical properties along the western Adriatic coast under different conditions of river discharge and wind stress in winter and spring.
In the winter cruise, the satellite images show a strong front in the northern part of the Adriatic extending from the Italian coast to the Istrian Peninsula. In situ measures showed that the northern water mass was characterized by low temperature and salinity, and high nutrient and chlorophyll concentrations due to a strong Bora event which expanded the Po River plume towards the Istrian Peninsula instead of southwards in the West Adriatic Current. During the spring cruise, wind forcing was quite weak and the volume flux from the Po River was about one third of its mean discharge for this period of the year. Off the Po River, the water column was characterized by a surface layer with low salinity and high dissolved inorganic nitrogen and chlorophyll. This water mass did not extend as far eastwards as in winter because the wind forcing was not nearly as important and the alongshore plume extended southward along the Italian Coast.

1 Introduction

The Adriatic Sea is the most continental basin of the Mediterranean Sea. It lies between the Italian peninsula and the Balkans and is elongated longitudinally, with its major axis (about 800 km by 200 km) in NW-SE direction. The basin shows clear morphological differences along both the longitudinal and the transversal axes and has been divided into northern, middle and southern sub-basins [1]. The Adriatic Sea has a complicated morphology and bathymetry. The western coast is low and generally sandy, while the eastern coast is rugged, with multiple islands and coves. The northern sub-basin, extending from the northernmost coastline to the 100 m bathymetric line, is extremely shallow (mean depth $\sim$30 m) with a very weak bathymetric gradient along its major axis. It is characterized by strong river runoff; indeed, the Po and the other northern Italian rivers are believed to contribute about 20% of the whole Mediterranean river runoff [2]. The middle Adriatic is a transition zone between northern and southern sub-basins, with the three Jabuka depressions reaching a depth of 270 m. The southern sub-basin is characterised by a wide depression about 1200 m in depth. Water exchange with the Mediterranean takes place through

the Otranto Straits, which has an 800 m deep sill. The present study focuses on the northern and central continental Adriatic margin, where circulation is mainly controlled by wind stress and river discharge. Two main currents are present in Adriatic: the West Adriatic Current (WAC), that flows towards south-east, along the western coast, and the East Adriatic Current (EAC) flowing towards north-west along the eastern cost [1, 3]. Being a continental basin, the Adriatic Sea circulation and water masses are strongly influenced by atmospheric conditions, primarily winds [4, 5]. The major winds blowing over the Adriatic Sea are Bora and Sirocco. Bora winds are generally from the northeast and are associated with a high-pressure system over central Europe [6]. Bora is a cold and dry wind where air spills through gaps in the Dinaric Alps (the mountain range situated along the Adriatic's eastern shore), resulting in intense wind jets due to catabatic effects at specific points of the Adriatic eastern coast [7]. The Bora wind system causes the sea surface to rise near the western coast generating a coastal current towards the south, the western adriatic current (WAC). Historical data and numerical simulations have demonstrated that Bora winds can cause the formation of a double gyre structure consisting in a larger cyclone in front of the Po River delta and a smaller anticyclone to the South [7]. In winter, the cold, dry Bora winds cause strong heat losses in the Northern Adriatic and formation of the Northern Adriatic Deep Water (NAdDW). Another factor influencing the NAdDW formation is the water flux, mainly governed by the Po River runoff, which can lower the salinity, and hence the density, of the NAdDW. Vilibic [8] demonstrated the relationships between NadDW formation, heat fluxes and autumn Po River runoff.

The Sirocco wind is generally from the southeast, and is associated with a low pressure system over the Tyrrhenian Sea. Sirocco is a warm and humid wind and often causes flooding events in the shallow lagoons along the Adriatic coast including Venice. Coming from the southeast over the sea, the Sirocco is less subject to local variations than the Bora, but it does show some geographical variations due to the coastal orography. It tends to be southerly in the strait of Otranto and off Istrian Peninsula (Pula), and more easterly at some places along the northern Adriatic coast near Ravenna and Pesaro [7].

River runoff is particularly strong in the northern basin and affects the circulation through buoyancy input and the ecosystem by introducing large fluxes of nutrients [9]. Freshwater is discharged into the northern Adriatic from major rivers along the North and Northwest coasts. The Po River represents the major buoyancy input with an annual mean discharge rate of 1500-1700 m^3/s, accounting for about one third of the total riverine freshwater input in the Adriatic [10]. Runoff is also responsible for making the Adriatic a dilution basin. The riverine water discharged into the northern Adriatic forms a buoyant coastal layer that flows southward along the Italian coast. Since the Po River is the main source of this water, the coastal layer is predominantly south of the Po River delta and is named Western Coastal Layer (WCL, [7]). It is associated with a strong near- surface current, which flushes the nutrient rich water out of the northern Adriatic along the Italian coast [11, 12, 13]. The principal compensating inflow occurs along the eastern boundary in the EAC where warm, high salinity modified Levantine Intermediate Water (LIW) is advected northward.

Kourafalou [14] elucidated the role of the major Adriatic rivers in creating buoyancy-driven coastal currents that are essential in maintaining the cyclonic circulation.
The intent of this study is to examine the Po River plume influence on nutrients and hydrological properties along the western Adriatic coast under varying conditions of river discharge and wind stress during winter and spring.

2 Material and Methods

The data for this study were gathered in the central and northern Adriatic Sea during two oceanographic cruises aboard the R/V Knorr (Woods Hole Oceanographic Institution) during the periods from January 31 to February 24, 2003 (winter) and from May 26 to June 15, 2003 (late spring) and during a cruise aboard the R/V G. Dallaporta (ISMAR-CNR) 12-20 February, 2003. Observations were gathered using three primary modes of sampling: underway mapping of near-surface seawater utilizing the ship's uncontaminated seawater distribution system, vertical profiling with a CTD/rosette system, and three-dimensional mapping using a towed undulating vehicle equipped with a CTD. Water samples were analyzed for nutrients and chlorophyll a. The surface water samples were collected using a bucket during underway mapping, and 10 L Niskin bottles at hydrographic stations. The CTD data were collected by a SeaBrid SBE 911-plus probe equipped with a Wetlabs ECO-AFL fluorometer. The 24 Hz CTD data were processed according to UNESCO [16] standards, obtaining pressure-averaged data (0.5 db intervals). Nutrient samples were filtered (GF/F Whatman) and stored at -22 °C in polyethylene vials, or analysed on board immediately after collection (winter cruise). Nutrient concentrations (ammonium-NH4, nitrite-NO_2, nitrate-NO_3, orthophosphate-PO4 and orthosilicate-Si(OH)4) were measured using a Technicon TRAACS 800 autoanalyzer. Data analyses was carried out using the AACE software supplied by Bran+Luebbe. Nutrient analyses utilized modifications of the procedures developed by Strickland and Parsons [17]. Dissolved inorganic nitrogen (DIN) was calculated as the sum of the NH4, NO_2 and NO_3 concentrations. Chlorophyll a concentrations were measured fluorometrically. One hundred ml. samples were filtered through a 25 mm Whatman GF/F filter. Filters were extracted for 24 hours in 90% acetone at -4°C, then analyzed on a Turner Designs 10-005 fluorometer. Chlorophyll was calculated according to Holm-Hansen et al. [18]. Contoured vertical sections of the data were plotted using the kriging interpolation method (software Surfer 8.0).
During each cruise, the sampling strategy was intended to focus on the basin response to strong physical forcing. During winter, Bora winds and the Po River freshwater input were the two major sources of forcing. The spring cruise was planned for the period when climatologically a freshet of the Po River flow occurs (Figure 1). The ships tracks / mapping grids were based on the analyses of meteorological data and on the location of specific features including the Po River plume observed from AVHRR and SeaWiFS imagery (Figures 2, 3, 5 and 6). Figure 1 shows the daily average Po River flow for the year of 2003 and the 14-year mean of the daily average flow from 1989-2002.

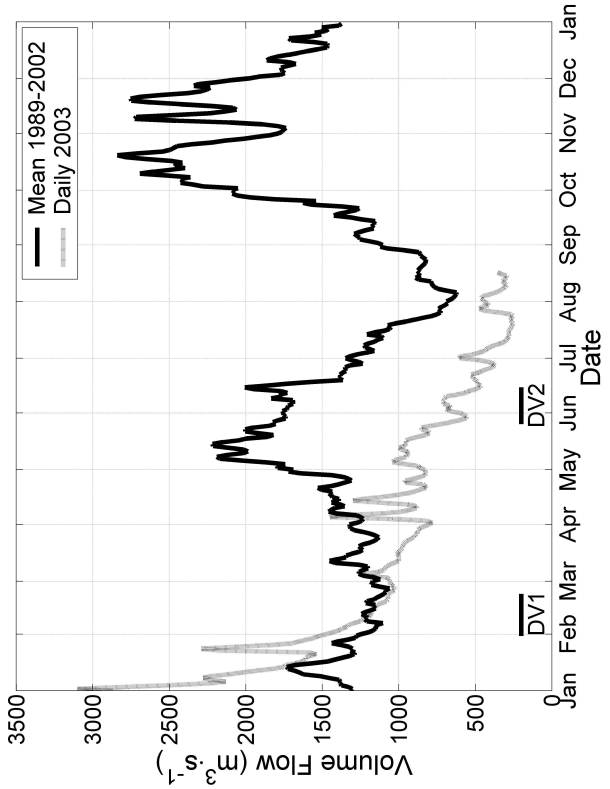

Figure 1: Daily averages of the Po River flow for the period 1989-2002. The solid line is the annual average for the period 1989-2002 and the dashed line is the daily flow for 2003 (DV1: period of the wintertime cruise, DV2: period of the springtime cruise), from [15].

3 Results

3.1 Physical characterization of the water masses

During the winter cruise (31 January – 23 February 2003) two Bora wind events occurred between 11 and 19 February resulting in distinct circulation patterns in the northern Adriatic [19, 6, 20]. Intense wind stress associated with Bora jets from Trieste and Senj drew a cold, fresh plume of Po River water across to northern basin. The Bora winds caused the plume to expand northeastward towards the Istrian coast between a northern cyclonic gyre and an anticyclonic circulation to the south ([19], Figure 1). Another front that extended westward from the southern tip of Istria separated the smaller anticyclonic gyre from a larger cyclonic gyre to the south. Remotely sensed surface temperature and ocean color showed a strong front in the northern part of the Adriatic extend-

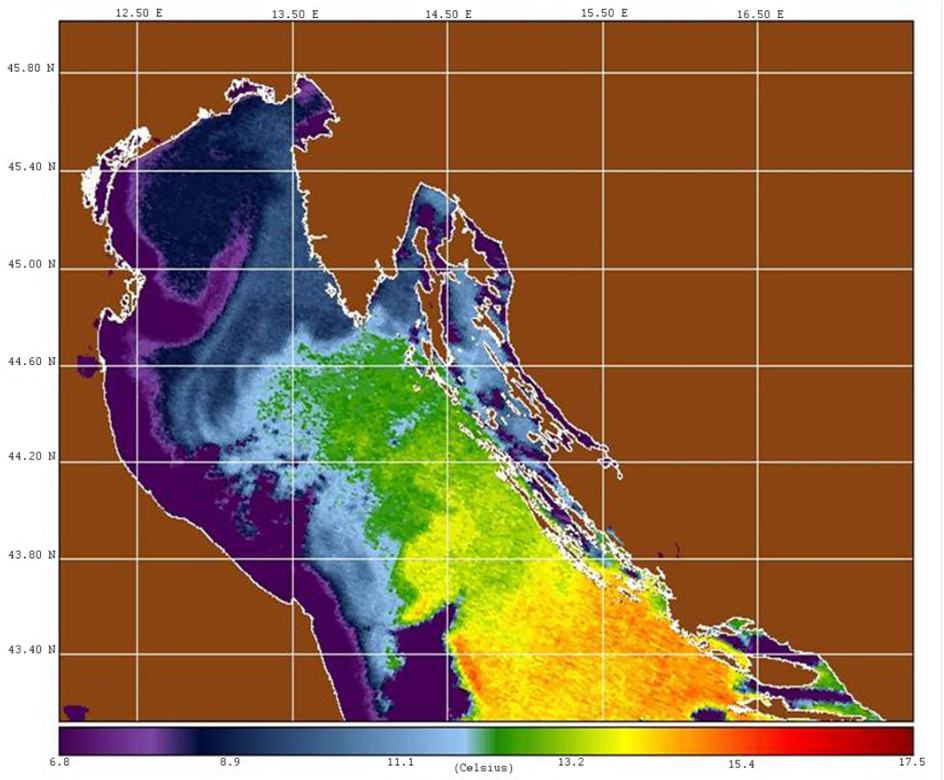

Figure 2: Sea surface temperature map from the AVHRR-NOAA-12, NRL (19 February 2003), from [15].

ing from Ravenna on the Italian coast to the northwestern corner of the Istrian Peninsula and southward along the western (Italian) boundary of the Adriatic Sea (Figures 2 and 3).In situ measurements indicated cooler, fresher water to the north and warmer, saltier water to the south of the front located southern tip of Istria (Figure 4 a and b).

During the late spring cruise (26 May – 15 June 2003), wind forcing was weak and volume flux from the Po River was about one third of its 14-year average discharge for this period (Figure 1). Despite the low discharge flux, from the river, the Po plume remained a significant feature in the northern and western Adriatic. Satellite images (Figures 5 and 6) showed a strong color front along the western boundary that divides the higher chlorophyll coastal water from the more oligotrophic mid-basin and eastern boundary Adriatic waters (Figure 6). Offshore from the mouth of the Po River, the surface layer was characterized by low salinity and high temperature (Figure 7a, b). The Po plume extended much more eastward in late spring than in winter because the vertical mixing is reduced

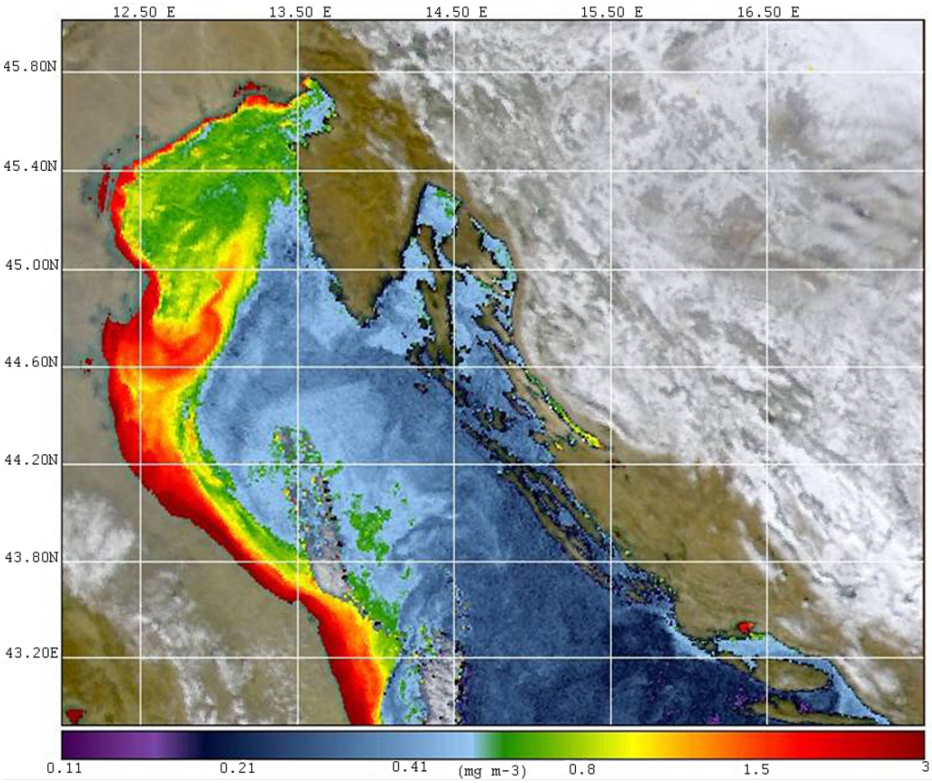

Figure 3: SeaWiFS image of chlorophyll concentration for 20 February 2003 (provide by NRL), from [15].

[7]. However, the plume extended southward along the Italian Coast.

3.2 Large Scale Surface Characterization of Biochemical properties

During the winter observations, DIN concentrations were high along the western boundary and decreased rapidly toward the east forming a strong front along the western side of the Adriatic (Figure 4c). This frontal structure extended southward from the Po River discharge consistent with the pattern of the seasonal circulation. The thermohaline circulation [7] advected the nitrate-rich river plume water southward, bound to a relatively narrow band along the Italian coast. The orthosilicate distribution was quite similar to that of nitrate (Figure 4d). On the eastern side of the basin, south of the Istrian Peninsula a strong temperature front and silicate gradient were present, resulting from the eastward extension of the Po River plume in response to the Bora winds. The phosphate distribution did not show such a clear gradient in the region south of the Istrian Peninsula (Figure 4e) because minimum concentrations were

sometimes found in the coastal waters and increase toward offshore. Thus, the northern Adriatic basin tended to be phosphorus limited despite the large river input.
During late spring the temperature and salinity patterns (Figure 7a,b) showed a broader warm, low salinity river plume band extending southward along the Italian coast. The central northern basin was better sampled during the spring cruise than during the winter cruise. Relatively low nutrient concentrations were detected in the offshore and eastern boundary regions of the northern basin (Figure 7c, d).
The overall pattern was similar between winter and summer with the nutrient-rich surface waters along the western boundary advected southward. Some mixing of this coastal water with middle Adriatic surface waters was evident; in particular during the winter a nutrient grading decreased toward offshore while in late spring filaments were present.

3.3 Vertical Characterization

3.3.1 Winter

In addition to the surface mapping and towed vehicle mapping carried out on this expedition several transects with CTD/rosette profiling were obtained. Two transects each from the winter cruise and from the spring cruise are shown in Figures 8 and 9 (winter) and Figures 10 and 11 (spring). The locations for the winter transects (indicated in Figure 4f) were across Po River plume (Figure 8) and off Pesaro (Figure 9). Similarly, the spring cruise transects (locations indicated in Figure 7f) were in the Po River plume (Figure 10) and in a filament extending eastward off Vasto (Figure 11). Nutrient concentrations and chlorophyll a concentrations are shown as color shading and salinity is overlaid as contour lines.
The core of the Po River plume during the winter was indicated by the nearsurface salinity minimum midway in the section. Salinity induced stratification was very strong in the core of the plume and relatively weak at the either end of this section (Figure 8). Except for a single sample near surface in the core of the plume, chlorophyll concentrations were lower within the plume and higher at the boundaries where salinity was greater than 38. The chlorophyll distribution was confirmed by the towed vehicle mapping that showed lower chlorophyll concentrations within the plume and higher chlorophyll values in the higher-salinity water masses to either side of the plume (not shown).The role of the Po plume in providing a significant flux of nutrients into the northern basin was indicated by the high DIN (about 10 μM) and orthosilicate (about 5 μM) concentrations associated with the salinity minimum of the plume (Figure 8, top and middle panels).
The Pesaro transect was about 100 km south of the Po River delta (Figure 4). During the winter cruise, the water column was well mixed vertically at each of the four stations in the transect (Figure 9). The salinity showed that the cross-shelf section was somewhat complex with lower salinities found both near shore and at the third station (about 18 km offshore), indicating confluence of different water masses. The lowest salinities ($<$38.1) and high levels of suspended particulate matter (beam attenuation $>$ 5 m-1, not shown) occurred nearest to the coast indicating the influence of the river input (Figure 9). The highest chlorophyll concentrations were also observed within the lower salinity water near-shore in this transect. The chlorophyll

a concentrations were vertically homogeneous in the station nearest to the coast and decreased to the east (0.5 μgl^{-1}). Nutrient values were higher (DIN $\sim$ 1.5-1.8 μM) near the coast and lowest offshore, consistent with the salinity gradient and the riverine source of the nutrients (Figure 9). Silicate concentrations were highest at the third station offshore (about 18 km in Figure 9) at middepth where salinities were less than 33.2. Nutrient values were much lower than those observed nearer the mouth of the Po River, presumably due mixing and perhaps uptake by phytoplankton.

3.3.2 Spring

During the spring cruise another section was made through the Po plume, but this time perpendicular to the coast rather than parallel to the coast. The wind forcing was much weaker during the spring cruise, and as a result stratification was much stronger. The highest chlorophyll a values from bottle samples, nearly 15 μgl^{-1}, occured near surface in the low salinity water and decreased monotonically offshore (Figure 10, bottom). The near-surface region where chlorophyll was high corresponded with the area where orthosilicate concentrations were quite low. Moderate values of 1–2 μgl^{-1} were observed near the bottom at the offshore end of the section. It was not clear from this hydrographic transect whether this near-bottom chlorophyll was the edge of a subsurface chlorophyll maximum typical of regions away from the direct influence of the Po plume.

The distribution of nutrient values (Figure 10) showed that, with strong water column stratification, DIN concentrations were highest (10-12 μM) near surface where the lowest salinities were observed. Orthosilicate distributions showed the opposite pattern with concentrations generally less than 2 μM in the surface layer and high values in the lower half of the water column (Figure 10, middle panel). The highest concentrations of $>$15 μM were observed where salinity was $>$38. The distribution of orthosilicate did not appear to be controlled by river inputs but by the active consumption by phytoplankton as reported by Cozzi et al. [21].

About 330 km southeast from the Po River delta in the southern part of the central basin, a transect was obtained through a filament distinguishable in ocean color (Figure 6) was observed extending offshore toward the east from the inshore region. A hydrographic section was obtained through the feature to determine its characteristics (Figure 7f). The filament was distinctly evident near-surface where salinities were less than 38.5, particularly near-surface at the two central stations (Figure 11). The thickness of this low salinity filament was less than 20 meters.Despite the evidence from the ocean color image, near-surface chlorophyll within the filament was low, $<$0.5 μgl^{-1} and maximum chlorophyll of up to 0.9 μgl^{-1} was observed in the chlorophyll maximum at depths of 70–75 m (Figure 11). Higher near-surface concentrations of DIN and orthosilicate values were associated with the low-salinity core of the filament. However, the highest concentrations of DIN and orthosilicate were observed below 100 m. There was some complexity to this distribution with higher DIN present near surface outside the filament in high-salinity surface at the station located at about 22 km, the southern end of the section. Below 100 m the silicate and DIN distributions also differ. Highest orthosilicate concentrations occurred at either end of the transect, whereas DIN values were lower at the southern end of the transect.

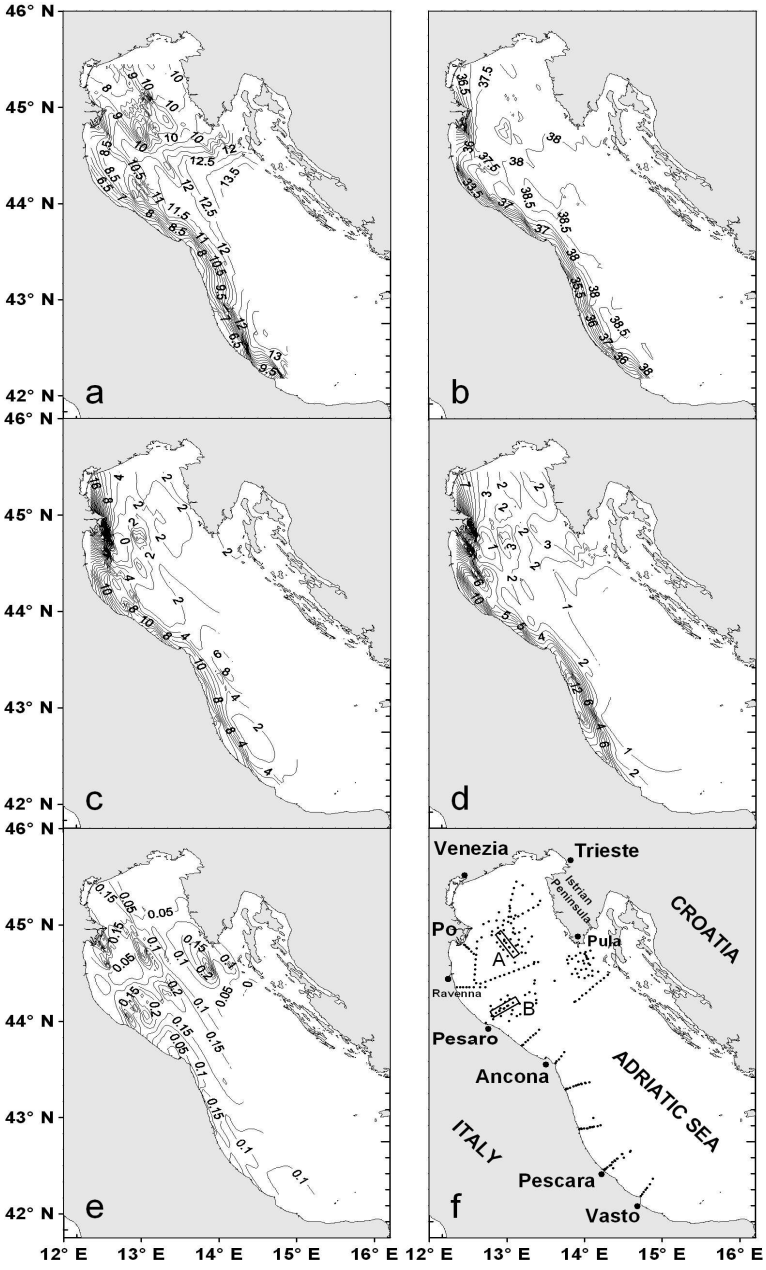

Figure 4: Winter surface field of: a) temperature (°C), contour interval is 0.5, b) salinity, contour interval is 0.5; c) DIN (μM), contour interval is 2; d) Orthosilicate (μM), contour interval is 1; e) Orthophosphate (μM), contour interval is 0.05; f) the rectangles indicate the Po (A) and Pesaro (B) transects. The dots represent the sampling points, from [15].

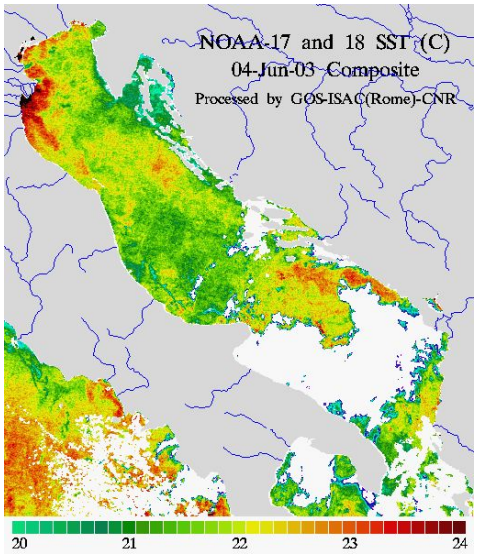

Figure 5: Sea surface temperature map from the NOAA-16, GOS-ISAC-CNR (04 June 2003), from [15].

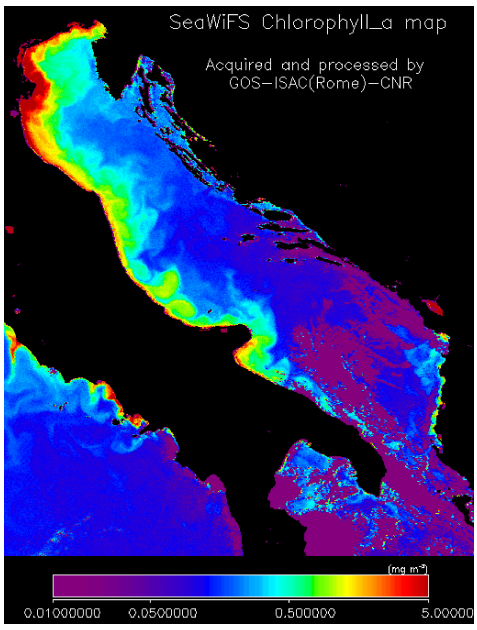

Figure 6: SeaWiFS image of chlorophyll concentration for 4 June 2003 (provide by GOS-ISAC-CNR), from [15].

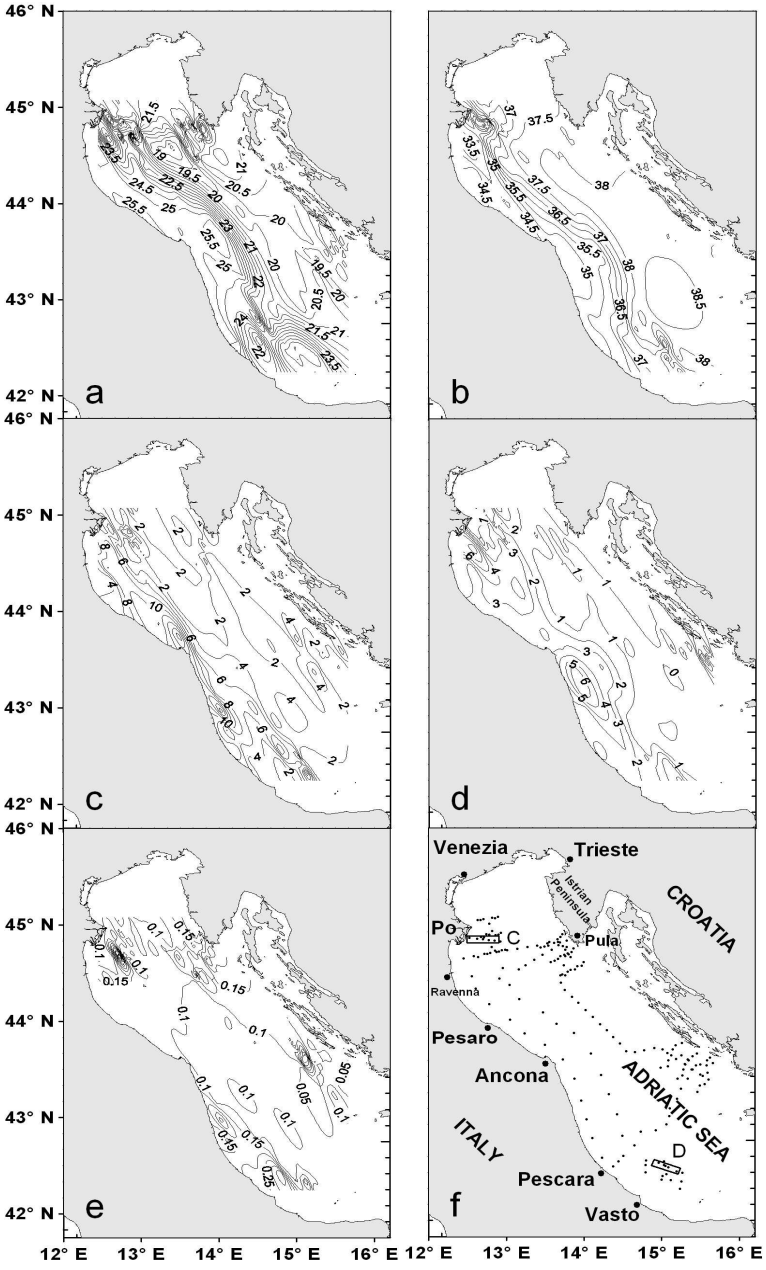

Figure 7: Late spring surface field of: a) temperature (°C), contour interval is 0.5, b) salinity, contour interval is 0.5; c) DIN (μM), contour interval is 2; d) Orthosilicate (μM), contour interval is 1; e) Orthophosphate (μM), contour interval is 0.05; f) the rectangles indicate the Po (C) and Vasto (D) transects. The dots represent the sampling points, from Marini et al. [15].

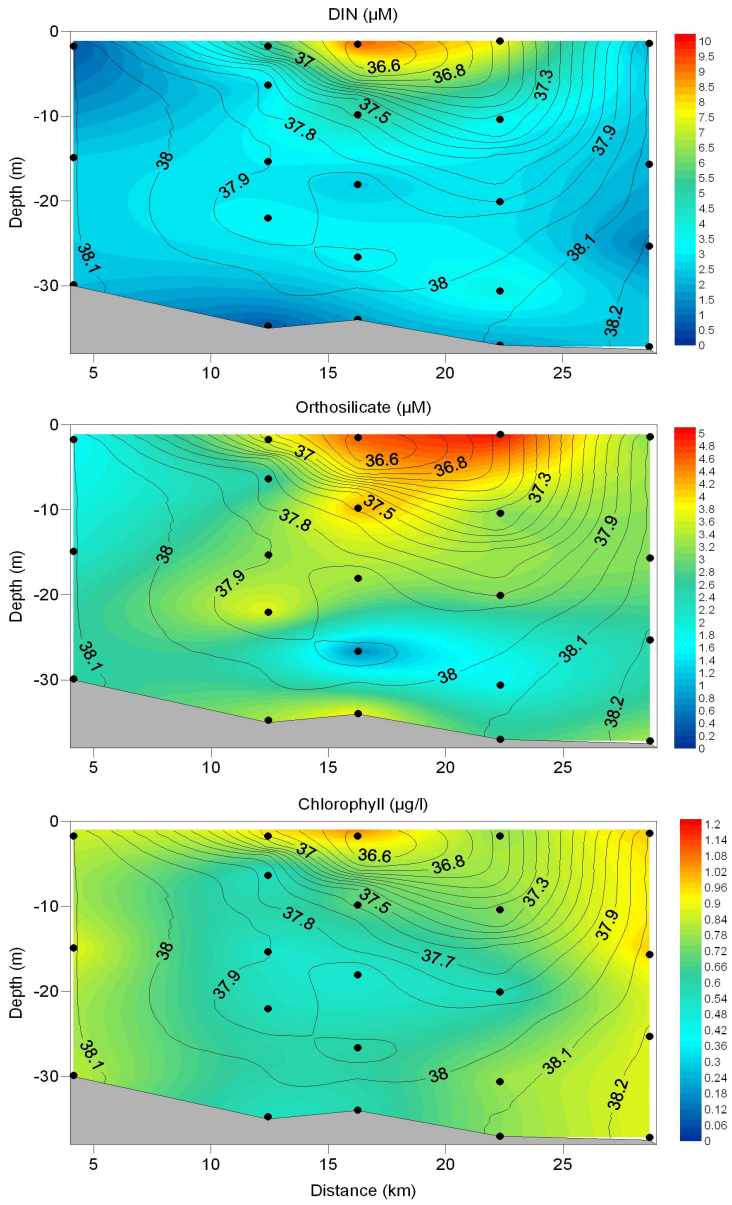

Figure 8: Po transect during winter cruise (February 21, 2003) of DIN, Orthosilicate and chlorophyll a concentration (colored shading). The black contours represent the salinity (contour interval 0.1) and the dots represent the sampling points. The position of the transect is plotted in Figure 4f, from Marini et al. [15].

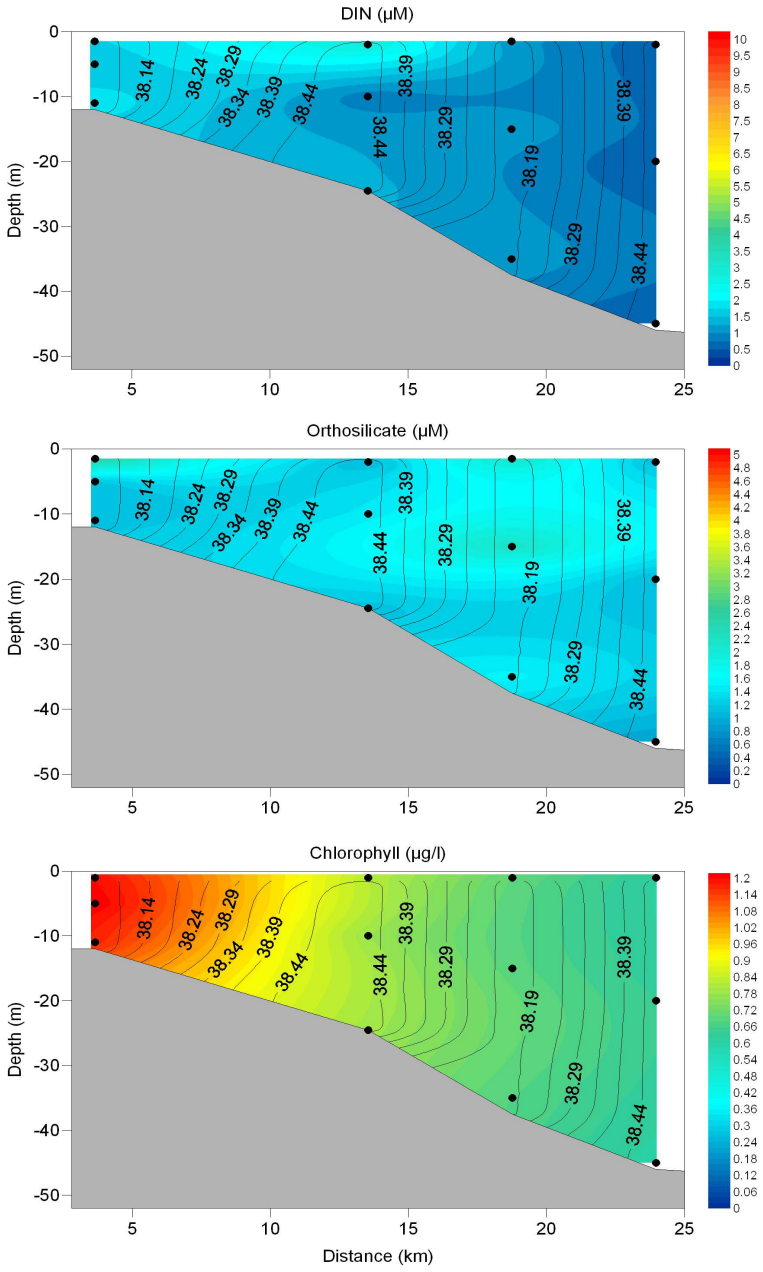

Figure 9: Pesaro transect during winter cruise (February 18, 2003) of DIN, Orthosilicate and chlorophyll a concentration (colored shading). The black contours represent the salinity (contour interval 0.1) and the dots represent the sampling points. The position of the transect is plotted in Figure 4 f, from [15].

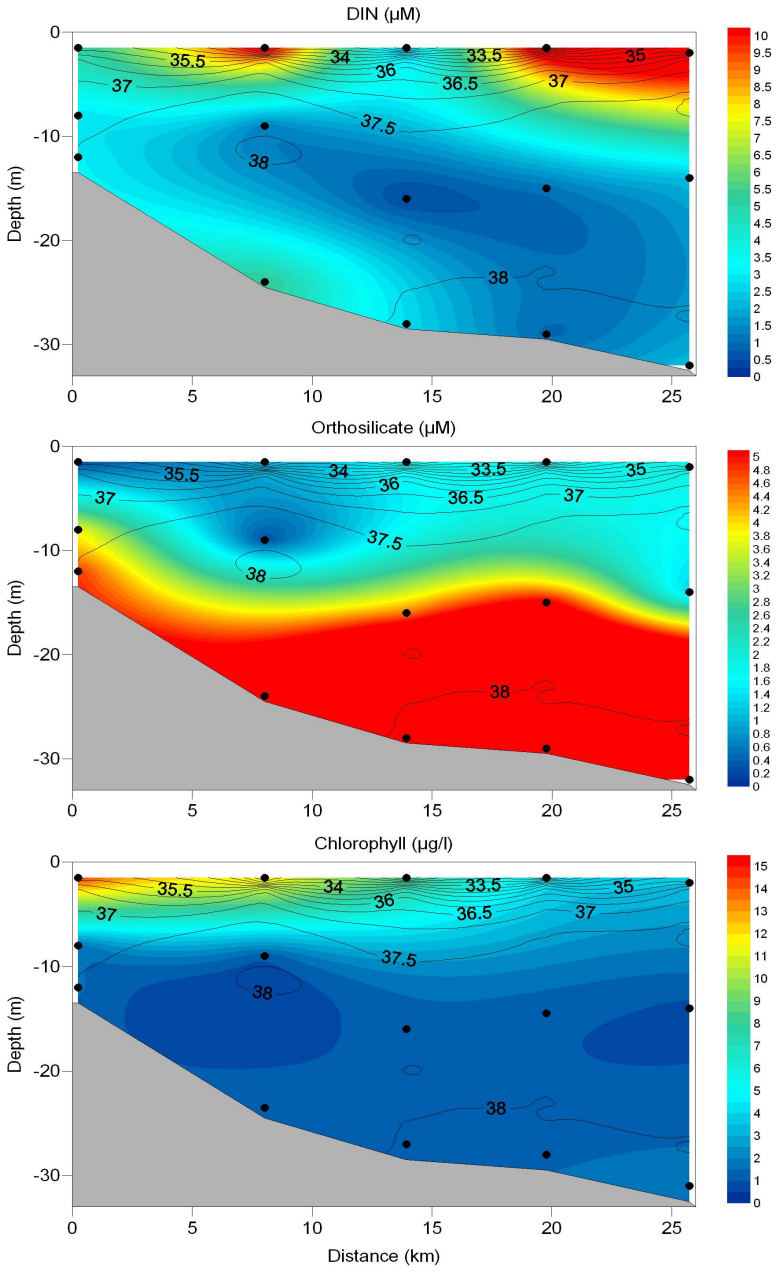

Figure 10: Po transect during late spring cruise (June 08, 2003) of DIN, Orthosilicate and chlorophyll a concentration (colored shading). The black contours represent the salinity (contour interval 0.1) and the dots represent the sampling points. The position of the transect is plotted in Figure 7f, from Marini et al. [15].

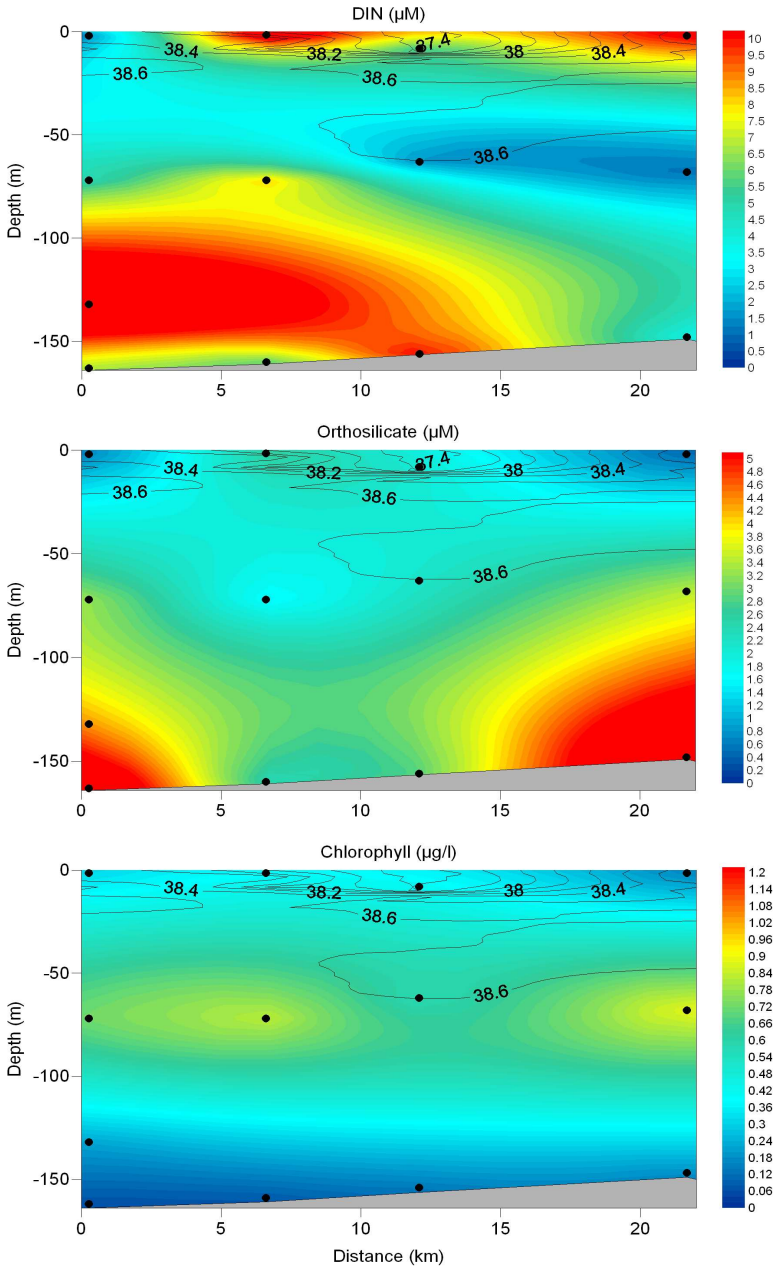

Figure 11: Vasto transect during late spring cruise (June 13, 2003) of DIN, Orthosilicate and chlorophyll a concentration (colored shading). The black contours represent the salinity (contour interval 0.1) and the dots represent the sampling points. The position of the transect is plotted in Figure 7f, from Marini et al. [15].

DVI January 31, 2003 - February 24, 2003							
	Temperature (*degree C*)	Salinity (*PSU*)	$Si(OH)_4$ (μM)	DIN (μM)	PO_4 (μM)	DIN/Si (μM)	Chl *a* ($\mu g/l$)
Po Survey (surface) S < 37.5	7.06 ± 0.34	37.02 ± 0.32	4.03 ± 1.12	6.51 ± 3.69	0.17 ± 0.12	1.51 ± 0.59	0.88(12) ± 0.20
Po Survey (surface) S > 37.5	8.71 ± 0.54	37.91 ± 0.11	2.20 ± 0.90	1.50 ± 0.83	0.11 ± 0.06	0.74 ± 0.42	0.79(20) ± 0.19
Istria Survey (Surface) S < 38.15	10.08 ± 0.46	37.84 ± 0.14	3.77 ± 0.51	1.97 ± 1.07	0.18 ± 0.12	0.53 ± 0.31	0.63(13) ± 0.05
Istria Survey (Surface) S > 38.15	12.17 ± 0.27	38.32 ± 0.03	1.95 ± 0.24	0.97 ± 0.29	0.15 ± 0.11	0.50 ± 0.15	0.45(13) ± 0.04
Pesaro Survey (Surface) S < 38.2	9.62 ± 0.76	37.94 ± 0.18	2.30 ± 0.94	2.17 ± 1.22	0.24 ± 0.07	1.07 ± 1.05	0.91(15) ± 0.32
Pesaro Survey (Surface) S > 38.2	11.39 ± 0.55	38.38 ± 0.07	1.60 ± 0.52	1.06 ± 0.60	0.22 ± 0.07	0.76 ± 0.61	0.63(13) ± 0.13

Table 1: The winter cruise (January 31- February 24, 2003) parameters for distinguished two water masses in three areas, in brackets number of data $\pm$ Standard Deviation.

4 Discussion

4.1 Winter characterization of northern and western Adriatic Sea

In the northern Adriatic Sea, during winter period, Bora winds are frequent, intense, narrow sea surface wind jets coming from the northeast through the mountain passages along the eastern side (e.g., [7]). During the winter cruise, two sequential Bora events occurred during 11-19 February [19, 6, 20].

In order to describe the simultaneous influence of Bora wind and Po plume on the distribution of the water masses in the northern and western part of the Adriatic Sea, three areas have been compared: Po plume area, Pula area and Pesaro area.

Some biochemical characteristics of the water masses have been described in this period. Salinity was used to discriminate water masses in the three areas investigated and two different water masses in each regions were found (Table 1). Water unaffected by river runoff generally had salinities equal to or greater than 38.5, which characterizes North Adriatic DeepWater (e.g., [3]). The water mass influenced by river runoff was fresher, colder, richer in chlorophyll a, orthosilicates, DIN, and DIN/orthosilicates ratio, and confined to the northern Adriatic, between the Po Delta and the Istrian peninsula, and along the western Adriatic coast. Farther offshore a more saline water mass was warmer and less nutrient-rich. The two water masses, always present in the three surveys, were compared and the results were summarized in Table 1. The northern region where salinity was less than 37.5 was strongly impacted by Po River runoff, in particular high concentrations of DIN, orthosilicates and DIN/orthosilicates ratio were found. A DIN/orthosilicate ratio close to 1 is good for diatom phytoplankton growth as examined by Redfield et al. [22] and Brzezinski [23]. High surface values of nutrients were evident in vertical transect across the Po river plume (Figure 8) concurrent with low salinity down to 20 m depth in the

DV2 March 26, 2003 - June 15, 2003							
	Temperature (*degree C*)	Salinity (*PSU*)	$Si(OH)_4$ (μM)	DIN (μM)	PO_4 (μM)	DIN/Si (μM)	Chl *a* ($\mu g/l$)
Po Survey (surface) S < 35.7	23.95 ± 1.94	34.18 ± 1.97	1.37 ± 0.86	2.74 ± 2.89	0.19 ± 021	4.19 ± 6.79	6.01(9) ± 4.49
Po Survey (surface) S > 35.7	23.00 ± 0.81	36.58 ± 0.46	1.75 ± 1.53	1.93 ± 1.98	0.13 ± 0.03	27.41 ± 71.60	2.97(2) ± 1.89
Vasto Survey (Surface) S < 37.42	24.40 ± 1.70	36.54 ± 0.87	2.43 ± 153	3.36 ± 1.86	0.14 ± 0.12	1.72 ± 1.18	0.81(3) ± 0.31
Vasto Survey (Surface) S > 37.42	25.52 ± 0.39	37.85 ± 0.43	1.86 ± 1.28	1.59 ± 1.58	0.12 ± 0.09	0.87 ± 0.47	0.15(6) ± 0.03
Pescara Survey (st. 24 to 32) S < 37.5	21.61 ± 1.12	36.21 ± 0.83	2.50 ± 0.58	4.64 ± 1.08	0.20 ± 0.02	1.88 ± 0.39	0.50(3) ± 0.02
Pescara Survey (st. 24 to 32) S > 37.5	20.29 ± 0.48	38.74 ± 0.02	0.15 ± 0.18	2.95 ± 2.06	0.09 ± 0.04	130.15 ± 121.69	0.32(4) ± 0.11

Table 2: The late spring cruise (March 26 - June 15, 2003) parameters for distinguished two water masses in three areas, in brackets number of data ± Standard Deviation.

core of the plume. South of the Po plume and east of Pesaro, DIN and orthosilicate values decrease and temperature and salinity increase (Table 1). In Figure 9, DIN, orthosilicates and chlorophyll a concentrations decrease from the cost toward offshore while the salinity increased. The influence of Po River discharge is quite evident in the northern Adriatic area and along the western coast in front of Pesaro (Figures 2, 3, and 4). DIN concentrations decrease threefold from north to south and orthosilicates decrease approximately twofold. Both temperature and salinity increase eastward and southward from the Po delta, whereas orthosilicates and DIN concentrations decrease (Table 1). South of the Istrian Peninsula, a strong front separated colder, fresher, and more DIN-rich water on the north from warmer, saltier, less DIN-rich water south of the front (Table 1). This front marks the eastern extension of the Po plume driven by strong Bora winds on either side of the plume.
Furthermore, Bignami et al. (2007) suggest that the Bora is the only wind capable of generating extensive offshore jets off the Po delta. Orthophosphate concentrations do not show much difference between the zones, indicating little or no contribution from the Po River runoff. The maximum of chlorophyll was at the edge of the plume owing to higher chlorophyll concentrations in waters outside the plume. The lower chlorophyll values within the plume may be due to cold temperature and low light concentrations within the plume, inhibiting growth of phytoplankton within the plume.

4.2 Late spring characterization of western Adriatic coast

During the late spring cruise strong stratification characterized the water column of the northern Adriatic (Figure 10). A SeaWiFS image of chlorophyll from June 4 showed the southward extension of the Po plume along the western boundary within the flow of the WAC (Figure 6). Despite the below average flow from the Po River, the buoyancy driven flow was evident along

the western boundary of the basin consistent with results from models and observations (e.g., [14, 24]).

In order to evaluate the influence of Po River runoff on biochemical properties of surface waters from three areas along the western Adriatic were compared: the Po plume area and the coastal regions off Pescara and Vasto (Figure 7). As in winter, salinity was used to distinguish between the different water masses. Two water masses were identified from the late spring cruise: fresher water where salinity was generally less than about 38.2 was indicative of the influence of river inputs along the western boundary, and more saline water, greater than 38.2, was present offshore. Water mass structure showed gradient from western coast to offshore. As in winter, salinity increased toward the east, but because of the strong vertical stratification, this gradient was confined mainly to the surface layer, in contrast to the winter situation. In the fresher water of the Po plume (salinity $<$ 35.7, Table 2) nutrient concentrations were variable. The highest concentrations of nutrients were found at intermediate salinities where S $>$ 35.7. The region of the Po plume where S$>$35.7, did not show marked differences in nutrient values from the fresher water where S$<$35.7. However, DIN/orthosilicate ratios were much higher in summer than in winter period when DIN/ Si ratios were nearly all less than 2.5. The much larger DIN/ Si ratios in the spring were most likely due to higher consumption of orthosilicate by diatom phytoplankton groups in response to high light availability near the surface and stratification. Diatoms were a dominated the phytoplankton community of the Po plume (I. Cetinic, personal communication, 2005). In the bottom plot in Figure 10 the maximum surface chlorophyll a of about 15 μgl^{-1} corresponded to a minimum of orthosilicate concentration as observed by Socal et al. [25].

The Pescara region showed larger differences in the water properties between the surface coastal water and the surface offshore water (Table 2). Orthosilicate and DIN concentrations decreased from near the coast toward offshore and DIN/orthosilicates ratio increased. In contrast to winter when concentrations of nutrients decreased southward from the Po River plume, concentrations off Pescara were greater than concentrations in the Po plume area.

In the most southern region off Vasto, a filament extending from the coast toward offshore was evident in the SeaWiFS image (Figure 6). In situ measurements across the filament (Figure 11) indicated that it included less saline surface water than the water into which it advected (Table 2, average S = 36.54 $\pm$ 0.87). Though the filament was generally characterized by water less than saline than 38.55, the salinity of hydrographic samples from the filament were $<$37.42. Outside of the filament where the salinity was greater and temperatures warmer; the mean concentrations of orthosilicates and DIN decreased (Table 2). In all regions chlorophyll a concentration was greater in the lower salinity coastal water than in the more saline water offshore and decreased from the area of Po plume southward along the coast. A deep chlorophyll a maximum at about 70–75 m depth was present in the offshore higher salinity water where deep penetration of the light field coincided with the top of the nutricline [26].

4.3 Characterization of the Seasonal Biochemical Variations

In general the basin was characterized by decreasing nutrient gradient in the surface layer from the western boundary eastward. Nutrient values in the northern Adriatic resulted from river input not only from the Po River, but from other smaller rivers along the Italian coast. Wintertime DIN and orthosilicates values were on average twice as high as late spring concentrations in the same region (Table 1 and 1). This could be due also to both low Po River discharge and high phytoplankton uptake of nutrients during the spring, indicated by the relatively high chlorophyll concentrations within the Po plume.

During the winter cruise the Po plume was more clearly defined extending northeastward toward the Istrian Peninsula in response to strong Bora winds from Trieste and Senj, and higher, but typical, river discharge rates. During the late spring cruise, although the Po plume spread more broadly, the area south of the Istrian Peninsula appeared less influenced by the Po plume (Figures 7c and 7d) perhaps because of below average river discharge rates and the absence of strong wind forcing. The middle Adriatic showed less influence from the Po River. During springtime local river inputs contributed to the nutrient concentrations along the coast [8, 13]; in particular the Pescara and Vasto regions were characterized by nutrient concentrations similar to the Po plume region (Table 2). Nutrient and chlorophyll values were highest in the western coastal areas of the Adriatic during both seasons.

5 Conclusions

The biochemical characteristics of water masses in the northern Adriatic and the western boundary of the Adriatic have been showed. Because temperature was very non-conservative in the shallow northern region of the Adriatic, salinity was a better discriminator of water mass variability. During winter the extent and shape of the Po plume appeared to respond to Bora winds, extending northeastward toward the Istrian Peninsula carrying highs concentrations of DIN and orthosilicate. In general, nutrient concentrations were negatively correlated with salinity, nutrients increasing with decreasing salinity. Little accumulation of phytoplankton biomass was observed within the Po plume, and nutrient values tended to be transported offshore with the freshwater. The Western Coastal Layer, observed in the Pesaro section, showed a decreasing nutrient concentrations and an increasing salinity in the offshore direction. Coastal advection transported freshwater, nutrients, and suspended material southward, dominated by physical mixing, and with limited phytoplankton growth.

In late spring, the western boundary coastal waters were characterized by lower salinity water near the coast and saltier water offshore, as in winter period. However, unlike the winter period, the onshore-to-offshore gradient is confined vertically mainly to the surface layer because of the strong stratification. During the spring cruise, low Po River runoff ($\sim$625 m^3/s) and weak wind forcing resulted in a broad spreading, vertically stratified river plume, where high phytoplankton abundance contributed to a rapid depletion of nutrients. In the central part of the Adriatic basin a filament extended offshore from the coast. In situ

measurements showed that this filament is characterized by lower salinity and temperature, and higher concentrations of orthosilicates and DIN compared to the surrounding water. Alongshore advection of the plume does occur, but because of the weak mixing, relatively slow advection, nutrients are relatively low in the advected plume, phytoplankton biomass is high relative to the offshore water, but decreases rapidly alongshore and in offshore filaments because of the lack of nutrients to sustain phytoplankton growth.

DIN/orthosilicate ratios were much typically less than 2–3 during the winter when phytoplankton growth was small. Low phytoplankton growth rates were probably the result of cold temperatures, low incident light, high attenuation of light in the plume, and deeper mixing than in spring. During the late spring the DIN/orthosilicate ratios were much higher. This higher ratio in spring is indicative of enhanced phytoplankton uptake in higher illumination and stratification conditions.

References

[1] A. Artegiani, D. Bregant, E. Paschini, N. Pinardi, F. Raicich, and A. Russo. The Adriatic Sea general circulation. Part I. Air-sea interactions and water mass structure. *J. Phys. Oceanogr*, 27:1492–1514, 1997.

[2] T.S. Hopkins. The structure of Ionian and Levantine Seas. Reports in Meteorology and Oceanography. Harvard Un. 41(II):35–56, 1992.

[3] A. Artegiani, , D. Bregant, E. Paschini, N. Pinardi, F. Raicich, and A. Russo. The Adriatic Sea general circulation. Part II: Baroclinic Circulation Structure. *J. Phis. Oceanogr.*, 27:1515–1532, 1997.

[4] M. Orlić, M. Gačić, , and P.E. La Violette. The Currents and Circulation of the Adriatic Sea. *Oceanol. Acta*, 15(2):109–124, 1992.

[5] M. Orlić, M. Kuzmić, and Z. Pasarić. Response of the Adriatic Sea to Bora and Sirocco forcings. *Cont. Shelf. Res.*, 14(1):91–116, 1994.

[6] C. E. Dorman, S. Carniel, L. Cavaleri, M. Sclavo, J. Chiggiato, J. Doyle, T. Haack, J. Pullen, B. Grbec, I. Vilibić, I. Janeković, C. Lee, V. Malačič, M. Orlić, E. Paschini, A. Russo, and R. P. Signell. February 2003 marine atmospheric conditions and the bora over the northern Adriatic. *J Geophys Res-Oceans*, 112:C03S03, 2007.

[7] P. M. Poulain and B. Cushman-Roisin. Observation of near- surface circulation. *In Cushman-Roisin, B., Gačić, M., Poulain, P. M. and Artegiani, A. (eds), Physical Oceanography of the Adriatic Sea. Kluwer Academic Publisher, Dordrecht*, pages 67–109, 2001.

[8] I. Vilibić. An analysis of dense water production on the North Adriatic shelf. *Estuar. Coast. Shelf Sci.*, 56:697–707, 2003.

[9] M. Zavatarelli, F. Raicich, D. Bregant, A. Russo, and A. Artegiani. Climatological biogeochemical characteristics of the Adriatic Sea. *J. Mar. Syst.*, 18:227–263, 1998.

[10] F. Raicich. On the fresh water balance of the Adriatic coast. *J. Mar. Syst.*, 9:305–319, 1996.

[11] T.S.Hopkins, A. Artegiani, F. Bignami, and A. Russo. Water-mass modification in the the Northern Adriatic. A preliminary assessment from the ELNA data set. pages 3–23, 1999.

[12] M. Marini, P. Fornasiero, and A. Artegiani. Variations of hydrochemical features in the coastal waters of Monte Conero:1982-1990. *P.S.Z.N.: Mar. Ecol.*, 23(1):258–271, 2002.

[13] A. Campanelli, P. Fornasiero, and M. Marini. Physical and Chemical Characterization of the Water Column in the Piceno Coastal Area (Adriatic Sea). *Fresenius Environmental Bulletin*, 13(5):430–435, 2004.

[14] V.H. Kourafalou. Process Studies on the Po River plume, North Adriatic Sea. *J. Geophys, Res.*, 104(C12):29963–2998, 1999.

[15] M. Marini, B.H. Jones, A. Campanelli, F. Grilli, and C. Lee. Seasonal variability and Po River plume influence on biochemical properties along western Adriatic coast. *J. Geophys. Res.*, 113(C05S90), 2008.

[16] UNESCO. The acquisition, calibration and analysis of CTD data. A report of SCOR WG 51. *Technical papers in Marine Sciences*, 54:1.59, 1988.

[17] J.D.H. Strickland and T.R. Parsons. A practical handbook of seawater analysis. *Bull. Fish. Res.*, 167:310 pp, 1972.

[18] O. Holm-Hansen, C. J. Lorenzen, R.W. Holmes, , and J.D.H. Strickland. Fluorometric determination of chlorophyll. *J. Cons. Perm. Int. Explor. Mer*, 30(1):3–15, 1965.

[19] C.M. Lee, F. Askari, J. Book, S. Carniel, B. Cushman, C.K. Harris, B.H. Jones, M. Kuzmic, P. Martin, A. Ogston, M. Orlic, H. Perkins, P.M. Poulen, J. Poulen, A. Russo, C. Sherwood, R.P. Signell, , and D. Thaler Detweiler. Northern Adriatic Response to a Wintertime Bora Wind Event. *EOS, Transaction American Geophysical Union*, 86(16):157–165, 2005.

[20] F. Bignami, R. Sciarra, S. Carniel, and R. Santoleri. Variability of Adriatic SEa coastal turbid waters fram SeaWIFS imagery. *J. Geophys. Res.*, 112:C03S10, 2007.

[21] S. Cozzi, M. Lipizer, C. Cantoni, and G. Catalano. Nutrient balance in the ecosystem of the north western Adriatic Sea. *Chemistry and Ecology*, 18(1/2):1–12, 2002.

[22] A.C. Redfield, B.H. Ketchum, and F.A. Richerds. The influence of organism on the composition of sea water. pages 26–77, 1963.

[23] M.A. Brzezinski. The Si:C:N Ratio of marine Diatoms: interspecific varaibility and the effect of some environmental variables. *J. Phycol*, 21:347–357, 1985.

[24] P. M. Poulain. Adriatic Sea surface circulation as derived from drifter data between 1990 and 1999. *J. Marine Syst.*, 29:3–32, 2001.

[25] G. Socal, A. Pugnetti, L. Alberighi, , and F. Acri. Observations on phytoplankton productivity in relation to hydrography in the northern Adriatic. *Chem. Ecol.*, 18(1-2):61–73, 2002.

[26] A. Boldrin, S. Carniel, M. Giani, M. Marini, F. Bernardi Aubry Campanelli, F. Grilli, and A. Russo. The effects of bora wind on physical and bio-chemical properties of stratified waters in the northern adriatic. *Journal of Geophysical Research, C08S92 doi:10.1029/2008JC004837*, 114, 2009.

Current Views and Open Problems on Sapropel Events

M. Ribera d'Alcalà[1], M. Sprovieri[2]
1, Zoological Station "Anton Dohrn", Napoli, Italy
2, Institute for Coastal Marine Environment, CNR, Capo Granitola (TP), Italy
mario.sprovieri@iamc.cnr.it

Abstract

Since many years the scientific community is devoting a large effort to describe, characterize and constrain seasonal to pluridecadal variability in climate dynamics. An important part of this effort is focused on reconstructing past climate events which may shed light on Earth system response to climate variability. In most cases the mutual interaction among abiotic and biotic components of the system is leaving tracks which are now used as clues to reconstruct past events. In this context, paleoclimate is among the most vital and creative fields of modern research and its method is intrinsically deductive. The Mediterranean Sea has been the site for, at least, the last $\sim$10 My (106 years) of recurrent events of increased carbon burial (sapropels and/or sapropelitic layers) which can be traced in the deep sea cores or in recently outcropped sedimentary successions. Because carbon burial is strongly linked with biotic carbon fixation and respiration, through biosynthesis, those events were certainly related to changes in the functioning of marine, and possibly, terrestrial food webs, which are generally coupled with variations in climate. This contribution aims at re-investigating the high number of available datasets and exploring new views on potential deep interaction between unbalanced Redfieldian chemistry of biota, systematic changes in the marine trophic web and climate/ocean variability as primary forcing of rhythmic increase of export production in the Mediterranean basin.

1 Background

Since many years the scientific community is devoting a large effort to describe, characterize and constrain seasonal to pluridecadal variability in climate dynamics. An important part of this effort is focused on reconstructing past climate events which, even if traceable at a much coarser scale, may shed light on Earth system response to climate variability. Marginal seas often display amplified responses to climate variations mostly because of their morphological constraints and the sharper gradients in the forcings. Mediterranean Sea (MED) is probably one of the clearest example. The MED has been the site for, at least, the last $\sim$10 My (106 years) of recurrent events of increased carbon burial which can be traced in the deep sea cores or in recently outcropped sedimentary successions. Because carbon burial is strongly linked with biotic carbon fixation and respiration, through biosynthesis, those events were certainly related to changes in the functioning of marine, and possibly, terrestrial food webs, which are generally coupled with variations in climate. Sapropels are "A discrete

layer, greater than 1 cm in thickness, set in open marine pelagic sediments containing greater than 2% organic carbon (Corg) by weight" [1]. The definitions apply to the layers as they are recovered and do not reflect the carbon content at the time of deposition, which may have been altered afterwards by secondary diagenetic processes. Besides being carbon richer than neighboring layers the striking feature of sapropels is of being recurrent. In some cores it is possible to find tens of them spanning over large time intervals ($10^4 \div 10^4$ years). Sapropels track shifts of the functioning of the MED. The increase in carbon burial can occur for different reasons: increase in carbon export production, decrease in mid/deep water consumption, increase in the efficiency of burial etc. Those changes may be due, in turn, to changes in the circulation, increase in the runoff, changes in the food web, etc.

2 The forcings

While processes regulating climate variability on decadal time scales and the causative changes in the forcing are still elusive, on the long time scale ($10^4 \div 10^4$ y) quasi-deterministic constraints, related to the mutual positions and interactions of the Earth, Sun and the other planets, exist. The Earth follows elliptic orbits around the Sun, contemporarily spinning on its axis. Because of the elliptic shape of the orbit, i.e., the Earth-Sun distance varies during the year, and because of the angle of the Earth axis with the plane of the orbit, the solar irradiance falling on the planet varies in time, generating the seasonality we observe. Gravitational interactions with all the components of the solar system and conservation laws of angular momentum cause quasi-periodic oscillations in the motion, the most relevant being those related to slight changes in the shape of orbital ellipse (eccentricity), in the angle of the Earth axis with the plane of the orbit (obliquity) and in the orientation of the Earth axis relative to the Sun at the time of perihelion (close to the Sun) and aphelion (far from the Sun) along the elliptic orbit (precession). The changes in movement and orientation of the Earth relative to Sun do in fact change the amount and location of solar radiation reaching the Earth, being the relative differences among the seasons and the regions the crucial factor. Land and ocean respond differently to solar radiation and they are unevenly distributed on the planet. This causes non linear responses with different seasonal contrasts in different regions, to the point of eventually favoring ice accumulations or thawing according to the phase of the cycle. Sapropels coincide with solar maxima and the response to increased gradients in heat transfer on the Earth surface is, for the uneven distribution of land and oceans mentioned before, far from being linear. Short et al. [2] analyzed the problem in great detail. The insolation is zonally symmetric, but the asymmetric land-sea distribution results in a seasonal temperature cycle with distinct zonal asymmetries (e.g., [3], Fig. 7.20). Over large mid-latitude continents the seasonal range can exceed 40°C. Over oceans it rarely exceeds 5°C because of the large heat capacity of the ocean mixed layer. Convenient formulae now available for calculating time series of earth's orbital configuration (e.g., [4, 5]) have facilitated detailed studies of orbit and insolation variations. For example, spectral analyses have shown that summer insolation variations in mid-latitudes are dominated by the eccentricity-modulated precession

cycle (significant power at periods near 19,000 and 23,000 yr). Because temperature contrasts among latitudes and among land and sea are among the main drivers of atmosphere dynamics and climate variations it was clear since the beginning that the coherence between the sapropel and orbital cyclicity held a causative link. The first to propose a conceptual mechanistic model was Rossignol-Strick [6, 7] who hypothesized that the strengthening of monsoons during solar irradiance maxima would have involved also the African Monsoon, causing and enhanced transport of wet air on the continent thus increasing the Nile runoff in the MED. While the fine mechanisms regulating the time course of those transitions, and their biogeochemical implications for sapropels deposition are still under debate, it can be definitely assumed that orbital cyclicity is the Pacemaker [8] of those events.

3 Physiography of the Mediterranean Sea

MED is an elongated semi-enclosed basin that extends between 6°E and 37°W, and 30°N and 46°N approximately and is connected to the Atlantic Ocean through the Gibraltar Strait and to the Black Sea through the Dardanelles Strait. The crucial feature of the MED is that the main connection among the two main sub-basins, Eastern and Western Mediterranean (EMED and WMED hereafter), and with neighboring seas are narrow and shallow sills hardly reaching 500 m depth. At particular sites, where the coupling of circulation and atmospheric forcing produces intense buoyancy extraction, convection is strong enough to make water reaching the intermediate depth or the sea bottom. The reason which makes this possible at such low latitudes is the unusually high salinity as compared to the open ocean. The Mediterranean is, in fact, a condensation basin, with evaporation exceeding the sum of precipitation and input from river runoff [9]. The resulting negative freshwater budget is partially compensated for by the Atlantic inflow at Gibraltar Strait, where a complex two layer system is at work. The long-term equilibrium of both water and salt budgets brings about an outflow across the strait of Gibraltar ranging from 0.8 to 1.6 Sv [10, 11], which, because of the shallow sills at Gibraltar strait (284 m), involves mostly the intermediate layers (a complex mixture of LIW, WMDW, etc.). A similar depth constraint works at the Straits of Sicily. Therefore the main connecting sills inhibit significant exchanges of deep waters [12]. LIW is the main driver of a large thermohaline cell encompassing the whole Mediterranean, with the inflow of the Atlantic Water (AW) through the Gibraltar strait compensating the LIW outflow. Deep circulations in the two main sub-basins are decoupled and are composed by two minor thermoaline cells forced by events of dense water formation occurring in the Gulf of Lions for the WMED, where Mistral bursts and cyclonic permanent circulation force the formation of the Western Mediterranean Deep Water (WMDW), and in the South Adriatic, where Bora bursts act on a permanent cyclonic structure, producing the source water for the Eastern Mediterranean Deep Water (EMDW). From the ecological point of view MED is considered an oligotrophic basin [13], with the EMED being classified as extremely oligotrophic. Current estimates of the total Primary Production (PP) utilizing different methods and data are re-

ported in D'Ortenzio [14]. Despite of the spread of PP estimates, a consistent difference between the two sub-basins with WMED export production possibly around $\sim$ 22 g·C·m^{-2} a^{-1} and EMED export production around $\sim$ 12 $\mathrm{g{\cdot}C \cdot m^{-2} \cdot a^{-1}}$. This difference is also reflected in a deeper Deep Chlorophyll Maximum (DCM) in the EMED than in the WMED [15, 16] and, therefore, a deeper nutricline in the former than in the latter. Moutin and Raimbault [17] showed that the depth of the DCM in the EMED makes its contribution to the depth integrated primary production very small while in the WMED at sites where the DCM was at 50 m or shallower its contribution was similar to the surface contribution. In addition, the prevailing recycled production in the EMED regime produced a carbon export in the EMED from 5 to 10 times lower than in the WMED.

4 The key issues

Sapropel deposition evidences inefficient carbon recycling in the water column and/or at the sea bottom. The simplest explanations for such inefficiency are the increase of carbon sedimentation rate and/or a lack of oxygen in the intermediate and deep layers. Neither one can taken for granted. A decisive support to the anoxic conditions (both in the column water and at the interface water/sediments) during sapropels deposition comes from i) the evidence of lamination and absence of burrowing (suggesting absence of living benthic fauna at the bottom of the basin), ii) the absence of tests of benthic foraminifera in the sapropels, iii) the distribution of redox sensitive elements indicating a highly reducing environment, and iv) the recovery of isorenieratenes. Considering that in the present MED oxygen supply to subsurface layers is very effective because of the deep water formation, anoxia at bottom implies a shut down either of lateral advection of newly formed dense water at the sites of the deposition or of the dense water formation tout court. The small scale of the basin and the spatial extension of sapropels, which span over most of the EMED (e.g. [18]), suggest that the latter is the most likely. This in turn calls for a more stagnant dynamics, especially in the vertical dimension. Since dense water formation in the present MED is driven by preconditioning the density through evaporative salinity increase, the process leading to Sapropel formation is assumed to be an alteration of fresh water budget with a surface salinity decrease such to prevent deep convection. The salinity decrease was primarily attributed to an increase of the fresh water input. Olaussen[19] hypothesized that the fresh water came from the melting of Scandinavian Ice sheet through continental Europe and the Black Sea. A more careful analysis of the timing of last sapropel event (S1) lead Rossignol-Strick [6, 7] to propose as the main source of fresh water the increase of precipitation in the African continent due to a more intense monsoonal activity with a consequent increase in the Nile runoff. Did the runoff increase to the extent of turning the inverse estuarine circulation of the present MED to a direct estuarine circulation, i.e., with surface water flowing out Sicily and Gibraltar Straits and intermediate waters flowing in? This has been another controversial issue for many years. A systematic and comprehensive analysis of processes leading to the deposition of most recent sapropels can be traced in the contributions by Rohling in collaboration with several colleagues of different expertise, spanning from modeling to iso-

tope and proxy analysis. The mechanistic reconstruction synthesizing the processes is described in detail by Rohling [20]. Very briefly, variation of the solar irradiance distribution in space and time over the Earth due to orbital cycles causes a change in the functioning of a Hadley cell which triggers a northward displacement of the Intertropical Convergence Zone (ITCZ). Such displacement is coupled with an increase of temperature contrast between sea and land which strengthens monsoonal dynamics, which carries more humidity on the continents. The humidity precipitates as rain in the Saharian-sub-Saharian (Sahel) region causing relevant increase in the runoff to the MED. Also, a significant contribution of freshwater from the North-Eastern Mediterranean borderland was proposed by Rohling and Hilgen [21] as an important component of the runoff input in the MED during deposition time of sapropels. Simulations of MED general circulation with an increased runoff, including changes in sea level and salinity due to glacial-interglacial transitions, showed that an inverse estuarine circulation could be kept as long as atmospheric forcing is similar to the present one and the salinity time course due the ice formation during the glacial period is taken into account ([22], [23] and references therein). Analysis of oxygen isotopes supports that scenario [24], which implies a shut-down of deep water formation while keeping intermediate circulation (i.e., LIW-like water mass) alive. If the intermediate circulation was still active then the depth of anoxia could hint at the thickness of the layers involved in surface and intermediate circulation. Cramp and O'Sullivan [25], on the basis of sapropel occurrence in cores sampled all around the EMED and Rohling et al. [26], on the basis of the distribution of isorenieratenes in sediments of Sapropel S1 collected from different sites of Eastern Mediterranean, inferred that the anoxic layer moved up to 300 m horizon. This implies that intermediate flow was higher in the water column than it is today [27]. Therefore a plausible scenario depicts the MED, particularly the EMED, as a basin with no water renewal in the deep layers, a sluggish dynamics in the intermediate layer with a relatively fresher upper layer exporting carbon at depth. Because of the stagnation of the deep layer, oxygen supply would have been sustained only by eddy diffusivity which would have been less effective in deeper layers. Assuming a slow remineralization rate in the anoxic water column, organic carbon accumulation rate in the sediments should have been more affected by oxygen supply than that by sedimentary flux. This in turn would reflect in a higher carbon accumulation rate in the deeper regions of the basin. This is what Murat and Got [28] argued in their analysis suggesting a more or less homogeneous regime of export production sinking to the sea bottom with a degradation rate proportional to the eddy oxygen diffusivity to the sea bottom. While this reconstruction fits well with observational evidence, it leaves unanswered three key questions. Did the export production increase during sapropels, thus suggesting a biotic response to regime change? Is that mechanism crucial for increased carbon burial? Can the possible increase in export production be explained on the basis of increased stratification and terrestrial inputs of nutrients?

5 Export production rates: a contrasting scenario

In the present EMED an acceptable estimate of export production is in the order 12 $\mathrm{g{\cdot}m^{-2}\cdot y^{-1}}$ (see above) which would correspond to an Oxygen Utilization Rate (OUR) at steady state of 0.40 $\mathrm{mmol{\cdot}m^{-3}\cdot y^{-1}}$ in deep (z>1000 m) EMED [29]. In the same study the authors derived from tracer data a value of 0.53 $\mathrm{mmol{\cdot}m^{-3}\cdot y^{-1}}$. Present oxygen concentration is around 185 $\mathrm{mmol{\cdot}m^{-3}}$ [30]. To drive anoxic at 1500 m layer using the classical Redfield ratio of 138/106, the time needed ranges between 350 and 460 years (the same values were previously calculated by Bethoux and Pierre, 1999 for the interval of sapropel S1), according to the value of OUR utilized (0.40 or 0.53 $\mathrm{mmol{\cdot}m^{-3}\cdot y^{-1}}$). This holds true if we assume no renewal of the deep waters and negligible vertical diffusion of oxygen. A different estimate may be based on the few measurements of gross primary production available for the EMED (e.g., [17]) and its export parametrized as in Betzer et al. [31]. With a primary production of 50 $\mathrm{g{\cdot}C\cdot m^{-2}\cdot y^{-1}}$ and only 2% to 10% reaching the stagnant layer i.e., 1 to 5 $\mathrm{g{\cdot}m^{-2}\cdot y^{-1}}$, approximately 500 to 2500 years are required to lead to anoxia. The discrepancy among the two estimates may depend on the presence of additional carbon forms, e.g., DOC, besides particulate carbon, that can be respired (e.g., [32]). In both scenarios the time scale for setting anoxia in the deep layer is compatible with the duration of sapropel events which is in order of 3000/5000 years. Therefore an increase in export production is not a prerequisite for leading deep EMED to anoxia. However it is disputable whether anaerobic respiration would not be able to recycle the organic carbon exported form the surface layer in the due time, thus preventing sapropel deposition. Thunnel et al. [33] argue that this would be the case. A convincing support to the increase of primary production comes from the increase of Ba:Al ratio in the sediments (e.g., [34]). The increase in the sedimentation of biogenic barite, taken as a proxy for the original C content suggests an increase of export production by 4 to 6 times the present one. This is a significant increase which calls for a proportional increase in nutrient supply. Where did the nutrients came from? Even using the higher Redfield ratio proposed by Takahashi et al. [35] (C/P = 169) to support an export production of 60 $\mathrm{g\cdot m^{-2}\cdot y^{-1}}$ as C $\approx$30 $\mathrm{mmol{\cdot}m^{-2}\cdot y^{-1}}$ of P are needed, while for N the flux should be around 750 $\mathrm{mmol{\cdot}m^{-2}\cdot y^{-1}}$. A three times increase in pre-anthropogenic terrestrial inputs, as assumed for the change in fresh water budget is far from filling the gap. A reasonable estimate of N and P inputs to the basin can be based on the two most recent studies on their fluxes and are reported in Markaki et al. [36] [DIN=45,7 $\mathrm{mmol{\cdot}m^{-2}\cdot y^{-1}}$ and DIP=0,23 $\mathrm{mmol{\cdot}m^{-2}\cdot y^{-1}}$] and Krom et al. [37] [DIN=74,5 $\mathrm{mmol{\cdot}m^{-2}\cdot y^{-1}}$ and DIP=0,63 $\mathrm{mmol{\cdot}m^{-2}\cdot y^{-1}}$]. The estimate based on Markaki et al. [36] analysis derives from averaging the fluxes at the sites monitored by them, i.e., Crete and Erdemli. Since the P supply is well below the Redfield ratio, P should be the limiting element. The observed external input supports at most 1.3 $\mathrm{g{\cdot}C\cdot m^{-2}\cdot y^{-1}}$ of new production, which is 10% of that estimated. By contrast the N supply seems to support around 50% of new production, but with a significant part of N input resulting from industrial activity. Ignoring the implications on the biogeochemical func-

tioning of the basin of the observed unbalance between N and P inputs, we may take as a specific feature of the basin that 50% of its export production derives from terrestrial and atmospheric inputs. If we extrapolate this to sapropel time a 5 times increase of export production implies at least a correspondent increase in external inputs. Indeed it requires much more than that because a correspondent increase in nutrient concentrations of Atlantic Water is unrealistic and the sluggish vertical dynamics within the basin should have prevented a large vertical transport of nutrients. However a 5 times increase in atmospheric and terrestrial inputs does not fit with the 3 times increase of runoff, unless a higher concentration in riverine waters is assumed. Moreover, this hypothesis would imply massive blooms, and deposition, nearby the river mouths, especially the Nile, which is not recorded in the sapropel record [28]. Therefore there is a missing source of nutrients. Phosphate constrain should be partially relaxed considering the release from sediments and the consequent upward diffusion as suggested by Slomp et al. [34]. According to their analysis the C/P ratio in the sediments suggests a release of P into the water column up to 2.7 mmol$\cdot \mathrm{P} \cdot \mathrm{m}^{-2} \cdot \mathrm{y}^{-1}$. This would mitigate the deficiency of P. As for N the dominant hypothesis is that it was supplied by nitrogen fixation ([38] and references therein). An alternative, though not exclusive hypothesis, was proposed by Rohling and colleagues (see [18] and [20] and references therein). Based on the observation of an enhanced percentage of the planktonic foraminifera group of Neogloboquadrinids (and in particular of the species N. acostaensis) in the sapropel layers they speculated that the peak of production occurred in the subsurface layer. More specifically they suggested that the change in the fresh water budget in an inverse estuarine dynamics would make the upper layer thinner [18] thus bringing the nutrient rich intermediate zone closer or within the photic zone, warranting a continuous nutrient supply in a very active Deep Chlorophyll Maximum [39]. Indeed this does not solve the problem of mass balance of nutrients but adds more complexity to the sapropel deposition dynamics. To date, several studies have been focused on the time course of sapropels deposition. Casford et al. ([40] and [41]) and Rohling et al. [26] provided a more dynamic reconstruction of the whole sapropel even. Based on a multiproxy analysis they described the deposition as a multiphase event, starting with freshwater-induced stratification that inhibited vertical mixing and deepwater ventilation, during the first 900 years. This phase developed anoxic to euxinic deepwater conditions up to 200 m. After this spin-up phase, the export production showed some ciclycity due to the depth/intensity of winter mixing and the consequent fluctuations in water column stability. Therefore sapropels deposition cannot be taken a unique catastrophic event. While from a biogeochemical point of view sapropels have been carefully analyzed, very little has been discussed on another crucial point. Did the food web changed during the sapropels? Were the organisms overwintering at depth, if any, impeded to migrate in the anoxic layer? Very little is known about this, even though accumulation of biogenic apatite suggests a vast fish kill [34]. Merging the knowledge on sapropels and that on anoxic and suboxic zone may be very effective not only for understanding their dynamics but to predict future scenarios in the present ocean.

6 Insights and future prospects

The astounding recurrence of sapropel deposition events in the MED during late Miocene through the Pleistocene, even considering the few exceptions, reveals the existence of a deterministic response of the basin to the change in heat, momentum and water fluxes which occurred also on a much larger scale in association with cyclic change in Earth orbital parameters. The regional impact of those cycles, during solar maxima, is always manifested as a positive change in the freshwater budget. The basin response to that change is not yet well constrained. While circulation reversal during the Pleistocene sapropels seems unlikely, it cannot be ruled out that such reversal took place before. Still, the rhythmicity of sapropels can hardly explained only on the basis of an enhanced fresh water flux. The shut down or oxygenation of the deep layers does not account for the increase of export production suggested by other proxies, e.g., Ba data. The increase of export production is generally explained in term of increased nitrogen fixation (e.g., [42]), although the absence of the 2, methyl-hopanoids biomarkers in sapropel sediments apparently does not confirm a massive component of nitrogen in the MED during those intervals. Moreover, the reasons of such an increase are not based on robust mechanistic reconstruction. They are an ex-post conjecture. In addition, other alterations of the fresh water budget have occurred in the MED region, e.g., at the time of Sarmatic basin, which did not depend on orbital cyclic modulations of fresh water budget and primary production. Sapropels likely reflect a change in the pelagic food web, triggered by the setup of anoxic conditions as well as non linear responses of a semi-enclosed morphologically constrained basin to quasi-periodic changes in the forcings. They might conceal more information than assumed to date on the biota response to changes in the water column dynamics forced by climate. Notwithstanding the huge research effort conducted until now, some crucial data need to be added to the picture. Were all the sapropels associated with an increase in export production? To which extent such an increase depended on a change in the structure of the pelagic food web? What fraction of the increased export production was due to an increase in nutrient fluxes? What mechanisms produced such an increase? Can the sapropels be a case of study for tracking, and possibly, predicting changes in the functioning of pelagic ecosystem due to climate change? Modern biogeochemistry, together with numerical geophysical models on coupled atmosphere-ocean dynamics (also considering the non-linear dynamical approaches of Rahmostorf [43], Thual and McWilliams [44] may allow advancing in answering the previous questions. But a better understanding of biota response, especially organized in food webs, is a prerequisite for reaching that goal.

References

[1] R.B. Kidd, M.B. Cita, and W.B.F. Ryan. Stratigraphy of eastern Mediterranean sapropel sequences recovered during Leg 42A and their paleoenvironmental significance. *Init. Rep. DSDP*, 42A:421–443, 1978.

[2] D.A. Short, J.G. Mengel, T.J. Crowley, W.T. Hyde, and G.R. North. Filtering of Milankovitch Cycles by Earth's Geography. *Quaternary Research*, 35:157–173, 1991.

[3] J.M. Wallace and P.V. Hobbs. Atmospheric Science: An Introductory Survey. *Academic Press, New York*, 1977.

[4] A.L. Berger. Long-term variations of daily insolation and Quatemary climate change. *Journal of the Atmospheric Sciences*, 35:2362–2367, 1978.

[5] J. Laskar, P. Robutel, F. Joutel, M. Gastineau, A.C.M. Correia, and B. Levrard. A long-term numerical solution for the insolation quantities of the Earth. *Astronomy & Astrophysics*, 428:261–285, 2004.

[6] M. Rossignol-Strick. African monsoons, an immediate climatic response to orbital insolation. *Nature*, 103:46–49, 1983.

[7] M. Rossignol-Strick. Mediterranean Quaternary sapropels: an immediate response of the African monsoon to variation of insolation. *Paleeogeogr., Palaeoclimatol., Palaeoecol.*, 49:237–265, 1985.

[8] J. D. Hays, J. Imbrie, and N.J. Shackleton. Variations in the earth's orbit: Pacemaker of the ice ages. *Science*, 194:1121–1132, 1976.

[9] A.E. Gill. Atmosphere-Ocean. *Dynamics, Academic Press, New York*, page 662, 1982.

[10] J.P. Bethoux. Budgets of the Mediterranean Sea. Their dependence on local climate and on characteristics of the Atlantic water. *Oceanologica Acta*, 2:157–163, 1979.

[11] T.S. Hopkins. The thermohaline forcing of the Gibraltar exchange. *Journal of Marine Systems*, 20:1–31, 1999.

[12] M. Astraldi, G.P. Gasparini, L. Gervasio, and E. Salusti. Dense water dynamics along the Strait of Sicily. *Journal of Physical Oceanography*, 31:3457–3475, 2001.

[13] D. Antoine, A. Morel, and J.M André. Algal pigment distribution and primary production in the eastern Mediterranean as derived from CZCS observations. 100:16193–1621, 1995.

[14] F. D'Ortenzio. Space and time occurrence of algal blooms in the Mediterranean: their significance for the trophic regime of the basin. *PhD Thesis, Open University of London, UK*, 2003.

[15] G. Crispi, A. Crise, and E. Mauri. A seasonal three-dimensional study of the nitrogen cycle in the Mediterranean Sea: Part II. Verification of the energy constrained trophic model. *Journal of Marine Systems*, 20:357–379, 1999.

[16] Thingstad and Rassoulzadegan. Conceptual models for the biogeo- chemical role of the photic zone microbial food web, with par- ticular reference to the Mediterranean Sea. *Prog. Oceanogr.*, 44:271–286, 1999.

[17] T. Moutin and P. Raimbault. Primary production, carbon export and nutrients availability in western and eastern Mediterranean Sea in early summer 1996 (MINOS cruise). *Journal of Marine Systems*, 842:273–288, 2002.

[18] E. Rohling. Review and new aspects concerning the formation of eastern Mediterranean sapropels. *Marine Geology*, 122:1–28, 1994.

[19] E. Olaussen. Studies of deep-sea cores. *Rep. Swed. Deep-Sea Exped., 1947–1948*, 8:323–438, 1961.

[20] E. Rohling. The dark secret of the Mediterranean - a case history in past. *environmental reconstruction*, 2005.

[21] E.J. Rohling and F.J. Hilgen. The eastern Mediterranean climate at times of sapropel formation: a review. *Geologie en Mijnbouw*, 70:253–264, 1991.

[22] P.G. Myers, K. Haines, and E. Rohling. Modeling the paleocirculation of the Mediterranean: the last glacial maximum and the Holecene with emphasis on the formation of sapropel S1. *Paleoceanography*, 13:586–606, 1998.

[23] P. Myers and K. Haines. Stability of the Mediterranean's thermohaline circulation under modified surface evaporative fluxes. *J. Geophys. Res.*, 107, 2002.

[24] E. Rohling. Environmental control on Mediterranean salinity and δ18O. *Paleoceanography*, 14:706–715, 1999.

[25] A. Cramp and G. O'Sullivan. Neogene sapropels in the Mediterranean: a review. *Marine Geology*, 153:11–28, 1999.

[26] E.J. Rohling, E.C. Hopmans, and J.S. Sinninghe-Damste. Water column dynamics during the last interglacial anoxic event in the Mediterranean (sapropel S5). *Paleoceanography*, 21:2018, 2006.

[27] P. Malanotte-Rizzoli, B.B. Manca, M. Ribera d'Alcalà, A. Teocharis, et al. A synthesis of the Ionian Sea Hydrography, Circulation and water mass pathways during POEM-phase I. *Progress in Oceanography*, 39:153–204, 1997.

[28] A. Murat and H. Got. Organic carbon variations of the eastern Mediterranean Holocene sapropel: a key for understanding formation processes. *Palaeogeography, Palaeoclimatology, Palaeoecology*, 158:241–257, 2000.

[29] W. Roether and R. Well. Oxygen consumption in the Eastern Mediterranean. *Deep-Sea Research I*, 48:1535–1551, 2001.

[30] B. Klein, W. Roether, N. Kress, B.B. Manca, M. Ribera d'Alcala, et al. Accelerated oxygen consumption in eastern Mediterranean deep waters following the recent changes in thermohaline circulation. *Journal of Geophysical Research*, 108:8107, 2003.

[31] P.R. Betzer, W.J. Showers, E.A. Laws, C.D. Winn, G.R. Ditullio, and P.M. Kroofnick. Primary productivity and partiele fluxes on a transect of the equator at 153 °W in the Pacific Ocean. *DeepSea Research*, 31:1–11, 1984.

[32] R. La Ferla, M. Azzaro, G. Civitarese, and M. Ribera d'Alcala'. Distribution patterns of carbon oxidation in the eastern Mediterranean Sea: Evidence of changes in the remineralization Processes. *Journal of Geophysical Research*, 108:8111, 2003.

[33] R.C. Thunnel, R. Varela, M. Llano, et al. Organic carbon fluxes, degradation, and accumulation in an anoxic basin: Sediment trap results from the Cariaco Basin. *Limnol. Oceanogr.*, 45:300–308, 2000.

[34] C. Slomp, J. Thomson, and G.J. De Lange. Enhanced regeneration of phosphorus during formation of the most recent eastern Mediterranean sapropel (S1). *Geochimica et Cosmochimica Acta*, 66:1171–1184, 2002.

[35] T. Takahashi, W.S. Broecker, and S. Langer. Redfield ratio based on chemical data from Isopycnal surfaces. *Journal of Geophysical Research*, 90:6907–6924, 1985.

[36] Z. Markaki, K. Oikonomou, M. Kocak, G. Kouvarakis, et al. Atmospheric deposition of inorganic phosphorus in the Levantine Basin, eastern Mediterranean: Spatial and temporal variability and its role in seawater productivity. *Limnology and Oceanography*, 48:1557–1568, 2003.

[37] M.D. Krom, B. Herut, and R.F.C. Mantoura. Nutrient budget for the Eastern Mediterranean: Implications for phosphorus limitation. *Limnology and Oceanography*, 49:1582–1592, 2004.

[38] U. Struck, K-C Emeis, M. Voss, M.D. Krom, and G.R. Rau. Biological productivity during sapropel S5 formation in the Eastern Mediterranean Sea: Evidence from stable isotopes of nitrogen and carbon. *Geochimica et Cosmochimica Acta*, 65:3249–3266, 2001.

[39] E.J. Rohling and W.W.C. Gieskes. Late Quaternary changes in Mediterranean Intermediate Water density and formation rate. *Paleoceanography*, 4:531–545, 1989.

[40] J.S.L. Casford, E.J. Rohling, R.H. Abu-Zied, S. Cooke, et al. Circulation changes and nutrient concentrations in the late Quaternary Aegean Sea: A nonsteady state concept for sapropel formation. *Paleocenaography*, 17:1024, 2002.

[41] J.S.L. Casford, E.J. Rohling, R.H.Abu-Zied, C. Fontanier, et al. A dynamic concept for eastern Mediterranean circulation and oxygenation during sapropel formation. *Palaeogeography, Palaeoclimatology, Palaeoecology*, 190:103–119, 2003.

[42] P. Meyers. Paleoceanographic and paleoclimatic similarities between Mediterranean sapropels and Cretaceous black shales. *Palaeogeography, Palaeoclimatology, Palaeoecology*, 235:305– 320, 2006.

[43] S. Rahmstorf. Bifurcations of the Atlantic thermohaline circulation in response to changes in the hydrological cycle. *Nature*, 378:145– 149, 1995.

[44] O. Thual and J. C. McWilliams. The catastrophe structure of thermohaline convection in a two-dimensional fluid model and comparison with low- order box models. *Geophysical and Astrophysical Fluid Dynamics*, 64:67–95, 1991.

Marine Organic Aerosol: Advances in Chemical Characterization and New Evidences of the Link with Oceanic Biological Activity

M. Rinaldi, S. Decesari, C. Carbone, E. Finessi, L. Giulianelli, S. Fuzzi, M.C. Facchini
Institute of Atmospheric Sciences and Climate, CNR, Bologna, Italy
m.rinaldi@isac.cnr.it

Abstract

Marine aerosol constitutes one of the most important natural aerosol systems at the global level and comprises both organic and inorganic components of primary and secondary origin. Primary aerosol particles are generated via wind driven bubble bursting processes at the ocean surface (sea-spray), while secondary components can be formed by gas-to-particle conversion or by chemical transformation of species present in the condensed phase. The work presents new results on organic marine aerosol and its link with oceanic biological productivity. Laboratory experiments have shown that sea-spray aerosol originating from highly biologically active sea water has a significant organic fraction, which increases with decreasing particle size, up to 77$\pm$5% below 0.25 μm diameter. Submicron sea-spray organic matter is mainly water-insoluble and composed of phytoplankton exudates (mainly lipopolysaccharides). With regard to secondary organic aerosols (SOA), new components have been detected: dimethyl and diethyl amine salts (DMA and DEA) turned out to be the most abundant organic species, alongside methanesulphonic acid, in fine marine particles over the North Atlantic. Clear evidence of a marine biological origin for DMA and DEA has been observed, pointing to a new atmospheric organic nitrogen global source, with a seasonality connected to oceanic biological productivity and an atmospheric cycle parallel to that of the organosulphur species.

1 Introduction

Marine aerosol constitutes one of the most important natural aerosol systems globally. It strongly influences the Earth's radiative budget, and biogeochemical cycling, with impacts on ecosystems and even on regional air quality [1].

Marine aerosol comprises both primary and secondary components. Primary aerosol production derives from the interaction of wind with the ocean surface and results in the mechanical production of sea-spray aerosol. A major source of primary marine aerosol is the bursting of air bubbles produced by breaking waves (e.g., [2]). Traditionally, sea-spray has been assumed as composed of sea salt and water, with water reaching equilibrium with the vapour phase after ejection. However, past evidence has been reported of scavenging of surface active organic material from bulk seawater, followed by its transport to the air-sea interface and then to the

atmosphere by rising bubbles [3, 4, 5, 6, 7]. The result of this process must be an internally mixed primary marine aerosol composed of sea salt and organics, in which the organic fraction can be a major component, at least when the sea surface layer is enriched in organic compounds (phytoplankton blooming periods). Chamber experiments and calculations indicate that the sea-to-air flux of organics via bubble bursting increases with decreasing bubble size [8, 9], and therefore the contribution of the scavenged organic matter to the total spray mass is expected to be more important in the submicron fraction.

Secondary aerosol production occurs in the marine boundary layer (MBL) in the following three ways: (a) new particle formation via the nucleation of stable clusters of the order of 0.5-1 nm in size (once formed, such clusters can grow to larger sizes via condensation processes); (b) cluster/particle growth via heterogeneous reactions and aqueous phase oxidation of dissolved gases or (c) chemical transformation of primary components present in the condensed phase. In terms of secondary marine aerosol production, sulphur species involved in the Dimethylsulphide (DMS) cycle are the most studied components [10, 11]. DMS produced by phytoplankton is released from the ocean into the atmosphere, where it undergoes oxidation to form SO_2, H_2SO_4 and organic compounds, the most important of which is methanesulfonic acid (MSA). DMS itself and DMS oxidation products can condense on pre-existing aerosols and cloud droplets, thereby contributing to the particulate phase and to non-sea-salt sulphate (nss-SO_4^{-2}) through liquid phase oxidation reactions (e.g. [12, 13]. Potential components of secondary aerosol in the MBL include secondary organic aerosols (SOA) produced by the oxidation of gaseous precursors emitted by the marine biota [14]. The oxidation process may take place in the gas-phase [15, 16], at the particle surface [17, 18] or in the aqueous phase [19, 20]. In this regard, marine aerosol has been found to contain carboxylic and dicarboxylic acids [21, 22] to which a secondary origin has been attributed. However, oxidized organics can also be produced by the oxidative degradation of primary particles generated by sea spray and rich in fatty acids [21]. Recently, the oxidation of isoprene produced by phytoplankton has been also proposed as an important source of SOA in marine particles [23]. Nevertheless, the observed high concentrations of oxidized organic matter in marine aerosol largely remain unexplained, suggesting that other formation processes and alternative SOA components should be considered.

In this work we provide an overview of the results on marine aerosol chemical composition obtained from measurements performed at Mace Head (Ireland), since 2002, with a main focus on the outcomes achieved within the framework of the EU project MAP (Marine Aerosol Production; http://macehead.nuigalway.ie/map/).

2 Experimental approach

Starting in 2002, the ISAC-CNR atmospheric chemistry group in collaboration with the University of Galway has been experimenting a specific sampling and analysis procedure for the chemical characterization of unperturbed marine aerosol at Mace Head research station (Figure 1). An automated sectorized sampling system was set up to control the aerosol sampling, allowing collection only in air masses (1)

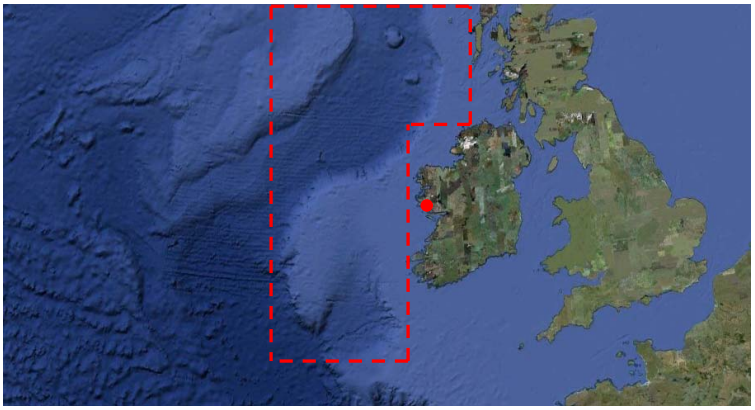

Figure 1: Map of the sampling sites: the red dot indicates the position of Mace Head atmospheric research station while the dashed red line delimits the area interested by the Celtic Explorer cruise (June-July 2006). Map from Google maps (http://maps.google.it).

reaching the site from a controlled oceanic clean sector between 180° and 300°, (2) with a total particle concentration below 700 cm^{-3}, and (3) with BC concentration lower than 50 $ng{\cdot}m^{-3}$, in order to avoid continental and anthropic influences. Aerosol has been collected on multistage impactors and high volume samplers, and analyzed for the main soluble ions (ion chromatography), water soluble and insoluble organic carbon and for water soluble nitrogen (C/N elemental analyzer). The organic characterization has been achieved through a set of analytical techniques, namely ^{1}H NMR [24], HPLC-TOC [25] and surface tension measurements [26].
In the framework of the EU project MAP, this expertise was applied to coastal measurements at Mace Head, for the entire year of 2006, and onboard the oceanographic vessel Celtic Explorer, during a campaign off the Irish coast between June and July 2006 (Figure 1).

3 Marine aerosol chemical composition

The most complete size segregated chemical characterisation of unperturbed marine aerosols was described in two papers based on measurements performed at Mace Head [27, 28]. Here, for the first time in literature, it was shown that marine aerosol chemical composition is influenced by the oceanic biological yearly cycle. Two different aerosol compositions were observed for the low biological activity period (LBA, winter) and the high biological activity period (HBA, spring to autumn). During the LBA period, sea-salt dominated all the aerosol size fractions, with a 74% (0.3 $\mu g \cdot m^{-3}$) contribution to the accumulation mode mass. The remainder of the mass in this mode comprised 10% (0.045 $\mu g \cdot m^{-3}$) non-sea-salt sulphate and 15% (0.070 $\mu g \cdot m^{-3}$) organic matter (OM). By contrast, in the HBA period, the OM fraction increased markedly, particularly for the submicrometre sizes, and this frac-

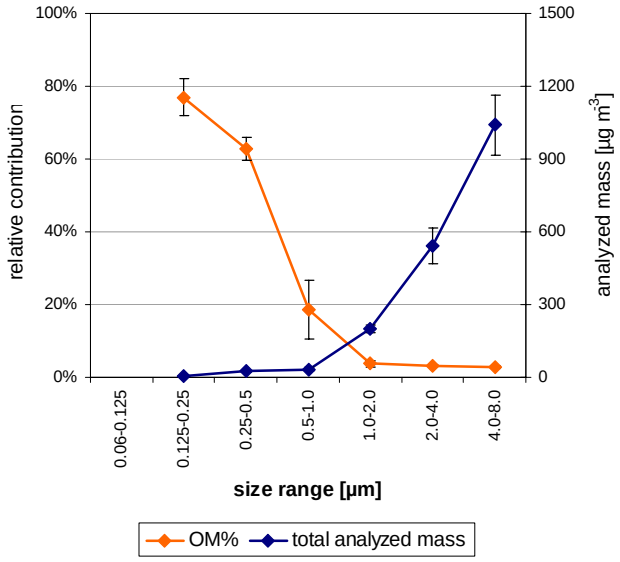

Figure 2: Average relative contribution of organic matter in sea-spray particles as a function of size (orange) and average mass size distribution of the sea spray samples (blue). Error bars represent ± 1 standard deviation.

tion increased with decreasing size. For the HBA period, OM in the accumulation mode accounted for 65% (0.619 $\mu g \cdot m^{-3}$) of the mass, whereas sea salt accounted for 10% (0.097 $\mu g \cdot m^{-3}$) and nss-sulphate for 23% (0.216 $\mu g \cdot m^{-3}$). The largest percentage contribution (83%) of OM occurred in the fine mode (0.06-0.125 μm). Across the size range from 0.06 to 0.5 μm, the average contributions of water insoluble (WIOM) and water soluble (WSOM) organics were 45% and 18%, respectively. It was also evidenced how seasonal concentration trends for the main marine aerosol components measured at Mace Head were related to the oceanic biological activity cycle, using satellite chlorophyll-a maps over the North Atlantic Ocean as a large scale proxy for biologic activity [29]. Very recently, similar observations were made in the Southern Hemisphere (Amsterdam Island), by [30], who observed a clear seasonal pattern for organic aerosols, with maximum values during the austral summer and minimum concentrations during winter. Such seasonal variation of organic concentration was found to be almost entirely related to the water-insoluble organic carbon fraction, in analogy with [27], thus suggesting an important primary origin for organics, most probably through bubble bursting processes.

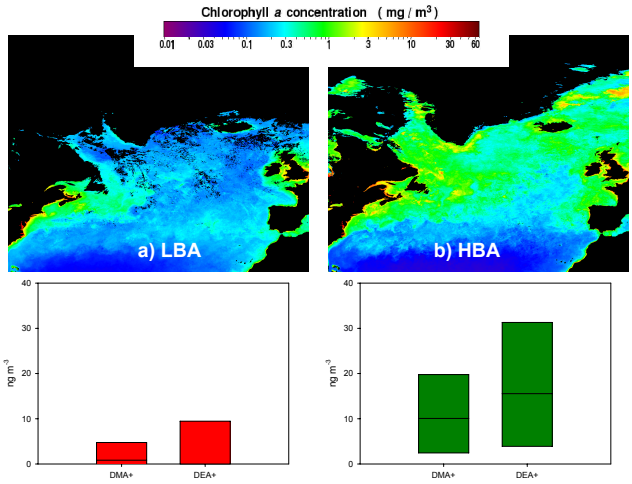

Figure 3: Top: average chlorophyll-a concentration over the North Atlantic Ocean during a) winter 2005-2006 and b) spring 2006. The chlorophyll map was obtained by level 3 products from MODIS (http://oceancolor.gsfc.nasa.gov/). Bottom: box plots indicating median, 25th and 75th percentiles of DMA^+ and DEA^+ aerosol concentrations measured in a) LBA and b) HBA conditions at Mace Head, during MAP. Concentrations below detection limit have been considered as zero in the plotting.

4 Chemical characterization of sea-spray organics

The chemical properties of sea-spray aerosol particles produced by artificially generated bubbles, using oceanic waters rich in organic matter, during periods of phytoplankton bloom, were investigated in an experiment carried out in the North Atlantic during the Celtic Explorer cruise (Figure 1). Details on the experimental setup can be found in [31]. Briefly, bubble bursting was induced in freshly collected, highly biologically active, oceanic water, and the resulting sea-spray particles were collected and analyzed.

The average relative contribution of organic matter in sea-spray particles, as a function of size, resulting from the experiment is shown in Figure 2, together with the average mass size distribution of the sea-spray samples. Spray particles exhibit a progressive increase in the organic matter (OM) content from 3 $\pm$ 0.4% up to 77 $\pm$ 5%, with decreasing particle diameter from 8 to 0.125 μm. The OM transferred within the submicron particles generated by bubble bursting was mainly water insoluble (WIOM) (on average 94 $\pm$ 4% of total carbon), while the organic water soluble fraction (WSOM) increased its contribution (up to 33 $\pm$ 3%) of total carbon in the coarse size interval (4-8 μm). Chemical characterization by ^{1}H NMR showed a striking similarity between WIOM and the seawater particulate organic carbon (POC)

fraction smaller than 10 μm, demonstrating that the less hydrophilic fraction of oceanic OM is preferentially transported into the atmosphere by the bubble bursting process. In addition, the ^{1}H NMR spectral fingerprint of WIOM was similar to that of macrogel samples collected from the Adriatic Sea surface [32] with a composition dominated by lipopolysaccharides. These compounds are known from the seawater chemistry literature for their various degrees of aggregation, ranging from colloids to microgels and to large POC particles [33] and for their surface active properties. The pattern of WIOM and sea-salt content in the different size intervals observed within the bubble bursting experiment was similar to that measured in atmospheric marine aerosol samples collected during periods of high biological activity (HBA), pointing to a WIOM/sea-salt fingerprint associated to submicron primary marine aerosol production in biologically rich waters. For this reason most of the WIOM was attributed here to primary production and, consequently, WSOM was mainly ascribed to secondary production.

The above findings are also in agreement with the work of [34], in which the authors reported the results of sea salt and organic carbon measurements in water extracts of nascent marine aerosol, showing a strong enrichment of organic matter in all size fractions, with the highest in the smallest size fractions ($\sim$ 80% of the measured mass for 0.13 μm particles). However, the authors did not distinguish between water soluble and insoluble organics, thus providing no information on the solubility and surface active properties of primary organic matter.

5 A newly identified SOA component in marine aerosol

Important organic aerosol components, dimethyl and diethyl-ammonium salts (DMA^+ and DEA^+), were identified over the North Atlantic Ocean, through coastal and onboard measurements, performed at Mace Head and during the Celtic Explorer cruise, respectively [35]. DMA^+ and DEA^+ were found to be the most abundant organic species, second only to MSA, detected in submicron marine particles, together ranging between $<$0.4 and 56 ng$\cdot$m^{-3}. During HBA periods alkyl-ammonium salts represented on average 11% of the marine SOA and a dominant fraction (35% on average) of the aerosol water soluble organic nitrogen (WSON).

There is considerable evidence that DMA^+ and DEA^+ are secondary aerosol components, and that they originate from biogenic gaseous precursors emitted by the ocean. Their size distributions exhibited maxima in the accumulation mode, as is also the case for other well known secondary components (nssSO_4^{-2}, NH_4^+, MSA), supporting the hypothesis that a gas-to-particle conversion process is responsible for the accumulation of alkyl-ammonium salts in the fine aerosol fraction. The most likely hypothesis is that gaseous dimethylamine and diethylamine react with sulphuric acid or acidic sulphates, accumulating within aerosol particles in close analogy with ammonia. Regarding the precursor origin, a main anthropogenic source of gaseous alkyl-amines over the ocean can be excluded, because the aerosol DMA^+ and DEA^+ concentrations measured at Mace Head, were always higher in clean marine samples (roughly double) than in pol-

luted air masses, in analogy with MSA. Like other reduced biogenic gases (DMS, CH_4) and in analogy to NH_3, DMA and DEA could be the end products of microbial turnover of marine labile organic matter [36, 37, 38]. Furthermore, alkyl-ammonium ions in submicron aerosol particles showed the typical seasonal variation of biogenic components, with high concentrations measured in the HBA period, and much lower concentrations in the LBA period (Figure 3).

The importance of amine salts in marine aerosol has recently been confirmed by [39], who reported similar concentrations of DEA^+ (10-50 $ng{\cdot}m^{-3}$) in clean air masses over the Pacific Ocean, also evidencing a qualitative correlation between DEA^+ aerosol concentrations and oceanic biological activity (chlorophyll-a surface concentration). Measurements performed at lower latitudes (Cape Verde) also confirm the presence of alkyl-ammonium salts in submicron marine particles associated to algal blooms, but in lower atmospheric concentrations [40]. This is probably related to the lower biological productivity of tropical waters.

6 Future perspectives

Notwithstanding recent advances in the chemical characterization and source identification of submicron marine aerosol, the present knowledge of the system remains incomplete.

Most recent results on sea-spray composition have shown that in conditions of intense oceanic biological productivity, submicron primary marine aerosol is mainly composed of insoluble and surfactant organic matter. Such information is currently not accounted for in most global models, determining a biased calculation of sea-spray mass and, consequently, of the direct and indirect radiative aerosol effect. Moreover, a potentially important atmospheric source of organic carbon is neglected in estimating the global carbon budget. A novel approach to developing a combined organic-inorganic submicron sea-spray source function for inclusion in large-scale models, with wind speed and surface ocean chlorophyll-a concentration as input parameters, has been presented [41] and tested with satisfactory results [42]. However, the modelling of primary marine organic production is still challenging and further data, from laboratory studies and worldwide field measurements, are necessary for function validation and improvement. The development of satellite measurements of dissolved and particulate organic matter at the ocean surface will probably provide tools to better predict the organic sea-spray production potential of the ocean as a function of space and time, improving current modelling capacity.

At present, nothing is known of the fate of primary marine organics once emitted in atmosphere. Their processing could be a source of oxygenated compounds in the condensed phase, but might also lead to the formation of volatile products possibly involved in SOA formation. Further investigations are required to address this issue.

As for secondary organics in the MBL, most marine aerosol WSOM is still uncharacterized at the molecular level. New insight on marine organic aerosol chemical composition is expected to be gained from the coupling of statistical methods (namely PMF) with traditional off-line (NMR, IR, etc.) or new on-line (AMS) aerosol analysis techniques (Decesari et al., in preparation). Water soluble organic nitrogen measurements showed an important fraction of

uncharacterised nitrogen-bearing organic compounds in marine aerosol: DMA^+ and DEA^+ accounted only for about one third of the WSON. A fraction of the unaccounted organic nitrogen, especially during the warm season, can reasonably be attributed to products of the oxidative degradation of the same alkyl ammonium salts. Nevertheless, alternative sources of unaccounted water soluble organic nitrogen, e.g. the oxidation of insoluble primary organic material emitted by sea-spray, cannot be ruled out at present, although further studies are necessary to clarify this point. Further work is also necessary to better characterise the marine aerosol water soluble organic nitrogen, in order to define its role in the marine boundary layer chemistry and in the global nitrogen biogeochemical cycle.

References

[1] C.D. O'Dowd and G. de Leeuw. Marine aerosol production: a review of the current knowledge. *Philosophic Transaction of the Royal Society A*, 365:1753–1774, 2007.

[2] D.C. Blanchard. The electrification of the atmosphere by particles from bubbles in the sea. *Progress in Oceanography*, 1:71–102, 1963.

[3] D.C. Blanchard. Sea to air transport of surface active material. *science*, 146:396–397, 1964.

[4] D.C. Blanchard. Bubble scavenging and the water-to-air transfer of organic material in the sea. *Adv. Chem. Series*, 145:360–387, 1975.

[5] E.J. Hoffman and R.A. Duce. Factors influencing the organic carbon content of marine aerosols: A laboratory study. *Journal of Geophysical Research*, 81:3667–3670, 1976.

[6] G.T. Wallace and R.A. Duce. Transport of particulate organic matter by bubbles in marine waters. *Limnology and Oceanography*, 23:1155–1167, 1978.

[7] R.A. Skop, W.G. Lindsley, and J.W. Brown. Radiotracer studies of surfactant transport to the sea-air interface by submillimeter-size bubbles. *Exp. Fluids*, 10:251–256, 1991.

[8] R.-S. Tseng, J.T. Viechnicki, R.A. Skop, and J.W. Brown. Sea-to air transfer of surface-active organic compounds by bursting bubbles. *Journal of Geophysical Research*, 97:5201–5206, 1992.

[9] C. Oppo, S. Bellandi, N. Degli Innocenti, A.M. Stortini, G. Loglio, E. Schiavuta, and R. Cini. Surfactant components of marine organic matter as agents for biogeochemical fractionation and pollutant transport via marine aerosols. *Marine Chemistry*, 63:235–253, 1999.

[10] G.E. Shaw. Bio-controlled thermostasis involving the sulfur cycle. *Climatic Change*, 5(3):297–303, 1983.

[11] R.J. Charlson, J.E. Lovelock, M.O. Andreae, and S.G. Warren. Oceanic phytoplankton, atmospheric sulfur, cloud albedo and climate. *nature*, 326(655-661), 1987.

[12] G.P. Ayers, M.E. Cainey, H. Granek, and C. Leck. Dimethylsulfide oxidation and the ratio of methanesulfonate to non sea-salt sulfate in the marine aerosol. *Journal of Atmospheric Chemistry*, 25:307–325, 1996.

[13] F.A. Campolongo, A. Saltelli, N.R. Jensen, J. Wislon, and J. Hjorth. The role of multiphase chemistry in the oxidation of dimethylsulphide (DMS): A latitude dependent study. *Journal of Atmospheric Chemistry*, 32:327–356, 1999.

[14] G.B. Ellison, A.F. Tuck, and V. Vaida. Atmospheric processing of organic aerosols. *Journal of Geophysical Research*, 104:11633–1164, 1999.

[15] B.K. Pun, S. Seigeur, D. Grajean, and P. Saxena. Gas-phase formation of water soluble organic compounds in the atmosphere: A retrosynthetic analysis. *Journal of Atmospheric Chemistry*, 35:199–223, 2000.

[16] R.J. Griffin, D. Dadbub, and J.H. Seinfeld. Secondary organic aerosols. 1: Atmospheric chemical mechanism for production of molecular constituents. *Journal of Geophysical Research*, 107, 2002.

[17] T.L. Eliason, J.B. Gilman, and V. Vaida. Oxidation of organic films relevant to atmospheric aerosols. *Atmospheric Environment*, 38:1367–1378, 2003.

[18] S.F. Maria, L.M. Russell, M.K. Giles, and S.C.B. Myneni. Organic aerosol growth mechanisms and their climate-forcing implications. *Nature*, 306:1921–1924, 2004.

[19] B. Ervens, C. George, J.E. Williams, G.V. Buxton, G.A. Salmon, M. Bydder, F. Wilkinson, F. Denter, P. Miranel, R. Wolke, and J. Hermann. CAPRAM2.4 (MODAC mechanism): An extended and condensed tropospheric aqueous phase mechanism and its application. *Journal of Geophysical Research*, 108, 2003.

[20] P. Warnick. In-cloud chemistry opens pathway to the formation of oxalic acid in the marine atmosphere. *Atmospheric Environment*, 37:2423–2427, 2003.

[21] K. Kawamura and F. Sakaguchi. Molecular distributions of water soluble dicarboxylic acids in marine aerosols over the Pacific Ocean including tropics. *Journal of Geophysical Research*, 104:3501–3509, 1999.

[22] V.-M. Kerminen, K. Teinilä, R. Hillamo, and T. Mäkelä. Size-segregated chemistry of particulate dicarboxylic acids in the Arctic atmosphere. *Atmospheric Environment*, 33(13):2089–2100, 1999.

[23] N. Meskhidze and A. Nenes. Phytoplankton and cloudiness in southern ocean. *Science*, 314:1419–1423, 2006.

[24] S. Decesari, M.C. Facchini, S. Fuzzi, and E. Tagliavini. Characterisation of water-soluble organic compounds in atmospheric aerosol: A new approach, Journal of Geophysical Research. *Journal of Geophysical Research*, 105:1481–1489, 2000.

[25] V. Mancinelli, M. Rinaldi, E. Finessi, L. Emblico, M. Mircea, S. Fuzzi, M.C. Facchini, and S. Decesari. An improved anion exchange chromatographic method for water-soluble organic carbon analysis in atmospheric samples. *Journal of Chromatography A*, 1149:385–389, 2007.

[26] S. Decesari, M.C. Facchini, M. Mircea, F. Cavalli, and S. Fuzzi. Solubility properties of surfactants in atmospheric aerosol and cloud/fog water samples. *Journal of Geophysical Research*, 108(21), 2003.

[27] C.D. O'Dowd, M.C. Facchini, F. Cavalli, D. Ceburnis, M. Mircea, S. Decesari, S. Fuzzi, Y.J. Yoon, and J.-P. Putaud. Biogenically driven organic contribution to marine aerosol. *Nature*, 431:676– 680, 2004.

[28] F. Cavalli, M.C. Facchini, S. Decesari, M. Mircea, L. Emblico, S. Fuzzi, D. Ceburnis, Y.J. Yoon, C.D. O'Dowd, J.-P. Putaud, and A. Dell'Acqua. Advances in characterisation of size resolved organic matter in marine aerosol over the North Atlantic. *Journal of Geophysical Research*, 109, 2004.

[29] Y.J. Yoon, D. Ceburnis, F. Cavalli, O. Jourdan, J.-P. Putaud, M.C. Facchini, S. Decesari, S. Fuzzi, S.G. Jennings, and C.D. O'Dowd. Seasonal characteristics of the physico-chemical properties of North Atlantic marine atmospheric aerosols. *Journal of Geophysical Research*, 112, 2007.

[30] J. Sciare, O. Favez, R. Sarda-Estève, K. Oikonomou, H. Cachier, and V. Kazan. Long-term observations of carbonaceous aerosols in the Austral Ocean atmosphere: Evidence of a biogenic marine organic source. *Journal of Geophysical Research*, 114, 2009.

[31] M.C. Facchini, M. Rinaldi, S. Decesari, C. Carbone, E. Finessi, M. Mircea, S. Fuzzi, D. Ceburnis, R. Flanagan, E.D. Nilsson, G. de Leeuw, M. Martino, J. Woeltjen, and C.D. O'Dowd. Primary submicron marine aerosol dominated by insoluble organic colloids and aggregates. *Geophysical Research Letters*, 35, 2008.

[32] N. Kovac, O. Bajt, J. Faganelli, B. Sket, and B. Orel. Study of macroaggregate composition using FT-IR and 1H NMR spectroscopy. *Marine Chemistry*, 78:205–215, 2002.

[33] J. Zhou, K. Mopper, and U. Passow. The role of surface-active carbohydrates in the formation of transparent exopolymer particles by bubble adsorption of seawater. *Limnology and Oceanography*, 43:1860– 1871, 1998.

[34] W.C. Keene, H. Maring, J.R. Maben, D.J. Kieber, A.A.P. Pszenny, E.E. Dahl, M.A. Izaguirre, A.J. Davis, M.S. Long, X. Zhou, L. Smoydzin, and R. Sander. Chemical

and physical characteristics of nascent aerosols produced by bursting bubbles at a model air-sea interface. *Journal of Geophysical Research*, 112, 2007.

[35] M.C. Facchini, S. Decesari, M. Rinaldi, C. Carbone, E. Finessi, M. Mircea, S. Fuzzi, F. Moretti, E. Tagliavini, D. Ceburnis, and C.D. O'Dowd. Important Source of Marine Secondary Organic Aerosol from Biogenic Amines. *Environmental Science Technology*, 42(24):9116–9121, 2008.

[36] S.W. Gibb, C. Mantoura, and P. Liss. Ocean-Atmosphere Exchange and Atmospheric Speciation of Ammonia and Methylamines in the Region of the NW Arabian Sea. *Global Biogeochemical Cycles*, 13(1):161–178, 1999.

[37] D.A. Hansell and C.A. Carlson. Biogeochemistry of Marine Dissolved Organic Matter. 2002.

[38] M. Johnson, R. Sanders, V. Avgoustidi, M. Lecas, L. Brown, D. Hansell, M. Moore, S. Gibb, P. Liss, and T. Jickells. Ammonium accumulation during a silicate-limited diatom bloom indicates the potential for ammonia emission events. *Marine Chemistry*, 106:63–75, 2007.

[39] A. Sorooshian, L.T. Padrò, A. Nenes, G. Feingold, A. McComiskey, S.P. Hersey, H. Gates, H.H. Jonsson, S.D. Miller, G.L. Stephens, R.C. Flagan, and J.H. Seinfeld. On the link between ocean biota emissions, aerosol, and maritime clouds: Airborne, ground, and satellite measurements off the coast of California. *Global Biogeochemical Cycles*, 23, 2009.

[40] C. Müller, Y. Iinuma, J. Karstensen, D. van Pinxteren, S. Lehmann, T. Gnauk, and H. Herrmann. Seasonal variation of aliphatic amines in marine sub-micrometer particles at the Cape Verde islands. *Atmospheric Chemistry and Physics*, 9:9587–9597, 2009.

[41] C.D. O'Dowd, B. Langmann, S. Varghese, C. Scannell, D. Ceburnis, and M.C. Facchini. A combined organic-inorganic sea-spray source function. *Geophysical Research Letters*, 35, 2008.

[42] E. Vignati, M.C. Facchini, M. Rinaldi, C. Scannell, D. Ceburnis, J. Sciare, M. Kanakidou, S. Myriokefalitakis, F. Dentener, and C.D. O'Dowd. Global scale emission and distribution of sea-spray aerosol: Sea-salt and organic enrichment. *Atmospheric Environment*, 2010.

Rare Earth Elements Behaviour in Marine Systems: the Mediterranean Sea, an Epicontinental Context

L.A. Randazzo[1,2,3], P. Zuddas[2,1], M. Raso[3], E. Tamburo[3], P. Aricò[1], P. Censi[3,1]

1, Institute for Coastal Marine Environment, CNR, Capo Granitola (TP), Italy

2, Department of Earth Sciences, University "Claude Bernard" Lyon 1, Villeurbanne, France

3, DiSTeM, University of Palermo, Palermo, Italy

censi@unipa.it

Abstract

This work synthesises the literature on the distribution of Rare Earth Elements (REE) between dissolved phases and suspended particulate matter in the seawater system. We focalize the attention on Mediterranean Sea, an epicontinental basin located at the shared of the boundary Europe, Africa and Asia that receives external input of anthropogenic and lithogenic origin. Sampling areas vary from coastal to open sea and from surface to deep-sea. Due to their particular chemical characters REE represent useful tracer in a wide range of geochemical processes leading to detailed descriptions of processes occurring at solid-liquid interface along the water columns. Their external electronic configuration, for example, allows us to differentiate between the scavenging reactions and the cation exchange at the dissolved phase / suspended media interface. These processes are traced through Y/Ho ratios, selected elemental anomalies and by shape and features of shale normalised REE patterns. The REE behaviour and distribution between suspended and dissolved media of Mediterranean seawater reveal that the majority of dissolved trace elements are due to atmospheric fallout. In the Eastern and Central part of the basin the input is driven by aeolian transport of Saharan dust whereas in the North-Western section it is associated with riverine loads and therefore, with a significant anthropic contribution. Moreover, delivery of large amounts of volcanic ejecta in recent years produced anomalous ratios of the REE behaviour in the Central Mediterranean. These comprehensive evidences highlighted the capability of Rare Earth Elements to represent a useful tool to trace geochemical processes in marine systems.

1 Inroduction

REE are a group of fourteen elements (La, Ce, Pr, Nd, Sm, Eu, Gd, Tb, Dy, Ho, Er, Tm, Yb and Lu) divided in light (LREE, from La to Pm), middle (MREE, from Sm to Ho) and heavy (HREE, from Er to Lu) REE. Pm, which can be produced by nuclear reactions, does not exist in nature in significant concentrations. REE occur in a trivalent oxidation state (except Ce and Eu) in natural environments and their chemi-

cal properties change systematically across the series from La to Lu. As a result of the f-electron shell being progressively filled, the effective ionic radii of REEs decreases systematically with increasing atomic number from La to Lu according to a phenomenon defined as "lanthanide contraction". Due to similar atomic dimensions and chemical behaviour induced by the same charge, also yttrium is associated to REE in geochemical investigations (REE).

REE distributions in marine environment were investigated during the last 30 years [1, 2, 3, 4], although these researches were often focused only on some REE due to analytical difficulties. More recently improvement of instrumental measurements (mainly based on Induced Coupled Plasma–Mass Spectrometry techniques) allowed the study all the REE series to investigate trace and ultra trace elements in several media and obtain a more complete information about the seawater system. Therefore, many chemical processes involving trace elements were described using lanthanides as tracers of hydrothermal processes [5, 6], ocean circulations and several other mechanisms that involved interface phenomena. Thus lanthanides began proxies of trace elements fluxes to seawater from surroundings, allowing to recognize aeolian inputs [7], river water outflows [8, 9, 10, 11, 12], vertical or horizontal migrations along the water columns or among different water masses also due to redox processes [13, 14, 15].

Byrne and Sholkovitz [16] carried out a detailed review of marine chemistry of lanthanides in marine systems with special attention to oceanic environments. Here we analyse the state of art of lanthanide geochemistry in coastal Mediterranean seawater systems to trace the origin and delivery of these trace elements to the water masses. The choice of Mediterranean Sea was strongly motivated by its particular geographical and geological characteristics. It is an epicontinental basin surrounded by densely populated and industrialised areas with a temperate climate at the northern side of basin and a large desert region at the southern side. In the former case, both lithogenic and anthropogenic materials are delivered to the basin involving both atmospheric and riverine inputs [17, 18]. On the contrary, the input from the South is essentially due to atmospheric fallout [19, 20, 21, 22]. In the Eastern Mediterranean sea delivery of continental waters occurs by means of Nile River that drained one of the world's largest watersheds before the building of the Aswan dam. Furthermore, large active volcanic structures with strong pyroclastic capabilities occur in the Central Mediterranean area in the Aeolian Islands, Pantelleria Island and Mount Etna, and REE can trace the effects of this particular atmospheric fallout. Although trace element geochemistry of marine systems in the Mediterranean Sea has been widely studied in the last two decades, the distribution of REEs was investigated only in limited areas (Figure 1). Therefore, the aim of this paper is to report the state-of-art of current knowledge about the distribution of REEs in the Mediterranean water system.

2 Dissolved REE distribution

In order to evaluate the processes involving REE distributions among different water column components, their shale-normalised concentrations [REE_i^{SN}] are generally considered. These can be calcu-

Figure 1: Location of sampling sites and studied area in the Mediterranean Sea.

lated according to the expression:

$$REE_i^{SN} = \frac{REE_i^{sample}}{REE_i^{shale}} \qquad (1)$$

where $[REE_i^{shale}]$ and $[REE_i^{sample}]$ are the content of each REE in the shales and samples, respectively. Resulting REE patterns can show elemental enrichments or depletions that are usually defined anomalies. Their amplitudes can be quantified based on the REE shale-normalised concentrations according to the following expression:

$$\frac{[REE_i]}{[REE_i]*} = \frac{2 * [REE_i]_n}{[REE_{i-1}]_n + [REE_{i+1}]_n} \qquad (2)$$

where subscript n represent the normalised concentration value of each REE, where $[REE_i]_n$ represents the normalised content of some REE, $[REE_{i-1}]_n$ and $[REE_{i+1}]_n$ represent the REE contents of the previous and the next REE and $[REE_i]$* is the expected value of some REE calculated as average between the previous and the next element.

The last twenty-five year investigations demonstrated that dissolved REE behaviour in marine systems is largely controlled by carbonate complexes [23, 24, 25] whose stability increases between La and Lu. Carbonate complexation maintains REE in the dissolved form under pH values close to 8, although REE are close to their solubility with respect to mixed-REE phosphate [26, 27, 28]. On the other hand, absorption removal processes generated by the stronger reactivity of suspended particles can locally modify the distribution of light and medium REE (LREE and MREE) with respect to HREE [29]. Moreover, oxidative Ce scavenging as insoluble Ce (IV) implies that shale-normalised REE patterns are also characterised by Ce negative anomalies, as shown in Figure 2. At the same time Y, which a similar distribution to Ho in crustal materials, is enriched in water in respect to the Ho due to the pref-

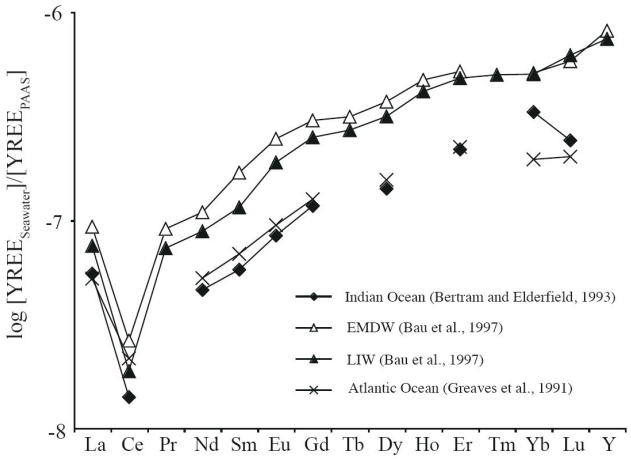

Figure 2: REE shale-normalised distributions in several seawater basins.

erential Ho removal onto suspended particulate matter from surface to deep seawater [30].

Circulation of water masses in the Mediterranean Sea is mainly characterised by the eastward inflow of shallow, less saline modified Atlantic water (MAW), through the Straits of Sicily and a westward outflow of the Levantine Intermediate Water (LIW). The last decade of oceanographic cruise investigations have been concentrated in this crucial area [31, 32, 33, 34, 35]. Bau et al.[36] demonstrate that there is an increase of REE concentrations due to dissolution of atmospheric particulate in water masses during their westward and eastward movements. This process is well evidenced in the Western basin where REE are punctually enriched in the shallow water layer with respect to Atlantic seawater as justified by dissolution of atmospheric particulate matter [37, 38].

In this scenario, that is quite usual in Mediterranean Sea, the effects of continental input from riverine sources, mainly expected in northern and western basins where the largest Mediterranean rivers are located, can influence REE distribution. Although the literature about REE distribution in Mediterranean coastal waters is poor [39], existing data account for the capability of REE to record anthropogenic signatures through the occurrence of positive Gd anomalies. These are related to discharges of wastewaters containing Gd-organic compounds used in medical practices [40, 41, 42]. Further evidences of anthropogenic signature in coastal waters are represented by shale-normalised MREE enrichments due to the delivery of continental waters that drained agricultural lands treated with phosphate-rich fertilisers [9, 10].

3 REE in suspended particulate matter (SPM)

The partitioning of trace elements between particles and seawater is controlled by the interplay of concurrent complexation onto

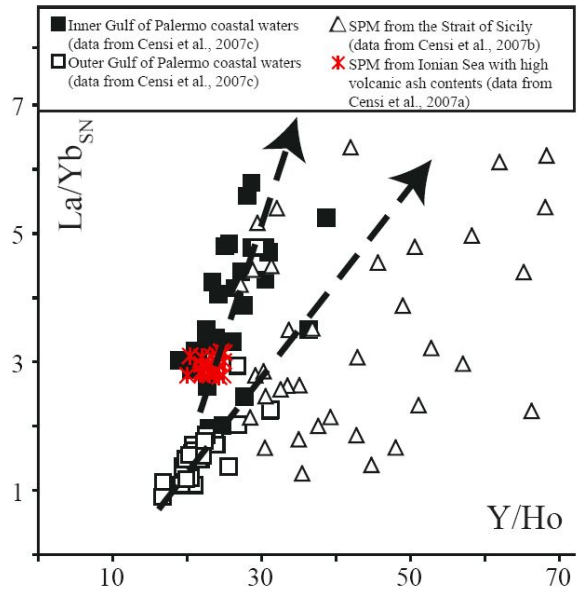

Figure 3: LREE/HREE fractionation (in terms of La/YbSN ratio) versus both Y/Ho ratio in SPM from several Mediterranean locations.

solid surfaces and solution [43, 44]. The extent to which trace elements are linked to different types of particles along the water column affects the kinetics of their removal. Therefore, the distribution of trace elements during these partitioning processes is usually defined in terms of elemental fractionation. In a marine environment, these mechanisms can be resumed in terms of LREE reactivity over SPM, due to their electron configurations, compared to the more soluble HREE [45]. Sholkovitz et al. [43] measured the differences in lanthanide contents of SPM (whose budget is dependent on local conditions) according to partial leaching experiments. Their results pointed out that the more soluble fraction has a flat behaviour, positive Ce anomaly, HREE depletion and the highest REE contents. On the contrary, in strong acid they observed a shale-like behaviour and a lack of Ce anomaly. Clearly, the last fraction represents the contribution of lithogenic materials to the REE budget in SPM, whereas the labile fraction corresponds to the organic-like authigenic matter coatings the lithogenic particulate. Moreover, the Ce anomaly values in labile fractions indicate that dissolved Ce(III) can be in situ oxidised to Ce(IV) that is scavenged along the upper water column. These results are confirmed by analogous studies carried out in Atlantic seawater where shale-normalised REE contents in SPM suggest that particulate Mn-oxides act as REE carriers from shallow to deep waters through an adsorption-desorption mechanism [14]. This agrees with results

showing an increase of the authigenic component with seawater depth [15].
Features of shale-normalised REE behaviour are an useful tool to discriminate authigenic from lithogenic fraction in SPM. This approach can be carried out according to several procedures based on selective digestion techniques, evaluation of LREE/HREE fractionations, or isotopic investigations of $^{143}Nd/^{144}Nd$ ratios. Grousset et al. [46] evidenced the influence of Saharan detrital aerosol particles on SPM budget in shallow waters, whereas the signature of Rhone river sediments was found in intermediate and bottom waters of Western Mediterranean margin. In the Eastern Mediterranean Basin, Tachikawa et al. [47], observed the effects of Nile River in terms of lithogenic suspended materials and the contribution of dissolved lanthanides in the water column. In the Central Mediterranean basin further investigations were carried out to discriminate different lithogenic materials from anthropic waste products and authigenic organic debris [48]. Figure 3 shows the effects of mixing among lithogenic products of volcanic origin, Saharan dust and authigenic particulate matter using La/YbSN ratios, representative of LREE/HREE fractionations, and Y/Ho ratio values. The increasing amount of authigenic particulate along the water column allows increasing of La/Yb for Y/Ho ratio values because authigenic particulates are mainly due to preferential LREE adsorption onto surfaces of lithogenic debris. Under these conditions also Y/Ho values are larger than "crustal" values (27-30) but La/Yb ratios represent by their primary origin. Therefore SPM enriched in lithogenic fraction fall along a different trend with respect to samples enriched in authigenic materials.

4 Summary and conclusion

The study of the whole REE series in different components of water column allows the assessment of input processes and fractionation mechanisms in marine system under different environmental conditions. These goals can be attained analysing features of shale-normalised REE patterns in terms of geochemical anomalies, fractionations of selected elements or groups of elements along the REE series in order to evaluate the effects of interface processes occurring along the water column that determine the dissolved composition of seawater.
In conclusion, we can say that the characterization of REE distribution in seawater is one of the most important tools for extensive geochemical examinations of the marine environment. It allows apprehending the wide range of processes and interactions between open sea, costal areas and atmosphere. This capability of REE to trace geochemical processes could be investigated in Mediterranean Sea due to the large environmental difference occurring in this basin as a consequence of its location and characters of surrounding. There results have been achieved involving extensively facilities offered by Italian Consiglio Nazionale delle Ricerche that usually carries out oceanographic cruises in the Mediterranean Sea.

References

[1] H. Elderfield and M.J. Greaves. The rare earth elements in seawater. *Nature*, 296:214– 219, 1982.

[2] C.R. German, T. Masuzawa, M.J. Greaves, H. Elderfield, and J.M. Edmond. Dissolved rare earth elements in the Southern Ocean: Cerium oxidation and the influence of hydrography. *Geochim. Cosmochim. Acta*, 59:1551–1558, 1995.

[3] C. Jeandel, D. Thouron, and Fieux M. Concentration and isotopic compositions of neodymium in the eastern Indian Ocean and Indonesian straits. *Geochim. Cosmochim. Acta*, 62:2597–2607, 1998.

[4] D.S. Alibo and Y. Nozaki. Rare earth elements in seawater: Particle association, shale-normalization, and Ce oxidation. *Geochim. Cosmochim. Acta*, 63:363–372, 1999.

[5] A.M. Olivarez and R.M. Owen. REE/Fe variations in hydrothermal sediments: Implications for the REE content of seawater. *Geochim. Cosmochim. Acta*, 53:757–762, 1989.

[6] R.M. Sherrell, M.P. Field, and G. Ravizza. Uptake and fractionation of rare earth elements on hydrothermal plume particles at 9°45'N, East Pacific Rise. *Geochim. Cosmochim. Acta*, 63:1709–1722, 1999.

[7] M.J. Greaves, H. Elderfield, and E.R. Sholkovitz. Aeolian sources of rare earth elements to the Western Pacific Ocean. *Mar. Chem.*, 68:31–37, 1999.

[8] E.R. Sholkovitz. The aquatic chemistry of rare earth elements in rivers and estuaries. *Aquatic Geochem.*, 1:1– 34, 1995.

[9] E.R. Sholkovitz, H. Elderfield, R. Smymczak, and K. Casey. Island weathering: river sources of rare earth elements to the Western Pacific Ocean. *Mar. Chem.*, 68:39–57, 1999.

[10] R.E. Hannigan and E.R. Sholkovitz. The development of middle rare earth element enrichments in freshwaters: weathering of phosphare minerals. *Chem. Geol.*, 175:495–508, 2001.

[11] P. Censi, S.E. Spoto, G. Nardone, M. Sprovieri, F. Saiano, D. Ottonello, and S.E. Di Geronimo. REE and yttrium distribution in mangrove coastal water systems. The western Gulf of Thailand. Chemistry and Ecology. *Chemistry and Ecology*, 21:255–277, 2005.

[12] P. Censi, M. Sprovieri, S.I. Di Geronimo, P. Aricò, D. Larocca, and F. Placenti. The REE behaviour in the Thailand's Maeklong estuary: suggestions from the Y/Ho ratios and YREE Tetrad Effects. *Estuarine, Coastal and Shelf Sciences*, 71:569–579, 2006.

[13] J. Schijf, H.J.W. De Baar, and F.J. Millero. Vertical distributions and speciation of dissolved rare earth elements in the anoxic brines of Bannock Basin, eastern Mediterranean Sea. *Geochim. Cosmochim. Acta*, 59:3285–3299, 1995.

[14] K. Tachikawa, C. Jeandel, A. Vangriesheim, and B. Dupré. Distribution of rare earth elements and neodymium isotopes in suspended particles of the tropical Atlantic Ocean (EUMELI site). *Deep Sea Res.*, 46:733–755, 1999.

[15] R. Arraes-Mescoff, L. Coppola, M. Roy-Barman, M. Souhaut, K. Tachikawa, C. Jeandel, R. Sempere, and C. Yoro. The behavior of Al, Mn, Ba, Sr, REE and Th isotopes during in vitro bacterial degradation of large marine particles. *Mar. Chem.*, 73:1–19, 2001.

[16] R.H. Byrne and E.R. Sholkovitz. Comparative complexation behavior of the rare-earths. Marine Chemistry and Geochemistry of the YREE. In: K.A. Gschneidner, Jr. and L. Eyring (Eds.), The Handbook on the Physics and Chemistry of the Rare Earths, Elsevier Science B.V. 23:497–593, 1996.

[17] F.E. Grousset, C.R. Quetel, B. Thomas, O.F.X. Donard, C.E. Lambert, F. Giullard, and A. Monaco. Anthropogenic versus lithogenic origins of trace elements (as, Cd, Pb, Rb, Sb, Sc, Sn, Zn) in water column particles in northwestern Mediterranean Sea. *Mar. Chem.*, 48:291–310, 1995.

[18] R. Chester, M. Nimmo, and P.A. Corcoran. Rain water-aerosol trace metal relationships at Cap Ferrat: A coastal site in the Western Mediterranean. *Mar. Chem.*, 58:293–312, 1997.

[19] R. Chester. Defining the chemical character of aerosols from the atmosphere of the Mediterranean Sea and surrounding regions. *Oceanologica Acta*, 16:231–246, 1993.

[20] R. Chester, K.J.T. Murphy, F.J. Lin, A.S. Berry, G.A. Bradshaw, and P.A. Corcoran. Factors controlling the solubilities of trace metals from non-remote aerosols deposited to the sea surface by the "dry" deposition mode. *Mar. Chem.*, 42:107–126, 1993.

[21] S. Guerzoni, E. Molinaroli, and R. Chester. Saharan dust inputs to the western Mediterranean Sea: Depositional patterns, geochemistry and sedimentological implications. *Deep-Sea Res. II*, 44:631–654, 1997.

[22] G.H. Gullu, I. Olmez, and G. Tuncel. Temporal variability of atmospheric trace element concentrations over the eastern Mediterranean Sea. *Spectrochimica Acta*, B55:1135–1150, 2000.

[23] J.H. Lee and R.H. Byrne. Examination of comparative rare earth element complexation behaviour using linear free-energy relationships. *Geochim. Cosmochim. Acta*, 57:295–303, 1992.

[24] J.H. Lee and R.H. Byrne. Complexation of trivalent rare earth elements (Ce, Eu, Gd, Tb, Yb) by carbonate ions. *Geochim. Cosmochim. Acta*, 57:295–303, 1993.

[25] F.J. Millero. Stability constants for the formation of rare earth inorganic complexes as a function of ionic strength. *Geochim. Cosmochim. Acta*, 56:3123–3132, 1992.

[26] Byrne R.H. and K.-H. Kim. Rare earth precipitation and coprecipitation behavior: The limiting role of PO43- on dissolved rare earth concentrations in seawater. *Geochim. Cosmochim. Acta*, 57:519–526, 1993.

[27] X. Liu and R.H. Byrne. Rare earth and yttrium phosphate solubilities in aqueous solution. *Geochim. Cosmochim. Acta*, 61:1625–1633, 1997.

[28] X. Liu, R.H. Byrne, and J. Schijf. Comparative Coprecipitation of Phosphate and Arsenate with Yttrium and the Rare Earths: The Influence of Solution Complexation. *J. Solution Chem.*, 26:1187–1198, 1997.

[29] D.S. Alibo and Y. Nozaki. Dissolved rare earth elements in the eastern Indian Ocean: chemical tracers of water masses. *Deep-Sea Res.*, 51:559–576, 2004.

[30] Y. Nozaki, J. Zhang, and H. Amakawa. The fractionation between Y anf Ho in the marine environment. *Earth Plan. Sci. Lett.*, 148:329–340, 1997.

[31] N.H. Morley, J.D. Burton, S.P.C. Tankere, and J.M. Martin. Distribution and behavior of some dissolved trace metals in the western Mediterranean Sea. *Deep Sea Res.*, 44:675–691, 1997.

[32] Y.Y. Yoon, J.M. Martin, and M.H. Cotté. Dissolved trace metas in the Western Mediterranean Sea: total concentration and fraction isolated by C18 Sep-Pak techique. *Mar. Chem.*, 66:129–143, 1999.

[33] P. Censi, S. Mazzola, B. Patti, F. Saiano, M. Sprovieri, G. Alonzo, and S.E. Spoto. Trace element distributions in the Straits of Sicily (Central Mediterranean Sea), I. Evidences of rock-water interactions and pollution. *Periodico di Mineralogia*, 71:255–272, 2002.

[34] P. Censi, S. Mazzola, M. Sprovieri, A. Bonanno, B. Patti, R. Punturo, S.E. Spoto, F. Saiano, and G. Alonzo. Rare Earth Elements distribution in seawater and suspended particulate of the Central Mediterranean Sea. *Chemistry and Ecology*, 20:323–343, 2004.

[35] P. Censi, D. Larocca, P. Aricò, M. Sprovieri, F. Saiano, S. Mazzola, and P. Ferla. Effects of alteration of volcanic ashes in seawater. I. Anomalous Y/Ho ratios in coastal waters of the Central mediterranean sea. *Geochim. Cosmochim. Acta*, 71:5405–5422, 2007.

[36] M. Bau, P. Moller, and P. Dulski. Yttrium and lantanides in eastern mediterranean seawater and their fractionation during redox cycling. *Mar. Chem.*, 56:123–143, 1997.

[37] M.J. Greaves, P.J. Statham, and H. Elderfield. Rare earth element mobilization from marine atmospheric dust into sea water. *Mar. Chem.*, 46:255–260, 1994.

[38] A.J. Thomas, C. Guieu, and J.M. Martin. Comment on "Rare earth elements in the Mediterranean Sea and mixing in the Mediterranean outflow" by M.J. Greaves, M. Rudnicki and H. Elderfield. *Earth Plan. Sc. Lett.*, 121:655–658, 1994.

[39] F. Elbaz-Poulichet, J.L. Seidel, and C. Othoniel. Occurrence of an anthropogenic gadolinium anomaly in river and coastal water of southern France. *Water Res.*, 36:1102–1105, 2002.

[40] M. Bau and P. Dulski. Anthropogenic origin of positive gadolinium anomalies in river waters. *Earth Plan. Sci. Lett.*, 143:245–255, 1996.

[41] P. Moller, P. Dulski, M. Bau, A. Knappe, Pekdeger A., and C. Sommer-Von Jarmersted. Anthropogenic gadolinium as a conservative tracer in hydrology. *J. Geochem. Explor.*, 69-70:409–414, 2000.

[42] Y. Zhu, M. Hoshino, H. Yamada, A. Itoh, and H. Haraguchi. Gadolinium anomaly in the distribution of rare earth elements observed for coastal seawater and river waters around Nagoya City. *Bull., Chem. Soc. Japan*, 77:1835–1842, 2004.

[43] E.R. Sholkovitz, W.M. Landing, and B.L. Lewis. Ocean particle chemistry: the fractionation of rare earth elements between suspended particles and seawater. *Geochim. Cosmochim. Acta*, 58:1567–1579, 1994.

[44] K.A. Quinn, R.H. Byrne, and J. Schijf. Comparative scavenging of Yttrium and the Rare Earth Elements in Seawater: Competitive influences of solution and surface chemistry. *Aquatic Geochemistry*, 10:59–80, 2004.

[45] R.H. Byrne and B.Q. Li. Comparative complexation behavior of the rare-earths. *Geochim. Cosmochim. Acta*, 59:4575–4589, 1995.

[46] F.E. Grousset, F. Henry, J.F. Minster, and A. Monaco. Nd isotopes as tracers in water column particles: the western Mediterranean Sea. *Mar. Chem.*, 30:389–407, 1990.

[47] K. Tachikawa, M. Roy-Barnam, A. Michard, D. Thouron, D. Yeghichenyan, and C. Jeandel. Neodymium isotopes in the Mediterranean Sea: comparison between seawater and sediment signals. *Geochim. Cosmochim. Acta*, 68:3095–3106, 2004.

[48] P. Censi, P. Zuddas, D. Larocca, F. Saiano, F. Placenti, and A. Bonanno. Recognition of water masses according to geochemical signatures in the Central Mediterranean sea: Y/Ho ratio and Rare Earth Elements behaviour. *Chemistry and Ecology*, 23:139–155, 2007.

Studies on the Interaction of the Ocean Upper Layer with the Atmosphere in the Mediterranean Sea Using the CNR-ODAS Italia 1 Buoy and the R/V Urania

S. Pensieri[1], R. Bozzano[1], M.E. Schiano[2], S. Sparnocchia[3]
1, Institute of Intelligent Systems for Automation, CNR, Genova, Italy
2, Institute of Marine Sciences, CNR, Genova, Italy
3, Institute of Marine Sciences, CNR, Trieste, Italy
sara.pensieri@ge.issia.cnr.it

Abstract

Although the climate evolution of our planet is strictly linked to the knowledge of air-sea interaction processes occurring in the ocean few experiments have been performed in order to investigate these phenomena.
A realistic assessment of atmospheric and marine parameters involved in these processes, their spatial and temporal scales, the analysis of their effects on water masses movements and atmospheric circulation as well as studies on the ecosystem remains one of the main open issues of scientific research. This is particularly valid for the Mediterranean basin, where knowledge of air-sea interaction processes is still inadequate.
Nowadays, ocean circulation models can reproduce with sufficient accuracy both currents dynamics on global scale and the major thermohaline stratifications of the Mediterranean Sea, but they don't provide yet a complete definition of the dynamics of the basin neither their variability at different spatio-temporal scales.
The lack of specific studies often leads to generalize the results obtained elsewhere without taking into account the temporal and geographical variability of the major marine and atmospheric parameters and the specificity of the involved processes.
By integrating various skills, a research group of the National Research Council (CNR) has developed tools and methodologies for accurately measuring the most important meteo-marine parameters from both fixed and mobile platforms.

1 Introduction

In order to realise social and economical politics that take into account the impact of human activities on the environmental conditions, there is the need to develop predictive climate models able to detect and assess the effects of abrupt climate change, whatever is its source.

Scenarios on the climate evolution at regional and global scale are proposed continuously, but the predictions often disagree. The main problem in the detection and description of climate change is that the natural variability existing in the ocean-atmosphere system because is still poor known. Without filling this gap, any climate study will be incomplete. At the

present, a better understanding of the space and time scales of the air-sea interactions and their effects on both ocean and atmosphere circulation is a major task of the scientific community.

The climate regime of the whole Europe is strongly influenced by the presence of the Mediterranean Sea. This is a semi-enclosed basin located between Europe and Africa with limited access to the World Ocean. Due to its geographic position, the Mediterranean Sea is subjected to the passage of continental and subtropical air masses. The combined effects of the large Atlantic Ocean, Eurasian and North African pressure systems as well as regional orography, control the main weather patterns. The marine and atmospheric features of this basin evidence strong variability on a broad range of time and space scales. The air-sea interactions, especially the intense evaporation processes that take place at the sea surface, greatly affect both ocean and atmospheric circulation. This ocean-atmosphere system is intrinsically coupled, although feedbacks across the air-sea interface are often masked by temporal and spatial differences.

Unfortunately, accurate atmospheric measurements over the Mediterranean Sea are scanty. The scarcity of data and the lack of an appropriate parameterization of the processes, able to take into account the Mediterranean peculiarities, lead to an incomplete knowledge of the air-sea energy exchanges, determining a strong limitation in the accuracy of the weather forecast and in the development of suitable Ocean General Circulation Model (OGCM) for this basin. This imposes research activities, mainly based on measuring campaigns, aiming at creating a comprehensive data base allowing answering to the different needs.

A CNR group is working in this field and its activity is briefly summarized in the following.

2 The Observing System

In order to achieve a significant data set of in situ measurements, several instrumentation packages have been developed for working on both fixed and moving platforms. Particularly, the CNR group has get ready an integrated system for meteorological and radiative measurements to be installed onboard of the ship during experimental cruises and has equipped and maintain a fixed offshore buoy with marine and meteorological sensors for supporting air-sea interaction observations. In detail:

1. The measurement system from ships includes: piranometers, pirgeometers, temperature and humidity probes, barometer, IR thermometers. All the data are acquired on a PC by using an ad hoc developed software. The system may be used onboard of any ship, but in order to reduce the influence of the ship's structure on the measurements, suitable locations on board have to be identified and apposite supports have to be realized for each different ship. Figure 1 shows the installation onboard of R/V Urania. This system was realized in close collaborations with the Institute of Marine Science (CNR-ISMAR) in La Spezia and the Institute of Atmospheric Sciences and Climate (CNR-ISAC) in Rome. Furthermore, in the last years, the observational capability onboard has been improved with a radiosounding system VAISALA DigiCORA III in order to obtain the atmospheric vertical profiles of temperature, humidity and wind vector over the open sea.

Figure 1: Sensors for meteorological and radiative measurements installed on board the R/V Urania.

2. The ”ODAS Italia 1” buoy (Figure 2), managed by CNR-ISSIA, is moored in the Central Ligurian Sea at 37 nm far from the coast, without any shield for winds and waves, and on a 1200 meter deep water. It is a pole-body buoy, about 50 meter long, with a small laboratory on its top. The buoy was specifically designed as a stable measuring platform: its design allows for negligible sensitivity of sea heave and height. Two complete sets of meteorological sensors are installed on the top of the buoy at a height of 13.5 m. The measured parameters are: wind speed and direction, air temperature, atmospheric pressure, relative humidity, global solar and infrared radiation, precipitation. The marine sensors are mounted along the buoy's body at various depths (0.5, 6, 12, 20, 28, 36 m) to collect sea temperatures and salinity data. Every 5 seconds the onboard system acquires the meteorological parameters, while marine data are sampled each 15 minutes. All the collected data are stored on board and transmitted each hour to the receiving station ashore. Acquired data are processed in near-real time by applying quality control procedures devel-

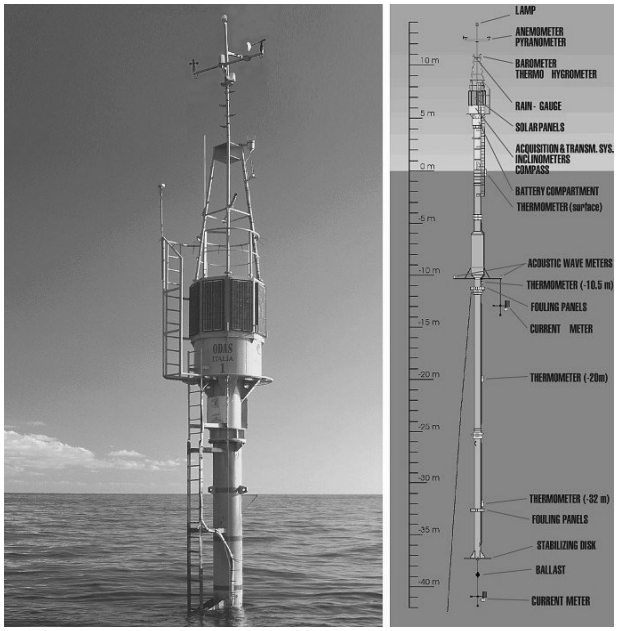

Figure 2: (leftt) Photo of the ODAS Italia 1 buoy (right) scheme of the instrumentation installed on board the buoy.

oped within the framework of the European project Mediterranean Forecasting System: Pilot Project (MFSPP). A database is updated as well as new web pages (http://www.odas.ge.issia.cnr.it) are created with a summary of the last received data and plots of past time series (last 24 hours, last week, last month). On a daily basis a subset of received data are converted into the MEDATLAS format and made available through the Coriolis data centre at Institut Francais de Recerche pour l'Exploitation de la Mer (IFREMER, France). Part of these data are also transmitted over the GTS making "ODAS Italia 1" the first buoy to fed the GTS with meteo-oceanographic data from the Italian seas. In addition, a mooring chain is located close to the buoy position for monitoring the marine currents in the upper sea layer and temperature and salinity data in the deeper levels. The sensors on the mooring self record the data. Every six months the chain is recovered for maintenance and for discharging the data. This chain has been realized and maintained thanks to a collaboration with ENEA CRAM.

3 Main Results

The data collected by both the buoy and on the ships have been used for several meteorological and marine studies. Particularly:

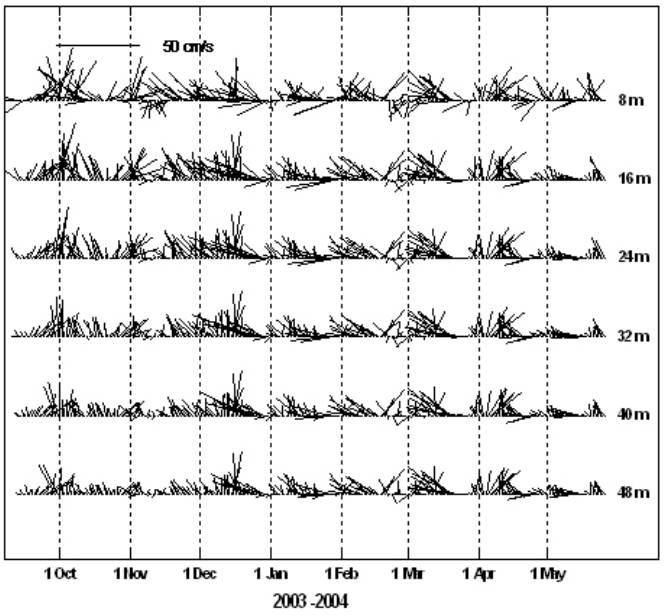

Figure 3: Time series of the vertical surface currents measured in the Ligurian Sea.

3.1 Marine upper layer

The continuous measurements of the upper marine layer performed by the buoy's sensors allowed the study of the anomalous warming period occurred during summer 2003, when the sea surface temperature of the Mediterranean Sea achieved the highest values of the last 50 years [1]. The data showed that the anomalous warming was prevalently confined to within a few meters below the surface while, on the contrary, temperatures in the underlying layers were lower than usual. The limited vertical propagation of heat was ascribed to the high temperature difference that arose between the surface and the deeper layers due to protracted calm weather conditions, particularly the low wind occurred during that period. Moreover, the long-time series of surface currents and meteorological parameters has been used to estimate the variability of the upper layer circulation of the Ligurian Sea [2]. Currents were mainly barotropic and directed NW, according to the general circulation of the area. Most of the observed sub-daily variability in the upper thermocline was determined by inertial currents and mesoscale activity due to the presence of the Ligurian Front. Local wind has a minor role in the near-surface circulation but induced internal waves propagating downward in the water column (Figure 3). These researches have been carried out in collaboration with the Italian National Agency for New Technologies, Energy and Sustainable Economic Development, Marine Environment Research Cen-

tre (ENEA-CRAM) in Lerici (La Spezia, Italy).

3.2 Atmospheric boundary layer

The success of any ocean-atmosphere coupled system crucially depends on the quality of the boundary layer parameterizations in the ocean and in the atmospheric models. Unfortunately, due to the complex nature of turbulent and convective flows in the boundary layer and in the ocean-atmosphere interface, there are still several scientific problems to be resolved in terms of boundary layer parameterization. Since the methodologies are often quite similar, a challenging idea was to pursue an approach that integrates the boundary layer parameterizations for both the ocean and the atmosphere. For this reason, in the last years, the measurements of the atmospheric vertical profile have been added to the observational set carried out from ship. Some of these data were used to study the evolution of the Marine Boundary Layer during a sequence of onshore-offshore-onshore events affecting the stability conditions at the surface [3]. These researches have been carried out in collaboration with CNR-ISAC in Lamezia Terme and Riso Technical Università of Denmark National Laboratory for Sustainable Energy (Riso) in Roskilde, Denmark.

3.3 Climate

A new climate index based on the surface water vapour density at sea has been defined by using the long term series of observations collected from both the buoy and on the ships [4]. This index, which is related to the surface ocean stratification also, can evidence when the tropical features of the Mediterranean climate predominate. It has been used to investigate the climate variability of the Mediterranean Sea [5]. The ERA-40 project of the European Centre for Medium-range Weather Forecast (ECMWF, Reading, UK) provided the long and unique time series of values that is needed for estimating the surface water vapour densities over the Mediterranean Sea. Since an analogous series does not exist, the use of model data was necessary, but any result must be viewed in the light of their obvious limitations. The results confirmed that the prevalence of tropical features of the Mediterranean climate is occurring more frequently in the last two decades, with a widening of the period affected by this condition and an enhancement of its character. This trend is detectable over the whole basin even if the signals are more evident in the regions located at the highest latitudes.

3.4 Algorithms for the Mediterranean Sea

More than ten years of direct measurements of solar and infrared radiation from research vessels permitted to demonstrate that the common used radiative bulk formulae fail when applied over the Mediterranean Sea and to develop specific algorithms which take into account the peculiarities of this basin [6, 7]. At the present, these are the radiative bulk formulae adopted by the scientific community working on the Mediterranean Sea. These researches have been carried out in collaboration with CNR-ISAC in Rome and ENEA-CRAM.

3.5 Data validation

The data gathered from the fixed buoy were used for the validation of forecasting model results as well as satellite measurements. Particularly, near-surface meteorological data (air temperature, relative humidity, barometric pressure, wind speed and direction) have been compared with the outputs of the ECMWF analysis in the two grid points closest to the buoy position from February through December 2000 [8]. The comparison showed that the model reproduces well the baric field while significant differences result for the other variables, which are more affected by local conditions. This suggested that the observed discrepancies may be due to the poor space resolution ($0.5625° \times 0.5625°$) of the model that probably is not sufficient to appropriately discriminate between land and ocean surfaces in a small basin such as the Ligurian Sea and to take into account local peculiarities. Meteorological data acquired by the ODAS Italia 1 buoy in the year 2000, had been used to validate over the Ligurian Sea some algorithms available in literature for SSM/I (passive microwave) surface humidity, wind speed and air temperature estimations [9]. From this comparison, it turned out that, over the Ligurian Sea, humidity and wind speed were systematically overestimated by the SSM/I algorithms; good agreements were obtained only after applying a linear correction, as results from the comparison with ECMWF and the ODAS Italia 1 buoy and two Aegean Sea POSEIDON system buoys. As far as SSM/I precipitation is concerned, no data at sea could confirm the reliability of the used precipitation algorithm, though a comparison with NCEP precipitation indicates a reasonable consistency, at least in the annual mean precipitation rates for the years 1999 and 2000. Furthermore, wind data collected from July 2006 to June 2007 were used to test the skill of the QuikSCAT products [10]. The results indicated that the QuikSCAT wind vectors satisfy the accuracy requirements for high speeds. On the contrary, the skill is lesser for low wind, in particular for the direction. These results are in agreement with those of previous comparisons but the analysis evidenced some issues until now mistreated. The first one is the scarceness of data. The satellite passages over the Ligurian Sea are only twice a day and data taken under rainy condition and for wind speed less than 3 $\mathrm{m \cdot s^{-1}}$ are not valid. Thus, the temporal sampling may be not adequate for monitoring wind fields and their evolution over this basin where calm condition often occurs and strong perturbations are generally associated to rain. Furthermore the comparison shows that it may be difficult to recognize spurious values obtained from QuikSCAT when the true wind speed is less than 3 $\mathrm{m \cdot s^{-1}}$ without a reference on sea.

Finally, data has been available for other groups working in different scientific fields, like marine biology and remote sensing, and industry.

4 Conclusion

Owing to the geographic position and to the semi-enclosed nature, the phenomenology of both the ocean and the atmosphere over the Mediterranean Sea is quite complex and not all the processes can be deal as it is done for those occurring over the open Oceans. Thus, in order to improve the knowledge of this basin, apposite studies are required and the experimental approach is essential.

Putting together different experiences, a CNR group has developed some facilities to carry out marine and meteorological measurements from both fixed and moving platforms and significant results has been obtained in several different fields.

References

[1] S. Sparnocchia, M.E. Schiano, P. Picco, R. Bozzano, and A. Cappelletti. The anomalous warming of summer 2003 in the surface layer of the central ligurian sea (western mediterranean). *Annales Geophysicae*, 24:443–452, 2006.

[2] P. Picco, M.Borghini, R. Bozzano, M.E. Schiano, and S. Sparnocchia. Near surface currents and wind observations in the open ligurian sea. In *proc. of LAPCOD Meeting*, 2005.

[3] A.M. Sempreviva, M.E. Schiano, S. Pensieri, R. Bozzano, M. Borghini, F. Grasso, A. Semedo, L. L. Soerensen, J. Teixeira, C. Transerici, and R. Tomé. Observed development of the vertical structure of the marine boundary layer during the lasie experiment in the ligurian sea. *Annales Geophysicae*, 27:17–25, 2009.

[4] M.E. Schiano, M. Borghini, S. Castellari, and C. Luttazzi. Climatic features of the mediteranean sea detected by the analysis of longwave radiative bulk formulae. *Annales Geophysicae*, 18:1482–1487, 2000.

[5] M.E. Schiano, S. Sparnocchia, C. Cappa, and R. Bozzano. An analysis of the climate variability over the mediterranean sea by means of the surface water vapour density. *International Journal on Climatology*, 25:1731–1784, 2005.

[6] F. Bignami, S. Marullo, R. Santoleri, and M. E. Schiano. Longwave radiation budget in the western mediterranean sea. *J. Geoph. Res.*, 100:2501–2514, 1995.

[7] M.E. Schiano. Insolation over the western mediterranean sea: a comparison of direct measurements and reed's formula. *Journal of Geophysical Research*, 101:3831–3838, 1996.

[8] R. Bozzano, A. Siccardi, M.E. Schiano, M. Borghini, and S. Castellari. Comparison of ecmwf surface meteorology and buoy observations in the ligurian sea. *Annales Geophysicae*, 22:317–330, 2004.

[9] F. Bignami, S.Marullo, P.Lionello, and R.Bozzano. Comparison of ssm/i-derived meteorological surface fields to ship/buoy observations and model results in the mediterranean sea. In *Remote Sensing of the Ocean and Sea Ice 2001, C.R.Bostater e R.Santoleri eds., proc. of SPIE*, volume 4544, pages 123–133, 2002.

[10] S. Pensieri, R. Bozzano, and M.E. Schiano. Comparison between quickscat and buoy wind data in the ligurian sea. *in press, Journal of Mar. Sys*, 2009.

Acetone Air-Sea Fluxes in the Atlantic Ocean

S. Taddei[1], P. Toscano[2], B. Gioli[2], A. Matese[2], F. Miglietta[2], F.P. Vaccari[2], A. Zaldei[2], T. Custer[3], J. Williams[3]
1, Institute for Biometeorology, CNR, Livorno, Italy
2, Institute for Biometeorology, CNR, Firenze, Italy
3, Max Planck Institute for Chemistry (Otto Hahn Institute), Mainz, Germany
s.taddei@ibimet.cnr.it

Abstract

Acetone and CO_2 fluxes have been measured over a high latitude phytoplankton bloom in the remote South Atlantic by using shipborne micrometeorological methods for direct atmospheric flux measurement. Previous results suggest that high latitude oligotrophic ocean regions are sinks of acetone, whereas high productivity regions are sources. While the observed CO_2 fluxes are into the ocean and of the order of 1 μmol$\cdot$m$^{-2} \cdot$ s^{-1} at most, the acetone fluxes measured show a significant relationship with chlorophyll in the region of the phytoplankton bloom. Although the uncertainty is very high due to the very low signal to noise ratio, significant, positive acetone mean fluxes of the order of 0.01 nmol$\cdot$m$^{-2} \cdot$ s^{-1} have been observed in bloom areas, whereas near zero, negative or highly variable low acetone fluxes have been measured elsewhere. These results support the idea that the global acetone source from bloom affected areas is small in comparison to the uptake from the much larger oligotrophic regions, and that the ocean is globally a net sink for acetone.

1 Introduction

Organic species play important roles in the Earth's atmosphere, impacting ozone chemistry and aerosol formation, thereby influencing the Earth's overall oxidation capacity and radiative budget. In particular acetone, which is ubiquitous in the troposphere and found at relatively high mixing ratios (ca. 200 ppt) even in the remote Pacific atmosphere, is recognised as an important precursor for hydrogen oxide radicals (HOx) and peroxyacetyl nitrate (PAN), especially in the cold, dry, upper troposphere.
Since elevated levels of HOx imply a more photochemically active upper troposphere, with enhanced rates of ozone formation, there has been interest in determining the sources and sinks of acetone worldwide.
Several budgets and numerous measurements of acetone have been published over the last ten years. Despite often intensive study at terrestrial sites, the budgets of acetone remain difficult to determine due to uncertainty in the role of the ocean, which is far less well characterised.
In fact, recent studies have modified drastically the overall budget of acetone from the estimates of Jacob et al. [1]. While the ocean was considered a net emitter of acetone (see [1]), it is now thought that acetone has a net sink in the ocean [2, 3, 4].
A detailed review of the most important contributions to this field is reported in the following.

In 2002, Jacob et al. published a global budget of acetone[1] which differed from all previous budget attempts in that it considered the role of the ocean for the first time. Through inverse modelling, [1] estimated that the ocean was an important net source of acetone. Indeed, from the total global source of 95 Tg, some 25 Tg was estimated to originate from the ocean in order to balance the known sources and sinks. However, in 2004 the model was revised following comparison with measurements over the remote Pacific [2] and the authors concluded that the ocean was a net global sink for 15 Tg, and moreover that the estimated sources and sinks were not balanced. In 2004, the first open ocean measurements of acetone in air and seawater were made [5]. The interhemispheric gradients and depth profiles shown by Williams et al. were consistent with uptake of acetone from the air to the sea and a microbial sink in the seawater although the calculated flux was highly variable. In 2004, the photolysis quantum yield of acetone was re-determined as a function of temperature and pressure [6]. It was found that the accepted acetone photolysis rates were significantly overestimated (factor 3-5), particularly for cold, low pressure conditions of the upper troposphere and therefore with the global acetone budget the photolysis sink term had to be significantly reduced [7]. In the same year, a shipborne study was published in which the flux of acetone at the ocean surface was measured directly for the first time using an eddy covariance (EC) method [3]. Interestingly, the authors consistently found uptake fluxes (from the air to the ocean) for acetone over the oligotrophic Pacific ocean which became stronger further from the equator. In mesocosm experiments [8] the acetone flux was found to be variable but systematic. In strong daylight and in the presence of significant biological activity, acetone was emitted from the ocean to the air. In low light or biologically poor regimes, however, acetone was taken up. These observations are consistent with previously observed photoproduction and microbial uptake of acetone e.g. [9]. These results are also partly consistent with the results of [3] who measured an acetone uptake in oligotrophic regions, however, biologically active regions (e.g. upwelling zones, ocean fronts, or large natural phytoplankton blooms) can be strong sources in daylight and depending on their size could to some extent offset the general sink. It is therefore important to investigate these biological hotspots in future to better constrain the global budget.

A variety of techniques exist for the measurement of fluxes including eddy covariance e.g. [10] and disjunct eddy covariance (DEC) e.g. [11]. A significant advance in air-sea turbulent flux measurements with respect to terrestrial applications is the ability to make such measurement on moving platforms such as airplanes and boats through use of inertial platform measurements [12].

In this study, a shipborne DEC system is used to determine the true direction and size of the acetone flux, while a shipborne EC system is used to measure CO_2 fluxes. These two distinct methods have been applied over a large-scale, naturally occurring high latitude phytoplankton bloom. The measurements were made in the remote South Atlantic near the Argentianian continental shelf as part of the OOMPH project (www.atmosphere.mpg.de/enid/oomph).

A more detailed description of the experiment, including schematics, pictures and plots about the flux measurement system, the EC and DEC methods, the spectral

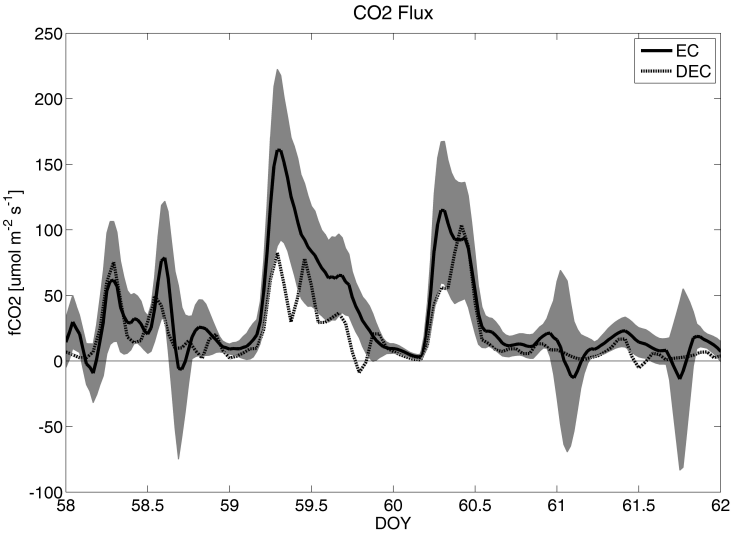

Figure 1: Filtered Eddy Covariance (continuous, darker line) and Disjunct Eddy Covariance (dashed, lighter line) CO_2 fluxes at the Ximeniano observatory. The filter is a moving average with a three hour time window. The grey band represents an estimation for the range of the probable values that can be obtained by the DEC method. DOY means day of year. (From [4]).

analysis, the cruise meteorological data, and the observed fluxes can be found in [4].

2 Materials and methods

The measurements were performed in the southern Atlantic Ocean on board the IPEV/TAAF research vessel Marion Dufresne. The cruise started in Cape Town (South Africa) on January 19th, 2007, and ended in Punta Arenas (Chile) on February 5th, 2007. The vessel traversed regions of relatively low marine biological productivity in the middle and South Atlantic, and a high productivity region of a natural phytoplankton bloom in the west. During the cruise wind was mostly westerly and the wind speed, the sea surface temperature and the chlorophyll a concentration varied approximately between 2-23 $\mathrm{m{\cdot}s^{-1}}$, 10-21 °C, and 0.1-5 $\mathrm{mg{\cdot}m^{-3}}$ respectively (the chlorophyll a concentrations are taken from the SEAWIFS database). The flux measurement system was mounted on the top of the atmospheric mast positioned on the foredeck.

The EC and the DEC methods allow directly scalar fluxes to be calculated by computing the covariance between the fluctuation in vertical wind speed and the fluctuations in the scalar quantity. The EC method represents the most direct method to determine turbulent fluxes [10]. For EC, fast sensors provide a quasi-continuous function of a scalar property of the atmo-

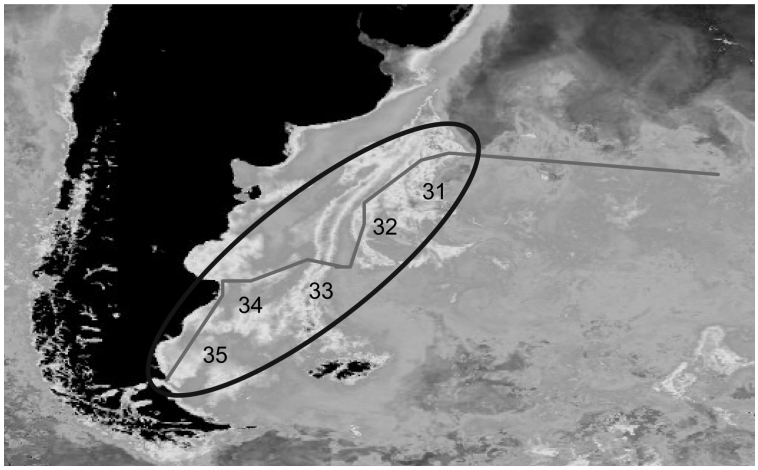

Figure 2: Satellite picture of the average values of Chlorophyll concentration. Lighter grey corresponds to higher concentration. The original colorscale is available at http://oceancolor.gsfc.nasa.gov/cgi/l3. Track and DOY of cruise are reported.

sphere (e.g., CO_2 mixing ratio) and vertical wind speed. Most of the vertical turbulent transport occurs with frequency below 5-10 Hz. The turbulent flux of the scalar is then calculated as the covariance between the scalar fluctuations and the vertical wind component fluctuation. In order to use the EC method, a fast response anemometer and gas analyzer are required. However for many trace gas species such fast analyzers are not available. If a slower response gas analyser is available for the target species a possible alternative for determining the in-situ flux is to apply the DEC method. In this technique, the covariance is calculated by using only a subset of the whole time series used in the conventional EC method. A slower sensor can be used for DEC because sampled points have a relatively long time interval between one another.

In our experiment a sonic anemometer was used for both the conventional and the disjunct eddy covariance methods. Wind measurements made on-board ship are complicated by the platform motion, and these effects must be measured and removed in order to obtain the true wind velocity. The ship motion data were measured at the same frequency as the wind (10 Hz) using an Inertial Navigation System combined with a global positioning system (INS/GPS), installed near the anemometer. The CO_2 measurements were made by pumping air into a closed path CO_2/H_2O infrared gas analyzer (IRGA LICOR 7500, LI-COR, USA). The air samples for acetone mixing ratio measurements were drawn into two, half-litre Teflon coated stainless steel flasks equipped with fast switching Teflon valves. Every 30 s, air was swiftly collected (duration $\sim$0.3 s) into one of the stainless steel containers, and after 5 s was sampled by a Proton transfer reaction mass spectrometer (PTR-MS) housed in the laboratory. Further specific details about the PTR-MS de-

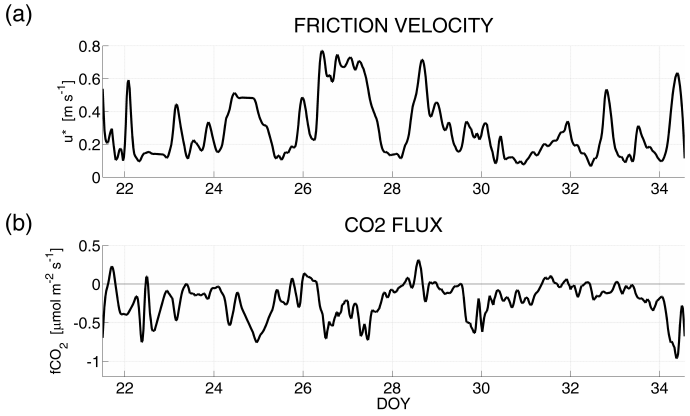

Figure 3: a) Corrected values of Eddy Covariance (EC) friction velocity. b) Corrected values of EC CO_2 flux. (From [4]).

tector can be found in [4]. While one stainless steel flask was being sampled, the second was being evacuated in preparation for the next sampling cycle 30 s later.
An experimental comparison between disjunct and conventional eddy covariance techniques can be found in the work of [13], but for validation purposes a comparison was also made between the disjunct and conventional eddy covariance methods in this study during a ground based experiment performed in an urban environment. Both methods were applied to measure CO_2 fluxes in Florence, Italy, at the Ximeniano Observatory in the centre of the city. The experiment started on February 26th, 2008, and ended on March 2nd, 2008. The disjunct system was the same used aboard the Marion Dufresne with the closed path IRGA used instead of the PTR-MS to measure CO_2 mixing ratio.

3 Results and discussions

The movements of the ship induced by the ocean waves generate flow distortion, and low frequency acoustic waves. As a consequence, vertical air velocity, air temperature, and air pressure oscillate with the same frequencies as the ocean waves. These oscillations generate fluctuations in both the CO_2 mixing ratio and the true vertical wind speed. Consistent peaks, due to the correlation between the components of the CO_2 spectrum corresponding to the ocean wave oscillations and the analogous components in the vertical wind speed spectrum, can be observed in the range 0.07-0.25 Hz in the typical cospectrum between vertical wind and CO_2 mixing ratio data. Since the integral of the cospectrum represents the flux, this correlation masks the true turbulence correlation signal and must be filtered out and the corresponding flux underestimation evaluated. Accurate corrections have been calculated in [4], and it has been found that the underestimation in the computed flux is of the

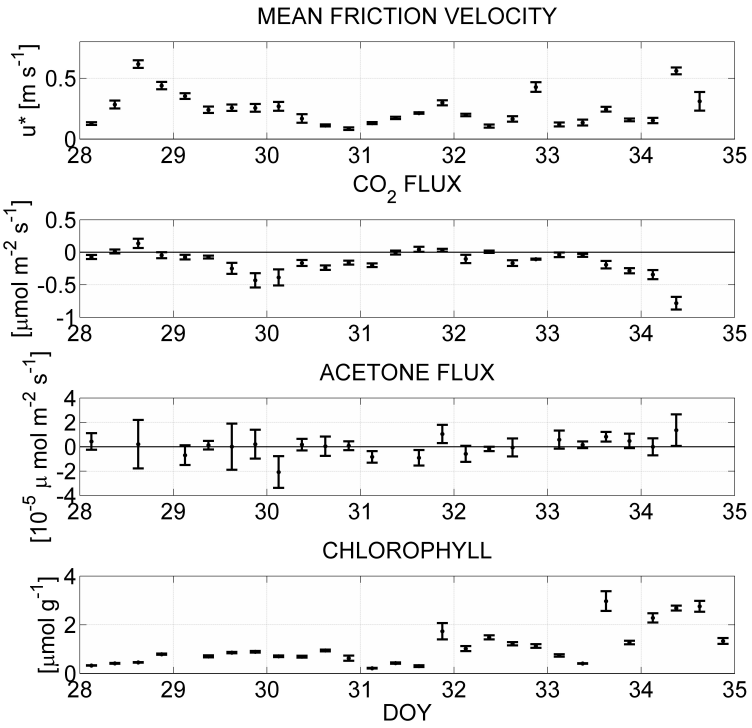

Figure 4: Six-hour average values of friction velocity, CO_2 fluxes, acetone fluxes, and chlorophyll a concentration. (From [4]).

order of 30%.

In order to verify the accuracy of the DEC method through a comparison with the ordinary EC results an experiment was performed in Florence. In Figure 1 a moving average filter with a three hour time window was applied to the raw CO_2 fluxes. The dashed line is the filtered DEC flux and the continuous line the filtered EC flux. The grey band is an estimation of the range of the probable values that can be obtained by the DEC method. This band was estimated as follows. Thirty subsamples of the high frequency EC data were taken. The time distance between two consecutive points in the same subsample was 30 s and the subsamples differ in their starting time. Therefore they represent thirty different virtual simulations of a DEC system. For each of them the time series of CO_2 fluxes was calculated. Finally at every time the average and the standard deviation of these fluxes were computed. The grey band represents the variation around the mean of the simulated DEC fluxes and its width is given by the standard deviations. The plot

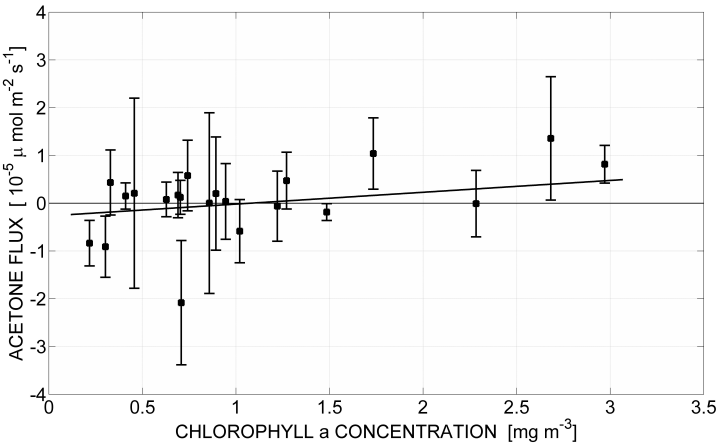

Figure 5: Six-hour average values of acetone fluxes versus chlorophyll a concentrations. (From [4]).

shows that the virtual simulated DEC allows reasonable flux estimation, although with higher uncertainty with respect to EC. The discrepancy between the true DEC and the EC results could be even larger for two reasons: a) the DEC data are obtained by a distinct and independent sampling system, while the virtual simulated DEC is based on a subsample of the EC data, b) there can be errors due to the pneumatic circuit (such as the incomplete evacuation of the sampling canisters). As shown in Figure 1, however, the observed DEC flux values are almost always inside the estimated error band, confirming the validity of the method, although these data suggest a possible underestimation of the true flux. In particular, the computation of the normalized mean bias error gives an underestimation of circa 39%.

The CO_2 measurement results have been reported in Figure 3. The values of friction velocity (u*) and CO_2 fluxes have been corrected for the underestimation due to the cospectrum filtration discussed above. The Marion Dusfresne cruise can, to a first approximation, be divided into two different oceanographic regions, an oligotrophic section with low nutrients, chlorophyll and primary production and the region of the phytoplankton bloom which is characterised by high chlorophyll and primary productivity. The period from day of year (DOY) 31 to 34 corresponds to time when the ship emerged from oligotrophic region and entered the high chlorophyll regions (see Figure 2). In both regions CO_2 fluxes were mainly into the ocean (Figure 3b). These EC CO_2 fluxes were indirectly validated against partial pressure measurements of dissolved and atmospheric CO_2. The CO_2 flux does not show any diel cycle and appears to correlate strongly with the friction velocity. The plots show that below a certain u* threshold, significant CO_2 fluxes were not observed, except on DOY 22 when the signal was very noisy. An estimation of the threshold was made and

an increase of the CO_2 fluxes for values of friction velocity above approximately 0.25 $\mathrm{m{\cdot}s^{-1}}$ was found [4]. This means that below the 0.25 $\mathrm{m{\cdot}s^{-1}}$ threshold, gas exchange between the water and the atmosphere encounters high resistance. Therefore the friction velocity above this threshold seems to be a necessary condition to have significant CO_2 fluxes. However, this is not the only factor in play since in some cases very low CO_2 fluxes were observed even though this condition was satisfied.

Acetone data were measured only from DOY 28 to DOY 34. In Figure 4 the six-hour average values of acetone fluxes are plotted. Since there were a few large gaps in the data, averages made on less than 70% of data were considered unreliable. As a consequence, four six-hour mean values have been discarded. The interval from DOY 28 to almost the end of DOY 31 is in the region with less pronounced biogenic activity, see Figure 4. In this area the average values of acetone fluxes are almost zero or negative. Negative acetone fluxes in non-bloom areas can be considered in agreement with the results of [3] who observed strong uptake of acetone in oligotrophic Pacific waters. The interval from DOY 31 to DOY 34 is in the region with stronger biogenic activity (bloom). In this interval some of the average values of the acetone fluxes are positive. In particular positive fluxes are observed for large values of chlorophyll concentration on DOY 31, DOY 33, and DOY 34. The correlation between chlorophyll concentration and acetone fluxes can be observed also in the scatter plot of Figure 5. In this figure negative or almost zero fluxes are found for lower chlorophyll concentration values, while mainly positive fluxes are observed for chlorophyll concentrations above 1.5 $\mathrm{mg{\cdot}m^{-3}}$. We considered fluxes negative or positive if they are at least one standard error different from zero. The value of the coefficient of determination for a simple linear least squares fit is 0.27. This value for a sample of 21 data points corresponds to a probability of null correlation of about 2% (two-tailed t-test). In the case of a weighted linear least squares fit, where the error bands are taken into account, the coefficient of determination is 0.16 with a two-tailed probability of null correlation of about 7%, while the value obtained for the slope is significantly different from zero with a 93% confidence interval: 0.0025 (0.0000, 0.0050) $\mathrm{nmol{\cdot}m \cdot mg^{-1} \cdot s^{-1}}$. Positive acetone fluxes in bloom areas can be considered in agreement with the results of [8] who showed light dependent acetone emission fluxes from phytoplankton blooms initiated in coastal mesocosms. Indeed the positive fluxes seen here over the phytoplankton blooms are also highest in the daylight hours. Median emission fluxes from the mesocosm experiment [8] show acetone emission fluxes of 0.4 $\mu\mathrm{mol{\cdot}m^{-2} \cdot day^{-1}}$ while in this study a mean flux of the order of 1 $\mu\mathrm{mol{\cdot}m^{-2} \cdot day^{-1}}$ was observed over the bloom which is about two time higher than the mesocosm results. It should be noted, however, that in the mesocosm experiments the fluxes are isolated from turbulence by the enclosures.

4 Conclusions

For the first time the atmospheric fluxes of CO_2 and acetone were measured during a cruise in the southern Atlantic ocean using respectively an EC system with an IRGA and a DEC with a PTR-MS. The effectiveness of the DEC system was tested in a ground experiment at the Ximeniano

observatory in Florence, Italy. During the cruise, regions with both high and low biogenic activity were encountered. The results described above clearly show that the exchange of CO_2 at the air-sea interface are mainly determined by the turbulence conditions. In particular it was shown that above a certain threshold (0.25 $\mathrm{m \cdot s^{-1}}$) for the friction velocity the fluxes can be significant. During the cruise this condition was satisfied for about half time. The observed CO_2 fluxes are into the ocean and they are of the order of 1 $\mu\mathrm{mol \cdot m^{-2} \cdot s^{-1}}$ at most. This is of the same order of magnitude as those measured by [14], 0.3-0.6 $\mu\mathrm{mol \cdot m^{-2} \cdot s^{-1}}$. Measured acetone fluxes show a significant relationship with biogenic activity. Although the uncertainty is very high due to the very low signal to noise ratio, positive acetone mean fluxes of the order of 1×10^{-5} $\mu\mathrm{mol \cdot m^{-2} \cdot s^{-1}}$, comparable to the results of [8], have been clearly observed in bloom areas, whereas near zero or negative acetone fluxes have been measured in the other areas. The order of magnitude of the sink in the oligotrophic ocean area is in general agreement with the sink reported in literature [3], who measured values ranging between -1 and -10 $\mu\mathrm{mol \cdot m^{-2} \cdot day^{-1}}$. Both our measurements and those of [3] have shown that the acetone fluxes are very small, quite close to the sensitivity of the current experimental methods. In conclusion, the source strength over the bloom seems comparable to the sink over the oligotrophic ocean. Bloom areas, however, represent circa 1% of the global ocean surface and therefore most of the ocean will be a sink and the estimated sink will not be significantly offset by the bloom source assuming that the bloom measured here is representative of all bloom/active areas. The flux from the phytoplankton rich region would have had to have been circa 100 times larger than the oligotrophic flux to offset the uptake elsewhere.

References

[1] D.J. Jacob and et al. Atmospheric budget of acetone. *Journal of Geophysical Research-Atmospheres*, 107(D10):10.1029, 2002.

[2] H.B. Singh et al. Analysis of the atmospheric distribution, sources, and sinks of oxygenated volatile organic chemicals based on measurements over the Pacific during TRACE-P. *Journal of Geophysical Research-Atmospheres*, 109(D15S07):10.1029, 2004.

[3] C.A. Marandino, W.J. De Bruyn, S.D. Miller, M.J. Prather, and E.S. Saltzman. Oceanic uptake and the global atmospheric acetone budget. *Geophysical Research Letters*, 32:L15806, 2005.

[4] S. Taddei, P. Toscano, B. Gioli, A. Matese, F. Miglietta, F. P. Vaccari, A. Zaldei, T. Custer, and J. Williams. Carbon Dioxide and Acetone Air-Sea Fluxes over the Southern Atlantic. *Environmental Science and Technology*, 43:5218–5222, 2009.

[5] J. Williams, R. Holzinger, V. Gros, X. Xu, E. Atlas, and D.W.R. Wallace. Measure-

ments of organic species in air and seawater from the tropical Atlantic. *Geophysical Research Letters*, 31(23):L23S06, 2004.

[6] M.A. Blitz, D.E. Heard, M.J. Pilling, S.R. Arnold, and M.P. Chipperfield. Pressure and temperature-dependent quantum yields for the photodissociation of acetone between 279 and 327.5 nm. *Geophysical Research Letters*, 31:L06111, 2004.

[7] S.R. Arnold, M.P. Chipperfield, M.A. Blitz, D.E. Heard, and M.J. Pilling. Photodissociation of acetone: Atmospheric implications of temperature-dependent quantum yields. *Geophysical Research Letters*, 31:L07110, 2004.

[8] V. Sinha, J. Williams, M. Meyerhoefer, U. Riebesell, A. I. Paulino, and A. Larsen. Air-sea fluxes of methanol, acetone, acetaldehyde, isoprene and DMS from a Norwegian fjord following a phytoplankton bloom in a mesocosm experiment. *Atmospheric Chemistry and Physics*, 7:739–755, 2007.

[9] X. Zhou and K. Mopper. Photochemical production of low molecular weight carbonyl compounds in seawater and surface microlayer and their air-sea exchange. *Marine Chemistry*, 56:201–214, 1997.

[10] M. Aubinet and et al. Estimates of the annual net carbon and water exchange of forest: the EUROFLUX methodology. *Advances in Ecological Research*, 30:113–175, 2000.

[11] H.J.I. Rinne, A.B. Guenther, C. Warneke, J.A. de Gouw, and S.L. Luxembourg. Disjunct eddy covariance technique for trace gas flux measurements. *Geophysical Research Letters*, 28:3139–3142, 2001.

[12] J.B. Edson, A.A. Hinton, K.E. Prada, J.E. Hare, and C.W. Fairall. Direct Covariance Flux Estimates from Mobile Platforms at Sea. *Journal of Atmospheric and Oceanic Technology*, 15:547–562, 1998.

[13] J. Rinne, T. Douffet, Y. Prigent, and P. Durand. Field comparison of disjunct and conventional eddy covariance techniques for trace gas flux measurements. *Environmental Pollution*, 152:630–635, 2008.

[14] W.R. McGillis, J.B. Edson, J.E. Hare, and C.W. Fairall. Direct covariance air-sea CO_2 fluxes. *Journal of Geophysical Research*, 106:16729–1674, 2001.

Double-Diffusive Layers in the Adriatic Sea

S. Carniel[1], M. Sclavo[1], L. Kantha[1,2]
1, Institute of Marine Sciences, CNR, Venezia, Italy
2, University of Colorado, Boulder, USA
sandro.carniel@ismar.cnr.it

Abstract

During the NURC/NRL DART06A cruise in late March 2006, a microstructure profiler was deployed to perform turbulence measurements in the upper layers of the Southern Adriatic Sea. Measurements in the Po river plume along the Italian coast displayed classic double-diffusive layers and staircase structures resulting from the relatively colder and fresher Po river outflow water masses overlying warmer and more saline water masses from the Adriatic Sea.
We report here the water mass and turbulence structure measurements of the casts made in the water columns undergoing double-diffusive convection (DDC).

1 Introduction

Double diffusive convection in the ocean is due to the large disparity between the heat and salt molecular diffusivities. Even though the water column may be statically stable overall, it is susceptible to instability because of the rapid diffusion of heat from a perturbed fluid mass relative to that of salt. When a relatively warm and salty water mass overlies a cooler and fresher but more dense one, narrow vertical finger like structures result. This is called salt finger (SF) type of DDC. When a relatively, cold and fresh water mass overlies a warmer, saltier but more dense one, oscillatory instability occurs leading to a series of well mixed layers, separated by sharp interfaces. This is called diffusive layer (DL) type of DDC. Diapycnal mixing due to double diffusive convection in the interior of the ocean has been the subject of many studies, since the discovery of salt fingers nearly 50 years ago. In the intervening time, much has been learnt about double diffusive mixing through many elegant laboratory experiments and a few salient oceanic observations. Nevertheless, field observations of double diffusion in the oceans are still very few, and even fewer are measurements of the resulting turbulent mixing. Most of the oceanic observations have been of diapycnal mixing due to salt fingers (SF) that produce the classic temperature, salinity and density staircase structures when a relatively warm and salty water mass overlies a cooler and fresher one. Observations and measurements of double diffusive layers (DL) and the resulting staircase structures when a cooler, fresher water mass happens to overlay warmer, more saline one are relatively scarce. We report here microstructure measurements of double diffusive layers we made in the southern Adriatic Sea during the late March 2006 DART06A cruise aboard the RV Alliance of the NATO Undersea Research Center (NURC).

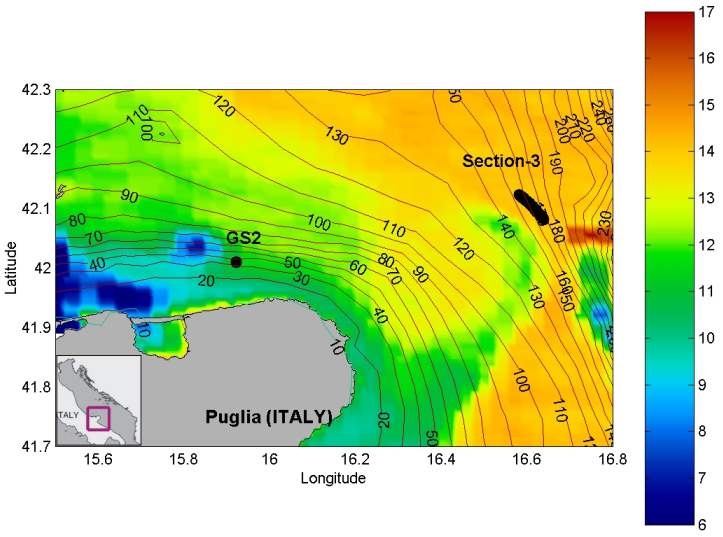

Figure 1: The positions and relative depths (m) of the 81 casts performed and analyzed in the present paper using the MSS profiler during the DART06A Cruise, superimposed to the surface temperature field as resulting from AVHRR satellite passage on 24th March, 2006, 07:46 UTC.

At the end of winter and before the onset of summer, the outflow from river Po, located in the NW area of the semi enclosed Adriatic Sea, tends to be colder than the basin water masses. The Po river water masses tend to flow southward along the Italian coast, and its plume and the associated front are clearly seen in satellite imagery as far south as the Gargano promentory before it rapidly mixes and disappears further downstream in the Southern Adriatic Sea. During the DART06A campaign, acoustic current meter moorings were deployed on the shelf along the coastal area shown in Figure 1, which shows local topography superimposed on the surface temperature field obtained from AVHRR satellite pass on 24th March, 2006, 07:46 UTC. During the mooring servicing cruise in late March 2006, we were able to deploy a microstructure profiler at these and other nearby stations to make temperature, salinity and turbulence measurements in the water column. In the northernmost station, called GS2 and located inside the Po river outflow, distinct staircase structures were observed due to DL. Along Section 3, located to the east, SF processes were detected. During the campaign, measurements were made at other locations besides those shown in Figure 1, but in those the layered structures were either nonexistent or not as distinct.

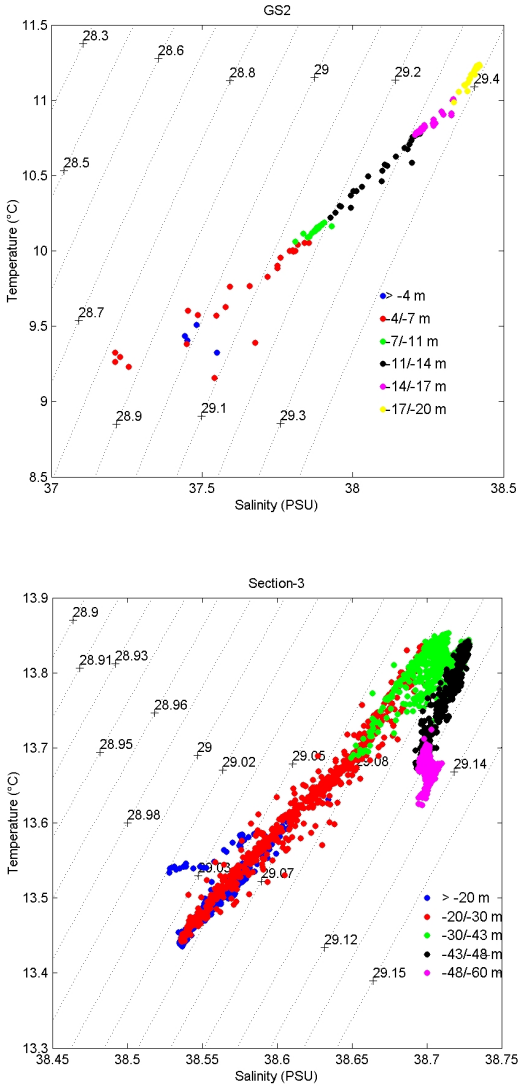

Figure 2: T and S diagrams for the two cases proposed, with water masses depicted at different depths. Top panel: Station GS2; bottom panel 3: Section 3.

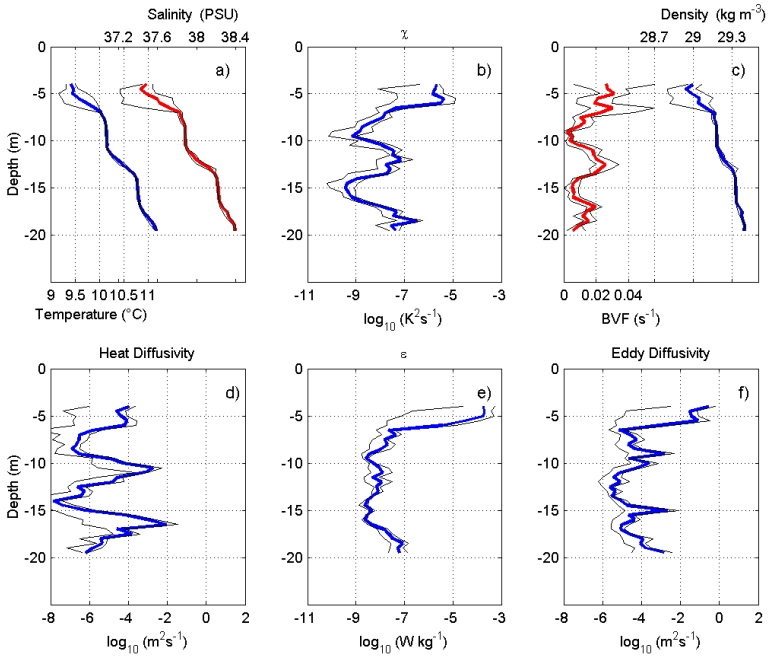

Figure 3: Staircase structures in the water column at station GS2. The water column depth is 27 m. Note the enhanced dissipation rate of thermal variance at the interface between well mixed layers. Measurements were made on March 20, 2006. Top panels: (a) temperature and salinity (red) in the water column, (b) temperature variance dissipation rate, (c) density (blue) and buoyancy frequency. Bottom panels: (d) heat diffusivity, (e) TKE dissipation rate, (f) eddy diffusivity. Color lines are the average, the two thin black lines represent the bootstrap confidence limits.

2 Observations

On March 20, 2006, four casts were made over a period of 7 minutes (between 08:50 and 08:57 UTC) at GS2 station, is in a shallow region (27 m deep) just 5 km away from the coast, and hence well within the Po river plume. Figure 2, top panel, shows the 0.5 m resolution TS relationship at different depth levels. Water masses are relatively fresh (never exceeding 38.5 PSU) and relatively cold (from 9 to 11.2 degree C), probably originating in the river Po outflow region.

Roughly 0.7 degrees to the east of stations GS2 (see again Figure 1), a total of 43 casts were made under moderate wind speeds in a water column roughly 160 m deep for 2.5 hours centered around the midnight of March 23rd-24th (22.40-01.18 UTC). Again Figure 2, bottom panel, is characterized mainly by a saltier (38.52-38.73 PSU)

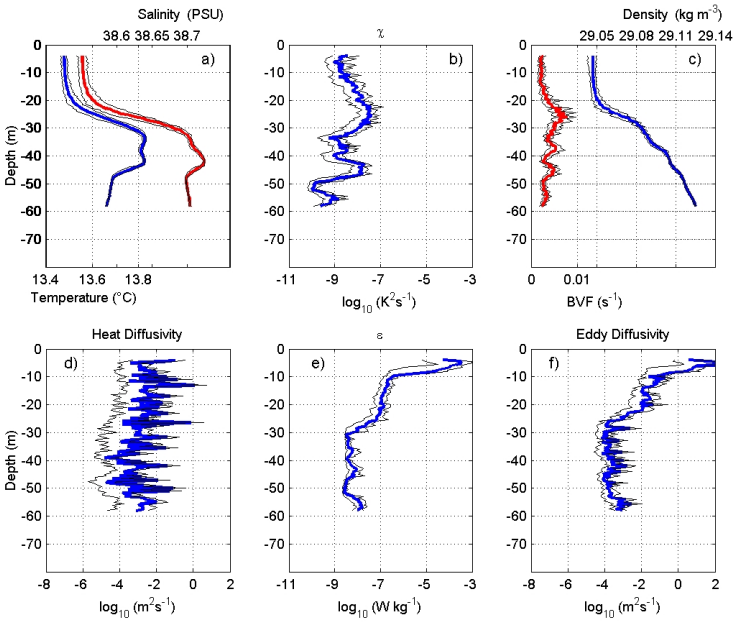

Figure 4: As in Figure 2, but along a short section (Section 3) to the east of Station GS2. The water column depth here is 160 m. A total of 43 casts were made here so that the inherent variability can be more clearly discerned. Color lines are the average, the two thin black lines represent the bootstrap confidence limits.

and much warmer (13.45-13.85 °C) water mass, thus leading a lighter water w.r.t. to the GS2 measurements (except the very surface ones). This is a signature of an off shore, open ocean water, that is less affected by the advection of the colder riverine water.

If we look more carefully at Figure 2, bottom panel, we have many cases in Section 3 where casts in the depth region between 43 and 48 m depict a decrease both in temperature and salinity with increasing density. SF processes are to be expected in this region.

Full details on the microstructure capabilities and turbulent variable derivation and analysis can be found in Carniel et al. [1].

Figures 3 and 4 show the vertical structure obtained from the microstructure profiler at station GS2 and Section 3. The mean and the confidence limits are presented, computed following the bootstrap analysis technique. Since the measurements were made from stern while the ship was moving forward very slowly, at a speed of 0.5 knots, roughly the upper 5 m of the profiles are discarded to avoid contamination by the wake of the ship.

The temperature and salinity profiles at GS2 indicate a clear staircase structure, with relatively cold and fresh waters over warm and salty ones, which is typical of

diffusive convection (DL) processes (see Figure 3a). The step-like structure is also evident in the density profile and rather prominent in the buoyancy frequency profile (Figure 3c, blue and red line respectively). The water column is stably stratified however, discounting the surface mixed layer, there are three well mixed layers in the water column each roughly 4 m thick with three roughly 3 m thick high gradient interfaces in between. The measured dissipation rate of thermal variance χ shows peaks at the interfaces between well mixed regions (Figure 3b), very much similar to measurements in staircase structures produced by for example double diffusive salt finger processes. Apart from the peak at the bottom of the upper mixed layer, prominent peaks can be seen at depths of 12 and 18 m. The dissipation rates χ reach values that are more than two orders of magnitude above the values in the bounding mixed layers, once again typical of staircase structures produced by DDC.
The dissipation rate ϵ of the turbulent kinetic energy (TKE, Figure 3e) also shows peaks at these depths, but they are rather less pronounced, smaller than 10^{-7} m^3 $s^{2,}$ while the background value of TKE is slightly higher. Also the peaks displayed at depths of 10 and 16 m by the thermal diffusivity derived from χ are well within the mixed layers adjoining the interfaces (see Figure 3, panel d). The peaks in the momentum diffusivity derived from ϵ are shown in panel f, and are located similarly but are less pronounced. Apparently then the measurements at GS2 show evidence of double diffusion, which is consistent with the fact that the station is well within the Po river plume (see Figure 1).
Figure 4 shows the vertical structure along Section 3. At this location, the upper mixed layer is slightly over 20 m deep. The interface below the mixed layer is rather diffuse and extends to a depth of roughly 30 m (see Figure 4a). Another well mixed layer, roughly 12 m deep and extending to a depth of 43 m, exists below this interface and is itself bounded below by an interface roughly 5 m deep, below which exists a deep mixed layer extending to the bottom.
The middle mixed layer contains a relatively warmer and more saline water mass than the upper and bottom mixed layers, so that the conditions are conducive to DC in the top interface and SF at the bottom interface. Again a step like structure is evident in the buoyancy frequency profile (Figure 4c, red line), while a peak in χ (Figure 4b) can be seen in the bottom interface at a depth of 45 m with a value slightly below 10^{-8} K^2 s^{-1} A more diffuse peak of similar value can be seen at the top interface, which is also rather diffuse.
The thermal and eddy diffusivities (panels d and f) exhibit rather high values, and the peaks associated with the region around 45 m are less evident w.r.t. those at GS2.

3 Conclusions

During the DART06A campaign in the Adriatic Sea, we were able to make measurements in layered staircase thermohaline structures resulting from double diffusive convection in the wintertime Po river plume in the Adriatic Sea. These measurements augment the sparse observations available on double diffusive convection, particularly diffusive layering type. The inferred turbulence diffusivities are consistent with those from earlier studies. We suggest that the wintertime Po river plume is a convenient and readily accessible location for studying these small scale mixing processes.

4 Acknowledgements

SC acknowledges partial support from the FIRB Project #RBFR08D825 (Project DECALOGO). MS and SC gratefully acknowledge support from EC FP7/2007-2013 under grant agreement n° 242284 (Project FIELD_AC).

References

[1] S. Carniel, M. Sclavo, L.H. Kantha, and H. Prandke. Double-diffusive layers in the Adriatic Sea. *Geophysical Research Letters*, 35(L02605), 2008.

Quantifying the Stokes Dissipation Wave Energy in the Global Ocean: Preliminary Estimates

M. Sclavo[1], S. Carniel[1], L. Kantha[1,2]
1, Institute of Marine Sciences, CNR, Venezia, Italy
2, University of Colorado, Boulder, USA
mauro.sclavo@ismar.cnr.it

Abstract

The turbulent Reynolds stresses in the upper layers of the ocean interact with the vertical shear of the Stokes drift velocity of the wave field to extract energy from the surface waves. This interaction is important for the dissipation of the low frequency part of the wave spectrum the effect of this Stokes dissipation is felt throughout the mixed layer, contributing also to Langmuir circulations. Unfortunately, this wave dissipation mechanism has hitherto been largely ignored. We present a preliminary estimate of the Stokes dissipation rate in the global oceans based on the results of the WAVEWATCH III model for the year 2007 to point out its potential importance seasonal and regional variations are also described.
The average for the year 2007 is about 2.5 TW, more than the 2.4 TW dissipation rate of wave energy in the surf zones around the ocean margins. Although it is small compared to the deep ocean dissipation rate by white capping of 68 TW it may be important to incorporate this mechanism into operational wave models.
The energy so extracted from waves is deposited in the mixed layer and, unlike energy injected by breaking waves it affects deeper parts of the mixed layer leading to enhanced turbulence, more uniform velocity profiles and higher deepening rate of the mixed layer.

1 Introduction

Surface gravity waves are frequently cited as a shining example of the very first successful application of the laws of fluid mechanics to a practical problem. However, for simplicity, most of the work over the past two centuries on oceanic surface gravity waves has considered the ocean to be inviscid. The interaction of waves with the turbulent motions in the upper layers has been ignored until recently. A proper treatment of the wave-mean current-turbulence interactions has only been accomplished in the past few years. The results show conclusively that very similar to the extraction of energy from mean currents by turbulence, turbulence can extract energy from the wave motions by the action of the Reynolds stresses on the vertical shear of the wave-induced Stokes drift.
Wind generated surface gravity waves travel on top of a turbulent and not an inviscid ocean as is commonly assumed. This implies that there is an inevitable interaction between the turbulent motions in the upper layers of the ocean and these gravity waves. Overall, such an interaction leads to extraction of energy from waves by turbulence in the oceanic mixed layer.

This interaction is particularly important for the dissipation of the low frequency part of the wave spectrum, swell. It acts as a source term for turbulent motions and a sink term for waves. This Stokes dissipation of wave energy is comparable to the dissipation of wave energy in the surf zones around the ocean basins. More importantly, unlike wave breaking (white capping), whose effects are confined to the top few meters, Stokes dissipation mechanism enhances upper layer turbulence with its effects felt potentially throughout the mixed layer. It also contributes to Langmuir circulation in the upper ocean. Unfortunately, the importance of this mechanism has not been fully appreciated and hence Stokes dissipation of waves has largely been ignored in wave modeling. In this note, we present a preliminary estimate of the Stokes dissipation in the global ocean based on the results of WAVEWATCH III model for 2007. Seasonal and regional variations are also described.

Needless to say that the Stokes mechanism of energy transfer from waves to turbulence constitutes an additional (in addition to the momentum and buoyancy fluxes at the air-sea interface) and important source of turbulent kinetic energy, and consequently, it enhances the intensity of turbulence in the oceanic mixed layer. One consequence of this is enhanced mixing and more uniform profiles in the mixed layer [1].

Based on LES simulations of Langmuir cells in the ocean, Kantha and Clayson (2004) have parameterized the extraction of energy from surface gravity waves by turbulence in the oceanic mixed layer. It is the working of the Reynolds stress on the vertical shear of the Stokes drift that extracts energy from the wave motion and transfers it to turbulence. It is rather analogous to working of the Reynolds stress against the mean shear in converting kinetic energy of the mean currents into TKE.

The wave directional spectrum from an operational wave model was integrated to estimate the Stokes drift velocity at the surface together with the wind stress this is needed to compute the Stokes dissipation rate.

We can therefore obtain a rough estimate of the wave dissipation rate due to wave and turbulence interactions without resorting to a second moment closure based global mixed layer model.

2 Wawewatch III model

As can be expected, observational data on the ocean surface wave field is inadequate to carry out this study. Instead appeal must be made to a global wave model. Using a version of the popular WAVEWATCH III (WW3) model, other authors [2] showed that on the average, the winds transfer energy into wave motions (which have a global energy content of about 1.52 EJ) at a rate of about 70 TW. Of this energy input, a majority of 67.6 TW goes into generating oceanic turbulence by breaking and other mechanisms, while 2.4 TW is dissipated in the surf zone. They did not however explore in detail the Stokes dissipation rate of the wave energy, reporting a value for Stokes dissipation of 6 TW. In this note, we intend to complement their work by computing the Stokes dissipation rate for the year 2007.

To estimate the Stokes drift over the global ocean, the WW3 Version 2.22 was run at 0.5 degree resolution (approximately 55 km at the equator) globally for the year 2007. This deep ocean wave model has been used at operational weather centers

since 2000, and there has been numerous verification studies, using wave buoys and satellite observations, documenting its performance over the years. It is a 3rd generation wave model, solving the non linear wave Interactions. The wave spectrum was discretized using 24 equally spaced directional bins and 25 logarithmically spaced wave number bins. The model was forced with 12 hourly surface winds from the Navy Operational Global Atmospheric Prediction System (NOGAPS), which have been archived on the Global Ocean Data Assimilation Experiment (GODAE) server. The time step was 3 hours.

3 Analysis and interpretation

The wave energy and the dissipation rate are summed up over the globe as well as the northern and southern hemispheres. In addition, values are computed for the longitudinal band between the Pacific sector, the Atlantic sector and the Indian sector. Figures 1 and 2 show the temporal variability of the energy in the global surface wave field and the Stokes dissipation rate of this wave energy. Black curves in Figures 1 and 2 denote the global values; the red curve in Figure 1 corresponds to the northern and the blue curve to the southern hemisphere; the blue curve in Figure 2 corresponds to the Pacific, the red curve to the Atlantic and the green curve to the Indian sectors. The average value of global wave energy of 1.68 EJ. Compare this to the total energy in barotropic ocean tides of only 0.6 EJ. The average Stokes dissipation rate of 2.5 TW is more than the 2.4 TW rate of dissipation of the wave energy in the surf zones at the ocean margins [2], but can reach values as high as 3.7 TW. Comparatively, the dissipation rate of tidal energy in the global oceans and hence of the gravitational energy of the Earth-Moon-Sun system, is only about 3.75 TW [3].

The Stokes dissipation rate of 2.5 TW is likely to be a slight underestimate due to issues related to the resolution of the high frequency end of the wave spectrum in wave models (The use of 24 frequency bands implies maximum frequency of 0.4 Hz instead of 0.7 Hz, which may reduce the surface Stokes drift value by a few tens of percent. While the global energy and dissipation rates show very little seasonal variability, the hemispheric values show a prominent seasonal variability, with values in the northern hemisphere being higher during the boreal winter than the boreal summer but exactly opposite behavior is evident in the southern hemisphere.

Majority of the contribution to Stokes dissipation (1.8 TW) is from the southern hemisphere, with the roaring fifties contributing significantly. During the boreal summer, the Stokes dissipation is mostly from the southern hemisphere. The average dissipation rate is 1.3 TW in the Pacific, 0.7 TW in the Atlantic and 0.6 TW in the Indian sectors. The Atlantic and Indian sectors contribute roughly equally to Stokes dissipation, with the Pacific sector contributing significantly more.

Figure 3 shows the distribution of the wave energy (in TJ) and Stokes dissipation rate (in MW) in each 0.5 x 0.5 degree box over the global oceans averaged over 2007. High dissipation rate regions are well correlated with high wave energy regions for example the roaring fifties in the southern hemisphere, and the Gulf Stream and Kuroshio extension regions as well as the Arabian Sea in the northern hemisphere. The average dissipation rates reach

as high as 70 MW and average wave energies as high as 36 TJ in the southern hemisphere. The southern latitudes, the Gulf Stream and Kuroshio extension regions contribute heavily to Stokes dissipation. In the North Indian Ocean, the summer monsoon-affected regions along the Arabian coast display high wave energy and dissipation rates.

Figures 4 and 5 show the seasonal variability. Figure 4 shows the boreal winter (from January to March) and Figure 5 the boreal summer (from July to September) averages. The seasonal contrasts are rather striking. For example, during the boreal winter, high dissipation rates are evident in the northern hemisphere, while during the boreal summer, the values there are very low. In contrast, the values remain high in the roaring fifties region of the southern hemisphere during both boreal summer and winter, although the boreal summer values are significantly higher. In the North Indian Ocean, summer monsoon winds cause high dissipation rates in the Arabian Sea region. The above findings are consistent with what could be expected based on what we know about the regional and seasonal characteristics of surface gravity waves in the global oceans. High wave regions tend also to be regions of high Stokes dissipation rates.

The study therefore highlights the importance of the Stokes dissipation mechanism in the global oceans.

4 Concluding remarks

We have provided a preliminary estimate of the Stokes dissipation rate of the surface gravity waves in the global oceans. The average for the year 2007 is about 2.5 TW, more than the 2.4 TW dissipation rate of wave energy in the surf zones around the ocean margins. More importantly, unlike wave breaking (white capping), whose effects are confined to the top few meters, Stokes dissipation mechanism enhances upper layer turbulence with its effects felt potentially throughout the mixed layer. It also contributes to Langmuir circulation in the upper ocean. Although it is small compared to the deep ocean dissipation rate by white capping of 68 TW, to improve the physical basis of parameterization of wave dissipation, it may be important to incorporate this mechanism into operational wave models.

The energy so extracted from waves is deposited in the mixed layer and unlike energy injected by breaking waves, which affects only the top few meters of the mixed layer, it affects deeper parts of the mixed layer leading to enhanced turbulence, more uniform velocity profiles and higher deepening rate of the mixed layer [1].

Needless to say that this study needs to be followed up by a more thorough in depth study using a reliable mixed layer model. The primary objective of this note is to merely point out the potential importance of the Stokes dissipation of surface gravity waves in the global ocean.

5 Acknowledgements

This work has been partially funded by the European Community's Seventh Framework Programme FP7/2007-2013 under grant agreement n° FP7-021338 (Project EQUIMAR).

References

[1] S. Carniel, M. Sclavo, L.H. Kantha, and C.A. Clayson. Langmuir cells and mixing in the upper ocean. *Il Nuovo Cimento*, 28:33–54, 2005.

[2] N. Rascle, F. Ardhuin, P. Queffeulou, and D. Croize-Fillon. A global wave parameter database for wave-current-turbulence interaction studies. *Ocean Modelling*, 25(3-4):154–171, 2008.

[3] L.H. Kantha and C.A. Clayson. Numerical Models of Oceans and Oceanic processes. page 912, 2000.

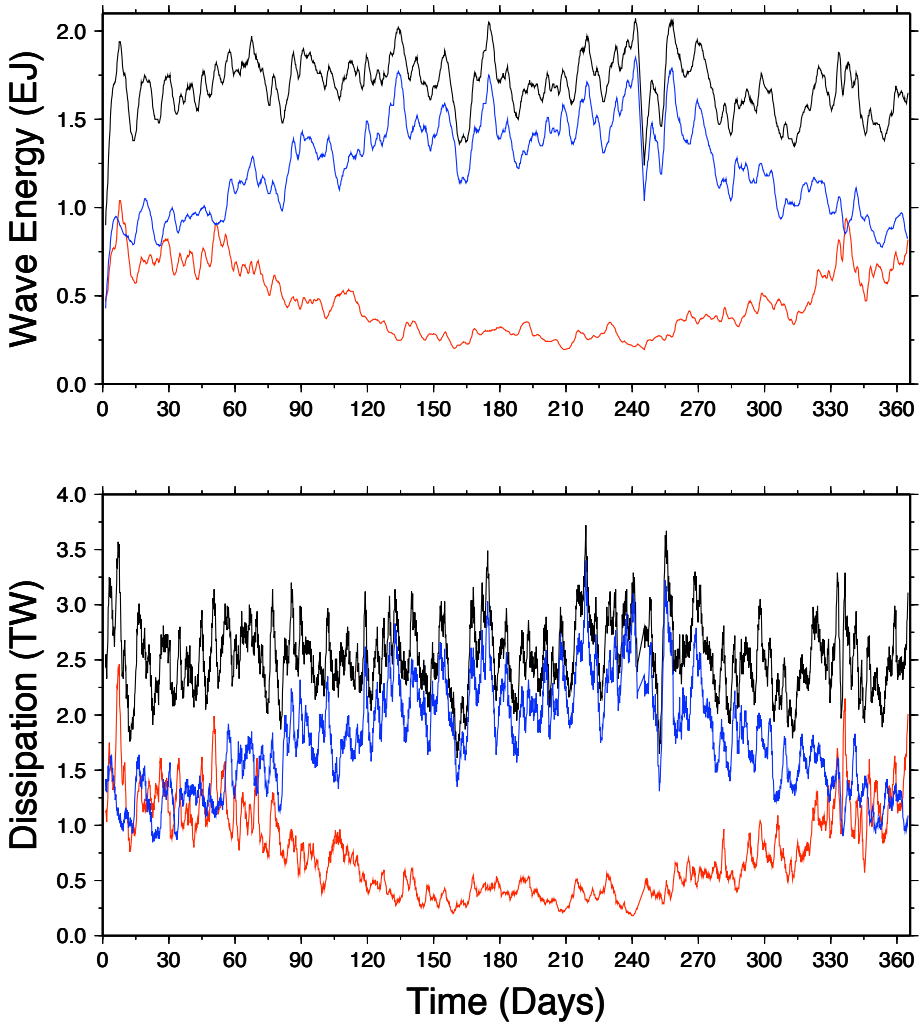

Figure 1: Time series of the energy in the global surface gravity wave field (in EJ) and the rate of dissipation of that energy by Stokes dissipation (in TW). Global average (black), Northern hemisphere (red), Southern hemisphere (blue)

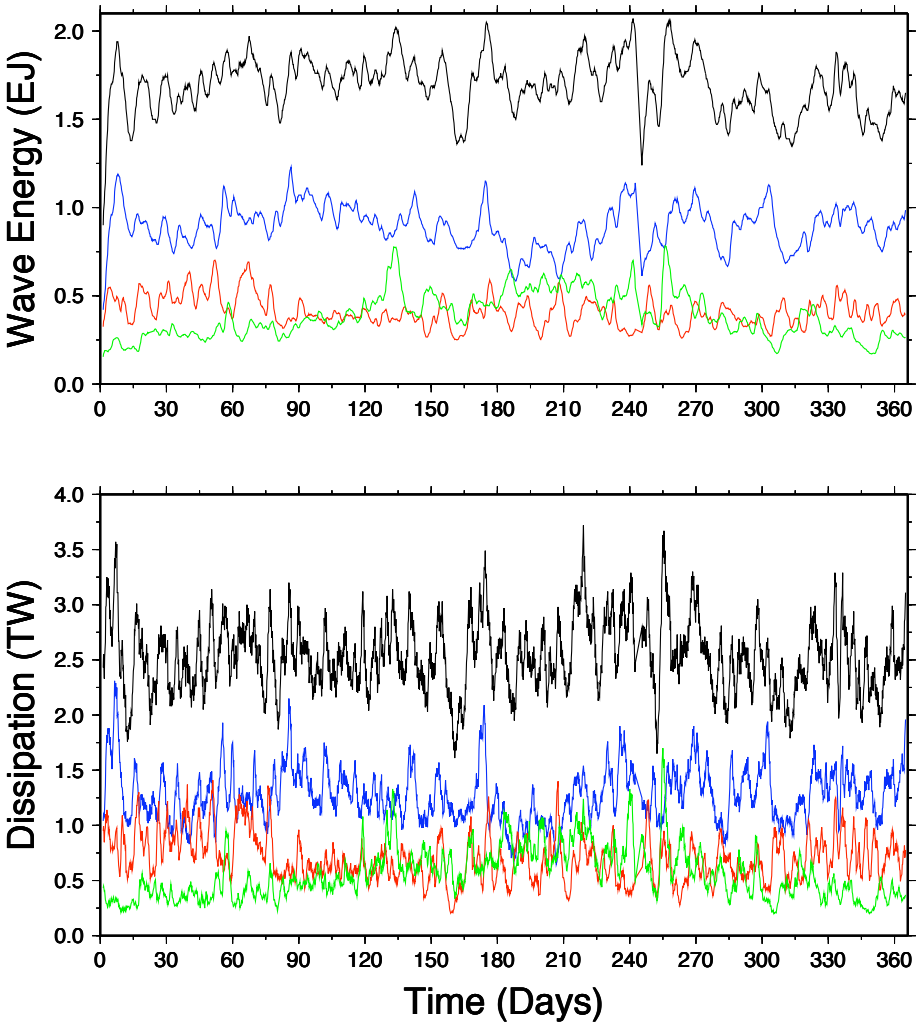

Figure 2: Time series of the energy in the global surface gravity wave field (in EJ) and the rate of dissipation of that energy by Stokes dissipation (in TW). Global average (black), Pacific (blue), Atlantic (red), Indian Ocean (green).

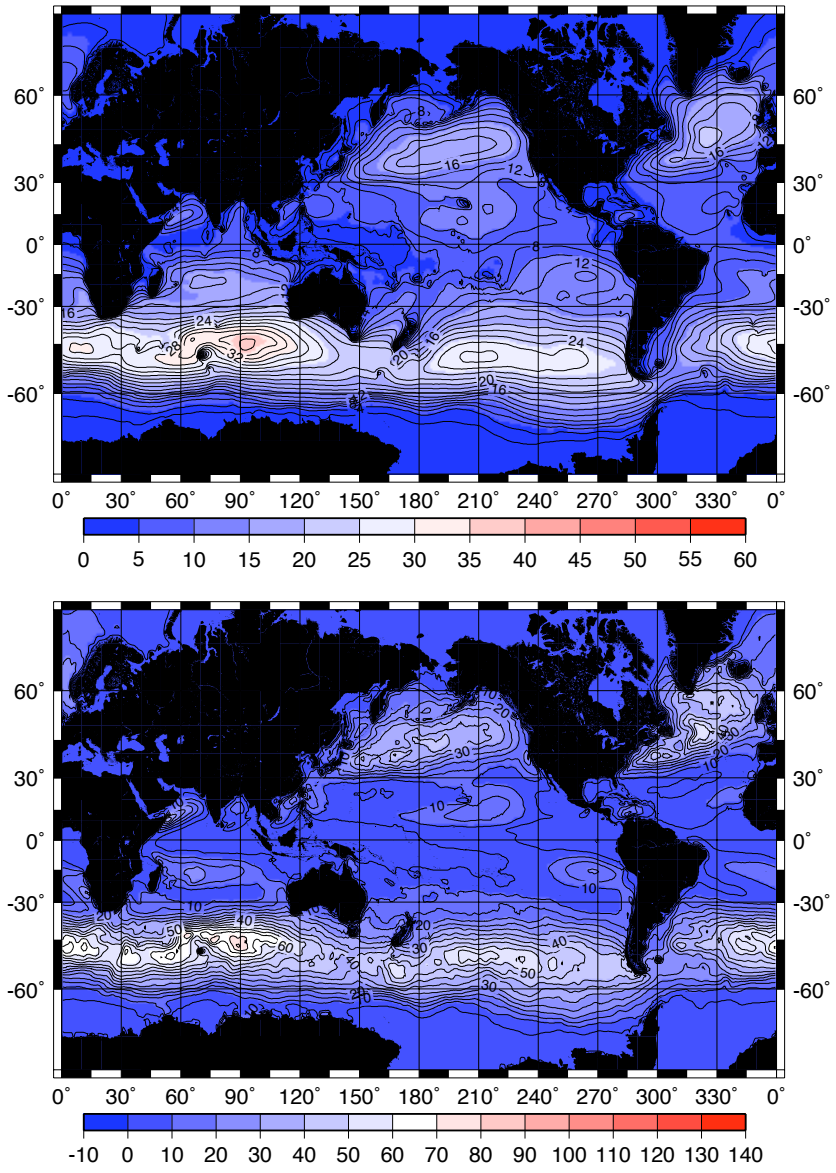

Figure 3: Spatial variability of the annual average of the wave energy (in TJ) (top panel) and the Stokes dissipation rate (MW) (bottom panel) in each 0.5 x 0.5 degree grid. Note the high dissipation rate regions are well correlated with high wave energy regions. The high dissipation rates in the southern latitudes are noteworthy.

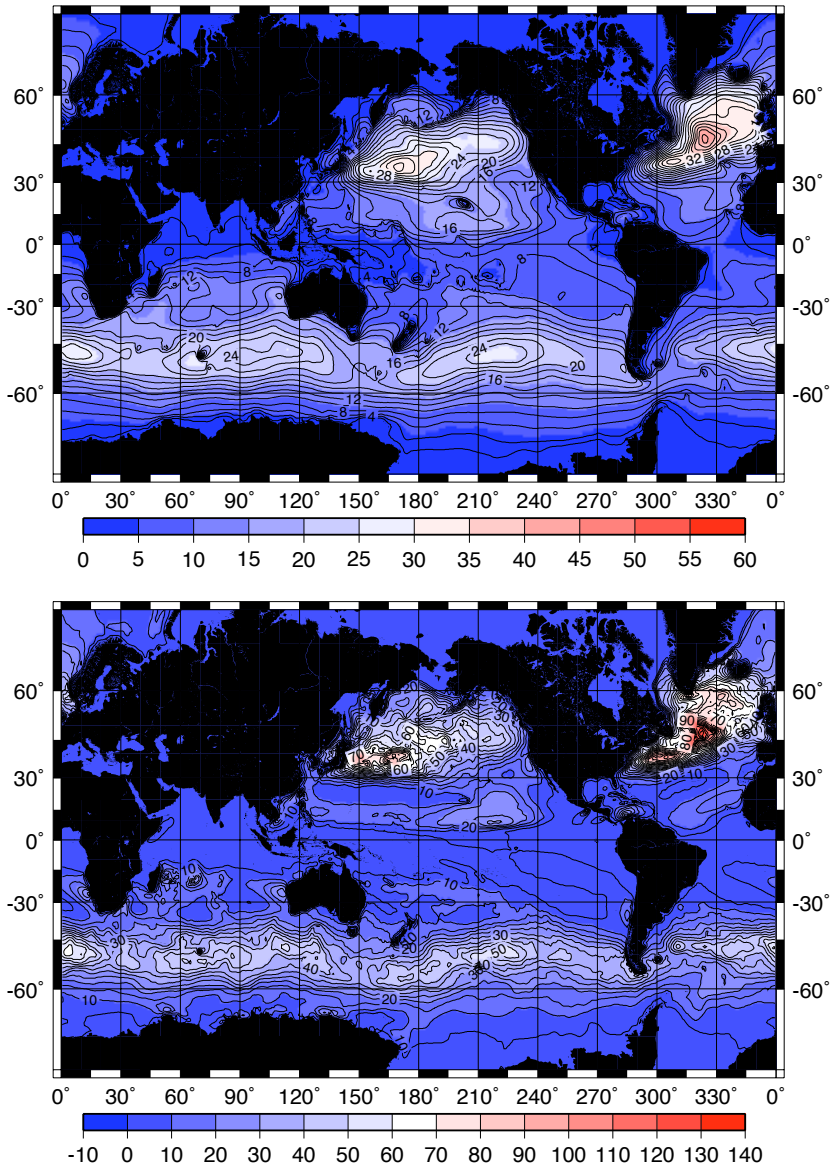

Figure 4: Spatial variability of the boreal winter (from January to March) average of the wave energy (in TJ) (top panel) and the Stokes dissipation rate (MW) (bottom panel) in each 0.5 x 0.5 degree grid. Note the high dissipation rates in the northern hemisphere.

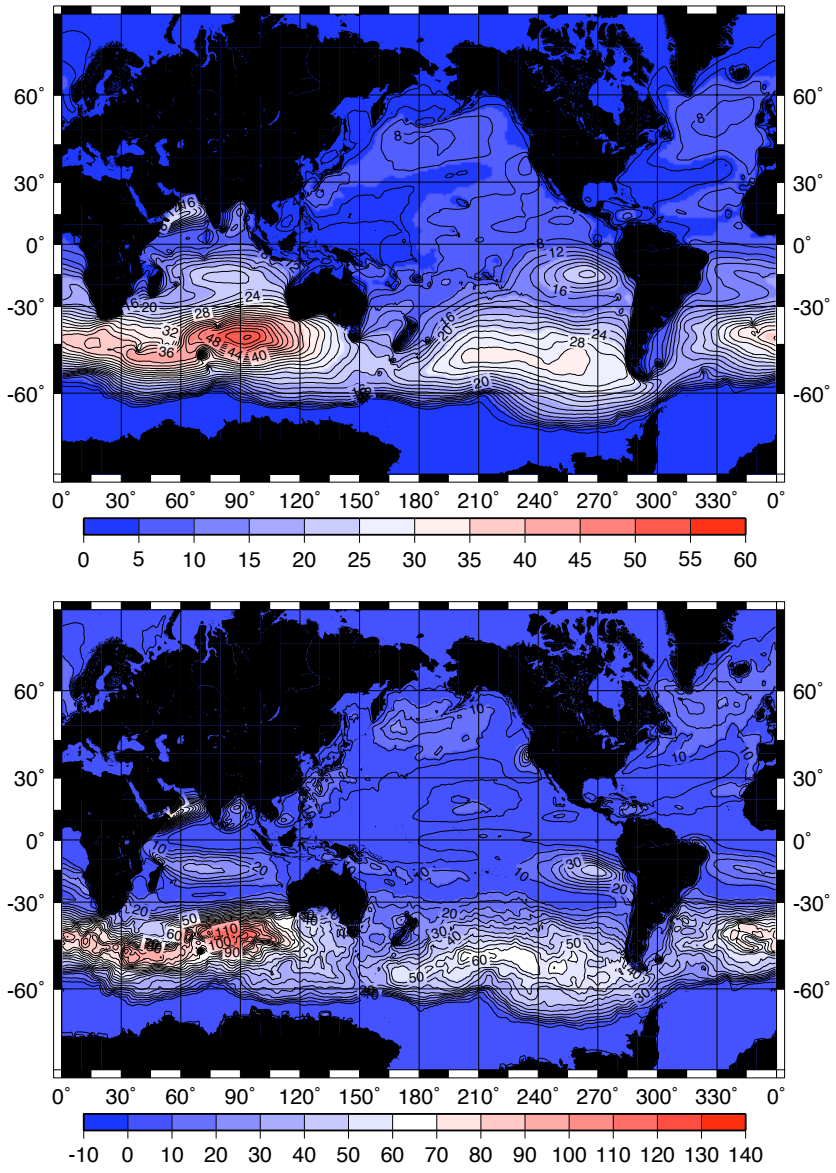

Figure 5: Spatial variability of the boreal summer (from July to September) average of the wave energy (in TJ) (top panel) and the Stokes dissipation rate (MW) (bottom panel)in each 0.5 x 0.5 degree grid. Note the high dissipation rate rates in the roaring fifties in southern hemisphere and the very low values in the northern.

Experimental Study of the Role of the Vertical Structure of the Marine Atmospheric Boundary Layer on the Air-Sea Exchange during the LASIE Campaign

A.M. Sempreviva[1], M.E. Schiano[2], S. Pensieri[3], R. Tomé[4,6], R. Bozzano[3], M. Borghini[5], F.M. Grasso[7], A. Semedo[8,4], L.L. Soerensen[4,9], J. Teixeira[10], C. Transerici[11]

1, Institute of Atmospheric Sciences and Climate, CNR, Lamezia Terme (CZ), Italy
2, Institute of Marine Sciences, CNR, Genova, Italy
3, Institute of Intelligent Systems for Automation, CNR, Genova, Italy
4, Risø National Laboratory for Sustainable Energy, Technical University of Denmark, Roskilde, Denmark
5, Institute of Marine Sciences, CNR, Pozzuolo di Lerici (SP), Italy
6, University of Azores, Açores, Portugal
7, Institute of Atmospheric Sciences and Climate, CNR, Lecce, Italy
8, Uppsala University, Uppsala, Sweden
9, National Environmental Research Institute, Aarhus University, Roskilde, Denmark
10, Jet Propulsion Laboratory, California Institute of Technology, Pasadena, California
11, Institute of Atmospheric Sciences and Climate, CNR, Roma, Italy
am.sempreviva@isac.cnr.it

Abstract

Several atmospheric parameters play a crucial role in the air-sea exchange of momentum and matter relevant for the ocean general and local circulations, biological activities and in monitoring the ocean from space-borne observations. Here, we address two issues: the height of the Atmospheric Boundary Layer (ABL) and its role in governing turbulent fluxes at the air-ocean interface, and the correlation amongst scalars used in assessing scalar transfer for estimating surface fluxes and in the atmospheric refraction index. We present a dataset spanning through the entire height of the Marine ABL collected during the Ligurian Air-Sea Interaction Experiment (LASIE) performed in the Western Mediterranean Sea. LASIE was organized to evaluate and develop parameterizations of the oceanic BL and ABL and their interactions. A detailed characterization of the mean and turbulent structure of the ocean and ABL has been carried out using ship and buoy -based meteorological and oceanographic observations. The main purpose of this contribution is to present this CNR's activity related to the air-sea exchange processes in an international context, and to draw the attention of the scientific community to the LASIE uncommon database. Here, we address the atmospheric part of the experiment In the meantime, we outline the on a case study of and present a case study of the evolution of the vertical structure of the ABL according to the synoptic conditions change, i.e. shift

offshore-onshore flow, and the work in progress to identify the relationship with surface air-sea exchange.

1 Introduction

Several atmospheric parameters play a crucial role in the air-sea exchange of momentum and matter of relevance for the ocean general and local circulations, biological activities and in monitoring the ocean from space-borne observation platforms. One of the relevant parameters is the height of the Atmospheric Boundary Layer (ABL),z_i, identified by a vertical increase of the potential temperature Θ and a vertical decrease of relative humidity RH and called temperature inversion which indicate the top of the ABL. During the last decade, z_i has been more and more recognized as governing the turbulent exchange of momentum and matter at the air-ocean interface [1, 2]. Recently, Gryning et al., [3] suggested that the wind speed U vertical profile above the surface within 50-80 meters height could be controlled by the surface conditions, z_i, and the conditions above the ABL.

Also the amount of water available in the air partly depends on the inversion height, affecting the evaporation from the sea surface as well as the cloud formation [4]. Latent heat fluxes through evaporation weaken the ocean stratification allowing for dense waters to sink and ventilate deep and intermediate water layers [5, 6, 7]. Furthermore, the transmission of radar and microwave signals over the ocean may be disturbed by the layered vertical structure of the Marine ABL (MABL) [8].

Another important issue is the mechanisms through which the atmospheric turbulent flow maintains strong scalar to scalar correlation that are also relevant for fluctuations of the refractive index of importance to short-path electromagnetic or acoustic wave propagation in the atmosphere. At the same time the correlation among turbulent fluctuations of scalars such as air temperature, T_a, moisture q and carbon dioxide c in the ABL has received significant attention because of its use in assessing similarities in bulk scalar transfer parameters Katul et al. [9], and consequently in the subgrid parameterizations employed in atmospheric models. Understanding scalar exchange mechanisms can highlight new dynamical processes modulating the structure of turbulence within the oceanic and the atmospheric boundary layers not readily detected by other approaches.

A complete set of measurements from the surface through the MABL entire height is even more seldom than over land especially in the Mediterranean Sea. The intensive Ligurian sea Air-Sea Interaction Experiment (LASIE), 16-22 June 2007 [10, 11] was organized to contribute filling this gap, for evaluating and developing parameterizations of the oceanic and ABL and to study their interactions. To achieve this goal, a detailed characterization of the mean and turbulent structure of the ocean and atmosphere boundary layers has been carried out using ship and buoy -based meteorological and oceanographic observations in the Ligurian Sea (Figure 1).

The main purpose of this contribution is to present the CNR's activity of investigating the air-sea interaction and exchange processes in the context of an international experimental effort, and to draw the attention of the scientific community to the LASIE complete and uncommon database. Here, we introduce the activity carried out within LASIE by analy$z_i$ng atmospheric data. We

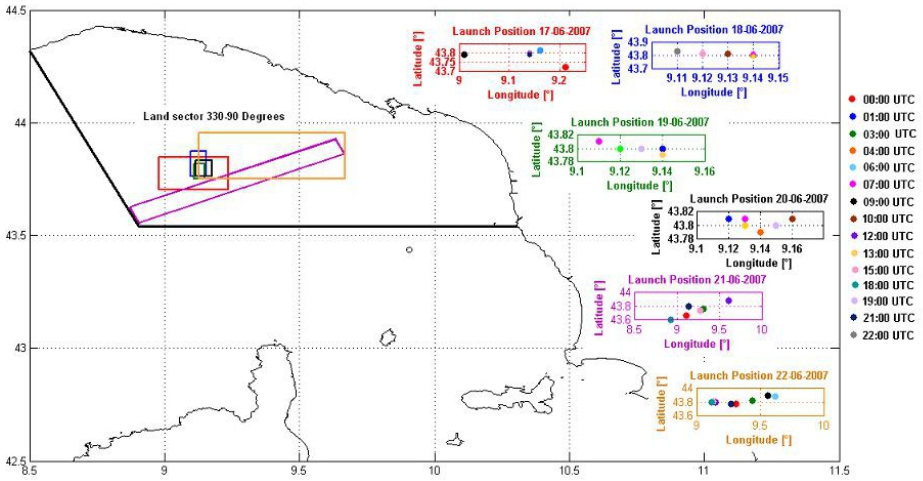

Figure 1: The R/V Urania operational areas during LASIE. Day 21 and 22 the ship was sailing within large areas back and forth from and to the coast. The black lines delimit the "land" sector with outflow from the coast.

outline the resuts of the main case study of the evolution of the vertical structure of the marine boundary layer following the evolution of z_i according to the change of synoptic conditions that induced a shift offshore - onshore flow, and the work in progress for identifying the relationship between z_i and the surface air-sea fluxes.
Details of instruments, methodologies and full results are presented in a recently produced paper by [11].

2 The experiment

In Figure 1, boxes of different colors show the operational areas during each of the six days. The LASIE atmospheric database consists in observations collected on two observation platforms, a ship and a buoy.
The CNR's buoy ODAS Italia 1 is moored in the Ligurian Sea at 43°47.36'N, 009°09.80' E, about 73 Km offhore the city of Genoa and on a water depth of 1377 m. It is a spar buoy about 50 m long and weighing 11 tons, with a small laboratory at the top, and a design (e.g. total mass, unity buoyancy at sea level, and damping disk) such as sensitivity to sea heave is negligible [12, 13].
Measurements are collected by an acquisition system installed on the small laboratory. Although the acquisition system can operate with any desired sampling interval, the employed default operating mode provides a data record every hour. The acquired records are transferred in real-time by a phone line to the shore station where they are quality checked. The sensors used in this work are listed in Table 1.
During LASIE, the onboard acquisition system collected at a frequency f = 0.2 Hz: - mean values of U and T and turbulent fluctuations of wind speed components u', v', w' and air temperature T', by a Gill research sonic anemometer;

Parameter	Manufacturer	Model	Height/Depth [m]
Meteorological Measurements			
Global solar radiation	Eppley	PSP	+14.6
Wind speed	Gill	WindSonic	+14.4
Wind direction	Gill	WindSonic	+14.4
Air temperature	Vaisala	HMP45A	+14.3
Relative humidity	Vaisala	HMP45A	+14.3
Atmospheric pressure	Vaisala	PTB100A	+7.8
Air temperature	Vaisala	WXT510	+14.5
Relative humidity	Vaisala	WXT510	+14.5
Precipitation	Vaisala	WXT510	+14.5
Atmospheric pressure	Vaisala	WXT510	+14.5
Oceanographic Measurements			
Water temperature	Seabird	SBE39	-0.5, -12.0, -28.0

Table 1: Equipment on the ODAS Buoy.

- T_a and the sea temperature T_s, radiation R, pressure P with standard sensors.

Heat fluxes were computed following Fairall et al. (1996). The evolution of surface U, DIR, RH, R, T_a and T_s, during LASIE is presented in Figure 2. On the second platform, the R/V Urania research vessel of the Italian National Council of Research (CNR), the equipment installed onboard collected at a sampling rate of 100 Hz:

- u', v' and w', and T', by a Gill research sonic anemometer and
- Turbulent fluctuations of humidity q' and carbon dioxide concentration c' by a LICOR 7500.

Furthermore, onboard of the Urania vessel, the vertical structure of the MABL was monitored by radiosondes (Vaisala DigiCORA Sounding System MW21) and a ceilometer (Vaisala CL31).

Radiosondes were released every 3 hours recording vertical profiles of U, DIR, Θ and RH, while the ceilometer was continuously measuring providing information on the vertical distribution of the atmospheric aerosols and of the height of the cloud bases.

During the late afternoon on June 18, the wind turned from onshore to offshore the Italian coast until late June 20 (shaded area in Figure 2). This caused the change of

the vertical structure of the MBL. Warm and dry air from land flowing over a colder sea induce a stably stratified atmospheric Internal Boundary Layer (IBL) that develops from the coast up to large distances. This stable IBL can be detected up to the buoy positions therefore it can develop and maintain to large distances from the coast ranging between 150-300m trapping the moisture in the Atmospheric Surface Layer (ASL) and the vertical structure of the MABL also present multiple inversions.

Figure 4 shows the development of the vertical structure of the ABL, in terms of Θ and RH vertical profiles, during the whole period; the shaded area corresponds to the same period as indicated in Figure 2.

Figure 4 shows the comparison between ceilometer and the radiosoundings for the 18 and 19 June when the air flow turned from onshore to offshore. Ceilometer plots show the intensity of the backscatter from the marine aerosols; the most intense backscatter (dark blue) indicates a discontinuity in the aerosol concentration, which delimits the MBL from the free atmosphere clean of aerosols. The vertical profiles of RH and Θ, from radiosondes allow detecting the inversion z_i delimiting the MABL. (in case of cloud free sky) Ceilometer and radiosoundings agree in showing the evolution of the vertical structure of the boundary layer following the change onshore-offshore flow shift when the marine surface layer becomes stable and dry modifying the airs-sea surface fluxes.

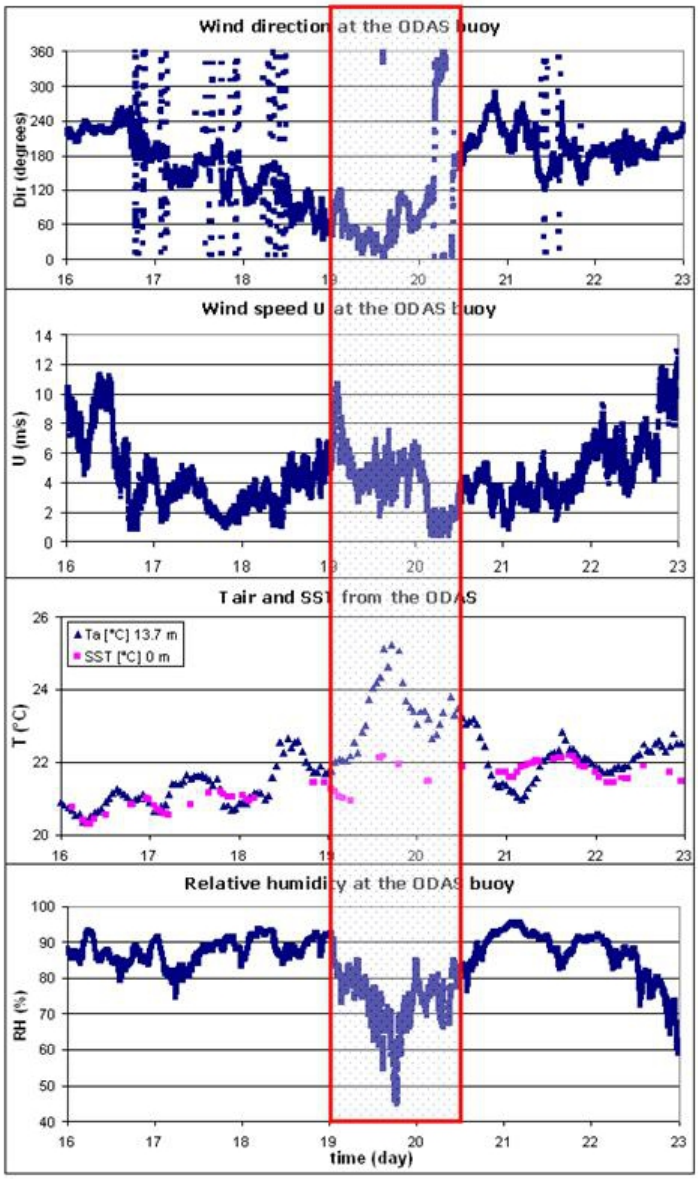

Figure 2: Evolution of surface DIR, U, ΔT and RH during LASIE. (From Top to Bottom). The shaded area corresponds to offshore flow of warm and dry air that caused the evolution of the vertical structure of the Atmospheric Marine Boundary Layer inducing a stable IBL.

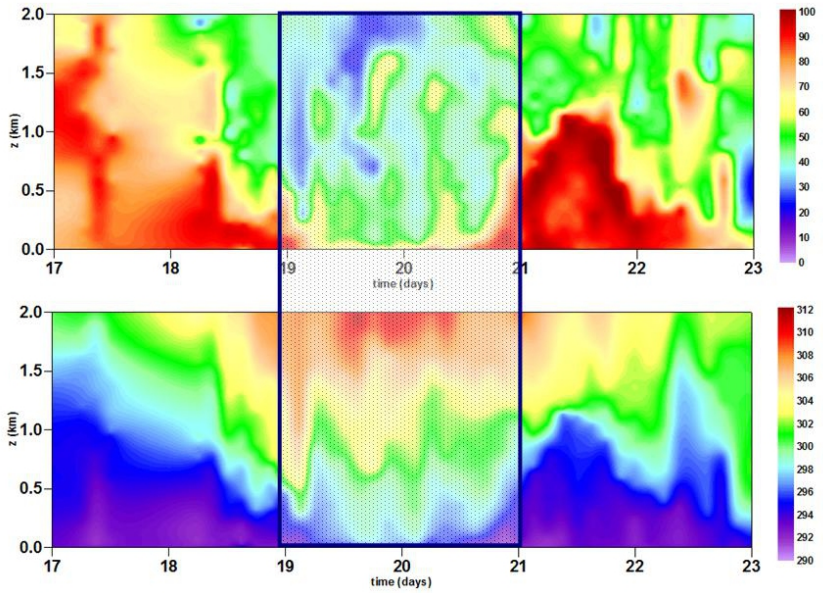

Figure 3: Evolution of the atmospheric vertical structure of the potential temperature Θ (Top) and relative humidity RH (Bottom) during LASIE. The shaded area corresponds to offshore flow as in Figure 2.

3 Work in progress

The correlation amongst scalars in the Marine Atmospheric surface layer in under investigation to understand the evolution of the air-sea exchange fluxes in time and space. The estimate of the correlation between two scalars x and y is their correlation coefficient R_{xy} defined as

$$R_{xy} = \frac{\overline{x'y'}}{\sigma_x \sigma_y},$$

where x and y in our case can be q, T and c, $\overline{x'y'}$ is their mean covariance and σ_x and σ_y are their variances.
As mentioned in the introduction, the correlation between T and q is a key parameter in obtaining the humidity flux using methods that strongly rely on a perfect correlation between the two variables, i.e. the flux-variance methods described in Katul et al. [9]. Katul et al. showed that using the flux variance method, the turbulent humidity flux, defined as the covariance between the fluctuations of the vertical wind speed and the fluctuations of humidity $\overline{w'q'}$, can be obtained from turbulent sensible heat defined as the covariance between the fluctuations of the vertical wind speed and the fluctuations of temperature $\overline{w'T'}$, which is more easily available. Actually, in the ABL, scalars such as T and q are supposed to be transported by local turbulence resulting in $|\mathrm{R_q T} = 1|$; however, a perfect correlation between scalars has long been questioned and studies on the correlation between q and T have been carried out for decades.

Therefore, if this basic assumption is not always correct, the flux parameterizations, based on it, will be limited to specific atmospheric conditions. In the marine environment, Sempreviva and Gryning [1] discussed the connection between the dissimilarity amongst scalars and the height of the inversion z_i. From this study, a consistent interpretation of the low q-T correlation in the surface layer over a homogeneous sea surface, suggests the important influence of processes outside the surface layer (non-local processes) i.e. entrainment of dry air from higher layers into the surface layer, through the mixing process of the larger eddies, sea-spray, and advection from land. In analogue to R_{xy}, it can be derived a spectral correlation coefficient $r_{xy}(n) = \frac{C_{xy}(n)}{S_x(n)S_y(n)}$ at the normalized frequency n = f_z/U, where z is the height of measurements, Cxy(n) is the co-spectrum of x and y, S_x(n) and S_y(n) are the root squared spectral values of x and y. Using this methodology, Asanuma et al., [14] showed that the low correlations of scalar can be correlated to atmospheric eddies of different sizes. Warm and dry outflow from land results in stable conditions and negative R_{xy} and r_{qT}. Therefore, studying the correlation of scalars allows exploring the limit of the application of new parameterizations and the interplay between the ABL structure and the surface processes, which influence the air-sea exchange.

4 Final remarks

The LASIE atmospheric and oceanic database will be of great value for future evaluation of ocean-atmosphere coupled model systems and atmospheric models at different spatial and temporal scales. It was found that during an offshore flow of warm and dry air over the sea, a stable internal boundary layer can develop and maintain up to large distances from the coast ranging between 150-300 m developing multiple inversions and trapping the moisture at the surface. Since the height of the MABL and the MABL vertical structure play a significant role on the surface turbulence and on wind speed profiles, future studies will address the relationship between surface fluxes, estimated using high frequency measurements of wind speed, temperature, moisture and CO_2, collected onboard of the buoy and the R/V Urania, and the vertical structure of the MABL including the use of spectral analyses.

5 Acknowledgments

We thank the Italian CNR for the availability of R/V Urania during the dedicated cruise "LIGURE2007", coordinated by Sandro Carniel (CNR-ISMAR, Venice). The captain and crew of the R/V Urania are also thanked for their excellent contributions to this successful campaign. We thank NURC for organi$z_i$ng the LASIE campaign and granting funding for shipping instruments and for the purchasing of radiosondes. Michael Courtney, Soeren Lund and Lars Christensen, from Risoe-DTU, are thanked for lending and setting up the ceilometer acquisition system. Daniele Contini and Antonio Donadeo from CNR-ISAC Lecce, are also thanked for useful discussions on the paper. Anna Maria Sempreviva, Fabio Grasso, Alvaro Semedo and Ricardo Tomé acknowledge funding from the FP6 Marie Curie Research Network ModObs, MRTN-CT-2006-019369. The ModObs Network www.modobs.windeng.net has been one of the sponsors of the LASIE Campaign and ISAC-CNR is one of the partners.

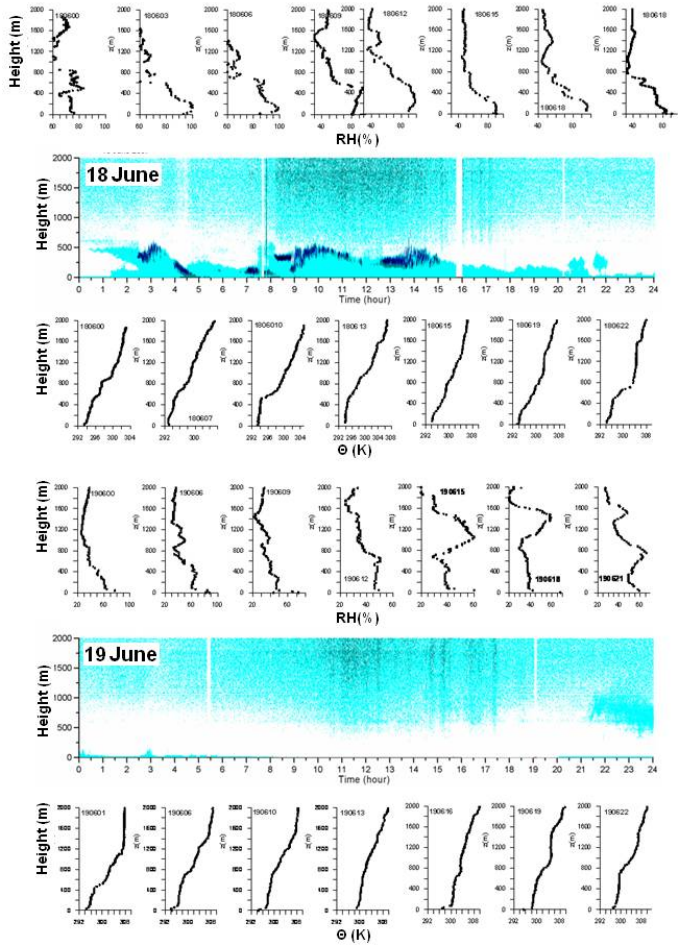

Figure 4: Example of the evolution of the vertical structure of the MABL detected by the ceilometer (Light blue figures in the middle) and vertical profiles of relative humidity (above the ceilometer plot) and potential temperature (below the ceilometer plot) by radiosoundings during 18-19 June 2007. During the late afternoon of the 18th the flow turned from onshore to offshore. Warm and dry air from land induced a stable IBL that trapped the water vapor content at the surface. Note the change in the backscatter signal of the ceilometer.

References

[1] A.M. Sempreviva and S.E. Gryning. Mixing height over water and its role on the correlation between temperature and humidity fluctuations in the unstable surface layer. *Boundary-Layer Meteor*, 97:273–291, 2000.

[2] G.G. Katul, A.M. Sempreviva, and D. Cava. The Temperature–Humidity Covariance in the Marine Surface Layer: A One-dimensional Analytical Model. *Boundary-Layer Meteorology*, 126(2):263–278, 2008.

[3] S.-E. Gryning, E. Batchvarova, B. Brümmer, HE. Jørgensen, and S.E. Larsen. On the extension of the wind profile over homogeneous terrain beyond the surface boundary layer. *Boundary-Layer Meteor.*, 124:251–268, 2007.

[4] S.-E. Gryning and E. Batchvarova. Marine boundary layer and turbulent fluxes over the Baltic Sea: Measurements and modelling. *Boundary-Layer Meteorol.*, 103:29–47, 2002.

[5] M.E. Schiano, M. Borghini, S. Castellari, and C. Luttazzi. Climatic features of the Mediterranean Sea detected by the analysis of the long-wave radiative bulk formulae. *Annales Geophysicae*, 18:1482–1487, 2000.

[6] Schiano et al. . 2005.

[7] A.S. Smedman, S.E. Gryning, K. Bumke, U. Högström, A. Rutgersson, et al. Precipitation and evaporation budgets over the Baltic Proper: observations and modelling. *Journal of Atmospheric and Ocean Science*, 10(3):163–191, 2005.

[8] I.M. Brooks, A.K. Goroch, and D.P. Rogers. Observations of Strong Surface Radar Ducts over the Persian Gulf. *J. Appl. Meteorol.*, 38:1293–1310, 1999.

[9] G.G. Katul S.M. Golz, C.I. Hsieh, Y. Cheng, F. Mowry, and J. Sigmon. Estimation of surface heat and momentum fluxes using the flux-variance method above uniform and non-uniform terrain. *Boundary-Layer Meteor*, 74:237–260, 1995.

[10] J. Teixeira. Ligurian Air-Sea Interaction Experiment (LASIE) trial plan. page 30, 2007.

[11] A.M. Sempreviva, M.E. Schiano, S. Pensieri, A. Semedo, R. Tomé, R. Bozzano, M. Borghini, F. Grasso, L.L. Soerensen, J. Teixeira, and C. Transerici. Observed development of the vertical structure of the marine boundary layer during the LASIE experiment in the Ligurian Sea. *Ann. Geophys.*, 28:17–25, 2010.

[12] H.O. Bertaux. Buoy Enginering. 1976.

[13] L. Cavaleri and E. Mollo-Christensen. Wave response of a spar buoy with and without a damping plate. *Oceanean Engineering*, 8:17–24, 1981.

[14] J. Asanuma, I. Tamagawa, H. Ishikawa, Y. Ma, T. Hayashi, Y. Qi, and J. Wang. Spectral similarity between scalars at very low frequencies in the unstable atmospheric surface layer. *Boundary-Layer Meteorol.*, 122:85–103, 2007.

Oceanographic Investigation in the Inner Kongsfjord (Svalbard, Artic Ocean)

S. Aliani, C. Galli, E. Lazzoni, C. Papucci
Institute of Marine Sciences, CNR, Pozzuolo di Lerici (SP), Italy
stefano.aliani@ismar.cnr.it

Abstract

The Kongsfjord (Svalbard) is a glacial fjord in the Arctic. Its circulation was studied for a long time except in the SE part, where the shoals of an emerging ancient moraine (Lovenøyane) separate the inner fjord and where seawater touches the glaciers. The outer circulation depends on the morphology and on offshore geostrophic circulation and wind patterns; under cross-fjord winds net transport occurs both in and out of the fjord, while along-fjord winds produce a tilt in the free surface and pycnocline and the total volume of water remains constant. This paper aims to investigate the hydrologic, sedimentary and biological processes in the inner fiord. In late summer the intrusion of the salty (>33psu) and warm (4.5°C) water into the inner fjord was visible all along the Southern coast as far as Kongsvegen. The core was at about 25 m depth. Flowing anticlockwise along the glaciers where water became colder and less saline, a layer of very cold fresh water produced by ice melting (5-10 m depth) was observed, and its northward outflow was through the passage between the Blomstrandbreen and Blomstrand island that recently opened due to the glacier's retreat. The depressions of the seabed between Lovenøyane moraine and the glaciers were filled with lenses of dense cold waters. Sedimentation processes are higher in the inner part of the fjord, close to the glacier-sea interface. In this area, the suspended load is high (up to 100 mg dm^{-3}). The residence time of particles in the water column is short (about 5 days) and the particle downward flux is consequently high (5-8 g m^{-2} d^{-1}, resulting in a huge sediment accumulation rate (exceeding 2 g cm^{-2} y^{-1}) close to Kongsvegen.

1 Introduction

The effects of Arctic climate change are expected to be most pronounced on the shelves with their tight cryo-pelagic-benthic coupling, and these changes will become a global problem when they further extend into the deep Arctic Ocean that receives a considerable portion of its carbon from the shelves [1] and from sea ice algal production [2].
Continental shelves represent about 50 percent of the Arctic Ocean: the Barents, Kara, Laptev, East Siberian and Chukchi shelves are shallow and broad (600-800km) while the shelves from Alaska to Greenland are narrow. The Arctic glaciers release every year millions of m^3 of fresh water from the ice reservoirs to the ocean and the total amount will probably increase in the next years following the global warming.
The melting zone of glaciers in the Arctic Sea has been poorly studied from the oceanographic point of view and the effects

produced by ice melting on the local hydrological features of the sea and on the transport pathways from the glacier to the open sea by currents deserve attention and monitoring.
The Kongsfjord (Figure 1) is a glacial fjord in the Arctic (Svalbard, 79°N), about 20 km long and its width varies from 4 to 10 km. It is elongated in southeast-northwest direction and exchanges with the open sea occur in the northwestern mouth. In the southeastern part, the shoals of an emerging ancient moraine (Lovenøyane) separate the inner fjord, where seawater mixes with the freshwater produced by melting of Blomstrandbreen, Kongsbreen, Kronebreen and Kongsvegen glaciers.
Some peculiar features of the Kongsfjord make it very "suitable" for climate change monitoring and assessment of "early warning". In spite of high latitude, the environment of the Kongfjord is a boundary region with Arctic and subarctic features due to warm oceanic currents from the south entering the fjord.
Because of the influence of North Atlantic water, and being an open fjord with no sill at the entrance, the exchange across the shelf-fjord boundary has a large impact on both the physical and biological environment and makes the area very sensitive to climate changes. In fact the cold and low salinity Western Svalbard coastal waters are periodically in contact with the northernmost extension of the warm North Atlantic Current, which carries relatively warm and salty water into the West Spitsbergen [3], [4]. In the inner part of Kongsfjord close to Ny Ålesund, large ice tongues (from Blomstrandbreen, Kongsbreen, Kronebreen and Kongsvegen glaciers) reach the sea.
The inner part is very interesting because is a major freshwater source for the fiord and important chemical-physical and biological processes (i.e. flocculation, algal blooms...) occur in this critical area.
Water circulation in the broad part of the fjord is well known [4] and depends on the morphology as well as on offshore geostrophic circulation and wind patterns [5]. When winds are across the fjord, net transport is in and out of the fjord resulting in flooding and emptying of the basin; when winds are along the fjord there is a tilt in free surface and pycnocline but the total volume of water in the fjord remains constant [6]. This paper aims to investigate: main oceanographic processes occurring in the inner part of the Kongsfjord close to the glaciers, the possible importance of the recently-opened passage in influencing the hydrographic, sedimentary and biological processes in the inner fjord.

2 Materials and Methods

Multidisciplinary investigations have then been carried out in September 2000 and 2001 in the inner part of the Kongsfjord at the glacier-sea interfaces, eastward to 12°E. Timeseries of water currents were collected in 2001-2002.

2.1 Hydrology and water currents

Small aluminium dinghies provided by local infrastructures in Ny Ålesund were equipped with a custom made crane and electric winch as well as GPS system. These arrangements allowed to deploy oceanographic equipment and to collect accurate positioning for CTD casting. Sea water temperature and conductivity were measured by a CTD probe IDRODAC-316 (Hydronaut) and by SBE (SeaBird). Cali-

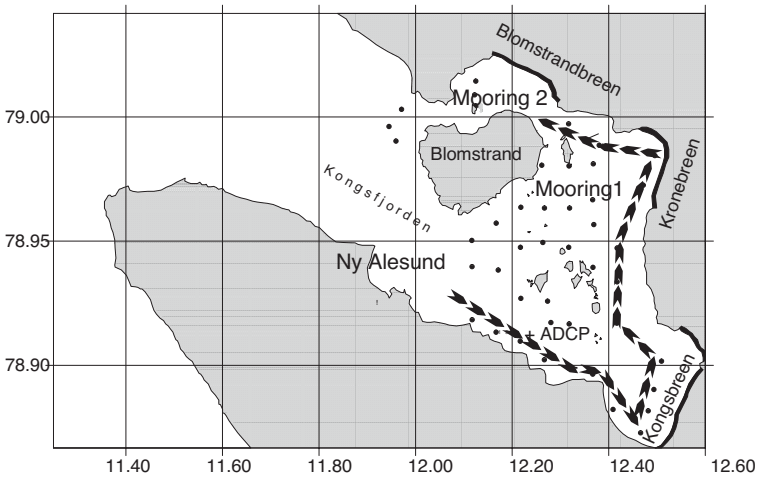

Figure 1: Map of study site. Mooring positions and CTD stations are also evidenced. Bold lines show the glaciers, the dashed line shows the transect of CTD stations reported further.

brations are done regularly by CNR staff.
Daily trips into the inner part of Kongsfjord and the recently opened Blomstrand passage were performed in the periods September 5-9-2000 and September 5-11-2001. About fifty CTD casts were performed each year. In 2001 short series were collected at the southern passage by Ånderaa RCM7 current meter and RDI ACDP. From September 2001 to September 2002 a self recording Ånderaa RCM7 current meter (Mooring 2) was deployed at 17 m depth in one of the northern openings of the moraine (GPS 78°56´58¨N 12°15´55¨E) where the major fresh water outflow toward the fjord was expected.

3 Results

3.1 Hydrology

In late summer (2000 and 2001) the intrusion of the salty (>33psu) and warm (4.5°C) water into the inner fjord was visible all along the Southern coast as far as Kongsvegen. The core was at about 25 m depth. Flowing anticlockwise along the glaciers front, the water became progressively colder and less saline; a layer of very cold fresh water produced by ice melting (5-10 m from the surface) was observed, and its northward outflow was visible out of the passage between Blomstrand and Blomstrandbreen.
This cold surface layer was not found in the areas out of the moraine.
Lenses of dense water occupied the deep inter-moraine depressions (Figure 2).

3.2 Timeseries

Short series from 5 September 2000 to 9 September 2000 were recorded at the northern passage of the moraine. Here velocity components of currents at 17 m in E-W direction were higher than in N-

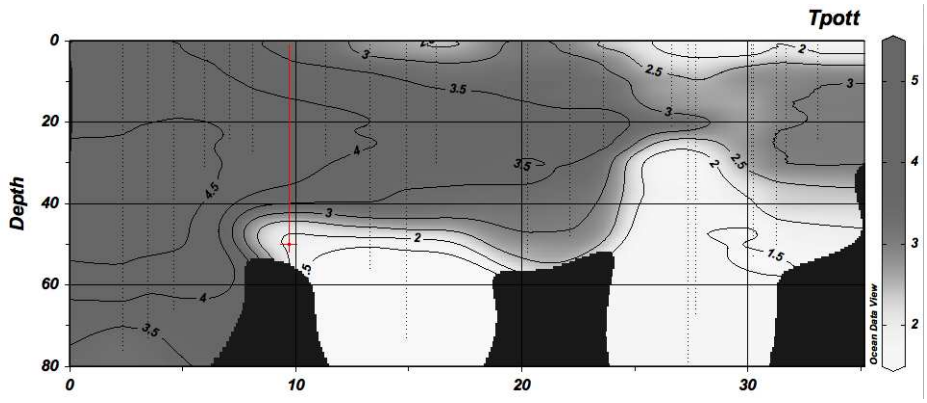

Figure 2: Plot of seawater temperature along a transect from West to East in the inner part of the fjord in September 2001. Warm layer entered the inter-morain depression at 25 m depth; cold layers were on the surface and on the bottom.

S direction by about one order of magnitude but despite eastward pulses were up up to 20 cm·s^{-1}, the progressive diagram showed a very poor net water transport with short distances covered. The year long timeseries were from the channel between Blomstrand and Blomstrandbreen (Mooring 2). Water regularly left the inner fjord at the surface with low speed (average 3.7$\pm$2.4 cm·s^{-1}) and progressive diagram of flow across this passage is reported in Figure 3. A small change in direction was recorded during winter probably because the flow was constrained by the winter ice covering the first meters of the water column at shallow depth. Seawater temperature ranged from seawater freezing point during winter to up to 5°C in summer (Figure 4) These values are consistent with those of Arctic and Atlantic water respectively, and they were found on the same spot in different periods of the year.

3.3 Primary production and suspended solids

In selected stations of the inner fjord and in a reference area in the outer fjord euphotic depths, total suspended solids (TSS), chlorophyll and phaeopigments have been determined (Figure 5).The southern part of the fjord is mainly influenced by oceanic water (low TSS, high values of PAR penetration and chlorophyll-*a*), but contributions from land are also evident: the presence of chlorophyll-*b* and -*c*, and of a lens of freshwater (evidenced by CTD profiles) suggest inputs from Brøgger Halvøya. In the inner part of the fjord, the melted glacier water is also marked by specific indexes characterising inputs of terrigenous origin: i) chlorophyll-*b* and -*c*, which are common in fresh water, ii) high values of suspended solids and, consequently, iii) strong attenuation of PAR penetration in the first few meters of the water column. The euphotic depth ranges from 10 to 2 meters [6].

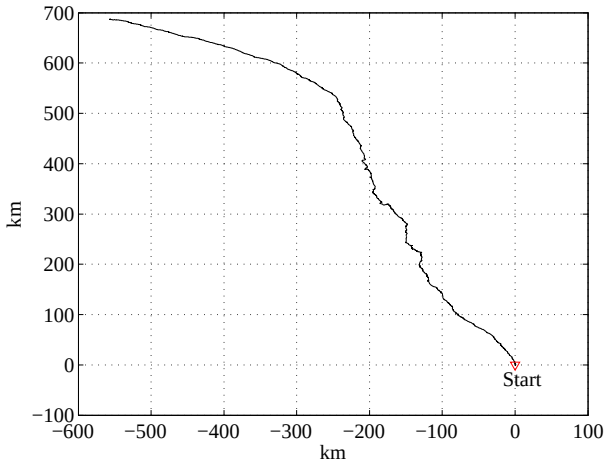

Figure 3: Progressive diagram of currents close to Blomstrand (sampling every 15 minutes). Current was directed northward exiting the inner fjord all year long.

3.4 Sedimentation

The highest concentrations of total suspended solids (up to 100 mg dm^{-3}) were found near Rundvika and Kongsvegen, while they significantly decreased in the Blomstrand passage. Data derived from the disequilibrium $^{238}U/^{234}Th$ indicated, in these areas, particle fluxes in the range 5 to 8 g $m^{-2}d^{-1}$ and very short particle residence times in the water column (about 5 days), suggesting fast sedimentation regime when approaching the glacier-sea interface. In contrast, the outer fjord was characterised by lower particle fluxes (2-4 g m^{-2} d^{-1}) and longer residence times (12-30 days) [7]. In the sediments of the inner fjord, the low POC/PON ratios (5 to 9) evidenced the input of fresh organic matter probably deriving from zooplankton that dies by osmotic shock in the contact with freshwater from the glacier outflow. They were also characterised by low concentrations of organic matter, due to its dilution into huge amounts of inorganic particles (Figure 6). The sill connecting Gerdøya to Lovenøyane seems to act as a trap for fine-grained particles that are aggregating and settling close to the glacier-sea interfaces, leading to preferential accumulation of sediments in the intermoraine depression. The sediment accumulation rates have been estimated by the analysis of the vertical profiles of $^{210}Pb_{ex}$ in sediment cores. The sedimentation rate is highest close to the Southern part of Kongsvegen (exceeding 1.8 g $cm^{-2}y^{-1}$), and it is one order of magnitude higher than in the trough between Ny Ålesund and Blomstrand (0.2 - 0.4 g $cm^{-2}y^{-1}$), and two orders of magnitude that found ($<$0.02 g $cm^{-2}y^{-1}$) in the outer fjord and on the continental shelf [6], [4].

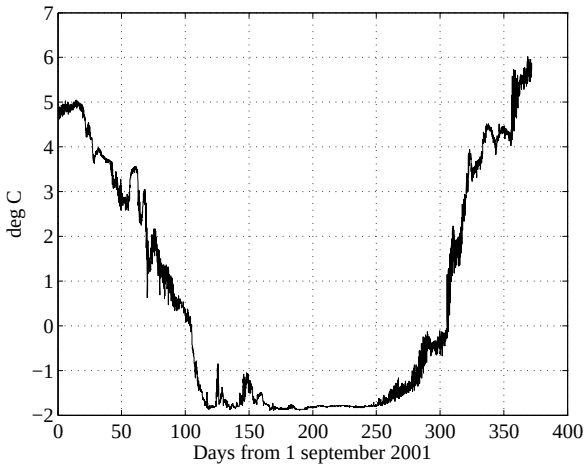

Figure 4: Plot of seawater temperature in from September 2001 to September 2002 at mooring 1. In winter seawater was close to freezing point and was up to 5°C during summer.

4 Discussion and Conclusion

The main marine features of the late-summer situation in the inner Kongsfjord, at the glaciers-sea interface, have been described. In September 2000, the net flux of water from the inner part of the fjord across the passages of the moraine was small. Ocean water entered the fjord at about 20-25 m depth and cooled interacting with the two marine ice tongues of the Kongsbreen and Kronebreen glaciers leaving cold lenses of fresh water at the surface. This surface layer diluted and temperature increased across the passage of Blomstrand where temperature was 5°C . This hydrological pattern is the result of the "recent" (early eighties) opening of the passage between Blomstrand and Blomstrandbreen, which activated a novel circulation regime, and likely influenced also sedimentation and biological processes in the inner part of Kongsfjord.

This change in the circulation regime which does not involve sea glacier interface in the Blomstrand area any more and has also important consequences for the heat balance.

In the areas where the ocean water touches the glaciers, as happens in the easternmost area in front where the lenses of cold and fresh waters were found, to melt the marine part of the glaciers about 3.340 J/kg are necessary. This heat should be provided by seawater, that in turn decreases its temperature forming the surface cold and fresh water layers we found. Ice temperature can be lower than melting temperature and a further source of heat is necessary to bring the ice tongue to 0°C. In the Blomstrand channel where the seawater doesn't touch the marine glaciers any more, assuming that the temperature of calving water from the now-terrestrial glacier Blomstrandbreen is

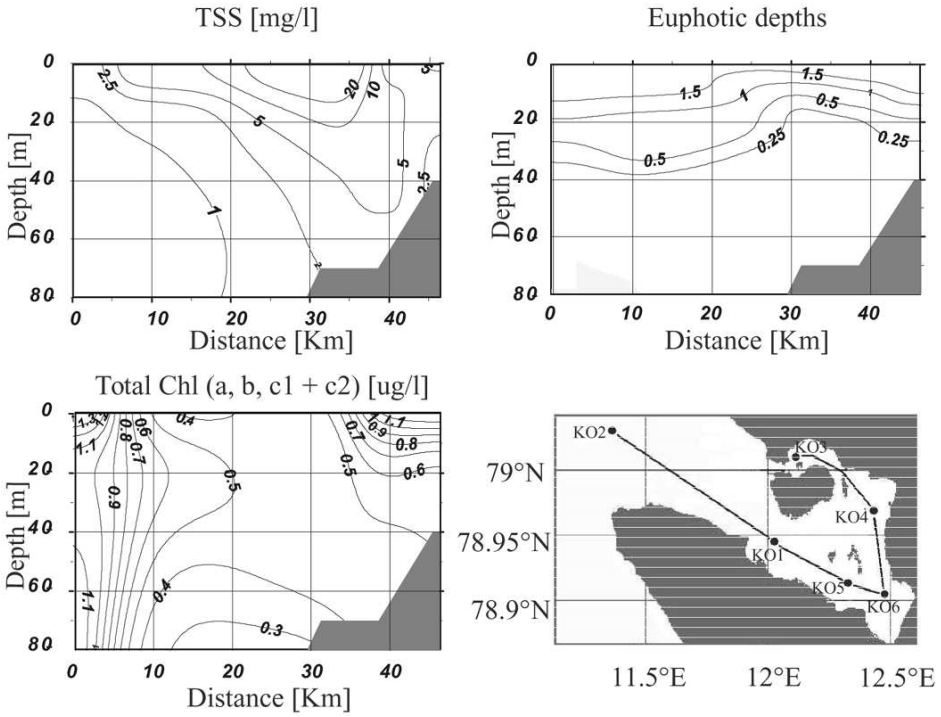

Figure 5: Distribution of euphotic depths, total suspended solids (TSS), chlorophyll and phaeopigments from the ocean (KO2) to the Blomstrand passage (KO3). From Aliani et al. 2004 modified.

higher than 0°C because of solar heating on the dark ground, seawater does not lose the latent heat and interact with warmer fresh water. The temperature across Bolmstrand passage doesn't locally decrease, nor are cold layers formed in this area as our data show. Cold surface lenses have important ecological and sedimentological roles and if they disappear an important process affecting the ecology of the fjord is lost. Cold fresh lenses also promote zooplankton alternation [8] storing in the sediments important paleoclimatic information to assess the climatic conditions in the recent past.

The annual monitoring of the swap of Arctic and Atlantic waters in the inner fjord in terms of timing and position penetration into the fjord is an important proxy to follow the change.

Changes in hydrographic conditions (e.g. warming of sea surface temperature, changes of the mixed layer, and reduction in sea ice extent), will have dramatic effects on the timing and spatial distribution of ice-associated and pelagic primary production, and subsequently on the deposition of carbon to the bottom sediments and the benthos.

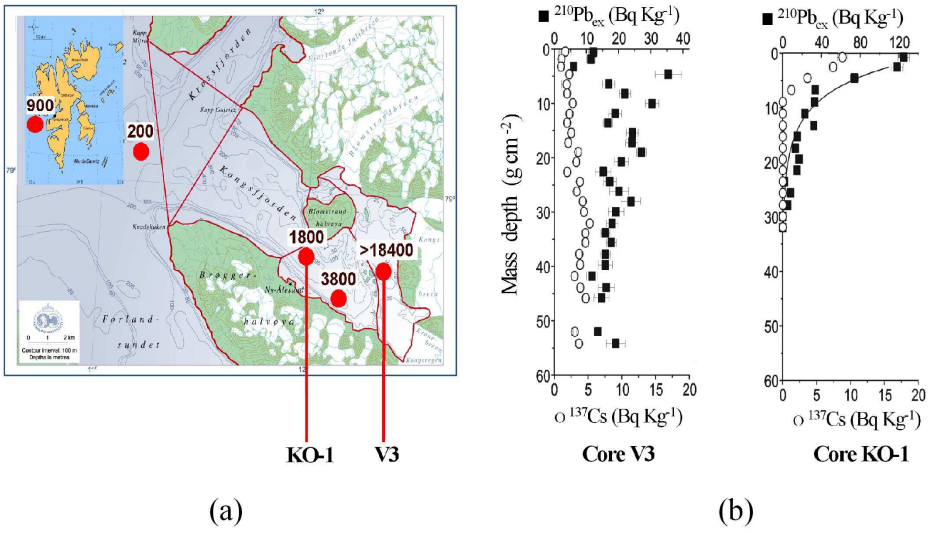

Figure 6: a) Sedimentation rates (g m^2 y^{-1}) in the Kongsfjord b) Vertical distribution of the anthropogenic radionuclide ^{137}Cs and the natural radionuclide $^{210}Pb_{ex}$ (Bq Kg^{-1}, d.w.)

4.1 Concluding remarks

The paths of water flows in the inner Kongsfjord have changed after the new passage close to Blomstrand has opened; the amount of heat lost by seawater in the inner fjord has reduced after marine ice tongues disappeared resulting in warmer waters in the fjord; temperature and currents are proposed as proxies of changes to be monitored over long periods.

5 Acknowledgments

We wish to thank the Open Source Community for the software we got from the web. We are also grateful to CNR Progetto Strategico Artico and to CNR POLARNET. Field work has been part-funded by EC-LSF program. One of the authors (CP) was involved (1996 2004) in the EU-funded Programs ARMARA and REMOTRANS through ENEA participation.

References

[1] K. Aagaard and E. Carmack. The role of sea ice and other fresh water in the Arctic circulation. Journal of Geophysical Research(94):14485–14498, 1989.

[2] M. Gosselin, M. Levasseur, P.A. Wheeler, R. A. Horner, and B. C. Booth. New measurements of phytoplankton and ice algal production in the Arctic Ocean. *Deep Sea Research Part II: Topical Studies in Oceanography*, 44(8):1623–1644, 1997.

[3] H. Loeng. Features of the physical oceanographic conditions of the Barents Sea. *Polar Research*, 10(1):5–18, 1991.

[4] H. Svendsen, A. Beszczynska-Moller, J.O. Hagen, B. Lefauconnier, V. Tverberg, S. Gerland, J.B. Orbak, K. Bischof, C. Papucci, M. Zajaczkowski, R. Azzolini, O. Bruland, C. Wiencke, J.G. Winther, and W. Dallmann. The physical environment of Kongsfjorden-Krossfjorden, an Arctic fjord system in Svalbard. *Polar Research*, 21(1):133–166, 2002.

[5] J.M. Klinck, J.J. O'Brien, and H. Svensen. A simple model of fiord and coastal circulation. *Journal of Physical Oceanography*, 11:1612–1626, 1982.

[6] S. Aliani, G. Bartholini, F. Deglinnocenti, R. Delfanti, C. Galli, E. Lazzoni, R. Lorenzelli, A. Malaguti, R. Meloni, C. Papucci, S. Salvi, and A. Zaborska. Multidisciplinary Investigations in the marine environment of the inner Kongsfiord, Svalbard Islands (September 2000 and 2001). *Chemistry and Ecology*, 20:19–28, 2004.

[7] C. Papucci, R. Delfanti, G. Bartho Andlini, L. Vintrò, K. J. Smith, and P.I. Mitchell. Scavenging and particle residence time at the glacier sea interface in Arctic fiords. *Proc. 5th Intern. Conf. on Environmental radioactivity in the Arctic and Antarctic*, 2002.

[8] M. Zajczkowski, W. Szczuciski, and R. Bojanowski. Recent changes sediment accumulation rates in Adventfjorden, Svalbard. 46(2):217–231, 2004.

The Role of Dissolved Organic Matter in the Global Carbon Cycle

C. Santinelli, R. Lavezza, A. Seritti
Institute of Biophysics, CNR, Pisa, Italy
chiara.santinelli@pi.ibf.cnr.it

Abstract

Dissolved organic matter (DOM) represents the most complex and the less understood reservoir of organic carbon on the Earth. The difficulty to describe and quantify marine DOM dynamics and cycle is due to the very scarce information on its numerous sources and sinks and to its variable and unknown composition. Dissolved organic carbon (DOC), representing the 93% of DOM pool, can give quantitative information on its pool. The study of DOC data, collected since 1999 during several field studies, in different regions of the Mediterranean Sea (from the Ionian to the Balearic Sea), underlines that DOC plays a significant role in carbon cycle. DOC distribution was studied in relation to water mass characteristics and circulation. Following the core of the Levantine Intermediate Water (LIW), a gradual DOC decrease going away from its source was observed. In the deep layer of some Mediterranean areas, close to deep water formation sites, DOC exhibited high concentrations ($>$ 55 μM) whereas in other Mediterranean regions, both in the intermediate and deep waters, DOC showed low values (30-45 μM), similar to those reported for the oceanic deep waters (34-48 μM). This finding opens intriguing questions on the role of DOC in carbon export to depth, during deep waters formation and on the DOC utilization processes in different layers of the Mediterranean waters.

1 Scientific background

Dissolved organic matter (DOM) is a complex mixture of molecules, most of them yet unknown. It plays a key role in the global carbon cycle as it represents one of the largest reservoir of reactive carbon on the Earth. It contains an amount of carbon ($700 \cdot 10^{15}$ g C), comparable to that occurring in the atmosphere ($720 \cdot 10^{15}$ g C). As a consequence, the oxidation of only 1% of DOM may determine a release of CO_2 in the atmosphere comparable to that released by the combustion of all fossil fuels ($5.5\ 10^{15}$ g C/y^{-1}) [1]. In addition, the enhancement of UV-B radiation reaching the Earth induces photochemical reactions that affect the quality and the quantity of DOM in the upper layer of the water column, with important implications for the CO_2 flux from the sea surface to the atmosphere [2]. DOM not only strongly affects CO_2 concentration in the atmosphere, but it also plays a key role in the microbial food web, as it is the main source of food for heterotrophic bacteria [3].

The fraction of DOM capable of absorbing light (PAR, UV-A and UV-B) is defined chromophoric DOM (CDOM). CDOM can represent an highly variable fraction of DOM and it plays a major role in marine ecosystem, in fact it determines the under-

water light availability in the open ocean and coastal waters. The absorption of the UV and blue portions of the solar radiation leads to the photodegradation of the original CDOM, with a consequent reduction of its absorbing light capacity. Through this process, CDOM is degraded into smaller compounds, with lower molecular weight, lower internal energy, and different optical properties. This kind of CDOM may be consumed by bacteria in a short time. CDOM also affects the accuracy of global satellite measurements of ocean chlorophyll and primary production. Despite the key role played by DOM and CDOM in marine ecosystems and in the global carbon cycle, the spatial distribution and variability of carbon sources and sinks at global scale is far from being precisely quantified. DOM concentration in oceanic waters is mainly the result of biological activity, while its distribution is mainly driven by water masses circulation [4]. Recently, a link between DOC distribution and circulation of the main water masses in the Mediterranean Sea has been detected and the occurrence of different DOC concentrations in different water masses was reported [5, 6]. Circulation changes, induced by climate change, may significantly affect DOM distribution. Due to the important role of DOM in the microbial food web, a change in the distribution of DOM, in particular of its semi-labile fraction, may have a strong impact on the functioning of the whole marine ecosystem.

2 Scientific research activity

2.1 Dynamics of Dissolved organic matter (DOM) in the Mediterranean Sea

The research activity is focused, since more than ten years, on the study of DOM dynamics in the Mediterranean Sea, with an holistic approach. This means that the study is carried out by measuring the concentration of dissolved organic carbon (DOC), that represents more than the 93% of DOM and, as a consequence, it can be considered representative of its concentration. More recently we combined DOC measurements with the analysis of the optical properties (absorption and fluorescence) of CDOM. These data can give some qualitative information on DOM pool, in particular: (i) the occurrence of different kind of chromophores; (ii) the changes in CDOM optical properties due to photodegradation or to bacterial transformation; (iii) the main sources of CDOM; (iv) an indirect estimation of its molecular weight and aromaticity degree.

This approach allows to study the behaviour of the whole pool of DOM, without going inside its molecular composition. It is important to stress that up to now only the 10 % of the DOM pool as been characterized at molecular level [7], so more than 90 % of the molecules constituting the DOM pool are unknown. The holistic approach tries to combine the DOC distribution with the other physical, chemical and biological parameters. A multi and interdisciplinary approach is fundamental to clarify DOM dynamics. During many cruises carried out in different areas of the Mediterranean Sea, seawater samples for

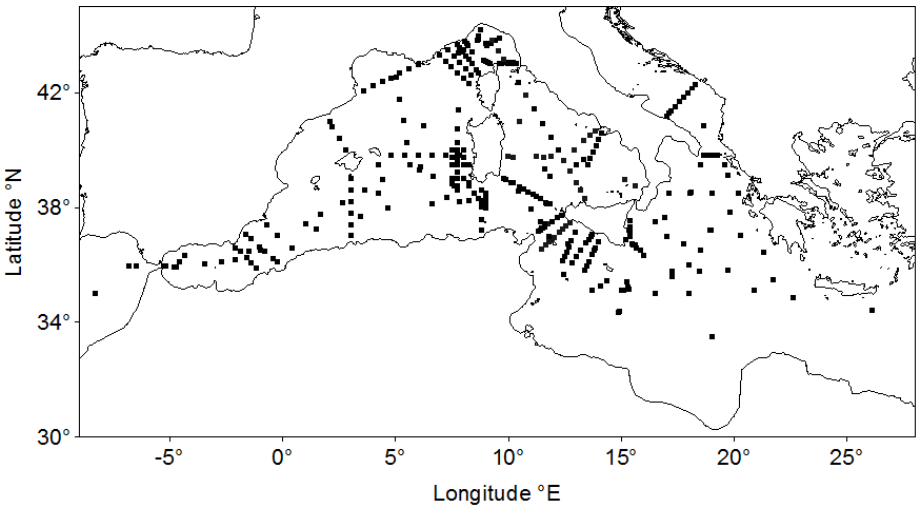

Figure 1: Map of the stations sampled since the 1999

DOC analysis were collected from the surface to the bottom. Figure 1 can give an idea of the spatial coverage of our data.
The research activity is focused on the Mediterranean Sea because it is a semi enclosed basin with peculiar biogeochemical characteristics. It can be considered as a natural laboratory for the study of physical processes, in fact here the main oceanographic processes occur on a reduced temporal and spatial scale and for this reason, it can respond very quickly to climate changes. In addition, it is a challenging site for the study of biogeochemical cycles, in fact it is a phosphorus limited basin, with peculiar N:P ratio.
At today we have a general picture of the DOC distribution in the intermediate and deep waters of the Mediterranean Sea [8], in contrast, only very few papers report the behaviour of the optical properties (absorption and fluorescence) of CDOM in the Mediterranean Sea and none of them refers to open sea areas [9, 10, 11].

3 Main results

3.1 DOC dynamics in meso and bathypelagic layers of the Mediterranean Sea

DOC distribution was studied in the different areas of the Mediterranean Sea reported in Figure 1 [8]. In general, the Mediterranean DOC pool showed a strong heterogeneity and dynamic nature together with an high variability both in the surface and deep layers. DOC distribution in the Mediterranean Sea is significantly affected by horizontal transport due to water masses circulation and vertical export due to winter deep convection. In most of the stations, DOC vertical profiles were similar to those observed for both oceanic waters [3, 4] and other Mediterranean Sea areas [12, 13, 14, 15, 16, 17, 6, 18]. DOC in the surface layer (0-100 m) showed the highest and most variable concentrations (46-100 μM), without significant dif-

ferences between the Western and the Eastern Mediterranean Sea. In the intermediate layer (200-500 m), DOC values ranged between 44 and 53 μM in most of the stations. Surprisingly, deep waters were characterized by high variability in the whole range of DOC (34-76 μM). In addition, in some areas, DOC showed a marked increase with very high values ($>$ 60 μM) close to the bottom [8]. High DOC and dissolved oxygen values were previously observed in the Mediterranean Sea in correspondence with newly formed deep waters [6, 5].

In order to better describe the DOC dynamics in the Mediterranean meso and bathypelagic layers, its distribution in the core of the Levantine Intermediate water (LIW) and in the bottom waters was detected [8]. The LIW is the only water mass that can be clearly identified by its salinity maximum. It forms in the northeastern Levantine basin and flows across the whole Mediterranean Sea, as far as Gibraltar, so it represents the Mediterranean contribution to the oceanic thermohaline circulation. LIW route is rather complicated and it follows different paths because it is trapped by eddies [19]. In general, DOC and apparent oxygen utilization (AOU, calculated by subtracting the concentration of dissolved oxygen from the oxygen at saturation) showed an opposite behavior moving from the Levantine Basin to the Western Mediterranean Sea: DOC decreased from 68 to $<$ 40 μM, while AOU increased from 10 to $>$ 90 μM, with an absolute minimum of DOC in the southern part of the Algerian Basin in correspondence to a maximum of AOU. These data suggest that in the core of LIW, both DOC and oxygen are consumed while the water goes away from its formation site. The contribution of DOC mineralization to the oxygen consumption was determined considering only the samples collected in the LIW core, that are those characterized by a S$>$ 38.70. The data indicated that DOC mineralization accounts for the 38% of oxygen consumption in the core of the LIW [8]. In addition the DOC removal rate in the core of LIW was estimated to be of about 2.2 μM·yr$^{-1\cdot}$ This value is about double than the highest values reported for the open ocean [3].

The DOC distribution in the bottom waters is very interesting too. Here, in fact, a marked increase of DOC ($>$ 60 μM) was observed in the Gulf of Lions, in the Southern Adriatic Sea and in the Ionian Sea; these maxima were associated with a minimum of AOU ($<$47 μM). All these regions are influenced by deep water formation. In contrast, low DOC concentrations were observed in the southwestern Mediterranean Sea in October 2004 ($<$49 μM) and in the Tyrrhenian Sea ($<$45 μM). In these areas old deep waters occurred as confirmed by the high AOU values (62-72 μM) [8].

A particularly strong event of deep water formation was observed in the Western Mediterranean Sea in the winter 2005 ([20, 21], so the high DOC concentrations (55-76 μM) detected in May 2005 in this area, can be attributed to the export of a large amount of DOC to depth during this particular event. An estimation of this amount was calculated by considering the mean production rate of DW reported by Shroeder et al. [22] (2.4 Sv, that is 2.4·10^6 m^3 $\cdot$ s^{-1}) and assuming that winter surface DOC concentrations ranged between 50 and 80 μM (the typical range of surface DOC values in the whole Mediterranean Sea). Considering 40 μM as representative of DOC in DW, a difference of 10-40 μM can be calculated between DOC at surface and DOC at depth. Given these assumptions, the export of DOC ranged between 0.29 and 1.15·10^6 g C·s^{-1} (0.76-3.02 Tg $\cdot$

C month^{-1}) [8]. Assuming that the lowest DOC concentration observed in Mediterranean waters (34 μM) represents the refractory fraction, all the DOC exported at depth should be in the semi-labile form [8]. This is a huge amount and underlines the importance of DOC in the global carbon cycle, both in terms of carbon sequestration and energy input for deep water ecosystems.

4 Work in progress

At today the general picture of DOC distribution in the meso and bathypelagic waters of the Mediterranean Sea has been widely described [8], so it is now very important to: (1) complete this scenario with DOC dynamics in the surface layer; (2) integrate these information with CDOM distribution and characteristics in the Mediterranean Sea; (3) study DOC and CDOM distribution in fixed locations in order to asses their seasonal and interannual variability. Concerning CDOM, the absorption coefficient at 355 nm (a_{355}) was chosen as representative of the whole absorbing dissolved organic compounds.

4.1 Seasonal dynamics of DOM in the coastal long-term ecological station "Mare Chiara" (Gulf of Naples)

DOC and CDOM data have been collected monthly (in 2007) or every two weeks (in 2008 and in 2009), in collaboration with the Zoological Station "A. Dhorn" of Naples (SZN), in the coastal long-term ecological station "Mare Chiara" (Gulf of Naples). The sample collection is still in course for the 2011. This is a very interesting site, in fact, it is located in an area strongly influenced by terrestrial inputs, mainly represented by urban discharge. Depending on the period and the circulation in the Gulf, it can behave as an oligotrophic station or a coastal site strongly influenced by the land.

The monthly vertical distribution of dissolved organic carbon (DOC) and CDOM (absorption at 355 nm, a_{355}) in the years 2007 and 2008 are reported in Figure 2. In general, DOC and the a_{355} showed values ranging from 40 to 140 μM and from 0.1 to 0.37 m^{-1}, respectively. If the highest values are excluded (>90 μM for DOC and $>$ 0.3 m^{-1} for a_{355}) the observed ranges are in agreement with the data reported for the Ocean and the Mediterranean open sea waters [24, 3, 8]. A strong seasonal and interannual variability, in particular in the surface layer (0-10 m), was observed. DOC and CDOM showed two maxima (DOC: 90-140 μM a_{355}: 0.22-0.37 m^{-1}): one more marked in the first 10 m of the water column in March-August 2007, the other in the first 5 m in April-July 2008. These maxima were observed in correspondence to the highest phytoplanktonic biomass abundance (data not reported), suggesting that phytoplankton could be a direct source of both DOC and CDOM and that the occurrence of a strong thermocline may determine their accumulation. On the other hand, the maxima of Chlorophyll a, DOC and CDOM were observed in correspondence of low salinity waters (data not reported), probably indicative of a terrestrial input (mainly urban discharge). The high DOC concentrations and the high values of a_{355} observed in the mixed layer are the result of a decoupling between production and removal processes. When the thermocline breaks, the DOC accumulated in the mixed layer is transported to depth, representing an im-

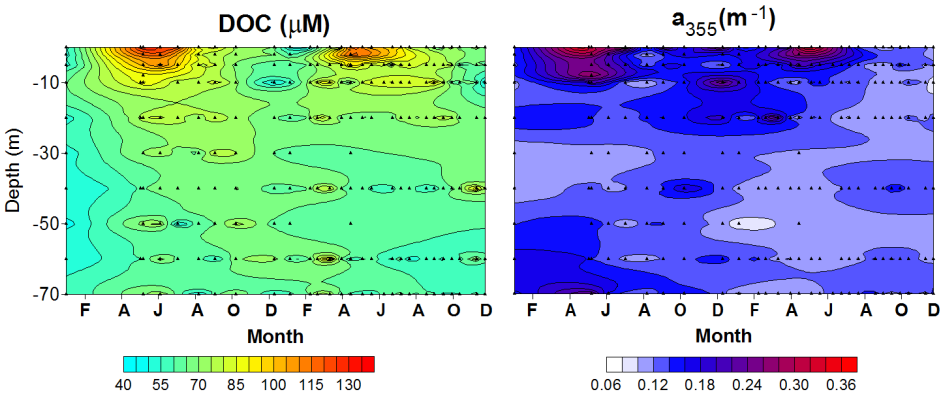

Figure 2: Vertical distribution of DOC (on the left) and a_{355} (on the right) in the years 2007 and 2008, in the Gulf of Naples (in collaboration with SZN).

portant source of energy for the microbial loop. As expected, in the winter, DOC and a_{355} showed low values, comparable to those reported for open sea waters, with a general homogeneity along the water column, due to the high extent of vertical mixing. The DOC trend is comparable to that observed in the Sargasso Sea [24]; in fact, the maximum was observed above the thermocline, in the period of strong stratification in both sites, even if the value of this maximum in the Gulf of Naples is about twice than that reported for the Sargasso Sea. In contrast, CDOM showed an opposite behavior in the two sites. In the Sargasso Sea a minimum in summer was observed in the surface layer and this was attributed to the effect of the photobleaching. In contrast, at "Mare Chiara" station, the high CDOM concentration observed in summer probably mask the effect of the photobleaching.

These data indicates that anthropogenic inputs can significantly affect the marine carbon cycle, determining an increase of primary production and an accumulation of DOC and CDOM. An interdisciplinary analysis of these data is still in course in collaboration with the SZN.

4.2 DOC seasonal variability in the Southern Adriatic Sea

In the framework of the Italian Project VECTOR ("VulnErabilità delle Coste e degli ecosistemi marini italiani ai cambiamenti climaTici e loro ruolO nei cicli del caRbonio mediterraneo"), six oceanographic cruises were carried out in the Southern Adriatic Sea, that is an important site of deep water formation for the Eastern Mediterranean Sea. Samples for DOC analysis were collected in nine stations, along the whole water column, in fall (November 2006, September 2007), winter (February 2007 and 2008), spring (April 2007) and summer (June 2008). CDOM absorption spectra were performed during the first three cruises. Figure 3 reports the DOC vertical distribution along this section (see inset map) during three cruises. Considering three periods, main features are: (i) seasonality mainly affects DOC distribution in the upper layer (0-200 m) of the

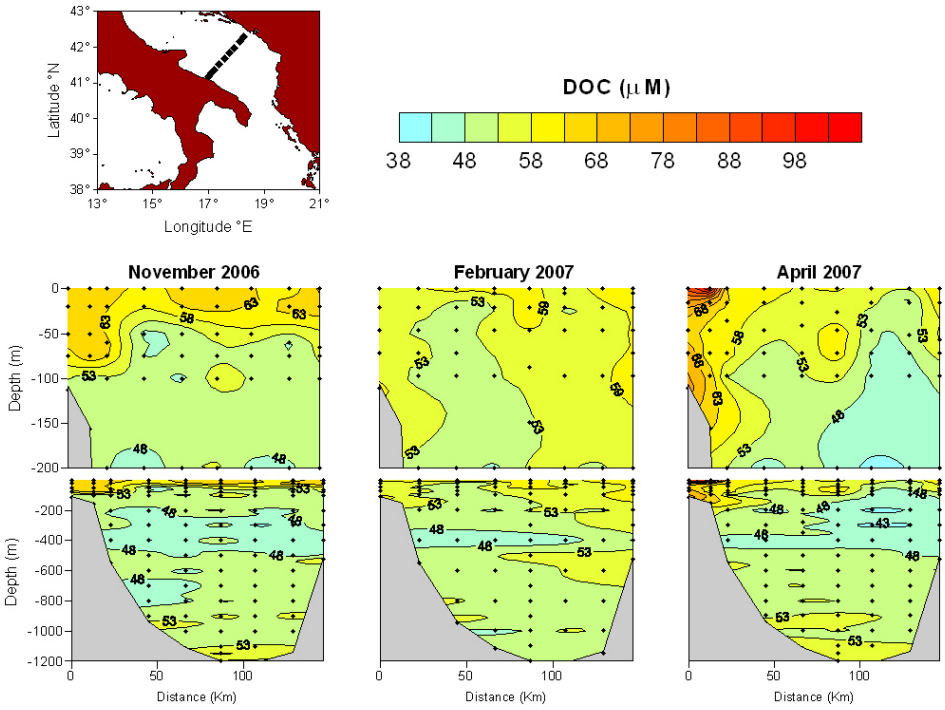

Figure 3: DOC vertical distribution in the Southern Adriatic Sea (see inset map) during three cruises. (Readapted from Santinelli et al.,[23]). The zoom of the surface layer (0-200 m) is reported for each month in the upper panel.

water column, but the range of values is almost comparable. (ii) Considering all the samples, DOC values ranged between 41 and 102 μM, with the highest values (>58 μM) in the surface layer (0-50 m) when the stratification of the water column was high (November 2006) and close to the Italian coast in April 2007. (iii) The minimum of DOC (41-48 μM) was always present in the intermediate layer interested by the occurrence of the LIW, recognizable by its salinity maximum and oxygen minimum (data not reported). (iv) High DOC values (>53 μM) were found in the deep waters (> 1000 m) in 2007 (November 2006) and in April 2007. This finding was attributed to the occurrence of young recently ventilated waters, in the central part of the section, advected from the Northern Adriatic Sea.

Table 1 reports the average values and the ranges for DOC and a_{355} for the first three cruises. Both parameters showed no significant differences between the different periods not even in the surface layer, confirming that seasonality affected the distribution of the DOC and CDOM more than their absolute values. In addition both DOC and a_{355} showed the lowest average values (DOC < 50 μM, $a_{355} < 0.13$ m^{-1}), in the intermediate waters, mainly characterized by the occurrence of the LIW. These a_{355} data are the first one reported

	Depth (m)	DOC (μM)	a_{355} (m^{-1})
November 2006	0-100	58±7	0.16±0.03
		46-69	0.10-0.23
	200-400	47±4	0.11±0.03
		41-54	0.07-0.15
	900-bottom	52±3	0.15±0.04
		48-59	0.11-0.21
February 2007	0-100	57±5	0.17±0.07
		48-65	0.10-0.52
	200-400	50±4	0.13±0.03
		44-57	0.11-0.17
	900-bottom	50±3	0.15±0.03
		46-55	0.12-0.20
April 2007	0-100	59±11	0.16±0.05
		46-102	0.09-0.32
	200-400	46±3	0.10±0.01
		41-53	0.08-0.11
	900-bottom	54±2	0.14±0.02
		49-56	0.12-0.18

Table 1: Average values and ranges of DOC and a_{355} for the cruises carried out in the southern Adriatic Sea in November 2006, February and April 2007.

for the open sea waters of the Mediterranean Sea; in general, they ranged from 0.07 to 0.23 m^{-1} during all the three periods and these values are comparable with those reported in the literature for the oceanic waters ([25] and literature there quoted). Some point maxima were also observed, one (0.52 m^{-1}) was found in February 2007, in correspondence to the deep chlorophyll maximum (DCM), even if further investigation are requested, this may suggest that this increase in CDOM could be explained by in situ production, probably due to phytoplankton activity. In addition, in April 2007, high values of a_{355} (0.32 m^{-1}) were found close to the Italian coast, these were associated to an increase in DOC. This observation may indicate an input of allocthonous DOM, probably transported from the Northern Adriatic Sea by the Western Adriatic current.

4.3 DOC and CDOM distribution in the surface layer of different areas of the Mediterranean Sea

As above reported one of the main goals of our study is to investigate the spatial distribution DOC and CDOM in open sea waters, in relation to the water masses circulation and to the biological and chemical pro-

cesses in the upper layer (0-150 m). Samples for DOC and a_{355} measurements were collected in open sea areas of the Mediterranean Sea (Western Mediterranean, Ionian Sea, Sicily Channel), in the framework of the European IP Project SESAME (Southern European Seas: Assessing and Modelling Ecosystem Changes). As an example, Figure 4 reports DOC and a_{355} distribution in one section located in the Ionian Sea in two periods, characterized by different physical characteristics: March 2008, after the winter mixing and September 2008 after summer stratification.

In general, CDOM (a_{355}=0.05-0.2 m^{-1}) and DOC (52-75 μM) showed values comparable to those reported in the literature for open oceanic waters and to those above reported for the Adriatic Sea and in the Gulf of Naples (in the fall and winter seasons). A clear change in their distribution is visible between the two periods although the range was almost the same. In March 2008, DOC showed an high vertical homogeneity, with high values ($>$ 64 μM) in the central part of the section and values of 54-58 μM in the other stations from the surface down to 150 m, a_{355} showed nor a clear trend neither a clear correspondence with the DOC distribution, if the high values in the northern station are excluded. In September, when the stratification was high, the highest DOC values ($>$64 μM) were observed in the upper 50 m, they decreased until 42-54 μM at 150 m. a_{355} showed a different distribution, with a maximum ($>$ 0.11 m^{-1}) between 20 and 90 m and low values ($<$ 0.09 m^{-1}) at the surface. This behaviour can be explained, according to the literature, with the photobleaching of CDOM, which is strong when the stratification and the solar irradiation are high, as happens in the summer. The same general features were evidenced also in the other areas of the Mediterranean Sea, in particular, the ranges of values are almost the same both for DOC and CDOM, and it is clearly evident the accumulation of DOC in the mixed layer in fall and the effect of photobleaching in determining a decrease of a_{355} at surface in summer. In addition, it has to be stressed that DOC and CDOM dynamics are clearly decoupled in open sea waters (Figure 4), in contrast to what observed in the Gulf of Naples (Figure 2). These preliminary data are under interpretation together with the other physical, chemical and biological parameters.

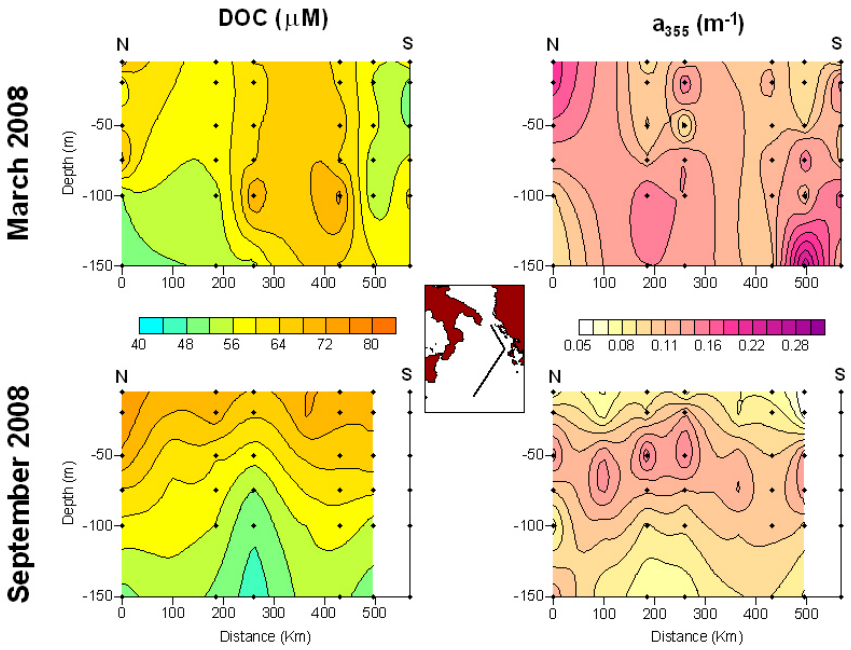

Figure 4: DOC and a_{355} distribution in a section located in the Ionian Sea in March 2008 (upper panels) and in September 2008 (lower panels).

5 Conclusions

Our data confirm that DOM plays a key role in the global carbon cycle, in fact, it can contribute to carbon sequestration through two processes: (1) during deep water formation an huge amount of carbon can be exported to depth, where it can remain many years before coming back to the atmosphere; (2) the DOM accumulated in the mixed layer after summer, is transported in the mesopelagic layer when the thermocline breaks. So, it can be consumed below 100 m and also in this case it needs some months or years to come back to the atmosphere. DOM can also significantly contributed to the atmospheric CO_2 pool, through the photoxidation processes, which are evident in summer in the open sea waters. The flux of CO_2 to the atmosphere due to DOM oxidation has not been yet correctly quantified.

Another feature that emerges from our data is that the range of concentration of DOC is almost the same in different areas of the Mediterranean Sea as in the Ocean, without significant changes in the different seasons; seasonality mainly affect its distribution. This finding evidences that this pool is stable, instead its dynamism.

6 Open questions

Many unresolved questions deal with DOM. How much DOM is refractory? How much is labile? How can we discriminate between fractions with different

biological lability? Which is the age of Mediterranean DOM? Which is its main origin? If we consider the exchanges at Gibraltar, the input of DOC from Atlantic is higher than the output, this suggests that the Mediterranean Sea is a remineralization basin, but is this true? The finding of an answer to these and many other unresolved questions is an intriguing challenge that could give key information on the processes determining the role of the Ocean as sink and/or source of CO_2 for the atmosphere.

7 Acknowledgments

This research is supported by the SESAME project, EC Contract No GOCE-036949, funded by the European Commission's Sixth Framework Programme under the priority "Sustainable Development, Global Change and Ecosystems" and by the VECTOR project funded by the Italian Ministry of Research and University. Part of the data were collected also in the framework of the research program "Ecosistemi Marini-SINAPSI" funded by the Italian Ministry of Research and University. We wish to thank the Area MECA (Dr. Saggiomo) of the SZN, for collecting samples for DOC and CDOM in the Gulf of Naples. Particular thanks are due to the captains and crews of the CNR RV "Urania" and RV "Dallaporta" and Conisma RV "Universitatis", for their assistance and continuous support during the cruises. Finally, we wish to thank Dr A. Porfido and Dr S. Puerari for their help in the analysis of CDOM absorption spectra.

References

[1] J.I. Hedges. Why dissolved organics matter. pages 1–33, 2002.

[2] N.V. Blough and R. Del Vecchio. Chromophoric dissolved organic matter (cdom) in the coastal environment. pages 509–546, 2002.

[3] C.A. Carlson, D.A. Hansell, N.B. Nelson, D.A. Siegel, W.M. Smethie Jr., S. Khatiwala, M.M. Meyers, and E. Wallner. Dissolved organic carbon export and subsequent remineralization in the mesopelagic and bathypelagic realms of the North Atlantic basin. *Deep-Sea Research Part II*, 57(16):1433–1445, 2010.

[4] D.A. Hansell. Doc in the global ocean carbon cycle. pages 685–715, 2002.

[5] A. Seritti, B.B. Manca, C. Santinelli, E. Murru, A. Boldrin, and L. Nannicini. Relationships between dissolved organic carbon (DOC) and watermass structures in the Ionian Sea (winter 1999). *Journal of Geophysical Research*, 108(C9)(8112), 2003.

[6] C. Santinelli, B.B Manca, G.P. Gasparini, L. Nannicini, and A. Seritti. Vertical distribution of dissolved organic carbon (DOC) in the Mediterranean Sea. *Climate Research*, 31:205–216, 2006.

[7] R. Benner. Chemical composition and reactivity. pages 59 – 90, 2002.

[8] C. Santinelli, L. Nannicini, and A. Seritti. DOC dynamics in meso and bathypelagic layers of the Mediterranean Sea. *Deep Sea Research Part II*, 57(16):1446–1459, 2010.

[9] A. Seritti, D. Russo, L. Nannicini, and R. Del Vecchio. DOC, absorption and fluorescence properties of estuarine and coastal waters of the Northern Tyrrhenian Sea. *Chemical Speciation and Bioavailability*, 10:95–106, 1998.

[10] M.G. Ferrari. The relationship between chromophoric dissolved organic matter and dissolved organic carbon in the European Atlantic coastal area and in the west Mediterranean Sea. *Marine Chemistry*, 70:339–357, 2000.

[11] S. Vignudelli, C. Santinelli, E. Murru, L. Nannicini, and A. Seritti. Distributions of dissolved organic carbon (DOC) and chromophoric dissolved organic matter (CDOM) in coastal waters of the northern Tyrrhenian Sea (Italy). *Estuarine, Coastal and Shelf Sciences*, 60:133–149, 2004.

[12] G. Cauwet, F. Gadel, M.M. De Souza Sierra, O. Donard, and M. Ewald. Contribution of the Rhone River to organic carbon inputs to the north-western Mediterranean Sea. *Continental Shelf Research*, 10(9 - 11):1025–103, 1990.

[13] G. Copin-Montegut and B. Avril. Vertical distribution and temporal variation of dissolved organic carbon in the north-western Mediterranean Sea. *Deep Sea Research Part I*, 40:1963–1972, 1993.

[14] E. Dafner, M. Gonzalez-Davila, J.M. Santana-Casiano, and R. Sempéré. Total organic and inorganic carbon exchange through the Strait of Gibraltar in September 1997. *Deep Sea Research Part I*, 48:1217–1235, 2001.

[15] E.V. Dafner, R. Sempéré, and H.L. Bryden. Total organic carbon distribution and budget through the Strait of Gibraltar in April 1998. *Marine Chemistry*, 73:233 – 252, 2001.

[16] B. Avril. DOC dynamics in the northwestern Mediterranean Sea (DYFAMED site). *Deep Sea Research Part II*, 49:2163 – 218, 2002.

[17] R. Sempéré, E. Dafner, F. Van Wambeke, D. Lefèvre, C. Magen, S. Allègre, F. Bruyant, M. Bianchi, and L. Prieur. Distribution and cycling of total organic carbon across the Almeria-Oran Front in the Mediterranean Sea: Implications for carbon cycling in the western basin. *Journal of Geophysical Research*, 108(C11)(3361), 2003.

[18] C. Santinelli, A. Ribotti, R. Sorgente, G.P. Gasparini, L. Nannicini, S. Vignudelli, and A. Seritti. Coastal dynamics and dissolved organic carbon in the western Sardinian shelf (Western Mediterranean). *Journal of Marine Systems*, 74:167–188, 2008.

[19] C. Millot. Circulation in the Western Mediterranean Sea. *Journal of Marine Systems*, 20:423–442, 1999.

[20] M. Canals, P. Puig, X. Durrieu de Madron, S. Heussner, A. Palanques, and J. Fabres. Flushing submarine canyons. *Nature*, 444:354 – 357, 2006.

[21] K. Schroeder, G.P. Gasparini, M. Tangherlini, and M. Astraldi. Deep and intermediate water in the western Mediterranean under the influence of the Eastern Mediterranean Transient. *Geophysical Research Letters*, 33(L21607), 2006.

[22] K. Schroeder, A. Ribotti, M. Borghini, R. Sorgente, A. Perilli, and G.P. Gasparini. An extensive western Mediterranean deep water renewal between 2004 and 2006. *Geophysical Research Letters*, 35(L18605), 2008.

[23] C. Santinelli, M. Ribera D'Alcalà, G. Civitarese, R. Lavezza, and A. Seritti. DOC export below the mixed layer in the Southern Adriatic Sea. *39th CIESM Congress proceedings*, 2010.

[24] N.B. Nelson and D.A. Siegel. Chromophoric dissolved organic matter (cdom) in the open ocean. pages 547 – 578, 2002.

[25] N.B. Nelson and D.A. Siegel. Chromophoric dissolved organic matter (cdom) in the open ocean. pages 423–442, 2002.